JOURNAL OF THE MECHANICS AND PHYSICS OF SOLIDS.

EDITORIAL ADVISORY BOARD

J. F. BAKER—Cambridge W. M. BALDWIN—Cleveland
E. BRANDENBERGER—Zürich G. BUSCH—Zürich
A. H. COTTRELL—Harwell C. CRUSSARD—Paris M. J. DRUYVESTEYN—Delft
A. KOCHENDÖRFER—Düsseldorf N. F. MOTT—Cambridge
A. NADAI—Pittsburgh, Pa. G. SACHS—Syracuse, N.Y. E. SIEBEL—Stuttgart

EDITOR-IN-CHIEF

R. HILL
University of Nottingham

Volume 4
1955—56

PERGAMON PRESS LTD LONDON & NEW YORK

Contents of Volume 4

Number 1

PAGE

R. Hill: On related pairs of plane elastic states 1

R. T. Shield: On Coulomb's law of failure in soils 10

G. Eason and R. T. Shield: The influence of free ends on the load-carrying capacities of cylindrical shells 17

R. A. Lad and F. I. Metz: An experimental investigation of the effect of vacancy and F-centre concentrations on the transient creep of sodium chloride single crystals 28

H. G. Hopkins: On the behaviour of infinitely-long rigid-plastic beams under transverse concentrated load 38

Number 2

G. Eason and R. T. Shield: Dynamic loading of rigid-plastic cylindrical shells 53

D. S. Berry and S. C. Hunter: The propagation of dynamic stresses in visco-elastic rods 72

L. W. Hu: An experimental study on the fracture of metals under hydrostatic pressure 96

M. R. Horne: The elastic-plastic theory of compression members .. 104

B. B. Muvdi and K. N. Tong: Yielding in compression of strip between smooth dies 121

A. P. Green and B. B. Hundy: Initial plastic yielding in notch bend tests 128

Number 3

P. G. Hodge, Jr. and F. Romano: Deformations of an elastic-plastic cylindrical shell with linear strain hardening 145

A. J. Kennedy: A reconciliation of certain recovery properties in metals.. 162

W. Prager: On conjugate states of plane strain 167

J. Hennephof: The tearing of aluminium foils 172

T. F. Jordan and E. G. Thomsen: Comparison of an unsymmetric slip-line solution in extrusion with experiment 184

W. Johnson: Extrusion through square dies of large reduction 191

J. E. Adkins: Associated problems in two-dimensional elasticity.. .. 199

NUMBER 3 (*continued*)

PAGE

Book Reviews:

" Probleme der Plastizitätstheorie " by W. PRAGER (Reviewed by R. HILL) 206

" X-ray Diffraction by Polycrystalline Materials," Technical editors, H. S. PEISER, H. P. ROOKSBY and A. S. C. WILSON (Reviewed by G. B. GREENOUGH) 207

" Building Materials, Their Elasticity and Inelasticity," Editor, M. REINER (Reviewed by R. H. EVANS) 208

NUMBER 4

D. R. BLAND: Elastoplastic thick-walled tubes of work-hardening material subject to internal and external pressures and to temperature gradients .. 209

J. WEERTMAN: Creep of polycrystalline aluminium as determined from strain rate tests 230

B. W. SENIOR: Flange wrinkling in deep-drawing operations 235

R. HILL: On the problem of uniqueness in the theory of a rigid-plastic solid – I 247

J. F. W. BISHOP, A. P. GREEN and R. HILL: A note on the deformable region in a rigid-plastic body 256

A. P. GREEN: The plastic yielding of shallow notched bars due to bending.. 259

W. JOHNSON: Experiments in plane-strain extrusion 269

J. E. GRIFFITH and JOSEPH MARIN : Creep relaxation for combined stresses 283

WALTER FREIBERGER and BEKIR TEKINALP : Minimum weight design of circular plates 294

Corrigenda 300

Author Index

(B) denotes a book review

ADKINS, J. E. p. 199.
BERRY, D. S. p. 72.
BISHOP, J. F. W. p. 256.
BLAND, D. R. p. 209.
EASON, G. pp. 17, 53.
EVANS, R. H. p. 208 (B).
FREIBERGER, W. p. 294
GREEN, A. P. pp. 128, 256, 259.
GREENOUGH, G. B. p. 207 (B).
GRIFFITH, J. E. p. 283
HENNEPHOF, J. p. 172.
HILL, R. pp. 1, 206 (B), 247, 256,
HODGE, P. G. Jr. p. 145.
HOPKINS, H. G. p. 38.
HORNE, M. R. p. 104.
HU, L. W. p. 96.
HUNDY, B. B. p. 128.
HUNTER, S. C. p. 72.
JOHNSON, W. pp. 191, 269.
JORDAN, T. F. p. 184.
KENNEDY, A. J. p. 162.
LAD, R. A. p. 28.
MARIN, J. p. 283
METZ, F. I. p. 28.
MUVDI, B. B. p. 121.
PRAGER, W. p. 167.
ROMANO, F. p. 145.
SENIOR, B. W. p. 235.
SHIELD, R. T. pp. 10, 17, 53.
TEKINALP, B. p. 294
THOMSEN, E. G. p. 184.
TONG, K. N. p. 121.
WEERTMAN, J. p. 230.

Journal of the Mechanics and Physics of Solids, 1935, Vol. 4, pp. 1 to 9. Pergamon Press Ltd., London.

ON RELATED PAIRS OF PLANE ELASTIC STATES

By R. Hill
Department of Mathematics, University of Nottingham

(*Received* 23*rd June*, 1935)

Summary

It is shown that remarkable connexions exist between solutions to certain superficially dissimilar boundary-value problems in plane strain of an elastic solid. Essentially, these connexions relate the displacement at a point in either state to the force resultant on a curve to the point in the other; as a consequence, related states can be recognized from their defining boundary-conditions alone. Many examples are given, including several problems not hitherto solved.

Analogous results in steady quasi-static viscous flow are discussed. These complement and complete the correspondences noted by Goodier (1934) between plane states of deformation in an elastic solid and a viscous fluid.

1. Outline of Paper

The purpose of this note is to draw attention to a remarkable connexion between the solutions to certain superficially dissimilar boundary-value problems for an elastically deformed solid.

Consider a state of plane strain with no body-forces in an incompressible elastic material (Poisson's ratio $\frac{1}{2}$). Then, as well as the Airy stress-function ϕ defined by

$$\sigma_x = 2\mu \frac{\partial^2 \phi}{\partial y^2}, \qquad \tau_{xy} = -2\mu \frac{\partial^2 \phi}{\partial x\, \partial y}, \qquad \sigma_y = 2\mu \frac{\partial^2 \phi}{\partial x^2}, \tag{1}$$

where μ is the shear modulus, there exists also a 'displacement-function' ψ such that the components of displacement are

$$u = \frac{\partial \psi}{\partial y}, \qquad v = -\frac{\partial \psi}{\partial x}. \tag{2}$$

It is well known that any stress function associated with an elastic state satisfies the biharmonic equation and can be expressed in the form

$$\phi = R\left[\bar{z} f(z) + g(z)\right]$$

where $f(z)$ and $g(z)$, sometimes called complex potentials, are analytic functions of $z = x + iy$ (R denotes the real part and the bar denotes the conjugate complex). The writer has, however, seen no mention of the fact that the negative imaginary part of the above complex function is actually ψ itself, *i.e.*

$$\phi - i\psi = \bar{z} f(z) + g(z). \tag{3}$$

This is proved in Section 2 below. ϕ and ψ are of course not harmonic conjugates, since the function is not an analytic function of z.

Suppose, now, that we have a certain state, defined by given boundary-conditions, such that the complex potentials are f and g. Consider another state defined by potentials

$$f^* = if, \qquad g^* = ig. \tag{4}$$

Then

$$\phi^* - i\psi^* = \bar{z}f^*(z) + g^*(z) = i(\phi - i\psi)$$

and so

$$\phi^* = \psi, \qquad \psi^* = -\phi. \tag{5}$$

We introduce functions $P(x, y)$ and $Q(x, y)$ such that

$$P = \frac{\partial \phi}{\partial y}, \qquad Q = -\frac{\partial \phi}{\partial x}, \qquad \frac{\partial P}{\partial x} + \frac{\partial Q}{\partial y} = 0. \tag{6}$$

with similar definitions for the corresponding starred quantities. By the use of (1) the differentials

$$\left.\begin{aligned} 2\mu\, dP &= 2\mu\left(\frac{\partial^2 \phi}{\partial x\, \partial y}\, dx + \frac{\partial^2 \phi}{\partial y^2}\, dy\right) = -\tau_{xy}\, dx + \sigma_x\, dy \\ 2\mu\, dQ &= -2\mu\left(\frac{\partial^2 \phi}{\partial x^2}\, dx + \frac{\partial^2 \phi}{\partial x\, \partial y}\, dy\right) = -\sigma_y\, dx + \tau_{xy}\, dy \end{aligned}\right\} \tag{7}$$

can immediately be recognized as the (x, y) components of the force acting across a line element dz; more exactly, if a positive sense be arbitrarily assigned to the element, the force is that exerted by material to the right of the element on material to the left (with respect to the positive direction). Hence $2\mu(P, Q)$ are the components of the resultant force acting across a curve from a certain origin to the point (x, y). It follows from (2), (5) and (6) that

$$\left.\begin{aligned} P^* &= \frac{\partial \phi^*}{\partial y} = \frac{\partial \psi}{\partial y} = u, & Q^* &= -\frac{\partial \phi^*}{\partial x} = -\frac{\partial \psi}{\partial x} = v, \\ u^* &= \frac{\partial \psi^*}{\partial y} = -\frac{\partial \phi}{\partial y} = -P, & v^* &= -\frac{\partial \psi^*}{\partial x} = \frac{\partial \phi}{\partial x} = -Q. \end{aligned}\right\} \tag{8}$$

Thus the displacement vector at a point in one state is directly related to the force on a curve to the point in the other.

The resultant moment of the stresses acting on a curve AB is

$$2\mu \int_A^B (x\,dQ - y\,dP) = 2\mu\,[xQ - yP + \phi]_A^B$$

from (6). The sense of the moment is anti-clockwise on material to the left of the curve when traversed from A to B. Hence, from (8),

$$2\mu \int_A^B (x\,dQ - y\,dP) = 2\mu\,[yu^* - xv^* - \psi^*]_A^B. \tag{9}$$

By examining whether the correspondence (8) is satisfied by those boundary tractions and displacements that uniquely define the respective internal fields,† we can at once recognize pairs of related states, *even though neither of the internal*

† Namely, either the displacement or the traction is given at each point, or a component of one and the perpendicular component of the other. In multiply-connected bodies the 'strengths' of dislocations, if any, have also to be considered (see Section 3).

fields (and remaining boundary-values) may have been determined. Put otherwise: the transforms of 'natural' boundary-conditions are themselves natural. This is a most important feature of the correspondence.

It is to be observed that two states are effectively related if (8) would be satisfied after the subtraction of a rigid-body translation from either; this is connected with the fact that, for given stresses, ϕ is arbitrary to within a linear combination of x and y, while P and Q are arbitrary to within additive constants. Again, a rigid-body rotation may need to be subtracted from one state, or a uniform hydrostatic stress added to the other, in view of the following equivalence of rotation and hydrostatic stress:

$$\left.\begin{aligned}\left(\frac{\partial v}{\partial x}-\frac{\partial u}{\partial y}\right) &= -\nabla^2\psi = -\nabla^2\phi^* = -(\sigma_x^*+\sigma_y^*)/2\mu \\ \left(\frac{\partial v^*}{\partial x}-\frac{\partial u^*}{\partial y}\right) &= -\nabla^2\psi^* = \nabla^2\phi = (\sigma_x+\sigma_y)/2\mu.\end{aligned}\right\} \tag{10}$$

There is yet a further correspondence to be noted. It is shown in Section 2 that

$$\sigma_x^*-\sigma_y^* = 2\tau_{xy}, \qquad 2\tau_{xy}^* = \sigma_y-\sigma_x. \tag{11}$$

Thus, the magnitude of the maximum shearing-stress at any point is the same in the two states, while the principal axes in one become the maximum shearing-stress directions in the other.

By means of the correspondences (5), (8), (10) and (11), any known solution may immediately be converted, in its entirety, into the solution of a different problem. Again, a boundary-value problem defined by surface displacements can be converted into one defined by surface tractions (or vice-versa) for which the method of solution may be more apparent (even though the problem is not thereby made intrinsically easier – as indeed the correspondence demonstrates). There may also be advantages in so transforming the boundary conditions when it is intended to employ the photo-elastic technique. Examples of related solutions are given in Section 4.

Finally, in Section 5 analogous results are stated for steady flow of a viscous fluid. In a later paper it is hoped to deal with generalizations to compressible media.

2. Proofs of Basic Theorems

It is advantageous to proceed by regarding z and $\bar{z}$ as independent variables instead of x and y. We formally define the operators

$$\frac{\partial}{\partial z} \equiv \tfrac{1}{2}\left(\frac{\partial}{\partial x}-i\frac{\partial}{\partial y}\right), \qquad \frac{\partial}{\partial \bar{z}} \equiv \tfrac{1}{2}\left(\frac{\partial}{\partial x}+i\frac{\partial}{\partial y}\right).$$

Then, if $f(z)$ is an analytic function of z, with derivative $f'(z)$,

$$\frac{\partial f}{\partial z} = f'(z), \qquad \frac{\partial f}{\partial \bar{z}} = 0,$$

in virtue of the Cauchy-Riemann relations. Conversely, if $\partial f/\partial\bar{z} = 0$ for a function $f(x, y)$ whose real and imaginary parts are differentiable functions of x and y, f is

an analytic function of z. In other words, we may treat the operators $\partial/\partial z$ and $\partial/\partial\bar{z}$ just as if z and $\bar{z}$ were a pair of independent variables. Moreover, this formal symbolism extends to the interchange of order of differentiation of any (non-analytic) function $\phi(x, y)$; for

$$\frac{\partial}{\partial\bar{z}}\left(\frac{\partial\phi}{\partial z}\right) = \tfrac{1}{4}\nabla^2\phi = \frac{\partial}{\partial z}\left(\frac{\partial\phi}{\partial\bar{z}}\right).$$

We shall also use the easily-verified formulae

$$\overline{\frac{\partial^2\phi}{\partial z^2}} = \tfrac{1}{4}\left[\left(\frac{\partial^2}{\partial x^2} - \frac{\partial^2}{\partial y^2}\right) + 2i\frac{\partial^2}{\partial x\,\partial y}\right]\phi = \frac{\partial^2\phi}{\partial\bar{z}^2},$$

where ϕ is real.

Equations (2) and (6) can now be written

$$u + iv = -2i\frac{\partial\psi}{\partial\bar{z}}, \qquad P + iQ = -2i\frac{\partial\phi}{\partial\bar{z}}. \tag{12}$$

From (7), or from (1) and (6),

$$\left.\begin{aligned}(\sigma_x - \sigma_y + 2i\tau_{xy})/2\mu &= -2i\frac{\partial}{\partial\bar{z}}(P + iQ) = -4\frac{\partial^2\phi}{\partial\bar{z}^2},\\ \text{and}\qquad \tfrac{1}{2}(\sigma_x + \sigma_y)/2\mu &= -i\frac{\partial}{\partial z}(P + iQ) = -2\frac{\partial^2\phi}{\partial z\,\partial\bar{z}}.\end{aligned}\right\} \tag{13}$$

Also, if the strain components are

$$\epsilon_x = \frac{\partial u}{\partial x}, \qquad \epsilon_y = \frac{\partial v}{\partial y}, \qquad \gamma_{xy} = \tfrac{1}{2}\left(\frac{\partial u}{\partial y} + \frac{\partial v}{\partial x}\right),$$

then

$$\left.\begin{aligned}\epsilon_x - \epsilon_y + 2i\gamma_{xy} &= 2\frac{\partial}{\partial\bar{z}}(u + iv) = -4i\frac{\partial^2\psi}{\partial\bar{z}^2},\\ \text{and}\qquad \tfrac{1}{2}\left(\frac{\partial v}{\partial x} - \frac{\partial u}{\partial y}\right) &= -i\frac{\partial}{\partial z}(u + iv) = -2\frac{\partial^2\psi}{\partial z\,\partial\bar{z}}.\end{aligned}\right\} \tag{14}$$

In an elastic state the left-hand sides of the first lines of (13) and (14) are equal. On equating the right-hand sides we obtain

$$\frac{\partial^2}{\partial\bar{z}^2}(\phi - i\psi) = 0. \tag{15}$$

Two integrations give

$$\phi - i\psi = \bar{z}f(z) + g(z)$$

where $f(z)$ and $g(z)$ are arbitrary analytic functions of z; this proves (8). The formal integration is justified by previous remarks, since ϕ, ψ, and their first derivatives are differentiable functions of x and y (the second derivatives of ϕ and ψ being continuous if the stress and strain fields are).

In passing, it may be noted that ψ, as well as ϕ, is biharmonic (if the stresses are twice differentiable). For

$$\tfrac{1}{4}\nabla^2(\phi - i\psi) = \frac{\partial^2}{\partial z\,\partial \bar{z}}\{\bar{z}f(z) + g(z)\} = f'(z).$$

Hence $\nabla^2\phi$ and $-\nabla^2\psi$ are harmonic conjugates and so ϕ and ψ are biharmonic. The previous equation can be written as

$$(\sigma_x + \sigma_y)/2\mu + i\left(\frac{\partial v}{\partial x} - \frac{\partial u}{\partial y}\right) = 4f'(z),$$

from which with the aid of (4) we could re-derive (10).

The elimination of ϕ and ψ from (13) and (14) in favour of the potentials f and g leads to the formulae of KOLOSOV (1909; see, for instance, MUSKHELISHVILI 1953, p. 114). However, for the present purpose, it is preferable to regard a solution as specified rather by the functions ϕ and ψ.

Consider, now, two elastic states related by the correspondence (5) or equivalently (8). From (13)

$$\sigma_y - \sigma_x + 2i\tau_{xy} = 8\mu\frac{\partial^2\phi}{\partial z^2}, \qquad \sigma_y^* - \sigma_x^* + 2i\tau_{xy}^* = 8\mu\frac{\partial^2\phi^*}{\partial z}.$$

But from (5) and (15)

$$\frac{\partial^2\phi^*}{\partial z^2} = \frac{\partial^2\psi}{\partial z^2} = i\frac{\partial^2\phi}{\partial z^2} = -i\frac{\partial^2\psi^*}{\partial z^2}.$$

Hence

$$\sigma_y^* - \sigma_x^* + 2i\tau^*_{xy} = i(\sigma_y - \sigma_x + 2i\tau_{xy})$$

in accord with (11). This completes the proof of theorems stated in Section 1.

3. MULTIPLY-CONNECTED REGIONS

When the body is singly connected, P and Q are single-valued functions of position and do not depend on the particular path from the origin; this is an obvious restatement of the fact that, in a state of equilibrium without body-force, the resultant traction on any closed circuit in the body is zero (since all circuits are reducible to zero within the body). If, however, the body is multiply-connected, and the stresses on one or more of the internal boundaries have non-vanishing resultants, then one or both of P and Q must be multi-valued. In such a case we imagine sufficient 'barriers' introduced to make the resulting domain singly-connected, and then consider only paths that do not cross the barriers. Within the new domain P and Q will be single-valued and continuous. However, their values at neighbouring points on opposite sides of certain barriers will be different; evidently, the 'jumps' in value depend only on the resultant forces applied to the internal boundaries, and are therefore of constant amount along each barrier.

Consider, now, the correspondence (8) applied to a continuous field of stress in a multiply-connected body. In the related state the strains are continuous, but the displacement vector has discontinuities similar to those in the original force vector; in particular the 'jump' in displacement is constant along each barrier. In other words, there are translational *dislocations* of Weingarten type (see LOVE, *Elasticity*, p. 222). Elastic states with dislocations arising from a relative rigid-

body rotation of opposite sides of a barrier cannot be transformed into (nor arise from) states in which the stress varies continuously. It would be necessary to suppose that in the transformed state a real cut replaces the barrier, and that the tractions applied to the two faces differ by a uniform normal pressure. The transforms of displacement fields involving dislocations of more complicated types can be similarly interpreted.

4. ILLUSTRATIONS

The following examples are a small selection from the many possible.

(i) Consider a body of rectangular section cemented along a pair of opposite faces to rigid dies, the other faces being free (Fig. 1a). The body is strained by translating the dies in opposite directions parallel to themselves through equal small distances s relative to the plane $x = 0$. The conditions defining this elastic state are

$$u = s, \quad v = 0 \quad \text{on} \quad y = b; \qquad u = -s, \quad v = 0 \quad \text{on} \quad y = -b;$$

$$2\mu P = \tfrac{1}{2}S, \quad Q = 0 \quad \text{on} \quad x = a; \qquad 2\mu P = -\tfrac{1}{2}S, \quad Q = 0 \quad \text{on} \quad x = -a;$$

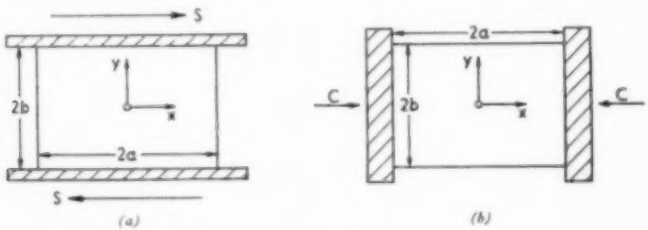

Fig. 1.

where S is the necessary shearing load on the dies (per unit thickness); no normal load is needed, by symmetry. (P, Q) is the force on a curve to the point (x, y) from the origin of co-ordinates. According to (8) the related state is defined by

$$P^* = s, \quad Q^* = 0 \quad \text{on} \quad y = b; \qquad P^* = -s, \quad Q^* = 0 \quad \text{on} \quad y = -b;$$

$$u^* = -S/4\mu, \quad v^* = 0 \quad \text{on} \quad x = a; \qquad u^* = S/4\mu, \quad v^* = 0 \quad \text{on} \quad x = -a.$$

This represents compression between rigid dies cemented to the body (Fig. 1b); the movement of each die relative to the plane $x = 0$ is $S/4\mu$, $= c$ say, and the compressive load per unit thickness is $4\mu s$, $= C$ say. Now $bS/2\mu as$ and $aC/8\mu bc$ are the respective constraint factors; that is, the actual loads, S and C, divided by the loads that would produce the same overall strains in *uniform* shear and compression respectively (under plane strain, with Poisson's ratio $\frac{1}{2}$). Hence, by the above correspondences, the product of the constraint factors is unity.

Exact solutions to either problem are apparently not available. From approximate summation of series solutions, partial information about the internal stresses in the shearing problem for particular values of a/b has been obtained by INGLIS (1923) and MANN (1949). By the aid of extremum principles, constraint factors have been estimated approximately for the shearing problem by READ (1950) for

Poisson's ratios between 0 and $\frac{1}{2}$ and values of a/b greater than about 3, and for the compression problem by GREENBERG and TRUELL (1948) for Poisson's ratio $\frac{1}{3}$ and $a/b = 1$.

(ii) Consider an infinite medium, free from dislocations, containing a traction-free cavity of circular section, and suppose that at infinity the rotation vanishes and the stress is a pure tension σ in the y direction (Fig. 2a). Let this be the unstarred state. The solution was found long ago by KIRSCH (see, for instance, TIMOSHENKO and GOODIER, 1951, p. 80). In the related state the stress at infinity is a shear of amount $\frac{1}{2}\sigma$ in the (x, y) directions and there is a rotation of amount

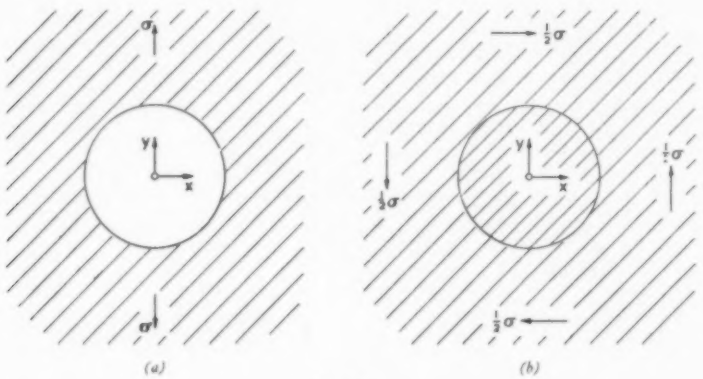

Fig. 2.

$\sigma/4\mu$ (cf. equations (10) and (11)). On the circle P and Q can be taken zero, and so, by (8), u^* and v^* both vanish there; accordingly, in the starred state we suppose that a rigid cylindrical inclusion is cemented within the cavity (Fig. 2b). Moreover (as would be expected from symmetry considerations) no resultant force is exerted by the material on the inclusion (cf. Section 3), which therefore need not be regarded as artificially fixed in position. Curiously enough, the solution to this related problem was stated only comparatively recently (MUSKHELISHVILI 1933; see, for instance, his book, 1953, p. 212).

Similarly, existing solutions for plates perforated by several holes† would furnish solutions (seemingly new) for a body containing a number of cemented inclusions, each free to move.

(iii) Consider an initially unstressed body of circular section having a concentric circular cavity filled by a rigid inclusion cemented to it. No displacement is permitted to elements on the external surface of the body when the inclusion is given a small translation. Let this be the unstarred state; the solution is known (STEVENSON, 1943). In the related state both surfaces are free from traction (since $dP^* = du = 0$, $dQ^* = dv = 0$ along them). However, according to the discussion in Section 3, the body must contain a dislocation whose discontinuity vector is parallel to the line of action of the force needed to move the inclusion. This related problem presents itself in the so-called 'dislocation theory' of plastic flow in metals; the solution has been discussed by COTTRELL (1953, pp.

† For references see TIMOSHENKO and GOODIER (1951, p. 83). In addition to these, mention may be made of DEAN and MANN (1949) for shear of a plate with two circular holes.

88-85, 87-88). Many other problems in this context, involving pairs or arrays of dislocations, have been investigated (an extensive review has been given by Nabarro, 1952). All such solutions could be translated in terms of inclusions, each under active load, or, in the limit, in terms of nuclei of force.

5. Viscous Flow Analogy

It is well known that the equations characterizing a state of equilibrium in an incompressible elastic solid are identical with those characterizing steady quasi-static flow of a Newtonian viscous fluid, if one merely replaces displacement and shear modulus in the former by velocity and coefficient of viscosity in the latter. This was probably first pointed out by Lord Rayleigh (*Theory of Sound*, Vol. II, Chap. 19). Thus, the previous theory can be immediately taken over for two-dimensional steady viscous flow problems. However, in practice the boundary-conditions for these are almost always that the fluid is contained by rigid surfaces (except perhaps at infinity), relative to which it does not slip. For this reason it is more profitable to regard a viscous flow as related to an *elastic* state in which the corresponding surfaces are free from traction (or under uniform normal pressure if the surface in the fluid is rotated).

As a very simple example of this method of procedure, steady flow between parallel walls under a uniform pressure-gradient corresponds to uniform bending of a rectangular beam by terminal couples. According to (9) the rate of discharge of fluid (given by the difference in the values of the stream-function on opposite walls) is directly related to the bending moment. Again, according to (10), the head of pressure is directly related to the angle of bend.

Essentially the same procedure for deriving solutions to a wide range of two-dimensional viscous flow problems from known elastic fields was formulated by Goodier (1934).† His starting-point was the remark that an elastic stress-function ϕ, being biharmonic, could be interpreted as the stream-function ψ^* of a slow viscous flow, since this is also biharmonic. He showed, moreover, that boundary-conditions on stresses in the solid could be simply related to those on velocities in the fluid (effectively as in the second line of (8), with u^* and v^* now denoting flow velocities, though he did not introduce the field functions P and Q). Goodier also derived (9), the second line of (10), and results equivalent to (11). However, he did not introduce the displacement-function ψ since there was no need to restrict the elastic material to be incompressible when applying the *partial* correspondence $\psi^* = \phi$. Thus, Goodier could not have been aware of the complementary half of the correspondence embodied in the first half of (8) or the first part of (5), nor of the important formula (3).

It is outside the scope of this note to pursue the viscous-elastic correspondence in more detail, but brief reference may be made to a few examples additional to those mentioned by Goodier, arising out of work of later date. For instance, laminar motion of a viscous fluid past a projection from an infinite plane boundary has been discussed by Dean (1940, 1944) and Scott-Hutton (1955) for various shapes of projection. Their results furnish solutions for the tension of a semi-infinite plate whose edge contains a notch (variously shaped). Weber (1942)

† It was Goodier's excellent paper which, in conjunction with Rayleigh's analogy, suggested to me the idea behind the present investigation.

and STEVENSON (1943) have discussed the tension of a semi-infinite plate whose edge has various wave-like contours. Their results can be translated in terms of viscous flow past a corrugated boundary. SCOTT-HUTTON has also solved the problem of laminar flow over an infinite plane boundary containing a hollow. This can be translated in terms of the tension of a semi-infinite plate whose edge has a projection.

REFERENCES

COTTRELL, A. H.	1953	*Dislocations and Plastic Flow in Crystals* (Clarendon Press, Oxford).
DEAN, W. R.	1940	*Proc. Camb. Phil. Soc.*, **36**, 300.
	1944	*Ibid.*, **40**, 19 and 214.
DEAN, W. R. and MANN, E. H.	1949	*Proc. Camb. Phil. Soc.*, **45**, 131.
GOODIER, J. N.	1934	*Phil. Mag.*, **17**, 554 and 800.
GREENBERG, H. J. and TRUELL, R.	1948	*Quart. Appl. Math.*, **6**, 52.
INGLIS, C. E.	1922	*Proc. Roy. Soc.* A **103**, 598.
MANN, E. H.	1949	*Proc. Camb. Phil. Soc.*, **45**, 258.
MUSKHELISHVILI, N. I.	1953	*Some Basic Problems of the Mathematical Theory of Elasticity*, 3rd Edition (Noordhoff Ltd., Groningen).
NABARRO, F. R. N.	1952	*Advances in Physics*, **1**, 269.
READ, W. T.	1950	*J. Appl. Mech.*, **17**, 349.
SCOTT-HUTTON, D. L.	1955	Ph.D. Thesis, University of Nottingham.
STEVENSON, A. C.	1943	*Phil. Mag.*, **34**, 766.
TIMOSHENKO, S. and GOODIER, J. N.	1951	*Theory of Elasticity* (McGraw-Hill).
WEBER, C.	1942	*Z. ang. Math. Mech.*, **22**, 29.

Journal of the Mechanics and Physics of Solids, 1955, Vol. 4, pp. 10 to 16. Pergamon Press Ltd., London.

ON COULOMB'S LAW OF FAILURE IN SOILS

By R. T. Shield
A.R.D.E., Fort Halstead, Sevenoaks

(*Received 2nd June*, 1955)

Summary

The Coulomb law of failure for an ideal cohesive soil is interpreted to obtain the yield surface for three-dimensional stress fields. The associated flow rule is derived under the assumption of perfect plasticity. As an application, limit analysis is used to obtain a lower bound for the bearing capacity of a rectangular footing on a soil.

1. Introduction

The work of Drucker and Prager (1952) on the implications of assuming that an ideal cohesive soil can be treated as a perfectly plastic material has been extended recently by Drucker (1953) to three-dimensional soil mechanics prob-problems. The Coulomb law was interpreted by Drucker as a modified Tresca as well as a modified Mises yield criterion. The yield surfaces obtained are valid generalizations of the Coulomb law to three dimensions, and there is no limit to the number of yield functions which reduce to the Coulomb law in two-dimensional problems. In the author's opinion, however, the interpretation of the Coulomb law leads to only one yield surface for three-dimensional stress fields. This yield surface is described in Section 2 below. The assumption of perfect plasticity is then made in order to derive the associated flow rule. As an application of the yield criterion a lower bound for the bearing capacity of a rectangular footing on a semi-infinite mass of soil is obtained. This bound applies to any footing which has a convex area of contact.

It should be remarked that application of this yield criterion and the associated flow rule to a problem will provide results which are correct for the ideal material, but which may bear no relation to the behaviour of a real soil. The value of the assumption of perfect plasticity must be estimated by the comparison of experiment with the predictions of the theory. Comparison between some theoretical results (Shield 1953) and experiment has been made by Sylwestrowicz (1953).

After the work described below had been completed, the author learnt that the yield surface and the associated flow rule were obtained previously by Professor W. Prager and Dr. J. F. W. Bishop in unpublished work.

2. The Coulomb Yield Criterion

In the theory of soil mechanics, it is usual to assume that the magnitude of the shearing stress τ on any section through a mass of an isotropic cohesive soil must

not be greater than an amount which depends linearly upon the normal stress σ acting on the section. This condition, which was suggested by COULOMB (1773), is written

$$\tau \leqslant c - \sigma \tan \phi, \tag{1}$$

where c is the cohesion and ϕ is the angle of friction of the soil. Failure can only occur when the equality sign holds in condition (1) for some section through the soil. Tensile stress is taken as positive so that clearly the stress σ must be less than $c \cot \phi$. Mention will be made later of soils which are unable to support a tensile stress.

In order to express the Coulomb yield condition (1) in terms of the principal stress components σ_1, σ_2 and σ_3, we use the graphical representation of stress due to MOHR (1882). In the MOHR diagram (Fig. 1) the normal stress σ and the shearing stress τ are used as co-ordinates. The stresses (σ, τ) acting at a point in the soil on any plane parallel to the second principal stress direction lie on the stress circle which passes through the points $(\sigma_1, 0)$, $(\sigma_3, 0)$, and which has its centre on the σ-axis. Similarly the stress circle through the stress points $(\sigma_1, 0)$, $(\sigma_2, 0)$ and the circle through $(\sigma_2, 0)$, $(\sigma_3, 0)$ represent states of stress acting on planes parallel to the third and first principal stress directions respectively. In Fig. 1, we have taken $\sigma_1 \leqslant \sigma_2 \leqslant \sigma_3$ for definiteness. At a point of the soil where the principal stresses have the values σ_1, σ_2, σ_3, the stress point (σ, τ) representing the traction across any section through the point lies on or within the largest stress circle in the MOHR diagram.

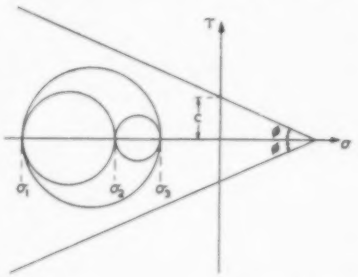

Fig. 1. MOHR's representation of a stress and the Coulomb yield criterion.

Values of σ, τ satisfying the COULOMB law (1) are represented in Fig. 1 by points in the region to the left of the two straight lines from the point $(c \cot \phi, 0)$ and inclined at angles of amount ϕ to the negative σ-axis. It follows that in order to satisfy condition (1), a state of stress σ_1, σ_2, σ_3 must be such that the MOHR's circles lie within the wedge-shaped region. Failure of the soil can occur when the largest of the circles touches the two straight lines, and in this case we have the well-known result

$$\sigma_3 - \sigma_1 = 2\, c \cos \phi - (\sigma_3 + \sigma_1) \sin \phi. \tag{2}$$

It can be seen from Fig. 1 that the principal stress σ_2 can have any value between σ_1 and σ_3 without violating the yield condition (1). Equation (2) can also be written

$$\sigma_1 = \sigma_3 \tan^2 (\tfrac{1}{4}\pi + \tfrac{1}{2}\phi) - 2c \tan (\tfrac{1}{4}\pi + \tfrac{1}{2}\phi). \tag{3}$$

In principal stress space the yield surface is a right hexagonal pyramid equally inclined to the σ_1, σ_2, σ_3 axes, and with its vertex V at the point $\sigma_1 = \sigma_2 = \sigma_3 = c \cot \phi$. Fig. 2 shows the section of the yield surface by the plane $\sigma_2 = 0$. Sections by other planes $\sigma_2 =$ constant (less than $c \cot \phi$) are similar in shape but are of varying size. The hexagon drawn with a full line in Fig. 3 is the section of the

pyramid by the plane

$$\sigma_1 + \sigma_2 + \sigma_3 = 0. \tag{4}$$

The hexagon is irregular since the yield stress in tension differs from the yield stress in compression. In contrast, the yield surface proposed by DRUCKER (1953) as a modified Tresca criterion is a right regular hexagonal pyramid. The inter-section of the plane (4) with this yield surface is a regular hexagon shown by the broken line in Fig. 3. This yield surface lies within the yield surface considered here.

If the soil is unable to take tension, then the pyramid is truncated by the three planes $\sigma_1 = 0$, $\sigma_2 = 0$, $\sigma_3 = 0$. Fig. 4 shows the section by the plane $\sigma_2 = 0$ of the pyramid with tension cut-offs.

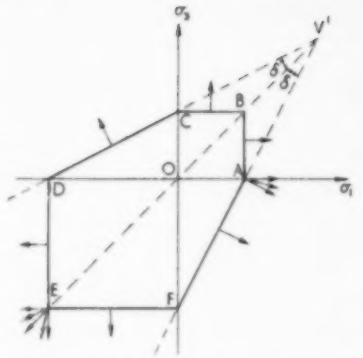

Fig. 2. Plane stress ($\sigma_2 = 0$) section of the yield surface. $OA = OC = 2c \tan(\frac{1}{4}\pi - \frac{1}{2}\phi)$, $OD = OF = 2c \tan(\frac{1}{4}\pi + \frac{1}{2}\phi)$, $\tan\delta = \sin\phi$.

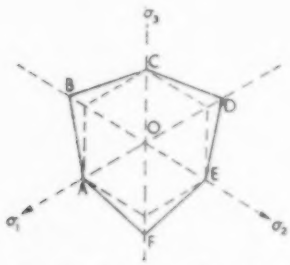

Fig. 3. Section of the yield surface by the plane $\sigma_1 + \sigma_2 + \sigma_3 = 0$. (The broken line shows the section of the yield surface proposed by DRUCKER).

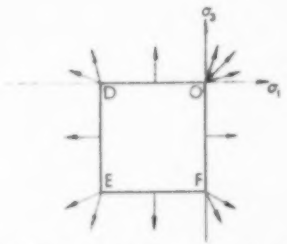

Fig. 4. Section of the pyramid with tension cut-offs by the plane $\sigma_2 = 0$.

$OD = OF = 2c \tan(\frac{1}{4}\pi + \frac{1}{2}\phi)$.

$$OA = \frac{2\sqrt{6}\, c \cos\phi}{3 + \sin\phi}, \qquad OB = \frac{2\sqrt{6}\, c \cos\phi}{3 - \sin\phi}.$$

3. THE FLOW RULE AND DISSIPATION FUNCTION.

As in recent work (see, for example, DRUCKER and PRAGER 1952) the concept of perfect plasticity is assumed to be applicable to the ideal soil under consideration. With this assumption, the vector representing the plastic strain rate is normal to the yield surface at a regular point (see VON MISES 1928 and DRUCKER 1950). At a singular point of the yield surface the plastic strain rate vector lies within the directions of the normals to the surface at adjacent points. For example, the normals drawn to the sides of the hexagon in Fig. 2 are the projections on the plane of Fig. 2 of possible plastic strain rates for stress points lying on the sides. When the stress point lies at a corner of the hexagon, e.g. point A in Fig. 2, the plastic strain rate vector lies in the fan bounded by the normals to the sides which meet at the corner.

For the faces of the pyramid, one of the principal components of the plastic strain rate is always zero, and the principal components if properly ordered are in the ratio

$$(1 + \sin\phi) : -(1 - \sin\phi) : 0. \tag{5}$$

At an edge of the pyramid, a possible plastic strain rate is a linear combination of the components for the faces which intersect at the edge. For example, for points on the edge which passes through the point A of Fig. 2, the principal components ϵ_1, ϵ_2, ϵ_3 of the plastic strain rate can be written

$$\epsilon_1 = (\lambda + \mu)(1 + \sin\phi), \quad \epsilon_2 = -\lambda(1 - \sin\phi), \quad \epsilon_3 = -\mu(1 - \sin\phi), \tag{6}$$

where λ and μ are positive scalars. Corresponding expressions apply for other stress points and it follows that for stress points on the faces and edges of the pyramid,

$$\epsilon_1 + \epsilon_2 + \epsilon_3 = (\epsilon_1 - \epsilon_2 - \epsilon_3)\sin\phi \geqslant 0, \tag{7}$$

where ϵ_1 is the (only) strictly positive principal component of the plastic strain rate. When ϕ is zero the Coulomb law reduces to the TRESCA yield criterion and equation (7) becomes the equation of incompressibility, but non-zero values of ϕ imply an increase in volume during plastic flow. From the equality in (7),

$$\epsilon_1 \tan^2(\tfrac{1}{4}\pi - \tfrac{1}{2}\phi) + \epsilon_2 + \epsilon_3 = 0, \tag{8}$$

where $\epsilon_1 \geqslant \epsilon_2, \epsilon_3$.

At the vertex of the cone, the plastic strain rate vector has more freedom, but the principal components must be such that the left hand side of equation (8) is positive, where ϵ_1 is the algebraically greatest principal strain rate.

In order to apply the limit analysis theorems (DRUCKER, GREENBERG and PRAGER 1952), it is necessary to calculate the rate of internal dissipation of energy per unit volume due to a plastic strain rate. For the yield surface considered here the dissipation function $D = \Sigma\sigma_i\epsilon_i$ has the simple form

$$D = c\cot\phi\,(\epsilon_1 + \epsilon_2 + \epsilon_3). \tag{9}$$

This form applies at all points of the pyramidal yield surface.

For a soil unable to take tension, the truncated pyramid, a section of which is shown in Fig. 4, is used to derive the flow rule. For stress points which do not lie on the cut-off planes, the principal components of the plastic strain rate satisfy (8), where ϵ_1 is the algebraically greatest component. Further, the dissipation function D is again given by (9). For stress points on the cut-off planes the left hand side of (8) is positive. When there is no compressive strain rate the rate of dissipation of energy is zero, but for stress points on the boundary of the cut-off planes a compressive strain rate is possible. In this case the dissipation function D is $2c\tan(\frac{1}{4}\pi + \frac{1}{2}\phi)$ times the modulus of the compressive strain rate (or the sum of the moduli of the compressive strain rates if two of the principal components are compressive).

4. RECTANGULAR FOOTING.

As an example of the application of the COULOMB yield criterion to three-dimensional soil mechanics problems, we obtain a lower bound for the bearing

capacity of a rectangular punch or footing on the plane surface of a semi-infinite mass of soil. The bound applies to a rough or smooth punch which is normally and centrally loaded. The bound is obtained by application of the following theorem of limit analysis for the case of all surface tractions increasing in proportion.

Theorem. Collapse will occur under the highest values of the surface tractions for which it is possible to find a statically admissible stress field.

In this theorem, the term "statically admissible stress field" is used to describe a stress field which satisfies the equations of equilibrium and the stress boundary conditions, and which does not violate the yield condition.

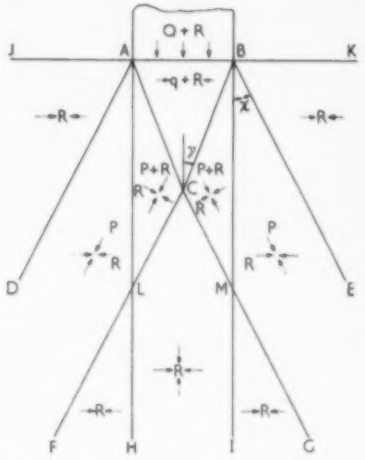

Fig. 5. Two-dimensional stress field for footing.

The stress field used is an adaptation of the statically admissible stress field used previously (SHIELD and DRUCKER, 1953) for the indentation of a TRESCA material by a rectangular punch. It is an extension into three dimensions of the two-dimensional stress field shown in Fig. 5. The stresses acting in the various regions are given in Fig. 5. The field is built up in the following way. A uni-axial compression of amount P in the regions ACFD, BCGE (which extend to infinity) produces a vertical compression Q and a horizontal compression q in the region ABC, AC and BC being lines of stress discontinuity. Superposed on this basic field are a horizontal compression of amount R throughout the soil, and a vertical compression of amount R in the region ABIH vertically below the line of indentation AB.

The largest permissible value is taken for the stress R. This value is

$$R = 2\,c \tan (\tfrac{1}{4}\pi + \tfrac{1}{2}\phi),$$

since this stress acts near the free surface where one principal component of stress is zero. The stress P and its inclination χ to the vertical are chosen so that regions BCM, BMGE are both at the point of yielding. Region BCM will be at yield if P has the value

$$P = 2\,c \tan^2 (\tfrac{1}{4}\pi + \tfrac{1}{2}\phi), \tag{10}$$

independently of the value of χ. Region BMGE will be at yield if P is given by

$$P = \frac{4c\,(\cos 2\chi + \sin \phi)}{\cos \phi\,(1 - \sin \phi)}. \tag{11}$$

Equating the values (10), (11) for P shows that χ is given by

$$\cos 2\chi = \tfrac{1}{2}\,(1 + \sin^2 \phi).$$

The compressions Q, q and the inclination γ of the stress discontinuities AC, BC to the vertical are chosen to satisfy the equilibrium conditions across AC, BC and to stress the region ABC to the point of yielding. It is found that

$$Q = \tfrac{1}{2}c \tan^3(\tfrac{1}{4}\pi + \tfrac{1}{2}\phi)\{4 + \sin\phi + \sin^2\phi + (1 + \sin\phi)(4 + \sin^2\phi)^{1/2}\},$$

$$q = \frac{QP\sin^2 x}{Q - P\cos^2 x}, \qquad \tan\gamma = \frac{P\sin x\cos x}{Q - P\cos^2 x}.$$

The extension of the two-dimensional field of Fig. 5 to a rectangular punch is shown in Fig. 6. LMNO is the rectangular area of contact between the punch and soil, LO and MN being the larger sides of the rectangle. The faces of the volume LMNOXY are inclined at an angle γ to the vertical; and the four prisms, two triangular and two trapezoidal, extending from the faces of the volume LMNOXY, are all inclined at an angle x to the vertical. Only two of the prisms are shown in Fig. 6. The pressure Q on the rectangular area is supported by compressions P in the four prisms. The addition of an all-round horizontal compression R throughout the soil, and a vertical compression R in the soil vertically below the rectangle LMNO, completes the stress field. Fig. 5 is then the vertical cross-section through the mid-points A, B of the longer sides of the rectangle.

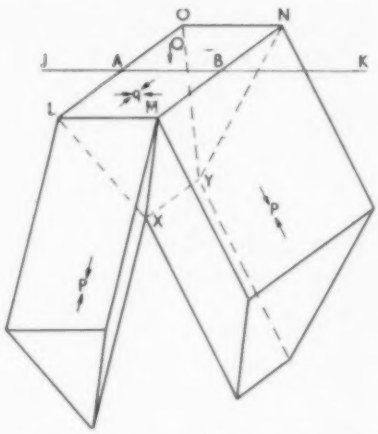

Fig. 6. Basis of stress field for rectangular footing.

Since the yield criterion is not violated in the plane of Fig. 5, it only remains to check that the stress applied normal to the plane of Fig. 5 is intermediate to the two principal stresses in that plane, in order that the yield criterion be not violated by the three-dimensional stress field. The verification is straightforward. We remark that the value R, which was chosen for the vertical compression added below the area of indentation, is the largest which can be taken without violating the yield condition in those parts of the prisms below the area of indentation.

It follows that the pressure $p = Q + R$, that is

$$p = \tfrac{1}{2}c \tan^3(\tfrac{1}{4}\pi + \tfrac{1}{2}\phi)\{4 + \sin\phi + \sin^2\phi + (1 + \sin\phi)(4 + \sin^2\phi)^{1/2}\} + 2c\tan(\tfrac{1}{4}\pi + \tfrac{1}{2}\phi), \tag{12}$$

on the area of contact can be supported by a statically admissible stress field. By the limit analysis theorem quoted above, p is therefore a lower bound for the average indentation pressure. The lower bound (12) is plotted against the angle of friction ϕ in Fig. 7. For comparison, the value given by Prandtl (1920),

$$c\cot\phi\{\exp(\pi\tan\phi)\tan^2(\tfrac{1}{4}\pi + \tfrac{1}{2}\phi) - 1\}, \tag{13}$$

for the indentation pressure for a very long rectangular punch (plane strain) is shown in the same diagram. The value (13) is an upper bound for the plane-strain indentation pressure for all values of ϕ, and is also a lower bound for values of ϕ less than 75° (Shield 1954).

As a special case, the lower bound (12) applies to a square punch. The points X and Y in Fig. 6 are then coincident. Further, the stress field of Fig. 6 can be

modified to apply to any convex area of indentation. The value (12) is therefore a lower bound for the average indentation pressure for any convex area.

The bound also applies to any uniformly loaded convex area as distinct from an area loaded by a punch. As remarked previously (SHIELD and DRUCKER, 1953) for a TRESCA material, the plane strain value (13) is an upper bound for any uniformly loaded area. This is because the soil immediately adjacent to the boundary of the loaded area can move in a manner which is essentially a plane strain motion.

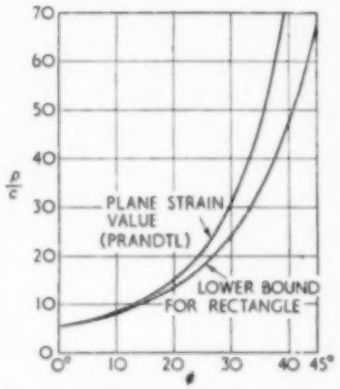

Fig. 7 Lower bound for the average indentation pressure for a rectangular footing and the average indentation pressure for a very long rectangle (plane strain).

ACKNOWLEDGMENT

The author would like to thank the Chief Scientist, Ministry of Supply, for permission to publish this paper. (Crown Copyright reserved. Reproduced with the permission of the Controller, H.M.S.O.)

REFERENCES

COULOMB, C. A.	1773	*Mém. Math. et Phys.*, **7**, 343.
DRUCKER, D. C.	1950	*Q. Appl. Math.*, **7**, 411.
	1953	*J. Mech. Phys. Solids*, **1**, 217.
DRUCKER, D. C., GREENBERG, H. J. and PRAGER, W.	1952	*Q. Appl. Math.*, **9**, 381.
DRUCKER, D. C. and PRAGER, W.	1952	*Q. App. Math.*, **10**, 157.
MISES, R. VON	1928	*Z. f. ang. Math. Mech.*, **8**, 161.
MOHR, O.	1882	*Zivilingenieur*, **28**, 113.
PRANDTL, L.	1920	*Göttinger Nachr., math. phys. Kl.*, **1920**, 74.
SHIELD, R. T.	1953	*Q. Appl. Math.*, **11**, 61.
	1954	*J. Appl. Mech.*, **21**, 193.
SHIELD, R. T. and DRUCKER, D. C.	1953	*J. Appl. Mech.*, **20**, 453.
SYLWESTROWICZ, W.	1953	*J. Mech. Phys. Solids*, **1**, 258.

Journal of the Mechanics and Physics of Solids, 1953, Vol. 4, pp. 17 to 27. Pergamon Press Ltd., London.

THE INFLUENCE OF FREE ENDS ON THE LOAD-CARRYING CAPACITIES OF CYLINDRICAL SHELLS

By G. Eason and R. T. Shield
A.R.D.E., Fort Halstead, Sevenoaks

(*Received 27th July*, 1953)

Summary

Previous work by Drucker on the axially symmetric plastic loading of thin circular cylindrical shells of infinite length is extended to shells of varying lengths. The ends of the shell are assumed to be stress free. The types of loading considered are a ring of force and a band of uniform pressure.

1. Introduction

The axially symmetric plastic loading of circular cylindrical shells has been considered by Drucker (1953). By applying the theorems of limit analysis (Hill 1951, and Drucker, Greenberg and Prager 1952), Drucker determined the appropriate yield condition in terms of force and moment resultants for a rigid-plastic material obeying Tresca's yield criterion. This work was extended by Hodge (1954) and Onat (1955) to include the effect of an axial force resultant on the yield condition.

Drucker solved the basic problems of an infinitely long shell acted upon by a ring of force or a band of uniform pressure. The following work considers the influence of free ends on the load-carrying capacities of cylindrical shells. The material of the shell is assumed to be rigid-plastic, and a simplified yield condition is used, effecting a considerable simplification in the analysis without a great loss in accuracy. For a material obeying the simplified yield condition used here, the solutions obtained to the problems considered are complete, *i.e.* they involve a plastic stress distribution and an associated mode of deformation. It follows from the theorems for a rigid-plastic material (Hill 1951) that the values obtained for the yield-point loads are the correct loads for a material obeying the simplified yield condition.

2. Basic Equations

The force and moment resultants acting upon an element of a thin cylindrical shell under axially symmetric lateral loading are shown in Fig. 1. The axial force resultant will be assumed to be zero in the following work, and the circumferential bending moment M_ϕ may be ignored since it does not enter explicitly into the equilibrium equations or the yield condition. The axial bending moment M, the shearing force resultant Q, the circumferential force N and the applied

lateral pressure p satisfy the equations of equilibrium

$$\frac{dQ}{dx} = p - \frac{N}{R}, \tag{1}$$

$$\frac{dM}{dx} = Q. \tag{2}$$

where R is the radius of the shell. It follows that

$$\frac{d^2M}{dx^2} = p - \frac{N}{R}. \tag{3}$$

For a material which obeys the TRESCA yield condition, the maximum permissible numerical values M_0, N_0 of M and N are given by

$$M_0 = \tfrac{1}{4}\sigma_0 h^2, \qquad N_0 = \sigma_0 h,$$

where σ_0 is the yield stress in tension or compression and h is the thickness of the shell. It will be assumed here that the shell remains rigid until the magnitude of M or N reaches the maximum value M_0 or N_0. In terms of the dimensionless quantities $m = M/\sigma_0 h^2$, $n = N/\sigma_0 h$, the shell will be rigid until $|m| = \frac{1}{4}$ or $|n| = 1$. The yield condition is then represented by the rectangle in Fig. 2, and is an approximation to the true yield condition derived by DRUCKER (1953) and indicated by the broken line in Fig. 2. The effect of the shearing force Q on the yield condition is neglected. The rectangular yield condition is chosen since it linearizes the yield condition, and effects a considerable simplification in the solution of particular problems without too severe a loss in accuracy in the values of the collapse loads. That the *deformations* predicted by a simplified yield condition may differ considerably from those in an actual material has been pointed out by HILL (1954). It should be remarked, however, that in principle the problems considered below could be solved with the exact yield condition.

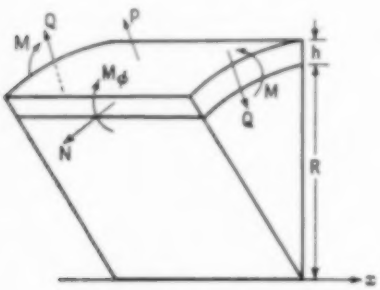

Fig. 1. Stresses on element of shell.

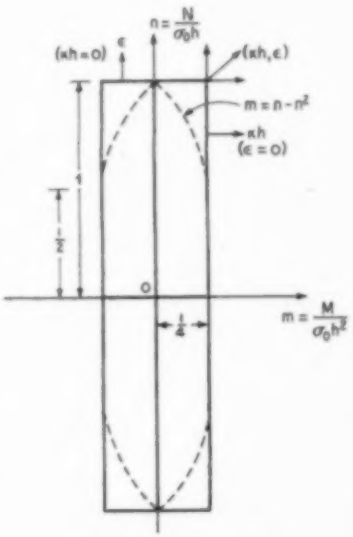

Fig. 2. Yield condition.

Since the rectangular yield condition used here overestimates the strength of

the shell, the approximation can be improved by using a suitably chosen value σ_0' less than σ_0 for the yield stress σ_0. Replacing σ_0 by $\sigma_0' = 0{\cdot}75\ \sigma_0$ is equivalent to using a yield rectangle which lies inside the exact yield curve of Fig. 2, and the load-carrying capacity of the shell would be underestimated (see DRUCKER 1953). With the value $\sigma_0' = 0{\cdot}875\ \sigma_0$, the rectangular yield condition will predict limit loads which do not differ from the values predicted by the exact yield conditions by more than 14%. Bounds for the error committed when any approximate theory of plasticity is used to estimate yield-point loads have been obtained by HILL (1952).

The radial velocity of the middle surface of the shell during plastic deformation will be denoted by u. Associated with the bending moment M and the force N are the rate of curvature κ and the rate of extensional strain ϵ, given by $\kappa = d^2u/dx^2$ and $\epsilon = u/R$. During plastic deformation under the 'stresses' m, n, the vector with components proportional to the 'strain' rates κh, ϵ is directed along the outwards-drawn normal to the yield rectangle at the stress point (m, n). At the corners of the rectangle the vector lies between the normals to the sides which meet at the corner. Thus, on the horizontal sides of the rectangle, $\kappa = 0$ and the shell deforms into a cone.

It is convenient (following DRUCKER) in the subsequent work to write equations (1), (2), (3) in the dimensionless forms

$$\frac{dq}{d\xi} = \psi - n, \tag{4}$$

$$\frac{dm}{d\xi} = q, \tag{5}$$

$$\frac{d^2m}{d\xi^2} = \psi - n, \tag{6}$$

where $\xi = x/\sqrt{Rh}$, $\psi = pR/\sigma_0 h$, $q = Q\sqrt{Rh}/\sigma_0 h^2$ and, as before, $m = M/\sigma_0 h^2$, $n = N/\sigma_0 h$.

3. RING OF FORCE

In this Section, the plastic loading of a cylindrical shell by a ring of lateral force is considered. The origin of the non-dimensional co-ordinate ξ is taken at the point of application of the force, the free ends of the tube being given by $\xi = -a$, $\xi = b$, where $b \geqslant a$. At the ends of the tube $m = q = 0$. The lateral pressure ψ is zero (except at $\xi = 0$) and the shearing force q has a discontinuity of amount P at the origin, where $P\sigma_0 h\sqrt{h/R}$ is the intensity per unit length of the ring of force. The values of a and b determine the number of hinge circles, *i.e.* sections at which $|m| = \frac{1}{4}$, which form in the tube during plastic deformation. The analysis is straightforward and it is found that the following cases arise.

(*i*) $a < 1/\sqrt{2}$, $\quad a \leqslant b < 1 + (a^2 + \frac{1}{2})^{\frac{1}{2}}$.

In this case, shown in Fig. 3, the moment m is everywhere less than the maximum value, $|m| < \frac{1}{4}$, and $|n| = 1$. The stress distribution is as follows:

For $-a \leqslant \xi < 0$,

$$m = -\tfrac{1}{2}(\xi + a)^2, \qquad n = 1, \qquad q = -(\xi + a). \tag{7}$$

For $0 < \xi < c$, where $c^2 = \frac{1}{2}(a^2 + b^2)$,

$$m = -\tfrac{1}{2}\xi^2 + \xi(2c - b) - \tfrac{1}{2}a^2, \qquad n = 1, \qquad q = -\xi + 2c - b. \tag{8}$$

For $c < \xi \leqslant b$,

$$m = \tfrac{1}{2}(\xi - b)^2, \qquad n = -1, \qquad q = \xi - b. \tag{9}$$

The value of P is

$$P = 2c + a - b = \sqrt{2}\,(a^2 + b^2)^{\frac{1}{2}} + a - b.$$

The form of the stress distribution is shown in Fig. 3. The circumferential force n is discontinuous at the point C distant c from O. Since $|m| < \frac{1}{4}$, the rate of curvature κ is zero. Where $n = 1$, $\epsilon \geqslant 0$ and where $n = -1$, $\epsilon \leqslant 0$ so that a permissible deformation mode is given by

$$u = V(c - \xi)/c,$$

where V is the radial velocity at O. The mode of deformation is indicated in Fig. 3.

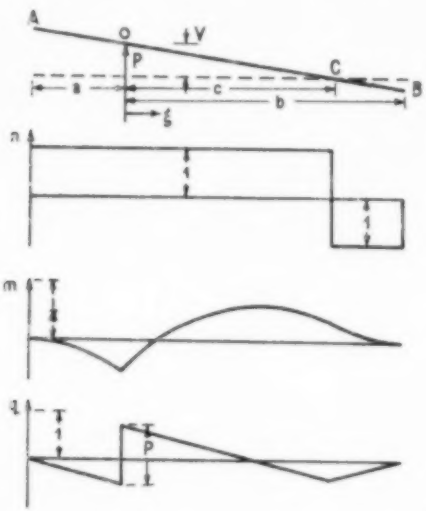

Fig. 3. Mode of deformation and stress distribution: $a < 1/\sqrt{2}$, $a \leqslant b < 1 + (a^2 + \frac{1}{4})^{\frac{1}{2}}$, $c^2 = \frac{1}{2}(a^2 + b^2)$, $P = 2c + a - b$.

(*ii*) $a < 1/\sqrt{2}$, $\quad b > 1 + (a^2 + \frac{1}{4})^{\frac{1}{2}}$.

In this case a yield-hinge at which $m = \frac{1}{4}$ develops at the point E in the length OB of the cylinder, Fig. 4. The stress distribution and deformation mode are as shown in the figure. For the length OA, the stresses are again given by equations (7). The distance ξ_1 of the hinge from O is given by $\xi_1 = (a^2 + \frac{1}{4})^{\frac{1}{2}}$.

For $0 < \xi < \xi_1$, the stresses are given by

$$m = \tfrac{1}{4} - \tfrac{1}{2}(\xi - \xi_1)^2, \qquad n = 1, \qquad q = -\xi + \xi_1, \tag{10}$$

and the value of P is

$$P = a + \xi_1 = a + (a^2 + \tfrac{1}{4})^{\frac{1}{2}}. \tag{11}$$

The portion EB of the shell remains rigid. Since the length of EB is greater than unity, $b - \xi_1 > 1$, the stress field can be extended into the portion EB without violating yield to give zero stress at the free end B. A permissible extension into EB is shown in Fig. 4.

(*iii*) $1/\sqrt{2} < a \leqslant b < 2$.

For this range of values for a and b, a hinge develops at the point O of application of the force,

Fig. 5. There are two discontinuities in the stress n at the points $\xi = -d$, $\xi = c$ where

$$c = \tfrac{1}{2}(2b^2 + 1)^{\frac{1}{2}}, \qquad d = \tfrac{1}{2}(2a^2 + 1)^{\frac{1}{2}}. \tag{12}$$

For $-a \leqslant \xi < -d$,

$$m = \tfrac{1}{2}(\xi + a)^2, \qquad n = -1, \qquad q = \xi + a. \tag{13}$$

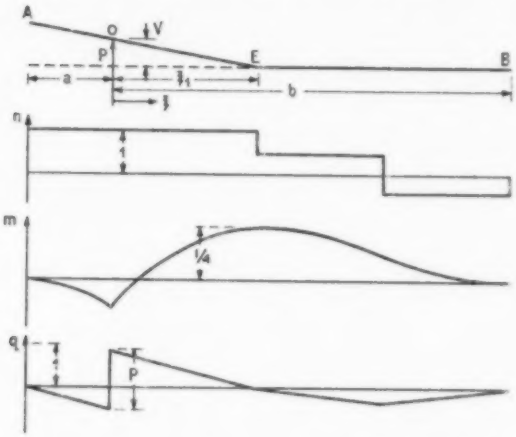

Fig. 4. Mode of deformation and stress distribution: $a < 1/\sqrt{2}$, $b > 1 + (a^2 + \frac{1}{2})^{\frac{1}{2}}$, $\xi_1 = (a^2 + \frac{1}{2})^{\frac{1}{2}}$, $P = a + \xi_1$.

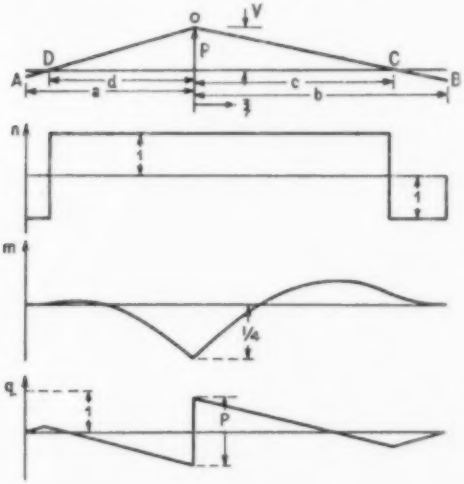

Fig. 5. Mode of deformation and stress distribution: $1/\sqrt{2} < a \leqslant b < 2$, $c = \frac{1}{2}(2b^2 + 1)^{\frac{1}{2}}$, $d = \frac{1}{2}(2a^2 + 1)^{\frac{1}{2}}$, $P = 2(c + d) - a - b$.

For $-d < \xi < 0$,

$$m = -\tfrac{1}{2}\xi^2 + \xi(a - 2d) - \tfrac{1}{2}, \qquad n = 1, \qquad q = -\xi + a - 2d. \tag{14}$$

For $0 < \xi < c$,

$$m = -\tfrac{1}{2}\xi^2 + \xi(2c - b) - \tfrac{1}{2}, \qquad n = 1, \qquad q = -\xi + 2c - b. \tag{15}$$

For $c < \xi \leqslant b$,

$$m = \tfrac{1}{2}(\xi - b)^2, \qquad n = -1, \qquad q = \xi - b. \tag{16}$$

The force P has the value

$$P = 2(c + d) - a - b = (2a^2 + 1)^{\frac{1}{2}} + (2b^2 + 1)^{\frac{1}{2}} - a - b.$$

The radial velocity u is zero at the points C, D, where n is discontinuous, and since $\kappa = 0$ everywhere except at the hinge, the deformation mode is given by

$$u = \begin{cases} V(\xi + d)/d \text{ for } -a \leqslant \xi \leqslant 0, \\ V(c - \xi)/c \text{ for } 0 \leqslant \xi \leqslant b, \end{cases}$$

where V is the velocity at the hinge.

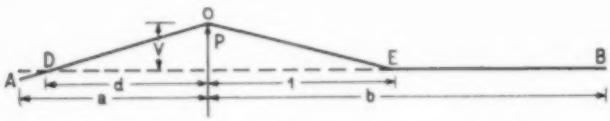

Fig. 6. Mode of deformation : $1/\sqrt{2} < a < 2 < b$, $d = \tfrac{1}{2}(2a^2 + 1)^{\frac{1}{2}}$, $P = 2d + 1 - a$.

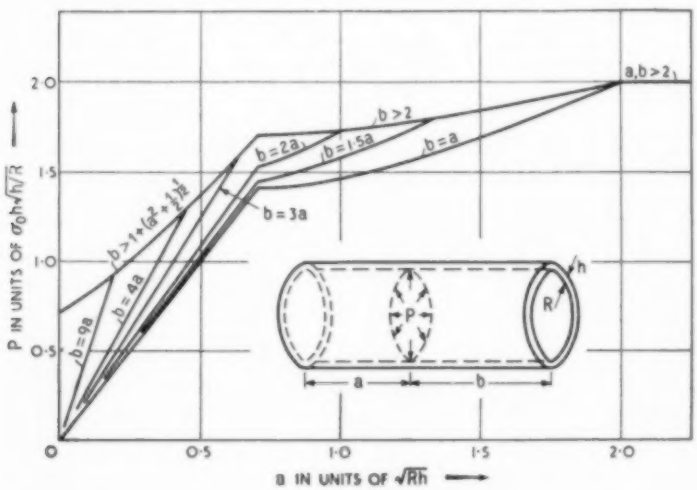

Fig. 7. Variation of P with a and b.

(iv) $1/\sqrt{2} < a < 2 < b$.

For this case there are two yield-hinges, one at the origin and one in the length OB, Fig. 6. The hinge at E in the length OB is at unit distance from O. The stresses in the portion OA of the shell are again given by equations (13), (14), and the stresses in OE are given by equations (10) in which ξ_1 is put equal to unity. The length of the rigid portion EB is greater than unity since $b > 2$, and the field can be extended into EB in a permissible way. The intensity of the force P is given by

$$P = 2d + 1 - a = (2a^2 + 1)^{\frac{1}{2}} + 1 - a.$$

The velocity field is given by

$$u = \begin{cases} V(\xi + d)/d & \text{for } -a \leqslant \xi \leqslant 0, \\ V(1 - \xi) & \text{for } 0 \leqslant \xi \leqslant 1. \end{cases}$$

(v) $a, b > 2$.

This is the case considered by DRUCKER (1953). The deformation is symmetrical about the point O. Hinges develop at O and at the sections at unit distance from O. The intensity of the force P is two units, $P = 2$. Fig. 7 shows the variation of P with a for various ratios of b to a.

4. Band of Pressure Applied to a Semi-infinite Tube

When the shell is loaded to yielding by a band of uniform pressure, various cases arise depending on the width of the band and the distance of the band from the free ends of the shell. The analysis is more difficult than that for the ring of force and only two particular cases are considered here, the semi-infinite tube and a shell of finite length loaded symmetrically.

Considering first the semi-infinite tube, the origin of the non-dimensional co-ordinate ξ is taken at the centre of the band, which is at a distance b from the free end $\xi = -b$. A uniform pressure of amount $P\sigma_0 h/R$ is applied over the band $-a \leqslant \xi \leqslant a$, where $a \leqslant b$.

(i) $b < [a^2(\sqrt{2} - 1)^2 + \frac{1}{2}]^{\frac{1}{2}} + a(2 - \sqrt{2})$.

In this case there is one yield hinge in the tube at the point E in Fig. 8a. The distance ξ_1 of the hinge from the centre of the band is given by

$$\xi_1 = (b^2 + \tfrac{1}{2})^{\frac{1}{2}}.$$

(a) $b < \{a^2(\sqrt{2}-1)^2 + \frac{1}{2}\}^{\frac{1}{2}} + a(2-\sqrt{2})$

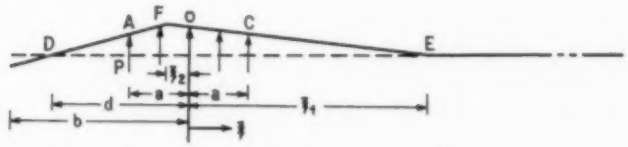

(b) $\{a^2(\sqrt{2}-1)^2 + \frac{1}{2}\}^{\frac{1}{2}} + a(2-\sqrt{2}) < b < \frac{1}{2}\{a+2+(a^2+4)^{\frac{1}{2}}\}$

Fig. 8. Semi-infinite tube.

For $-b \leqslant \xi \leqslant -a$, the stresses are given by

$$m = -\tfrac{1}{2}(\xi + b)^2, \qquad n = 1, \qquad q = -(\xi + b).$$

For $-a \leqslant \xi \leqslant a$,

$$m = \tfrac{1}{2}(P - 1)(\xi + a)^2 - (\xi + a)(b - a) - \tfrac{1}{2}(b - a)^2,$$

$$n = 1, \qquad q = (P - 1)(\xi + a) - (b - a).$$

For $a \leqslant \xi \leqslant \xi_1$,

$$m = -\tfrac{1}{2}(\xi - \xi_1)^2 + \tfrac{1}{2}, \qquad n = 1, \qquad q = -\xi + \xi_1. \tag{17}$$

The value of P is given by

$$Pa = \tfrac{1}{2}(b + \xi_1) = \tfrac{1}{2}\{b + (b^2 + \tfrac{1}{2})^{\frac{1}{2}}\}.$$

Since $n = 1$ in the plastic region, the radial velocity u is positive. The mode of deformation is given by

$$u = V(\xi_1 - \xi)/\xi_1,$$

and is shown in Fig. 8a. The stress field can be extended into the rigid region $\xi > \xi_1$ without violating the yield condition.

(*ii*) $[a^2(\sqrt{2} - 1)^2 + \tfrac{1}{2}]^{\frac{1}{2}} + a(2 - \sqrt{2}) < b < \tfrac{1}{2}\{a + 2 + (a^2 + 4)^{\frac{1}{2}}\}$.

For values of b in this range, there are two yield hinges at the points E and F in Fig. 8b. Also the stress n has a discontinuity at the point D; $n = -1$ in BD and $n = 1$ in DE. The distances of the points D, E, F from the centre O of the band are denoted by d, ξ_1, ξ_2, respectively.

For $-b \leqslant \xi < -d$, the stresses are given by

$$m = \tfrac{1}{2}(\xi + b)^2, \qquad n = -1, \qquad q = (\xi + b).$$

For $-d < \xi \leqslant -a$,

$$m = -\tfrac{1}{2}(\xi + d)^2 + (b - d)(\xi + d) + \tfrac{1}{2}(b - d)^2,$$

$$n = 1, \qquad q = -(\xi + d) + b - d.$$

For $-a \leqslant \xi \leqslant -\xi_2$,

$$m = \tfrac{1}{2}(P - 1)(\xi + a)^2 + (\xi + a)(a + b - 2d) - \tfrac{1}{2}(d - a)^2 + (b - d)(d - a) + \tfrac{1}{2}(b - d)^2,$$

$$n = 1, \qquad q = (P - 1)(\xi + a) + a + b - 2d.$$

For $-\xi_2 \leqslant \xi \leqslant a$,

$$m = \tfrac{1}{2}(P - 1)(\xi - a)^2 - (a - \xi_1)(\xi - a) - \tfrac{1}{2}(a - \xi_1)^2 + \tfrac{1}{2},$$

$$n = 1, \qquad q = (P - 1)(\xi - a) - (a - \xi_1).$$

For $a \leqslant \xi \leqslant \xi_1$, region CE in Fig. 8b, the stresses are again given by equations (17). The distances ξ_1, ξ_2 are given in terms of a, b, d, by

$$\xi_1 = (\tfrac{1}{2} + 2d^2 - b^2)^{\frac{1}{2}}, \qquad \xi_2 = \frac{(2d^2 - 2ad - b^2 + ab - \tfrac{1}{2})}{2d - a - b}, \tag{18}$$

and the value of P is given by

$$Pa = \tfrac{1}{2}(2d - b + \xi_1). \tag{19}$$

The distance d is found from the equation

$$2a(2d - b - \xi_2) = (2d - b + \xi_1)(a - \xi_2),$$

in which ξ_1 and ξ_2 have the values (18), subject to the condition $0 \leqslant b - d \leqslant 1/\sqrt{2}$.

The radial velocity is negative in BD and positive in DE. The mode of deformation is indicated in Fig. 8b.

(*iii*) $b > \tfrac{1}{2}\{a + 2 + (a^2 + 4)^{\frac{1}{2}}\}$.

This is the case considered by Drucker (1953). The deformation is symmetrical about the centre O of the band. Yield-hinges form at O and at distances ξ_1 from O, where

$$\xi_1 = \tfrac{1}{2}\{a + (a^2 + 4)^{\frac{1}{2}}\}.$$

The value of Pa is given by

$$Pa = \xi_1 = \tfrac{1}{2}\{a + (a^2 + 4)^{\frac{1}{2}}\}.$$

The variation of Pa with a and b is indicated in Fig. 9.

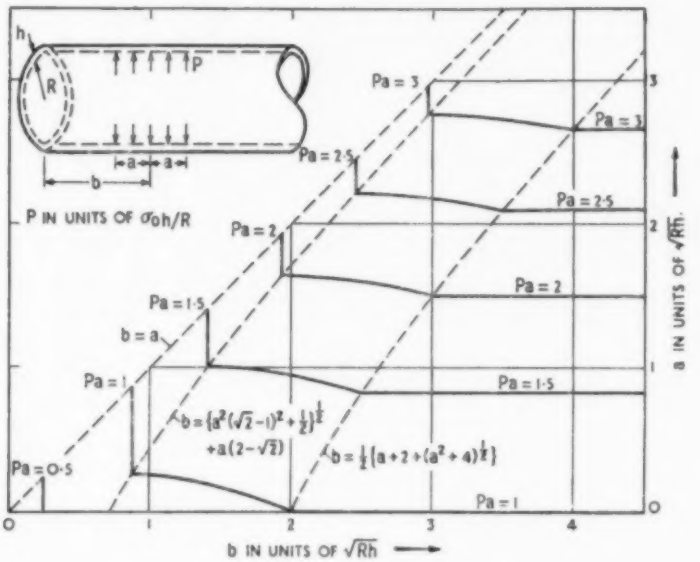

Fig. 9. Semi-infinite tube.

5. Band of Pressure Symmetrically Applied to a Short Tube

As before the width of the band is denoted by $2a$. The centre O of the band, Fig. 10, is at the middle of the tube, distant b from the free ends.

(i) $b < \tfrac{1}{2}\{a + (a^2 + 2)^{\frac{1}{2}}\}$.

In this case there are no yield-hinges, and $n = 1$ everywhere. The stresses in the length AB, Fig. 10a, are given by

$$m = -\tfrac{1}{2}(\xi - b)^2, \qquad n = 1, \qquad q = -(\xi - b).$$

In the length OA,

$$m = \tfrac{1}{2}(P - 1)(\xi - a)^2 + (b - a)(\xi - a) - \tfrac{1}{2}(b - a)^2,$$

$$n = 1, \qquad q = (P - 1)(\xi - a) + (b - a).$$

The value of P is given by

$$Pa = b.$$

Permissible modes of deformation must be such that the radial velocity u is positive everywhere and is a linear function of ξ.

(ii) $\tfrac{1}{2}\{a + (a^2 + 2)^{\frac{1}{2}}\} < b < \tfrac{1}{2}\{a + 2 + (a^2 + 4)^{\frac{1}{2}}\}$.

In this case a yield-hinge forms at the centre O of the band. Fig. 10b. The stress n is discontinuous at points distant c from O in the unloaded portions of the tube. The value of c is given by

$$c = \tfrac{1}{2}\{(b - a)^2 + b^2 + 1\}^{\frac{1}{2}} + \tfrac{1}{2}a,$$

and the pressure P by

$$Pa = 2c - b.$$

For $c < \xi \leqslant b$,

$$m = \tfrac{1}{2}(\xi - b)^2, \qquad n = -1, \qquad q = \xi - b.$$

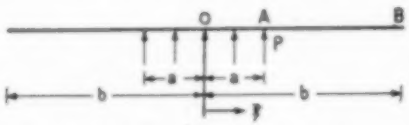

(a) $b < \frac{1}{2}\{a + (a^2+2)^{\frac{1}{2}}\}$

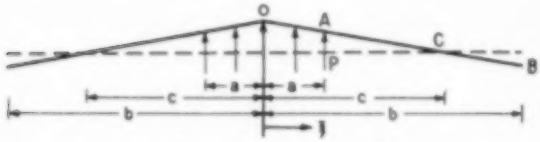

(b) $\frac{1}{2}\{a + (a^2+2)^{\frac{1}{2}}\} < b < \frac{1}{2}\{a + 2 + (a^2+4)^{\frac{1}{2}}\}$

Fig. 10. Symmetrical loading of short tube.

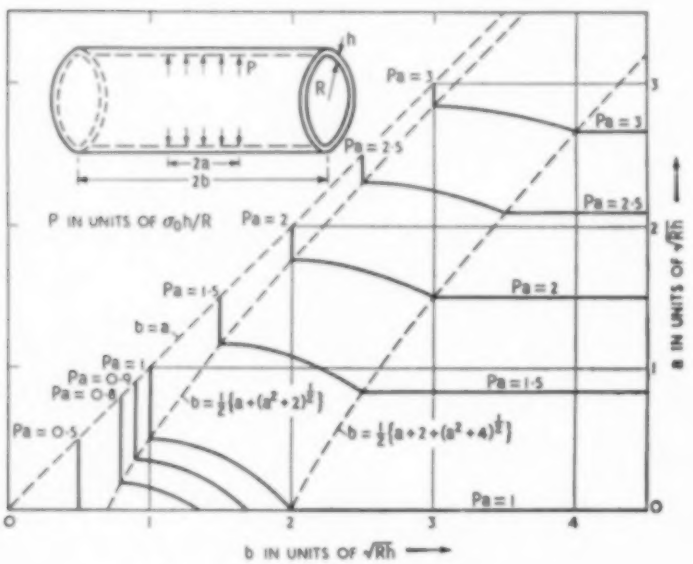

Fig. 11. Symmetrical loading of short tube.

For $a \leqslant \xi < c$,

$$m = -\tfrac{1}{2}(\xi - c)^2 - (b - c)(\xi - c) + \tfrac{1}{2}(b - c)^2,$$

$$n = 1, \qquad q = -(\xi - c) - b + c.$$

For $0 \leqslant \xi \leqslant a$,

$$m = \tfrac{1}{2}(P - 1)\xi^2 - \tfrac{1}{4}, \qquad n = 1, \qquad q = (P - 1)\xi.$$

The deformation mode is indicated in Fig.10b. The radial velocity is positive where $n = 1$ and negative where $n = -1$.

(*iii*) $b > \frac{1}{2}\{a + 2 + (a^2 + 4)^{\frac{1}{2}}\}$.

This is again the case examined by DRUCKER (1953) and described in the previous section. Fig. 11 shows the variation of Pa with the distances a and b.

(Crown Copyright reserved. Reproduced with the permission of the Controller, H.M.S.O.)

REFERENCES

DRUCKER, D. C.	1953	Proc. 1st Midwestern Conference on Solid Mech., Urbana, Ill., p. 158 (*A.S.M.E.*, New York).
DRUCKER, D. C., GREENBERG, H. J. and PRAGER, W.	1952	*Quart. Appl. Math.*, **9**, 381.
HILL, R.	1951	*Phil. Mag.*, **42**, 868.
	1952	*Phil. Mag.*, **43**, 353.
	1954	*J. Appl. Mech.*, **21**, 93.
HODGE, P. G., JR.	1954	*J. Appl. Mech.*, **21**, 336.
ONAT, E. T.	1955	*Quart. Appl. Math.*, **13**, 63.

Journal of the Mechanics and Physics of Solids, 1955, Vol. 4, pp. 28 to 37. Pergamon Press Ltd., London.

AN EXPERIMENTAL INVESTIGATION OF THE EFFECT OF VACANCY AND F-CENTRE CONCENTRATIONS ON THE TRANSIENT CREEP OF SODIUM CHLORIDE SINGLE CRYSTALS*

By R. A. Lad and F. I. Metz
Lewis Flight Propulsion Laboratory, National Advisory Committee for Aeronautics, Cleveland

(*Received 15th May*, 1955)

Summary

The effects of vacancy and F-centre concentrations on the room temperature creep properties of NaCl single crystals were studied. Under a load of 1,200 gm/mm^2, logarithmic creep behaviour was found for both annealed and quenched crystals before or after irradiation. Irradiation with 50 kV X-rays was found to have a marked effect on both initial deformation and subsequent creep, causing an initial softening followed by a hardening as irradiation is continued. The behaviour after irradiation can be explained on the basis of the changes in vacancy concentration and distribution which accompany F-centre formation. Experiments in which the vacancy concentration was changed by quenching from various temperatures indicate that the creep rate may depend in a simple way on the number of vacancies.

1. Introduction

It has long been known that one of the effects of ionizing radiation on the alkali halides is to increase brittleness, and recent work has shown that marked changes in hardness (Westervelt 1954), yield stress (Podaschewsky 1935; Li 1953), and internal friction (Frankl 1953) also occur. These considerations, together with the fact that much is known about F-centre formation (Seitz 1954; Pohl 1937; Markham 1952), instigated this study of the creep properties of sodium chloride as affected by radiation. A stress range was chosen which yielded transient creep to which the Mott-Nabarro exhaustion theory (Mott and Nabarro 1948; Cottrell 1953) might be expected to apply.

In the Mott-Nabarro theory, the plastic flow is considered to be the result of the motion of a large number of dislocations. A dislocation moves when the sum of the applied stress and thermal activation stress is great enough to overcome its internal stress. It is generally assumed that both the number and distribution of lattice vacancies have a pronounced effect on the internal stress, and on the contribution to the strain made by a dislocation jump. Consequently the changes in vacancy concentration and distribution which are believed to result when F-centres are produced by X-irradiation might be expected to affect the creep properties.

* Taken in part from a thesis submitted by Florence I. Metz to the faculty of the Western Reserve University in partial fulfilment of the requirements for the Master of Science Degree.

In this investigation, the creep properties of NaCl single crystals under compression were studied as a function of irradiation time. Compression was used rather than tension because grips were not required and because an accurate measurement of the initial deformation was possible. The strain range studied (< 10 per cent) was small enough to minimize the deviations from uniaxial stress. The effect of incremental loading was studied before and after irradiation. Changes in vacancy concentration and distribution were also effected by the use of crystals quenched from temperatures which ranged from 150°C to just below the melting point.

Both F-centre production and creep are complex processes, and the results of the experiments described herein are not sufficient to enable one to set forth a unique explanation of their interrelations. However, an interpretation is given of the observed phenomena which is consistent with some of the current ideas about F-centre formation and of creep.

2. Experimental

(i) *Preparation of Specimens*

Harshaw sodium chloride single crystals were used in the form of $10 \times 2{\cdot}5 \times 2{\cdot}5$ mm blocks. The initial cleaving and grinding were to dimensions slightly larger. Further surface treatment after annealing resulted in the proper final dimensions. A fresh specimen was used for each creep experiment. The annealing treatment involved heating in a bed of powdered NaCl at 600°C for 24 hours, then a slow cooling to room temperature over a period of 36 hours. The annealed crystals were stored at room temperature in a desiccator. Prior to irradiation, the specimen surface was removed by a stream of water from a burette (4 ml were used), and the crystal immediately rinsed with ethanol followed by acetone. Air drying for 10 minutes resulted in a smooth surface, which microscopic examination showed to resemble an electropolished metal surface (smooth and free of steps or abrupt changes in level). The surface treatment described was adopted as a standard procedure in all except the quenching experiments because, although the nature of the surface was found to have no systematic effect on the magnitude of the creep constants, the reproducibility of the creep data was increased.

The quenched crystals were heated at temperatures between 150° and 700° before quenching. Prior to heating at the desired temperature, each specimen was maintained at 720° for at least 100 hours. The time at the lower temperature was long enough to ensure that further heating would have no effect on the creep behaviour after quenching to room temperature : it varied from 150 hours at 500° to 300 hours at 150°. Quenching was accomplished by air cooling the combustion boat containing the crystal imbedded in powdered NaCl.

(ii) *Irradiation Procedure*

The depth of penetration of X-rays which are effective in colouring the crystals is small. The intensity of the effective wavelengths has been estimated (Estermann, Leivo and Stern 1949) to decrease to 37 per cent of the initial intensity in approximately 0·05 mm. Specimens of thickness 0·05 mm could not easily be

adapted to creep measurements. Consequently the alternative procedure of irradiating larger specimens on all four sides was adopted.

The specimens were mounted on the shaft of a 4 rpm clock motor, and rotated around an axis normal to the X-ray beam and parallel to the large faces of the specimen. The irradiation was performed in an atmosphere of helium at room temperature. The X-ray tube was a Machlett AEG-50 having a tungsten target and a beryllium window, and was operated at 50 kv and 30 ma. The radiation intensity as measured on a Gamma survey meter was 75,000 r per hr at the position of the crystal.

(iii) *Creep Measurement*

The creep tests were performed in the apparatus shown in Fig. 1. Granulated lead was used in order that the load could be applied gradually and without an initial shock. The creep strain was measured on a dial indicator which was sensitive to changes in length of 5×10^{-4} mm. The experiments were carried out in red light having a cut-off at 6,000 Å. No detectable diminution in the F-band occurred due to the illumination for the period of time required to obtain a creep curve (60 to 100 minutes).

The general procedure was to mount the crystal in position with a small load (piston plus platform amounting to 150 g/mm^2), and adjust the dial indicator to zero. The quantity of lead required for an applied stress of 1,200 gm/mm^2 was poured into the funnel, and readings were then taken at appropriate intervals. The time required for loading was of the order of 15 seconds. Incremental loading experiments were carried out in the same fashion, except that further increments in load of 20-60 gm/mm^2 were added after times of 50 to 100 minutes. The alignment of the piston, anvil and the ends of the specimen were good enough, so that the measured strain can be taken to be the total strain of the specimen.

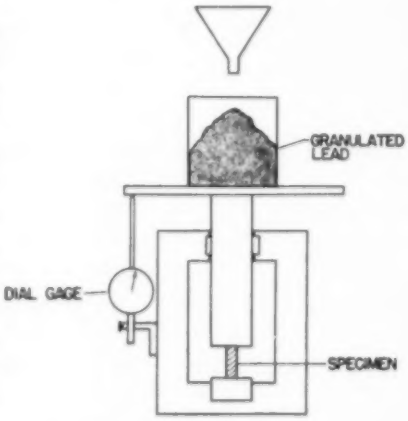

Fig. 1. Creep apparatus.

The creep tests showed the variations characteristic of creep tests in general. The reliability of the observed effects of irradiation was increased by the use of a large number of specimens. The variations from specimen to specimen will be discussed in more detail in the section on radiation effects.

3. RESULTS AND DISCUSSION

(i) *Time Law for Creep*

The creep data were found to be represented satisfactorily by an equation of the type

$$\gamma = a \log t + b \tag{1}$$

where γ is the creep strain, t is time in minutes, and a and b are dimensionless constants. This functional dependence was obtained by MOTT and NABARRO (1948; COTTRELL 1953) in their theory of exhaustion creep, and found to prevail for a number of metals by DAVIS and THOMPSON (1950) and by WYATT (1953). The equation derived by MOTT and NABARRO is

$$\gamma - \gamma_i = \frac{vNkT}{A} \log \nu t \tag{2}$$

where γ_i is the "instantaneous" strain, v is the incremental contribution to the creep strain due to a single dislocation jump, N is the number of dislocations, A is the activation energy, ν is the vibration frequency of the dislocation loop against its obstacle, and kT has its usual connotation. In the present investigation, a logarithmic dependence of strain on time was found for all three types of specimens – annealed, quenched, and irradiated. Typical data are shown in Fig. 2, where

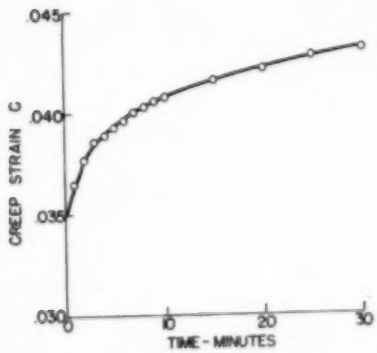

Fig. 2. A typical creep curve. The points are experimental and the curve represents the equation $c = a \log t + b$.

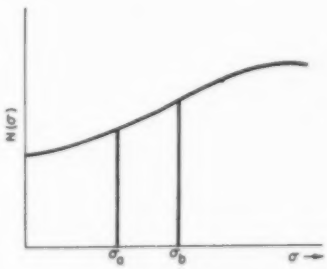

Fig. 3. Activation stress distribution. The number of dislocations which will start to move under stresses between σ and $\sigma + d\sigma$ is $N(\sigma)\, d\sigma$.

the points are experimental and the curve is that obtained from equation (1). The constants a and b were obtained from a plot of γ versus $\log t$; b is the value of the strain at the intersection of the line with the $\log t = 0$ axis. The satisfactory fit obtained with the equation led to the adoption of the two constants as characterizations of the creep curve; a is equal to the creep rate at unit time and b is a measure of the extent of initial deformation. The discussion below indicates that a value of the initial deformation which might have a greater physical significance may be obtained by computing the strain at the time required for the passage of a dislocation through the crystal. However, the assumption that the dislocations which move immediately would do so with the velocity of sound yielded a value of the strain substantially the same as that for $t = 1$, and the latter value was adopted for convenience.

The exhaustion theory of creep (MOTT and NABARRO 1948; COTTRELL 1953) is based on the idea that plastic deformation is the result of the individual movements of dislocations which are fixed in number and which move but once. For a given

applied stress, every dislocation has an activation stress which is the minimum required to induce motion. A dislocation will move only when thermal activation supplies the stress needed in addition to the applied stress to overcome the internal stresses. The distribution of activation stresses might be as in Fig. 3; the number of dislocations having an activation stress between σ and $\sigma + d\sigma$ is $N(\sigma)\,d\sigma$. When a stress σ_a is applied, the number of dislocations represented by the area under the curve to the left of σ_a will move immediately. Subsequently, as activation energy is supplied by thermal vibrations, the dislocations to the right of σ_a will move so that at a later time the stress necessary for motion will in effect be σ_b. If now an increase is made in the applied stress to a value greater than σ_b, the activation stress will be reduced to a value equal to that existing at an earlier time. The effect of the increment would therefore be to reproduce the portion of the creep curve which continues from that time. Incremental loading experiments by

TABLE 1
Dislocation energies obtained in incremental loading experiments on NaCl

Initial load, σ, g/mm^2	*Increment*, $\Delta\sigma$, g/mm^2	$F = \dfrac{kT\sigma(\Delta \log t)}{\Delta\sigma}$ *e.v.*
960	60	0·54
1100	20	0·65
1200	40	0·62
1200	60	0·57

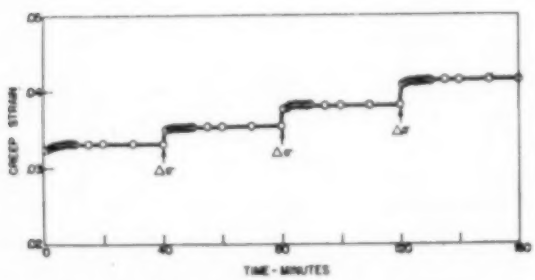

Fig. 4. Incremental loading curve for unirradiated NaCl. The initial stress was 1,200 gm/mm^2 and the increments were 60 gm/mm^2.

WYATT (1958) on aluminium, copper and cadmium indicated that the curves after the increments in load were applied were indeed similar to segments of the parent curve. The structural theory of COTTRELL (1953) based on WYATT's results predicted that the relation

$$\frac{\Delta\sigma}{\sigma\Delta \log t} = \frac{kT}{F} \tag{3}$$

should hold where σ and $\Delta\sigma$ are the applied stress and incremental stress, while $\Delta \log t$ is the distance along the $\log t$ axis which is equivalent in strain to the

effect of $\Delta\sigma$. F is the energy per unit length of dislocation. Good agreement was obtained for WYATT's data on copper when F was taken as equal to μb^3, where μ is the shear modulus and b is the atomic dimension in the shear direction.

In this investigation, incremental loading experiments were carried out after the manner of WYATT for both unirradiated and irradiated crystals. With unirradiated crystals, it was found (Fig. 4) that the successive increments of the

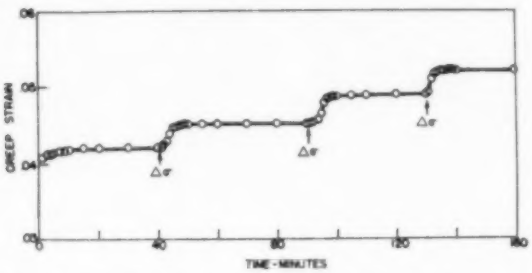

Fig. 5. Incremental loading curve for a crystal irradiated for 24 hours. Initial load of 1,200 gm/mm^2 and increments of 60 gm/mm^2.

creep curve could be superimposed on the parent curve. Quenched and annealed crystals behaved in the same manner. Average values of F computed by equation (8) for various loading conditions are listed in Table 1. The values so obtained are of the correct order of magnitude; μb^3 is 5 e.v. in this case, and HUNTINGTON's (1941) computations, which take into account the electrostatic energy between sodium and chloride ions in a dislocation, predict a value of F lower than μb^3 by a factor of 3.

Incremental loading experiments on crystals irradiated for 30 to 60 hours gave a notably different result. In every case, an induction period in the creep was obtained on the addition of a load increment (Fig. 5).

(ii) *The Effect of Radiation*

Irradiation of sodium chloride with X-rays results in marked changes in its mechanical properties. The variations in the initial deformation (which we take to be approximately equal to b) and the creep coefficient a with irradiation time are illustrated in Figs. 6 and 7. As mentioned above, the variations in the values of a and b from specimen to specimen for the same irradiation time required that a large number of experiments be run. The points plotted in Figs. 6 and 7 are averages obtained from a total of 64 creep tests. It is believed that the value of b at any point is reliable to $\pm$ 0·010, and the value for a to $\pm$ 0·0009.

The initial softening of the crystals, followed by a hardening, indicates that there may be several pertinent processes occurring during irradiation. Current theories regarding the role of dislocations in creep and the interaction of X-rays with dislocations and vacancies suggest an approach to the explanation of these two effects.

The annealed crystal before irradiation contains both dislocations and vacancies. The vacancies are believed to be distributed as pairs and larger clusters at random

throughout the crystal, and also as clusters around dislocations. Since vacancies clustered around dislocations contribute most to the relief of the internal stresses due to the dislocations, it may be concluded that an appreciable number of vacancies will be so located.

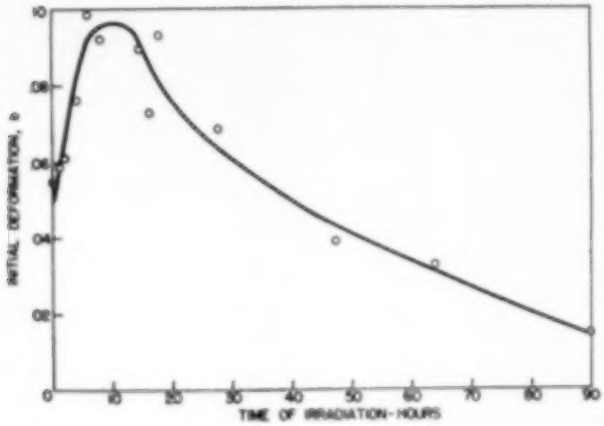

Fig. 6. Variation of the initial deformation, b, with irradiation time for an annealed crystal.

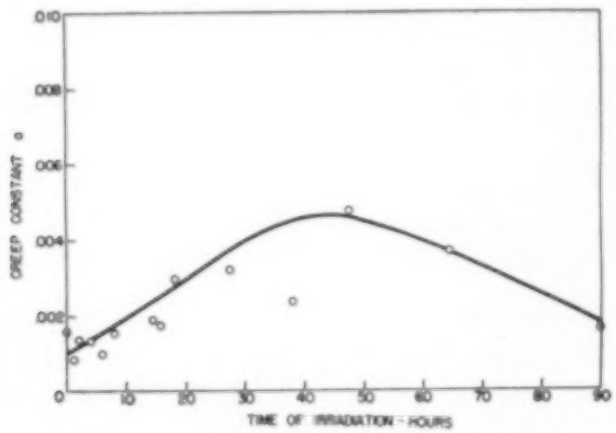

Fig. 7. Variation of the creep constant, a, with irradiation time for an annealed crystal.

The dislocation theory as applied to creep would lead one to assume that both the number and distribution of lattice vacancies have an effect on the internal stresses and on the contribution to the strain made by a dislocation jump. The vacancies closely associated with a dislocation effect the ease with which it can be made to move on the application of external stress, while the others may act as blocks when in the path of moving dislocations.

Two important processes which are believed to occur concurrently during X-irradiation of an alkali halide involve vacancy concentration and distribution. The first of these processes, and the one which is probably predominant at short

irradiation times, is the formation of F-centres by the combination of X-ray produced electrons with existent negative ion vacancies. The second process is the production of additional vacancies at dislocation jogs by the NABARRO-SEITZ (NABARRO 1948; SEITZ 1950) mechanism followed by the conversion of the negative ion vacancies so produced to F-centres.

The long term effect observed in this investigation, namely an increase in creep resistance, is analogous to the effects observed on irradiation of metals with high energy neutrons (KUNZ and HOLDEN 1954). In metals, the increase in hardness, yield point and early flow stress have been ascribed to the formation of vacancies and interstitials; these imperfections being thought of as impediments to the motion of dislocations. It might be expected that the additional vacancies introduced by the NABARRO-SEITZ process would have a similar effect in the alkali halides.

The initial softening of the crystals is more difficult to understand. It might be thought of as the result of a temporary predominance of the cluster dispersal which accompanies the formation of F-centres from existent negative ion vacancies (SEITZ 1954). Such a dispersal would tend to reduce the number and effectiveness of the impediments to dislocation motion.

(iii) *Experiments with Quenched Crystals*

It was also of interest to study the behaviour of crystals in which the vacancy concentration and distribution were varied by a means other than radiation. A convenient way in which to vary them is to quench the specimens to room temperature after equilibration at some higher temperature. Because vacancies can be lost during quenching, such crystals can be expected to have a concentration and distribution characteristic of the temperature from which they were quenched, but not necessarily the equilibrium number at that temperature. The need for an easily reproduced initial state for all specimens led to the adoption of a pretreatment of 700°, since diffusion rates at temperatures near the melting point are high enough so that crystals can be equilibrated in relatively short times. The procedure was to heat the crystals at 700° for a long time (in excess of 100 hr), and then to reduce the temperature to the desired value before quenching to room temperature. The time at the second temperature was long enough to achieve reproducible creep behaviour. Some of the vacancies present at 700° are in excess at the lower temperatures and must be lost by diffusion, possibly, as suggested by STRAUMANIS (1958), to form voids. These may not be of importance as sources of F-centres, but they can play a role in the deformation behaviour of the crystal.

The specimens therefore were assumed to have a vacancy concentration characteristic of the temperature from which they were quenched, as well as voids which were the result of the condensation of the excess vacancies introduced at 700°. There is no doubt that there were present stresses arising from the quenching procedure, and that they would have an unpredictable effect on the creep behaviour. However, it is believed that these were small in comparison to the stress applied in our experiments.

The variation in the creep constants of quenched crystals which have not been irradiated is illustrated in Fig. 8. The lack of variation of the initial deformation, b, with the heat treatment, suggests that the changes in vacancy concentration

did not alter the stress distribution around the dislocations. The large decrease in the creep coefficient, a, with temperature prior to quench, suggests that some of the randomly distributed vacancies, introduced at 700° may have been converted to voids, and that the voids are not so effective in interfering with the motion of dislocations. The dashed line in the Figure is an exponential curve and suggests that the creep rate may depend in a simple way on the number of vacancies.

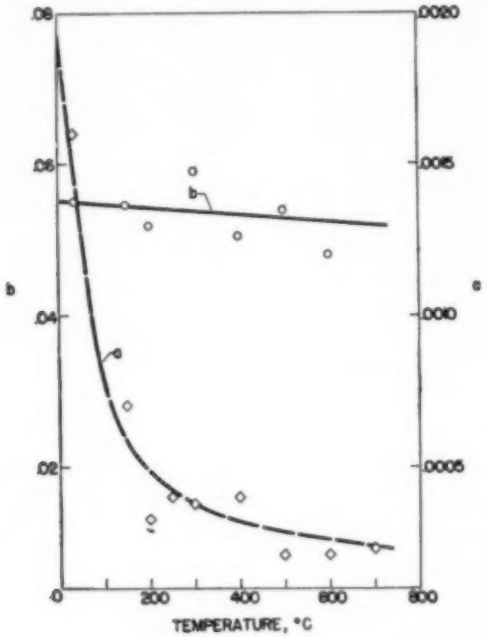

Fig. 8. Variation of the constants a and b, with temperature prior to quenching.

Conclusions

The results of this investigation may be summarized as follows :

1. Alkali halide single crystals exhibit logarithmic creep at room temperature under a load of 1,200 gm/mm^2. The logarithmic equation was found to fit equally well for crystals which were annealed, quenched, or irradiated with X-rays.

2. Irradiation with X-rays has a marked effect on creep behaviour, causing an initial softening followed by a hardening as irradiation is continued.

3. The behaviour after irradiation can be explained on the basis of the changes in vacancy concentration and distribution with accompanying F-centre formation.

4. Studies in which the vacancy concentration was changed by quenching from higher temperatures indicate that the creep rate may depend in a simple way on the number of vacancies.

References

Cottrell, A. H. 1952 *J. Mech. Phys. Solids*, **1**, 53.
1953 *Dislocations and Plastic Flow in Crystals* (Oxford).

Davis, M. and Thompson, N.	1950	*Proc. Phys. Soc.* B **63**, 847.
Estermann, I., Leivo, W. J. and Stern, O.	1949	*Phys. Rev.*, **75**, 627.
Frankl, D. R.	1953	*Phys. Rev.*, **92**, 573.
Huntington, H. B.	1941	*Phys. Rev.*, **59**, 942A.
Kunz, F. W. and Holden, A. N.	1954	Report KAPL-1066 Knolls Atomic Power Laboratory, General Electric Co.
Li, Y.	1953	*Acta Metallurgica*, **1**, 455.
Markham, J. J.	1952	*Phys. Rev.*, **88**, 500.
Mott, N. F. and Nabarro, F. R. N.	1948	*Conference on the Strength of Solids*, Physical Society (London), p. 1.
Nabarro, F. R. N.	1948	*Conference on the Strength of Solids*, p. 75 (Physical Society, London).
Podaschewsky, M. N.	1935	*Phys. Z. Sowjetunion*, **8**, 81.
Pohl, R. W.	1937	*Proc. Phys. Soc.* **49** (extra part), 4.
Seitz, F.	1950	*Phys. Rev.*, **80**, 239.
	1954	*Rev. Mod. Phys.*, **26**, 7.
Straumanis, M. E.	1953	*Am. Mineralogist*, **38**, 662.
Westervelt, D. R.	1954	Report NAA-SR-888 Atomic Energy Research Department, North America Aviation, Inc.
Wyatt, O. H.	1953	*Proc. Phys. Soc.* B **66**, 459.

Journal of the Mechanics and Physics of Solids, 1955, Vol. 4, pp. 38 to 52. Pergamon Press Ltd., London.

ON THE BEHAVIOUR OF INFINITELY LONG RIGID-PLASTIC BEAMS UNDER TRANSVERSE CONCENTRATED LOAD

By H. G. Hopkins
Armament Research and Development Establishment, Fort Halstead

(*Received* 12*th August*, 1955)

Summary

This paper is concerned with the behaviour of an infinitely long uniform beam, made of a non-hardening plastic-rigid material, under the action of a single transverse concentrated load. The effects of transverse shearing deformation and rotatory inertia are assumed negligible, and the yield condition is assumed to depend only upon the bending moment. This problem is solved subject to the condition that the ratio of the impact velocity of the concentrated load to the time is non-increasing in time. The impact velocity is allowed to vary with the time. The associated problem concerning the motion of the beam following the removal of the concentrated load is also solved. Hitherto the only problem of the present type whose solution has been published is that involving constant impact velocity, but even there the solution of the unloading problem was not found. The general analysis of this paper is applied to solve completely the constant impact velocity problem, and some detailed results for other cases are also given. The motion, subject to the above restriction upon the impact velocity, is such that there are always a central, fixed yield-hinge and two lateral, outwards-moving yield-hinges, and is also such that the beam does not come to rest in any finite time.

1. Introduction

The general problem of plastic deformations in structures subjected to dynamic loading is very complicated. So far only the simplest possible physical situations have been treated theoretically. These include the propagation of plane waves along a rod, the propagation of spherical waves in an infinite medium, and transverse impact on cables, beams, frames and membranes. The compilation of a bibliography of published work in this field is not within the scope of this paper, but the reader may note that some representative references are given in a recent paper by Hopkins and Prager (1954).

The only theoretical work on the behaviour of infinitely long plastic beams under transverse concentrated load of which the author is aware is that of Bohnenblust (1950) and Conroy (1952). The reader is referred to Prager (1955) for a summary of the theoretical treatments that have been made of corresponding problems for finite beams. In this latter field the work of Lee and Symonds and their collaborators is especially important.

This paper is concerned with the behaviour of an infinitely long uniform beam, made of a non-hardening rigid-plastic material, under the action of a single trans-

verse concentrated load. The analyses of BOHNENBLUST (1950) and CONROY (1952) exhibit a similarity in that attention is restricted to the special problem of constant impact velocity, the associated problem concerning the motion following the removal of the concentrated load not being solved. These analyses also exhibit a dissimilarity in the choice of mechanical behaviour of the material, this being taken as elastic-plastic by BOHNENBLUST (1950) and as rigid-plastic by CONROY (1952), with arbitrary moment-curvature relationship. The analysis of BOHNENBLUST (1950) is essentially an extension of that by BOUSSINESQ (1885) for infinitely long beams, made of a material exhibiting linear elastic behaviour, to cover the completely general case of non-linear elastic behaviour. This extension is possible because no unloading of beam elements is involved, and then any distinction between elastic and plastic mechanical behaviour is immaterial. The success of the extension devolves from the fact that the transverse velocity and bending moment distributions in the beam can be expressed when there is constant impact velocity, and independently of mechanical behaviour, simply in terms of a single independent variable which is the ratio of the distance from the point of impact to the square root of the time. The same mathematical situation occurs in the problem studied by CONROY (1950), but, although its exploitation enables a compact elegant analysis to be given, it appears to have obscured the fact that there also exists a relatively simple solution of the present problem in other circumstances. Here the problem is solved subject to the condition that the ratio of the impact velocity of the concentrated load to the time is non-increasing in time. The impact velocity is allowed to vary with the time. As will be seen later the motion is then such that there are always a central, fixed yield-hinge and two lateral, outwards-moving yield-hinges. The associated problem concerning the motion of the beam following the removal of the concentrated load is also solved. The purpose of this paper is to give the general analysis of these problems, and to apply this analysis to solve completely the constant velocity impact problem, and to give some detailed results for some other prescribed velocity distributions of interest.

In the present paper, the usual assumption of the theory of thin beams is adopted, according to which the transverse normal stress and the shear stress are, on the average, regarded as small when compared to the bending stress. Although the shear force resulting from the shearing stresses is taken into account in the equation of motion, these shearing stresses are neglected in the yield condition. It is supposed that the line of action of the concentrated force coincides with a principal axis of the beam cross-section, and thus there is no twisting action under load. Fig. 1 shows the relationship between the bending moment M and the curvature κ for a beam made of a non-hardening rigid-plastic material. Such a beam can bend only at cross-sections where the absolute value of the bending moment is equal to the limit moment $M_0\,(>0)$; and, at other cross-sections, $|M| < M_0$, and there the beam is rigid. As a rule, the limit moment is first reached only at isolated

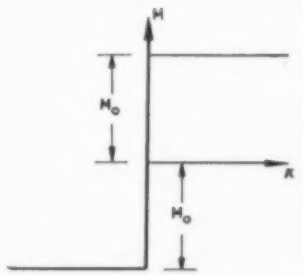

Fig. 1. Bending moment v. curvature relationship for a perfectly plastic-rigid beam.

cross-sections, and accordingly bending is therefore initially concentrated at these yield-hinges. Since the beam segments between these yield-hinges must initially remain straight, deformation of a statically indeterminate beam first becomes possible only when yield-hinges have been formed in a number sufficient to transform the beam into a mechanism. The flow limit at which the non-hardening rigid-plastic beam begins to deform is therefore, in general, different from the elastic limit at which the limit moment is first reached at some cross-section. Once the flow limit has been achieved, although the velocity distribution depends only upon the instantaneous disposition of the yield-hinges, the deformation depends upon the past positions of the yield-hinges. Only in relatively simple situations do all the yield-hinges remain fixed, and, for example, in the present problem it is necessary to consider the complications due to moving yield-hinges. Lee and Symonds (1952) and Symonds and Leth (1954) have discussed the circumstances in which the present type of analysis is likely to provide results that are a satisfactory approximation to those obtaining in experimental studies of the permanent deformation of a beam of ductile material subjected to transverse impact load. These authors observe that the assessment of the reliability of such an analysis must perforce rest ultimately upon comparison with either experimental results or predictions of more complete elastic-plastic solutions when these are developed, but the results may be expected to be valid when the plastic deformations are large enough.

In Sections 2 to 4, attention is given to the general problem of the deformation of a non-hardening rigid-plastic beam under distributed transverse load. The basic concepts involved here are now well established in the literature. Here, for completeness, the derivation of the formal mathematical statement of the problem is included. In Section 5, analysis is given of the problem involving a single concentrated transverse load and also of the associated unloading problem. In Section 6, as an illustration, the general analysis of Section 5 is applied to solve the problem for the variable impact velocity $v = \text{const. times } t^{\alpha}$ $(0 \leqslant \alpha \leqslant 1)$. This includes the constant velocity impact problem as the special case $\alpha = 0$, and some results of Conroy (1950) are recovered.

2. Dynamical Equations, Yield Condition and Flow Rule

Let x be distance measured along the neutral axis from some arbitrary cross-section; and let t be the time. Let $p(x, t)$ denote the applied load intensity, the direction of p everywhere coinciding with a principal axis of cross-section and pointing vertically downwards, and let m be the mass per unit length of the beam. Let $y(x, t)$ be the downwards deflection of material points lying on the neutral axis and $M(x, t)$ be the bending moment caused by the bending stresses parallel to the neutral axis. Here M is reckoned positive when the lower half of the beam is in tension. Finally, let $Q(x, t)$ be the shear force caused by the shearing stresses normal to the neutral axis. Here the shear force transmitted across a section $x = \text{const.}$ from the side of larger values of x to the side of smaller x values is reckoned positive if it is directed vertically downwards. The variation of the states of deflection and stress will then be specified by giving y, M and Q as functions of the co-ordinates x and the time t.

In the spirit of the theory of thin beams, the dynamical equations are expressed in terms of the bending moment M and shear force Q. Here the effects on the motion of shearing deformation and rotatory inertia are assumed negligible, and then the dynamical equations are well known to be

$$Q_x = -(p - my_{tt}), \tag{1}$$

$$Q - M_x = 0, \tag{2}$$

where, for simplicity, p is supposed finite. Here, as elsewhere, suffixes denote derivatives. Equations (1) and (2) yield

$$M_{xx} = -(p - my_{tt}), \tag{3}$$

which is taken as the fundamental dynamical equation, and then, once M is known, Q is given directly by (2). Equation (3) is independent of the mechanical properties of the material. These properties are specified by the yield condition and flow rule. The yield condition specifies those states of stress M under which plastic flow can occur. For each of these yield states the flow rule makes a statement regarding the rate of curvature

$$\kappa = -y_{xxt} \tag{4}$$

that can occur under a given yield state. Here the situation is an especially simple one because there are only two possible yield states, viz.

$$M = \pm M_0, \tag{5}$$

and the corresponding flow rules are respectively

$$\kappa \lesseqgtr 0. \tag{6}$$

There is of course the possibility that some parts of the beam are not yielding at a particular instant. Since elastic deformations are neglected in the present analysis such a part must move instantaneously as a rigid body, i.e. the rate of curvature κ vanishes. According to (4), this means that, at this particular instant, the rate of deflection is linear in x.

3. Yield-hinges

A cross-section across which y_{xt} is discontinuous is called a yield-hinge. A yield-hinge is best regarded as the limiting case of a very thin slice of the beam through which y_{xt} varies rapidly although in a continuous manner. It is clear that for non-hardening rigid-plastic material, yield-hinges can form only at cross-sections where $|M| = M_0$, and elsewhere y_{xt} must be continuous.

If the entire beam were at all times exhibiting the same mechanical behaviour, then the determination of y, M and Q as functions of x and t would not constitute a difficult problem. For most problems, however, the beam is sub-divided into segments separated by cross-sections at which there is a yield-hinge. Moreover, the number of these segments and the associated yield-hinges may vary with time. It therefore becomes necessary to establish relations between the various mechanical quantities on the two sides of a yield-hinge separating two such segments of the beam.

Let H denote a yield-hinge. Dynamical considerations establish that the bending moment M and the shear force Q are continuous across H. The cohesion of the beam material requires that the deflection y is continuous across H. If the velocity y_t were not continuous across H then large transverse shear strain-rates would occur. Therefore inasmuch as the present theory altogether neglects such strain-rates, it is accordingly necessary for consistency to demand that y_t is continuous. The acceleration y_{tt} may be discontinuous across H, and this will be shown below. By definition, y_{xt} is discontinuous across H.

In general, the distance $x = \xi$ to a yield-hinge varies with the time. The yield-hinge is stationary whenever $\xi_t = 0$. In order to discuss the possible discontinuities of the derivatives of y across a yield-hinge H, represent the variation of ξ by the curve Γ with equation $x = \xi(t)$ in terms of rectangular cartesian co-ordinates x and t. Since the deflection y is continuous across Γ, the derivative of y along Γ is also continuous across Γ. Thus

$$[y_t] + \xi_t [y_x] = 0 \tag{7}$$

where the brackets denote discontinuities, if any, of the enclosed quantities across Γ. Now y_t is continuous across Γ, and (7) therefore shows that the slope y_x can be discontinuous only across a stationary yield-hinge. If the yield-hinge H is not stationary, then y_x must be continuous across Γ. The same reasoning leading to (7) now shows that

$$[y_{xt}] + \xi_t [y_{xx}] = 0, \tag{8}$$

where, by hypothesis, $\xi_t \neq 0$. Now return to the general case of either a stationary or moving yield-hinge. Since the velocity y_t is continuous across Γ, it follows similarly that

$$[y_{tt}] + \xi_t [y_{xt}] = 0. \tag{9}$$

Thus the acceleration y_{tt} must be continuous across a stationary yield-hinge, but is discontinuous across a moving yield-hinge because y_{xt} is, by definition, discontinuous across a yield-hinge. Finally, since the bending moment M is continuous across Γ, it is established similarly that

$$[M_t] + \xi_t [M_x] = 0. \tag{10}$$

It follows from (2), and the fact that Q is continuous across Γ, that M_t is continuous across Γ. In the derivation of (7) to (10) it has been tacitly assumed that only one yield-hinge occurs within a certain length of the beam. If there were two yield-hinges H and H', one moving faster than the other and eventually catching up with it, it would be necessary to give special consideration to the conditions at the point of intersection of the corresponding curves Γ and Γ' that represent the motions of the two yield-hinges.

4. The Mathematical Problem

It is now possible to formulate the mathematical problem of the motion of a beam under piece-wise continuous, distributed, time-dependent loading $p(x, t)$. It is assumed that the beam is initially straight $[y(x, 0) = 0]$ and at rest $[y_t(x, 0) = 0]$, and the origin of time is so chosen that the beam begins to yield at $t = 0$. The

deflection $y(x, t)$ and the bending moment $M(x, t)$ are then to be determined in such a manner that certain conditions are fulfilled throughout the entire length of the beam for all time. In the enumeration of these conditions it will be assumed first that $p(x, t)$ is continuous in t. There are then the following conditions.

(1) The quantities y and y_t are continuous in x and t, and the derivatives y_x, y_{xx}, y_{xt} and y_{tt} are piece-wise continuous in x and continuous in t, x-discontinuities occurring only at yield-hinges. Across a stationary yield-hinge y_x, and hence y_{xx} and y_{xt}, may be discontinuous, but y_{tt} must be continuous. Across a moving yield-hinge y_x must be continuous, but y_{xx}, y_{xt} and y_{tt} may have discontinuities satisfying (8) and (9).

(2) The bending moment M is continuous in x and t, and the derivatives M_x and M_t are continuous in x and t.

(3) The quantities y and M satisfy (3). If the loading $p(x, t)$ is symmetrical about $x = 0$, then, at $x = 0$, $|M| = M_0$ unless a neighbourhood of the centre moves as a rigid body with y_{xt} identically zero in x.

(4) The bending moment satisfies either $|M| < M_0$ or $|M| = M_0$. In the first case $y_{xt} = 0$, and in the second case the rate of curvature must satisfy the flow rules (6).

(5) At an end $x = l$ that is either (i) simply-supported, $y(l, t) = M(l, t) = 0$; (ii) clamped, $y(l, t) = 0$, and $|M(l, t)| = M_0$; or (iii) free, $M(l, t) = M_x(l, t) = 0$.

(6) Initially $y(x, 0) = y_t(x, 0) = 0$.

When $p(x, t)$ is allowed to have t-discontinuities, all quantities considered above, except y and y_t, must be allowed to have corresponding discontinuities in t.

5. Infinite Beam under Concentrated Load. General Analysis

In this Section, the problem of an infinitely long beam subjected to the action of a single transverse concentrated load $P(t)$ is solved for an impact velocity $v(t)$ (> 0) of the concentrated load; v satisfying only the condition that v/t is non-increasing, and otherwise v is arbitrarily prescribed. The associated problem concerning the motion of the beam following the removal of the concentrated load is also solved. The direction of P coincides with a principal axis of the cross-section $x = 0$, and points vertically downwards. The beam is held rigidly at infinity. In view of the symmetrical deflection of the beam about the cross-section $x = 0$, it is sufficient to confine attention to the semi-infinite beam $x \geqslant 0$ subjected of course to shear force and bending moment at the left-hand end cross-section.

The procedure adopted here is to assume first an appropriate linear form for the velocity distribution along the beam, and then integrate the dynamical equations satisfied at all sections of the beam. This procedure differs slightly from that adopted elsewhere (see for example Lee and Symonds 1952) which is to assume first that the beam is divided into rigid segments, and then integrate the dynamical equations for these segments.

Two phases of the complete motion are distinguished, *viz.* the loading phase (I) for which $P(t) > 0$ $(0 \leqslant t < \tau)$ and the unloading phase (II) for which $P(t) = 0$ $(t > \tau)$.

Phase I: $0 \leqslant t < \tau$, $P(t) > 0$. Attention is confined to the case in which there is a central yield-hinge at $x = 0$ and an outwards-moving, lateral yield-hinge at $x = \xi(t)$. This is the simplest situation, and it will be seen that the impact velocity $v(t)$ or alternatively the concentrated force $P(t)$ must satisfy a certain condition for this to be the case. The solution of the problem has not been investigated when this condition is violated. Consider the motion described by the velocity distribution

$$y_t(x,t) = \begin{cases} v(t)\{1 - x/\xi(t)\} & (0 < x < \xi(t)), \\ 0 & (x > \xi(t)). \end{cases} \tag{11}$$

This motion satisfies the conditions $y_t(0,t) = v(t)$ and $y_t(\xi,t) = 0$. Note that y_t is everywhere continuous. According to (11),

$$y_{xt} = \begin{cases} -v/\xi & (0 < x < \xi), \\ 0 & (x > \xi), \end{cases} \tag{12}$$

so that y_{xt} is discontinuous at the points $x = 0, \xi$ where there must be yield-hinges, and then clearly $M(0,t) = -M(\xi,t) = M_0$. Further,

$$y_{tt} = \begin{cases} v_t(1 - x/\xi) + v\xi_t x/\xi^2 & (0 < x < \xi), \\ 0 & (x > \xi), \end{cases} \tag{13}$$

and so y_{tt} is discontinuous at $x = \xi$. Note that the jump condition (9) is satisfied.

The integration of (3) gives

$$M_x = -\tfrac{1}{2}P + m\int_0^x y_{tt}\,dx, \tag{14}$$

when the concentrated load $P(t)$ is regarded as a limiting case, say $P(t)\,\delta(x)$ where δ is the Dirac delta function, of a distributed loading $p(x,t)$. Then from (13) it follows that

$$M_x = -\tfrac{1}{2}P + m\{v_t(x - x^2/2\xi) + v\xi_t x^2/2\xi^2\}. \tag{15}$$

Integration of (15) with use of the condition $M(0,t) = M_0$ gives

$$M = M_0 - \tfrac{1}{2}Px + m\{v_t(x^2/2 - x^3/6\xi) + v\xi_t x^3/6\xi^2\}. \tag{16}$$

The condition $M(\xi,t) = -M_0$ gives

$$2M_0 - \tfrac{1}{2}P\xi + m(\tfrac{1}{3}v_t\xi^2 + \tfrac{1}{6}v\xi\xi_t) = 0. \tag{17}$$

The quantities M and $Q = M_x$ are both continuous across the yield-hinge $x = \xi(t)$. Now $M(\xi,t) = -M_0$ and $M(x,t) \geqslant -M_0$ near $x = \xi(t)$, and it therefore follows that $Q(\xi,t) = 0$. From (2) and (15) this additional condition gives

$$P/m = (v\xi)_t. \tag{18}$$

The elimination of P between (17) and (18) gives

$$12M_0/m = (v\xi^2)_t, \tag{19}$$

and therefore, if $\xi(0) = 0$ so that the deformation spreads out from the centre,

$$\xi = (12M_0 t/mv)^{1/2}. \tag{20}$$

Also from (18) it now follows that

$$P = (12M_0 m)^{1/2}\{(vt)^{1/2}\}_t. \tag{21}$$

The general results for the position of the moving yield-hinge and for the magnitude of the concentrated force in terms of the prescribed velocity are notably simple. Note that if v is discontinuous then ξ and P are discontinuous.

The necessary restrictions upon $v(t)$, for the present solution to be valid, arise from the requirement that $|M| < M_0\,(0 < x < \xi)$. That some conditions are necessary is perhaps suggested by the form of (20), because if v is such that v/t is an increasing function then ξ is a decreasing function. Therefore it may be conjectured that the present solution is valid only if v is such that v/t is a non-increasing function in order that, by (20), ξ is a non-decreasing function. Further, it seems reasonable to conjecture that for an increasing velocity v the condition $|M| < M_0$ $(0 < x < \xi)$ is likely to be first violated near $x = \xi$. Now $M_0 + M(\xi,t) = M_x(\xi,t) = 0$, and therefore near $x = \xi$ it follows from Taylor's theorem that $M(x,t) \simeq -M_0 + \tfrac{1}{2}(x - \xi)^2 \times M_{xx}(\xi,t)$, and consequently $M_{xx}(\xi,t) > 0$ is a necessary condition. Now from (3), $M_{xx} = my_{tt}$

($x > 0$), and therefore from (13), $\xi_t > 0$ is a necessary condition. Equation (15) together with the condition $M_x(\xi, t) = 0$ gives

$$-M_x/m = (\xi - x)\{v_t - \tfrac{1}{2}(\xi + x)(v/\xi)_t\}. \tag{22}$$

Therefore M will decrease monotonically from M_0 to $-M_0$ as x increases from 0 to ξ only if $v_t > \max.\{\frac{1}{2}(\xi + x)(v/\xi)_t\} = \xi(v/\xi)_t$, i.e. only if $\xi_t > 0$. Thus the conjecture is proved correct. Therefore the present solution is valid if and only if v/t is a non-increasing function of t. Then ξ is a non-decreasing function of t, and M is a monotonic decreasing function of x.

Instead of regarding P and ξ to be determined in terms of a given v, consider now the inverse problem of the determination of v and ξ in terms of a given P. Equation (21) may be integrated to give

$$v = \left\{\int_0^t P(t)\,dt\right\}^2 \Big/ 12M_0 mt, \tag{23}$$

and then substitution of this result in (20) gives

$$\xi = (12M_0 t) \Big/ \int_0^t P(t)\,dt. \tag{24}$$

The solution is valid if and only if $P(t)$ is such that $\left(\int_0^t P(t)\,dt\right) \Big/ t$ is a non-increasing function of t.

Finally it remains to determine the deflection of the beam. Suppose that the moving yield-hinge reaches the cross-section x at a time $T(x)$ determined from (20). Then the displacement at this cross-section at later times is

$$y(x, t) = \int_{T(x)}^t y_t\,dt \quad (t > T), \tag{25}$$

and therefore, from (11) and (20),

$$y(x, t) = \int_{T(x)}^t v\{1 - x(mv/12M_0 t)^{1/2}\}\,dt \quad (t > T), \tag{26}$$

where

$$x = \{12M_0 T/mv(T)\}^{1/2}. \tag{27}$$

The jump condition (8) together with (12) gives

$$[y_{xx}] = -v/\xi\xi_t, \tag{28}$$

and it is straightforward to show that (26) and (27) are consistent with this result.

Phase II : $t > \tau$, $P(t) = 0$. In this part of the motion no concentrated load is applied, but the beam must continue in further motion for some period of time during which the kinetic energy acquired during Phase I is dissipated by plastic work. At time τ, continuity of displacement and velocity is required. Consider the motion described by (11) to (13) where ξ, different from before, is as yet unknown. Equation (3), after setting $p \equiv 0$, together with (13), gives

$$M_{xx} = m\{v_t(1 - x/\xi) + v\xi_t x/\xi^2\}. \tag{29}$$

The bending moment distribution $M(x, t)$ satisfying (29) and the conditions $M(0, t) = M_0$ and $M_x(0, t) = 0$ is

$$M = M_0 + m\{v_t(x^2/2 - x^3/6\xi) + v\xi_t x^3/6\xi^2\}. \tag{30}$$

Further, exactly as before, $M_x(\xi, t) = 0$, and therefore from (30),

$$(v\xi)_t = 0. \tag{31}$$

Therefore

$$v\xi = v(\tau)\,\xi(\tau) = v_1\,\xi_1 \tag{32}$$

because the velocity is continuous at $t = \tau$, the suffix 1 denoting evaluation at time τ. Moreover

$M(\xi, t) = -M_0$, and therefore from (20),

$$2M_0 + m(v_t \xi^2/3 + v\xi_t \xi/6) = 0. \tag{33}$$

From (32) and (33),

$$\xi_t = 12M_0/mv_1 \xi_1. \tag{34}$$

Then after integration and with use of (20),

$$\xi/\xi_1 = t/\tau, \tag{35}$$

and hence from (32),

$$v/v_1 = \tau/t. \tag{36}$$

The results (35) and (36) are notably simple, and state that the distance from the origin of the moving yield-hinge is directly proportional to the time and the central velocity is inversely proportional to the time. The latter result means that the beam does not come to rest in any finite time.

The above solution is valid only if the condition $|M| < M_0$ $(0 < x < \xi)$ is satisfied. From (30), (32) and (36),

$$M_x/m = -v_1(\tau/t^2)x(1 - x/\xi), \tag{37}$$

and accordingly M monotonically decreases from M_0 to $-M_0$ as x increases from 0 to ξ. Therefore the above condition is satisfied.

Finally, it remains to determine the deflection of the beam. Two cases need to be considered here according as $x \lessgtr \xi_1$.

(i) The case $0 < x < \xi_1$. The displacement is continuous at $t = \tau$, and therefore

$$y(x, t) = y(x, \tau) + \int_\tau^t y_t \, dt, \tag{38}$$

where $y(x, \tau)$ is given by (26) and (27) and y_t is given by (11), (35) and (36). Thus

$$y(x, t) = y(x, \tau) + v_1 \tau \{ln(t/\tau) - (x/\xi_1)(1 - \tau/t)\} \tag{39}$$

or alternatively

$$y(x, t) = y(x, \tau) + v_1 \tau \{ln(\xi/\xi_1) + x(1/\xi - 1/\xi_1)\}. \tag{40}$$

(ii) The case $\xi_1 < x < \xi(t)$. The displacement is continuous at $t = \tau$, and it is then zero. The moving yield-hinge reaches the cross-section x at time $\tau x/\xi_1$ (see (35)). At later times t the displacement is

$$y(x, t) = \int_{\tau x/\xi_1}^t y_t \, dt \quad (t \geqslant \tau x/\xi_1), \tag{41}$$

i.e. from (11), (35) and (36),

$$y(x, t) = v_1 \tau \{ln(t\xi_1/\tau x) + (\tau x/\xi_1 t - 1)\} \quad (t \geqslant \tau x/\xi_1) \tag{42}$$

or alternatively

$$y(x, t) = v_1 \tau \{ln(\xi/x) + (x/\xi - 1)\}. \tag{43}$$

This completes the general analysis.

6. Variable Impact Velocity : $v(t)$ = const. times t^a

The results of the general analysis of Section 5 are now specialized to the case when there is a variable impact velocity of the form

$$v = v_0 (t/\tau)^a, \tag{44}$$

where $v_0 = v(\tau) = v_1$, *i.e.* the central velocity at the end of Phase I. Now the present solution requires that v/t is a non-increasing function of t, and thus it is

necessary that $\alpha \leqslant 1$. Further, restrict v to be finite, and then $\alpha \geqslant 0$. Then in (44) take

$$0 \leqslant \alpha \leqslant 1. \tag{45}$$

Phase I : $0 \leqslant t \leqslant \tau$. From (20),

$$\xi = (12M_0\, t^{1-\alpha}\, \tau^{\alpha}/mv_0)^{1/2}, \tag{46}$$

so that the distance to the moving yield-hinge varies directly as $t^{(1-\alpha)/2}$. Also from (21),

$$P = \{3\,(1+\alpha)^2\, M_0\, mv_0/\tau^{\alpha}\, t^{1-\alpha}\}^{1/2} \tag{47}$$

so that the magnitude of the concentrated force varies inversely as $t^{(1-\alpha)/2}$. Thus $P\xi$ remains constant. Note from (47) that, although an infinite force is required, save in the special case $\alpha = 1$, to initiate the motion envisaged, the impulse $I(t)$ of this force is finite,

$$I(t) = \int_0^t P(t)\, dt = (12M_0\, mv_0\, t^{\alpha+1}/\tau^{\alpha})^{1/2}. \tag{48}$$

The deflection of the beam is found from (26) and (27),

$$y(x,t) = \begin{cases} v_0\, \tau\, (t/\tau)^{1+\alpha} \left\{ \dfrac{1}{1+\alpha} - \dfrac{2}{1+3\alpha}(x/\xi) + \dfrac{1-\alpha}{(1+3\alpha)(1+\alpha)}(x^2/\xi^2)^{(1+\alpha)/(1-\alpha)} \right\} & (0 \leqslant x \leqslant \xi), \\ 0 & (x \geqslant \xi), \end{cases} \tag{49}$$

where ξ is given by (46). Therefore, for any fixed t the deflection of the beam is given in terms of a simple algebraic expression. The discontinuity in slope of the beam at the central cross-section, *viz.* $2\theta\,(>0)$, is given from (46) and (49) by

$$\theta = (mv_0^3\, \tau/3M_0)^{1/2}\, (t/\tau)^{(1+3\alpha)/2}/(1+3\alpha). \tag{50}$$

Further, from (49) it is clear that there is no discontinuity in slope of the beam at the lateral yield-hinge. Also from (46) and (49) the change in curvature $\varkappa\,(>0)$ at the lateral yield-hinge is

$$\varkappa = \{mv_0^2/6\,(1-\alpha)\, M_0\}\, (t/\tau)^{2\alpha}. \tag{51}$$

Phase II : $t > \tau$. The results found in Section 5 under (b) apply, and it is only necessary to note that $y(x, \tau)$ occurring in (38) to (40) is given from (46) and (49) by

$$\left.\begin{aligned} y(x,\tau) = v_0\, \tau \left\{ \frac{1}{1+\alpha} - \frac{2}{1+3\alpha}(x/\xi_1) + \frac{1-\alpha}{(1+3\alpha)(1+\alpha)}(x^2/\xi_1^2)^{(1+\alpha)(1-\alpha)} \right\} \\ (0 \leqslant x \leqslant \xi_1 = (12M_0\, \tau/mv_0)^{1/2}). \end{aligned}\right\} \tag{52}$$

The formulae for the deflection of the beam, (40), (43) and (52), now involve algebraic and logarithmic expressions. The discontinuity in slope 2θ of the beam at the central cross-section is given from (39), (46) and (49) by

$$\theta = (mv_0^3\tau/3M_0)^{1/2} \left\{ \frac{1}{1+3\alpha} + \tfrac{1}{2}\,(1-\tau/t) \right\}, \tag{53}$$

and therefore

$$\lim_{t\to\infty} \theta(t) = 3\,[(1+\alpha)/2\,(1+3\alpha)]\, (3\, mv_0^3\, \tau/M_0)^{1/2}. \tag{54}$$

Further, from (43) it is clear that there is no discontinuity in slope of the beam at the lateral yield hinge. Also, from (35), (43) and (46) the change in curvature $\varkappa$ at the lateral yield-hinge is

$$\varkappa = (mv_0^2/12M_0)\, (\tau/t)^2, \tag{55}$$

and, as expected, $\varkappa \to 0$ as $t \to \infty$. Further, from (40), (43) and (52) it is clear that there is no discontinuity in slope of the beam at the cross-section $x = \xi_1$. The change in curvature at this cross-section is given by (40) and (52),

$$x = \left(\frac{1+\alpha}{1-\alpha}\right)(mv_0^2/12M_0), \tag{56}$$

and is accordingly constant.

It is of some interest to investigate the rate of dissipation of kinetic energy by plastic work. During Phase I, the work W_1 done by the concentrated load is

$$W_1 = \int_0^\tau P(t)\, v(t)\, dt, \tag{57}$$

i.e. from (44) and (47),

$$W_1 = \left(\frac{1+a}{1+3\alpha}\right)(12M_0\, mv_0^3\, \tau)^{1/2}. \tag{58}$$

At the end of Phase I, the kinetic energy T_1 acquired by the beam is

$$T_1 = \int_0^{\xi_1} \tfrac{1}{2}\, m y_t^2\,(x, \tau)\, dx, \tag{59}$$

i.e. from (11) and (46),

$$T_1 = (M_0\, mv_0^3\, \tau/3)^{1/2}. \tag{60}$$

Therefore from (58) and (60),

$$1 - T_1/W_1 = (5 + 3\alpha)/6\,(1+\alpha), \tag{61}$$

i.e. between 5/6 and 2/3 of the work done by the concentrated forces has been dissipated. In general, throughout the motion in Phase I, only between 1/6 and 1/3 of the work done by the concentrated force is available to produce changes in the kinetic energy of the beam, the remainder (between 5/6 and 2/3) being continually dissipated at the yield-hinges. During Phase II the kinetic energy $T(t)$ of the beam is

$$T(t) = \int_0^\xi \tfrac{1}{2}\, m y_t^2\,(x, t)\, dx, \tag{62}$$

i.e. from (11), (35), (26) and (46),

$$T(t) = (M_0\, mv_0^3\, \tau^3/3t^2)^{1/2}, \tag{63}$$

or, from (60),

$$T(t)/T_1 = \tau/t. \tag{64}$$

Thus from (61) and (64),

$$T(t)/W_1 = \{(1 + 3\alpha)/6\,(1+\alpha)\}\,(\tau/t). \tag{65}$$

The rate of dissipation of kinetic energy is therefore relatively low, and an unloading time interval of between $15\frac{1}{3}\,\tau$ and $32\frac{1}{3}\,\tau$ is required to dissipate all but 1% of $W(\tau)$.

The above detailed results are given as an illustration, and the derivation of results for many other types of impact velocity distribution should be quite straightforward.

This Section is concluded with some discussion of special cases. First consider the case of constant velocity impact $v = v_0 = \text{const}$. The solution of the loading problem was given first by CONROY (1952), and the main results are easily recovered by setting $\alpha = 0$. From (46),

$$\xi = (12M_0\, t/mv_0)^{1/2}, \tag{66}$$

so that the distance to the moving yield-hinge varies directly as the square root of the time. Also from (47),

$$P = (3M_0\, mv_0/t)^{1/2}, \tag{67}$$

so that the magnitude of the concentrated force varies inversely as the square root of the time. The impulse of this force is

$$I = (12 M_0 m v_0 t)^{1/2}, \tag{68}$$

and thus varies directly as the square root of the time. The displacement of the beam is given from (49) by

$$y(x,t) = \begin{cases} v_0 t (1 - x/\xi)^2 & (0 \leqslant x \leqslant \xi), \\ 0 & (x \geqslant \xi), \end{cases} \tag{69}$$

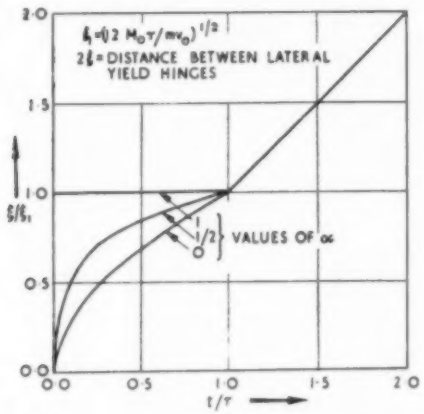

Fig. 2. Variation of position of lateral yield-hinge with time for three types of impact velocity - $v = v_0 (t/\tau)^\alpha$ $(0 \leqslant t/\tau \leqslant 1)$ where $\alpha = 0$, 1/2 or 1.

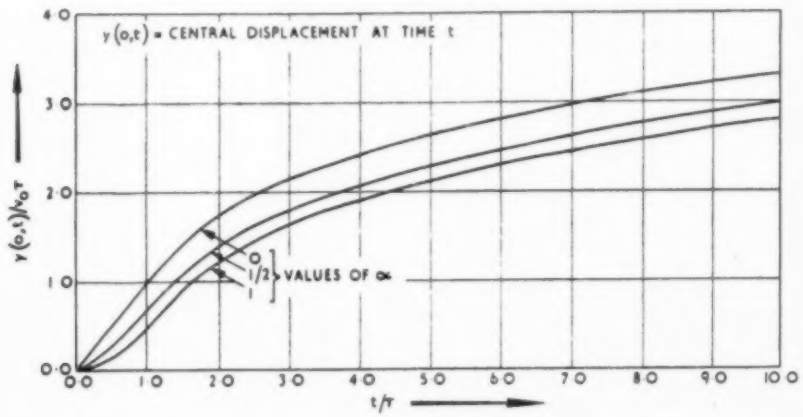

Fig. 3. Variation of central displacement with time for three types of impact velocity - $v = v_0 (t/\tau)^\alpha$ $(0 \leqslant t/\tau \leqslant 1)$ where $\alpha = 0$, 1/2 or 1.

where ξ is given by (66), and therefore, for any fixed t, the beam has a parabolic shape.

Now consider the case of velocity impact varying directly as the time, *i.e.* $v = v_0 t/\tau$. The results corresponding to (66) to (69) are

$$\xi = \text{const.} = (12M_0\,\tau/mv_0)^{1/2}, \tag{70}$$

$$P = \text{const.} = (12M_0\,mv_0/\tau)^{1/2}, \tag{71}$$

$$I = Pt, \tag{72}$$

$$y(x,t) = \begin{cases} v_0\,(t^2/2\tau)\,(1 - x/\xi) & (0 \leqslant x \leqslant \xi), \\ 0 & (x \geqslant \xi). \end{cases} \tag{73}$$

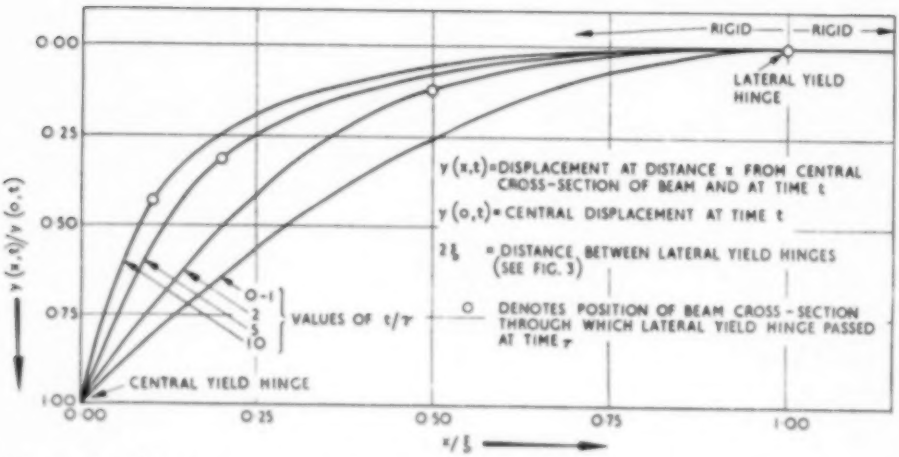

Fig. 4. Variation of displacement along beam, expressed in terms of that at beam centre, with time-case of constant impact velocity $v = v_0\ (0 \leqslant t/\tau \leqslant 1)$.

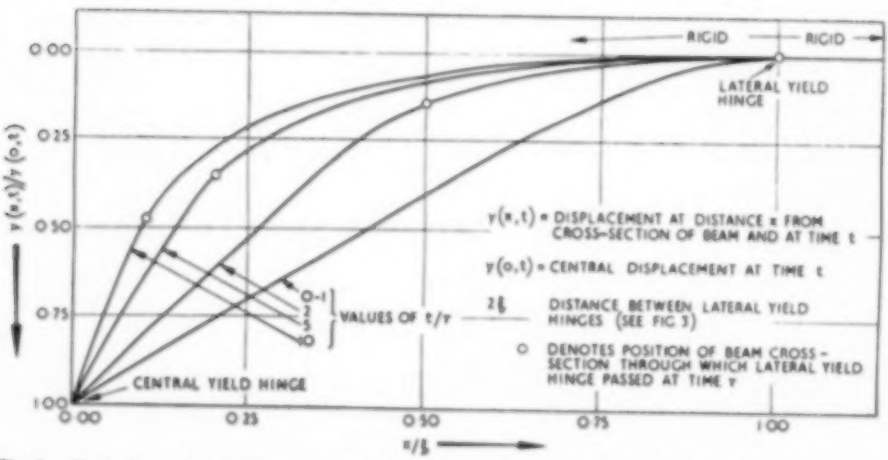

Fig 5. Variation of displacement along beam, expressed in terms of that at beam centre, with time-case of variable impact velocity $v = v_0\,(t/\tau)^{1/2}\ (0 \leqslant t/\tau \leqslant 1)$.

The lateral yield-hinges are stationary, the transverse concentrated force is constant, and the beam assumes a triangularly shaped deformation increasing in height as the square of the time.

Some of the more important of the results obtained above are shown in Figs. 2 to 6. In Fig. 2 there is given the variation of the position of the lateral yield-hinges with time for the three types of impact velocity corresponding to $\alpha = 0$, $\frac{1}{2}$ and 1. The three curves coalesce, of course, for $t/\tau > 1$. In Fig. 3 there is given the variation of the central displacement with time for the same types of impact velocity. Note that the curves have a similar asymptotic behaviour for $t/\tau \to \infty$. Finally, in Figs. 4 to 6 there is given the variation of the displacement along the

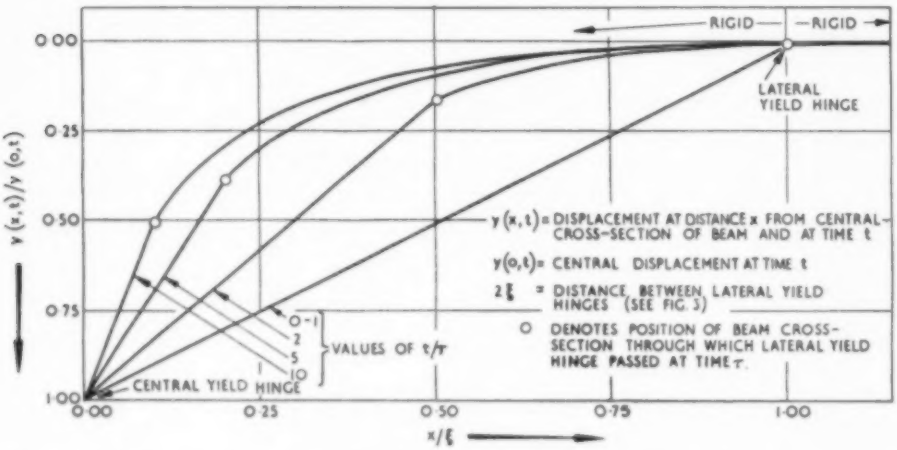

Fig. 6. Variation of displacement along beam, expressed in terms of that at beam centre, with time-case of variable impact velocity $v = v_0\,(t/\tau)$ $(0 \leqslant t/\tau \leqslant 1)$.

beam in terms of the central displacement, already given in Fig. 3, again for the same types of impact velocity. When taken together the numerical results plotted in these Figures give a complete picture of the plastic deformation of the beam for a fairly general impact velocity distribution. In retrospect it should be noted that the special cases $\alpha = 0, 1$ have certain distinctive features so that they are best regarded as limiting cases $\alpha \to 0, 1$, respectively.

Note added in proof (*7th September*, 1955).

If, as stated in the paper, the condition on the impact velocity $(v/t)_t \leqslant 0$ is violated then the present analysis does not apply. The recent work by P. S. Symonds on finite beams [*Proc. Sec. United States Congr. Appl. Mech., Ann Arbor, Mich.*, 1954 (*Amer. Soc. Mech. Engrs., New York*, 1954), pp. 505-515] indicates that lateral yield-hinges will no longer occur at isolated cross-sections of the beam. Instead two lateral yield bands, throughout which $M = -M_0$, must develop. The analysis for this case is needed if the solution of the problem is to be quite free from restriction. This further analysis will be given elsewhere.

Acknowledgments

This paper was written when the author was Visiting Professor of Applied Mathematics at Brown University, Providence, R.I. The research was sponsored

by Watertown Arsenal under Contract DA-19-020-ORD-2598. The author is indebted to Professors W. PRAGER and P. S. SYMONDS for comments on the analysis.

REFERENCES

BOUSSINESQ, J.	1885	*Applications des Potentiels à l'Etude de l'Equilibre et du Mouvement des Solides Elastiques*, 435 (Gauthier-Villars, Paris).
CONROY, M. F.	1952	*J. Appl. Mech.*, **19**, 465.
DUWEZ, P. E., CLARK, D. S. and BOHNENBLUST, H. F.	1950	*J. Appl. Mech.*, **17**, 27.
LEE, E. H. and SYMONDS, P. S.	1952	*J. Appl. Mech.*, **19**, 308.
PRAGER, W.	1955	*Proc. Instn. Mech. Engrs.*, **169**, 41.
SYMONDS, P. S. and LETH, C. F. A.	1954	*J. Mech. Phys. Solids*, **2**, 92.

Journal of the Mechanics and Physics of Solids, 1956, Vol. 4, pp. 53 to 71. Pergamon Press Ltd., London.

DYNAMIC LOADING OF RIGID-PLASTIC CYLINDRICAL SHELLS

By G. Eason and R. T. Shield
Armament Research and Development Establishment, Fort Halstead

(*Received 12th September*, 1955)

Summary

The behaviour of an infinitely long, rigid-plastic cylindrical shell under impulsive loading by a ring of concentrated force and a band of uniform pressure is discussed. The loads are assumed to be greater than the statical collapse values and to act for a short period of time. Numerical results are obtained for rectangular and triangular pulse shapes for the ring of force and for a rectangular pulse shape for a band of uniform pressure. In the final section of the paper, the steady-state motion which would be produced by a constant load greater than the statical value moving along the shell with constant velocity is obtained for the particular cases of a ring of force and a band of uniform pressure.

1. Introduction

In analysing the behaviour of cylindrical shells under dynamic loading, certain simplifying assumptions must be made in order to reduce the problem to manageable proportions. In the analogous theory of the dynamic loading of beams (see, for example, Lee and Symonds 1952) and the dynamic loading of plates (see, for example, Hopkins and Prager 1954), it is usual to assume that the elastic deformations are negligible compared with the plastic deformations. At the same time it is assumed that the strains produced are small compared with unity, so that changes in shape may be neglected. Further, an approximation is made to the plastic behaviour of the beam or plate by using a simplified yield condition. Similar assumptions are made here to predict the behaviour of an infinitely long cylindrical shell under certain types of dynamic loading. It is not within the scope of the present paper to assess the extent to which the results predicted for an ideal material will differ from those for a real material. Such an assessment can only be made when a more exact analysis has been performed or when experimental results are available.

The statical loading of a cylindrical shell by axially symmetric lateral pressure was considered by Drucker (1953), who obtained the appropriate yield condition for a material obeying Tresca's yield criterion. Later work by Hodge (1954) and Onat (1955) included the effect of an axial force. Recently, Hodge (1955) has applied the rigid-plastic theory to the impact pressure loading of cylindrical shells, under the assumptions mentioned above. Hodge considered the loading by a uniform radial pressure pulse of an infinitely long cylindrical shell reinforced by equally spaced rigid reinforcing rings. After a statement of the basic equations

in Section 2 of the following work, the impulsive loading of an infinitely long shell by a ring of force is examined in Section 3. The two types of possible deformation modes and stress patterns are discussed and applied to rectangular and triangular pulses of force. Section 4 treats impulsive loading by a band of uniform pressure, particular application being made to a rectangular pressure pulse. In Section 5 we consider a different type of dynamic loading. The loads are constant in magnitude but move along the shell with constant velocity. For simplicity it is assumed that the motion has settled down to a steady state, and the loads considered are a ring of force and a band of uniform pressure.

2. Basic Equations

The stress and moment resultants acting upon an element of a cylindrical shell under axially symmetric loading are shown in Fig. 1. In the following it will be assumed that the axial stress resultant N_x is zero. Also the circumferential bending moment M_ϕ can be ignored, since it does not enter explicitly into the equations of motion or the yield condition. The remaining resultants are the axial bending moment M, the shearing force resultant Q, and the circumferential force resultant N. The applied lateral pressure is denoted by p and is considered positive if it is directed outwards. The types of loading to be considered will produce radial motion only of the shell. The equations of motion are therefore

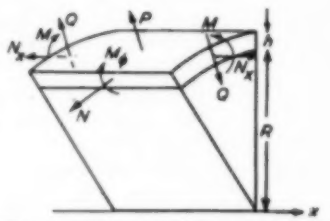

Fig. 1. Stresses on element of shell.

$$\left.\begin{aligned} \frac{\partial Q}{\partial x} &= p - \frac{N}{R} - \rho \frac{\partial u}{\partial t}, \\ \frac{\partial M}{\partial x} &= Q. \end{aligned}\right\} \tag{1}$$

In these equations the surface density of the shell is denoted by ρ, the radius of the shell by R, and the radial velocity by u. The quantities t and x represent time and distance along the shell.

It is convenient to introduce dimensionless variables defined by

$$\left.\begin{aligned} m = \frac{M}{\sigma_0 h^2}, \qquad n = \frac{N}{\sigma_0 h}, \qquad q = \frac{Q}{\sigma_0 h}\sqrt{R/h}, \qquad \psi = \frac{pR}{\sigma_0 h}, \\ \eta = \frac{u\rho R}{\sigma_0 h T}, \qquad \xi = \frac{x}{\sqrt{Rh}}, \qquad \tau = \frac{t}{T}, \end{aligned}\right\} \tag{2}$$

where σ_0 is the yield stress of the material of the shell, h is the thickness of the shell, and T is a time interval associated with the particular problem under consideration. Equations (1) can now be written in the dimensionless forms

$$\left.\begin{aligned} \frac{\partial q}{\partial \xi} &= \psi - n - \frac{\partial \eta}{\partial \tau}, \\ \frac{\partial m}{\partial \xi} &= q. \end{aligned}\right\} \tag{3}$$

Elimination of the shearing stress q, which is ignored in the yield condition, between these two equations gives

$$\frac{\partial^2 m}{\partial \xi^2} = \psi - n - \frac{\partial \eta}{\partial \tau}. \tag{4}$$

As in previous work (HODGE 1955 and EASON and SHIELD 1955), we shall use a simplified yield condition on the reduced stress resultants m and n. The yield condition to be used is an approximation to the exact yield condition obtained by DRUCKER (1953) for a material which obeys Tresca's yield criterion of constant maximum shearing stress during plastic deformation. The shell is assumed to remain rigid until the magnitude of M or N reaches the maximum permissible value M_0 or N_0 given by

$$M_0 = \tfrac{1}{4}\sigma_0 h^2, \qquad N_0 = \sigma_0 h.$$

Thus plastic deformation is possible if $|m| = \frac{1}{4}$ or $|n| = 1$, i.e. if the state of stress in the shell is represented by a point on the rectangle ABCD in Fig. 2. The true yield condition derived by DRUCKER (1953) is shown by the broken line in Fig. 2. During plastic deformation, the strain rate vector with components proportional to $\partial^2 \eta/\partial \xi^2$, η must be normal to the yield curve at the stress point in question. At a corner, the vector must lie between the normals at adjacent points. The plastic regions in the following work will all be represented by points on the side AB of the rectangle in Fig. 2, including the end points A and B. Thus n will have the value $+1$ throughout the plastic regions. It follows that the radial velocity must be positive, $\eta \geqslant 0$, and where $|m| < \frac{1}{4}$,

$$\partial^2 \eta/\partial \xi^2 = 0 \tag{5}$$

and the velocity depends linearly on ξ. Sections of the shell at which $|m| = \frac{1}{4}$ will be called hinge circles. At these sections the magnitude of $\partial^2 \eta/\partial \xi^2$ is unrestricted, but the derivative must have the same sign as m.

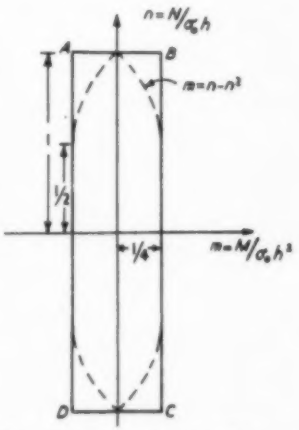

Fig. 2. Rectangular yield condition (full line) and exact yield condition (broken line).

Since the magnitude of $\partial^2 \eta/\partial \xi^2$ is unrestricted at a section where $|m| = \frac{1}{4}$, discontinuities in the velocity slope $\partial \eta/\partial \xi$ can occur at a hinge circle. The radial displacement must be continuous at a hinge circle since it is assumed that fracture of the material does not occur. If the hinge circle is stationary, it also follows that the radial velocity and acceleration must be continuous. Conditions at a moving hinge circle can be obtained in the same way that LEE and SYMONDS (1952) obtained the conditions at a moving hinge in a beam. It can easily be shown that the velocity η must be continuous across a moving hinge circle, but in general the acceleration is discontinuous. The discontinuity in the acceleration $\partial \eta/\partial \tau$ across a moving hinge circle at the section ξ_H is given by

$$\left(\frac{\partial \eta}{\partial \tau}\right)_1 - \left(\frac{\partial \eta}{\partial \tau}\right)_0 = \frac{d\xi_H}{d\tau}\left\{\left(\frac{\partial \eta}{\partial \xi}\right)_0 - \left(\frac{\partial \eta}{\partial \xi}\right)_1\right\}, \tag{6}$$

where suffices 0, 1 refer to sections just to the right and just to the left of the hinge section. Equation (6) may be obtained by equating the total time derivatives, expressed in terms of partial derivatives with respect to ξ and τ, of the velocities η_0 and η_1 on either side of the hinge circle.

3. Ring of Force

When an infinitely long shell is acted upon by a ring of force, no plastic deformation takes place unless the magnitude of the force exceeds the statical collapse value. For the rectangular yield condition used here the collapse value P_s is given by

$$P_s = 2\sigma_0 h\sqrt{h/R},$$

per unit length (see Drucker 1953). When a ring of force of intensity P is applied, accelerated plastic flow will occur if P is greater than P_s. We shall use the notation

$$P = \Psi P_s,$$

where Ψ is a non-negative function of the time, $\Psi = \Psi(\tau)$. The ring of force is applied to the section $\xi = 0$, and the stress and deformation patterns are symmetrical about this section. Because of the symmetry, only the half-shell $\xi \geqslant 0$ need be considered.

Depending upon the form of the loading function Ψ, two types of motion can occur. In the first type, which will be called the first phase, there is a hinge circle at the loaded section $\xi = 0$ and a hinge circle at some distance ξ_1 from the loaded section. In general the distance ξ_1 varies with the time. The deforming region $0 \leqslant \xi \leqslant \xi_1$ of the shell is in a plastic state of stress represented by points on the side AB of the rectangle in Fig. 2; the states of stress at the hinge sections $\xi = 0$, $\xi = \xi_1$ are represented by points A and B respectively, and the bending moment m attains the maximum numerical value $\frac{1}{4}$ at the hinge circles only. At a given time the radial velocity of the shell is greatest at the loaded section and decreases linearly to zero at the section $\xi = \xi_1$. When the shell first deforms under the action of the ring of force, the motion is always in the first phase. However, if the loading function Ψ increases at a sufficiently large rate the motion cannot continue in the first phase without violating the condition $|m| \leqslant \frac{1}{4}$ in the deforming region $0 \leqslant \xi \leqslant \xi_1$. In order to prevent this violation, the hinge circle at the section $\xi = \xi_1$ spreads so that there is a finite region $\xi_1 \leqslant \xi \leqslant \xi_2$ of the shell in which m has the maximum value $\frac{1}{4}$. The region where $m = \frac{1}{4}$ is called a hinge band, and when the width of the hinge band is finite the motion is said to be in the second phase. During motion in the second phase, the velocity in the region $0 \leqslant \xi \leqslant \xi_1$ is again a linear function of ξ. The form of the velocity in the rest of the deforming region, i.e. in the hinge band $\xi_1 \leqslant \xi \leqslant \xi_2$, depends upon the history of the motion, but the deceleration is constant throughout the hinge band. Since the elements of the shell in the hinge band are decelerating, the boundary $\xi = \xi_2$ of the plastic region moves towards the section $\xi = 0$. The first and second phases will now be discussed in more detail, and the equations governing the motion in the phases will be derived.

(i) *First phase*

When the loading function Ψ first exceeds unity hinge circles develop at the section of application of the force and at the section $\xi = \xi_1$. The bending moment m has the value $-\frac{1}{4}$ at $\xi = 0$ and $m = \frac{1}{4}$ at $\xi = \xi_1$, where ξ_1 is a function of the time τ. The shearing stress $q = \partial m/\partial \xi$ has a discontinuity of amount 2Ψ at $\xi = 0$, and q is zero at $\xi = \xi_1$ where m has a maximum value. Since $|m| < \frac{1}{4}$ for $0 < \xi < \xi_1$, the velocity η is a linear function of ξ from (5). Also $\eta = 0$ at the boundary $\xi = \xi_1$ of the plastic region, and it follows that

$$\eta = \eta_0 \left(1 - \frac{\xi}{\xi_1}\right), \tag{7}$$

where η_0 is the velocity at $\xi = 0$. The acceleration is obtained by differentiation of (7), giving

$$\frac{\partial \eta}{\partial \tau} = \frac{d\eta_0}{d\tau}\left(1 - \frac{\xi}{\xi_1}\right) + \eta_0 \frac{\xi}{\xi_1^2}\frac{d\xi_1}{d\tau}. \tag{8}$$

The equation of motion is obtained by substituting $\psi = 0$ and $u = 1$ in (4), and with the value (8) for the acceleration term we obtain

$$\frac{\partial^2 m}{\partial \xi^2} = -1 - \frac{d\eta_0}{d\tau} + \frac{\xi}{\xi_1}\left(\frac{d\eta_0}{d\tau} - \frac{\eta_0}{\xi_1}\frac{d\xi_1}{d\tau}\right). \tag{9}$$

Integrating this with respect to ξ and using the conditions at $\xi = 0$, there results, for $0 < \xi \leqslant \xi_1$,

$$\left.\begin{aligned} \frac{\partial m}{\partial \xi} &= \Psi - \xi\left(1 + \frac{d\eta_0}{d\tau}\right) + \tfrac{1}{2}\frac{\xi^2}{\xi_1}\left(\frac{d\eta_0}{d\tau} - \frac{\eta_0}{\xi_1}\frac{d\xi_1}{d\tau}\right), \\ m &= -\tfrac{1}{4} + \Psi\xi - \tfrac{1}{2}\xi^2\left(1 + \frac{d\eta_0}{d\tau}\right) + \tfrac{1}{6}\frac{\xi^3}{\xi_1}\left(\frac{d\eta_0}{d\tau} - \frac{\eta_0}{\xi_1}\frac{d\xi_1}{d\tau}\right). \end{aligned}\right\} \tag{10}$$

The conditions $m = \frac{1}{4}$ and $\partial m/\partial \xi = 0$ at $\xi = \xi_1$ provide two equations for the functions ξ_1, η_0, and after re-arrangement the equations can be written

$$\left.\begin{aligned} \eta_0 \xi_1 \frac{d\xi_1}{d\tau} &= -2\Psi\xi_1 + 3 - \xi_1^2, \\ \xi_1^2 \frac{d\eta_0}{d\tau} &= 4\Psi\xi_1 - 3 - \xi_1^2. \end{aligned}\right\} \tag{11}$$

With (11) the derivatives with respect to τ can be eliminated from (10). Since m is a cubic function of ξ, and since $\partial m/\partial \xi = 0$ at $\xi = \xi_1$, a necessary and sufficient condition that $|m| \leqslant \frac{1}{4}$ in the range $0 \leqslant \xi \leqslant \xi_1$ is that

$$\partial m/\partial \xi \geqslant 0 \text{ for } 0 \leqslant \xi \leqslant \xi_1. \tag{12}$$

This condition can easily be shown to require that the loading function Ψ (assumed positive) must be such that

$$\Psi\xi_1 \leqslant 3/2 \tag{13}$$

during the motion. Thus the first phase only applies if condition (13) is satisfied.

During the first phase, equations (11) for the functions ξ_1, η_0 apply whenever Ψ exceeds the collapse value unity and satisfies condition (13). They also apply

if the shell is in motion and the loading function Ψ is less than unity, for the shell will continue to deform until the kinetic energy has been dissipated into plastic work. For the case when the force is removed while the shell is in motion during the first phase, Ψ is set equal to zero in (11), and the solution of the equations is found to be

$$\left.\begin{aligned} \xi_1 &= A\tau + B, \\ \eta_0 &= (3 - \xi_1^2)/A\xi_1. \end{aligned}\right\} \tag{14}$$

The constants A, B are determined by the values of ξ_1 and η_0 at the instant the force is removed. The hinge distance ξ_1 has the value $\sqrt{3}$ at the time

$$\tau = (\sqrt{3} - B)/A, \tag{15}$$

and at this instant η_0 is zero and the motion ceases.

(ii) *Second Phase*

The second phase arises if the loading function Ψ is such that at some stage during the first phase of the motion, Ψ increases and violates condition (13). In the second phase of the motion, there is a hinge circle at $\xi = 0$ where $m = -\frac{1}{4}$, and a hinge band in the region $\xi_1 \leqslant \xi \leqslant \xi_2$, so that

$$m = \tfrac{1}{4} \text{ for } \xi_1 \leqslant \xi \leqslant \xi_2. \tag{16}$$

The bending moment m has magnitude less than $\frac{1}{4}$ in the region $0 < \xi < \xi_1$, and the shell is rigid for $\xi > \xi_2$. As before, $\psi = 0$ and $n = 1$ in the plastic region, and $q = \partial m/\partial \xi$ has a discontinuity of amount 2Ψ at $\xi = 0$. The shearing stress q is zero in the region $\xi_1 \leqslant \xi \leqslant \xi_2$.

Since $\partial^2 m/\partial \xi^2 = 0$ for $\xi_1 < \xi \leqslant \xi_2$, the equation of motion (4) shows that in this region the deceleration is unity, $\partial \eta/\partial \tau = -1$, so that

$$\eta = -\tau + f(\xi), \qquad \xi_1 \leqslant \xi \leqslant \xi_2. \tag{17}$$

The function $f(\xi)$ is determined by the velocity at the section ξ at the instant the section enters the hinge band. Since m and n are positive in the hinge band, the function $f(\xi)$ must be such that $d^2 f/d\xi^2$ and η are positive. The boundary $\xi = \xi_2$ of the plastic region is given by the equation

$$-\tau + f(\xi_2) = 0, \tag{18}$$

since the velocity is zero at this section. Because of the conditions on the function f, ξ_2 will be a decreasing function of τ.

In the region $0 \leqslant \xi \leqslant \xi_1$, the velocity is a linear function of ξ so that

$$\eta = \eta_0 - (\eta_0 - \eta_1)\frac{\xi}{\xi_1}, \tag{19}$$

where η_0, η_1 are the velocities at the sections $\xi = 0$, $\xi = \xi_1$, respectively. Continuity of velocity at $\xi = \xi_1$ requires that

$$\eta_1 = -\tau + f(\xi_1). \tag{20}$$

The acceleration in this region is found by differentiation of (19) with respect to τ, and the equation of motion (4) becomes

$$\frac{\partial^2 m}{\partial \xi^2} = -1 - \frac{d\eta_0}{d\tau} + \frac{\xi}{\xi_1}\left\{\frac{d\eta_0}{d\tau} - \frac{d\eta_1}{d\tau} - \frac{1}{\xi_1}(\eta_0 - \eta_1)\frac{d\xi_1}{d\tau}\right\}.$$

With the conditions at $\xi = 0$, integration of this equation with respect to ξ gives, for $0 < \xi \leqslant \xi_1$,

$$\left.\begin{aligned} \frac{\partial m}{\partial \xi} &= \Psi - \xi\left(1 + \frac{d\eta_0}{d\tau}\right) + \tfrac{1}{2}\frac{\xi^2}{\xi_1}\left\{\frac{d\eta_0}{d\tau} - \frac{d\eta_1}{d\tau} - \frac{1}{\xi_1}(\eta_0 - \eta_1)\frac{d\xi_1}{d\tau}\right\}, \\ m &= -\tfrac{1}{4} + \Psi\xi - \tfrac{1}{2}\xi^2\left(1 + \frac{d\eta_0}{d\tau}\right) + \tfrac{1}{6}\frac{\xi^3}{\xi_1}\left\{\frac{d\eta_0}{d\tau} - \frac{d\eta_1}{d\tau} - \frac{1}{\xi_1}(\eta_0 - \eta_1)\frac{d\xi_1}{d\tau}\right\}. \end{aligned}\right\} \quad (21)$$

At $\xi = \xi_1$, $m = \frac{1}{4}$ and $\partial m/\partial \xi = 0$, and it follows from (21) that

$$\left.\begin{aligned} &\Psi - \xi_1\left(1 + \frac{d\eta_0}{d\tau}\right) + \tfrac{1}{2}\xi_1\left\{\frac{d\eta_0}{d\tau} - \frac{d\eta_1}{d\tau} - \frac{1}{\xi_1}(\eta_0 - \eta_1)\frac{d\xi_1}{d\tau}\right\} = 0, \\ &-\tfrac{1}{2} + \Psi\xi_1 - \tfrac{1}{2}\xi_1^2\left(1 + \frac{d\eta_0}{d\tau}\right) + \tfrac{1}{6}\xi_1^2\left\{\frac{d\eta_0}{d\tau} - \frac{d\eta_1}{d\tau} - \frac{1}{\xi_1}(\eta_0 - \eta_1)\frac{d\xi_1}{d\tau}\right\} = 0. \end{aligned}\right\} \quad (22)$$

These equations hold only if $|m| \leqslant \frac{1}{4}$ in the region $0 \leqslant \xi \leqslant \xi_1$, and as in the discussion of the first phase it can be shown that Ψ and ξ_1 must be such that condition (13) is satisfied, i.e. $\Psi\xi_1 \leqslant 3/2$.

Suppose now that at an instant of time, $\tau = 0$ say, the shell is in motion in this second phase and the velocity η is known for $0 \leqslant \xi \leqslant (\xi_2)_{\tau=0}$. Then the function $f(\xi)$ is known in the region $(\xi_1)_{\tau=0} \leqslant \xi \leqslant (\xi_2)_{\tau=0}$ since (17) holds at the time $\tau = 0$. If in the subsequent motion, $d\xi_1/d\tau$ is positive, $f(\xi)$ will be known in the interval $\xi_1 \leqslant \xi \leqslant \xi_2$ since ξ_1 will increase and ξ_2 decrease from their values at $\tau = 0$. The four functions ξ_1, ξ_2, η_0, η_1, which specify the motion, will be given by the four equations (18), (20), (22). When ξ_1 becomes equal to ξ_2, the motion will re-enter the first phase. On the other hand, if $d\xi_1/d\tau$ is negative during the motion after the time $\tau = 0$, the function $f(\xi)$ must be determined in the region $\xi_1 \leqslant \xi \leqslant (\xi_1)_{\tau=0}$ as part of the solution. Thus at first sight it appears that there are only four equations, (18), (20), (22), for the determination of the quantities ξ_1, ξ_2, η_0, η_1 and the function $f(\xi)$ in the interval $\xi_1 \leqslant \xi \leqslant (\xi_1)_{\tau=0}$. However, a closer examination of the equations, described below, shows that $d\xi_1/d\tau$ can be negative only if

$$\Psi\xi_1 = 3/2, \quad (23)$$

and this additional equation enables the motion to be determined. (It follows from (23) that Ψ must be an increasing function of the time τ for $d\xi_1/d\tau$ to be negative). Equation (23) gives the hinge distance ξ_1 in terms of the known loading function Ψ, and with (23), equations (22) reduce to

$$\left.\begin{aligned} \frac{d\eta_0}{d\tau} &= \frac{3}{\xi_1^2} - 1, \\ \frac{d}{d\tau}\left(\frac{\eta_0 - \eta_1}{\xi_1}\right) &= \frac{3}{\xi_1^3}. \end{aligned}\right\} \quad (24)$$

When η_0 and η_1 have been determined from these equations, the function $f(\xi)$ in the interval $\xi_1 \leqslant \xi \leqslant (\xi_1)_{\tau=0}$ is obtained from (20).

It remains to show that negative values of $d\xi_1/d\tau$ imply (23). Eliminating $d\eta_0/d\tau$ between equation (22) gives

$$1 + \frac{d\eta_1}{d\tau} + \frac{1}{\xi_1}(\eta_0 - \eta_1)\frac{d\xi_1}{d\tau} = 2\left(\tfrac{3}{2} - \Psi\xi_1\right)/\xi_1^2. \tag{25}$$

From (20) and (17) it follows that

$$1 + \frac{d\eta_1}{d\tau} = \frac{d\xi_1}{d\tau}\left(\frac{df}{d\xi}\right)_{\xi=\xi_1^-} = \frac{d\xi_1}{d\tau}\left(\frac{\partial\eta}{\partial\xi}\right)_{\xi=\xi_1^+},$$

and from (19),

$$\frac{1}{\xi_1}(\eta_0 - \eta_1) = -\left(\frac{\partial\eta}{\partial\xi}\right)_{\xi=\xi_1^-},$$

where ξ_1^- and ξ_1^+ designate sections just to the left and just to the right, respectively, of the hinge section $\xi = \xi_1$. Equation (25) can now be written

$$\frac{d\xi_1}{d\tau}\left\{\left(\frac{\partial\eta}{\partial\xi}\right)_{\xi=\xi_1^+} - \left(\frac{\partial\eta}{\partial\xi}\right)_{\xi=\xi_1^-}\right\} = 2\left(\tfrac{3}{2} - \Psi\xi_1\right)/\xi_1^2. \tag{26}$$

(As can be seen by comparison with equation (6), the left hand side of this equation is the jump in the value of the acceleration across the hinge circle $\xi = \xi_1$ from left to right). Because of the inequality (13), the right hand side of (26) is non-negative. Further, the quantity multiplying $d\xi_1/d\tau$ on the left hand side is non-negative since $\partial^2\eta/\partial\xi^2$ is positive at the hinge section $\xi = \xi_1$. It follows that $d\xi_1/d\tau$ can be negative only if (23) holds and

$$\left(\frac{\partial\eta}{\partial\xi}\right)_{\xi_1^+} = \left(\frac{\partial\eta}{\partial\xi}\right)_{\xi=\xi_1^-}.$$

The above discussion of the motion of the shell due to loading by a ring of force is now applied to the cases of rectangular and triangular pulses of force.

(iii) *Rectangular Pulse*

In this case it is assumed that a ring of force of constant magnitude P_m (greater than the collapse value P_s) is applied at the time $t = 0$ for a time T and then removed. Thus the quantity Ψ has the constant value Ψ_m during the interval $0 \leqslant \tau \leqslant 1$, and is then zero (Fig. 3a). The motion is confined to the first phase so that equations (11) apply. The initial condition that $\eta_0 = 0$ at $\tau = 0$ determines the initial value of ξ_1 from the first of equations (11). During the application of the force, ξ_1 remains constant at this initial value given by

$$\xi_1 = (\Psi_m^2 + 3)^{1/2} - \Psi_m.$$

This value of ξ_1 satisfies the inequality (13). The radial acceleration $d\eta_0/d\tau$ is constant during the interval $0 \leqslant \tau \leqslant 1$, and the velocity at the section $\xi = 0$ is found to be given by

$$\eta_0 = 2\{2\Psi_m - (\Psi_m^2 + 3)^{1/2}\}\tau/\{(\Psi_m^2 + 3)^{1/2} - \Psi_m\}$$

during this part of the motion.

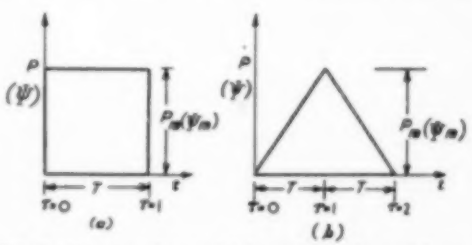

Fig. 3. Rectangular and triangular pulses of force.

After the force has been removed at the time $\tau = 1$, the motion is given by (14). From the values of ξ_1 and η_0 and at the time $\tau = 1$, the constants A and B have the values

$$A = \Psi_m \frac{\{(\Psi_m^2 + 8)^{1/2} - \Psi_m\}}{\{2\Psi_m - (\Psi_m^2 + 8)^{1/2}\}},$$

$$B = (\Psi_m^2 + 8)^{1/2} - \Psi_m - A.$$

The motion ceases when η_0 becomes zero at the instant of time (15).

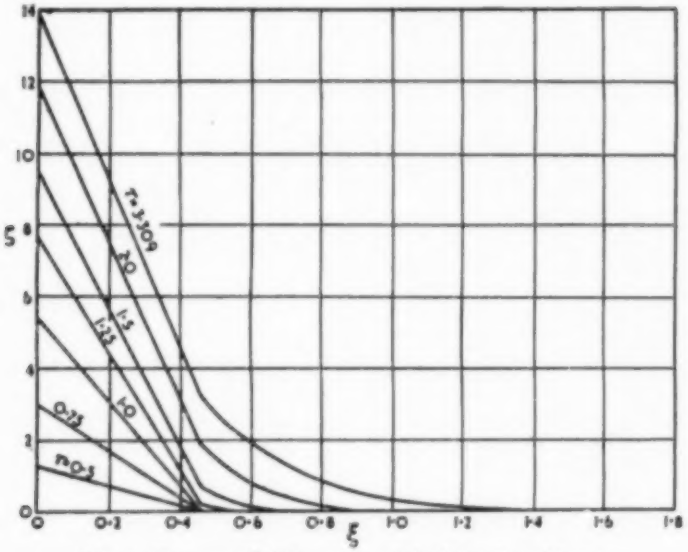

Fig. 4. Progress of deformation of shell for ring of force.
Rectangular pulse of magnitude 3 times static collapse load.
Load removed at $\tau = 1$.
Deformation stops at $\tau = 3{\cdot}309$.

The progress of the deformation of the shell for the particular case $\Psi_m = 3$ is shown in Fig. 4 for illustration. In the figure, ζ denotes the non-dimensional displacement of the shell, so that $\eta = \partial\zeta/\partial\tau$, and the displacement w of the shell is given by

$$w = \zeta \frac{\sigma_0 h T^2}{\rho R}. \tag{27}$$

The final value of the radial displacement ζ_0 at the section $\xi = 0$ after the motion has ceased is shown graphically in Fig. 5 for values of the load Ψ_m. In the same figure is shown the radial displacement ζ_0 at the instant the load is removed (i.e. when $\tau = 1$) in order to show the extent to which deformation occurs after removal of the load. For a pressure pulse of magnitude ten times the collapse load ($\Psi_m = 10$), 80 per cent. of the displacement at the section $\xi = 0$ occurs after the removal of the load.

(iv) *Triangular Pulse*

When a triangular pulse of force is applied to the section $\xi = 0$, the analysis is more complicated. The loading function Ψ is assumed to increase linearly with time to the maximum value Ψ_m (greater than unity) in the interval $0 \leqslant \tau \leqslant 1$, and then to decrease linearly to zero in the interval $1 \leqslant \tau \leqslant 2$, (Fig. 3b). Thus we have

$$\Psi = \begin{cases} \Psi_m \tau & 0 \leqslant \tau \leqslant 1, \\ \Psi_m (2 - \tau) & 1 \leqslant \tau \leqslant 2, \\ 0 & \tau \geqslant 2 \end{cases} \tag{28}$$

The shell remains at rest until the load Ψ reaches the collapse value unity at the time $\tau = 1/\Psi_m$. The shell then moves according to the first phase. At the time $\tau = 1/\Psi_m$ the hinge distance ξ_1 is unity, and as the force increases the hinge circle $\xi = \xi_1$ moves towards the section of application of the force $\xi = 0$. For small enough values of Ψ_m, $\Psi_m \leqslant 2{\cdot}391$, the motion is confined to the first phase. For values of Ψ_m greater than 2·391, the motion enters the second phase when Ψ reaches the value 2·391, and (23) is satisfied. As the load increases from the value 2·391 to the value Ψ_m, $d\xi_1/d\tau$ is negative and the width of the hinge band increases. After the time $\tau = 1$ when the peak load is reached, $d\xi_1/d\tau$ is positive and the width of the hinge band decreases. When the width of the hinge band becomes zero the motion re-enters the first phase and eventually ceases.

In greater detail, the analysis proceeds as follows. When the motion begins at the time $\tau = 1/\Psi_m$, equations (11) apply in which Ψ has the value (28). It is convenient at this stage to introduce a new time variable s defined by

$$s = \Psi_m \tau - 1. \tag{29}$$

The loading function Ψ defined by (28) is now given by

$$\Psi = \begin{cases} 1 + s & 0 \leqslant s \leqslant s_1, \\ 2\Psi_m - 1 - s & s_1 \leqslant s \leqslant s_2, \\ 0 & s_2 \leqslant s, \end{cases} \tag{30}$$

during the motion which starts at the time $s = 0$. The time s_1 when the peak load is reached and the time s_2 when the force becomes zero are given by

$$s_1 = \Psi_m - 1, \qquad s_2 = 2\Psi_m - 1. \tag{31}$$

Equations (11) now become, in the interval $0 \leqslant s \leqslant s_1$,

$$\left.\begin{aligned} \Psi_m \eta_0 \xi_1 \frac{d\xi_1}{ds} &= -2\xi_1 (1 + s) + 3 - \xi_1^2, \\ \xi_1^2 \Psi_m \frac{d\eta_0}{ds} &= 4\xi_1 (1 + s) - 3 - \xi_1^2. \end{aligned}\right\} \tag{32}$$

the initial conditions being $\xi_1 = 1$ and $\eta_0 = 0$ at $s = 0$. These equations were integrated numerically to give ξ_1 and $\Psi_m \eta_0$ as functions of s. The integration was started with a series solution and completed with GILL's form of the Runge-Kutta process (GILL 1951) on the high-speed digital computer AMOS. It was found that the inequality (13) was satisfied until s reached the value $s_0 = 1{\cdot}391$, when the equality sign held. Since the load decreases after $s = s_1$, the motion remains entirely in the first phase if $s_1 \leqslant s_0$, i.e. if $\Psi_m \leqslant 2{\cdot}391$, from (31).

The motion in the interval $s_1 \leqslant s \leqslant s_2$ for the particular cases $\Psi_m = 1{\cdot}5$, 2 was obtained by numerical integration of (11) on AMOS. The motion ceased before the load became zero for the case $\Psi_m = 1{\cdot}5$, and the motion after the removal of the load for the case $\Psi_m = 2$ was found from equations (14).

For values of Ψ_m greater than 2·391, the motion enters the second phase at the time s_0. The values of ξ_1 and $\Psi_m \eta_0$ at this time s_0 will be denoted by α and β, respectively. The numerical values of α and β were found to be

$$\alpha = 0{\cdot}627, \qquad \beta = 4{\cdot}065.$$

The hinge band starts at the section $\xi = \alpha$ and has zero width at the time s_0. As the force increases during the ensuing motion, i.e. in the interval $s_0 \leqslant s \leqslant s_1$, the width of the hinge band increases, $d\xi_1/d\tau$ being negative. From the discussion of the second phase, this part of the motion is given by (18), (20), (23) and (24). The distance ξ_1 is given by

$$\xi_1 = 3/2\Psi = 3/2\,(1 + s), \tag{33}$$

from (23) and (30). The velocities η_0 and η_1 can now be obtained from (24) and (33), and with the conditions $\Psi_m\,\eta_0 = \beta$ and $\eta_1 = 0$ at $s = s_0$, there results

$$\left.\begin{aligned} \Psi_m\,\eta_0 &= \frac{3}{2}\left(\frac{1}{\xi_1^3} - \frac{1}{\xi_1} - \frac{1}{\alpha^3} + \frac{1}{\alpha}\right) + \beta, \\ \Psi_m\,\eta_1 &= \frac{3}{8\xi_1^3} - \frac{3}{2\xi_1} + \frac{\xi_1}{\alpha}\left(\frac{9}{8\alpha^3} - \beta\right) - \frac{3}{2\alpha^3} + \frac{3}{2\alpha} + \beta. \end{aligned}\right\} \tag{34}$$

The function $f(\xi)$ is determined by the continuity of velocity at the section $\xi = \xi_1$, equation (20), and is found to be given by

$$\Psi_m f(\xi) = \frac{3}{8\xi^3} + \frac{\xi}{\alpha}\left(\frac{9}{8\alpha^3} - \beta\right) - \frac{3}{2\alpha^3} + \beta + s_0 + 1. \tag{35}$$

The boundary $\xi = \xi_2$ of the plastic region is given by (18) in which $f(\xi)$ has the value given by (35). The resulting equation for ξ_2 is, after re-arrangement,

$$\xi_2^4\left(\frac{9}{8\alpha^3} - \beta\right) + \xi_2^3\left\{\alpha\beta + \frac{3}{2} - \frac{3}{2\alpha^2} - \alpha\,(1 + s)\right\} + \frac{3\alpha}{8} = 0. \tag{36}$$

The relevant root of this equation is the root which has the value $\xi_2 = \alpha$ at the time $s = s_0$.

At the time s_1, i.e. the time $\tau = 1$, the loading function Ψ becomes a decreasing function of time and (23) no longer applies in the subsequent motion. The width of the hinge band decreases and $d\xi_1/d\tau$ is positive. The motion is described by equations (20) and (22) in which $f(\xi)$ is given by (35) and Ψ is given by (30). The distance ξ_2 is still given by (36). At the time $\tau = 1$, ξ_1 has the value $3/2\Psi_m$, and the value of η_0 at $\tau = 1$ can be found from (34). The details are omitted here, but it can be shown that the quantities ξ_1 and η_0 are given by

$$\left.\begin{aligned} \Psi_m\,\xi_1 &= 3/2\,\{1 - (\sqrt{2} - 1)\,(\tau - 1)\}, \\ \eta_0 &= (\eta_0)_{\tau=1} - (\tau - 1) + \frac{4}{3}\,\Psi_m{}^2\,(\tau - 1)\{1 - (\tau - 1) + \tfrac{1}{4}\,(\tau - 1)^2\,(4\sqrt{2} - 5)\}. \end{aligned}\right\} \tag{37}$$

The velocity η_1 is given by (20) and (35). This part of the motion, in which ξ_1 and η_0 are given by (37), continues until either the hinge band width or the load becomes zero. When the hinge band width becomes zero, the motion reverts to the first phase and equations (11) apply. It was found that for $\Psi_m \leqslant 9{\cdot}310$, the first phase is re-entered before the load becomes zero at the time $\tau = 2$, and for the cases $\Psi_m = 3, 4, 6, 8$ this part of the motion was obtained by integrating (11) numerically on AMOS. The final part of the motion when Ψ is zero was then found from equations (14).

For $\Psi > 9{\cdot}310$, the motion is still in the second phase when the load becomes zero at the time $\tau = 2$, and equations (22) apply in which Ψ is zero and η_1 is given by (20) and (35). While the motion is in the second phase after the time $\tau = 2$, ξ_1 and η_0 were found to be given by

$$\left.\begin{aligned} \Psi_m\,\xi_1 &= \tfrac{1}{2}\,\{\tau + (\tau^2 - 2)^{1/2}\}, \\ \Psi_m\,\eta_0 &= \frac{3}{2\alpha} - \frac{3}{2\alpha^3} + \beta - \Psi_m\,\tau + \frac{2}{9}\,\Psi_m{}^3\,\{\tau - (\tau^2 - 2)^{1/2}\}\,\{6 - [\tau - (\tau^2 - 2)^{1/2}]^2\}. \end{aligned}\right\} \tag{38}$$

The boundary $\xi = \xi_2$ is again given by (36) and the motion re-enters the first phase when ξ_1 and ξ_2 become equal. The last part of the motion is then given by (14). Numerical results were obtained for the case $\Psi_m = 10$.

The final values of the radial displacement ζ_0 at the section $\xi = 0$, after the motion has ceased for the cases $\Psi_m = 1{\cdot}5, 2, 3, 4, 6, 8, 10$ are joined by a smooth curve in Fig. 5. The radial displacement ζ_0 at the instant the load becomes zero, i.e. the time $\tau = 2$, is also shown in the figure. It should be noted that the quantity T is the time of duration of the rectangular pulse and half

the time of application of the triangular pulse (see Fig. 3). It follows that for both the rectangular and triangular pulses

$$P_m T = \int P \, dt,$$

P_m being the peak value of the load, so that Fig. 5 compares the final value of ζ_0 for two shapes of pulse which have the same impulse $P_m T$. The final value of ζ_0 may be considered as a damage parameter specifying the amount of permanent deformation produced by the force pulse.

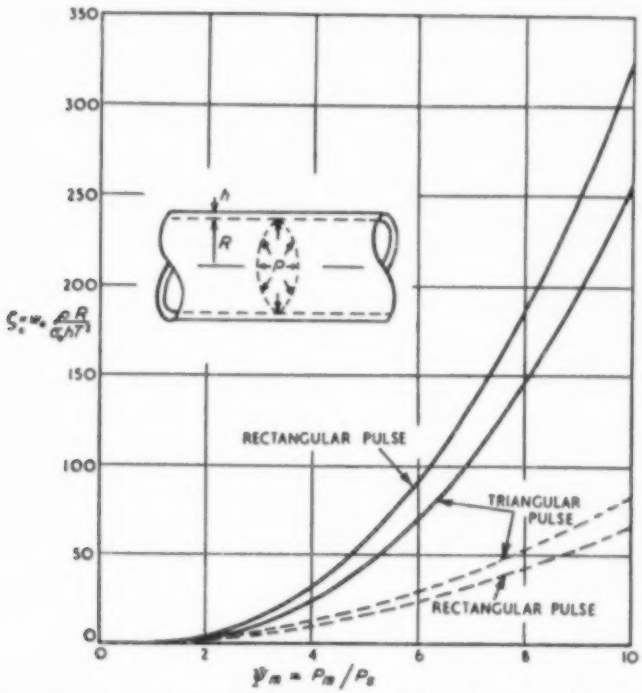

Fig. 5. Displacement at section of application of the ring of force as a function of maximum load.
———— Final displacement.
- - - - Displacement at instant load is removed.

In the analogous problem of the transverse dynamic loading of rigid-plastic beams, a convenient damage parameter to take is the amount of permanent relative rotation of the sections of the beam on either side of the loaded section. The values of the damage parameter for a centrally loaded beam have been obtained by SYMONDS (1953) for rectangular, triangular and sinusoidal pulses ; it was found that for the same impulse the rectangular pulse produced the greatest amount of deformation and the triangular pulse produced the least. The deformations produced by a sinusoidal force pulse (half sine wave) were found to be approximately the averages of the deformations for the rectangular and triangular pulses for the same impulse. It is to be expected that a similar result will hold in the present problem.

4. BAND OF UNIFORM PRESSURE

We now consider loading of the shell by a band of uniform pressure. The central section of the band of pressure is taken to be the section $\xi = 0$ so that the applied lateral pressure ψ is given by

$$\psi = \begin{cases} \psi(t) & |\xi| \leqslant a, \\ 0 & |\xi| > a, \end{cases}$$

where $2a$ is the width of the band. The loading function $\psi(t)$ is assumed to be positive and accelerated plastic flow involving outward radial motion of the shell occurs if $\psi(t)$ exceeds the statical collapse load ψ_s. The value of ψ_s for the rectangular yield condition used here has been determined by DRUCKER (1953), and is given by

$$a\psi_s = \tfrac{1}{2}\{a + (a^2 + 4)^{1/2}\}. \tag{39}$$

Depending upon the loading function $\psi(t)$ and the band width $2a$, four types of motion can occur. The first two types, designated the first and second phases, are similar to the types of motion produced by a ring of force and discussed above. More explicitly, in the first phase there is a hinge circle where $m = -\frac{1}{4}$ at the section $\xi = 0$, and hinge circles where $m = \frac{1}{4}$ at the sections $\xi = \pm\xi_1$, where ξ_1 is greater than a; in the second phase $m = -\frac{1}{4}$ at $\xi = 0$ and also $m = \frac{1}{4}$ in the regions $\xi_1 \leqslant |\xi| \leqslant \xi_2$. For large enough values of the band width $2a$, the third and fourth phases are possible in which a central hinge band where $m = -\frac{1}{4}$ develops in the region $-\xi_3 \leqslant \xi \leqslant \xi_3$, where ξ_3 is less than a. In the third phase there are also hinge circles where $m = \frac{1}{4}$ at the sections $\xi = \pm\xi_1$, while in the fourth phase $m = \frac{1}{4}$ in the regions $\xi_1 \leqslant |\xi| \leqslant \xi_2$.

The equations governing the motion in each of these phases are not difficult to obtain, although the analysis is more complicated than that for the ring of force. The fourth phase includes the other three phases as special cases in which ξ_3, or $\xi_2 - \xi_1$, or both, are zero, and all equations for motion in one of the first three phases can be derived from the equations for the fourth phase. For this reason, only the equations governing the fourth phase are given here.

During the fourth phase the bending moment m is such that

$$m = -\tfrac{1}{4} \text{ for } 0 \leqslant \xi \leqslant \xi_3,$$
$$|m| \leqslant \tfrac{1}{4} \text{ for } \xi_3 \leqslant \xi \leqslant \xi_1,$$
$$m = \tfrac{1}{4} \text{ for } \xi_1 \leqslant \xi \leqslant \xi_2,$$

where ξ_3 is less than a and ξ_1 is greater than a. The shearing force $q = \partial m/\partial\xi$ and m are continuous functions of ξ. The velocity η is given by

$$\eta = \begin{cases} (\psi - 1)\tau + g(\xi) & 0 \leqslant \xi \leqslant \xi_3, \\ \eta_3 - (\eta_3 - \eta_1)\dfrac{(\xi - \xi_3)}{(\xi_1 - \xi_3)} & \xi_3 \leqslant \xi \leqslant \xi_1, \\ -\tau + f(\xi) & \xi_1 \leqslant \xi \leqslant \xi_2, \end{cases}$$

where η_1 and η_3 are the velocities at the sections $\xi = \xi_1$ and $\xi = \xi_3$ respectively. The functions $f(\xi)$ and $g(\xi)$ must be such that η is positive and $d^2 f/d\xi^2 \geqslant 0$, $d^2 g/d\xi^2 \leqslant 0$. Continuity of velocity at the sections $\xi = \xi_1$, $\xi = \xi_3$ requires that

$$\left.\begin{aligned} \eta_1 &= -\tau + f(\xi_1), \\ \eta_3 &= (\psi - 1)\tau + g(\xi_3). \end{aligned}\right\} \tag{40}$$

The boundary $\xi = \xi_2$ of the plastic region is given by

$$-\tau + f(\xi_2) = 0, \tag{41}$$

since the velocity is zero at this section. Integration of the equation of motion (4) with respect to ξ and the continuity conditions on m and $\partial m/\partial\xi$ provide two equations which can be written in the form

$$\left.\begin{aligned}(\xi_1-\xi_3)^2\left\{1-\psi+\frac{d\eta_3}{d\tau}+\frac{\eta_3-\eta_1}{\xi_1-\xi_3}\frac{d\xi_3}{d\tau}\right\} &= \psi(\xi_1-\xi_3)\left[4(a-\xi_3)-(\xi_1-\xi_3)\right]\\ &\quad -3\left[1+\psi(a-\xi_3)^2\right],\\ (\xi_1-\xi_3)^2\left\{1+\frac{d\eta_1}{d\tau}+\frac{\eta_3-\eta_1}{\xi_1-\xi_3}\frac{d\xi_1}{d\tau}\right\} &= 3\left[1+\psi(a-\xi_3)^2\right]\\ &\quad -2\psi(a-\xi_3)(\xi_1-\xi_3).\end{aligned}\right\} \tag{42}$$

The condition $|m| \leqslant \frac{1}{4}$ in the region $\xi_3 \leqslant \xi \leqslant a$ requires

$$3\left[1+\psi(a-\xi_3)^2\right] \geqslant \psi(\xi_1-\xi_3)\left[4(a-\xi_3)-(\xi_1-\xi_3)\right]. \tag{43}$$

In the region $a \leqslant \xi \leqslant \xi_1$, the same condition requires

$$3\left[1+\psi(a-\xi_3)^2\right] \geqslant 2\psi(a-\xi_3)(\xi_1-\xi_3). \tag{44}$$

Suppose now that the velocity η is known at some instant of time, $\tau = \tau_0$ say, throughout the plastic region. If $d\xi_1/d\tau$ is positive and $d\xi_3/d\tau$ is negative in the subsequent motion, the quantities η_1, η_3, ξ_1, ξ_3 in the subsequent motion will be determined by (40) and (42), since the functions $f(\xi)$ and $g(\xi)$ will be known from the conditions at the instant τ_0. Since $\partial^2\eta/\partial\xi^2$ is negative at the section $\xi = \xi_3$ where $m = -\frac{1}{4}$, it can be shown from the first of equations (42) that $d\xi_3/d\tau$ must be negative unless the equality sign holds in (43). Hence if $d\xi_3/d\tau$ is positive in the subsequent motion after the time τ_0, the second of equations (40) is replaced by the equation obtained by taking the equality sign in (43). The second of equations (40) still applies, but is now used to determine the function $g(\xi)$ for values of ξ greater than the value of ξ_3 at the time τ_0 Similarly, if $d\xi_1/d\tau$ is negative during the subsequent motion, the equality sign holds in (44), and the first of equations (40) is used to determine $f(\xi)$ for values of ξ less than the value of ξ_1 at the time τ_0.

As an illustrative exam|le, we briefly consider the case when the loading function $\psi(t)$ has the form of a rectangular pulse. The loading function ψ is assumed to be given by

$$\psi = \begin{cases}\psi_m & 0 \leqslant \tau \leqslant 1,\\ 0 & 1 < \tau,\end{cases}$$

in the region $|\xi| \leqslant a$, where ψ_m is a constant greater than the statical collapse load ψ_s.

If the width $2a$ of the band and the magnitude ψ_m of the pressure pulse are such that

$$a^2 \leqslant 3(1+\psi_m)^2/\psi_m(\psi_m-1)(\psi_m+3), \tag{45}$$

the motion is confined entirely to the first phase. During the motion, $m = -\frac{1}{4}$ at $\xi = 0$ and $m = \frac{1}{4}$ at $\xi = \pm\xi_1$. In the interval $0 \leqslant \tau \leqslant 1$, i.e. during the application of the band of pressure, ξ_1 has a constant value given by

$$\xi_1 = \left\{\psi_m{}^2 a^2 + 3(1+\psi_m a^2)\right\}^{1/2} - \psi_m a. \tag{46}$$

The radial velocity η, which is symmetrical about the centre section $\xi = 0$, decreases linearly with ξ from the value η_0 at $\xi = 0$ to zero at $\xi = \xi_1$. For $0 \leqslant \tau \leqslant 1$, η_0 is given by

$$\eta_0 = 2\left\{\psi_m a - \xi_1\right\}\tau/\xi_1,$$

where ξ_1 has the value (46). After the removal of the load at the time $\tau = 1$, the motion is given by (14), the constants A and B being determined from the values of ξ_1 and η_0 at $\tau = 1$.

If the inequality (45) is not satisfied by the quantities a, ψ_m, the motion begins in the third phase. That is a hinge band in which $m = -\frac{1}{4}$ develops in the region $-\xi_3 \leqslant \xi \leqslant \xi_3$, where ξ_3 is less than a, and also $m = \frac{1}{4}$ at the sections $\xi = \pm\xi_1$. During the application of the pressure pulse, the distances ξ_1 and ξ_3 remain constant and are given by

$$\left.\begin{aligned}(a-\xi_3)^2 &= 3(1+\psi_m)^2/\psi_m(\psi_m-1)(\psi_m+3),\\ (\xi_1-\xi_3)^2 &= 12\psi_m/(\psi_m-1)(\psi_m+3).\end{aligned}\right\} \tag{47}$$

The radial velocity η in the hinge band $-\xi_3 \leqslant \xi \leqslant \xi_3$ has the value η_3, where

$$\eta_3 = (\psi_m - 1)\tau.$$

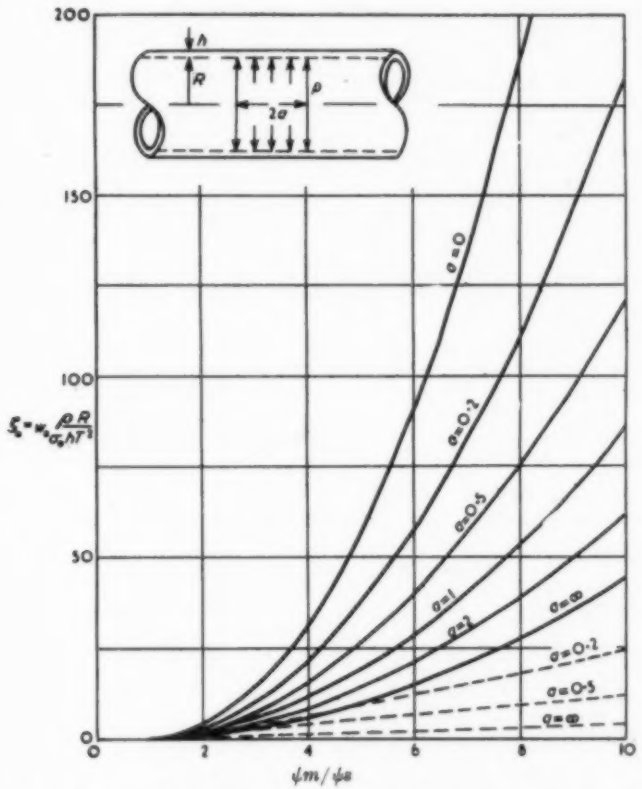

Fig. 6. Displacement at centre of loaded region due to a rectangular pulse of uniform pressure ψm applied to a band of width $2a$.
———— Final displacement.
- - - - Displacement at instant load is removed a in units of $\sqrt{Rh}$.

The velocity η is a linear function of ξ in the remainder of the plastic region, i.e. the region $\xi_3 \leqslant |\xi| \leqslant \xi_1$, and is zero at $\xi = \pm\xi_1$. When the load is removed at the time $\tau = 1$, the motion continues in the third phase, kinetic energy of the shell being dissipated through plastic work. The motion is governed by the second of equations (40) and equations (42), in which the function $g(\xi)$ is set equal to ψ_m and ψ and η_1 are set equal to zero. The quantities ξ_1, ξ_3, η_3 are found to be given by

$$\left.\begin{aligned}\eta_3 &= \psi_m - \tau,\\ a-\xi_3 &= B + \tfrac{1}{2}\sqrt{6}\,\mathrm{sech}^{-1}\{A(\psi_m-\tau)\},\\ (\xi_1-\xi_3)^2 &= 6\{1-A^2(\psi_m-\tau)^2\}.\end{aligned}\right\} \tag{48}$$

where the constants A and B are determined by the values of ξ_1 and ξ_3 at $\tau = 1$. When ξ_3 becomes zero the motion enters the first phase and is given by (14).

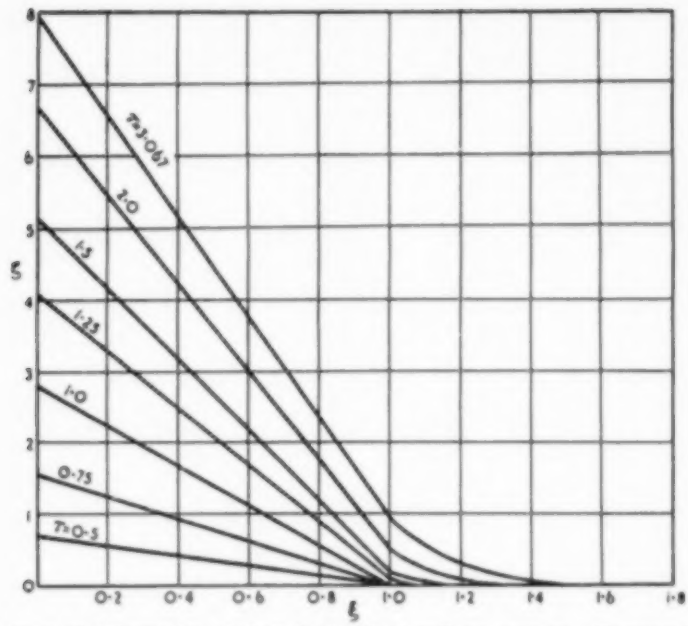

Fig. 7. Progress of deformation of shell for band of uniform pressure. Rectangular pulse of magnitude 3 times static collapse load applied to band of width 1 ($a = 0{\cdot}5$).
Load removed at $\tau = 1$.
Deformation stops at $\tau = 3{\cdot}067$.

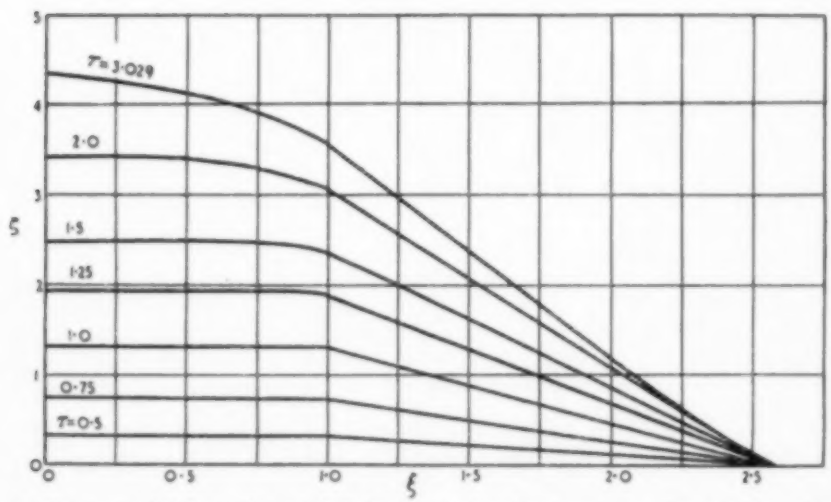

Fig. 8. Progress of deformation of shell for band of uniform pressure. Rectangular pulse of magnitude 3 times static collapse load applied to band of width 4 ($a = 2$).
Load removed at $\tau = 1$.
Deformation stops at $\tau = 3{\cdot}029$.

Fig. 6 shows the variation of the final value of the displacement ζ_0 at the section $\xi = 0$ with ψ_m for the cases $a = 0{\cdot}2, 0{\cdot}5, 1, 2$. For comparison, the curve for the case $a = 0$, i.e. the ring of force, is also shown in the diagram, together with the curve for the case when the width of the pressure band is infinite ($a = \infty$). The value of the radial displacement ζ_0 at the instant the load is removed is also shown for the cases $a = 0{\cdot}2, 0{\cdot}5, \infty$.

Fig. 7 shows the progress of the deformation of the shell for a rectangular pulse of pressure of magnitude three times the statical collapse load applied to a band of unit width (i.e. $\psi_m = 3\psi_s$, $a = 0{\cdot}5$). The motion in this case is confined to the first phase. The general features of the deformation are similar to those of the deformation indicated in Fig. 4 for a ring of force. Fig. 8 shows the progress of the deformation for a band of width four units ($a = 2{\cdot}0$), the load again being three times the statical load. In this case the motion begins in the third phase. After the removal of the load at the time $\tau = 1$, the motion continues in the third phase until the time $\tau = 2{\cdot}261$. The motion then enters the first phase and ceases at the time $\tau = 3{\cdot}029$.

5. Moving Loads

In the problems considered so far, the applied loads were stationary in that the loaded region of the shell was independent of the time. In this Section we consider a load of constant magnitude which moves along the tube with constant velocity. It is to be expected that after the initial application of the load the motion will eventually reach a steady state. In order to simplify the analysis it is assumed here that the steady state has been reached.

We first consider a ring of force of constant intensity moving along the shell with constant velocity V. Deformation of the tube occurs if the intensity P of the ring of force exceeds the statical collapse value P_s given above. We shall use the notation $\Psi = P/P_s$, and assume that Ψ is greater than unity. The origin of the non-dimensional co-ordinate ξ defining distance along the tube is taken at the section of application of the force at the time $\tau = 0$. If the force is assumed to move in the direction of increasing ξ, the section of application of the force at later times is given by $\xi = v\tau$, where v is given by

$$v = VT/\sqrt{Rh}. \tag{49}$$

Here T is the quantity used in defining the dimensionless variables η, τ by (2) and is an arbitrary interval of time.

Since the motion is assumed to be steady it is convenient to use a co-ordinate system which moves with the force, and we write

$$y = \xi - v\tau. \tag{50}$$

The force is applied to the section $y = 0$ and the radial velocity η and the stresses are functions of y only. With (50), the equation of motion (4) then becomes

$$\frac{d^2 m}{dy^2} = -1 + v\frac{d\eta}{dy}, \tag{51}$$

since $\psi = 0$ (except at $y = 0$) and $n = 1$ in the plastic region. It is found that the solution to the problem is obtained by assuming a hinge circle where $m = -\frac{1}{4}$ at the section $y = 0$, and hinge circles where $m = \frac{1}{4}$ at the sections $y = A$, $y = -B$. The distances A and B are given by

$$A = \frac{1}{B} = \Psi - (\Psi^2 - 1)^{1/2}. \tag{52}$$

The radial velocity in the deforming region is given by

$$\eta = \begin{cases} \eta_0 (A - y)/A & 0 \leqslant y \leqslant A, \\ \eta_0 (B + y)/B & -B \leqslant y \leqslant 0, \end{cases} \tag{53}$$

where η_0 is the radial velocity at the section $y = 0$ and is given by

$$v\eta_0 = 2 (\Psi^2 - 1)^{1/2}. \tag{54}$$

The bending moment m is given by

$$m = \begin{cases} \frac{1}{4} - (A - y)^2/2A^2 & 0 \leqslant y \leqslant A, \\ \frac{1}{4} - (B + y)^2/2B^2 & -B \leqslant y \leqslant 0. \end{cases} \tag{55}$$

The shearing force $q = dm/dy$ has a discontinuity of amount 2Ψ at the section $y = 0$.

The radial displacement is obtained from (53). The displacement is zero in the undisturbed region $y \geqslant A$, and in the rigid region $y \leqslant -B$ the non-dimensional displacement ζ defined by (27) has the value

$$\zeta = 2\Psi (\Psi^2 - 1)^{1/2}/v^2. \tag{56}$$

In the deforming region ζ is given by

$$\zeta = \begin{cases} \eta_0 (A - y)^2/2Av & 0 \leqslant y \leqslant A, \\ \Psi\eta_0/v - \eta_0 (B + y)^2/2Bv & -B \leqslant y \leqslant 0. \end{cases} \tag{57}$$

The problem of a band of uniform pressure moving along the shell with constant velocity V can be solved in a similar manner. The centre of the band of pressure is taken to be the section $y = 0$, and the width of the band is denoted by $2a$. In the steady state there is a hinge circle where $m = -\frac{1}{4}$ at the section $y = -y_1$ inside the loaded region, and hinge circles where $m = \frac{1}{4}$ at the sections $y = A$, $y = -B$ outside the loaded region. The distances y_1, A, B are given by

$$\left.\begin{aligned} y_1 &= \{a^2 - 1/\psi (\psi - 1)\}^{1/2}, \\ A &= \psi a - (\psi - 1) y_1, \\ B &= \psi a + (\psi - 1) y_1, \end{aligned}\right\} \tag{58}$$

where ψ is the constant value of the pressure inside the band. The value ψ must be greater than the statical value ψ_s for deformation to occur. The radial velocity in the deforming region is given by

$$\eta = \begin{cases} \eta_0 (A - y)/(A + y_1) & -y_1 \leqslant y \leqslant A, \\ \eta_0 (B + y)/(B - y_1) & -B \leqslant y \leqslant -y_1, \end{cases} \tag{59}$$

where η_0 is the velocity at the section $y = -y_1$ and is given by

$$v\eta_0 = 2 (\psi - 1) y_1. \tag{60}$$

The value of the displacement ζ in the region $y \leqslant -B$ which has ceased to deform is given by

$$\zeta = 2\psi a (\psi - 1) y_1/v^2. \tag{61}$$

(Crown Copyright reserved. Reproduced with the permission of the Controller, H.M.S.O.).

References

Drucker, D. C.	1953	*Proc. 1st. Midwest. Conf. on Solid Mech.*, 158.
Eason, G. and Shield, R. T.	1955	*J. Mech. Phys. Solids*, **4**, 17.
Gill, S.	1951	*Proc. Camb. Phil. Soc.* **47**, 96.
Hodge, P. G., Jr.	1954	*J. Appl. Mech.*, **21**, 336.
	1955	*J. Mech. Phys. Solids*, **3**, 176.
Hopkins, H. G. and Prager, W.	1954	*Z. angew. Math. Phys.*, **5**, 317.
Lee, E. H. and Symonds, P. S.	1952	*J. Appl. Mech.*, **19**, 308.
Onat, E. T.	1955	*Q. Appl. Math.*, **13**, 63.
Symonds, P. S.	1953	*J. Appl. Mech.*, **20**, 475.

Journal of the Mechanics and Physics of Solids, 1956, Vol. 4, pp. 72 to 95. Pergamon Press Ltd., London.

THE PROPAGATION OF DYNAMIC STRESSES IN VISCO-ELASTIC RODS

By D. S. Berry* and S. C. Hunter†

(*Received* 14*th November*, 1955)

Summary

An account is given of the propagation of stress in thin visco-elastic rods when the ends of the rods satisfy a wide variety of boundary conditions. It is assumed that the material of the rods satisfies a stress-strain relation of either of the types

$$\epsilon(t) = \int_{-\infty}^{t} \chi(t-\tau)\frac{d\sigma(\tau)}{d\tau}\,d\tau, \qquad \sigma(t) = \int_{-\infty}^{t} \phi(t-\tau)\frac{d\epsilon(\tau)}{d\tau}\,d\tau$$

and that the strains are infinitesimal. General solutions of the equations of motion are derived by use of the theory of Laplace transforms and their applicability demonstrated by the consideration of special problems. The theory of possible experiments to determine the functions $\chi(t)$, $\phi(t)$ for any given material is also developed.

1. Introduction

The object of the present paper is to discuss the propagation of mechanical waves in thin rods of visco-elastic material. It is assumed throughout that the strains are infinitesimal so that variations in the cross-section of the rod during the motion may be neglected, and also that the effect of the inertia of the associated lateral motion on the longitudinal motion may be neglected. To simplify the analysis dimensionless quantities are used throughout, a characteristic time τ being taken as the unit of time, a quantity, E, with the dimensions of a Young's modulus, being taken as the unit of stress. A suitable unit of length is then $(\rho/E)^{\frac{1}{2}}\tau^{-1}$, where ρ is the density of the material of the rod. It is assumed that the material of the rod satisfies a general linear relation based on Boltzmann's principle of superposition as developed by Leadermann (1943) and Gross (1953), and that there are no body forces operative in the rod.

The stress patterns in semi-infinite rods and in rods of finite length are discussed. In the former instance it is assumed that either the displacement of the free end or the pressure applied to it is prescribed, and that the rod is ' held at infinity ' in such a way that the displacement and the strain are zero there. In the case of the finite rod it is assumed that one end is free of stress and that either the stress or the displacement at the other end is prescribed, or that one end rests on a rigid foundation so that the displacement there is zero and the stress or displacement applied to the other end is prescribed.

* Department of Mathematics, University College of North Staffordshire.
† Armament Research and Development Establishment, Ministry of Supply, London.

Special boundary-value problems corresponding to a rod satisfying a less general stress-strain relation than those of LEADERMANN and GROSS have been solved recently by LEE and KANTER (1953) by converting the equations of motion and the stress-strain relation for the material under discussion into a single partial differential equation and solving the appropriate boundary-value problem for that equation. In the present paper the theory of the Laplace transform is applied to convert the equations of motion and the stress-strain relation, and the equation relating displacement to strain, into a system of ordinary differential equations. The prescribed boundary conditions are converted similarly to yield a two-point boundary-value problem for this set of ordinary differential equations. The solution of these equations is readily found and the required solution of the problem considered is then expressible as a contour integral by making use of the inversion theorem for Laplace transforms.

The general solution is applied to the discussion of the distribution of stress in semi-infinite and finite rods of various physical types and subjected to a variety of end conditions. A method is also described (in Section 8) by means of which it might be possible to determine the form of the stress-strain relation from suitable experimental measurements. Because of the difficulty of evaluating the contour integral in the general solution it is not always possible to obtain a simple closed expression for the stress at any point in the rod. For that reason some consideration has been given to the case of a 'nearly elastic' solid for which the integral may be evaluated approximately. The steady-state solution corresponding to the imposition of a sinusoidal displacement on one end of the rod is also considered in some detail.

2. THE EQUATIONS OF MOTION

We shall work throughout in dimensionless quantities. If we denote by x^*, t^*, σ^*, X^* measures of length, time, stress and body force respectively, then we define a reduced, or dimensionless, length through the equation

$$x = (\rho/E)^{\frac{1}{2}} x^*/\tau$$

where ρ is the density of the material, τ is a characteristic time, and E is a constant which has the dimensions of a Young's modulus. In a similar way we can introduce a reduced time through the equation

$$t = t^*/\tau,$$

a reduced stress through the equation

$$\sigma = \sigma^*/E,$$

and a reduced body force through the equation

$$X = (\rho/E)^{\frac{1}{2}} \tau X^*.$$

In the subsequent analysis we refer always to these reduced quantities unless the contrary is stated explicitly.

We consider a thin rod with spatial co-ordinate x measured along its length. If u denotes the displacement, in the direction of x increasing, of a section of the rod

specified by the co-ordinate x in the unstrained state, the equation of motion in the x-direction is, in dimensionless form,

$$\frac{\partial \sigma}{\partial x} + X = \frac{\partial^2 u}{\partial t^2}, \tag{2.1}$$

where σ is the nominal stress, that is, the tensile force per unit initial cross-sectional area. If the co-ordinate x is of Lagrangian type and the stress is nominal, equation (2.1) is valid for large strains; but if, instead, use is made of the *true* stress, that is, the tensile force per unit current cross-sectional area, this equation is valid only for infinitesimal strains for which variations in the cross-sectional area of the rod may be neglected. The equation of motion (2.1) ignores the effect on the longitudinal motion of the inertia of the associated lateral motion; this is negligible if the wavelengths of all significant Fourier components of the stress pulse are appreciably greater than the diameter of the rod. The strain ϵ is expressed in terms of the reduced displacement u and the reduced co-ordinate x by means of the equation

$$\epsilon = \frac{\partial u}{\partial x}, \tag{2.2}$$

and the reduced particle velocity v is given by means of the equation

$$v = \frac{\partial u}{\partial t}. \tag{2.3}$$

3. The General Linear Stress-Strain Relation

The most general kind of linear stress-strain relation is deduced by means of Boltzmann's principle of superposition and takes the form of an integral equation. Both Leadermann (1943) and Gross (1947) give the relation in two alternative forms. In the dimensionless units employed here these are

$$\epsilon(t) = a\sigma(t) + \int_{-\infty}^{t} x'(t-\tau)\,\sigma(\tau)\,d\tau \tag{3.1}$$

and

$$\sigma(t) = a'\epsilon(t) + \int_{-\infty}^{t} \phi'(t-\tau)\,\epsilon(\tau)\,d\tau \tag{3.2}$$

where a and a' are numerical constants and $x'(t)$ and $\phi'(t)$ (the primes denoting differentiation) are functions often described as " memory " functions. Elsewhere, Gross (1953) uses equivalent equations which can be written

$$\epsilon(t) = \int_{-\infty}^{t} x(t-\tau)\frac{d\sigma(\tau)}{d\tau}\,d\tau \tag{3.3}$$

$$\sigma(t) = \int_{-\infty}^{t} \phi(t-\tau)\frac{d\epsilon(\tau)}{d\tau}\,d\tau. \tag{3.4}$$

If, following Gross, we put

$$x(t) = a + bt + \theta(t) \tag{3.5}$$

and

$$\phi(t) = a' + b'\delta(t) + \psi(t) \tag{3.6}$$

where a, b, a', b' are numerical constants (which may assume the value zero), and $\delta(t)$ is the Dirac delta function, then the functions $\theta(t)$ and $\psi(t)$ correspond, respectively, to the creep and relaxation functions of Gross, which have the properties that $\theta(t)$ is zero at $t = 0$ and is monotonic increasing, and that $\psi(t)$ is monotonic decreasing and zero at $t = \infty$. Gross (1953) derives the conditions under which the equations (3.3) and (3.4) are compatible.

The creep function $\theta(t)$ is often represented in terms of a distribution function of retardation times of strain, $F(\tau)$, thus :

$$\theta(t) = \theta(\infty) \int_0^\infty F(\tau)\,(1 - e^{-t/\tau})\,d\tau \tag{3.7}$$

where $\theta(\infty)$ serves as a normalizing factor. In a similar way the relaxation function $\psi(t)$ can be expressed in terms of a distribution function of relaxation times, $G(\tau)$, thus :

$$\psi(t) = \psi(0) \int_0^\infty G(\tau)\, e^{-t/\tau}\, d\tau. \tag{3.8}$$

When the distributions degenerate into line spectra, that is, when

$$\theta(\infty)\, F(\tau) = \sum_i A_i\, \delta(\tau - \tau_i) \tag{3.9}$$

and

$$\psi(0)\, G(\tau) = \sum_i B_i\, \delta(\tau - \tau_i'), \tag{3.10}$$

we find that

$$\theta(t) = \sum_i A_i\,(1 - e^{-t/\tau_i}) \tag{3.11}$$

and

$$\psi(t) = \sum_i B_i\, e^{-t/\tau_i'}. \tag{3.12}$$

In this case it can be shown that the stress-strain relation can be written as the partial differential equation

$$a_0\,\sigma + a_1 \frac{\partial \sigma}{\partial t} + \ldots + a_m \frac{\partial^m \sigma}{\partial t^m} = b_0\,\epsilon + b_1 \frac{\partial \epsilon}{\partial t} + \ldots + b_n \frac{\partial^n \epsilon}{\partial t^n} \tag{3.13}$$

where the $a_0, \ldots a_m$, $b_0, \ldots b_m$ are numerical constants, with $m = n$ except when $a = 0$ in (3.5) or $b' \neq 0$ in (3.6), and $b_0 = 0$ when $b \neq 0$ in (3.5) or $a' = 0$ in (3.6). Gross (1953) shows that the line spectra correspond to generalizations of the Voigt or Maxwell models of spring and dash-pot systems, and gives methods for deriving the constants A_i, τ_i of equation (3.11) from the B_i, τ_i' of equation (3.12) and vice versa.

Later in this paper we shall consider a three-parameter model obtained by putting

$$x(t) = a + c\,(1 - e^{-t/d}). \tag{3.14}$$

If we substitute this expression into either equation (3.1) or equation (3.3), differentiate with respect to t, and eliminate the integral between the two equations, we form an equation of the type (3.13), namely :

$$\kappa^2 \left(\alpha\sigma + \frac{\partial \sigma}{\partial t}\right) = \beta\epsilon + \frac{\partial \epsilon}{\partial t} \qquad (\alpha > \beta > 0). \tag{3.15}$$

where $\kappa^2 = a$, $\alpha = (a + c)/ad$, $\beta = 1/d$. This equation has been used extensively as a model for the study of internal friction phenomena by Alfrey (1948), Zener (1948), and Kolsky (1953). When $\alpha = \beta$, (3.15) simplifies to that for a purely elastic material :

$$\kappa^2 \sigma = \epsilon,$$

provided that $\sigma = \epsilon = 0$ when $t = 0$. We shall investigate the behaviour of a solid which we shall describe as ' nearly elastic.' By this term we mean that the solid has a stress-strain relation of the type (3.15) with $(\alpha - \beta) \ll \beta$, that is, $c \ll a$ in equation (3.14).

The simple Maxwell solid is given by

$$x(t) = a + bt \tag{3.16}$$

leading to the partial differential equation

$$\kappa^2 \left(\alpha\sigma + \frac{\partial\sigma}{\partial t}\right) = \frac{\partial\epsilon}{\partial t} \qquad (\alpha > 0) \tag{3.17}$$

where, now, $\kappa^2 = a$, $\alpha = b/a$; and the simple Voigt solid is given by

$$x(t) = c\,(1 - e^{-t/d}) \tag{3.18}$$

leading to the partial differential equation

$$k^2 \sigma = \epsilon + q \frac{\partial\epsilon}{\partial t} \tag{3.19}$$

where $k^2 = c$, $q = d$.

Another form of $x(t)$ which we shall consider has been postulated by Kuhn, Künzle, and Preissmann (1947), and may be derived by assuming the distribution

$$\theta(\infty)\, F(\tau)\, d\tau = \begin{cases} 0, & \tau < \tau_0 \\ k d\tau/\tau, & \tau > \tau_0 \end{cases} \tag{3.20}$$

in which k is a constant, in (3.7). Performing the integration we find that

$$\theta(t) = k\left[\gamma + \log(t/\tau_0) - Ei(-t/\tau_0)\right] \tag{3.21}$$

where γ is Euler's constant and

$$Ei(-t/\tau_0) = -\int_{t/\tau_0}^{\infty} s^{-1} e^{-s}\, ds$$

defines the exponential integral. The pair of equations (3.20) does not properly define $F(\tau)$ since, unlike a creep function derived from the line spectrum (3.9), $\theta(t)$ is here unbounded as $t \to \infty$. This is due to the extension of the distribution (3.20) to $\tau = \infty$, and can be avoided by cutting it off at $\tau = T$ (sufficiently large), so that, for $\tau > T$,

$$\theta(\infty)\, F(\tau)\, d\tau = 0,$$

and then

$$\theta(t) = k\left[\log(T/\tau_0) + Ei(-t/T) - Ei(-t/\tau_0)\right], \tag{3.22}$$

which tends to the expression (3.21) as $T \to \infty$. In both cases the value of $\theta(0)$ has to be defined as the limit, as $t \to 0$, of $\theta(t)$ and is found to be zero. The expression (3.22) gives

$$\theta(\infty) = k \log (T/\tau_0)$$

from which it follows that

$$F(\tau) = \begin{cases} 0, & \tau < \tau_0 \\ \dfrac{1}{\tau \log (T/\tau_0)}, & \tau_0 < \tau < T \\ 0, & \tau > T. \end{cases} \tag{3.23}$$

4. Boundary Value Problems

We shall enumerate here the combinations of boundary conditions with which we shall deal later. We assume throughout the analysis that there are no body forces acting on the rod, and that the time $t = 0$ is chosen so that $\sigma = u = 0$ for $t < 0$. The boundary value problem then consists of solving the equation

$$\frac{\partial \sigma}{\partial x} = \frac{\partial^2 u}{\partial t^2}, \qquad t \geqslant 0, \tag{4.1}$$

with a stress-strain relation of the form (3.3) or (3.4) for each of the sets of boundary conditions listed below :

I. *Semi-Infinite Rod.* We consider the case $x \geqslant 0$, with the assumption that both the stress and the displacement tend to zero as $x \to \infty$. We specify either

(*a*) the displacement of the surface $x = 0$,

or (*b*) the pressure at the surface $x = 0$.

We therefore have the boundary conditions :

(I*a*) $u = u(0, t)$ at $x = 0$; $\sigma, u \to 0$ as $x \to \infty$;

(I*b*) $\sigma = \sigma(0, t)$ at $x = 0$; $\sigma, u \to 0$ as $x \to \infty$.

II. *Finite rod.* We consider the rod $0 \leqslant x \leqslant l$ with the four cases :

(*a*) Displacement prescribed at $x = 0$, displacement zero at $x = l$;

(*b*) Stress prescribed at $x = 0$, displacement zero at $x = l$;

(*c*) Displacement prescribed at $x = 0$, stress zero at $x = l$;

(*d*) Stress prescribed at $x = 0$, stress zero at $x = l$.

The boundary conditions are therefore :

(II*a*) $u = u(0, t)$ at $x = 0$, $u = 0$ at $x = l$;

(II*b*) $\sigma = \sigma(0, t)$ at $x = 0$, $u = 0$ at $x = l$;

(II*c*) $u = u(0, t)$ at $x = 0$, $\sigma = 0$ at $x = l$;

(II*d*) $\sigma = \sigma(0, t)$ at $x = 0$, $\sigma = 0$ at $x = l$.

5. Solutions of the Equations of Motion

We shall solve the set of equations (2.1), (2.2), (2.3) and (3.3) – or, what is equivalent, (3.4) – by means of the Laplace transform. We shall use the notation

$$\boldsymbol{f}(x, s) = \int_0^\infty f(x, t)\, e^{-st}\, dt \tag{5.1}$$

to denote the Laplace transform with respect to t of the function $f(x, t)$. Assuming that the body force X is zero and that $\sigma = u = 0$ when $t < 0$, we find that (2.1), (2.2), and (2.3) transform to

$$\frac{d\boldsymbol{\sigma}}{dx} = s^2\, \boldsymbol{u}, \tag{5.2}$$

$$\boldsymbol{\epsilon} = \frac{d\boldsymbol{u}}{dx}, \tag{5.3}$$

$$\boldsymbol{v} = s\boldsymbol{u}. \tag{5.4}$$

In addition, we may replace the infinite lower limits in the integrals occurring in (3.3) and (3.4) by zero, in which case we find from the theory of the Laplace transform that

$$\boldsymbol{\epsilon} = \mathbf{X}\, s\, \boldsymbol{\sigma} \tag{5.5}$$

and that

$$\boldsymbol{\sigma} = \boldsymbol{\Phi}\, s\, \boldsymbol{\epsilon} \tag{5.6}$$

from which it follows that

$$s^2\, \mathbf{X}(s) \boldsymbol{\Phi}(s) = 1. \tag{5.7}$$

If, therefore, we write

$$\mu^2 = s^3\, \mathbf{X} = s/\boldsymbol{\Phi} \tag{5.8}$$

we find that either of the forms (5.5) or (5.6) of the transformed stress-strain relation can be written as

$$\boldsymbol{\epsilon} = \frac{\mu^2}{s^2}\, \boldsymbol{\sigma}. \tag{5.9}$$

If we eliminate $\boldsymbol{u}$ and $\boldsymbol{\epsilon}$ from (5.2), (5.3), and (5.9) we find that the Laplace transform $\boldsymbol{\sigma}$ of the stress σ satisfies the second-order ordinary linear differential equation

$$\frac{d^2\boldsymbol{\sigma}}{dx^2} = \mu^2\, \boldsymbol{\sigma} \tag{5.10}$$

whose general solution is

$$\boldsymbol{\sigma} = Ae^{\mu x} + Be^{-\mu x} \tag{5.11}$$

where the constants A and B are functions of the parameter s alone. It follows from (5.2) that the Laplace transform of the displacement is then of the form

$$\boldsymbol{u} = \frac{\mu}{s^2}\, (Ae^{\mu x} - Be^{-\mu x}) \tag{5.12}$$

and from (5.4) that the Laplace transform of the particle velocity is given by the equation

$$v = \frac{\mu}{s}(Ae^{\mu x} - Be^{-\mu x}). \tag{5.13}$$

In terms of the transformed quantities the boundary conditions of Section 4 become :

(I*a*) $u = u(0, s)$ at $x = 0$; $\sigma, u \to 0$ as $x \to \infty$;

(I*b*) $\sigma = \sigma(0, s)$ at $x = 0$; $\sigma, u \to 0$ as $x \to \infty$;

(II*a*) $u = u(0, s)$ at $x = 0$; $u = 0$ at $x = l$;

(II*b*) $\sigma = \sigma(0, s)$ at $x = 0$; $u = 0$ at $x = l$;

(II*c*) $u = u(0, s)$ at $x = 0$; $\sigma = 0$ at $x = l$;

(II*d*) $\sigma = \sigma(0, s)$ at $x = 0$; $\sigma = 0$ at $x = l$.

In each case the number of boundary conditions is sufficient to enable us to determine the constants A and B uniquely when the relevant functions $u(0, t)$, $\sigma(0, t)$ are prescribed. The general expression for the stress is then found from the Laplace inversion theorem to be

$$\sigma(x, t) = \frac{1}{2\pi i}\int_{\gamma-i\infty}^{\gamma+i\infty}(Ae^{\mu x} + Be^{-\mu x})\,e^{st}\,ds. \tag{5.14}$$

Corresponding integral expressions for $u(x, t)$ and $v(x, t)$ can be obtained from (5.12) and (5.13) using the Laplace inversion theorem.

6. Solutions of the Equations of Motion for a Semi-Infinite Rod

In order that the stress and displacement should tend to zero as $x \to \infty$ we must obviously take the constant of integration A in (5.11) to be zero. The remaining boundary conditions then give the two cases :

(I*a*) $u = u(0, s)\,e^{-\mu x}$; $\quad \sigma = -(s^2/\mu)\,u(0, s)\,e^{-\mu x}$; (6.1)

(I*b*) $u = -(\mu/s^2)\,\sigma(0, s)\,e^{-\mu x}$; $\quad \sigma = \sigma(0, s)\,e^{-\mu x}$; (6.2)

where μ is the root of either of the equations

$$\mu^2 = s^3\,\mathsf{X}(s), \qquad \mu^2 = s/\Phi(s)$$

which is positive for real positive s. It is clear that such a root exists for functions $x(t)$, $\phi(t)$ which are positive for positive values of t.

If we set

$$\Theta_1(x, t) = \mathcal{L}^{-1}(e^{-\mu x}), \quad \Theta_2(x, t) = \mathcal{L}^{-1}(s^2\,\mu^{-1}\,e^{-\mu x}), \quad \Theta_3(x, t) = \mathcal{L}^{-1}(\mu s^{-2}\,e^{-\mu x}), \tag{6.3}$$

where $\mathcal{L}^{-1}$ denotes the inverse Laplace operator, we can make use of the convolution theorem for Laplace transforms to express the solutions corresponding to conditions (I*a*) in the forms :

$$\left.\begin{aligned} u(x,t) &= \int_0^t \Theta_1(x, t-\tau)\, u(0,\tau)\, d\tau, \\ v(x,t) &= \int_0^t \Theta_1(x, t-\tau)\, \frac{\partial}{\partial\tau}\, u(0,\tau)\, d\tau, \\ \sigma(x,t) &= -\int_0^t \Theta_2(x, t-\tau)\, u(0,\tau)\, d\tau. \end{aligned}\right\} \tag{6.4}$$

Similarly the solutions corresponding to conditions (I*b*) can be expressed in the forms

$$\left.\begin{aligned} u(x,t) &= -\int_0^t \Theta_3(x, t-\tau)\, \sigma(0,\tau)\, d\tau, \\ v(x,t) &= -\int_0^t \Theta_3(x, t-\tau)\, \frac{\partial}{\partial\tau}\, \sigma(0,\tau)\, d\tau, \\ \sigma(x,t) &= \int_0^t \Theta_1(x, t-\tau)\, \sigma(0,\tau)\, d\tau. \end{aligned}\right\} \tag{6.5}$$

7. Solutions of the Equations of Motion for A Rod of Finite Length

If we make use of the four sets of conditions for a rod of finite length defined by $0 \leqslant x \leqslant l$ to determine the constants A and B we obtain the following solutions of (5.10) :

$$(\text{II}a)\quad u = \frac{u(0,s)\sinh\left[\mu(l-x)\right]}{\sinh(\mu l)}, \qquad \sigma = -\frac{u(0,s)\, s^2 \cosh\left[\mu(l-x)\right]}{\mu\sinh(\mu l)}; \tag{7.1}$$

$$(\text{II}b)\quad u = -\frac{\sigma(0,s)\,\mu\sinh\left[\mu(l-x)\right]}{s^2\cosh(\mu l)}, \quad \sigma = \frac{\sigma(0,s)\cosh\left[\mu(l-x)\right]}{\cosh(\mu l)}; \tag{7.2}$$

$$(\text{II}c)\quad u = \frac{u(0,s)\cosh\left[\mu(l-x)\right]}{\cosh(\mu l)}, \qquad \sigma = -\frac{u(0,s)\, s^2 \sinh\left[\mu(l-x)\right]}{\mu\cosh(\mu l)}; \tag{7.3}$$

$$(\text{II}d)\quad u = -\frac{\sigma(0,s)\,\mu\cosh\left[\mu(l-x)\right]}{s^2\sinh(\mu l)}, \quad \sigma = \frac{\sigma(0,s)\sinh\left[\mu(l-x)\right]}{\sinh(\mu l)}. \tag{7.4}$$

If we write

$$\left.\begin{aligned} \Phi_1(x,t) &= \mathcal{L}^{-1}\left\{\frac{\sinh\left[\mu(l-x)\right]}{\sinh(\mu l)}\right\}, \qquad \Phi_2(x,t) = \mathcal{L}^{-1}\left\{\frac{\cosh\left[\mu(l-x)\right]}{\cosh(\mu l)}\right\}, \\ \Phi_3(x,t) &= \mathcal{L}^{-1}\left\{\frac{s^2\cosh\left[\mu(l-x)\right]}{\mu\sinh(\mu l)}\right\}, \quad \Phi_4(x,t) = \mathcal{L}^{-1}\left\{\frac{\mu\sinh\left[\mu(l-x)\right]}{s^2\cosh(\mu l)}\right\}, \\ \Phi_5(x,t) &= \mathcal{L}^{-1}\left\{\frac{s^2\sinh\left[\mu(l-x)\right]}{\mu\cosh(\mu l)}\right\}, \quad \Phi_6(x,t) = \mathcal{L}^{-1}\left\{\frac{\mu\cosh\left[\mu(l-x)\right]}{s^2\sinh(\mu l)}\right\}, \end{aligned}\right\} \tag{7.5}$$

and make use of the convolution theorem for Laplace transforms, we find the following sets of solutions relevant to the boundary conditions stated :

$$\text{(II}a\text{)}: \quad \left.\begin{aligned} u(x,t) &= \int_0^t \Phi_1(x, t-\tau)\, u(0,\tau)\, d\tau, \\ v(x,t) &= \int_0^t \Phi_1(x, t-\tau) \frac{\partial}{\partial \tau} u(0,\tau)\, d\tau, \\ \sigma(x,t) &= -\int_0^t \Phi_3(x, t-\tau)\, u(0,\tau)\, d\tau ; \end{aligned}\right\} \tag{7.6}$$

$$\text{(II}b\text{)}: \quad \left.\begin{aligned} u(x,t) &= -\int_0^t \Phi_4(x, t-\tau)\, \sigma(0,\tau)\, d\tau, \\ v(x,t) &= -\int_0^t \Phi_4(x, t-\tau) \frac{\partial}{\partial \tau} \sigma(0,\tau)\, d\tau, \\ \sigma(x,t) &= \int_0^t \Phi_2(x, t-\tau)\, \sigma(0,\tau)\, d\tau ; \end{aligned}\right\} \tag{7.7}$$

$$\text{(II}c\text{)}: \quad \left.\begin{aligned} u(x,t) &= \int_0^t \Phi_2(x, t-\tau)\, u(0,\tau)\, d\tau, \\ v(x,t) &= \int_0^t \Phi_2(x, t-\tau) \frac{\partial}{\partial \tau} u(0,\tau)\, d\tau, \\ \sigma(x,t) &= -\int_0^t \Phi_5(x, t-\tau)\, u(0,\tau)\, d\tau ; \end{aligned}\right\} \tag{7.8}$$

$$\text{(II}d\text{)}: \quad \left.\begin{aligned} u(x,t) &= -\int_0^t \Phi_6(x, t-\tau)\, \sigma(0,\tau)\, d\tau, \\ v(x,t) &= -\int_0^t \Phi_6(x, t-\tau) \frac{\partial}{\partial \tau} \sigma(0,\tau)\, d\tau, \\ \sigma(x,t) &= \int_0^t \Phi_1(x, t-\tau)\, \sigma(0,\tau)\, d\tau. \end{aligned}\right\} \tag{7.9}$$

8. The Determination of the Stress-Strain Relation

The stress-strain relations (3.3) and (3.4) are specified for a particular material if we know the form of either the function $x(t)$ or the function $\phi(t)$. In circumstances in which the conditions are $\sigma = u = 0, t < 0$, these functions are determined by means of (5.8) if the function $\mu(s)$ is known. From the general solutions (5.11) and (5.12) it follows that, if x_1 and x_2 are the co-ordinates of any two points of the rod, then

$$\frac{[u(x_1, s)]^2 - [u(x_2, s)]^2}{[\sigma(x_1, s)]^2 - [\sigma(x_2, s)]^2} = \frac{\mu^2}{s^4}. \tag{8.1}$$

Perhaps the most useful form of this relationship is obtained by setting $x_1 = 0$ and $x_2 = l$. We then obtain the formula

$$\mu^2 = s^4 (u_0^2 - u_l^2)/(\sigma_0^2 - \sigma_l^2) \tag{8.2}$$

where $u_0 = u(0, s)$, $u_l = u(l, s)$, $\sigma_0 = \sigma(0, s)$, $\sigma_l = \sigma(l, s)$. Eq. (8.2) is valid for each set of the sets of conditions. In the semi-infinite case $u_l = \sigma_l = 0$ so

that we have

$$\mu^2 = s^4 u_0^2/\sigma_0^2 \tag{8.3}$$

and either u_0 or σ_0 is prescribed. A knowledge of the other therefore should enable us to calculate μ. For the finite case, either u_l or σ_l is zero, and one of u_0 or σ_0 is prescribed so that a knowledge of the two remaining quantities is sufficient for the determination of the function $\mu(s)$.

From (5.8) and (8.2), it follows that

$$x(t) = \mathcal{L}^{-1}\left[s(u_0^2 - u_l^2)/(\sigma_0^2 - \sigma_l^2)\right] \tag{8.4}$$

and that

$$\phi(t) = \mathcal{L}^{-1}\left[s^{-2}(\sigma_0^2 - \sigma_l)^2/(u_0^2 - u_l^2)\right]. \tag{8.5}$$

Explicit formulae for μ^2 may be obtained by other methods, notably by considering two rods of the same material of lengths l and $2l$. As an example we derive such an expression under conditions (IIa) and (IIa') where by (IIa') we mean the set of boundary conditions :

$$u = u_0 \text{ at } x = 0, \qquad u = 0 \text{ at } x = 2l$$

for the rod $0 \leqslant x \leqslant 2l$. We have then for the first rod

$$\sigma_l = -\frac{u_0 s^2}{\mu \sinh(\mu l)} \tag{8.6}$$

and for the second

$$\sigma_{2l}' = -\frac{u_0 s^2}{\mu \sinh(2\mu l)}. \tag{8.7}$$

Eliminating the hyperbolic functions from (8.6) and (8.7) we find that

$$\mu^2 = \frac{4u_0^2 s^4 \sigma_{2l}'^2}{\sigma_l^2(\sigma_l^2 - 4\sigma_{2l}'^2)}, \tag{8.8}$$

an expression which does not require a knowledge of the stress at the end $x = 0$ at which the displacement is prescribed.

9. Steady-State Solutions

When a visco-elastic rod is subjected to a sinusoidal displacement at the end $x = 0$, we expect on physical grounds that, as $t \to \infty$, the stress and the displacement at any point will become sinusoidal, with the same period as the applied displacement but with a change of phase.

We shall begin by stating the implications of some restrictions we may reasonably impose on the function $x(t)$. If $x(0) \geqslant 0$ and $x'(t) > 0$ and non-increasing for $t \geqslant 0$, then it can be shown that μ, $\sinh(\mu l)$ and $\cosh(\mu l)$ are each regular and non-zero in the half-plane $\mathcal{R}(s) > 0$. Also $\mu/s \to [x(0)]^{\frac{1}{2}}$ as $|s| \to \infty$ in the sector $|\arg s| < \frac{1}{2}\pi$. If, in addition, $x(t)$ is regular for complex values of t lying within the sector $|\arg t| < \frac{1}{2}\pi$, all the singularities of μ^2 lie on the negative real axis (including the origin), and $\mu/s \to [x(0)]^{\frac{1}{2}}$ as $|s| \to \infty$ in the sector $|\arg s| < \pi$.

(i) *Semi-Infinite Rod*

We consider the displacement at the point x when a sinusoidal displacement $u(0, t) = Ae^{i\omega t}$ is applied at the end $x = 0$ of a semi-infinite rod. In this case

$$u(0, s) = A/(s - i\omega) \tag{9.1}$$

and, substituting this expression in the first of (6.1) and making use of the Laplace inversion formula, we find that

$$u(x, t) = \frac{A}{2\pi i} \int_{\gamma - i\infty}^{\gamma + i\infty} (s - i\omega)^{-1} e^{-\mu x + st}\, ds. \tag{9.2}$$

Assuming that the function $x(t)$ is regular in the sector $|\arg t| < \frac{1}{2}\pi$, we find that :

(*a*) When $x[x(0)]^{\frac{1}{2}} > t$, $\quad \mathcal{R}(-\mu x + st) \to -\infty$ as $|s| \to \infty$ in $|\arg s| < \frac{1}{2}\pi$,

$\to +\infty$ as $|s| \to \infty$ in $\frac{1}{2}\pi < |\arg s| < \pi$.

(*b*) When $x[x(0)]^{\frac{1}{2}} < t$, $\quad \mathcal{R}(-\mu x + st) \to +\infty$ as $|s| \to \infty$ in $|\arg s| < \frac{1}{2}\pi$,

$\to -\infty$ as $|s| \to \infty$ in $\frac{1}{2}\pi < |\arg s| < \pi$.

In case (*a*) we can show by a simple application of Cauchy's theorem that $u(x, t) = 0$. In case (*b*) the integral expression for $u(x, t)$ may be evaluated by considering the integral of the same function round a closed contour consisting of the infinite line $\mathcal{R}(s) = \gamma$ and the infinite arc obtained by letting $R \to \infty$ in the equations $|s| = R$, $(\frac{1}{2}\pi - \delta) \leqslant |\arg s| \leqslant \pi$, where $\delta = \sin^{-1}(\gamma/R)$, the contour being deformed in such a way as to exclude branch points of the function $\mu(s)$. We assume that the contributions to the integral due to the branch points will be decreasing functions of t. The remaining contribution results from the residue at the simple pole $s = i\omega$, and gives the steady state solution, as $t \to \infty$,

$$u_s(x, t) = Ae^{-\mu(i\omega)x + i\omega t} \tag{9.3}$$

Putting

$$\mu(i\omega) = \xi(\omega) + i\eta(\omega),$$

we have the expression

$$u_s(x, t) = Ae^{-\xi x}\, e^{i(\omega t - \eta x)} \tag{9.4}$$

showing that, in the steady state, the displacement is transmitted with an attenuation coefficient $\xi(\omega)$ and a phase lag $x\eta(\omega)$.

Consideration of the two cases, $x[x(0)]^{\frac{1}{2}} \lesseqgtr t$, shows that the wave front is propagated with a velocity $[x(0)]^{-\frac{1}{2}}$. This holds for other forms of the imposed displacement $u(0, t)$. If the material exhibits no instantaneous elastic effect, so that $x(0) = 0$, the velocity of propagation is infinite ; but such materials are unlikely to exist.

(ii) *Finite Rod*

Applying the displacement $u(0, t) = Ae^{i\omega t}$ to a finite rod under conditions (II*a*), we find, from (9.1), and the second of (7.1), that

$$\sigma(x, t) = -\frac{A}{2\pi i} \int_{\gamma - i\infty}^{\gamma + i\infty} \frac{s^2 \cosh[\mu(l - x)]}{(s - i\omega)\,\mu \sinh(\mu l)}\, e^{st}\, ds. \tag{9.5}$$

In this instance, with the full restrictions on the functions $x(t)$, the integrand tends to zero exponentially as $|s| \to \infty$ within the sector $\frac{1}{2}\pi < |\arg s| < \pi$ for all positive values of t, and we consider the integral of this function round the same closed contour as in the semi-infinite case, modified as necessary. Besides contributions from possible branch points on the negative real axis, we need to consider those from residues at the zeros of μ^2/s^2 and $\sinh(\mu l)$. We must assume that these zeros lie in the half-plane $\mathcal{R}(s) < 0$ if the residues are to decrease exponentially with t. This imposes a more stringent condition than that derived from the restrictions on $x(t)$. Then, as $t \to \infty$, we derive, from the residue at $s = i\omega$, the steady-state solution

$$\sigma_s(x, t) = \frac{A\omega^2 \cosh\left[\mu_0 (l - x)\right] e^{i\omega t}}{\mu_0 \sinh(\mu_0 l)}, \qquad \mu_0 = \mu(i\omega). \tag{9.6}$$

When $x = l$, this may be put in the form

$$\sigma_s(l, t) = -\frac{A\omega^2 e^{i(\omega t - \delta)}}{(\xi^2 + \eta^2)^{\frac{1}{2}} [\sinh^2(\xi l) + \sin^2(\eta l)]^{\frac{1}{2}}} \tag{9.7}$$

where $\mu(i\omega) = \xi(\omega) + i\eta(\omega)$ and the phase lag δ is given by the equations

$$\sin\delta = -\frac{\xi \cosh(\xi l) \sin(\eta l) + \eta \sinh(\xi l) \cos(\eta l)}{(\xi^2 + \eta^2)^{\frac{1}{2}} [\sinh^2(\xi l) + \sin^2(\eta l)]^{\frac{1}{2}}},$$

$$\cos\delta = \frac{\eta \cosh(\xi l) \sin(\eta l) - \xi \sinh(\xi l) \cos(\eta l)}{(\xi^2 + \eta^2)^{\frac{1}{2}} [\sinh^2(\xi l) + \sin^2(\eta l)]^{\frac{1}{2}}}.$$

(iii) *Determination of* $\mu(i\omega)$

If we suppose that steady-state solutions of the types illustrated by (9.4) and (9.6) may be obtained for each of the sets of conditions (I) and (II), it is possible to derive expressions for $\mu(i\omega)$ corresponding to those for $\mu(s)$ given by (8.2) and (8.3). Assuming appropriate behaviour of $\mu(s)$, we see that the steady-state solutions are derived from the transform solutions (6.1), (6.2), (7.1) to (7.4) by the substitution of $Ae^{i\omega t}$ for $u(0, s)$ or $\sigma(0, s)$ and of $i\omega$ for s. Then each pair of steady-state solutions satisfies the relation

$$\frac{[u_s(x_1, t)]^2 - [u_s(x_2, t)]^2}{[\sigma_s(x_1, t)]^2 - [\sigma_s(x_2, t)]^2} = \frac{[\mu(i\omega)]^2}{\omega^4} \tag{9.8}$$

where x_1 and x_2 are any two points of the rod. We take the convenient case $x_1 = 0$, $x_2 = l$ ($= \infty$ in the semi-infinite case), and suppose that the amplitudes and phase angles of displacement and stress are known at each end as functions of the frequency $\omega/2\pi$. We then have that

$$[\mu(i\omega)]^2 = \omega^4 (A_1^2 e^{2i\delta_1} - A_2^2 e^{2i\delta_2})/(A_3^2 e^{2i\delta_3} - A_4^2 e^{2i\delta_4}) \tag{9.9}$$

where $A_i(\omega)$, $(i = 1, 2, 3, 4)$ are the amplitudes of the displacement at $x = 0$ and $x = l$, and of the stresses at $x = 0$ and $x = l$, in that order; and $\delta_i(\omega)$, $(i = 1, 2, 3, 4)$ are the phase angles of the displacement at $x = 0$ and $x = l$, and of the stresses at $x = 0$ and $x = l$, in that order. If the phase angles are determined so that that of the applied displacement or stress is zero, we have, under the various boundary conditions :

(Ia) $A_2 = A_4 = 0, \quad A_1 = A, \quad \delta_1 = 0;$

(Ib) $A_2 = A_4 = 0, \quad A_3 = A, \quad \delta_3 = 0;$

(IIa) $A_2 = 0, \quad A_1 = A, \quad \delta_1 = 0;$

(IIb) $A_2 = 0, \quad A_3 = A, \quad \delta_3 = 0;$

(IIc) $A_4 = 0, \quad A_1 = A, \quad \delta_1 = 0;$

(IId) $A_4 = 0, \quad A_3 = A, \quad \delta_3 = 0;$

where A is the amplitude of the displacement or stress which is applied to the end $x = 0$ of the rod.

10. Wave Propagation in a Semi-Infinite Rod for Special Cases

We now apply the Laplace inversion theorem to (6.1) and (6.2) to obtain solutions of the equations of motion corresponding to known impact conditions at the end $x = 0$ for prescribed forms of the function $\mu(s)$ corresponding to the Voigt and Maxwell solids, and to the 'nearly elastic' solid defined earlier. It will be seen, in the first two examples, that the velocity of propagation of the wave front is $[x(0)]^{-1}$, as we shewed in the previous section.

(i) *Maxwell solid impacted at constant velocity*

For this boundary condition

$$u(0, t) = v_0 t H(t)$$

where v_0 is the constant velocity and $H(t)$ denotes the Heaviside unit function. It follows immediately that

$$\mathfrak{u}(0, s) = v_0 s^{-2}.$$

For the Maxwell solid we have, from (3.16) and (5.8), that

$$\mu^2 = s^3 \mathrm{X}(s) = \kappa^2 s(s + \alpha)$$

where $\kappa^2 = a$, and $\alpha = b/a$. Substituting these results in the second of (6.1) and inverting by means of the Laplace inversion formula, we find that

$$\sigma(x, t) = \frac{v_0}{2\pi i \kappa} \int_{\gamma - i\infty}^{\gamma + i\infty} [s(s + \alpha)]^{-\frac{1}{2}} \exp\left\{ - \kappa [s(s + \alpha)]^{\frac{1}{2}} x \right\} e^{st}\, ds.$$

This integral can be evaluated readily from tables of the Laplace transform (Erdélyi *et al.* 1954) to give the expression

$$\sigma(x, t) = - v_0 \kappa^{-1} e^{-\frac{1}{2}\alpha t} I_0\left[\tfrac{1}{2}\alpha (t^2 - \kappa^2 x^2)^{\frac{1}{2}}\right] H(t - \kappa x) \qquad (10.1)$$

derived previously by Lee and Kanter (1958).

(ii) *The 'nearly elastic' solid impacted at constant stress*

The 'nearly elastic' solid is defined in Section 3 by equation (3.14) with the condition $c < a$, giving

$$\mu^2 = s^3 \mathrm{X}(s) = \kappa^2 s^2 (s + \alpha)/(s + \beta), \qquad \alpha - \beta < \beta$$

where $\kappa^2 = a$, $\alpha = (a + c)/ad$, $\beta = 1/d$. The inequality stated above will be used later in this example in order to simplify the form of the final integrals obtained from the formal solution.

For a constant compressive stress, $-\sigma_0$, applied at $t = 0$, we have $\sigma(0, t) = -\sigma_0 H(t)$, so that $\sigma(0, s) = -\sigma_0 s^{-1}$. Substituting these values for $\sigma(0, s)$ and $\mu(s)$ into the second of (6.2) and inverting by means of the Laplace inversion theorem, we find that

$$\sigma(x, t) = -\frac{1}{2\pi i}\int_{\gamma-i\infty}^{\gamma+i\infty} \sigma_0 s^{-1} \exp\left[-\kappa s\left(\frac{s+\alpha}{s+\beta}\right)^{\frac{1}{2}} x + st\right] ds. \tag{10.2}$$

The integrand in (10.2) has a simple pole at $s = 0$ and two branch points at $s + \alpha = 0$, $s + \beta = 0$. To evaluate this integral we complete the path of integration as shown in Fig. 1, where ultimately the radii of the two large circular quadrants tend to infinity and the radii of the small circles tend to zero. Denoting the integrand of the integral (10.2) by I we have, by Cauchy's theorem,

$$(2\pi i)^{-1}\int_{\Gamma} I\,ds = \sigma_0 \tag{10.3}$$

where Γ is the completed contour.

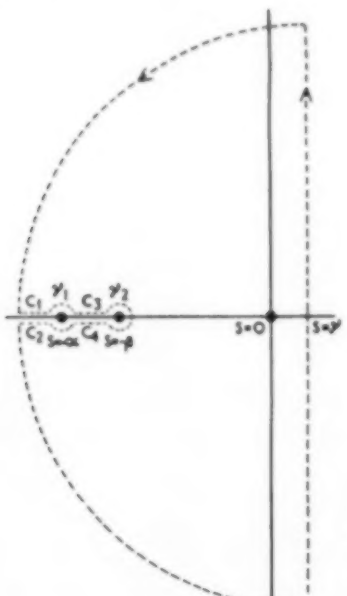

Fig. 1.

Provided $t - \kappa x > 0$, the integrals round the two circular arcs tend to zero as the radii of the circles tend to infinity. Further, since $\mu(s)$ is a single-valued function along C_1 and C_2 the sum contribution from these two paths is zero. For the integrals round the semi-circles γ_1 enclosing the singularity $s + \alpha = 0$ we write $s + \alpha = \rho e^{i\theta}$, $|\theta| < \pi$, which yields the result

$$\lim_{\rho\to 0}\int_{\gamma_1} I ds = \lim_{\rho\to 0}\left[1+O(\rho)\right]\int_{-\pi}^{\pi}\sigma_0\,\alpha^{-1}\exp\left[\kappa\alpha x\left(\frac{\rho}{\beta-\alpha}\right)^{\frac{1}{2}}e^{\frac{1}{2}i\theta}\right]e^{-\alpha t}\,\rho i e^{i\theta}\,d\theta.$$
$$= 0.$$

For the integral round the circle γ_2 enclosing the point $s = -\beta$, we substitute $s+\beta = e^{i\theta}$, and then it can be shown that

$$\lim_{\rho\to 0}\int_{\gamma_2} I ds = \lim_{\rho\to 0}\left[1+O(\rho)\right]\int_{-\pi}^{\pi}\sigma_0\,\beta^{-1}\exp\left[\kappa\beta x\left(\frac{\alpha-\beta}{\rho}\right)^{\frac{1}{2}}e^{-\frac{1}{2}i\theta}\right]e^{-\beta t}\,\rho i e^{i\theta}\,d\theta$$
$$= 2\pi i\sigma_0(\alpha-\beta)\,\beta\kappa^2x^2e^{-\beta t}.$$

Finally along C_3 and C_4 we put $s+\beta = qe^{i\pi}$, $s+\beta = qe^{-i\pi}$ respectively to obtain the contribution ,

$$(2\pi i)^{-1}\left\{\int_{C_3}+\int_{C_4}\right\} I ds = \sigma_0\,\pi^{-1}\int_0^{\alpha-\beta}(\beta+q)^{-1}\sin\left[\kappa(\beta+q)\left(\frac{\alpha-\beta-q}{q}\right)^{\frac{1}{2}}x\right]e^{-(\beta+q)t}\,dq.$$

Combining these results and making an obvious change of variable in the integral we find that

$$-\frac{\sigma(x,t)}{\sigma_0} = 1-(\alpha-\beta)\beta\kappa^2x^2e^{-\beta t}$$
$$-\frac{2(\alpha-\beta)}{\pi}\int_0^{\infty}\frac{\xi}{(1+\xi^2)(\alpha+\beta\xi^2)}\sin\left[\kappa\left(\frac{\alpha+\beta\xi^2}{1+\xi^2}\right)\xi x\right]\exp\left[-\left(\frac{\alpha+\beta\xi^2}{1+\xi^2}\right)t\right]d\xi \quad (10.4)$$

provided that $t-\kappa x>0$. If $t-\kappa x<0$ we complete the contour by the addition of a large semi-circle lying in the half-plane $\mathcal{R}(s)>0$. Since the new contour contains no singularities of the integrand, and the integral round the semi-circle tends to zero as the radius tends to infinity, we find that

$$\sigma(x,t) = 0, \qquad t-\kappa x<0. \quad (10.5)$$

The corresponding expression for the displacement, obtained by a similar procedure, is

$$u(x,t) = \sigma_0\kappa\Big\{(\alpha/\beta)^{\frac{1}{2}}\left[t-(\alpha/\beta)^{\frac{1}{2}}\kappa x-(\alpha-\beta)/2\alpha\beta\right]+2\beta^{-1}(\alpha-\beta)\kappa x e^{-\beta t}$$
$$+\frac{2(\alpha-\beta)}{\pi}\int_0^{\infty}\frac{\xi^2}{(\alpha+\beta\xi^2)^2}\cos\left[\kappa\left(\frac{\alpha+\beta\xi^2}{1+\xi^2}\right)\xi x\right]\exp\left[-\left(\frac{\alpha+\beta\xi^2}{1+\xi^2}\right)t\right]d\xi\Big\}H(t-\kappa x). \quad (10.6)$$

In the limit $\alpha=\beta$ (10.4), (10.5) and (10.6) reduce to the well known results

$$\sigma(x,t) = -\sigma_0 H(t-\kappa x), \qquad u(x,t) = \sigma_0\kappa(t-\kappa x)H(t-\kappa x)$$

for an elastic rod. A first-order approximation for $(\alpha-\beta)\ll\beta$ is obtained by substituting $\alpha=\beta$ in the definite integrals occurring in (10.4) and (10.6) which may then be evaluated to yield the approximate solutions

$$\sigma(x,t) = -\sigma_0\left[1-(\alpha-\beta)\kappa x\left(\beta\kappa x+\tfrac{1}{2}e^{-\beta\kappa x}\right)e^{-\beta t}\right]H(t-\kappa x)+O\left[(\alpha-\beta)^2\right] \quad (10.7)$$

$$u(x,t)=\sigma_0\kappa(\alpha/\beta)^{\frac{1}{2}}\{t-\kappa(\alpha/\beta)^{\frac{1}{2}}x-\frac{\alpha-\beta}{2\beta^2}+\frac{\alpha-\beta}{2\beta^2}[4\beta\kappa x+(1-\beta\kappa x)e^{-\beta\kappa x}]e^{-\beta t}\}H(t-\kappa x)$$

$$+O[(\alpha-\beta)^2]. \qquad (10{\cdot}8)$$

The approximations (10.7) and (10.8) are valid for $(\alpha - \beta)\, t \ll 1$. However, for larger values of t, βt is large enough to make the terms with the factor $e^{-\beta(t+\kappa x)}$ negligible. Since this is also true of the integrals in (10.4) and (10.6) to which these terms are approximations, the expressions (10.7) and (10.8) may be used for all values of t.

In the remaining examples it has been found possible to derive explicit solutions only for the impacted end $x = 0$ of the rod.

(iii) *Maxwell solid impacted at constant stress*

In this instance $\sigma\,(0, s) = -\sigma_0\, s^{-1}$, $\mu\,(s) = \kappa\,[s\,(s + \alpha)]^{\frac{1}{2}}$, so that the first of (6.2), taken with the relation (5.4) and the Laplace inversion theorem, leads to the expression

$$v\,(x, t) = (2\pi i)^{-1} \int_{\gamma-i\infty}^{\gamma+i\infty} \sigma_0\, s^{-2}\, \kappa\,[s\,(s + \alpha)]^{\frac{1}{2}} \exp\{-\kappa\,[s\,(s + \alpha)]^{\frac{1}{2}}\, x + st\}\, ds$$

for the particle velocity in the rod. In particular the velocity of the impacted end is given by the equation

$$v\,(0, t) = \frac{\sigma_0\,\kappa}{2\pi i} \int_{\gamma-i\infty}^{\gamma+i\infty} s^{-3/2}\,(s + \alpha)^{\frac{1}{2}}\, e^{st}\, ds$$

$$= \sigma_0\, \kappa e^{-\frac{1}{2}\alpha t}\,[\alpha t I_1\,(\tfrac{1}{2}\alpha t) + (1 + \alpha t)\, I_0\,(\tfrac{1}{2}\alpha t)]\, H\,(t) \qquad (10.9)$$

where I_0 and I_1 are, in the usual notation, modified Bessel functions of the first kind of order zero and unity.

(iv) *Voigt solid impacted at constant stress*

Again, $\sigma\,(0, s) = -\sigma_0\, s^{-1}$, while from (3.18) and (5.8) we find that $\mu\,(s) = ks\,(1 + qs)^{-\frac{1}{2}}$ for the Voigt solid. Proceeding as in the previous example we find that

$$v\,(x, t) = \frac{\sigma_0 k}{2\pi i} \int_{\gamma-i\infty}^{\gamma+i\infty} s^{-1}\,(1 + qs)^{-\frac{1}{2}} \exp\,[-ks\,(1 + qs)^{-\frac{1}{2}}\, x + st]\, ds, \qquad (10.10)$$

which, for $x = 0$, may be evaluated to yield the expression

$$v\,(0, t) = \sigma_0\, k\, \mathrm{erf}\,[(t/q)^{\frac{1}{2}}]. \qquad (10.11)$$

(v) *Voigt solid impacted at constant velocity*

The expression for $u\,(0, s)$ is the same as in case (i) above, and the expression for $\mu\,(s)$ is the same as in the last case. Substituting these expressions in the second of (6.1) and making use of the Laplace inversion theorem, we find that the distribution of stress in the rod is described by the equation

$$\sigma\,(x, t) = -\frac{v_0}{2\pi i k} \int_{\gamma-i\infty}^{\gamma+i\infty} s^{-1}\,(1 + qs)^{\frac{1}{2}} \exp\,[-ks\,(1 + qs)^{-\frac{1}{2}}\, x + st]\, ds$$

which yields, in the particular case, $x = 0$, the expression

$$\sigma(0, t) = -(v_0/k)\{\operatorname{erf}[(t/q)^{\frac{1}{2}}] + (\pi t/q)^{\frac{1}{2}} e^{-t/q}\} \tag{10.12}$$

for the stress at the impacted end.

One method of generalizing these solutions to problems in which pulses of arbitrary shape are applied to rods of finite length has been given by LEE and KANTER (1953). In the examples that follow a more direct method of solution is employed for problems involving rods of finite length.

11. WAVE PROPAGATION IN RODS OF FINITE LENGTH FOR A SPECIAL CASE

We consider in this Section the variation with time of the stress at the end $x = l$ of the ' nearly elastic ' rod $0 \leqslant x \leqslant l$ when the end $x = 0$ is displaced with a uniform velocity for a finite time, and the displacement of the end $x = l$ is kept zero. The conditions are (IIa) with

$$u(0, t) = \begin{cases} v_0 t, & 0 < t < t_1 \\ v_0 t_1, & t > t_1 \end{cases}$$

for which

$$\boldsymbol{u}(0, s) = v_0 s^{-2}(1 - e^{-st_1}). \tag{11.1}$$

Substituting from (11.1) into the second of (7.1) and applying the Laplace inversion theorem we find that, at the end $x = l$, the stress is given by the equation

$$\sigma(l, t) = -\frac{v_0}{2\pi i}\left\{\int_{\gamma-i\infty}^{\gamma+i\infty} \frac{e^{st}\,ds}{\mu \sinh(\mu l)} - \int_{\gamma-i\infty}^{\gamma+i\infty} \frac{e^{s(t-t_1)}\,ds}{\mu \sinh(\mu l)}\right\} \tag{11.2}$$

When $t < t_1$, the second integral is zero and

$$\sigma(l, t) = \sigma_0(l, t), \qquad t < t_1$$

where

$$\sigma_0(l, t) = -\frac{v_0}{2\pi i}\int_{\gamma-i\infty}^{\gamma+i\infty} \frac{e^{st}\,ds}{\mu \sinh(\mu l)}. \tag{11.3}$$

When $t > t_1$,

$$\sigma(l, t) = \sigma_0(l, t) - \sigma_0(l, t - t_1) = \sigma_1(l, t), \tag{11.4}$$

say. The expressions (11.3) and (11.4) tend to the same limit as $t \to t_1$ provided that $\sigma_0(l, 0) = 0$, which we shall find to be so in the present case.

The ' nearly elastic ' case is given, as in Section 10, case (ii), by writing

$$\mu(s) = \kappa s(s + \alpha)^{\frac{1}{2}}(s + \beta)^{-\frac{1}{2}}, \qquad \alpha - \beta \ll \beta. \tag{11.5}$$

We find that, as $R \to \infty$,

$$\int_{\Gamma} \frac{e^{st}\,ds}{\mu \sinh(\mu l)} \to 0$$

where Γ is the arc of $|s| = R$, $(\frac{1}{2}\pi - \delta) \leqslant |\arg s| \leqslant \pi$, $\delta = \sin^{-1}(\gamma/R)$. The only singularities of the integrand are poles lying in the half-plane $\mathscr{R}(s) \leqslant 0$. Hence, $\sigma_0(l, t)$ is equal to $-v_0$ times the sum of the residues at the poles. The double pole at $s = 0$ has residue

$$R_0 = (\alpha\beta t + \alpha - \beta)/\alpha^2 l\kappa^2, \tag{11.6}$$

and the simple pole at $s = -\alpha$ has residue

$$R_{-\alpha} = -(\alpha - \beta)\, e^{-\alpha t}/\alpha^2\, l\kappa^2. \tag{11.7}$$

The remaining poles are at the other zeros of $\sinh(\mu l)$, which are the roots of

$$\mu^2 l^2 + n^2 \pi^2 = 0, \qquad n = 1, 2, 3, \ldots.$$

that is

$$s^3 + \alpha s^2 + m^2 s + m^2 \beta = 0, \qquad m = n\pi/l\kappa. \tag{11.8}$$

It can be shown that this cubic equation has complex roots for all values of n whenever $\alpha < 9\beta$, so that the poles fall into three groups: s_n, the real poles, s_n' and $\bar{s}_n'$, the complex poles. The residues at the poles s_n are

$$R_n = \frac{(-1)^n\, 2\,(s_n + \beta)^2\, e^{s_n t}}{l\kappa^2\, s_n \left[2{s_n}^2 + s_n(\alpha + 3\beta) + 2\alpha\beta\right]}, \tag{11.9}$$

while those at the poles s_n', $\bar{s}_n'$, denoted by R_n', $\bar{R}_n'$ are similar but with s_n', $\bar{s}_n'$ substituted for s_n.

We can prove the following inequalities concerning the roots of equation (11.8):

$$-\alpha < s_n < -\beta,$$

$$-\tfrac{1}{2}(\alpha - \beta) < \mathcal{R}(s_n') < 0,$$

$$(m^2 - \tfrac{1}{3}\alpha^2) < |\mathcal{I}(s_n')|^2 < m^2.$$

Furthermore, in the purely elastic case, where $\alpha = \beta$, the roots of (11.8) become $-\beta, \pm mi$. We therefore make the assumption that for α and β nearly equal the roots of (11.8) are close to these values. In fact we have the following approximations, valid at least for $l\kappa\beta \leqslant 1$:

$$s_n = -\beta\left\{1 + \frac{\beta(\alpha - \beta)}{m^2 + \beta^2} + O\left[\left(\frac{\alpha - \beta}{\beta}\right)^2\right]\right\}, \tag{11.10}$$

$$s_n', \bar{s}_n' = -\frac{m^2(\alpha - \beta)}{2(m^2 + \beta^2)} \pm im\left[1 - \frac{\beta(\alpha - \beta)}{2(m^2 + \beta^2)}\right] + O\left[\left(\frac{\alpha - \beta}{\beta}\right)^2\right]. \tag{11.11}$$

Substituting these expressions in (11.9) we have

$$R_n = -\frac{(-1)^n 2\beta^2(\alpha - \beta)e^{-\beta t}}{l\kappa^2(m^2 + \beta^2)^2} \exp\left\{-\frac{\beta^2 t(\alpha - \beta)}{m^2 + \beta^2}\left[1 + O\left(\frac{\alpha - \beta}{\beta}\right)\right]\right\}\left[1 + O\left(\frac{\alpha - \beta}{\beta}\right)\right], \tag{11.12}$$

and

$$R_n' + \bar{R}_n' = 2\mathcal{R}(R_n') = \frac{(-1)^n 2e^{-\frac{1}{2}t(\alpha-\beta)}}{l\kappa^2\, m} \exp\left\{\frac{\beta^2 t(\alpha - \beta)}{2(m^2 + \beta^2)}\left[1 + O\left(\frac{\alpha - \beta}{\beta}\right)\right]\right\} \times$$

$$\times\left\{\left[1 + \frac{\beta(\alpha - \beta)(m^2 - \beta^2)}{2(m^2 + \beta^2)^2} + \ldots\right]\sin\left[(m - h)t\right] + \frac{m\beta^2(\alpha - \beta)}{(m^2 + \beta^2)^2}\left[1 + \ldots\right]\cos\left[(m - h)t\right]\right\} \tag{11.13}$$

where

$$h = \frac{m\beta(\alpha - \beta)}{2(m^2 + \beta^2)}\left[1 + O\left(\frac{\alpha - \beta}{\beta}\right)\right]$$

and $m = n\pi/l\kappa$ with $n = 1, 2, 3, \ldots$.

When $(\alpha - \beta)\, t \ll 1$, we show that $\sigma(l, t)$ approximates to the solution for the purely elastic case. With this restriction on t,

$$\sum_{n=1}^{\infty} R_n = -\frac{2\beta^2(\alpha-\beta)e^{-\beta t}}{l\kappa^2} \sum_{n=1}^{\infty} (-1)^n (m^2+\beta^2)^{-2}\left[1+o(1)\right]$$

$$= -\frac{2\beta^2(\alpha-\beta)e^{-\beta t}}{l\kappa^2}\left\{\frac{l\kappa\left[\sinh(l\kappa\beta)+l\kappa\beta\cosh(l\kappa\beta)\right]}{4\beta^3\sinh^2(l\kappa\beta)} - \frac{1}{2\beta^4}\right\}\left[1+o(1)\right]. \quad (11.14)$$

Also, we find that

$$\sum_{n=1}^{\infty} (R_n' + \overline{R}_n') = \frac{2\left[1-\frac{1}{2}t(\alpha-\beta)+\ldots\right]}{l\kappa^2} \sum_{n=1}^{\infty} (-1)^n \times$$

$$\times \left\{\sin(mt)\left[\frac{1}{m} + \frac{\beta^2 t(\alpha-\beta)}{2m(m^2+\beta^2)} + \frac{m\beta(\alpha-\beta)}{2(m^2+\beta^2)^2} - \frac{\beta^3(\alpha-\beta)}{2m(m^2+\beta^2)^2} + \ldots\ldots\right]\right.$$

$$\left. + \cos(mt)\left[\frac{\beta^2(\alpha-\beta)}{(m^2+\beta^2)^2} - \frac{\beta t(\alpha-\beta)}{2(m^2+\beta^2)} + \ldots.\right]\right\}. \quad (11.15)$$

Using the periodic properties of the series and introducing the symbol t' such that $t'/2l\kappa$ is the integral part of $\frac{1}{2}(1 + t/l\kappa)$, we find that this sum reduces to

$$\sum_{n=1}^{\infty} (R_n' + \overline{R}_n') = -\frac{1}{l\kappa^2}\left\{(t-t') - \frac{\alpha-\beta}{\beta}(t-\tfrac{1}{2}t') + \frac{\alpha-\beta}{\beta^2}\right.$$

$$\left. - \frac{l\kappa(\alpha-\beta)e^{-\beta(t-t')}}{2\beta\sinh^2(l\kappa\beta)}\left[(1-\beta t')\sinh(l\kappa\beta) + l\kappa\beta\cosh(l\kappa\beta)\right] + \ldots..\right\} \quad (11.16)$$

for all $t \ll (\alpha - \beta)^{-1}$ except when $t = (2r-1)\, l\kappa$, $r = 1, 2, 3, \ldots$, where the series is discontinuous.

Collecting these results together we find that

$$\sigma_0(l, t) = -\frac{v_0}{l\kappa^2}\left(\frac{\beta}{\alpha}\right)^{\frac{1}{2}} t' - \frac{v_0(\alpha-\beta)\, e^{-\beta t}}{2\kappa\beta\sinh^2(l\kappa\beta)} \times$$

$$\times \left\{(e^{\beta t'} - 1)\left[\sinh(l\kappa\beta) + l\kappa\beta\cosh(l\kappa\beta)\right] - \beta t'\, e^{\beta t'}\sinh(l\kappa\beta)\right\}$$

$$+ \text{higher order terms}, \qquad t \ll (\alpha-\beta)^{-1}. \quad (11.17)$$

When $t < l\kappa$, $t' = 0$, and $\sigma_0(l, t) = 0$; this is to be expected since we saw that, in the semi-infinite case, the wave front is propagated with a velocity $[\chi(0)]^{-\frac{1}{2}}$, that is, for this solid, κ^{-1}. When $t > l\kappa$, the second term is $o(1)$ compared with the first, which itself differs from the purely elastic result only by the factor β/α.

To find an approximate solution for large values of t, we return to the expressions for the residues, (11.6), (11.7) and (11.9) above. Since both s_n, and $\mathcal{R}(s_n')$ are negative for all n, all residues tend exponentially to zero as $t \to \infty$, except R_0, giving the result

$$\sigma_0(l, t) \to -v_0(\alpha\beta t + \alpha - \beta)/(\alpha^2 l\kappa^2) \qquad \text{as} \qquad t \to \infty \quad (11.18)$$

for all $\alpha > \beta > 0$.

When $t_1 < t \ll (\alpha - \beta)^{-1}$, we have, from (11.4) and (11.17) the equation

$$\sigma_1(l,t) = -\frac{v_0}{l\kappa^2}\left(\frac{\beta}{\alpha}\right)^{\frac{1}{2}}\left[t' - (t-t_1)'\right] -$$

$$-\frac{v_0(\alpha-\beta)\left[\sinh(l\kappa\beta) + l\kappa\beta\cosh(l\kappa\beta)\right]e^{-\beta t}}{2\kappa\beta\sinh^2(l\kappa\beta)}\left\{e^{\beta t'} - 1 - e^{\beta t}\left[e^{\beta(t-t_1)'} - 1\right]\right\}$$

$$+\frac{v_0(\alpha-\beta)e^{-\beta t}}{2\kappa\sinh(l\kappa\beta)}\left\{t'e^{\beta t'} - (t-t_1)'\,e^{\beta[t_1+(t-t_1)']}\right\} + \text{higher order terms.} \tag{11.19}$$

where $(t-t_1)'/2l\kappa$ is the integral part of $\frac{1}{2}(1 + \overline{t-t_1}/l\kappa)$. In the purely elastic case, $\alpha = \beta$, this reduces, for all $t > t_1$ to

$$\sigma_1(l,t) = -(v_0/l\kappa^2)\left[t' - (t-t_1)'\right]. \tag{11.20}$$

If $t_1 = 2rl\kappa$, $r = 1, 2, 3, \ldots$, the expression (11.20) remains constant at the value $-v_0 t_1/l\kappa^2$ for all $t > t_1$; otherwise it alternates between the values $-v_0(t_1 - l\kappa)'/l\kappa^2$ and $-v_0(t_1 + l\kappa)'/l\kappa^2$, with a mean value of $-v_0 t_1/l\kappa^2$. In the non-elastic case, when t is greater than t_1 and sufficiently large, we have, from the relations (11.4) and (11.18), that

$$\sigma_1(l,t) \to -v_0\beta t_1/\alpha l\kappa^2 \qquad \text{as} \qquad t \to \infty \tag{11.21}$$

for all $\alpha > \beta > 0$, and we see that, for $\alpha - \beta \ll \beta$, $\sigma_1(l,t)$ tends to the mean value of the elastic case, to a first approximation.

12. Steady-State Solutions for Special Cases

In the steady-state solutions we shall derive in this section we shall suppose that the function $x(t)$ is composed of a purely elastic term together with the function $\theta(t)$ of (3.22) In other words, we assume that

$$x(t) = a + k\left[\log(T/\tau_0) + Ei(-t/T) - Ei(-t/\tau)_0\right], \qquad T > \tau_0. \tag{12.1}$$

with the Laplace transform

$$\mathrm{X}(s) = \frac{1}{s}\left[a + k\log\left(\frac{s+1/\tau_0}{s+1/T}\right)\right]. \tag{12.2}$$

It follows from eq. (5.8) that

$$\mu(s) = s\left[a + k\log\left(\frac{s+\alpha}{s+\beta}\right)\right]^{\frac{1}{2}} \tag{12.3}$$

where $\alpha = 1/\tau_0$ and $\beta = 1/T$, $\alpha > \beta$. The real and imaginary parts of $\mu_0 = \mu(i\omega)$ are then readily shown to be given by the equations

$$\xi(\omega) = \mathcal{R}(\mu_0) = 2^{-\frac{1}{2}}\,\omega\left[r - a - \tfrac{1}{2}k\log\left(\frac{\omega^2+\alpha^2}{\omega^2+\beta^2}\right)\right]^{\frac{1}{2}},$$

$$\eta(\omega) = \mathcal{J}(\mu_0) = 2^{-\frac{1}{2}}\,\omega\left[r + a + \tfrac{1}{2}k\log\left(\frac{\omega^2+\alpha^2}{\omega^2+\beta^2}\right)\right]^{\frac{1}{2}}, \tag{12.4}$$

where $$r^2 = \left[a + \tfrac{1}{2}k\log\left(\frac{\omega^2+\alpha^2}{\omega^2+\beta^2}\right)\right]^2 + \left[k\tan^{-1}\frac{\omega(\alpha-\beta)}{\omega^2+\alpha\beta}\right]^2.$$

By putting $T = \infty$, i.e. $\beta = 0$, we have expressions appropriate to the function $\theta(t)$ of (8.21).

(i) *Semi-Infinite Rod*

When a displacement $u(0, t) = Ae^{i\omega t}$ is applied to the end of the semi-infinite rod, we find, by substituting from (12.3) into (9.2), that

$$u(x, t) = \frac{A}{2\pi i} \int_{\gamma - i\infty}^{\gamma + i\infty} (s - i\omega)^{-1} \exp\left\{ - sx \left[a + k \log\left(\frac{s + \alpha}{s + \beta} \right) \right]^{\frac{1}{2}} + st \right\} ds. \qquad (12.5)$$

The singularities of the integrand are a simple pole at $s = i\omega$ and branch points at $s = -\alpha$, $s = -\beta$, and $s = s_1$, the zero of $a + k \log (\overline{s + \alpha}/\overline{s + \beta})$. It is an elementary calculation to show that $s_1 = (\beta - \alpha e^{a/k})/(e^{a/k} - 1) < -\alpha$. When $t < xa^{\frac{1}{2}}$, the integral round the contour $|s| = R$, $-\frac{1}{2}\pi < \arg s < \frac{1}{2}\pi$ tends to zero as $R \to \infty$, so that $u(x, t) = 0$ if $t < xa^{\frac{1}{2}}$. When $t > xa^{\frac{1}{2}}$, the integral tends to zero on $|s| = R$, $(\frac{1}{2}\pi - \delta) \leqslant |\arg s| \leqslant \pi$, $\delta = \sin^{-1}(\gamma/R)$, as $R \to \infty$. The integrand is single-valued in the plane cut from s_1 to $-\infty$ and from $-\alpha$ to $-\beta$, so that in this case we consider the integral of the same function taken round the contour shown in Fig. 2, with R allowed to tend to infinity and the small circles to shrink to points.

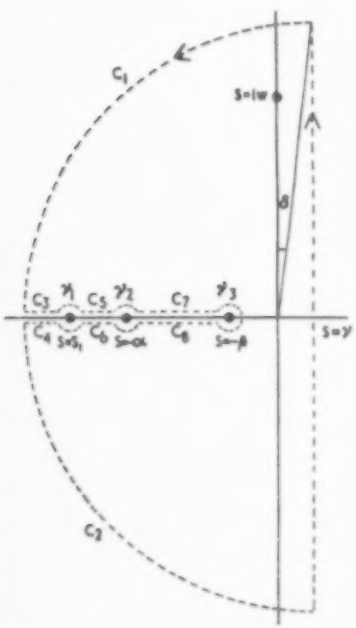

Fig. 2.

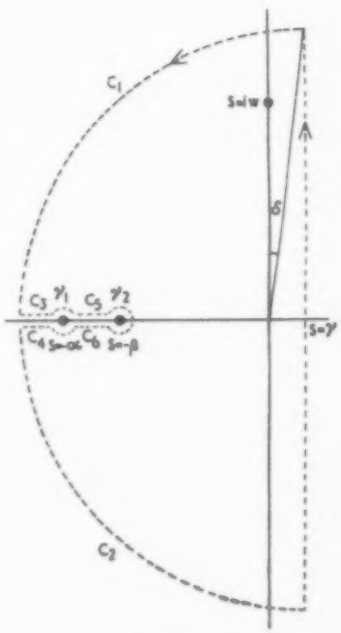

Fig. 3.

As we have seen, for $t > xa^{\frac{1}{2}}$, the integrals along the contours C_1 and C_2 tend to zero, so also do those round the circles γ_1, γ_2 and γ_3, while the sum contribution from the contours C_3 and C_5 vanishes identically. We can show that the sum of the integrals along C_3 and C_4 is less than $O(e^{s_1 t})$ with respect to t, while the

sum of the integrals along C_7 and C_8 is less than $O(e^{-\beta t})$. Hence as $t \to \infty$, $u(x,t)$ tends to a limiting value given by A times the residue of the integrand at the point $s = i\omega$. It follows from (9.4) that the steady-state solution is

$$u_s(x, t) = Ae^{-\xi x} e^{i(\omega t - \eta x)} \tag{12.6}$$

where $\xi(\omega)$ and $\eta(\omega)$ are given by the expressions (12.4).

(ii) *Rod of Finite Length*

When $u = 0$ at the end $x = l$ and $u(0, t) = Ae^{i\omega t}$, we find from (9.5) that

$$\sigma(l, t) = -\frac{A}{2\pi i} \int_{\gamma - i\infty}^{\gamma + i\infty} \frac{s^2 e^{st}}{(s - i\omega)\,\mu \sinh(\mu l)}\, ds \tag{12.7}$$

where $\mu(s)$ is given by (12.3). The singularities of the integrand are poles at $s = i\omega$ and at the zeros of $\sinh(\mu l)$, and branch points at $s = -\alpha$ and $s = -\beta$. The integral round the contours C_1 and C_2 of Fig. 3 tends to zero as $R \to \infty$ for all values of t, and the integrand is single-valued in the plane cut from $-\alpha$ to $-\beta$, so that the sum contribution from the contours C_3 and C_4 is zero. The integrals round the contours γ_1 and γ_2 tend to zero as the radii of the circles tend to zero, and the sum of the integrals along C_5 and C_6 is less than $O(e^{-\beta t})$. The zeros of $\sinh(\mu l)$ can be shewn to lie in the half-plane $\mathcal{R}(s) < 0$, and it follows that the residues at these zeros are $O(e^{\delta_n t})$ where δ_n are the real parts of the zeros. We find then that as $t \to \infty$, the stress $\sigma(l, t)$ tends to the value $-A$ times the residue of the integrand at the point $s = i\omega$, and the steady-state solution (9.7) holds, i.e., after substituting for $(\xi^2 + \eta^2)^{\frac{1}{2}}$ from (12.4),

$$\sigma_s(l, t) = -\frac{A\omega e^{i(\omega t - \delta)}}{r^{\frac{1}{2}} \left[\sinh^2(\xi l) + \sin^2(\eta l)\right]^{\frac{1}{2}}} \tag{12.8}$$

where the phase lag δ is given by eq. (9.7) and $\xi(\omega)$, $\eta(\omega)$ and $r(\omega)$ are given by (12.4).

Acknowledgments

One of us (D.S.B.) is indebted to the Research Association of British Rubber Manufacturers for a Research Grant enabling him to work at the University College of North Staffordshire. We are grateful to Professor I. N. Sneddon for discussions during the course of the work described here.

References

Alfrey, T. 1948 *Mechanical Behaviour of High Polymers* (New York, Interscience Publishers Ltd.).

Erdelyi, A., Magnus, W., Oberhettinger, F. and and Tricomi, F. G. 1954 *Tables of Integral Transforms*, Vol. 1 (New York, McGraw-Hill Book Co. Ltd.).

Gross, B. 1947 *J. Appl. Phys.*, 18, 212.

1953 *Mathematical Structure of the Theories of Viscoelasticity* (Paris, Hermann et Cie.).

KOLSKY, H.	1953	*Stress Waves in Solids* (Oxford, Clarendon Press).
KUHN, W., KÜNZLE, O. and PREISSMANN, A.	1947	*Helv. Chim. Acta*, **30**, 307. (See also *Rubber Chem. and Tech.*, **27** (1954), 36).
LEADERMANN, H.	1943	*Elastic and Creep Properties of Filamentous Materials and other High Polymers* (Washington, Textile Foundation).
LEE, E. H. and KANTER, T.	1953	*J. Appl. Phys.*, **24**, 1115.
ZENER, C.	1948	*Elasticity and Anelasticity of Metals* (Chicago, University Press).

Journal of the Mechanics and Physics of Solids, 1956, Vol. 4, pp. 96 to 108. Pergamon Press Ltd., London.

AN EXPERIMENTAL STUDY ON THE FRACTURE OF METALS UNDER HYDROSTATIC PRESSURE

By L. W. Hu
Department of Engineering Mechanics, Pennsylvania State University.

(*Received* 12*th November*, 1955)

Summary

Experimental investigation on the plastic behaviour of an aluminium alloy Alcoa 61S-T6 subjected to triaxial stresses was conducted. It was found that fracture strength was not affected by hydrostatic pressure but ductility decreased as hydrostatic pressure increased.

1. Introduction

The plastic behaviour of metals under combined stresses has been of great interest to engineers for many years. To verify the assumptions and postulations made in the mathematical theory of plasticity as well as to achieve a better understanding of the actual plastic behaviour of metals, numerous experimental investigations have been conducted to study the mechanical properties of metals under both simple and biaxial stress states. Little work has been done to study the behaviour of metals under a triaxial stress state, which is the most general condition of combined stresses.

In recent years, more and more interest has been shown in the study of mechanical properties of metals under the triaxial stress state. Mainly there are two objectives to such studies. First, information obtained will serve as a means for checking the validity of some of the assumptions made in the mathematical theory of plasticity, such as the assumption that hydrostatic pressure produces no plastic deformation. Secondly, the knowledge of the plastic behaviour of metals under high pressure may give us a better understanding of the metal cutting and forming processes and of the fracture phenomena under impulsive loading. A summary of previous investigations of the mechanical properties of metals under the triaxial stress state will first be given.

2. Summary of Previous Work

In 1893 Voigt conducted an investigation on the effect of hydrostatic pressure on the breaking strength of sodium chloride crystals. This investigation is one of the earliest attempts to study the mechanical properties of crystalline materials under triaxial stresses. An interesting experimental study on the fracture of marbles and sandstones subjected to compression under constant hydrostatic pressure was made by von Karman in 1911. In this study, a triaxial stress state

with two equal principal stress components as shown in Fig. 1 (a) was produced in specimens of various materials. A second series of tests was conducted by BOKER in 1914 to study the fracture of marble, sandstone, and zinc subjected to constant load with gradually increasing hydrostatic pressure. As shown in Fig. 1 (b), a triaxial stress state consisting of one tensile stress component with superimposed

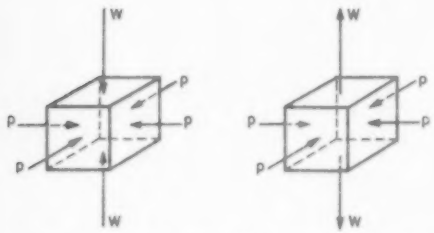

Fig. 1. Triaxial stress tests : (a) Compression with superimposed hydrostatic pressure; (b) Tension with superimposed hydrostatic pressure.

Fig. 2. Tension test in the presence of hydrostatic pressure.

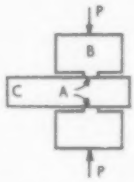

Fig. 3. Shear test under hydrostatic pressure.

hydrostatic compressive stresses was produced. A comprehensive series of triaxial stress experiments to study the plastic behaviour of metals was first conducted by ROS and EICHINGER in 1929. Since then, several methods for studying the plastic behaviour of metals under triaxial stresses have been developed. Outstanding work has been done by BRIDGMAN (1949, 1952) who to date has tested metals at the highest hydrostatic pressure. BRIDGMAN devised three different

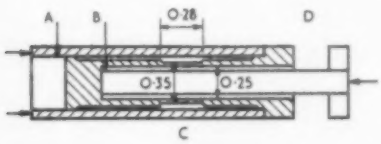

Fig. 4. Tension test under hydrostatic pressure.

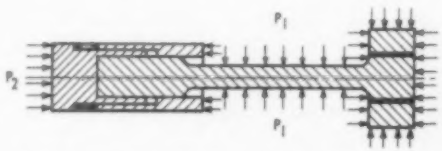

Fig. 5. Tension test under hydrostatic pressure using differential pressure principle.

types of test to investigate the plastic behaviour of metals under triaxial stresses. (1) Tension with superimposed hydrostatic pressure (by means of a yoke arrangement, *B*, as shown in Fig. 2, a compressive load is converted to a tensile load and is applied to a specimen *A* subjected to hydrostatic pressure.) (2) Shear under high pressure (the thin specimen *A* in Fig. 3 is subjected to a shear deformation as anvil *C* is rotated manually while an axial load is applied through stationary parts *B*.) (3) Two-dimensional tension under high pressure. (As shown in Fig. 4, an axial load is applied by means of ramrod *D* to thin-walled tubular specimen *C* which is immersed in the pressure medium.) The stress state in the reduced section is interpreted as two-dimensional tension according to the hypothesis he derived from studies on " necking " of materials. In 1954 WISEMAN and MARIN studied the plastic behaviour of an aluminium alloy which was subjected to a

tensile load with superimposed hydrostatic pressure. They produced a tensile load in the specimen by using the principle of pressure differential as shown in Fig. 5. The torsion test on metals under hydrostatic pressure was first conducted by CROSSLAND in 1955. As shown in Fig. 6, a torsional load was applied to a solid cirucular specimen immersed in the pressure medium. In general, the axial load was measured by an indirect means in which the frictional force was not well determined, and the deformation was measured either by an intermittent load method or by an indirect method to measure the change in overall dimensions. Furthermore, in all tests, the stress state was essentially just a simple stress with super-imposed hydrostatic pressure. In other words, in the three principal stress components, at least two of them were equal to each other. This stress state is a special case which is considered theoretically to be equivalent to a simple stress test only, if the hydrostatic pressure component causes no plastic deformation.

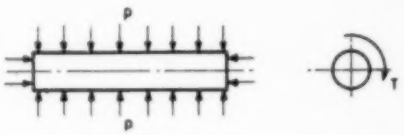

Fig. 6. Torsion test in the presence of hydrostatic pressure.

In this paper, a new type of triaxial stress test is reported. The specimen is so designed that the three principal stress components produced are different from each other. Due to the nature of the geometrical configuration of the specimens, the stress state in the specimen can be considered to be well defined. The purpose of the investigation is to study the effect of this general triaxial stress state on the fracture of metals.

3. DESCRIPTION OF EXPERIMENT

Material—The material tested in this investigation was an aluminium alloy designated as Alcoa 61S-T6. The material was received in solid rod form. The nominal chemical composition, in addition to aluminium and nominal impurities, consisted of 0·25% copper, 0·6% silicon, 1·0% magnesium, and 0·25% chromium. The typical mechanical properties given by the manufacturer were: ultimate strength = 45,000 psi, yield strength = 40,000 psi, and elongation in 2 in. = 17%.*

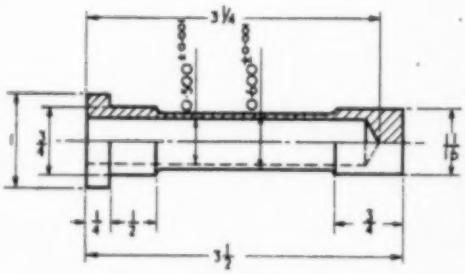

Fig. 7. Test specimen.

Specimen—The specimen was of thin-walled tubular shape with a closed end. The dimensions of the finished specimen are shown in Fig. 7. The diameter-wall thickness ratio of the specimen was about 10, so that the stress state throughout the wall in the plastic range could be assumed to be essentially uniform. The diameter-reduced length ratio was about 0·25, so that the test section of the specimen was free from end effects.

* *Alcoa Structural Handbook*, Aluminium Company of America, 1950.

Test Machine—In this investigation, a triaxial stress-testing machine was used. A general description of the original design of the testing machine was given by WISEMAN and MARIN. However, some essential modifications were made in order to conduct the present investigation.

Essentially, the triaxial stress-testing machine consists of two major parts : the pressure-generating section and the testing section as shown in the block diagram (Fig. 8). The pressure generating section is composed of two 10,000 psi

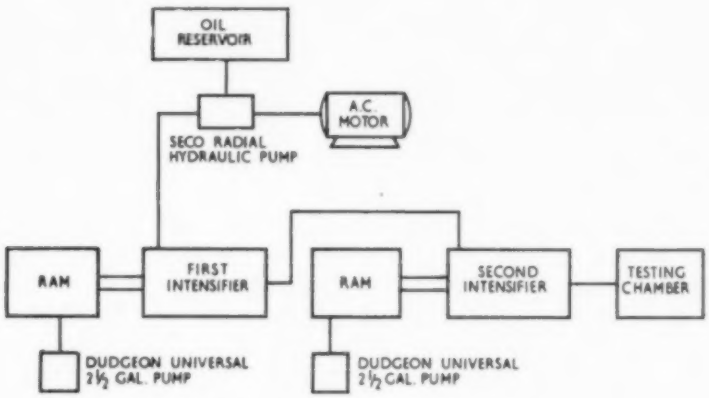

Fig. 8. Block diagram of triaxial stress-testing machine.

Seco Radial Hydraulic Pumps, two pressure intensifiers with two 15,000 psi Dudgeon Universal 2½ gallon pumps. The testing chamber with specimen assembly is shown in Fig. 9. With an inside bore of 1 in., the testing chamber is a 12 inch in length and 10 inch in diameter steel forging of SAE 6140. The two ends of the testing section in the testing chamber are connected by a U-shape conduit of $\frac{1}{16}$ in. in diameter. The U-shape conduit is controlled by a bypass needle valve which is operated manually outside the testing chamber. By this arrangement, it is possible to generate different pressures at the two ends of the testing section. The pressure medium used is XCT White oil, supplied by the Esso Company. This oil was selected because it will not solidify up to a pressure of 200,000 psi – the safe operating pressure of the present design. Two manganin coils were used to measure the pressure magnitudes at both ends of the testing section. The coils were calibrated by using a 50,000 psi dead weight tester and the variation of coil resistance was found to be linearly proportional to applied pressure. For

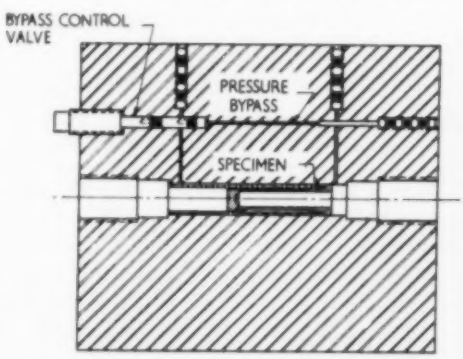

Fig. 9. Testing chamber.

measuring hydrostatic pressure beyond this range, a linear relationship between the resistance change and the pressure magnitude was assumed. The validity of this assumption was first checked by Bridgman (1949). The resistance change of the manganin coil was determined by using a SR-4 Portable Strain Indicator with a dummy coil.

Test Procedure—The specimen assembly is placed in the testing section of the testing chamber (Fig. 9) with the bypass needle valve in the open position. When a pressure p is applied to the interior of the specimen from the right hand side, the pressure is transmitted to the left hand side at the same time through the U-shape conduit. In other words, the specimen is subjected to a hydrostatic pressure p. After a certain pressure p' is reached, the U-shape conduit is disconnected by closing the bypass needle valve. Then a higher pressure p is applied from the right hand side. Due to the pressure increase, the rubber seal in the specimen assembly becomes effective and the left hand side of the testing section becomes a closed region. The pressure p' in the closed region will remain essentially constant until the specimen expands greatly. Then the applied pressure p is increased gradually until fracture of the specimen occurs. The pressures at both ends of the specimen at fracture are then recorded. The pressure at the left hand side of the testing section is the external pressure p_0 applied to the specimen at fracture, and the pressure at the right hand side is the internal pressure p_i applied. The principal stress components in the thin-walled specimen at fracture can be shown to be

$$\sigma_a = \frac{d_i}{4t}(p_i - p_0) - p_0, \qquad \sigma_t = \frac{d_i}{2t}(p_i - p_0) - p_0, \qquad \sigma_r = -\tfrac{1}{2}(p_i + p_0) \tag{1}$$

where σ_a, σ_t and σ_r are the axial, tangential, and radial stress components respectively, d_i is the inside diameter of the specimen, and t is the wall thickness.

After the pressure is released, the fractured specimen is removed from the testing chamber. The outside circumferential length S of the cross-section at the middle of the crack is measured, and a mean value of the final outside diameter $\overline{D_0}$ is obtained by dividing the measured circumferential length S by 2π. The length of the crack of the fractured specimen is also measured.

4. Test Results and Discussion

In this investigation, eighteen tests were conducted. The initial and final dimensions of the tested specimens and the internal pressure p_i and the external pressure p_0 at fracture are given in Table 1.

Due to the applied pressure, the stress state in the specimen is defined by (1). However, if the stress state is expressed as a reduced stress state with a superimposed hydrostatic pressure component, the following equation defines the state of stress (Nadai 1950) :

$$\begin{aligned}
\sigma_a &= -\tfrac{1}{2}(p_i + p_0)I + \sigma_a' = -\tfrac{1}{2}(p_i + p_0)I + \left(\frac{d_i}{4t} + \tfrac{1}{2}\right)(p_i - p_0) \\
\sigma_t &= -\tfrac{1}{2}(p_i + p_0)I + \sigma_t' = -\tfrac{1}{2}(p_i + p_0)I + \left(\frac{d_i}{2t} + \tfrac{1}{2}\right)(p_i - p_0) \\
\sigma_r &= -\tfrac{1}{2}(p_i + p_0)I + \sigma_r' = -\tfrac{1}{2}(p_i + p_0)I + 0
\end{aligned} \tag{2}$$

where I is the unit matrix. Therefore, if the hydrostatic pressure component $= -\frac{1}{2}(p_i + p_0)I$ has no effect on the plastic behaviour of metals (as postulated in the mathematical theory of plasticity), the plastic behaviour of the specimens under triaxial stresses will be the same as one subjected to a biaxial stress state

TABLE 1. *Test data.*

No.	d_0 (*in.*)	d_i (*in.*)	p_i (*psi*)	p_0 (*psi*)	σ_t' (*psi*)	$\bar{D}_0$ (*in.*)	Σ_t'' (*in./in.*)	L_c (*in.*)
1	·6260	·5001	10,770	0	42,740	·6990	·1166	1·312
4	·6247	·4997	29,800	19,240	42,220	·6539	·0586	0·616
5	·6255	·4996	49,950	39,280	42,310	·6695	·0676	0·485
6	·6005	·4998	55,690	47,400	41,110	·6290	·0483	0·390
7	·5993	·4996	61,290	53,040	41,290	·6317	·0549	0·436
8	·5985	·4997	76,310	68,260	40,710	·6243	·0473	0·243
9	·5998	·4998	78,270	70,540	38,620	·6278	·0485	0·255
10	·5984	·4997	100,420	91,960	42,820	·6225	·0443	0·331
11	·5992	·4998	60,000	51,710	41,670	·6234	·0397	0·250
12	·5998	·5005	133,210	117,860	77,360	·6209	·0350	0·384
13	·5996	·5002	8,900	0	44,800	·6559	·1091	1·165
15	·6003	·5023	9,040	0	46,330	·6881	·1757	1·310
16	·6003	·5015	9,000	0	45,690	·6893	·1653	1·578
17	·6009	·4998	9,090	0	40,880	·6795	·1579	1·368
18	·5995	·4996	15,600	6,690	44,580	·6391	·0422	0·795
19	·6004	·4998	15,260	8,450	30,490	·6363	·0793	0·775
20	·6006	·4996	19,450	10,350	40,960	·6370	·0723	0·830
21	·6009	·4995	15,550	6,720	39,630	·6397	·0792	0·849

as defined by the reduced stress components in (2). In other words, the fracture will occur once the reduced stress state reaches a critical stage which depends only on the difference between the internal and external pressures regardless of the absolute values of the internal and external pressures. In Table 1, the reduced tangential stresses σ_t' at fracture are given. The variation of reduced tangential stresses σ_t' at fracture against internal pressure p_i is plotted in Fig. 10, and shows a certain amount of scattering. However, the general features of Fig. 10 indicate that the reduced tangential stress σ_t' at fracture is not affected by the hydrostatic pressure in the range investigated. Since the nominal ratio of the reduced tangential stress σ_t' to the reduced axial stress σ_a' is equal to 1·88 for all tests, this conclusion is, therefore, also valid in so far as the reduced axial stress σ_a' is concerned. The plastic tangential strain ϵ_t'' at fracture can be

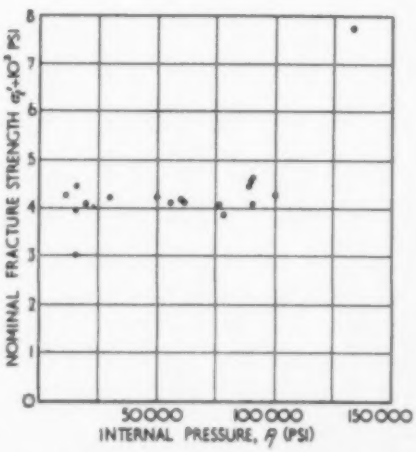

Fig. 10. Variation of reduced tangential stress σ_t' at fracture with applied pressure.

found once the mean value of the final outside diameter $\bar{D}_0$ is determined as described in the previous section. That is

$$\epsilon_t'' = \frac{\bar{D}_0 - d_0}{d_0}. \tag{3}$$

In this manner the tangential strains ϵ_t'' given in Table 1 are evaluated. According to the postulate that the hydrostatic pressure does not produce any plastic deformation, the plastic strain state at fracture should be the same, regardless of the pressure level. In Fig. 11, the variation of the plastic tangential strain ϵ_t'' at fracture against the internal pressure p_i is plotted. Because of the scattering observed, two curves are plotted in Fig. 11 as an upper limit and a lower limit respectively. For the pressure range investigated, it can be concluded that the plastic tangential strain ϵ_t'' at fracture decreases as the applied pressure increases.

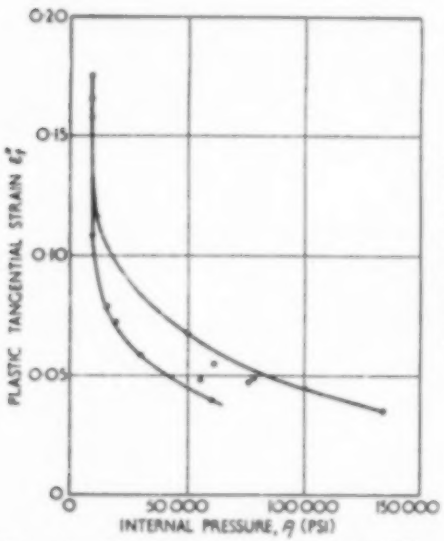

Fig. 11. Variation of plastic tangential strain ϵ_t'' at fracture with applied pressure.

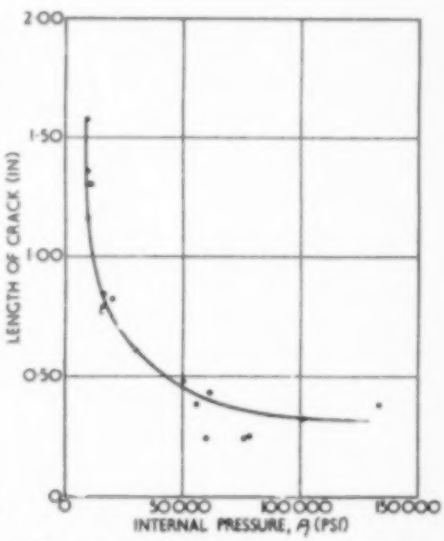

Fig. 12. Variation of length of crack at fracture with applied pressure.

A similar conclusion can be drawn that the length of the crack L_c caused by fracture decreases as the applied pressure increases, as shown in Fig. 12 where the length of the crack is plotted against the internal pressure p_i at fracture. If the ductility of metals is measured by the amount of plastic deformation at fracture, it can be concluded that the ductility of metals exposed to hydrostatic pressure decreases as the magnitude of pressure increases. This conclusion seems to be in contradiction to the findings of Bridgman (1945). He found that the ductility of metals increased with increasing hydrostatic pressure. However, this difference may be attributed to the fact that different concepts of ductility were used. Bridgman employed the area change at the neck in a tension specimen as a measure of ductility. In other words, he used the concept of zero gauge length, and neglected the effect of the complicated stress state at the neck. In

this paper, on the other hand, the concept of finite gauge length is used, and the localized deformation at the vicinity of the crack is not considered important.

After a careful examination of the fractured specimens, one finds that the opening of the crack becomes smaller as the pressure increases. The deformation in the reduced section is found to be more uniform at the high-pressure level than at the low-pressure level. From the appearance of the crack, one may conclude that the specimens broke in a more ductile manner at high-pressure level than at low-pressure level. These phenomena may be very helpful in the study of fractures under impulsive load.

5. Conclusion

In this investigation, the fracture of an aluminium alloy designated as Alcoa 61S-T6 subjected to triaxial stresses with three different principal stress components was studied. For the pressure range tested, it was found that the hydrostatic pressure component did not affect the magnitude of the reduced stress components at fracture. This confirms an important assumption made in the theory of plasticity. The ductility of the material tested was found to decrease as the applied pressure increased. The length of the crack caused by fracture decreased as the magnitude of hydrostatic pressure increased. However, the appearance of the crack indicated that the material tested fractured in a more ductile manner as the magnitude of applied pressure became higher.

6. Acknowledgments

The investigation presented in this paper is a part of a project on " Theoretical and Experimental Studies on the Mechanical Properties of Metals Subjected to Triaxial Stresses," sponsored by the Office of Ordnance Research, U.S. Army. The author wishes to express his appreciation to the Office of Ordnance Research and to Mr. Dan Snyder who helped in conducting the tests.

References

Bridgman, P. W.	1945	*Rev. Mod. Phys.*, **17**, 3.
	1949	*The Physics of High Pressure* (Bell and Sons, Ltd.).
	1952	*Studies in Large Plastic Flow and Fracture* (McGraw-Hill Book Co.).
Crossland, B.	1954	*Proc. Inst. Mech. Eng.*, **168**, 935.
Karman, Th. von	1911	*Z. Ver. deuts. Ing.*, **55**, 1749.
Nadai, A.	1950	*Theory of Flow and Fracture of Solids*, **1** (McGraw-Hill Book Co.).
Ros, M. and Eichinger, A.	1929	*Eidgenoss. Mat. pruf. Versuchanstalt Ind. Bauw. Gewerbe, Zurich*, No. 34.
Voigt, W.	1893	*Gottinger Nachrichter*, 521.
Wiseman, H. A. B. and Marin, J.	1954	*Proc. Amer. Soc. Test. Mat.*, **54**, 1365-1382.

Journal of the Mechanics and Physics of Solids, 1956, Vol. 4, pp. 104 to 120. Pergamon Press Ltd., London.

THE ELASTIC-PLASTIC THEORY OF COMPRESSION MEMBERS

By M. R. Horne
Department of Engineering, Cambridge

(*Received* 21*st November*, 1955)

Summary

Expressions are first derived for the curvature of an initially straight prismatic member of rectangular cross-section subjected to any combination of axial load and bending moment about a principal axis. The material is assumed to show elastic-pure plastic behaviour, with a finite drop of stress at yield. Using these results, expressions for the shape of elastic-plastic compression members at all stages of plasticity are derived. It is shown how solutions for the collapse loads of eccentrically loaded struts and of members with ends restrained in fixed directions may be obtained. Complete numerical results are given for the case in which there is no drop of stress at yield, and these are compared with the loads at which the elastic limit is just reached in the member. Finally, a method is presented by which the collapse load of a member subjected to terminal moments combined with any degree of elastic end restraint may be derived.

1. Introduction

The elastic-plastic theory of compression members has been studied by several investigators. The subject is difficult because, although the local plastic strains are not large compared with the elastic strains, the overall change of geometry of the member is usually large enough to be of primary importance. The limit theorems of the theory of plasticity are thus inapplicable, and it becomes necessary, in deriving collapse loads, to follow the detailed behaviour of any member under a gradually increasing axial force combined with transverse forces and bending moments.

The simplified problem of an initially straight member carrying only an axial load acting through the centroid has been discussed by Shanley (1947) who has shown that, for continuously strain-hardening materials, the member can begin to develop curvature at the tangent modulus load. Behaviour beyond this point is calculated by a step-by-step process. Theoretically, a member composed of an ideal 'elastic-plastic' material with the stress-strain relation shown in Fig. 1 (a) (that is, with no strain-hardening), will, if axially loaded between pin-ended connections, remain straight until either the Euler buckling load or the yield stress f_L is reached. This idealized problem is, however, of little significance for real structures, in which the members will scarcely ever be subjected to pure axial load acting through the centroid. Some consideration has been given to the problem of an eccentrically loaded, pin-ended member. The first analysis was given by von Karman (1908), and this was later developed by Chwalla (1928)

to derive the behaviour of struts, using a stress-strain relation with a limit of proportionality below the general yield stress. JEZEK (1934) has shown that good results may be obtained for mild steel from an analysis based on the simplified stress-strain relation of Fig. 1 (a).

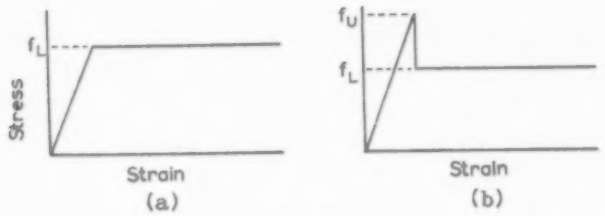

Fig. 1.

Elastic-plastic theories of compression members have particular interest when used to explain the behaviour of stanchions in continuous rigid-jointed structures. BAKER, HORNE and RODERICK (1949) have developed a theory for mild-steel members with the stress-strain curve shown in Fig. 1 (b), and have used it to interpret a series of tests on compression members with elastic end restraints (see BAKER and RODERICK, 1942, 1948a, b). Unfortunately, the theory as given by BAKER *et al.* is cumbersome, and can only be applied to particular cases by carrying out a lengthy trial-and-error process.

It is first shown below that the equations for elastic-plastic bending of a mild-steel member of rectangular cross-section can be expressed in a much more convenient form than that previously adopted. These equations are then used to derive the collapse loads of pin-ended members with equal terminal eccentricities, numerical results being given for the stress-strain relation in Fig. 1 (a). The critical loads of members with ends at fixed angles to the straight line joining the ends are discussed in the following Section. Finally, a description is given of general curves from which may be obtained the collapse loads of compression members loaded by terminal moments in the presence of elastic end-restraints.

The theory here developed is based on the approximation that cross-sections which are plane before bending remain so after bending. This is the usual approximation made in the elastic theory of structures, and is generally accepted as sufficiently accurate for the length-to-depth ratios usually encountered. While the extension of this approximation to the elastic-plastic range is more difficult to justify than its use in purely elastic structures, test results have shown (BAKER *et al.*, 1949) that it leads to a satisfactory prediction of both deformations and collapse loads. It is at the same time assumed that the transverse component of the force acting anywhere on a member is small compared with the longitudinal component, and the influence of the transverse force on the distribution of stresses at any cross-section is neglected.

A second approximation made in the present treatment is that unloading of material stressed into the plastic range does not take place. Provided the loads on an initially stress-free structure are increased proportionately from zero, the degree of unloading appears to be small. A previous investigation (BAKER *et al.*, 1949) has indicated that, if the unloading which does occur is neglected, plastic

straining being assumed to be reversible, then the predicted collapse loads will be conservative. Since a theory which takes account of the irreversibility of plastic deformation in compression members soon becomes impossibly complicated, it is not here attempted.

2. The Equations of Bending for Rectangular Members under Axial Load

The curve AB in Fig. 2 (a) represents the longitudinal centre line of a member, initially straight and free from stress, subjected to terminal loads and bending moments. The forces P_A and R_A and the bending moment M_A acting at end A are equivalent to some force P acting along some line ST as shown, the loading at B being equivalent to an equal and opposite force P'. In deriving the form of the curve AB, it is convenient to take the line of action of the forces P and P' as the OX axis, as shown in Fig. 2 (b). The position of the origin O along OX is arbitrary, OY being perpendicular to OX.

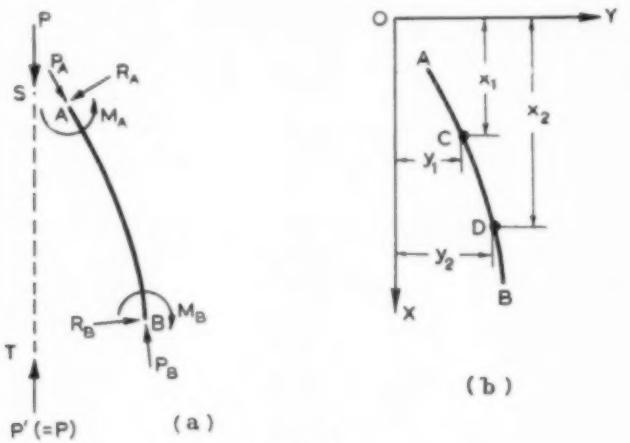

Fig. 2.

It is characteristic of the loading conditions in compression members that transverse (shear) forces are small compared with longitudinal forces. Hence, in Fig. 2 (a), R_A and R_B are to be assumed small in comparison with P_A and P_B. If x, y are the co-ordinates of any point in AB, it follows that y' $(= dy/dx)$ is small compared with unity, and that the curvature of the centre line in the plane XOY is given with sufficient accuracy by the second differential y''.

The possible states of plasticity in a member are shown in Fig. 3 (a). Over the length EF, the yield point is nowhere exceeded. At F yield occurs in the extreme compression fibres, while at G yield in tension occurs on the outside face. Over the length FH there is a region of the member which is plastic in compression, while over GH there is also a region which has become plastic in tension. The lengths EF, FG and GH are described as 'elastic,' 'primary plastic,' and 'secondary plastic' zones respectively. The equations for the centre line of the member differ in the three zones, which therefore have to be considered separately.

The cross-section of the member is shown in Fig. 3 (b), the axis $\zeta\zeta$ being perpendicular to the plane XOY in Fig. 2 (b). The stress-strain relationship, the same in tension and compression, is that shown in Fig. 1 (b). The ratio of the upper yield stress f_U to the lower yield stress f_L is denoted by β.

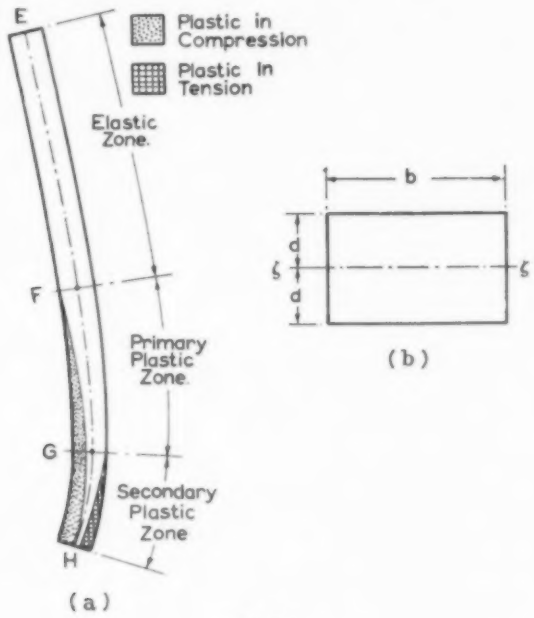

Fig. 3.

Elastic zone

The curvature y'' of the longitudinal axis is linearly related to the bending moment M about this axis, viz. $EIy'' = -M$ where E is the elastic modulus and $I\ (= \frac{1}{12}bd^3)$ is the moment of inertia about the axis $\zeta\zeta$. It is convenient to express M as αM_p where α is a non-dimensional quantity and M_p is the full plastic moment $(bd^2 f_L)$ of the member under zero axial load. Hence

$$y'' = -\frac{1}{2a^2 d}\alpha \tag{1}$$

where $a^2 = E/3f_L$. The bending moment M is related to the ordinate y by the relation $M = Py$. If nf_L denotes the mean longitudinal stress in the member, then since y' is everywhere small, $P = 2bdnf_L$. Hence, expressing M and P in terms of the non-dimensional quantities α and n respectively in the relationship $M = Py$, it is found that

$$y = \frac{d}{2}\frac{\alpha}{n}. \tag{2}$$

If y' is denoted by θ, then the value of θ may be derived from (1) and (2), since $\theta^2 = 2\int y''\,dy$. If (y_1, θ_1) and (y_2, θ_2) denote the values of (y, θ) at any two points

C and D in the elastic zone (Fig. 2 b), then

$$\theta_1^2 + \frac{n}{a^2 d^2} y_1^2 = \theta_2^2 + \frac{n}{a^2 d^2} y_2^2 = \theta_e^2 \tag{3}$$

where θ_e is the value of θ at the section (real or imaginary) where AB cuts the axis OX. Moreover, since $x = \int dy/\theta$, it follows that, if x_1 and x_2 are the abscissae of the points C and D in Fig. 2 (b),

$$x_2 - x_1 = \frac{ad}{\sqrt{2}} \left\{ \sin^{-1} \left(\frac{\sqrt{n} y_2}{ad\theta_e} \right) - \sin^{-1} \left(\frac{\sqrt{n} y_1}{ad\theta_e} \right) \right\}. \tag{4}$$

If y and θ are known for any section in the elastic zone, (3) and (4) enable values at any other section in the elastic zone to be determined.

The boundary between the elastic and primary plastic zones occurs where the bending moment is just sufficient to cause yield in the extreme fibres in compression, that is where $M = \frac{2}{3} bd^2 (f_U - nf_L)$. Hence at this section $\alpha = \frac{2}{3} (\beta - n)$ and $y = (\beta - n)\, d/3n$. Equations (3) and (4) apply when the elastic zone extends to negative values of y down to $y = -(\beta - n)\, d/3n$. At $y = 0$, the bending moment is zero, and there is a point of contraflexure.

Primary Plastic Zone

A typical stress distribution in the primary plastic zone is shown in Fig. 4 (b), the cross-section being plastic in compression over the region *efkj* in Fig. 4 (a). The total depth of elastic material is denoted by $2\xi d$, while the distance of the neutral

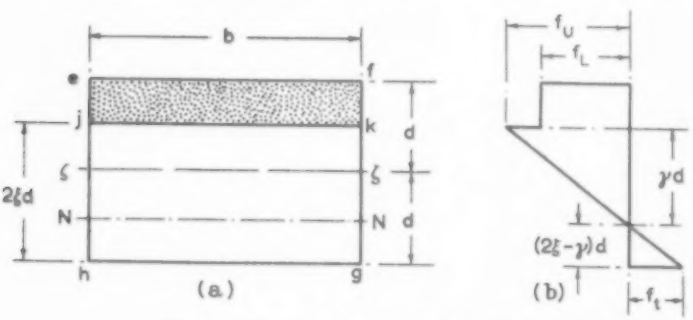

Fig. 4. Stress distribution in primary plastic zone.

axis NN from the boundary jk of the plastic region is γd. If f_t is the tensile stress in the extreme fibres opposite to the plastic region, it follows from similar triangles in Fig. 4 (b) that $f_t = (2\xi - \gamma) f_U/\gamma$. The total axial force P may be derived from the stress distribution, and remembering that $P = 2bdnf_L$, we find that

$$\gamma = \frac{\beta \xi^2}{(1 - n) + (\beta - 1)\, \xi} \tag{5}$$

The bending moment M (about the central axis $\zeta\zeta$) may be derived, and equated to $\alpha bd^2 f_L$. After eliminating γ by using (5), it follows that

$$\alpha = \tfrac{2}{3} \left[(1 - n)\, (3 - 2\xi) + (\beta - 1)\, \xi^2 \right] \tag{6}$$

The longitudinal strain at the boundary jk of the plastic region in Fig. 4 (a) is f_U/E, and hence the curvature of the longitudinal axis in the plane XOY (Fig. 2 b) is $f_U/E\gamma d$. Since $a^2 = E/3f_L$ it follows that

$$y'' = -\frac{\beta}{3a^2\,\gamma d} \tag{7}$$

The value of θ may now be derived from the relation $\theta^2 = 2\int y''\,dy$, using (2), (5), (6) and (7). If (θ_1, ξ_1) and (θ_2, ξ_2) are the values of (θ, ξ) at any two sections in the same primary plastic zone, it is found that

$$\theta_1^2 + \frac{C^2}{a^2}\left\{\frac{1}{\xi_1} + B^2\,\xi_1\right\} = \theta_2^2 + \frac{C^2}{a^2}\left\{\frac{1}{\xi_2} + B^2\,\xi_2\right\} = \theta_p^2 \tag{8}$$

where

$$B = \frac{\beta - 1}{1 - n}, \qquad C^2 = \frac{4}{9}\frac{(1-n)^2}{n}$$

and θ_p is a constant for the member.

The use of (2), (6) and (8) in conjunction with the relation $x = \int dy/\theta$ leads to the integral

$$x = \frac{adC}{\sqrt{n}}\int \frac{(B\xi - 1)\sqrt{\xi}\,d\xi}{\sqrt{a^2\,\theta_p^2\,\xi - C^2 - B^2\,C^2\,\xi^2}}. \tag{9}$$

The solution of equation (9) involves elliptic integrals of the first and second kinds, namely

$$F(k, \phi) = \int_0^{\phi} \frac{d\phi}{\sqrt{1 - k^2\sin^2\phi}} \qquad \text{and} \qquad E(k, \phi) = \int_0^{\phi} \sqrt{1 - k^2\sin^2\phi}\,d\phi.$$

The distance $x_2 - x_1$ between any two sections in the primary plastic zone may be expressed as

$$\left\{\frac{1 - k^2}{adA^5\,BC}\right\}(x_2 - x_1) = \left\{\frac{3}{A^2\,B} - 2\frac{2 - k^2}{1 - k^2}\right\}\left\{E(k, \phi_2) - E(k, \phi_1)\right\}$$

$$+ \left\{F(k, \phi_2) - F(k, \phi_1)\right\} - \frac{a}{AC}\left\{\xi_2\,\theta_2 - \xi_1\,\theta_1\right\} \tag{10}$$

where if

$$\theta_q^2 = \sqrt{\theta_p^4 - 4\frac{B^2\,C^4}{a^4}},$$

then

$$A^2 = \frac{\theta_p^2 - \theta_q^2}{2B^2\,C^2}\,a^2,$$

$$k^2 = \frac{2\theta_q^2}{\theta_p^2 + \theta_q^2},$$

$$\phi_1 = \tfrac{1}{2}\cos^{-1}\left\{\frac{2B^2\,C^2\,\xi_1 - a^2\,\theta_p^2}{a^2\,\theta_q^2}\right\},$$

and ϕ_2 is similar to ϕ_1, but involving ξ_2 in place of ξ_1.

When $f_U = f_L$, then $\beta = 1$ and $B = 0$. The analysis is then much simplified, and (9) may be integrated using only elementary functions. Equation (8) becomes

$$\theta_1^2 + \frac{C^2}{a^2 \xi_1} = \theta_2^2 + \frac{C^2}{a^2 \xi_2} = \theta_p^2, \tag{11}$$

while (10) becomes

$$x_2 - x_1 = \frac{dC}{\sqrt{n}\theta_p} \left\{ \frac{\xi_1 \theta_1 - \xi_2 \theta_2}{\theta_p} + \frac{C^2}{2a^2 \theta_p^2} \log_e \frac{\xi_1 (\theta_p + \theta_1)^2}{\xi_2 (\theta_p + \theta_2)^2} \right\}. \tag{12}$$

At the boundary between the elastic zone and the primary plastic zone, the whole depth of the section is elastic. Hence $\xi = 1$ and $\alpha = \frac{1}{3}(\beta - n)$. At the boundary between the primary and secondary plastic zones, yield first occurs in the extreme fibres on the tension side, and hence $f_t = f_U$. Since $f_t = (2\xi - \gamma) f_U / \gamma$ in the primary plastic zone, then $\xi = \gamma$ at this boundary, whence from (5), $\xi = (1 - n)$. Equation (6) then shows that at the boundary between the primary and secondary plastic zones, $\alpha = \frac{1}{3}(1 - n)\{\beta + (3 - \beta)n\}$.

The solution which has been obtained applies only to primary plastic zones with positive values of y. When y is negative, there has to be a change of sign in (7). Equations (8) and (11) remain valid, but $(x_2 - x_1)$ must be replaced by $(x_1 - x_2)$ in (10) and (12).

Secondary Plastic Zone

The stress distribution in the secondary plastic zone is of the type shown in Fig. 5 (b). The regions *efkj* and *mngh* are plastic in compression and tension respectively. The total depth of elastic material is denoted by $2\xi d$. The neutral axis *NN* is midway between the boundaries *jk* and *mn*, and at a distance from the central axis $\zeta\zeta$ of λd.

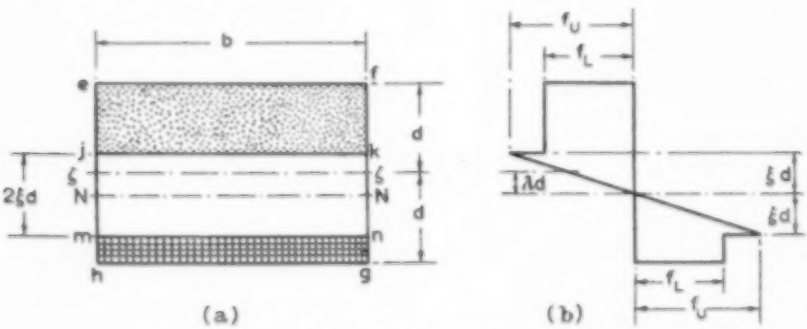

Fig. 5. Stress distribution in secondary plastic zone.

Equating the resultant longitudinal force represented by the stress distribution to the axial load $P\ (= 2bdnf_L)$, it is found that $\lambda = n$. When the resultant bending moment about the axis $\zeta\zeta$ is equated to $M\ (= \alpha bd^2 f_L)$, it is found that

$$\alpha = (1 - n^2) - \frac{(3 - 2\beta)}{3} \xi^2. \tag{13}$$

The curvature of the longitudinal axis is

$$y'' = -\frac{\beta}{3a^2 \, d\xi}. \tag{14}$$

The value of θ being obtained from $\theta^2 = 2\int y''\,dy$, using (2), (13), and (14), it is found that, for two sections in the same secondary plastic zone,

$$\theta_1^2 - \frac{N^2}{a^2}\xi_1 = \theta_2^2 - \frac{N^2}{a^2}\xi_2 = \theta_s^2, \qquad \text{where} \qquad N^2 = \frac{2}{9}\frac{(3-2\beta)\,\beta}{n}. \tag{15}$$

The use of (2), (13) and (15) in the relation $x = \int dy/\theta$ leads finally to

$$x_2 - x_1 = \frac{3a^2\,d}{\beta}\left[\left\{\frac{2}{3}\frac{a^2\,\theta_2^2}{N^2} - \xi_2\right\}\theta_2 - \left\{\frac{2}{3}\frac{a^2\,\theta_1^2}{N^2} - \xi_1\right\}\theta_1\right]. \tag{16}$$

The secondary plastic zone extends from the section at which $\xi = (1-n)$ and $\alpha = \frac{2}{3}(1-n)\{\beta + (3-\beta)\,n\}$ to that at which full plasticity occurs, namely $\xi = 0$ and $\alpha = (1-n^2)$. When the value of y is negative, (15) remains valid, but $(x_2 - x_1)$ has to be replaced by $(x_1 - x_2)$ in (16).

3. Application to Pin-Ended, Eccentrically Loaded Struts

The eccentrically loaded strut AB in Fig. 6 is of length L, and has a rectangular cross-section of width b and depth $2d$, the dimension b being at right-angles to

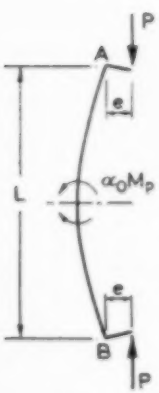

Fig. 6.

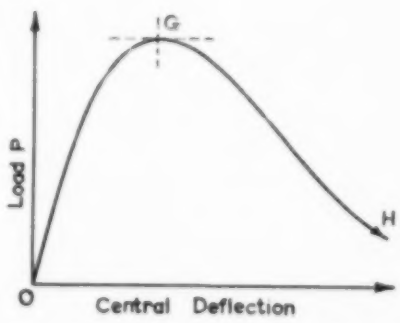

Fig. 7.

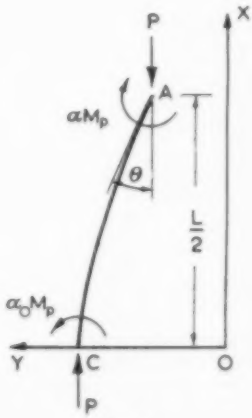

Fig. 8.

the plane of eccentricity. If the load P, acting at a constant eccentricity e at each end of the member, is increased from zero, the graph of load against central deflection is of the form OG in Fig. 7. The point G, where the curve becomes horizontal, corresponds to the maximum load which the member can support, and at greater deflections, the resistance of the strut decreases, as indicated by the curve GH. Let the bending moment at the centre of length (point C in Fig. 6) be denoted by $\alpha_0 M_p$, and that at each end by αM_p, where M_p is the full plastic moment of the member under zero axial load. If $P = 2bdnf_L$, then at point G on the load-deflection curve, the relation

$$\left(\frac{\partial\alpha}{\partial\alpha_0}\right)_{n,\,L\ \text{constant}} = 0 \tag{17}$$

is satisfied. This condition may be used to derive the collapse loads of eccentrically loaded struts.

The compression member AC in Fig. 8 has $\theta = 0$ at C and is of length $L/2$. The axial load is P, and the moments at A and C are αM_p and $\alpha_0 M_p$ respectively. The theory already developed may be applied in order to derive L for given values of n, α and α_0. The results of such calculations, taking $n = 0{\cdot}6$ and $\beta = 1{\cdot}0$, are shown in Fig. 9, in which the curves show the relationship between α and L for

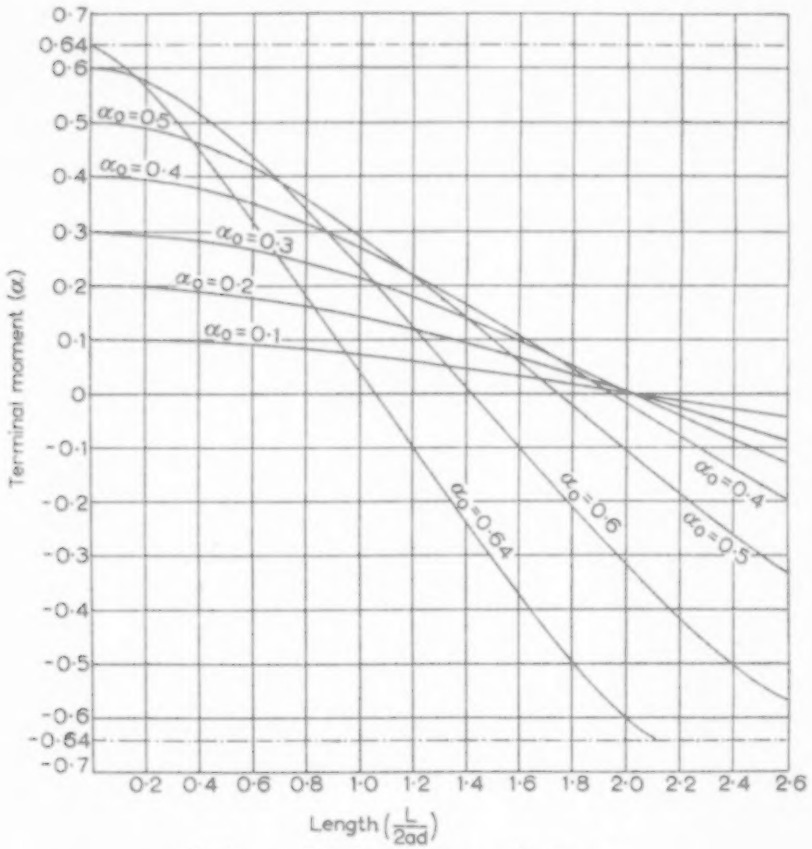

Fig. 9. $\alpha - L/2ad$ curves for $n = 0{\cdot}6$, $\beta = 1{\cdot}0$.

successive values of α_0. The values of L have for convenience been plotted non-dimensionally in terms of $L/2ad$. The curves have an envelope along which (17) is satisfied. Hence the envelope represents combinations of length L and eccentricity e (given by $\alpha d/2n$) for which the critical load would have the value $P = 2bdnf_L$ corresponding to the value of n for which the curves are drawn.

The envelopes for nine values of n when $\beta = 1{\cdot}0$ are collected in Fig. 10. The dotted curves correspond to constant values of the eccentricity ratio e/d. The length may be derived by multiplying the horizontal scale by $2ad$ where $a = \sqrt{(E/8f_L)}$. It may be noted that, if $E = 18{,}500$ tons per sq. in. and $f_L = 15$

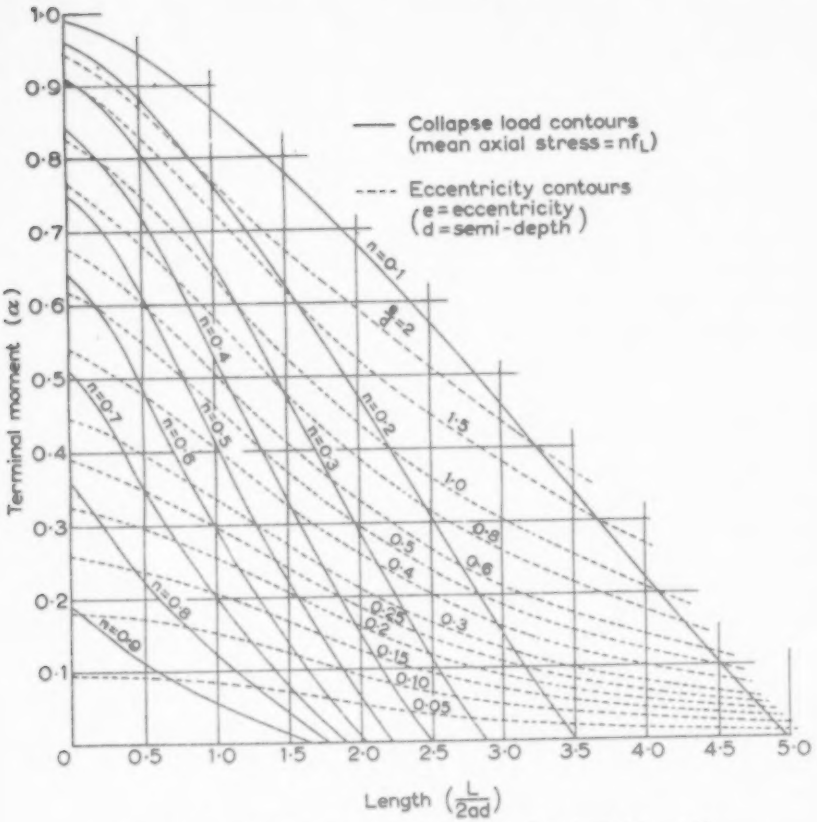

Fig. 10. Collapse loads for eccentrically loaded struts ($\beta = 1{\cdot}0$).

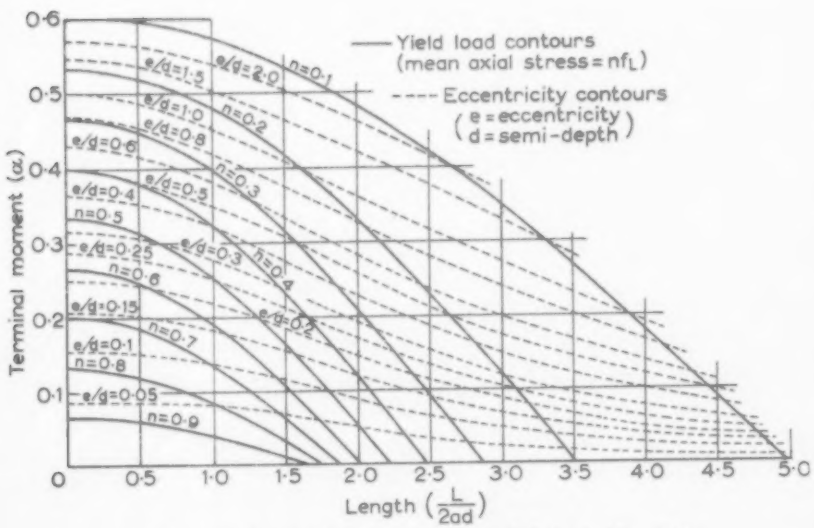

Fig. 11. Yield loads for eccentrically loaded struts ($\beta = 1{\cdot}0$).

tons per sq. in., the slenderness of the strut (length divided by radius of gyration, or $\sqrt{8}L/d$), is sixty times the horizontal scale.

It is interesting to compare the critical loads given by the plastic theory with the loads at which the yield stress is just reached in the most highly stressed fibres. These latter loads are often taken as an approximation to the critical loads, and are shown in the chart in Fig. 11. The yield loads and collapse loads are not very different for slender members and low eccentricities, but differ appreciably when the members are short and the eccentricities high. At zero eccentricity ($\alpha = 0$) the yield and collapse conditions coincide, the load P then being equal to the Euler critical load $EI\pi^2/L^2$, except when this gives a mean stress greater than the yield value. In terms of n and α, the Euler critical load corresponds to $L/2ad = \pi/2\sqrt{n}$.

4. Application to Members with Ends Fixed in Given Directions

The ends A and B of the member ACB in Fig. 12 are restrained in fixed directions, making an angle θ with the straight line AB. The member carries an axial load P, which attains a critical value in the same way as does the load in an eccentrically loaded strut. If the bending moment at mid-height C is again denoted by α_0, the critical condition is given by

$$\left(\frac{\partial\theta}{\partial\alpha_0}\right)_{n,\,L\text{ constant}} = 0. \qquad (18)$$

In some cases, the critical load is found to occur when full plasticity has occurred at C, where there arises an angle of discontinuity. If θ_0 denotes the slope of the centre line at C under such conditions, then the collapse load occurs when

$$\left(\frac{\partial\theta}{\partial\theta_0}\right)_{n,\,L\text{ constant}} = 0. \qquad (19)$$

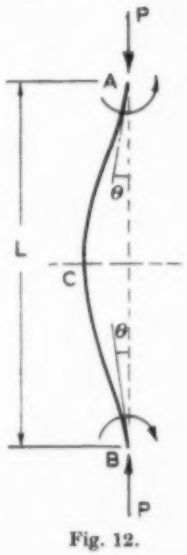

Fig. 12.

Consider now the member AC in Fig. 8, and let L be calculated for given values of n, θ and α_0 when the tangent at C is vertical, and for given values of n, θ and θ_0 when full plasticity occurs at C and the tangent is there inclined at an angle θ_0 to the vertical. The curves in Fig. 13 have been calculated for $n = 0{\cdot}6$ and $\beta = 1{\cdot}0$, and give, for specific values of α_0 or $a\theta_0$, the relationship between $a\theta$ and $L/2ad$. The envelope to these curves satisfies (18) and (19), and thus shows the lengths of those members which, when restrained in direction at either end at given angles, will collapse under a critical load of $n = 0{\cdot}6$. The envelopes thus obtained for a series of values of n are collected in Fig. 14.

Under zero axial load ($P = 0$, or $n = 0$), a member with ends fixed in direction as envisaged above will bend in uniform curvature, with a corresponding uniform bending moment. The curvature induced is most conveniently expressed in terms of the equivalent extreme fibre bending stress as derived by elastic theory,

this stress being less than the upper yield value when the critical member is elastic at the given curvature, and greater than the yield stress when the member is actually plastic. If this equivalent stress is denoted by mf_L, it is readily shown that $m = 3a\theta/(L/2ad)$. The values of m are indicated in Fig. 14 by the dotted lines. It is seen that, except for slender members, very high stresses may be induced by the initially imposed curvature and yet leave the member with a high carrying capacity for axial loads.

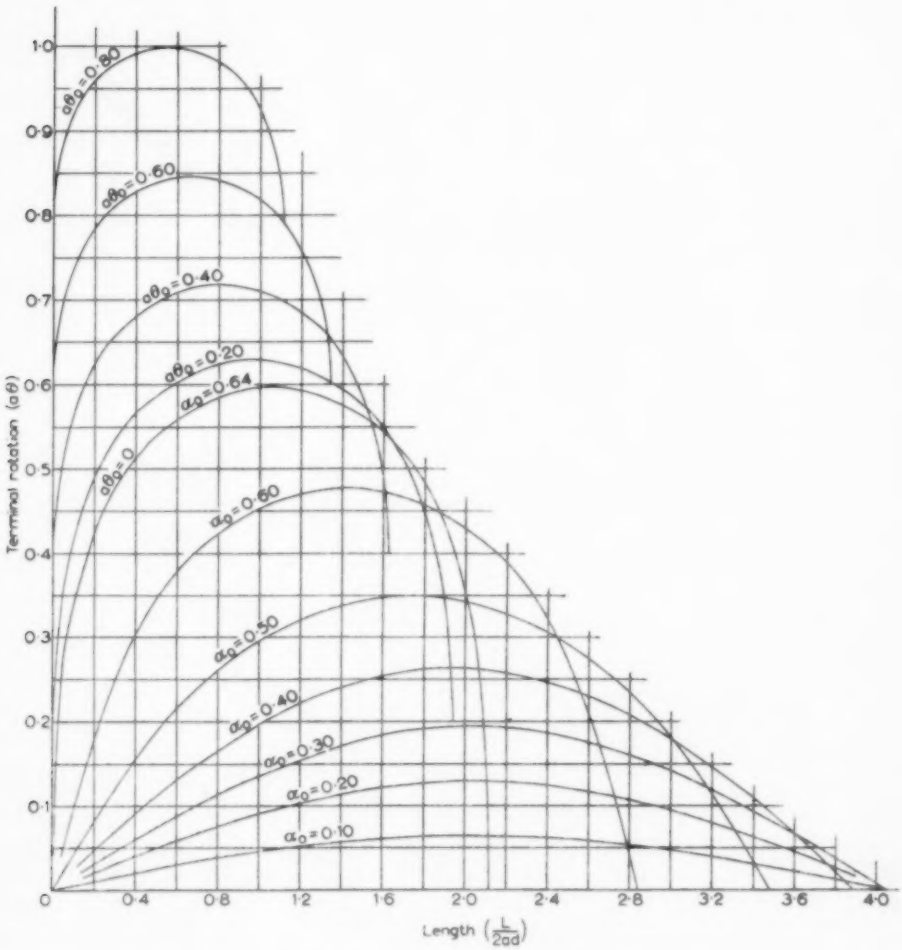

Fig. 13. $a\theta - L/2ad$ curves for $n = 0{\cdot}6$, $\beta = 1{\cdot}0$.

The axial loads at which yield first occurs in members with direction-fixed ends are given in Fig. 15. The contrast between this chart and that giving the collapse loads (Fig. 14) is striking, and shows that if end fixity is present, the load at which yield occurs shows no relationship to that necessary to cause com-

plete collapse. The loads given by the two charts coincide when $m = 0$ and $\theta = 0$, and give the solution corresponding to the Euler crippling load for a fixed-ended member of length L, namely $L/2ad = \pi/\sqrt{n}$.

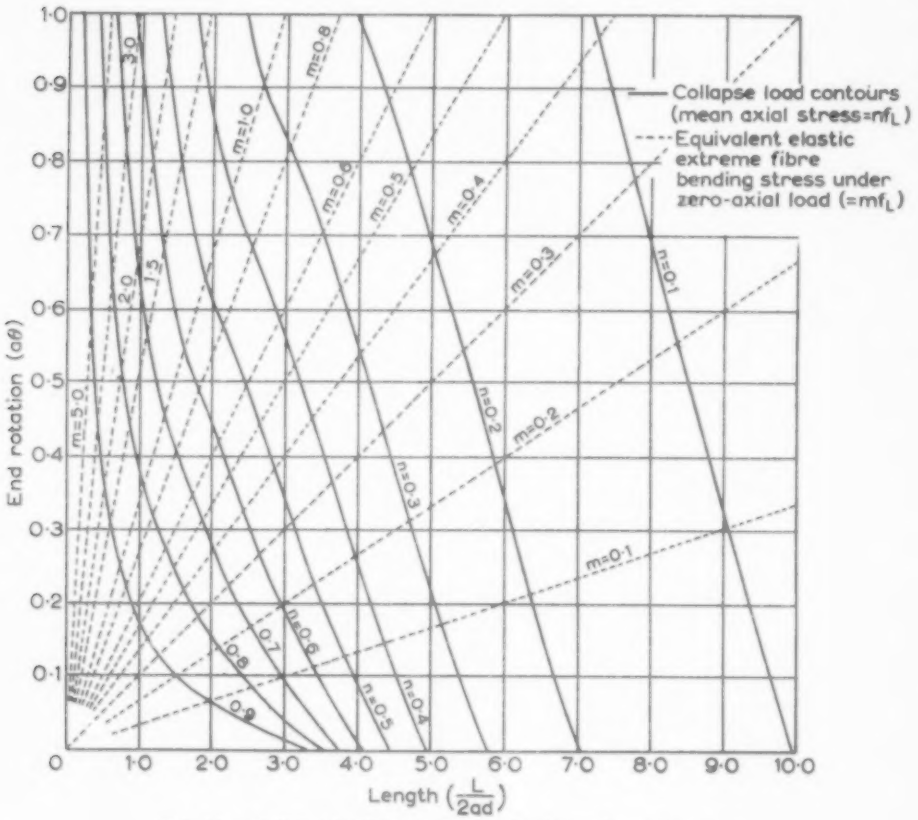

Fig. 14. Collapse loads for end-restrained members ($\beta = 1{\cdot}0$).

5. Members with Elastic End-Restraints

The member AB (Fig. 16) of length L, is rigidly connected at A and B to elastic beams DAE and $D'BE'$ which carry transverse loads only. If the members DAE and their connections at D and E are antisymmetrical about a horizontal plane relative to the members $D'BE'$ and their connections, and if the loading on these members is also antisymmetrical, then the compression member ACB will behave antisymmetrically about the central section C. If all loads are increased uniformly from zero, the relation between the axial load P in the member and its central deflection will follow some curve OG as shown in Fig. 7, and thereafter the resistance of the member to axial load will decrease. At the point G, the loading intensity is stationary and so also is the axial load P.

Consider now the length AC in Fig. 8, now regarded as representing the upper half of the member AB in Fig. 12. It is possible to derive, for a particular length of member and any given value of n, the relationship between the terminal moment

αM_p and the terminal rotation θ at A as the central moment $\alpha_0 M_p$ is varied. If full plasticity occurs at C, the moment there is constant, but the slope θ_0 varies. Let $Oabc$ and $Oa'b'c'$ in Fig. 17 (a) represent the $\alpha - \theta$ relationship for a given length of member for $n = n_1$ and $n = n_2$ respectively, where $n_1 < n_2$. By considering now the elastic members to which the member AB is attached in Fig. 16,

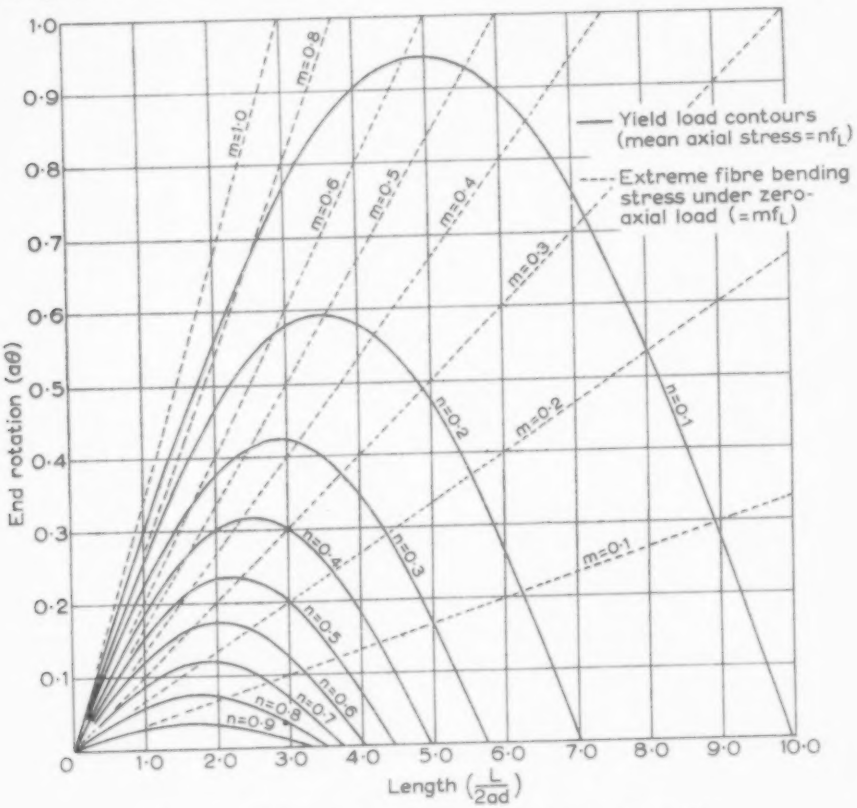

Fig. 15. Yield loads for end-restrained members ($\beta = 1{\cdot}0$).

other relationships between α and θ are obtained. At any given value of n the axial load in the compression member, and hence also the general intensity of loading, are defined. For any such value of n, the $\alpha - \theta$ relationship derived from the elastic members is a straight line of negative slope. Let de and $d'e'$ represent the required relationships when $n = n_1$ and $n = n_2$ respectively. The points of intersection, s and t, of de with the curve $Oabc$, represent possible states of compatibility between the compression member and the surrounding elastic members at the load intensity corresponding to $n = n_1$. Hence if the curve in Fig. 17 (b) is part of the load-deflection relationship for the compression member, points s and t, corresponding to the points s and t in Fig. 17 (a), are obtained. The peak u of the load-deflection curve in Fig. 17 (a) thus corresponds to the n value at which the $\alpha - \theta$ curve $Oa'b'c'$ in Fig. 17 (a) just touches the line $d'e'$ representing the behaviour of the surrounding members.

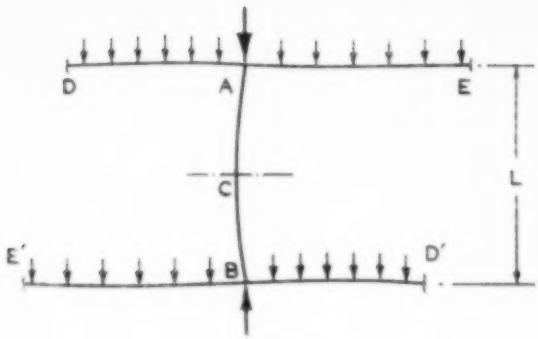

Fig. 16.

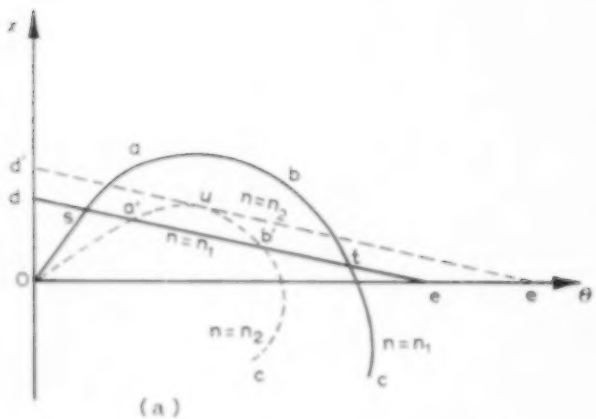

(a)

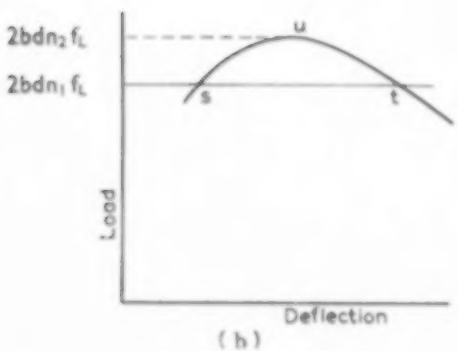

(b)

Fig. 17.

It is thus apparent that the collapse loads of elastically restrained symmetrically loaded compression members may be derived by constructing $\alpha - \theta$ charts, and noting points of tangency between the curves for the compression members and the straight lines representing the elastic restraint. The number of variables involved is too great to make any attempt at a summary worthwhile, but a typical $\alpha - \theta$ chart is shown in Fig. 18. This chart has been calculated for $\beta = 1{\cdot}0$ and a fixed value of n (0·6), taking for each contour a different value of the length L. The rotations are expressed in terms of $a\theta$ and $a\theta_0$, while the length is given in terms of $L/2ad$.

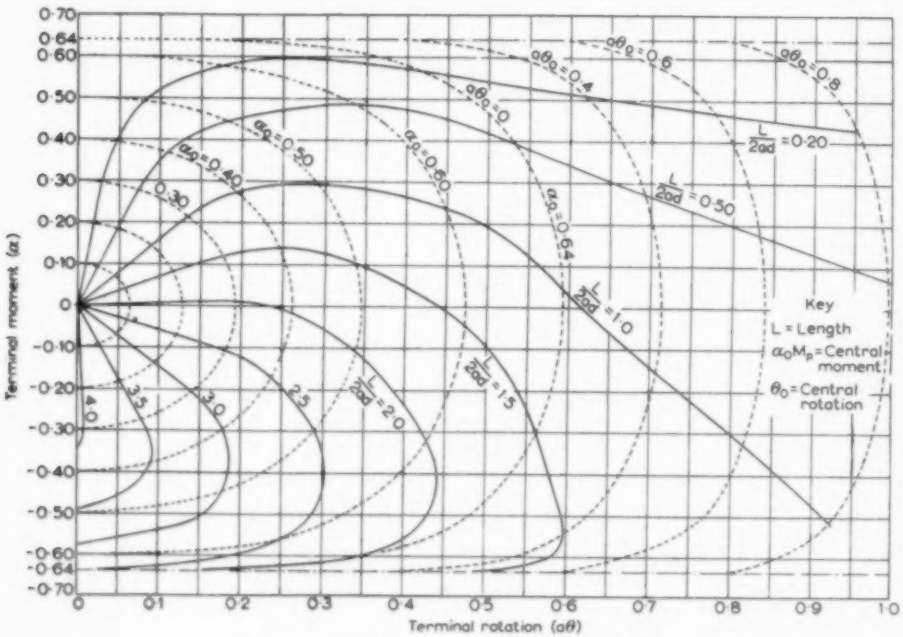

Fig. 18. $\alpha - a\theta$ curves for $n = 0{\cdot}6$, $\beta = 1{\cdot}0$.

The chart may also be used to derive collapse loads when the surrounding members in Fig. 16 are partially plastic, but in this case the lines *de* and *d'e'* in Fig. 17 (a) become curved, and very much more difficult to calculate. The case when the loading on the compression member is unsymmetrical about the mid-section *C* presents considerable difficulties, and has not been attempted.

6. Conclusions

The elastic-plastic theory of compression members outlined above leads to a better understanding of their behaviour than is possible either from a study of elastic behaviour only, or from a consideration of the elementary problem of a member loaded concentrically into the plastic range. The collapse loads of eccentrically loaded, pin-ended struts are shown to lie close to the yield-point loads for slender members, but somewhat above these loads for stocky members. There is, however, a close resemblance between the charts for the collapse and the yield-point loads (Figs. 10 and 11). The collapse loads for members with ends

fixed in given directions are shown to bear no relation to the yield-point loads, the charts for the two sets of loads having completely different forms (see Figs. 14 and 15). The condition of elastic restraint lies between the two extreme cases of terminal eccentricity with pinned ends and terminal fixity at given angles, and may be solved by constructing suitable charts (see Fig. 18). The variables involved in this problem are too numerous for general conclusions to be drawn.

NOTATION

A, B, C = constants in the equations for the primary plastic zone (see equations 8 and 10).
E = modulus of elasticity.
I = moment of inertia of section about axis of bending.
L = length of compression member.
M, M_A, M_B = bending moments.
M_p = full plastic moment under zero axial thrust.
N = constant in the equations for the secondary plastic zone (see equation 15).
P, P', P_A, P_B = axial thrust.
R_A, R_B = shear force.
a = $\sqrt{(E/3f_L)}$.
b = width of section.
d = half-depth of section.
e = eccentricity of axial thrust at end sections.
f_U = upper yield stress.
f_L = lower yield stress.
f_t = tensile stress in the extreme elastic fibres in the primary plastic zone (see Fig. 4).
k see equation (10).
m = extreme fibre elastic stress induced in a direction fixed member under zero axial load divided by f_L.
n = mean axial stress divided by f_L.
x, y = co-ordinates of the centroid at any cross-section of a member relative to axes in plane of the bending.
α = ratio of bending moment to full plastic moment under zero axial load.
α_0 = value of α at the mid-section of a member.
β = ratio of yield stresses f_U/f_L.
γ γd is the distance between the neutral axis and the edge of the plastic region in the primary plastic zone (see Fig. 4).
ξ $2\xi d$ is the depth of elastic material in a cross-section in the primary and secondary plastic zones (see Figs. 4 and 5).
λ λd is the distance between the central axis and the neutral axis in the secondary plastic zone (see Fig. 5).
θ = slope (dy/dx).
θ_0 = value of θ at the mid-section of a member.
$\theta_e, \theta_p, \theta_s$ = constants in the equations for the elastic, primary and secondary plastic zones respectively (equations 3, 8 and 15).
θ_q, ϕ see equation (10).

REFERENCES

BAKER, J. F., HORNE, M. R. and RODERICK, J. W. 1949 *Proc. Roy. Soc.* A, **198**, 493.
BAKER, J. F. and RODERICK, J. W. 1942 *Trans. Inst. Welding*, **5**, 97.
1948a *Welding Res.*, **2**, 2.
1948b *Welding Res.*, **2**, 110.
CHWALLA, E. 1928 *Sitzungsberickte d. Akademie d. Wissenschaften im Wien*, 11a, 469.
JEZEK, K. 1934 *Sitzungsber. Akad. Wiss. Wien*, **143**.
KARMAN, T. v. 1908 *Physikal. Z.*, **9**, 136.
SHANLEY, F. R. 1947 *J. Aero. Sci.*, **14**, 261.

Journal of the Mechanics and Physics of Solids, 1956, Vol. 4, pp. 121 to 127. Pergamon Press Ltd., London.

YIELDING IN COMPRESSION OF STRIP BETWEEN SMOOTH DIES

By B. B. Muvdi and K. N. Tong
Metallurgical Research Laboratories, Syracuse University

(*Received 5th December*, 1955)

Summary

This paper describes an experiment in compressing a flat high-strength steel between two smooth dies. The object was to compare the yielding loads determined experimentally with those from analysis based upon the plastic-rigid theory of plasticity. Except for very thin plates where the experimental scatter obscures the test results, it was found that the theory and experiments agree well.

1. Introduction

Under the assumption of an ideally plastic-rigid material, the mathematical theory of plasticity has succeeded in obtaining solutions to many problems in plane strain by the method of characteristics or slip lines. While such solutions should give fairly accurate descriptions of an actual steady-state process or of a non-steady-state process after a certain amount of plastic deformation has taken place, their validity in predicting the beginning of plastic flow is not entirely certain. This is because in an analysis based upon the plastic-rigid theory the starting slip-line field generally does not correspond to the elastic stress distribution established by loading from a stress-free state. For instance, in the indentation of a semi-infinite block by uniform pressure distributed along an infinite strip of width b, on the surface, the theory of elasticity gives the yielding load per unit length along the strip to be πbk (Sneddon 1951) where k is the yield stress in pure shear, while the starting slip-line field for the same problem in the plastic-rigid theory corresponds to a load of $(2 + \pi)\, bk$ (Hill 1950). Although at the termination of the purely elastic process, there could be no observable plastic deformation in the specimen, it is rather certain that the plastic region produced by a further steady increase of the pressure to a value of $(2 + \pi)\, bk$ would be substantially different from that postulated in the plastic-rigid theory (Hill 1950). Therefore, the validity of predicting the load at which visible plastic deformation begins by the use of the plastic-rigid theory needs to be experimentally verified. Aside from purely academic interest, the validity of the theoretical solution would furnish a simple means for the determination of yield strength of strip materials. Early experimental work, (Nadai 1921; Sachs 1927; Körber and Siebel 1928; Mesmer 1930) performed after Prandtl (1921) first suggested the possible slip-line fields for the problem, was mostly devoted to the study of the geometry of the plastic region. Recently Watts and Ford (1952) performed tests on specimens

of cold-rolled copper and cold-rolled brass. They reported yielding loads determined from the experiments to be within ± 1 per cent. of the theoretical predictions. This is particularly astounding in view of the anisotropy of the materials used.

This paper describes the determination of the yielding load in compressing a strip between smooth dies. The yielding load is a function of the ratio of plate

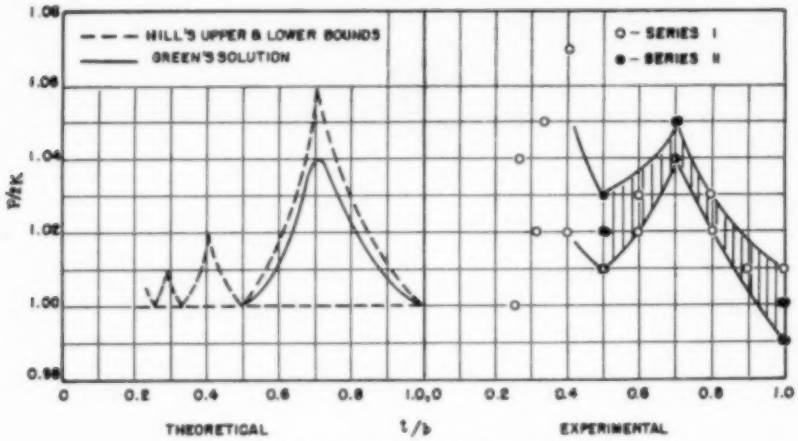

Fig. 1. Variation of $p/2k$ with t/b. $(t/b \leqslant 1)$.

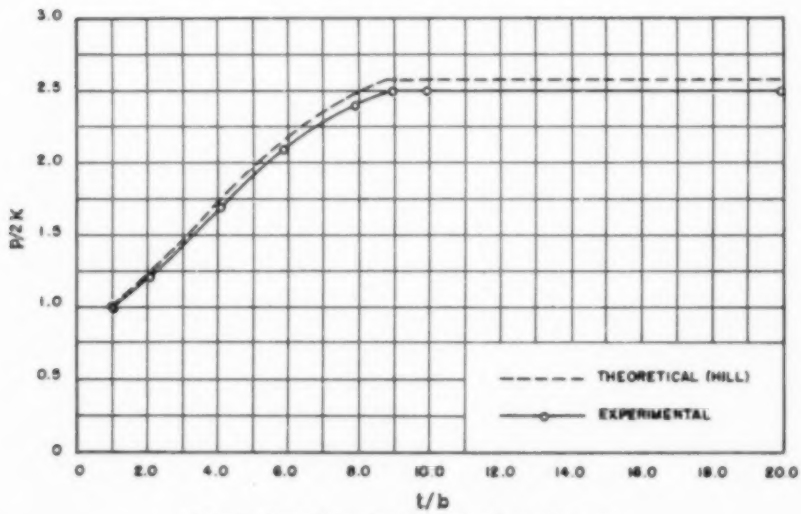

Fig. 2. Variation of $p/2k$ with t/b. $(t/b \geqslant 1)$.

thickness to die breadth, t/b. The plastic-rigid theory gives the relations shown in Figs. 1 and 2 (Hill 1950; Green 1951). The corresponding slip-line fields are presented in Fig. 3.

The present work differs from that of Watts and Ford in the test procedure used as well as in the material investigated. It is undertaken to determine a

suitable technique to be used on specimens of higher-strength ferrous metals as well as to verify the validity of the theoretical analysis when applied to such metals.

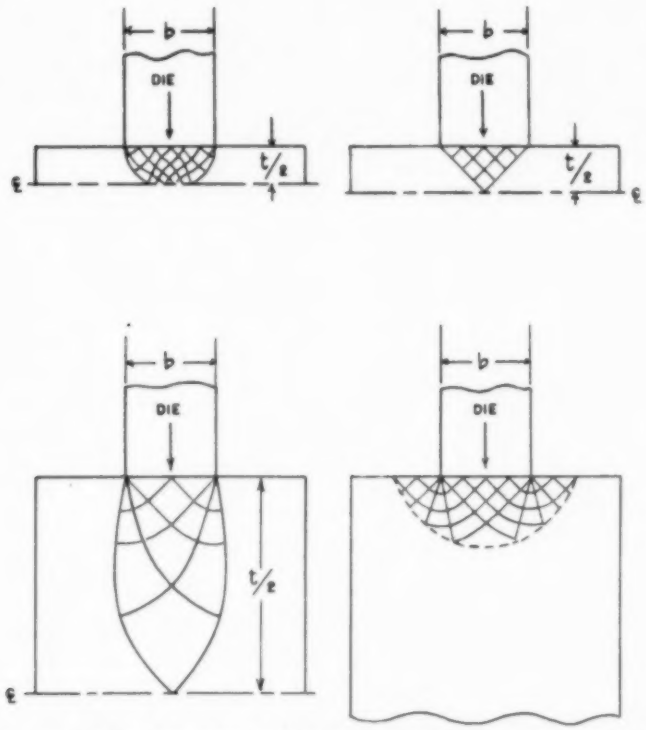

Fig. 3. (a) Slip-line field at the yield point for the range $1/2 < t/b < 1$ (Green).
(b) Slip-line field at the yield point for $t = b$ (Hill).
(c) Slip-line field at the yield point for the range $1 < t/b < 8{\cdot}75$ (Hill).
(d) Slip-line field at the yield point for a semi-infinite block $t/b > 8{\cdot}75$ (Hill).

2. Procedure

Material and Specimens

The material used in this investigation is a 0·1 per cent. carbon, 5 per cent. chromium, tool steel known under the trade name of "Supersamson." It also contains 0·9 per cent molybdenum and 0·25 per cent. vanadium. It has a well-defined yield strength but no sharp yield point, and is much less anisotropic than cold-rolled materials.

The specimens were sliced off from a 1in. × 1in. square hot-rolled bar stock and heat-treated at 1,750°F for 1h., air-cooled and tempered at 1,200°F for 1h. to yield a hardness of 21 Rc. They were subsequently surface-ground to proper dimensions and hand-polished with No. 3/0 emery paper to a smooth surface finish. The finished specimens measured 1in. wide and 1in. long, and varied in thickness from 0·0220in. to 1·0080in. corresponding to t/b ratios of about 0·20 to 20*. The thickness dimension of the specimens was along the axis of the original bar.

* The 1·0080 in. specimen was indented by one punch only while the other face rested on a rigid surface. Hence, the equivalent thickness was twice the actual thickness.

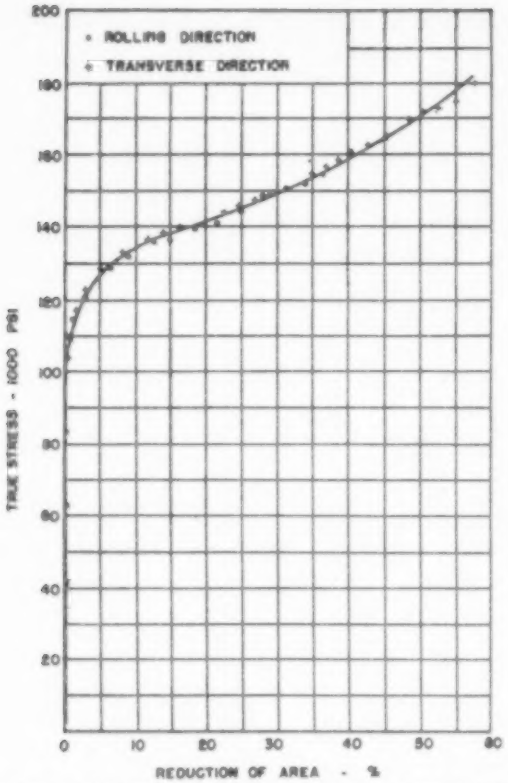

Fig. 4. True stress-reduction of area diagram for the material used in series I.

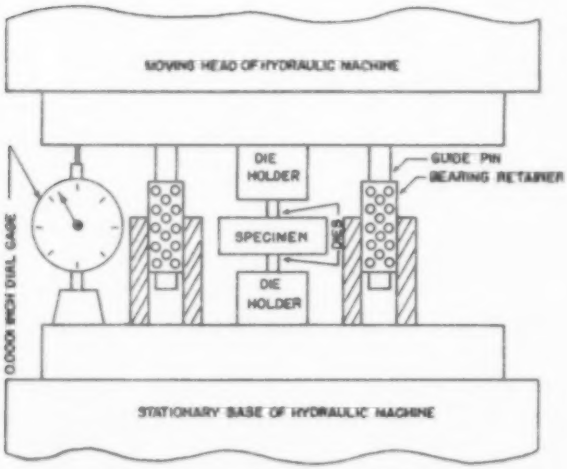

Fig. 5. Schematic diagram of die set.

Tensile specimens were also obtained from the same bar along and perpendicular to the direction of rolling. The results of the tension tests, shown in Fig. 4, indicate negligible anisotropy in the material.

Apparatus

The apparatus used is shown schematically in Fig. 5. It consists of a precision, antifriction, die set modified to take two rectangular carboloy indenters. The indenters measured 0·101in. in width, $1\frac{9}{16}$ in. in length and $\frac{3}{16}$ in. in height, and were provided with carefully polished flat surfaces. The die set was placed between the heads of a universal hydraulic testing machine with the centre line of the indenters collinear with the axis of the heads of the machine.

A dial gauge, graduated to 0·0001in., was used to measure the indentation depth.

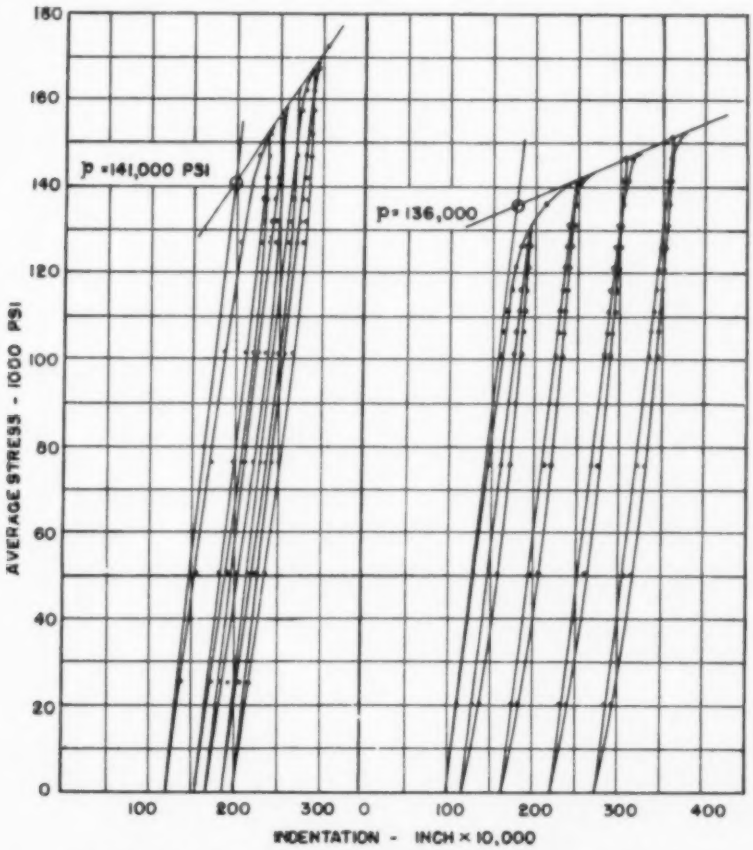

Fig. 6. (a) Stress-indentation curve for $t/b = 0{\cdot}265$ – series I.
(b) Stress-indentation curve for $t/b = 0{\cdot}998$ – series I.

Tests Performed

In this investigation two different series of tests were performed. Series I covered the range $0{\cdot}217 \leqslant t/b \leqslant 19{\cdot}910$, while series II covered the range

$0.497 \leqslant t/b \leqslant 1.000$. Series II served to check certain results obtained in Series I. Except for a slightly higher hardness reading (26 Rc) the material used was the same as that used in series I (21 Rc).

Determination of Average Yield Pressure

The procedure followed can be portrayed by a typical load-indentation curve shown in Fig. 6. The specimens were indented in stages by a succession of loading and unloading cycles. The maximum load in each cycle was maintained for a duration of about 10 sec. The purpose of breaking up the loading process was two-fold : (i) to reduce friction by repeated applications of a dry lubricant, molybdenum disulphide, to all the contact surfaces after each loading and (ii) to establish a consistent elastic modulus for the specimens and the assembly. It was observed that the elastic portion of the loading curve had a smaller slope in the first cycle than those in the subsequent ones, which had essentially the same elastic modulus considered as the true elastic modulus. This change in the slope after the first loading cycle may be due to the removal of surface imperfections as well as a slight amount of initial warping and misalignment in the specimens.

As apparent from Fig. 6, the plastic portions of each cycle have a straight-line envelope which intersects another straight line drawn through the point of zero indentation with a slope equal to the true elastic modulus defined above. The average indentation pressure corresponding to this point of intersection was taken to be the yield pressure of the specimen tested. Watts and Ford took the intercept of the envelope at the ordinate on the stress axis to be the average yield pressure. Owing to the relatively large amount of strain hardening in the steel used, this definition was considered to be unsatisfactory for the present work.

Determination of the Yield Strength of the Material

In order to present the results in a useful non-dimensional form, it was necessary to determine the yield strength k of the material in pure shear (plane strain). To avoid the inaccuracy inherent in tension or compression tests of small specimens, as well as to avoid the choosing of a yielding criterion, it was decided to take the value $2k$ to be the average yield stress of a specimen with $t/b = 1$ as postulated by Hill's theory. The value thus obtained was 135,000 psi for series I and 150,000 psi for series II.

3. Results and Discussion

The results of the two series of tests performed in this investigation are presented in dimensionless form in Figs. 1 and 2. Fig. 1 shows the results for $t/b \leqslant 1$, while Fig. 2 assembles the results for $t/b \geqslant 1$. In both instances the theoretical solutions arrived at by Hill and Green are also presented.

It can be seen that for thicker specimens ($t/b > 0.6$) the experimental results agreed well with the theoretical predictions. For the thinner ones ($t/b < 0.6$) the experimental scatter overshadowed the theoretically expected variation which was less than 2 per cent. The slightly larger scatter in the thinner specimens could be due to the larger effects of surface irregularities in the indenters and in the specimen, of the misalignment and friction ever present, and of the strain hardening

of the material. It is interesting to note, however, that for t/b greater than one the experimental values fell consistently below the theoretical curve, while the reverse was true for t/b less than one. The experiment also showed that the limiting condition of a semi-infinite block was reached at about the theoretical value of $t/b = 8{\cdot}75$, in spite of the elastic deformation of the material outside the plastic region.

Acknowledgments

The work described in this paper was carried out in the Metallurgical Research Laboratories, Syracuse University, under the direction of Dr. G. Sachs and Dr. E. P. Klier, and was sponsored by Watertown Arsenal Laboratory under contract DA-30-115-ORD-376. The authors wish to thank Dr. R. Beeuwkes Jr. of Watertown Arsenal for his valuable suggestions.

References

Green, A. P.	1951	*Phil. Mag.* (7), **42**, 900.
Hill, R.	1950	*Mathematical Theory of Plasticity*, pp. 254-257. (Clarendon Press).
Korber, F. and Siebel, E.	1928	*Mitt. Kaiser Wilhelm Inst. Eisenfor., Dusseldorf*, **10**, 15.
Mesmer, G.	1930	*Tech. Mech. Thermodynamik*, **1**, 85.
Prandtl, L.	1921	*Z. ang. Math. Mech.*, **1**, 15.
	1923	*Z. ang. Math. Mech.*, **3**, 401.
Sneddon, I. N.	1951	*Fourier Transforms*, p. 408 (McGraw-Hill).
Watts, A. B. and Ford, H.	1952	*Proc. Inst. Mech. Eng.*, **1B**, 448.

Journal of the Mechanics and Physics of Solids, 1956, Vol. 4, pp. 128 to 144. Pergamon Press Ltd., London.

INITIAL PLASTIC YIELDING IN NOTCH BEND TESTS

By A. P. Green* and B. B. Hundy†

(*Received 9 November*, 1955)

Summary

Theoretical plane-strain solutions are presented for the initial plastic yielding of notched bars bent either under four-point loading or as in the Izod or Charpy tests, and having either a V notch or a notch whose root is a circular arc. These solutions provide estimates of the stresses in the plastic regions, the mode of yielding, and the corresponding yield-point loads. Calculations are made of the maximum tensile stress below the notch root and of the smallest depth of notch for which initial yielding does not extend to the notched surface. The theoretical solutions are confirmed by experimental observations of the yield-point loads in slow bend tests, and of the modes of deformation in slow and impact tests; the latter are found to be very similar. The ductility transition is discussed in relation to this and other work.

1. Introduction

Since the early part of the present century notch bend tests of various types, particularly impact tests, have come to play an increasingly important role in the testing of metals, and many hundreds of Charpy and Izod tests, the most popular of these, are carried out each day. The aim of these tests is to assess the "toughness" of the metal, i.e. its ability to resist fracture under severe conditions of fabrication or service; with steels this often includes the estimation of a transition range of temperature below which the energy absorbed in the test is low and the metal behaves in a dangerously brittle manner under the high triaxial state of stress that may occur in the vicinity of a notch, groove, sharp angle, or fillet.

In spite of their extensive use, no complete theory of such tests has yet been formulated. Without a fundamental understanding of the test it is, of course, difficult to assess its precise physical significance in relation to the fabrication or use of the metal which is tested. A separate empirical assessment of the test results has to be made for each separate application, and this, although valuable, is a lengthy and expensive process which still leaves the situation somewhat obscure.

Unfortunately even a qualitative analysis of the tests is difficult because the behaviour of a test specimen depends in a complex way on so many factors. For example, it depends in the first place on the shape of the specimen and the system of loading used; it depends on the elastic and plastic properties of the metal and on the laws governing its brittle and ductile fracture; and these properties in turn depend on the speed and temperature at which the test is carried out.

* Tube Investments Research Laboratories, Hinxton Hall, Cambridge.
† Steel Peech and Tozer branch of the United Steel Companies, Sheffield.

The present paper is concerned in detail with only one aspect of the problem : the macroscopic plastic deformation and stresses in the plastic regions of the specimen which occur in the initial stages before fracture is initiated. This aspect has not been treated before in detail, but it is an essential preliminary to an understanding of subsequent fracture behaviour. Theoretical plane strain solutions for certain notched bar tests are presented, based on the assumption of a plastic-rigid materal. These solutions provide estimates of the stresses in the plastic regions, the mode of overall yielding that will occur if this is not forestalled by the start of a crack, and the applied loads corresponding to the start of overall yielding (the yield-point). Theoretical estimates are calculated of the maximum tensile stress below the notch root and of the critical minimum depth of notch for which initial yielding does not extend to the notched surface. The theoretical solutions are confirmed by experimental observations of the applied loads at the yield-point in slow bending tests, and of the plastic deformation which occurs up to this stage in both slow and impact tests. The overall deformation is shown to be very similar under slow and impact loading conditions. Finally, the relevance of this theoretical and experimental work to a better understanding of the tests is discussed.

2. Bending by Pure Couples

Let us first consider a wide rectangular bar, deeply notched through its thickness t on one side, and subjected to four-point loading so that the bending tends to open the notch (Fig. 1). The bending moment per unit width over the central length of the bar at the yield-point is denoted by M, and the thickness of the minimum section of the bar at the notch by a. The notch is assumed to be deep enough to prevent the region of plastic deformation from spreading to the notched surface of the bar before the yield-point.

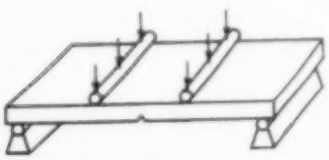

Fig. 1. Loading system for pure bending.

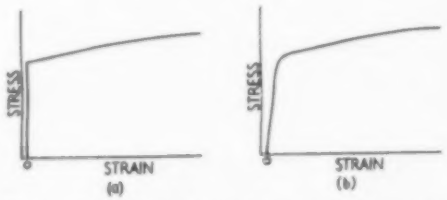

Fig. 2. Stress-strain curves for (a) a plastic-rigid material ; and (b) a real plastic-elastic material.

One of the authors (Green 1953) has obtained theoretical yield-point solutions to this problem, assuming that the material is uniform and plastic-rigid (i.e. Young's modulus is infinitely large), and that the strain is zero across the width of the bar parallel to the length of the notch (plane strain). Two shapes of notch were considered, a V notch and a notch whose root is a circular arc.

Before describing these solutions let us first compare the behaviour of a plastic-rigid notched bar with that of a similar real plastic-elastic bar, as each is bent by pure couples increasing steadily from zero. Only a qualitative comparison is possible based on a general understanding of the kind of differences that occur,

since in neither case do solutions for the complete loading sequence exist.* Uniaxial stress-strain curves for the two types of material are shown diagrammatically in Figs. 2 (a) and 2 (b).

Let τ_m be the maximum shear stress at any point and let σ be the tensile stress perpendicular to the minimum section of the bar. The moment when the bar first becomes *locally* plastic (i.e. the stresses first satisfy the yield criterion in a small element but no macroscopic plastic deformation has occurred) is known as the elastic limit. Before this, neglecting elastic changes of shape, the distribution of elastic stresses is the same in each bar for the same bending moment and could be calculated by relaxation methods. There is a stress concentration at the root of the notch; τ_m is a maximum on the surface at the root, and τ_m and σ decrease along the minimum section with increasing distance from the root. Hence, the bars first become locally plastic at the root. Subsequently the plastic-elastic boundary spreads outwards from the root, increasing in width at the notch surface and depth into the bar. It is reasonable to suppose that at some stage one or more plastic regions start to spread from the opposite flat side of the bar, and that all these regions eventually join together.

For the plastic-rigid bar the yield-point is precisely defined as the moment when deformation begins. Between the elastic limit and the yield-point the body remains entirely rigid, the plastic regions being constrained from deforming by the surrounding non-plastic material. Only when the plastic region has spread far enough to contain within itself an *overall* plastic deformation mode does deformation begin. This initial region of deformation, however, is not likely to cover the whole of the plastic region, some parts of which will still be constrained. These constrained plastic regions roughly correspond to regions in a real body where the plastic strain is of an elastic order of magnitude. The subsequent loading and deformation history depends on both the rate of hardening and the changes of shape of the bar, including of course the development of any cracks. It is important to note that at any stage before overall yielding, the stress distribution in a plastic-rigid bar can be calculated in the part of that plastic region near the notch where the state of stress depends only on the shape of the surface (HILL 1950, p. 144, and pp. 242-245).

The definition of the yield-point for a real plastic-elastic body must be somewhat arbitrary, and the plastic rigid material is not much use as a theoretical model for a material with a well rounded stress-strain curve. If, however, as in mild steel, there is a sharp bend in the stress-strain curve, after which the rate of hardening is small, there will be a corresponding sharp bend in a small loading interval in the bending moment-deflection curve for the notched bar (see Fig. 10). It is then convenient to define the yield-point load as that corresponding to the backward extrapolation of the curve immediately following the bend to the forward extrapolation of the elastic part of the curve; the initial uniaxial yield stress is defined in the same manner from the uniaxial stress-strain curve. The construction is illustrated in Fig. 10 and has been used in deriving experimental values in this paper. The yield stress for a material such as annealed mild steel which has an upper yield-point is taken to be the lower yield stress, and throughout this paper the upper yield-point is ignored.

* There is, however, a detailed approximate analysis of the spread of the plastic region in a notched plastic-elastic bar under steadily increasing tension by SOUTHWELL and ALLEN, 1950, *Phil. Trans. Roy. Soc.* A 242, 379.

The yield-point load for a real body defined as above is found to be reasonably reproducible experimentally and to correspond approximately to the theoretical yield-point load for a similar plastic-rigid body, the material of which has the same uniaxial yield stress. The *overall* deformation occurring after the elastic limit but before the yield-point is of an elastic order of magnitude due to the constraint of the non-plastic material. The *local* plastic deformation is also constrained and will usually be small; there are, however, important exceptions. In the region near the root of the notch it is clear that the local strain, when overall yielding commences, increases with decreasing r/a, where r is the radius of the notch, and it may be quite large when r/a is small, as it is in practice with a V notch. If so, the *local* stresses may be appreciably raised by local hardening under the notch, and these stresses are likely to be underestimated by methods, such as those described below, which neglect this. Nevertheless the overall pattern of yielding observed experimentally is, as we shall see, remarkably similar to that predicted for the plastic-rigid material. The sort of differences that occur are discussed later, following a description of GREEN's theoretical solutions.

These solutions take the form of slip-line fields* in the plastically deforming regions, which satisfy the boundary conditions, and consist of two families of orthogonal slip lines coinciding at all points with the directions of maximum shear stress and strain-rate (see for example Fig. 3). In the plastic region the state of stress in any element is a hydrostatic pressure p, combined with a pure shear. At the yield-point the maximum shear stress has the same value k throughout the plastic region, but p varies. The ratio of k to the yield stress in uniaxial tension Y, depends on the yield criterion e.g. $k = Y/\sqrt{3}$ or $Y/2$ for the Mises and Tresca yield criteria respectively. Once the slip-line field is known, the values of p and hence of M, and the mode of deformation, are readily calculated in the deforming region with the aid of the Hencky and Geiringer relations along the slip lines.

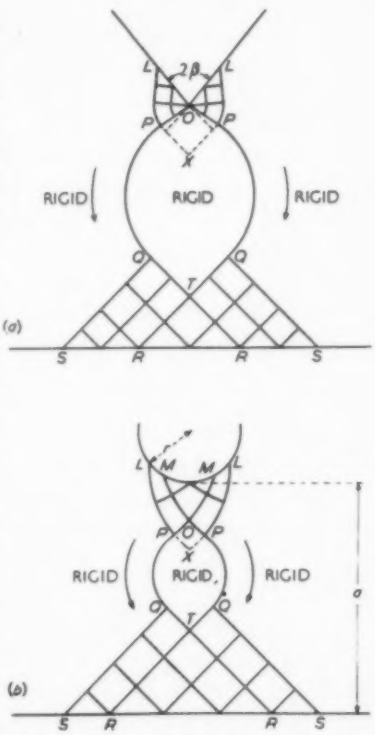

Fig. 3. Slip-line fields for pure bending with (a) a V notch, and (b) a notch with a circular root.

In Fig. 3 are shown the types of slip-line fields proposed for a bar with (a) a V notch of total angle $2\beta \leqslant 114{\cdot}6°$, and (b) a notch whose root is a circular arc of radius r, where $a/(a+r) \geqslant 0{\cdot}398$. All notch tests used in practice have notches whose dimensions fall within the limits stated, so we shall not concern ourselves here with the different types of solution proposed for less sharp notches. According to the solutions shown, there is at the yield-point a central pivot *OPQTQPO*

* For a detailed account of the theory of plane plastic strain see R. HILL, The Mathematical Theory of Plasticity, 1950, Chapters 6 and 11 (Clarendon Press, Oxford).

which remains rigid, around which the rigid parts of the bar or either side rotate by shearing over the circular arcs PQ, so that, roughly speaking, the material near the root in $LPOPL$ is stretched ($p - ve$) and that near the flat side in $SQTQS$ is compressed ($p + ve$). Thus there is a constant velocity discontinuity across the lines $(M)OPQQTR$, and along them the instantaneous rate of shear is infinite, These discontinuities correspond to what in a real slowly hardening material is a narrow band within which the strain-rate is large.

It is assumed that the yield criterion is nowhere violated in the rigid regions, where no stress distribution has been constructed. However, as was remarked above, parts of these rigid regions are likely to be incipiently plastic, and this must be taken into account in any attempt to estimate the position and value of the maximum tensile stress across the minimum section. *If* the plastic region extends below POP, the stress distribution is uniquely obtained by extending the slip-line field into this rigid region. It must be emphasized that this extension is meaningless beyond the plastic-elastic boundary, the position of which is unknown. In Fig. 3 the field for each kind of notch has been extended, as indicated by the dashed lines, as far as the slip-lines through P meeting at X on the minimum section. As far as X the field is determined only by the shape of the notch. Below PXP it depends also on the radius of the arc PQ. From the geometry of the field and the Hencky relations it can be shown (HILL 1950, p. 248) that near the notch whose root is a circular arc the slip-lines are logarithmic spirals and the tensile stress σ, perpendicular to the minimum section of the bar, is distributed *in the plastic region* according to the formula

$$\sigma = 2k\left[1 + \ln\left(1 + x/r\right)\right] \tag{1}$$

down to the point X, where x is the distance measured from the root. Below X, σ decreases. Hence, σ increases from the value $2k$ at the root to a maximum value at X, σ_X say, assuming that the plastic region extends so far. Thus the elastic stress concentration near the root is dispersed by plastic yielding, and the gradient of the distribution of σ is reversed. This process starts at the elastic limit. At any subsequent stage up to the yield-point, equation (1) is valid down to the point Y, say, somewhere between the root and X, which is the meet of the two most extreme slip lines that can be drawn from the notch surface lying entirely within the plastic region. Now it seems most likely that Y lies on the plastic-elastic boundary, and that below Y in the non-plastic region σ decreases with increasing x as it does before the root becomes plastic. Assuming that this is so, Y is the point at which σ is a maximum and the kind of distributions of σ which occur near the root, between the elastic limit and the yield-point, are shown diagrammatically in Fig. 4. If, then, the extent of the plastic region could

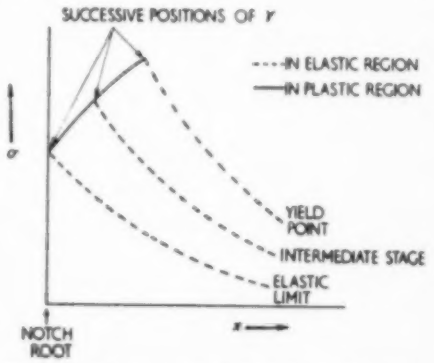

Fig. 4. Diagram of the kind of distribution postulated for the longitudinal stress, σ, across the minimum section of the bar.

be found theoretically or experimentally at any stage, this maximum value of σ can be estimated with the aid of (1). However, without a knowledge of the position of the plastic-elastic boundary we can only say that before the yield-point the maximum value of σ lies between $2k$ and σ_X, and at the yield-point it lies between σ_O and σ_X, where σ_O is the value of σ at the point O.

The situation is simpler in a bar with a V notch. By extending the slip-line field below O, we find that, between O and X,

$$\sigma = 2k\left[1 + \pi/2 - \beta\right] = \text{constant} \tag{2}$$

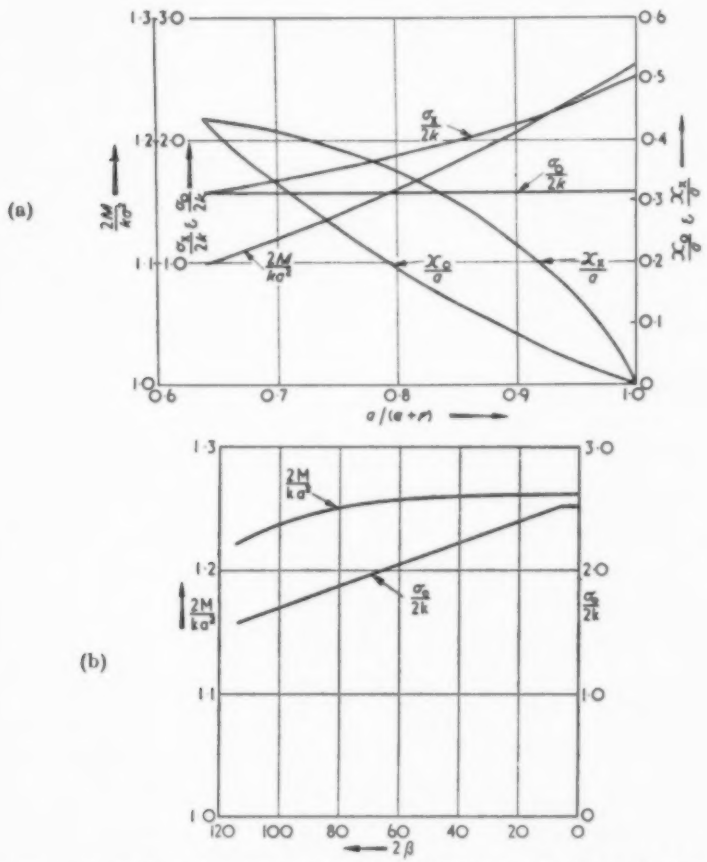

Fig. 5. Theoretical calculations for pure bending with (a) a notch with a circular root, and (b) a V notch.

and that below X, σ decreases (incidentally X coincides with O if $\beta \leqslant 3{\cdot}2°$). Therefore, neglecting work-hardening, the maximum value of σ is given by equation (2) between the elastic limit and the yield-point. In practice, of course, a so-called V notch has a small but finite curvature at its root, with the result that the maximum value of σ actually occurs a very short distance below the root, the stress gradient being large between this point and the surface ; the stress-distribution and deformation elsewhere will not be much affected.

The theoretical results for circular notches are given in Fig. 5 (a). The constraint factor $2M/ka^2$ is plotted against $a/(a+r)$. This factor is the ratio of M to the yield-point moment per unit width for an unnotched bar of the same cross-section as that of the notched bar at its minimum section. Plotted against $a/(a+r)$ on the same figure are $\sigma_O/2k$, $\sigma_X/2k$, x_O/a, and x_X/a, where x_O and x_X are the distances measured from the notch root to O and X respectively. Similarly for V-notched bars, $2M/ka^2$, and $\sigma_O/2k = \sigma_X/2k$ are plotted against 2β in Fig. 5 (b).

Tests were carried out on V-notched specimens of mild steel to check the accuracy of the theoretical predictions of mode of deformation and constraint factor (see GREEN 1953 for full details). Fig. 6 (a) shows the region of plastic deformation obtained when a wide specimen with a 60° notch was bent in the manner shown in Fig. 1. This region was revealed by bending the bar past the yield-point, ageing it at 250°C for 30 minutes, polishing a section cut from the centre down to 2/0 emery paper, and etching this section in a mixture of 45 g cupric chloride, 180 ml hydrochloric acid, and 100 ml water. All the experimental patterns of yielding shown in this paper were produced in this way. The etching darkens the regions of plastic deformation and is believed to be sensitive down to plastic strains of an elastic order of magnitude. One would therefore expect the pattern to cover most if not all of the plastic region, i.e. to extend beyond the region of deformation predicted by the theory for a plastic-rigid material. If Fig. 6 (a) is compared with Fig. 3 (a) it can be seen that the overall mode of deformation is close to that suggested by the theoretical slip-line field; though, as one would

TABLE 1.

Comparisons of the theoretical and experimental yield-point load for pure bending of a bar with a 60° notch.

Metal	*Theoretical Bending Moment per inch width at Yield*	*Measured Bending Moment per inch width at Yield*
	(*ton. in.*)	(*ton. in.*)
Cold Worked Copper	0·700	0·715
Annealed Copper	0·048	0·049
Annealed Stainless Steel	0·860	0·770

expect in practice, the single arc PQ is replaced by a narrow band. The detailed appearance of the experimental pattern was found to depend on the amount of plastic strain to which the specimen was subjected. Fig. 6 (b) shows the pattern obtained when a similar specimen to that shown in Fig. 6 (a) was bent only very slightly past the yield-point; the overall pattern is roughly the same as in the more severely bent specimen and even closer to the theory, though not all of the theoretical deformation zone has yielded at this stage. This " banded " mode of yielding is typical of yielding in a mild steel with a sharp yield-point such as that used in this work (HUNDY 1954).

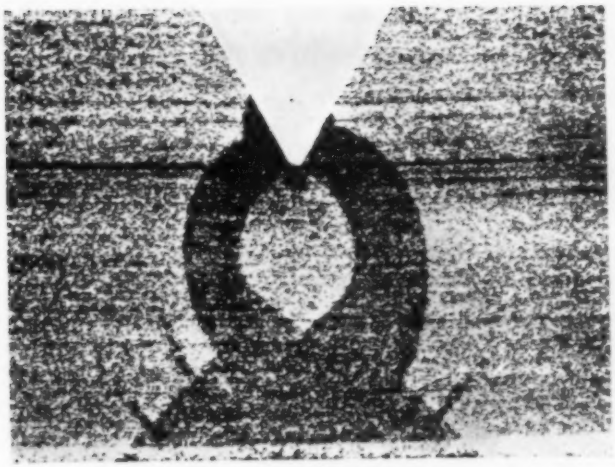

(a)

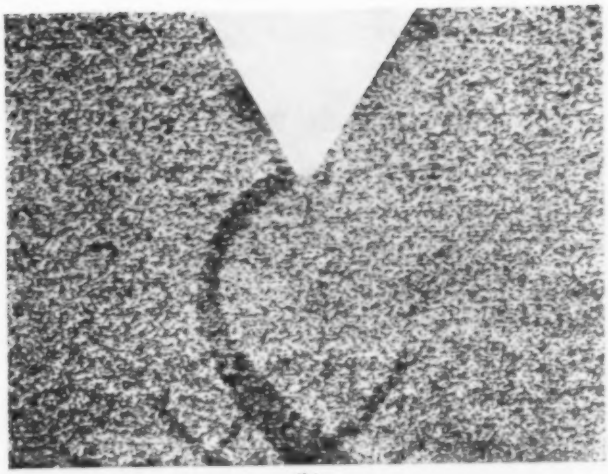

(b)

Fig. 6. Deformation patterns for pure bending with a V notch ; (a) well past the yield-point, (b) close to the yield-point.

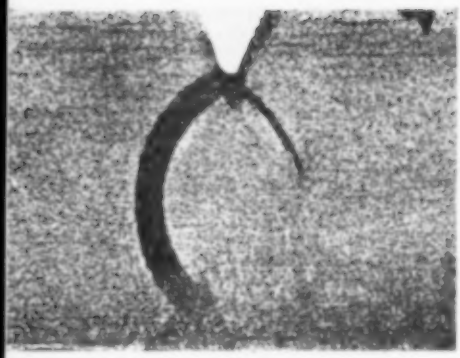

(a)

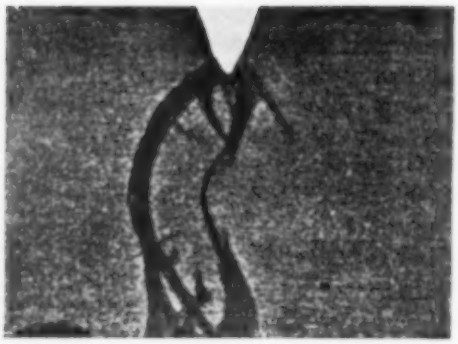

(b)

25′

(c)

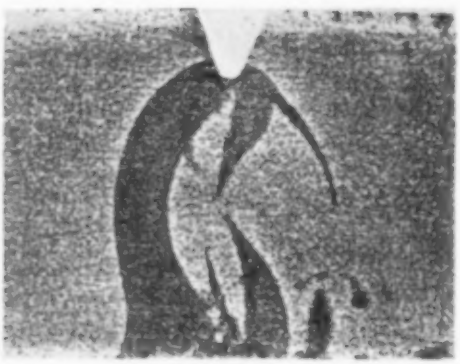

(d)

50′

(e)
Centre

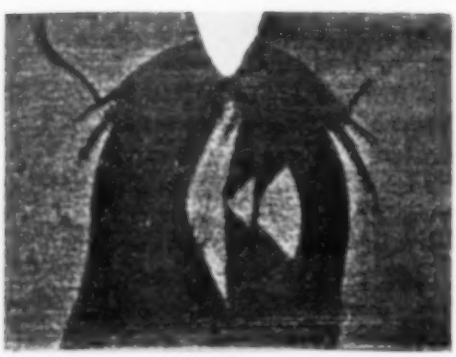

(f)
Outer edge

2°40′

Fig. 9. Deformation patterns for slow Izod tests.

Table 1 compares the theoretical bending moments at the yield-point for a 60° notched bar with those measured in experiments with annealed and work-hardened copper and annealed stainless steel specimens. There is good agreement between theory and experiment with the copper specimens, but not so good with the stainless steel. However, only the work-hardened copper corresponded closely to the theoretical plastic-rigid material with a sharp yield-point, and the good agreement for the annealed copper is probably fortuitous.

3. Izod and Charpy Tests

The general parts of the discussion in the previous section are immediately applicable to the Izod and Charpy notch bend tests, and only the points of difference are dealt with in this section. As before, yielding starts at the root of the notch, and σ may be estimated by means of (1) or (2), provided that the assumption of plane strain is not greatly in error. The systems of loading are, however, different, and this affects the overall mode of deformation and stress distribution, including the position of the plastic-elastic boundary. We now consider the two tests separately.

(a) *The Izod Test*

The Izod test is probably the most popular of the many notched bar impact tests used in Great Britain. The specimen has a square cross-section* with a 45° notch on one face. It is firmly clamped in position and direction up to the minimum cross-section and is loaded as a cantilever so that the impact load opens the notch. The details of the specimen and manner of testing are shown diagrammatically in Fig. 7 (a).

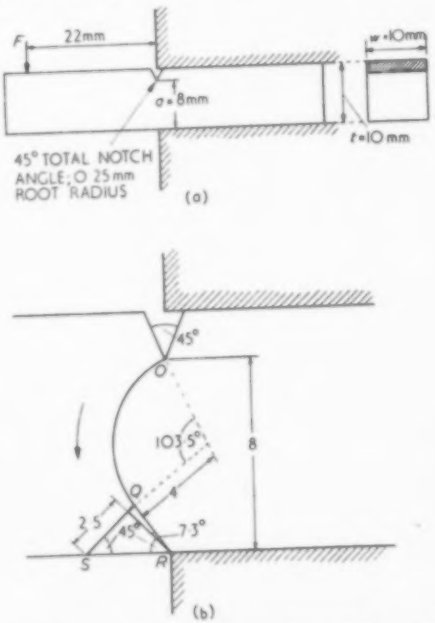

Fig. 7. The Izod tests; (a) specimen and loading system, (b) slip-line field (all dimensions in mm).

Let us for the moment ignore any complications which may arise because of the impact loading conditions and consider the problem as quasi-static. The effect of impact conditions is discussed later. The slip-line field solution is shown in Fig. 7 (b). The assumption of plane strain may appear at first sight to be far too crude an approximation for such a narrow specimen, but the experimental results described below suggest otherwise. In constructing the field it was also assumed that the clamped part of the bar remains entirely rigid, that the notch is perfectly sharp and is sufficiently deep for initial overall yielding not to spread to the surface on the notched side, and that there is a stress singularity at the

* Sometimes a specimen of circular cross-section is used but this type is not considered here.

point R on the flat surface where the clamping block ends. Apart from the latter the form of the field was suggested by and is similar to one half of that for pure bending of a similar bar; the deformation is also similar. The dimensions of the field which are given in Fig. 7 (b) are governed by the conditions that the longitudinal load is zero and that the yield-point bending moment M is related to the shear load F, by the equation $M/F = 22$ mm. From equation (2) the maximum stress σ_O just below the notch root is $\sigma_O = 4{\cdot}36\,k$. The value of F/wa is found to be $0{\cdot}223\,k$, where w is the width of the bar.

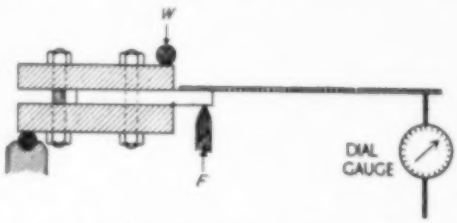

Fig. 8. Experimental set up used for Izod tests.

To check the theory, standard square Izod specimens of mild steel were bent slowly, using an Amsler Universal testing machine. The method of loading is shown in Fig. 8. The deflections were measured by means of a dial gauge situated as shown, and load-deflection curves were plotted for three specimens. After being bent to various amounts, the specimens were sectioned, polished and etched to reveal the plastic regions in the centre of the bar and on the outer faces. Small compression specimens were cut from the unstrained portions of the bars, and were tested under good conditions of lubrication to determine the uniaxial yield stress, Y.

TABLE 2.

Comparison of theoretical and experimental yield-point loads for the Izod and Charpy tests.

Test	F/wa (tons/in^2)	
	Theory	*Experiment*
Izod V-notch	2·09	2·07 2·11 2·15
Charpy V-notch	2·15	2·01 1·98
Charpy Keyhole Notch	1·32	1·31 1·30

Fig. 9 (a) shows the deformed region in the centre of a specimen bent only slightly past the yield-point, and comparing this with Fig. 7 (b) it can be seen that the theoretical slip-line field is closely confirmed. In more severely bent bars (Figs. 9 (c), (e)) the deformed region spread further into the previously elastic region below the notch, and the circular band of shear broadened; in the most severely deformed bar (Fig. 9 (e)) a second circular shear band formed and yielding also extended to the notched surface of the bar. This new mode of deformation started at a load of about 20% above the yield-point load. The deformed regions

on the outer faces of the specimens (Figs. 9 (c), (d), (f)) are similar to those in the centre of the bar, though they show certain differences. The main difference is that at the outer faces the material yields to a greater extent below the notch.

A typical load-deflection curve for an Izod specimen is shown in Fig. 10 ; the yield-point is quite sharply defined. In Table 2 the experimental values for F/wa are compared with the theoretical value which was calculated using the mean value of $k = 9{\cdot}38$ tons/in^2 obtained from the compression tests, assuming the Mises yield criterion ($Y = \sqrt{3}k$).

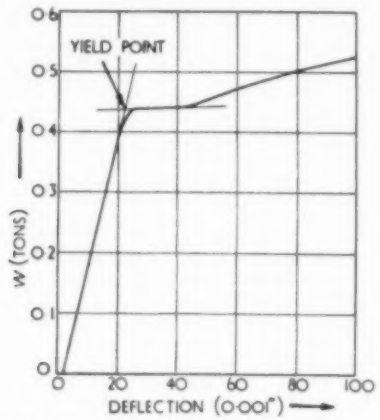

Fig. 10. A typical load-deflection curve for an Izod specimen.

The good agreement between theory and experiment for the overall pattern of yielding and the yield-point loads justifies the assumptions made in constructing the slip-line field, and in particular the basic assumption of plane strain, though the magnitude of σ will, of course fall off near the outer faces. The reasons why conditions approximate so closely to plain strain are thought to be firstly that the breadth of the region of deformation is everywhere considerably smaller than the width of the bar, and secondly that the tendency for lateral contraction in the stretched part of the bar is opposed by the tendency for lateral expansion in the compressed part.

(b) *The Charpy Test*

The Charpy notch impact test, which is probably the most widely used of all notch tests, differs from the Izod test in two main ways : (i) the specimen is loaded as a beam under symmetrical three-point loading instead of as a cantilever ; and (ii) the notch is either a V notch or a keyhole type (circular root). There are other minor differences such as the speed of testing, but we are not concerned with those here. The details of the specimen and manner of testing are shown diagrammatically in Figs. 11 (a) and (b).

The slip-line fields constructed for the quasi-static problem for both shapes of notches are shown in Figs. 11 (c) and (d). Half the field for the V-notched bar is identical in form to that for the Izod test, though slightly different in dimensions since the end loads are applied at 20 mm instead of 22 mm from the minimum

section; the other field is similar except near the notch. In practice the central load would have to be supported over a finite length of surface spanning the point R and local deformation would fit the load 'point' to this surface. Thus the two singularities shown coinciding at R in Fig. 11 (c) and (d) should be separated by a small distance; in fact, with them coinciding, the yield criterion is certainly violated in the 'rigid' corner QRQ (Hill 1954). However, the effect of neglecting this local disturbance is not likely to lead to much error in the overall pattern or loads, or in the stress distribution towards the notch root.

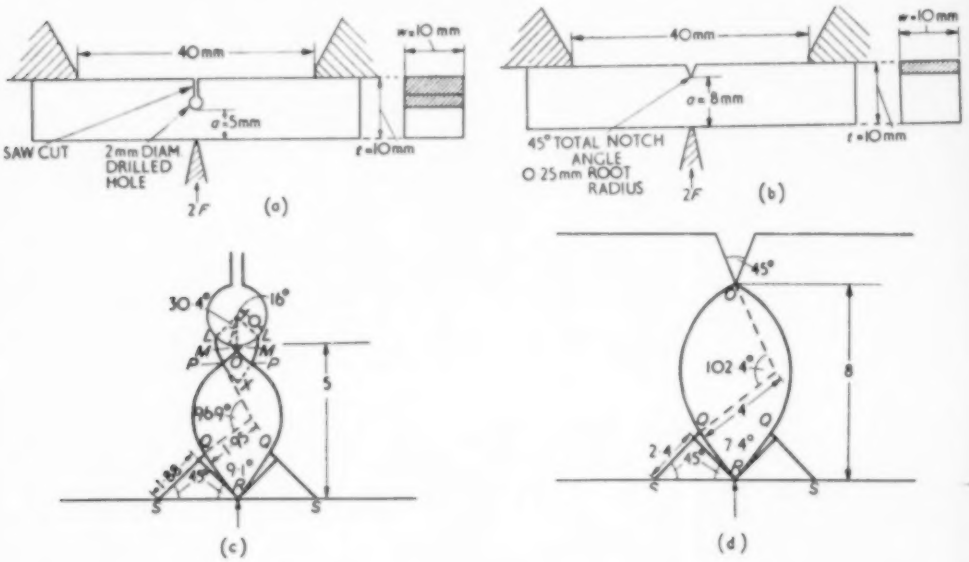

Keyhole notch. V notch

Fig. 11. The Charpy test. (a) and (b)—Specimen and loading system. (c) and (d)—Slip-line Field (all dimensions in mm).

With the same notation as in Section 2, σ_O and σ_X are found from (2) to be $1{\cdot}50\,k$, and $3{\cdot}62\,k$, for the keyhole notch, and these values occur at distances $x_O = 0{\cdot}06a$ and $x_X = 0{\cdot}23a$ below the notch root; at the yield-point $F/wa = 0{\cdot}151k$. For the V notch, $\sigma_O = 4{\cdot}36\,k$, the same as in the Izod test, and $F/wa = 0{\cdot}242\,k$.

Slow bending Charpy tests were carried out on mild steel specimens of both types, using an Amsler testing machine, with a dial gauge below the notch to measure deflections. Figs. 12 (a) and 13 (a) show that the modes of deformation at the central sections, for specimens bent only just past the yield-point, agree closely with the theory (c.f. Figs. 11 (c), (d)). The main difference is that deformation extends below the notch into the theoretically rigid region, and this is much more noticeable at an early stage in the specimen with a keyhole notch. The patterns for severely bent specimens (Fig. 12 (c), 13 (c)) show that, as in the Izod test, the region of deformation spreads as bending continues, but that only in the V-notched specimen does it eventually extend to the notched surface. The patterns on the outer edges of the specimens (Figs. 12 (b), (d), and 13 (b), (d))

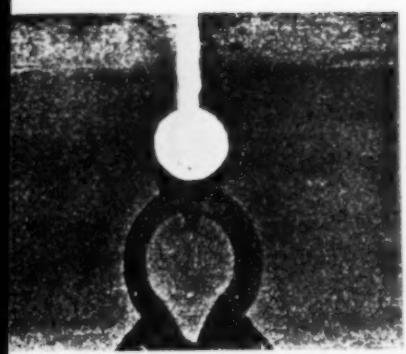

(a)

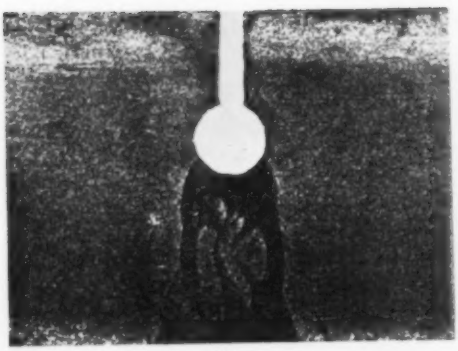

(b)

35′

Angles of bending

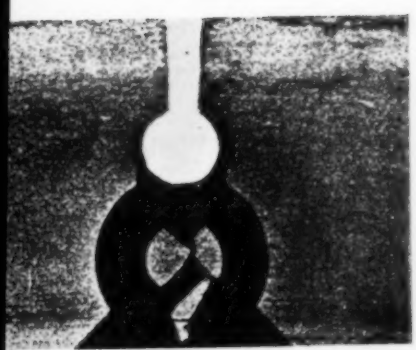

(c)
Centre

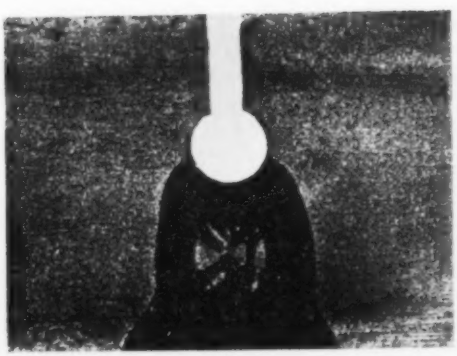

(d)
Outer edge

1°20′

Fig. 12. Deformation patterns for slow Charpy tests (keyhole notch).

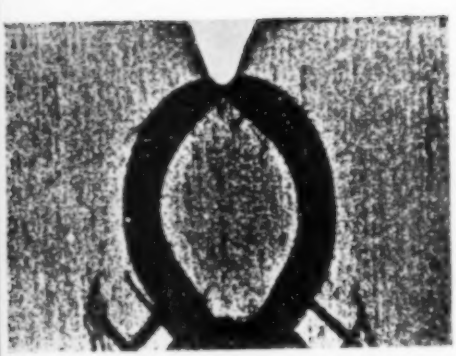

(a)

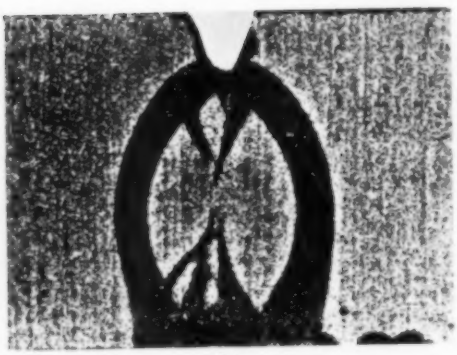

(b)

35′

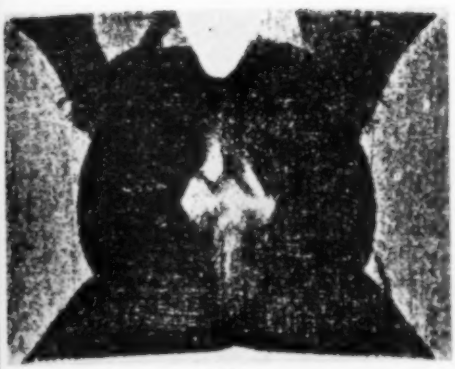

(c)
Centre

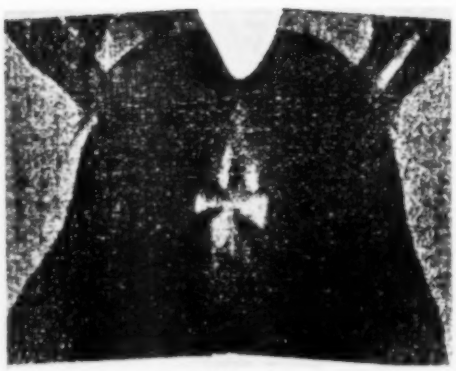

(d)
Outer edge

2°20′

Fig. 13. Deformation patterns for slow 3′ Charpy tests (V notch).

exhibit the same kind of differences from those at the central section as were observed in the Izod specimens.

The yield-point loads F were quite sharply defined on the load-deflection curves, and were found to be in reasonably good agreement with theory. The comparison is made in Table 2; the theoretical values were calculated using mean values of $k = 8{\cdot}90$ tons/in^2 (V notch), and $k = 8{\cdot}74$ tons/in^2 (keyhole notch), obtained from compression tests.

4. The Effect of Impact and Temperature

The experiments described so far show that the slip-line field theory predicts with reasonable accuracy the overall modes of deformation and yield-point loads for notched mild steel bars bent slowly at room temperature. Before this theory can be applied to notch impact testing, however, it is necessary to enquire whether its predictions are still valid under conditions of impact loading and at temperatures lower than room temperature.

A few Charpy V notch specimens were tested under impact conditions, using an Avery impact machine, to investigate their modes of deformation. The first tests were carried out at room temperature (22°C). The hammer was released from heights such that (i) 2ft. lb., and (ii) 6 ft. lb., of energy were absorbed in bending the specimens. Since neither specimen broke, the energy was all absorbed in plastic and elastic deformation. The deformation patterns revealed by etching are shown in Fig. 14. The overall mode of deformation was very similar to that which occurred in the slow tests at room temperature (Fig. 13). The main difference is that the pattern in the impact specimens is more diffuse, containing a network of fine bands with undeformed material in between : these bands, at least on the central section, appear to run in the directions of maximum shear stress, i.e. they coincide with the theoretical slip-line directions.

Two other Charpy V-notch specimens were then broken in impact at − 15°C and − 50°C. The former specimen absorbed about 8 ft. lb. of energy, and its deformation region is shown in Fig. 15. Even at this low temperature plastic deformation occurred along the circular slip-line before fracture took place across the minimum section. The deformation pattern appears to be identical to that in the specimen tested in impact at room temperature (Fig. 14). The specimen broken at − 50°C absorbed only about 3 ft lb. of energy, examination of it after etching showing that the bulk of it had not been deformed plastically before fracture, though local deformation had occurred around the root of the notch and the part hit by the striker. The fracture appeared to be entirely brittle. A taper section revealed that there was also a thin band, about 0·01 in. thick, of yielded material running along the fractured surface, which was presumably caused by the propagation of the fracture.

These experimental results are discussed in Section 6.

5. Critical Notch Depth

The results obtained with the slowly bent Izod and Charpy V notch specimens show that if the bar is bent far enough, yielding will eventually spread to the

notched surface of the bar. If the notch was very shallow, then the initial overall yielding pattern would differ from that in a specimen with a deep notch, and would extend to the notched surface in a manner similar to that shown in Figs. 9 (e) and 18 (c). Now, in order that the stress distribution across the minimum section should be independent of the precise depth of the notch it is important to confine the initial deformation to the material below the notch. It is of some interest, therefore, to find the critical minimum depth of notch above which the initial deformation does not extend to the notched surface, but below which it does.

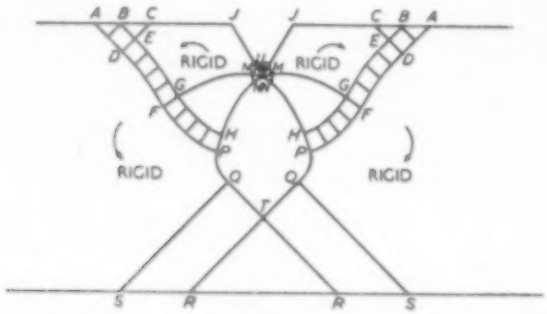

Fig. 16. Form of the slip-line field for pure bending with a shallow V-notch.

The form of the slip-line field when yielding extends to the surface was first suggested by etched patterns (Fig. 17) obtained on bars with shallow V notches bent by pure couples (HUNDY 1954). The type of field for this loading system is shown in Fig. 16, and is discussed in detail in another paper (GREEN 1956). The solutions given for the Izod and Charpy tests may be modified in a similar manner. Deformation extends over the whole field, the material in *ABHP* undergoes simple shear, and the rigid part *CJLMGE* rotates at a smaller angular velocity than the corresponding rigid end of the bar, but in the same direction. As the depth of the notch is decreased the straight slip lines between *ADFP* and *BEGH* decrease in length until at the critical depth their length is zero, yielding does not extend to the surface, and the solution in the centre of the bar is the same as that already proposed for deep notches.

From this type of solution, the critical ratio of the thickness of the bar t to the thickness at the minimum section a is deduced to be $t/a = 1{\cdot}39$, for a bar with a 60° V notch bent by pure couples, and $t/a = 1{\cdot}22$ for a bar with a 45° notch bent as in the Izod test. The latter value should be a reasonable approximation for a similar bar bent as in the Charpy test, since the ratio M/F differs by only 10% from that in the Izod test.

Slow bending tests were carried out on wide specimens with 60° notches of different depths bent by pure couples, and two of the deformation patterns obtained are shown in Fig. 17. These patterns confirm the suggested form of slip-line field. The critical ratio t/a was found to be about 1·35 (estimated possible error ± 5%), which is slightly less than the theoretical value.

The actual value of t/a in the Izod and Charpy tests is 1·25. One would expect, therefore, that the initial deformation pattern would be that for a deep notch,

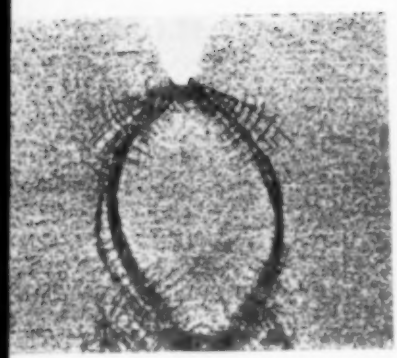

(a)

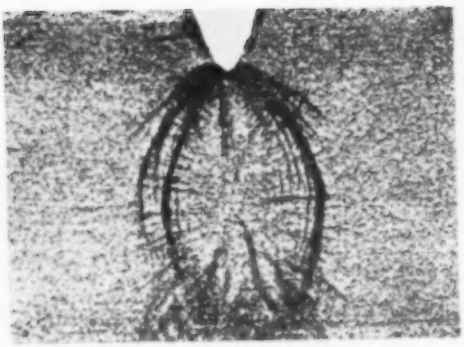

(b)

20′

Angles of bending

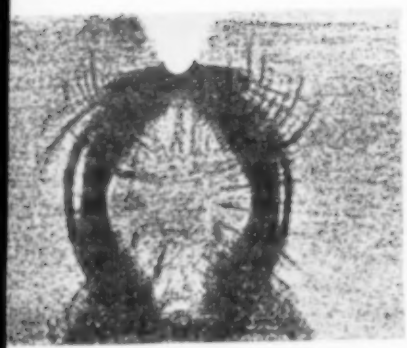

(c)
Centre

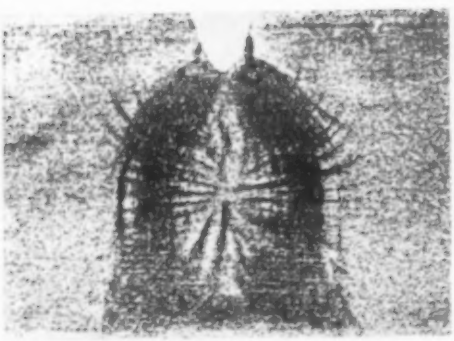

(d)
Outer edge

1°20′

Fig. 14. Deformation patterns for Charpy impact tests (V notch).

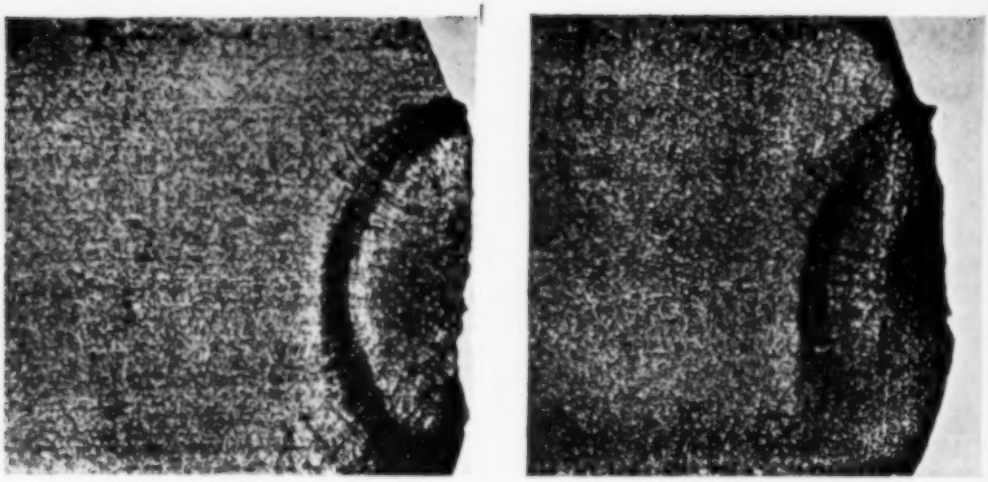

(a)
Centre

(b)
Outer-edge

Fig. 15. Deformation patterns for a Charpy V notch specimen broken at − 15°C.

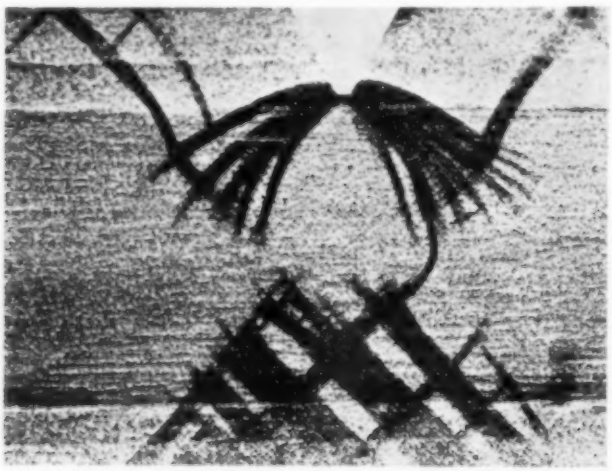

(a)
$t/a = 1{\cdot}24$

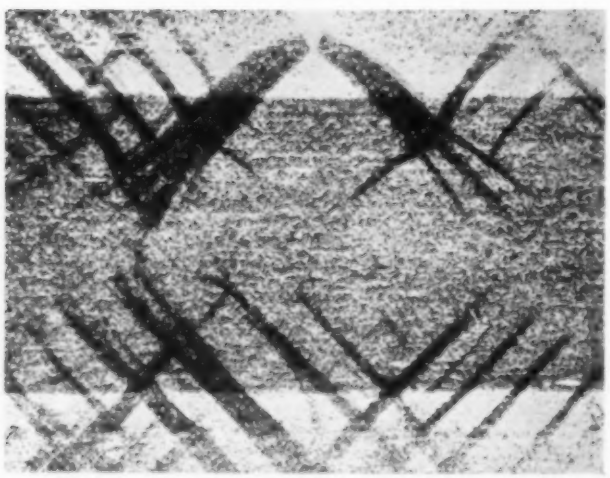

(b)
$t/a = 1{\cdot}1$

Fig. 17. Deformation patterns for pure bending with shallow V notches.

and that as deformation proceeds and work-hardening takes place, the type of deformation mode for a shallow notch would become apparent. Figs. 9 and 13 show that this is what actually happens.

Harris, Rinebolt and Raring (1951) bent some Charpy V-notch bars under impact loading at temperatures such that appreciable plastic deformation occurred, and found that yielding eventually reached the notched surface in bars with t/a ratios up to 1·36; but in bars with t/a ratios of 1·46 or more the deformation region never extended to the notched surface, no matter how great the amount of plastic bending.

Bumps (1952) examined a number of Charpy V notch impact specimens in a similar way to the present work and obtained similar deformation patterns. He carried out ordinary impact tests at various temperatures and found that yielding only spread to the notched surface in specimens tested above the transition temperature of the steel, because below this temperature only a small amount of deformation occurred before fracture started. Harris *et al.* (1951) observed the same feature and claimed that the lowest temperature at which yield markings could be seen on the notched face of the specimen was roughly the lower or ductility transition temperature for the steel. If this is so, it provides an alternative method of finding this transition temperature of steel in Izod and Charpy V notch testing, in place of the usual method of measuring energy absorbed.

6. Discussion

The basic problem of the general conditions which determine the ductile and brittle fracture of metals is still largely unsolved. The various theories proposed conflict with each other and consequently all current theories of notch bend and impact tests are somewhat uncertain. Nevertheless, reasonable qualitative explanations have been advanced, and the work described in the present paper serves both to confirm and amplify these explanations.

It is now clearly recognized that there are two kinds of transition which can be observed in steel as the temperature of testing is decreased, other conditions of the test remaining constant (Osborn *et al.* 1949; Stout and McGeady 1949; Vanderbeck and Gensamer 1950): the *fracture* transition involving a change from fibrous (ductile) to cleavage (brittle) type fracture and corresponding to a modification of the mode of *propagation* of the fracture; and the *ductility* transition corresponding to a modification of the mode of *initiation* of the fracture, the appearance of the fracture surface changing only over a small zone at the base of the notch. The former transition is outside the scope of the present work, involving as it does deformation well beyond the yield-point, associated with the propagation of a crack, and hence for the most part not determined by the original shape of the specimen. We therefore confine our attention to the ductility transition which, it has been suggested by some French workers (Borione 1955), could more appropriately be called the 'initiation' transition. It is of interest to note that brittle fracture in structures such as ships frequently involves little plastic deformation. In the opinion of Vanderbeck and Gensamer (1950) the behaviour of steel in a ship is best evaluated by consideration of the low levels of energy absorption corresponding to the ductility transition. This is confirmed

by the extensive investigations of WILLIAMS and ELLINGER (1953) on steel plates taken from ships that failed in service.

The following account of the ductility transition closely follows that given by BORIONE (1955). The transition corresponds to the coexistence at the same temperature of two modes of initiation of fracture, one brittle, the other ductile. After initiation both types of crack propagate in a brittle manner. The initiation of ductile fracture requires considerable local plastic deformation whereas brittle fracture does not. The local strain necessary to initiate ductile fracture was found by HARRIS *et al.* (1951) to be independent of temperature at all testing temperatures above the ductility transition in their Charpy V notch impact tests.

The mode of initiation can, therefore, be differentiated by any observation which detects whether or not appreciable plastic deformation occurs. The most commonly measured parameter is the total energy absorbed in complete fracture, most of which, according to BORIONE, is absorbed either before an initially ductile fracture changes over to propagate in a brittle manner (high energy level), or before brittle fracture is initiated (low energy level); other quantities measured are the small lateral contraction at the notch root, or the bending angle at complete failure. All of these parameters are found to be grouped about two levels in the transition range of temperature. The greater the value of r/a the greater is the separation between these two levels since the local deformation at the notch root occupies a greater volume (c.f. Figs. 12 (a) and 13 (a)) and greater overall deformation is required to produce a local strain sufficient to cause ductile fracture. Thus the transition is readily observed with a keyhole notch but not with a V notch unless an especially sensitive testing technique is used. HARRIS *et al.* (1951) have shown that the transition is much more readily observed with a V notch if the specimen is broken by a series of low-energy impacts instead of by one high-energy blow.

The picture, then, at the ductility transition, is that either a crack originates in a brittle manner with little or no prior macroscopic plastic deformation and therefore little energy absorption, or the development of large plastic strains at the notch root, with correspondingly higher energy absorption, leads to an initially ductile fracture, which thereafter propagates in a brittle manner. According to BORIONE (1955) a brittle fracture originates *inside* the specimen at some point below the notch, whereas a ductile fracture starts at the surface due to tearing of the notch root. This agrees well with the theoretical analysis presented in this paper which shows that after plastic deformation has commenced at the notch root the maximum tensile stress across the minimum section occurs a small distance below the notch root, whereas the maximum plastic strain develops at the surface.

However, although the macroscopic state of stress in the bar undoubtedly influences the initiation of a cleavage fracture, it seems unlikely that the initiation is determined *solely* by a stress criterion such as the commonly assumed maximum tensile stress criterion. According to explanations of brittle fracture based on dislocation theory (e.g. see ZENER 1947; STROH 1955) brittle fracture cannot occur without some plastic deformation, though this deformation may be so small that it is confined to individual crystals and may even not amount to a local macroscopic plastic strain of the polycrystalline aggregate, which is only recognized when it occurs over a region containing many crystals (BISHOP and HILL 1951). Nevertheless, the effect of the notch in creating a triaxial state of stress which

enables a high tensile stress σ to be reached below it at the start of yielding is clearly of great importance. Without postulating a fracture stress criterion, the increase in ductility transition temperature observed experimentally due to increasing notch sharpness (i.e. decreasing β and/or r/a), or increasing yield stress due to pre-strain of the material (VANDERBECK and GENSAMER 1950), may reasonably be explained by the theoretical observation that all these factors increase the maximum value of σ. The neglect of the upper yield-point, which would be difficult to take account of in the theoretical analysis, should not invalidate this qualitative explanation, though the actual maximum values of σ are likely to be greater because of it, and to occur just outside the plastic-elastic boundary.

In specimens whose fracture is initiated in a ductile manner, overall yielding is likely to commence (i.e. the yield-point is reached) before the local strain at the notch root is sufficient to initiate the fracture, except possibly if the notch is unusually sharp. Brittle specimens, however, almost certainly break before the yield-point (c.f. the specimen broken at $-50°C$ referred to in Section 4, and a similar etched specimen reported by BUMPS). This, combined with the theoretical calculation showing that the critical notch depth at which initial overall yielding extends to the surface is very close to that used in standard Izod and Charpy specimens, explains the correlation observed by HARRIS *et al.* (1951) between the ductility transition and the occurrence of surface markings. If a slightly shallower notch were used the correlation might be even closer.

A ductility transition is observed in both slow and impact bending tests, but the transition temperature range is lower for the former than the latter, and the absorbed energy jump is less (BORIONE 1955). From the present experiments it appears that the mode of deformation and hence the type of stress distribution (but not necessarily the magnitudes of the stresses) is not affected by the speed of testing, within the limits used in practice. The rise in transition temperature might be explained by an effective increase in plastic yield stress due to the increase in speed of testing. But here again it seems that the role of the macroscopic stress will be clearly understood only on the basis of a more fundamental theory of fracture (see for example STROH's (1955) dislocation model for the effect of speed and temperature of testing on the nature of the fracture.)

In conclusion, this study of initial plastic behaviour contributes to the understanding of the ductility transition. The analysis of plastic stresses and deformation clarifies the effects of notch shape and system of loading, and explains the observations of HARRIS *et al.* on the spread of yielding to the surface. It also agrees with the observations reported by BORIONE of the position in the bar at which the two different types of fracture originate. A more exact and quantitative analysis of the tests depends mainly on a clearer understanding of the laws of fracture, and it is hoped that, given this, it will be possible to apply the present work more effectively to the problem than is possible at present.

ACKNOWLEDGMENTS

The authors would like to thank Tube Investments Ltd. and the United Steel Companies Ltd. for permission to publish this paper. Most of the experimental work was carried out while one of the authors (B.B.H.) was with the British

Iron and Steel Research Association. The authors are grateful to Mr. T. D. BOXALL, Mr. D. BURTON, and Mr. B. COLDWELL for their help with this experimental work.

REFERENCES

BISHOP, J. F. W. and HILL, R.	1951	*Phil. Mag.*, **42**, 414.
BORIONE, R.	1955	Joint American Metallurgical Societies Meeting, France, 14-19 June.
BUMPS, E. S.	1952	*Trans. A.I.M.E.*, **194**, 1067.
GREEN, A. P.	1953	*Qu. J. Mech. Appl. Maths.*, **6**, 223.
	1956	To be published.
HARRIS, W. J., Jnr., RINEBOLT, J. A. and RARING, R.	1951	*Welding J.*, **30**, Research Suppl., 417-s.
HILL, R.	1950	*Mathematical Theory of Plasticity* (Clarendon Press).
	1954	*J. Mech. Phys. Solids*, **2**, 278.
HUNDY, B. B.	1954	*Metallurgia*, **49**, 109.
OSBORN, C. J., SCOTCHBROOK, A. F., STOUT, R. D. and JOHNSTON, B. G.	1949	*Welding J.*, **28**, Research Suppl., 24-s.
STOUT, R. D. and MCGEADY, L. J.	1949	*Ibid.*, 1-s.
STROH, A. N.	1953	*Phil. Mag.*, **46**, 968.
VANDERBECK, R. W. and GENSAMER, M.	1950	*Welding J.*, **29**, Research Suppl., 37-s.
WILLIAMS, M. L. and ELLINGER, G. A.	1953	*Welding J.*, **32**, Research Suppl., 498-s.
ZENER, C.	1948	*Fracture of Metals*, p. 3 (A.S.M., Cleveland).

Journal of the Mechanics and Physics of Solids, 1956, Vol. 4, pp. 145 to 161. Pergamon Press Ltd., London.

DEFORMATIONS OF AN ELASTIC-PLASTIC CYLINDRICAL SHELL WITH LINEAR STRAIN HARDENING*

By P. G. Hodge Jr.† and F. Romano‡

(*Received 11th January*, 1956)

Summary

A thin-walled circular cylindrical shell of finite length is subjected to a slowly increasing uniform radial pressure. The tensile stress-strain diagram of the material of the shell consists of two straight-line segments, the first representing elastic behaviour and the second plastic. A certain simplified piecewise-linear yield function between the stress resultants in the shell is assumed, and the strain-hardening is taken to be isotropic. The stress-strain law is a flow-type law determined by the plastic potential.

The complete solution to this problem is obtained directly from the governing equations. Various limiting cases are considered, including elastic perfectly plastic and rigid strain hardening. The results are applied to an example, and salient features are shown graphically.

1. Introduction

Within the past few years, the behaviour of circular cylindrical shells which are symmetrically loaded beyond the elastic limit has received considerable attention. Rigid perfectly plastic shells with and without end loads have been considered by Drucker (1953), Onat (1955), and Hodge (1954), and Hodge (1956a) has also considered elastic perfectly plastic shells. In addition, several papers by Hodge (1955a, 1955b, 1956b) have been written on the response of rigid perfectly plastic shells to blast-type loads in excess of the static yield load.

The present paper is an extension of the static solutions just mentioned to account for linear strain hardening. In principle the methods used can be generalized to apply to any piecewise-linear stress-strain curve, and hence to any desired approximation to a given stress-strain curve. In practice, however, it does not appear feasible to consider more than one such plastic segment.

The problem at hand is conveniently expressed in terms of the stress resultants of the shell. Within the limits of small deformations and in the absence of end load, the only resultants which need to be considered are the circumferential direct stress and axial bending moment (Hodge 1954). If these are treated as generalized stress variables, the corresponding strain variables must be the circumferential extension and axial curvature of the middle surface (Prager 1952).

For uniaxial states of stress and strain, the mechanical behaviour is completely characterized by the stress-strain curve. For multiaxial states, however, it is

* The results presented in this paper were obtained in the course of research sponsored by the Office of Naval Research.

† Associate Professor of Applied Mechanics, Polytechnic Institute of Brooklyn.

‡ Research Group Leader, Polytechnic Institute of Brooklyn, currently on leave to Zurich, Switzerland.

necessary to specify in addition a yield criterion and a flow rule. Since strain hardening is allowed, the yield condition involves both initial yield and the dependence of further yield upon the state of stress. As far as the flow rule is concerned, it will be shown that under the hypotheses of the problem this can be integrated with respect to time to furnish a direct relation between the generalized stresses and strains. These concepts will be developed in the next section.

Section 3 will contain the remaining equations and boundary conditions necessary to define the problem. If the shell is everywhere elastic, the problem reduces to the solution of a simple fourth-order linear equation with constant coefficients, as is well known. It is shown that the general plastic solution can be obtained from the same equation with a suitable modification of the coefficients.

The particular problem of an unsupported shell which is subjected to a constant exterior pressure p and to concentrated interior ring loads πpL at either end is considered in Section 4. Specific equations are obtained for the elastic and elastic-plastic solution.

Section 5 is concerned with the limiting case when the rate of strain hardening tends to zero. It is shown that this leads to the same results as are obtained from an elastic-perfectly plastic material. A second limiting case when the elastic strain contributions tend to zero is considered in Section 6.

Two numerical examples are evaluated in the next section both for the general solution and for the various limiting cases. Finally, the conclusions are summarized and the limitations discussed in Section 8.

2. Yield Condition and Flow Law

As mentioned in the introduction, it is convenient to define the problem of a cylindrical shell in terms of the stress resultants

$$N_\phi(x) = \int_{-h}^{h} \sigma_\phi(x, z)\, dz, \qquad M_x(x) = \int_{-h}^{h} z\sigma_x(x, z)\, dz. \tag{2.1}$$

Here $2h$ is the thickness of the shell and moments are taken about the central surface. If Y represents the initial yield stress of the material in simple tension, then the maximum direct stress and moment which can be carried by the shell regardless of any possible interaction are

$$N_0 = \int_{-h}^{h} Y\, dz = 2Yh,$$

$$M_0 = 2\int_{0}^{h} zY dz = Yh^2. \tag{2.2}$$

It will prove convenient to define dimensionless stress resultants by

$$n = N_\phi/N_0, \qquad m = M_x/M_0. \tag{2.3}$$

If the state of stress (i.e., stress resultants) of the shell is plotted in a two dimensional space with Cartesian co-ordinates n, m, then the condition for initial yield will appear as a closed convex interaction curve. Various such curves have been proposed by Drucker (1953) and Hodge (1954). Here the so-called "square" interaction curve will be assumed, as shown in Fig. 1. Points inside this curve

represent elastic behaviour, so that the initial condition for elasticity is

$$-1 < n < 1, \qquad -1 < m < 1. \tag{2.4}$$

If the stress point reaches the interaction curve and continues to move outwards, then plastic behaviour must ensue. It will be assumed that the strain hardening is isotropic, so that at any time the current yield curve is similar in shape to the initial curve and differs only in size. Thus, if at a point in the material, n say had reached the value $-k$ while m was less than k in magnitude, the current condition for elasticity would be

$$-k < n < k, \qquad -k < m < k. \tag{2.5}$$

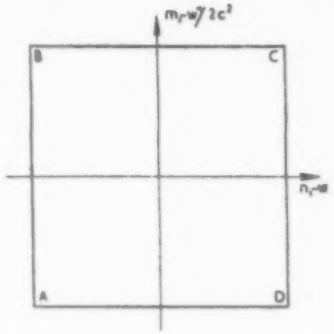

Fig. 1. Interaction curve for initial yield.

For the problems to be discussed in the following it will be assumed and verified *a posteriori* that

$$n < -|m| \leqslant 0. \tag{2.6}$$

Therefore the face AB of the interaction curve (Fig. 1) is the only operative one. It follows that the initial elasticity condition (2.4) is equivalent to

$$-1 < n. \tag{2.7}$$

The generalized strain rates associated with the generalized stresses must be such that the specific power is of the form stress $\times$ strain rate (Prager 1952). Thus, since the power per unit volume is

$$\begin{aligned} D &= (N_\phi \dot{e}_\phi + M_x \dot{\kappa}_x)/2h \\ &= n(Y\dot{e}_\phi) + m(Yh\kappa_x/2), \end{aligned} \tag{2.8}$$

the correct generalized strain rates are

$$\dot{e} = Y\dot{e}_\phi, \qquad \dot{\kappa} = Yh\dot{\kappa}_x/2. \tag{2.9}$$

Here e_ϕ and κ_x are the circumferential extension and axial curvature of the middle surface, and dots indicate differentiation with respect to time.

When the material is straining plastically, the total strain rate may be divided into an elastic and plastic part :

$$\dot{e} = \dot{e}_e + \dot{e}_p, \qquad \dot{\kappa} = \dot{\kappa}_e + \dot{\kappa}_p. \tag{2.10}$$

The elastic parts are given by Hooke's law. Since the circumferential curvature is neglected and the axial direct stress vanishes, the elastic components of generalized strain are

$$\begin{aligned} e_\phi &= N_\phi/2Eh = Yn/E, \\ \kappa_x &= 3(1-\nu^2)M_x/2Eh^3 = 3(1-\nu^2)Ym/2Eh. \end{aligned} \tag{2.11}$$

Therefore, differentiation with respect to time and substitution of (2.9) lead to

$$\dot{e}_e = Y^2\dot{n}/E, \qquad \dot{\kappa}_e = 3(1-\nu^2)Y^2 m/4E. \tag{2.12}$$

The plastic parts are given by the plastic potential law which states that the strain rate vector with components $(\dot{e}, \dot{\kappa})$ is normal to the yield curve. Together with the isotropy of the yield condition this is expressed by

$$\dot{e}_p = F(n, m)(\partial f/\partial n)\dot{f}, \qquad \dot{\kappa}_p = F(n, m)(\partial f/\partial m)\dot{f}. \tag{2.13}$$

Here F is a function which respresents the rate of hardening and f is the yield function. In the present problem the hardening is linear so that F is a constant. The yield function f is such that $f < 0$ corresponds to initial elasticity and $f = 0$ to initial yield. Thus, in view of (2.7),

$$f = -(n + 1). \tag{2.14}$$

Therefore, equations (2.13) become

$$\dot{e}_p = F\dot{n}, \qquad \dot{\kappa}_p = 0. \tag{2.15}$$

The constant F may be related to the observed slope of a tensile stress-strain test. Let this latter be as given in Fig. 2. Then, on the plastic portion of the curve,

$$\dot{\sigma} = E'\dot{\epsilon} = E'(\dot{\epsilon}_e + \dot{\epsilon}_p),$$

hence

$$\dot{\epsilon}_p = \dot{\sigma}/E' - \dot{\epsilon}_e = \dot{\sigma}(1/E' - 1/E). \tag{2.16}$$

If dimensionless variables are introduced by

$$s = \sigma/Y, \quad e = Y\epsilon, \tag{2.17}$$

equation (2.16) becomes

$$\dot{e}_p = (Y^2/E)(\rho - 1)\dot{s}, \tag{2.18}$$

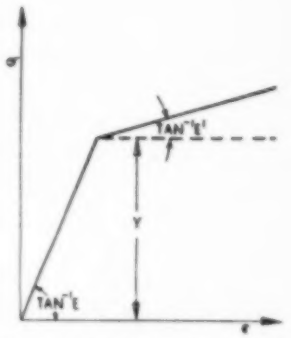

Fig. 2. Tensile stress-strain curve.

where ρ is defined by

$$\rho = E/E'. \tag{2.19}$$

Since s is analogous to n in the first equation (2.15), it follows that

$$F = (Y^2/E)(\rho - 1). \tag{2.20}$$

Addition of (2.12) and (2.15), together with the above value for F, furnishes the total strain rates:

$$\dot{e} = (Y^2/E)\rho\dot{n}, \qquad \dot{\kappa} = (3/4)(1 - \nu^2)(Y^2/E)\dot{m}. \tag{2.21}$$

Evidently the above equations are linear in time and may be trivally integrated. The constants of integration are determined by the condition that at the instant a particle first becomes plastic, $n = -1$ and the strains must be continuous with the elastic strains. In view of (2.11) and (2.9), this leads finally to

$$e = (Y^2/E)(\rho n + \rho - 1),$$
$$\kappa = (3/4)(1 - \nu^2)(Y^2/E)m. \tag{2.22}$$

Equations (2.22) are valid so long as n is less than -1 and always decreasing,

while the magnitude of m is less than that of n. It must be verified *a posteriori* that these conditions are always fulfilled after the onset of yielding at each point. Previous to the onset of yielding the elastic equations

$$e = (Y^2/E)\, n, \qquad \kappa = (3/4)\ (1 - \nu^2)\ (Y^2/E)\, m \tag{2.23}$$

will be valid.

3. Defining Equations

The stresses occurring in (2.22) and (2.23) must be in equilibrium with the external loads, and the strains must be derivable from a displacement field. In terms of the dimensionless stress variables (2.3), the equilibrium equations may be written

$$m''/2c^2 + n + P = 0, \tag{3.1}$$

where

$$c = L/\sqrt{ah}, \qquad P = pa/2Yh, \qquad y = x/L, \tag{3.2a}$$

and primes indicate differentiation with respect to y. Here L is the half-length, a the radius, and h the half-thickness of the shell.

The only displacement of interest is the radial displacement w, taken positive inwards. If a dimensionless displacement is defined by

$$W = (E/Y)\ (w/a), \tag{3.2b}$$

then it follows from (2.9) that

$$\begin{aligned} e &= Ye_\phi = -Yw/a = -(Y^2/E)\, W, \\ \kappa &= Yh\kappa_x/2 = -(Yh/2)\ (d^2w/dx^2) = -(Y^2/E)\ (W''/2c^2). \end{aligned} \tag{3.3}$$

If (3.3) are substituted into the elastic stress-strain law (2.23) the resulting equations are easily solved for the stresses, which in turn can be substituted into the equation (3.1). The results are the well-known expressions

$$n = -W, \quad m = -2W''/\left[3c^2(1 - \nu^2)\right], \tag{3.4a, b}$$

$$W'''' + 4\beta^4 W = 4\beta^4 P, \tag{3.4c}$$

where

$$\beta^4 = 3c^4(1 - \nu^2)/4, \qquad n > -1. \tag{3.4d, e}$$

In similar fashion the plastic equations are determined from (3.3), (2.22), and (3.1):

$$n = -(W + \rho - 1)/\rho, \tag{3.5a}$$

$$m = -2W''/\left[3c^2(1 - \nu^2)\right], \tag{3.5b}$$

$$W'''' + (4\beta^4/\rho)\, W = 4\beta^4\left[P - (\rho - 1)/\rho\right], \qquad n < -1 \tag{3.5c, d}$$

where β is still defined by (3.4d).

Equations (3.4) and/or (3.5) must be solved subject to boundary conditions. Since according to either the elastic or plastic stress strain law (equations 3·4b, 3·5b) the bending moment is proportional to the second derivative, it follows that in a homogeneous boundary condition m may be replaced by W''. Similarly,

vanishing of the shear implies vanishing of W'''. Therefore, the commonly encountered end conditions are as follows* :

$$\text{No support :} \qquad W'' = W''' = 0 \tag{3.6a}$$

$$\text{Centre of symmetry :} \qquad W' = W''' = 0 \tag{3.6b}$$

$$\text{Simple support :} \qquad W = W'' = 0 \tag{3.6c}$$

$$\text{Built in end :} \qquad W = W' = 0 \tag{3.6d}$$

Since the shell has two ends, the necessary four conditions are obtained for the solution of a fourth-order equation.

If part of the shell is elastic and part plastic, then certain continuity conditions must be satisfied at the interface separating the solutions. Physically, W, W'', n, m, and m' can all be shown to be continuous. Since the form of m is the same on both sides of the interface, the last two conditions are equivalent to continuity of W''' and W''''. Also, since n and W are both continuous, it follows from the equations (3.4a) and (3.5a) that at the interface

$$n = -(W + \rho - 1/)\rho = -W. \tag{3.7}$$

These two equations imply that the continuous value of W at the interface is $W = 1$. Thus, if the shell is elastic for $y < u$ and plastic for $y > u$, then at $y = u$,

$$W(u^-) = W(u^+) = 1 \tag{3.8a}$$

$$W'',\ W''',\ W'''',\ \text{all continuous.} \tag{3.8b}$$

These five conditions determine the four additional constants of integration and the location of the interface $y = u$. In practice it is usually more convenient to assume a value of u and regard the associated pressure P as an unknown quantity.

4. Example

The preceding analysis will now be applied to an unsupported shell of total length $2L$ which is subjected to a uniform pressure p over its entire length and to outwardly directed ring loads αLp per unit length of circumference applied at either end. If the end of the shell is taken as $y = 0$, then $y = 1$ will be a centre of symmetry, and it is sufficient to discuss only the half shell $0 \leqslant y \leqslant 1$. The appropriate boundary conditions are

$$\text{at } y = 0, \qquad m = 0, \qquad m' = 2c^2 \alpha P \tag{4.1a}$$

$$\text{at } y = 1, \qquad W' = 0, \qquad m' = 0. \tag{4.1b}$$

If P is sufficiently small, the shell will be everywhere elastic. Application of the boundary conditions (4.1) to equations (3.4) then leads to the elastic solution :

$$W_e = P\{1 - 4\beta\alpha[\cosh\beta\cos\beta\cosh\beta(1-y)\cos\beta(1-y) + \sinh\beta\sin\beta\sinh\beta(1-y)\sin\beta(1-y)]/(\sinh 2\beta + \sin 2\beta)\} \tag{4.2}$$

The stresses are now easily determined from (3.4a, b). It is convenient to plot the resulting "stress profile" in the n, m plane. Fig. 3 shows this for the particular case $\alpha = 0{\cdot}1$, $\beta = 2$. Evidently the general character of the curve will be the same for all $0 < \beta < \pi$ and all sufficiently

* It must be mentioned that for some boundary combinations the inequality (2.6) will not be satisfied and the analysis must be modified accordingly.

small α. Further, for α and β fixed, the curve will grow proportionally out from the origin as P increases. Therefore, the elastic analysis will first become invalid when $n(1) = -1$. An elementary computation shows the limiting elastic load to be

$$P_1 = [1 - 4\beta\alpha \cosh \beta \cos \beta/(\sinh 2\beta + \sin 2\beta)]^{-1}. \tag{4.3}$$

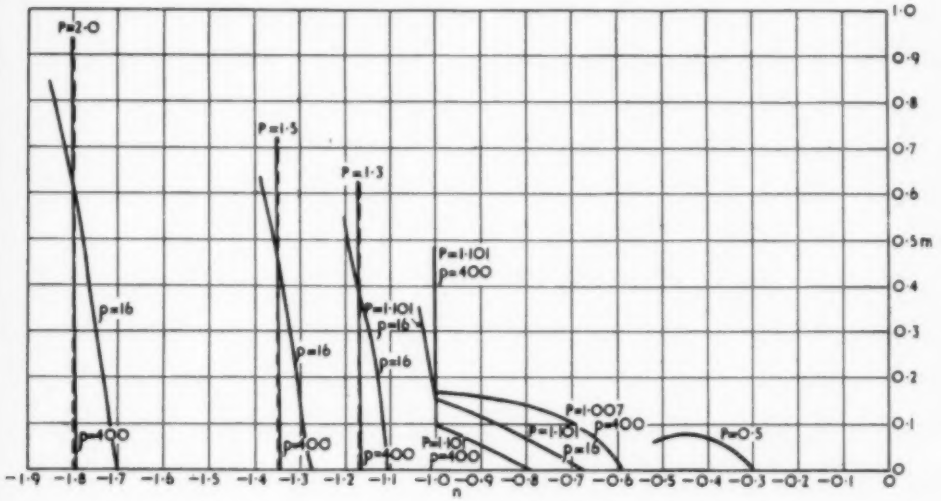

Fig. 3. Stress profiles for selected values of P and ρ.
———— Elastic-strain hardening.
– – – – – – – – – – – Rigid-strain hardening.

For $P > P_1$, that part of the shell near $y = 1$ will be plastic and that part near $y = 0$ will still be elastic. Therefore, (3.4) apply for $0 < y < u$, and (3.5) for $u < y < 1$. At $y = 0$, the boundary conditions (4.1a) apply, at $y = 1$ (4.1b) apply, and at $y = u$ (3.8) must be satisfied. The resulting solution may be written

$$0 < y < u: \quad W_{es} = P - (P-1)(\cosh \beta y/\cosh \beta u)\cos \beta(u-y) + B \cosh \beta y \sin \beta(u-y)$$
$$+ [(P-1)(\sin \beta u/\cosh \beta u) - 2\beta\alpha P + B \cos \beta u] \sinh \beta(u-y)(\cos \beta y/\cosh \beta u) \tag{4.4a}$$

$$u < y < 1: \quad W_{es} = \rho[A - (P-1)] \cosh \beta_1(1-y) \cos \beta_1(1-y) + \rho(P-1) + 1$$
$$- \rho[A \coth \lambda \cot \lambda + (P-1)(\operatorname{csch} \lambda \csc \lambda - \coth \lambda \cot \lambda)] \cdot$$
$$\sinh \beta_1(1-y) \sin \beta_1(1-y) \tag{4.4b}$$

Here

$$\beta_1 = \beta\rho^{-1/4}, \qquad \lambda = \beta_1(1-u). \tag{4.4c}$$

Equations (4.4) are readily shown to satisfy the appropriate differential equations and the boundary conditions (4.1a), (4.1b) and (3.8a). It remains to determine the constants A and B and the pressure P so as to satisfy the continuity conditions (3.8b) for a given u. The values of the first three derivatives of W are easily computed at either side of $y = u$ with the following results :

$$W'(u^-) = \beta\{-(P-1)(\tanh\beta u + \sin\beta u\cos\beta u/\cosh^2\beta u)$$
$$+ (2\beta\alpha P)(\cos\beta u/\cosh\beta u) - B(\cosh\beta u + \cos^2\beta u/\cosh\beta u)\},$$
$$W''(u^-) = 2\beta^2\{(P-1)(\sin^2\beta u/\cosh^2\beta u) - (2\beta\alpha P)(\sin\beta u/\cosh\beta u)$$
$$+ B(-\sinh\beta u + \sin\beta u\cos\beta u/\cosh\beta u)\},$$
$$W'''(u^-) = 2\beta^3\{(P-1)(\tanh\beta u + \sin\beta u\cos\beta u/\cosh^2\beta u)$$
$$- (2\beta\alpha P)(\cos\beta u/\cosh\beta u) + B(-\cosh\beta u + \cos^2\beta u/\cosh\beta u)\}; \tag{4.5}$$
$$W'(u^+) = \beta\rho^{3/4}[A(\cosh\lambda/\sin\lambda + \cos\lambda/\sinh\lambda)$$
$$- (P-1)(\cosh\lambda - \cos\lambda)(\csc\lambda - \operatorname{csch}\lambda)],$$
$$W'''(u^+) = -2\beta^2\rho^{1/2}[A(\coth\lambda\cosh\lambda/\sin\lambda - \sin\lambda/\sinh\lambda)$$
$$+ (P-1)(\coth\lambda\cot\lambda - \coth\lambda\cosh\lambda/\sin\lambda + \sin\lambda/\sinh\lambda)],$$
$$W'''(u^+) = 2\beta^3\rho^{1/4}[A(\cosh\lambda/\sin\lambda - \cos\lambda/\sinh\lambda)$$
$$- (P-1)(\cosh\lambda - \cos\lambda)(\csc\lambda + \operatorname{csch}\lambda)]. \tag{4.6}$$

The constants A, B and P are easily found by equating the corresponding derivatives in (4.5) and (4.6). These values could be exhibited as determinants by use of Cramer's rule, but the expressions are so lengthy that it appears more practicable to assign values to u and evaluate A, B and P numerically. This has been done for a particular example in Section 7.

The preceding solution is valid for all values of u between zero and one. However, as the load is increased it will eventually reach a value P_0 which corresponds to $u = 0$. If P is increased still further above P_0, the entire shell will be plastic. In this case, (3.5) are valid over the entire shell. Together with the four boundary conditions (4.1) they determine the solution

$$W_s = 1 + \rho(P-1) - 4\beta\alpha\rho^{3/4}P[\cosh\beta_1\cos\beta_1\cosh\beta_1(1-y)\cos\beta_1(1-y)$$
$$+ \sinh\beta_1\sin\beta_1\sinh\beta_1(1-y)\sin\beta_1(1-y)][\sinh 2\beta_1 + \sin 2\beta_1]^{-1} \tag{4.7}$$

The value P_0 which separates the domains of validity of (4.4) and (4.7) is more easily determined from the latter equations. The smallest value of P for which (4.7) is valid is the value for which $n(0) = -W(0) = -1$. Therefore,

$$P_0 = [1 - 2\beta\alpha\rho^{-1/4}(\cosh 2\beta_1 + \cos 2\beta_1)/(\sinh 2\beta_1 + \sin 2\beta_1)]^{-1}. \tag{4.8}$$

5. Elastic Perfectly Plastic Shell

An elastic perfectly plastic material is characterized by no strain hardening. Therefore, it may be considered as the limiting case of strain hardening material where $E' \to 0$, i.e., $\rho = E/E' \to \infty$.

Before discussing this limiting process it will prove instructive to find the solution directly. The elastic equations are unaffected by the change so that (4.2), (4.4a) and (4.5) all hold. In the plastic region $u < y < 1$, n cannot decrease below -1 but remains fixed at that value. With $n = -1$, the equilibrium equation (3.1) is easily solved for m. Thus,

$$m = c^2[D - (P-1)(1-y)^2] \tag{5.1}$$

where one constant was determined from the condition $m'(1) = 0$. The first equation (2.21) (the strain hardening stress-strain law) is now meaningless, since $n = 0$ and $\rho = \infty$ in the plastic region. However, the second equation (2.21) is independent of ρ and hence is still valid. Since it is also valid in the elastic region, the integrated form may be used, as given by (3.5b). With m known from (5.1), the stress-strain law may be integrated twice with respect to y and solved for W. The resulting complete solution is

$$u < y < 1: \quad W_{ep} = \beta^4\{[(P-1)/6][(1-y)^4 - (1-u)^4] - D[(1-y)^2 - (1-u)^2]\} + 1$$
$$m = c^2[D - (P-1)(1-y)^2], \qquad n = -1. \tag{5.2}$$

Equations (4.4a) and (5.2) satisfy all required equations, the boundary conditions at $y = 0$ and $y = 1$, and the conditions $W(u^{\pm}) = 1$. It remains to determine B, D and P so that (3.8b) will be satisfied. From (5.2) the results

$$W'(u^+) = 2\beta^4\left[-(P-1)(1-u)^3/3 + D(1-u)\right], \tag{5.3a}$$

$$W''(u^+) = 2\beta^4\left[(P-1)(1-u)^2 - D\right], \tag{5.3b}$$

$$W'''(u^+) = 2\beta^4\left[-2(P-1)(1-u)\right] \tag{5.3c}$$

are easily obtained. The equating of corresponding members of (4.5) and (5.3) then furnishes the integration constants B and D and the pressure P as functions of u.

The solution will remain valid so long as u is between zero and one. For $u = 0$, the shell is everywhere plastic and (5.1) applies throughout. The four boundary-conditions (4.1) determine a unique value of P, but leave W indeterminate. The complete solution is

$$m = c^2(P-1)(2y - y^2), \quad n = -1 \tag{5.4a, b}$$

$$W = W_0 + (1/6)\beta^4(P-1)(8y - 4y^3 + y^4), \tag{5.4c}$$

$$P = P_0 = 1/(1-\alpha)$$

Obviously, for $P > P_0$ there does not exist any equilibrium configuration.

Next, it is desired to show that the same results can be obtained by letting $\rho \to \infty$ in the solution of Section 4. To this end, it is first observed that (5.3) may be combined to give two relations independent of D. Thus

$$W'(u) + (1-u)W''(u) = (4/3)\beta\mu^3(P-1), \tag{5.5a}$$

$$W'''(u) = -4\beta^3\mu(P-1), \tag{5.5b}$$

where the notation

$$\mu = \beta(1-u) \tag{5.6a}$$

has been introduced. Since (5.5) hold at $y = u^+$ the same combinations of derivatives in (4.5) must hold. Thus there are two equations available to determine P and B, independent of the value of D.

It will now be shown that as $\rho \to \infty$ equations (4.6) satisfy (5.5) and hence the same two equations determine P and B independently of the value of A. To this end, let

$$x = \rho^{-1/4}, \qquad \lambda = \mu x \tag{5.6b}$$

where the second equation follows from (4.4c). While μ remains fixed $x \to 0$ as $\rho \to \infty$. Equations (4.6) may thus be expanded in powers of x :

$$W'(u) = (2\beta/\mu x^4)\left\{\left[A + (P-1)\right] + \left[13A - 2(P-1)\right](\mu^4 x^4/90) + \ldots\right\},$$

$$W''(u) = -(2\beta^2/\mu^2 x^4)\left\{\left[A + (P-1)\right] + \left[61A - 14(P-1)\right](\mu^4 x^4/90) + \ldots\right\},$$

$$W'''(u) = (4\beta^3\mu/3)\left[2A - (P-1)\right] + \ldots \tag{5.7}$$

As $x \to 0$, $W'(u)$ must remain finite. This implies that A may be written in the form

$$A = -(P-1) + A^*\mu^4 x^4/90 \tag{5.8}$$

were A^* is bounded as $x \to 0$. Substitution of (5.8) into (5.7) and evaluation of the limits as $x \to 0$ leads to

$$W'(u) = (2\mu^3\beta/90)\left[A^* - 15(P-1)\right] \tag{5.9a}$$

$$W''(u) = (-2\mu^2\beta^2/90)\left[A^* - 75(P-1)\right] \tag{5.9b}$$

$$W'''(u) = -4\beta^3\mu(P-1). \tag{5.9c}$$

Obviously the functions of u defined by (5.9) satisfy (5.5). Therefore, the values of P and B for any given u will be the same in the limit as for the perfectly plastic case computed directly. It follows that the elastic solutions will be identical in the two cases. This being the case, the

values $W'(u)$ on the left-hand sides of (5.3a) and (5.9a) must be the same. This can only be so if the constants A^* and D are related by

$$A^* = D\,\beta^2\,\mu^2 - (P-1)\,\mu^4/6. \tag{5.10}$$

Finally, if (5.6), (5.8) and (5.10) are substituted into (4.4b), and the limit taken as x tends to zero, the expression (5.2) for W is again obtained. Therefore, as $\rho \to \infty$ the strain-hardening solution (4.3b) approaches the perfectly plastic solution (5.2) in the plastic region as well as in the elastic.

If $\rho \to \infty$ in the fully plastic solution (4.7) the limiting value of W is infinite, corresponding to the fact that there does not exist any equilibrium configuration for $P > P_0$ in the absence of strain hardening. However, if $\rho \to \infty$ in (4.8), then the value of (5.4d) for P_0 is obtained in the limit.

6. Rigid Strain Hardening Shell

A rigid strain hardening material remains rigid at stresses less than the elastic limit and thereafter undergoes plastic strains only. The appropriate flow law is obtained from (2.15) if $\dot{e}_p$ and κ_p are replaced by the total strain rates. Therefore, using the value of F given by (2.20),

$$e = (Y^2/E)\,(\rho - 1)\,\dot{n}, \qquad \dot{\kappa} = 0. \tag{6.1}$$

Equations (6.1) are not yet in a usable form, since for a rigid material, Young's modulus E tends to infinity. Therefore, since $\rho = E/E'$ (equation (2.19), (6.1) must be written

$$\dot{e} = (Y^2/E')\,\dot{n}, \qquad \dot{\kappa} = 0. \tag{6.2}$$

Finally, since the material undergoes no straining until $n = -1$, the correct integrated form of (6.2) is

$$e = (Y^2/E')\,(n+1), \qquad \kappa = 0, \qquad n \leqslant -1. \tag{6.3}$$

As E tends to infinity, the dimensionless displacement W defined by (3.2b) becomes infinite for any nonzero actual displacement. Therefore, in dealing with a rigid strain-hardening material it is necessary to use a new dimensionless displacement defined by

$$W^* = (E'/Y)\,(w/a) = W/\rho. \tag{6.4}$$

In terms of these displacements the stress-strain law becomes, see (3.3),

$$E'\,e/Y^2 = -W^* = n+1, \tag{6.5a}$$

$$E'\,\kappa/Y^2 = -W^{*\prime\prime}/2c^2 = 0. \tag{6.5b}$$

Integration of (6.5b) together with the boundary condition $W^{*\prime}(1) = 0$ (4.1) furnishes

$$W^* = G = \text{const.} \tag{6.6}$$

throughout the plastic region. Continuity of W^* then shows immediately that this constant is zero unless the entire shell is plastic. Therefore, the shell remains rigid until load the P_0 is reached, at which time it becomes everywhere plastic and deforms according to (6.6).

Next, substitution of (6.6) and (6.5a) into the equilibrium equation (3.1) leads to the solution

$$m = c^2\,(G + 1 - P)\,(y^2 - 2y), \tag{6.7}$$

where the two homogeneous boundary conditions on m (4.1) have been accounted for. Finally, the condition $m'(0) = 2c^2\,\alpha P$ determines the constant G and leads to the complete solution

$$m = 2c^2\,P\alpha\,(y - y^2/2), \tag{6.8a}$$

$$n = -P\,(1-\alpha), \tag{6.8b}$$

$$W^* = P\,(1-\alpha) - 1. \tag{6.8c}$$

Equations (6.8) are valid only if the predicted value of n is less than -1, hence the critical load is given by

$$P_0 = 1/(1 - \alpha) \tag{6.9}$$

in agreement with (5.4d).

As in the previous section, the above solution can also be obtained as the limiting case of the elastic strain-hardening solution as $E \to \infty$. For $P < P_0$, (4.2) or (4.4) simply yield the result $W^* = 0$, as would be expected. However, if u is set equal to zero in (4.4), then the continuity conditions can be shown to predict the value of P_0 given by (6.9). The same result is also obtained by letting $E \to \infty$ (i.e., $\rho \to \infty$) in (4.8). Finally, if $E \to \infty$ in (4.7), the last equation (6.8) is obtained.

As a final example, the limiting conditions of the present and preceding sections may be combined to yield a rigid perfectly plastic material. Since $E' \to 0$ and $E \to \infty$ the proper dimensionless displacement is

$$W^{**} = w/a. \tag{6.10}$$

For $P < P_0$, W^{**} is identically zero since the material is rigid below the yield limit, while if $P > P_0$, W^{**} is infinite since there is no strain hardening. Thus, the only interesting case is $P = P_0$, and the corresponding complete solution is

$$m = c^2 (P - 1)\ (2y - y^2), \qquad n = -1,$$

$$W^{**} = W_0^{**}, \qquad P = P_0 = 1/(1 - \alpha). \tag{6.11}$$

This may be obtained directly, as a limiting case of equations (5.4) as $E \to \infty$, or as a limiting case of equations (6.8) as $E' \to 0$.

7. Numerical Example

As mentioned in Section 4, the particular shell under consideration is subjected to a uniform pressure, p over its entire length, and to outwardly directed ring loads αLp per unit length of circumference applied at both ends. Also, for the numerical examples considered, the values $\alpha = 0{\cdot}1$, $\beta = 2{\cdot}0$ are assumed. If Poisson's ratio is $\nu = 0{\cdot}3$, then it follows from (3.4d) that the geometric parameter $c = L/\sqrt{ah}$ has a value of 2·200. Therefore, the specific applications are to "short" shell theory since a thickness-of-shell to radius ratio of $1/100 \leqslant 2h/a \leqslant 1/25$ leads to a length-radius ratio of $0{\cdot}311 \leqslant 2L/a \leqslant 0{\cdot}622$.

In order to investigate the effect of strain hardening on the load-carrying capacity of the shell as well as on the deflections and stress distributions, the ratio $\rho = E/E'$ was assigned two different values of 400 and 16. The equation for linear strain hardening in the case of a uniaxial stress-strain curve, Fig. 2, may be written as

$$\sigma/\sigma_0 = 1 + (\epsilon/\epsilon_0 - 1)/\rho \tag{7.1}$$

where σ_0 and ϵ_0 represent the elastic stress and strain limits respectively, and ρ the ratio of the modulii of the elastic and plastic ranges. Hence, for the values of ρ selected, (7.1) indicates that for any given strain past the elastic limit, the stress increase in one case is 25 times as large as in the other. Moreover, when $\rho = 400$, the stress increase at a value of the strain equal to, say, five times the elastic limit is 1%, a characteristic similar to that exhibited by mild steel. For an appreciable amount of strain hardening, the value of ρ chosen was 16, thus leading to a stress increase, at the same value of the strain of 25%. Certain alloys of aluminium and cast iron approximate this physical characteristic.

Sections 4, 5, and 6 were devoted to the development of theory applicable to four types of materials, i.e., elastic strain hardening, elastic plastic, rigid strain hardening and rigid plastic. For an elastic strain hardening material, the theory indicates that in order to obtain the deflection configuration and stress distribution

over the entire shell, three separate solutions are required depending on the value of the applied load, P. The two limiting loads $P = P_1$ and $P = P_0$, defined by (4.3) and (4.8) respectively, help to characterize the condition of the shell. For the present examples, the maximum elastic load was found to be $P_1 = 0{\cdot}9555$, independently, of course, of the value of ρ. The load P_0 at which the shell becomes fully plastic depends upon the strain hardening and is found to be $P_0 = 1{\cdot}114$

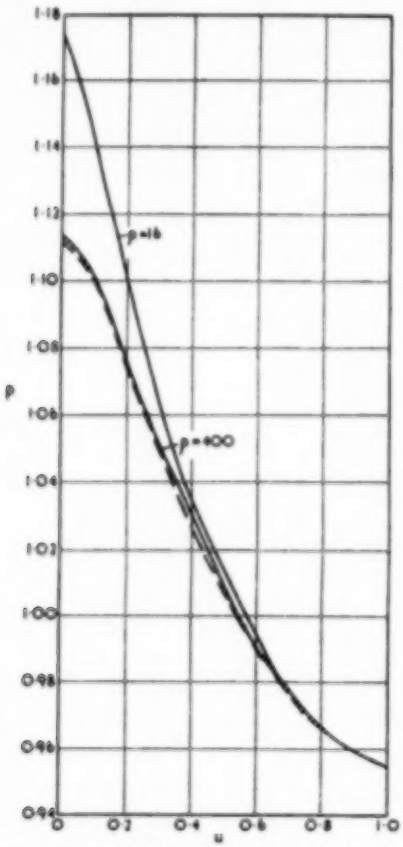

Fig. 4. Relation between pressure and elastic-plastic interface for shell under uniform pressure and ring loads.

———————— Elastic-strain hardening.

– – – – – – – – – – – Elastic-perfectly plastic.

for $\rho = 400$, and $P_0 = 1{\cdot}173$ for $\rho = 16$. For the perfectly plastic material, corresponding to an infinite value of ρ, $P_0 = 1{\cdot}111$.

With the magnitude of the applied load such that the shell becomes partly elastic and partly plastic, $P_1 < P < P_0$, selected values of u, the interface parameter, are chosen, and the load P as well as the constants of integration are then determined from a set of simultaneous equations as described in Sections 4 and 5. The solid curves in Fig. 4 show the relation between P and u for an elastic strain hardening material for the two values of ρ, while the dashed curve does the same for the elastic perfectly plastic material.

The complete solution is now known for selected values of P between P_1 and P_0, while for P less than P_0 or greater than P_1 all quantities can be directly expressed as functions of the load. Salient features are shown in Figs. 8, 5 and 6, in which the stress profiles, the maximum deflection $W(1) = (E/y)(w/a)$, and the maximum hoop stress, $n(1)$, are plotted respectively against the applied load P.

For a rigid strain hardening material (Section 6) the shell remains rigid at stresses less than the elastic limit, the deflections being zero until the hoop stress everywhere in the shell achieves a value equal to $n = -1$. The value of the load corresponding to this stress distribution is $P_0 = 1/(1-\alpha) = 1{\cdot}111$. As the

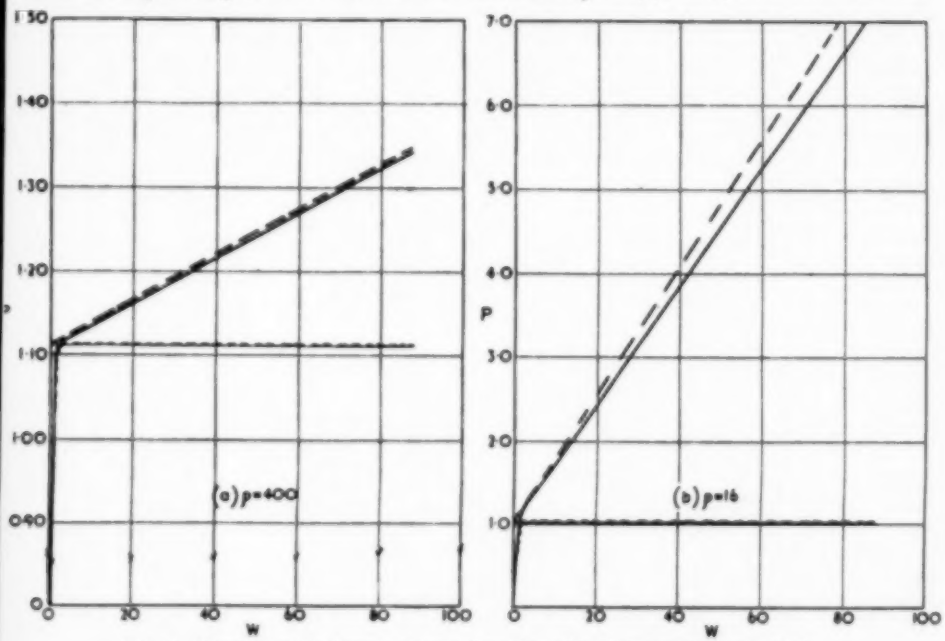

Fig. 5. Maximum displacement as a function of load for various materials.

Elastic-strain hardening.
Rigid-strain hardening.
Rigid-perfectly plastic.
Elastic-perfectly plastic.

the load increases beyond P_0, the stress n becomes less than -1 at all points in the shell. The corresponding bending moment distribution m is given by (6·8a), while the deflection which is a constant and is given by (6·8c).

The stress profiles plotted in Fig. 3 are superimposed on those for the elastic strain hardening case. Figs. 5 and 6 also show the deflection and hoop stress distribution at the centre of the shell as a function of the load. It is to be noted that, although the deflection as defined by (6.8c) is given as $W = (E'/y)(w/a)$, the variation of the quantity $\rho W^* = W$ with the load is meaningful if ρ is considered here as a pure number with no physical connotation. This allows a direct comparison of the deflections to be made.

Finally, for the rigid perfectly plastic material, as in the rigid strain hardening case, the displacement for loads less than $P_0 = 1/(1-\alpha) = 1{\cdot}111$ is everywhere

zero. At $P = P_0$, however, the deflection becomes indeterminate as was the case for the elastic perfectly plastic material. For $P > P_0$ the deflections become infinite. The light solid curve in Fig. 5 shows the resulting deflection as a function of the load.

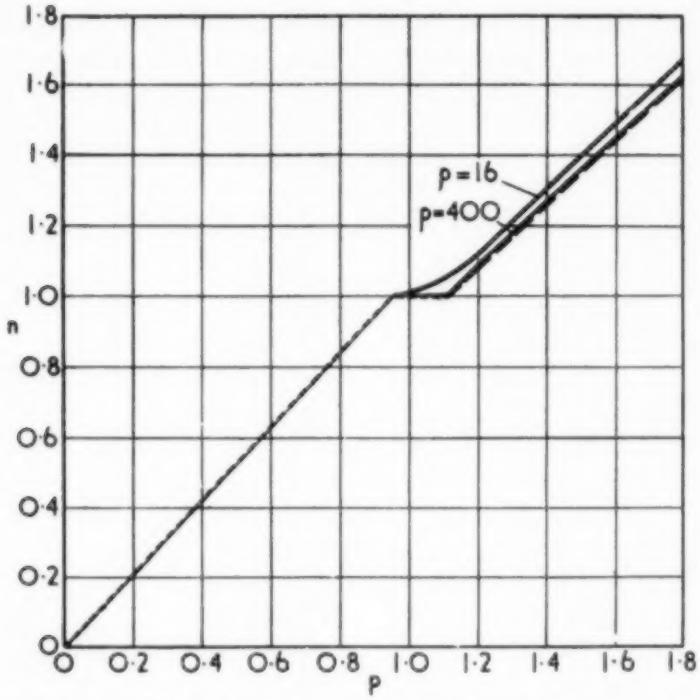

Fig. 6. Maximum hoop stress as a function of load for various materials.
——————— Elastic-strain hardening.
——— ——— ——— Rigid-strain hardening (independent of ρ).
- - - - - - - - - - - Elastic-perfectly plastic.

8. Discussion of the Results

Fig. 3 shows the variation of stress profiles corresponding to several choices of loads for an elastic strain-hardening material as well as for a rigid strain-hardening material. In the former case, for values of the load resulting in a purely elastic shell, $P < P_1$, the hoop stress n increases monotonically in magnitude from some finite value at the free end of the shell to a maximum value at the centre. The bending stress m which is always zero at the free end reaches its maximum value at some intermediate point in the shell, as is shown for $P = 0{\cdot}50$. As the load is increased further, i.e. : $P_1 < P < P_0$, the shell becomes partly elastic and partly plastic and the hoop stress, slightly greater than the elastic limit in magnitude, is practically constant throughout the entire plastic region. Thus, for $P = 1{\cdot}101$ the shell is elastic for $0 \leqslant u < 0{\cdot}10$ and plastic for $0{\cdot}10 < u \leqslant 1$ when $\rho = 400$. For $\rho = 16$, the elastic range is increased to $0 \leqslant u < 0{\cdot}20$ for the same value of the loads. In the elastic portion of the shell, the hoop stress and the bending moment increase monotonically in magnitude until the plastic region is reached.

At the elastic-plastic interface and throughout the entire plastic region, the hoop stress varies from $n = -1$ to $n = -1{\cdot}0004$ for $\rho = 400$, and from $n = -1$ to $n = -1{\cdot}043$ for $\rho = 16$. This condition persists despite the fact that, because of the presence of strain hardening, the elastic limit stress could be substantially exceeded. The conclusion is therefore that, as the load increases, (causing the plastic region of the shell to spread out), the hoop stress in the entire plastic region remains at practically the same value as the elastic limit stress. Moreover, once the entire shell has become plastic, for $P > P_0$, the hoop stress is almost uniformly distributed over the entire shell.

It is of interest to note that stresses of the same order of magnitude, for loads resulting in completely plastic shells, can be derived by making the assumption that the hoop stresses are uniformly distributed. Considering the equilibrium of one-half of a uniformly loaded shell obtained by passing a plane through the axis of the cylinder, the well-known hoop formula is obtained as

$$\sigma_\phi = -\frac{pa}{2h}(1 - \alpha) \tag{8.1}$$

where $2h$ is the thickness and αLp are the additionally applied outwardly directed ring loads per unit length of circumference. In terms of the dimensionless variables used, this may be written

$$n = \sigma_\phi / Y = -P(1 - \alpha) \text{ where } P = pa/2hY. \tag{8.2}$$

The bending moment distribution, obtained by considering equilibrium of a longitudinal element of the shell, when properly nondimensionalized becomes

$$m = M_x / Yh^2 = 2c^2 P\alpha y - c^2 y(P + n), \tag{8.3}$$

or, in view of (8.2),

$$m = 2c^2 P\alpha (y - y^2/2). \tag{8.4}$$

Equations (8.2) and (8.3) for the stresses are exactly those obtained for the rigid strain hardening material. Fig. 3 indicates how slightly the stress profiles vary for $P > P_0$.

Also, for both the elastic perfectly plastic and rigid perfectly plastic materials, the maximum hoop stress possible is $n = -1$. Hence, from (8.2)

$$P_0 = 1/(1 - \alpha). \tag{8.5}$$

These results are in agreement with (5.4a, b, d), (6.8a, b) and (6.11).

Fig. 4 shows a plot of the position of the elastic-plastic interface defined by u as a function of the load P for an elastic perfectly plastic material as well as for the two types of elastic strain hardening material denoted by $\rho = 400$ and $\rho = 16$. It is noted that, for a given value of the load, the plastic region is smallest for the elastic strain hardening material possessing the greatest amount of strain hardening, i.e., for $\rho = 16$. The reason for this can be explained by noting that, in a strain-hardening material, the hoop stress n in the plastic portion of the shell is not restricted to the elastic limit stress value of -1 as is true of the zero strain-hardening case. Thus, for a strain-hardening material, part of the applied load is in equilibrium with that part of the hoop stress in the plastic region which is in excess of the elastic limit. Hence, if two geometrically similar shells are considered,

one of which is made of elastic perfectly plastic material and the other of elastic strain-hardening material, an increment to the elastic-limit load P_1 would in the first case create a plastic region whose stress distribution is precisely equal to -1 everywhere. In the latter case, a stress distribution slightly less than -1 in the plastic region would be created, necessitating a smaller plastic region in order for the slightly larger stresses to be in equilibrium with the applied loads.

Fig. 5 shows how the deflection W varies with the load P for both the elastic and rigid strain-hardening materials as well as for the elastic and rigid perfectly plastic materials. It is immediately evident that, while the elastic deflections contribute to the overall picture for large enough loads, a suitable approximation would have been to assume the materials as initially rigid. Of course, if the applied loads are small enough, the elastic deflections are of significance.

It is of particular interest to note the appreciable increase in load-carrying capacity of the shell with strain hardening. For a typical deflection, say of $W(1) = 40$, the ratio of the loads necessary to cause this deflection in the two cases of strain hardening is approximately 3 : 1.

The quantity W is defined by (3.2b) as

$$W = (E/Y)\ (w/a) = (E/Y)\ (2h/a)\ (w/2h),$$

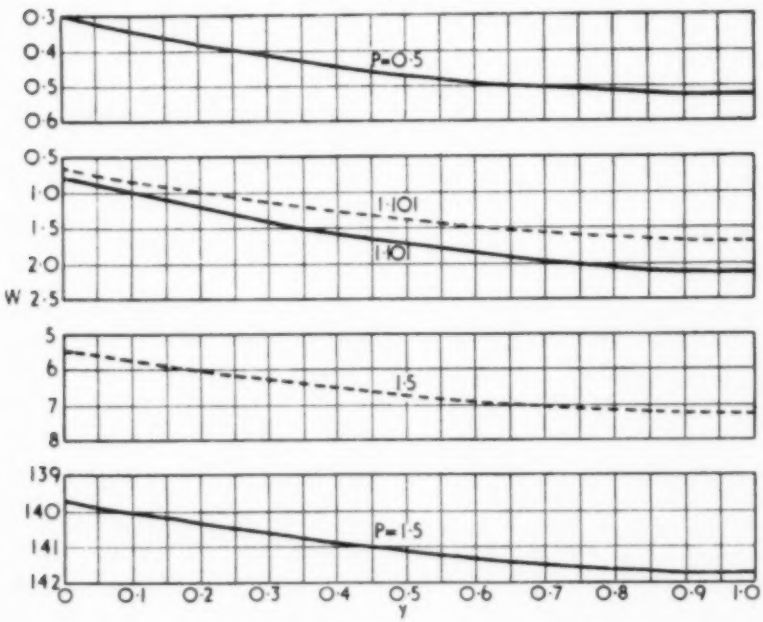

Fig. 7. Deflected shape of elastic strain hardening shell.
——————— $\rho = 400.$
- - - - - - - - - - $\rho = 16.$

and it appears at first glance that the theory is invalid in this region of load-displacement because, for typical values of $E = 30 \times 10^6/\text{in}^2$, $Y = 30 \times 10^3/\text{in}^2$ and $2h/a = 1/100$,

$$w/2h = 4.$$

This means that the deflection at the centre of the shell is four times the thickness of the shell. However, it must be remembered that the ends of the shell are unsupported and as a matter of fact also deflect considerably. This is shown in Fig. 7. For the case considered above, $W(1) = 40$ and $W(0) = 38{\cdot}4$ for an elastic strain-hardening material characterized by $\rho = 400$. Since the displacements vary monotonically, the maximum relative displacement is $\Delta W = 1{\cdot}6$ or $\Delta w/2h = 0{\cdot}16$. Because the slopes are therefore small, the neglect of the effect of the induced axial stress in the equations of equilibrium is justified. Of course, this is true only because the problem under consideration is one of axial symmetry. If the problem were not a symmetric one, it would no longer be correct, despite small slopes, to say that large deflections can be tolerated in this type of theory.

Fig. 6 shows the maximum hoop stress, occurring at the centre of the shell, as a function of the applied load. For the elastic strain-hardening material, $\rho = 400$, the hoop stress increases linearly in magnitude with the load until the elastic limit for the stress is reached, $n = -1$ at $P = P_1 = 0{\cdot}955$. Then, despite an increase in load, causing the plastic region to spread, the hoop stress remains practically constant. It is only after the entire shell is plastic for $P > P_0 = 1{\cdot}114$ that the magnitude of the hoop stress increases again with the load. Even with a substantial increase in strain hardening, $\rho = 16$, the hoop stress for the completely plastic shell, $P > P_0 = 1{\cdot}173$, does not differ significantly from those stresses due to slight strain hardening.

Also of interest is the stress load curve for the rigid strain-hardening material which is independent of the amount of strain hardening existing. An explanation for this lies in the fact that the whole shell remains perfectly rigid until the load P_0 is reached, after which the entire shell deforms uniformly in a plastic state. The hoop stress distribution must then be a constant throughout the entire shell and hence, regardless of the amount of strain hardening, the applied load can be in equilibrium with only one possible stress distribution which is uniform. Of course, the deflections for a material whose strain hardening is small will be larger than those of a material possessing appreciable strain hardening as is indicated in Fig. 5.

In conclusion, it appears that, as long as any part of the shell is elastic, the neglect of even a substantial amount of strain hardening will yield a reasonably accurate solution. On the other hand, for values of P such that the shell is fully plastic, the elastic strains do not contribute significantly and rigid strain-hardening theory can be used. Thus, depending upon the magnitude of the applied load, one or another of the approximate theories discussed in Sections 5 and 6 can be used to advantage in place of the exact theory of Section 4.

References

Drucker, D. C.	1953	*Proc. 1st Midw. Conf. on Solid Mech.*, 158.
Hodge, P. G., Jr.	1954	*J. Appl. Mech.* **21**, 336.
	1955a	*J. Mech. Phys. Solids* **3**, 176.
	1955b	*Proc. 2nd Midw. Conf. on Solid Mech.* (to be published).
	1956a	*J. Appl. Mech.* **23**, 73.
	1956b	*J. Appl. Mech.* (to be published).
Onat, E. T.	1955	*Qu. Appl. Math.* **13**, 63.
Prager, W.	1952	*Proc. 8th Internat. Congr. Appl. Mech.* (to be published).

Journal of the Mechanics and Physics of Solids, 1956, Vol. 4, pp. 162 to 166. Pergamon Press Ltd., London.

A RECONCILIATION OF CERTAIN RECOVERY PROPERTIES IN METALS

By A. J. KENNEDY
The British Iron and Steel Research Association

(*Received 8th December*, 1955)

SUMMARY

A VARIETY of time and temperature functions have been proposed to express the mechanical and electrical properties of metals. It is demonstrated that these can be reconciled with the behaviour of a particular kind of physical model built up from relaxation-type elements.

1. INTRODUCTION

IN recent years, the search for a suitable physical model to provide a basis for the time-dependent processes observed in solids has proceeded broadly along two lines. The first of these has sought for explanations in terms of the elements of the microstructure (such as dislocations, subgrains or grain boundaries), and has attempted to established the dependence of these elemental processes on such quantities as stress and temperature. The second line of enquiry starts by viewing the behaviour of solids in a much more general way. In this case, the observed behaviour, as expressed by empirical laws, provides the basis for speculation and mathematical development, the object being the construction of a framework within which the behaviour of a variety of systems may be defined, and, indeed, predicted. Generally speaking, this is the viewpoint adopted by rheology. The difference between these two attitudes resides, then, in what each takes as fundamental. In one case, reasonable physical elements are necessary for the logical development of the subject, and close agreement with observed behaviour, over wide ranges of the experimental parameters, is not accepted as an important objective. In the other case, empirical behaviour is taken as both important and fundamental, and the break-down of the observed laws into simple individual processes is not accepted as a necessary end. Indeed, although at times some such analyses are made, the simplifications usually involved are accepted with mistrust. The philosophy here is that the complexities of the subject demand special mathematical forms which become false and meaningless when the aggregate behaviour is viewed from the classical physical standpoint.

It is not the purpose of the present note to offer evidence for or against either of these two interpretations; indeed, both have their value. The object rather is to show how one kind of physical element already widely used in mechanical and electrical theory, namely the condenser or KELVIN element, may be more generally applicable than is at present believed. A reconcilation between complex rheological laws and elementary physical mechanisms may therefore become a much more reasonable possibility.

2. Reconciliation of Certain Empirical Formulae for Recovery-type Processes

Some of the time and temperature functions proposed for the mechanical and electrical properties of metals can be reconciled with the behaviour of models treated according to rate-process or dislocation theory, although it is true that no wholly unified theory has yet been achieved. Some recent experimental results, on various recovery processes, may be expressed by similar functions, and it is possible to correlate these results by adopting a particular type of physical approach.

One form of recovery of some practical importance is that by which a metal recovers from the work-hardening brought about previous creep. The transient creep period, during which this hardening occurs, satisfies an empirical relation of the form.

$$\epsilon = \beta t^p, \tag{1}$$

ϵ being the strain at a time t after loading, with β and p constants. The case $p = \frac{1}{3}$ (Andrade 1910, 1914) is of wide occurrence in both metallic and non-metallic materials (Kennedy 1953; Wyatt 1953; Feltham 1954). Mott (1953) has provided a theory for this so-called cubic creep, one consequence of which is that temperature T is introduced into the equations according to a function of the form

$$\epsilon = \beta' [t \exp(-H/RT)]^{\frac{1}{3}} \tag{2}$$

where H is the activation energy for transient creep, and R the Gas Constant. This approach is supported by Feltham (1954). An extensive experimental investigation has led Dorn (1954) to the same results, the quantity $t \exp(-H/RT)$ being termed by him 'temperature-compensated time.'

In measuring the recovery of this transient creep (that is, the re-softening during a period of zero stress) Kennedy (1952) deduced certain empirical time functions relating a quantity n with τ the period of previous creep, and with ρ the period of off-load. The relation was of the form

$$n/(1-n) = A(\rho/\tau)^p \tag{3}$$

where A is a constant. The quantity n, a fraction, was a measure of the magnitude of the new transient exhibited on re-loading; this was of the form $n\beta t^p$, starting, obviously, from the time $t = (\tau + \rho)$.

An equation such as (3) predicts complete recovery ($n = 1$) at $\rho = \infty$. As complete recovery does not necessarily occur, even over very prolonged times (unless the temperature is raised sufficiently) equation (3) must be modified for long ρ-periods to

$$n/(\alpha - n) = A'(\rho/\tau)^p \tag{4}$$

where α is a limiting fraction.

It will be evident that the model behaves as if the metal were composed of fully-recovered regions, occupying a fraction n of the whole, with the remaining fraction $(1 - n)$ behaving as if no recovery at all had occurred. This is useful as a practical device, but is difficult to accept fundamentally.

In subsequent work on materials which showed recrystallization as well as recovery (Kennedy 1955a) it became necessary to introduce temperature into

equations such as (3) or (4). The tests in question were made under identical conditions of stress and of time (τ and ρ values), but the temperature T during the recovery period was varied. From the subsequent behaviour on reloading, a value of n was deduced, and it was found that empirically

$$n/(1-n) = K \exp(-E/RT) \tag{5}$$

where K and E are constants.

In order to introduce the time of recovery ρ into equation (5) we use equation (4), and obtain

$$n/(\alpha - n) = B\,\rho^{p} \exp(-E/RT) \tag{6}$$

where B is a constant embodying the τ^{-p} factor. Clearly we can now rewrite (6) in a form similar to (2), and obtain, for the case of cubic creep,

$$n/(\alpha - n) = B\,[\rho \exp(-Q/RT)]^{\frac{1}{3}} \tag{7}$$

where, Q the activation energy for the recovery process, equals $3E$.

Thus the use of the quantity "temperature-compensated time" appears in the recovery equation (6) just as it does in the creep equation (2), and with the same fractional power ($\frac{1}{3}$). Because of this, the observed experimental invariance of n with stress and temperature (for fixed τ and ρ) leads to the conclusion that $H \simeq Q$ (KENNEDY 1955b). All such deductions are based on the empirical validity of equations (2) and (6) and on the MOTT theory which supports equation (2).

Some recent results by LINDE (1954) on the recovery of electrical resistivity in cold-worked alloys have been expressed by functions of an identical form. Thus LINDE finds that, after cold-working certain alloys by about 5% strain, the resistivity recovered with time according to

$$\Delta r/r_0 = C\,[t \exp(-P/RT)]^{m} \tag{8}$$

where Δr is the resistivity change in the time t, r_0 the cold-worked resistivity (i.e., at $t = 0$), P the activation energy of the recovery process and C and m constants. As LINDE points out, equation (8) cannot apply over long times because it predicts a continuous increase in Δr towards infinity. Clearly some modified function Δr is to be preferred that approximates to $\Delta r/r_0$ when t is small (i.e., when Δr is small), and which can also provide a limit to Δr. This can be achieved by the use of functions similar to the left-hand side of equation (6).

Thus we write (8) as

$$\frac{r_0 - r}{r - r'} = \frac{\Delta r}{r - r'} = \frac{\Delta r}{\gamma - \Delta r} = C'\,[t \exp(-P/RT)]^{m} \tag{9}$$

where r is the resistivity at time t, r_0 the cold-worked and r' the fully-recovered resistivity, with $\gamma = (r_0 - r')$. We thus obtain an equation of a similar form to (7) with Δr replacing n. Clearly, when Δr is small, $\Delta r/(\gamma - \Delta r)$ varies as Δr, and thus equation (9) then conforms with LINDE's equation (8). LINDE notes that complete recovery does not necessarily occur, i.e., $\gamma < (r_0 - r')$ even over very prolonged periods, which is just what is observed in the mechanical case ($\alpha < 1$). The values of m were found to range from 0·12 to 0·43, a value of 0·22 being the most common. This is also the range of p-values, equation (1) encountered

in creep ; usually p is near to 0·33 (ANDRADE or cubic creep) but values as extreme as 0·1 and 0·5 have been reported.

The next question is how the converse processes of mechanical and electrical hardening compare. The most direct reconcilation of resistivity and creep hardening is that of ANDRADE and CHALMERS (1932). Their results revealed a striking linearity, for hexagonal metals, between the value of Δr and the transient creep extension [ϵ in equation (1)]. Thus, during transient creep, Δr varies with time according to the same time function as the strain, and we may write $\Delta r = \beta' t^p$. No Δr change was detected by them in cubic metals. In general, for rapid cold-working (as distinct from creep) the rate of increase in Δr falls off as the amount of cold work increases (BROOM 1952). This is similar to the effect on the mechanical properties of previous cold-work (KENNEDY 1949). The same experiments also show that greater effects are produced, for some given degree of cold-work, as the working temperature is reduced.

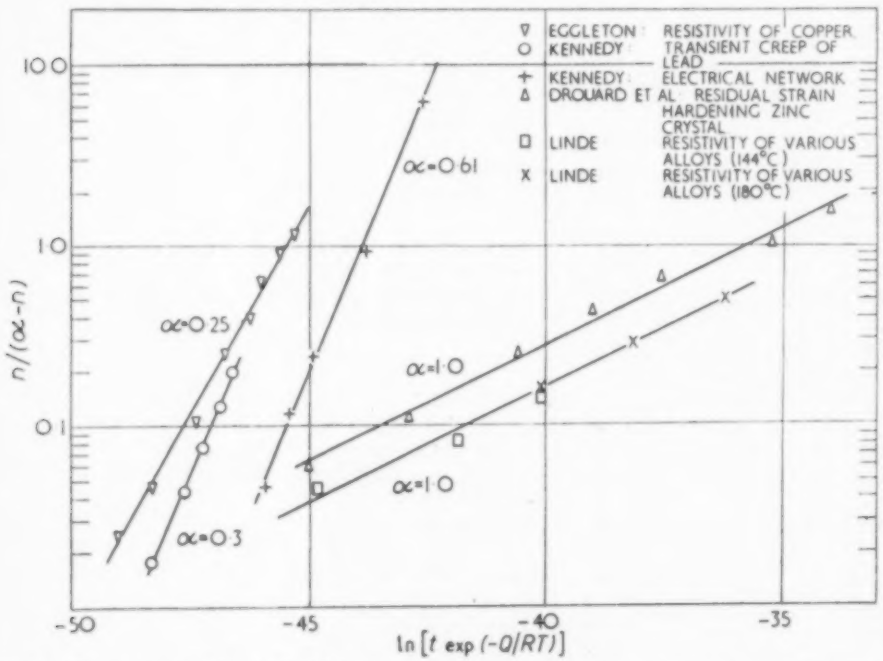

Fig. 1. Demonstrating the similarity in recovery behaviour of various properties. The numerical scale of the abscissa is correct for the results of DROUARD *et al.*, but is otherwise irrelevant.

The common features of electrical and mechanical hardening and recovery support the view that they are aspects of the same process, very possibly a dislocation mechanism of the kind proposed by BROOM (1952) in which faults are produced by the dissociation of two half dislocations. MOTT (1951) favours vacancies as the agents for the electrical properties, as these are mobile even at very low temperatures, and can thus explain low-temperature recovery.

The general application of a function of the form $n/(\alpha - n)$ to a variety of recovery results is shown in Fig. 1 plotted against the quantity $\ln [t \exp (-Q/RT)]$.

A similar empirical relationship (see Fig. 1) is displayed by an electrical network model (KENNEDY 1955c) of the transmission line type, the exact analysis of which we know to be extremely complex. Such a model also exhibits analogue creep curves of a similar form to that shown by solids. These results underline the approximate nature of some of the empirical formulations : the development of physical theories specially to satisfy such simplified laws may be seriously misleading. The model in question may not be a valid physical analogue of the processes occurring in solids, but it does at least demonstrate how simple exponential type elements can exhibit, in the aggregate, time-functions closely similar to those encountered in creep and recovery in solids.

4. CONCLUSION

The general conclusion is that a variety of hardening and recovery processes exhibit similar time and temperature functions, and that such results can be interpreted in terms of the behaviour of an aggregate composed of simple relaxation type elements.

REFERENCES

ANDRADE, E. N. da C.	1910	*Proc. Roy. Soc.* A, **84**, 1.
	1914	*Proc. Roy. Soc.* A, **90**, 329.
ANDRADE, E. N. da C. and CHALMERS, B.	1932	*Proc. Roy. Soc.* A, **138**, 348.
BROOM, T.	1952	*Proc. Phys. Soc.* B, **65**, 871.
DORN, J. E.	1954	*N.P.L. Symposium on Creep and Fracture of Metals at High Temperatures.*
DROUARD, R., WASHBURN, J. and PARKER, E. R.	1953	*Trans. Amer. Inst. Metall. Engrs.* **197**, 1226.
EGGLESTON, R. R.	1952	*J. Appl. Phys.* **23**, 1400.
FELTHAM, P.	1954	*Proc. 2nd Int. Congress on Rheology* (Butterworth's Scientific Publications, London).
	1954	*Phil. Mag.* **45**, 9.
KENNEDY, A. J.	1949	*Proc. Phys. Soc.* B, **62**, 501.
	1952	*Proc. Roy. Soc.* A., **213**, 492.
	1953	*J. Mech. Phys. Solids* **1**, 172.
	1955a	*Proc. Phys. Soc.* B, **63**, 257.
	1955b	*Nature* **175**, 674.
	1955c	*Brit. J. Appl. Phys.* **2**, 49.
LINDE, J. O.	1954	*Appl. Sci. Research* B, **4**, 73.
MOTT, N. F.	1953	*Phil. Mag.* **44**, 742.
WYATT, O. H.	1953	*Proc. Phys. Soc.* B, **66**, 459.

Journal of the Mechanics and Physics of Solids, 1956, Vol. 4, pp. 167 to 171. Pergamon Press Ltd., London.

ON CONJUGATE STATES OF PLANE STRAIN

By W. Prager
Brown University

(*Received 19th December*, 1955)

Summary

The dual correspondence between states of plane strain in incompressible elastic solids, which was recently described by Hill (1955), is shown to be a special case of a general dual correspondence between states of plane strain in pairs of incompressible solids such that the relation between the stresses and the strains in one solid has the same mathematical structure as the relation between the strains and the stresses in the other.

1. Introduction

Hill (1955) recently described an interesting dual correspondence between states of plane strain in an incompressible elastic solid. Roughly speaking, the forces and stresses of one state correspond to the displacements and strains of the other. In establishing this duality, Hill used a complex notation that incorporates the elastic stress-strain law and thereby restricted the discussion to elastic solids. In the present note, this restriction is shown to be unnecessary : the duality principle applies quite generally to pairs of incompressible solids such that the relation between the stresses and the strains in one solid has the same mathematical structure as the relation between the strains and the stresses in the other. If, for example, one is a Maxwell solid, the other is a Voigt solid. While this particular example involves linear stress-strain relations, as does Hill's example of elastic solids, the duality principle does not require the stress-strain law to be linear.

The uses of the duality principle are obvious. From any known solution of a problem of plane strain in an incompressible solid, the solution of another such problem may be immediately derived. Also, a boundary value problem on plane strain in an incompressible solid may be converted into another problem of this kind that may suggest a method of solution more readily than the original problem.

2. Notations and Fundamental Equations

Using rectangular Cartesian co-ordinates x, y, denote the components of the displacement by u, v, the stress components by σ_x, σ_y, τ, the components of the strain tensor by

$$\epsilon_x = \frac{\partial u}{\partial x}, \qquad \epsilon_y = \frac{\partial v}{\partial y}, \qquad \gamma = \tfrac{1}{2}\left(\frac{\partial v}{\partial x} + \frac{\partial u}{\partial y}\right), \tag{1}$$

and the mean rotation by

$$\omega = \tfrac{1}{2}\left(\frac{\partial v}{\partial x} - \frac{\partial u}{\partial y}\right). \tag{2}$$

The incompressibility of the solid requires that

$$\epsilon_x + \epsilon_y = 0, \tag{3}$$

so that we may set

$$\epsilon_x = -\epsilon_y = \epsilon. \tag{4}$$

It follows from these equations that

$$\frac{\partial u}{\partial x} = \epsilon, \qquad \frac{\partial u}{\partial y} = \gamma - \omega, \tag{5}$$

and hence

$$\frac{\partial \gamma}{\partial x} - \frac{\partial \omega}{\partial x} - \frac{\partial \epsilon}{\partial y} = 0. \tag{6}$$

Similarly,

$$\frac{\partial \epsilon}{\partial x} + \frac{\partial \gamma}{\partial y} + \frac{\partial \omega}{\partial y} = 0. \tag{7}$$

Denoting the mean normal stress $\frac{1}{2}(\sigma_x + \sigma_y)$ by σ, we write $\sigma_x = \sigma + s$, $\sigma_y = \sigma - s$, where s and $-s$ are the normal components of the stress deviation in the x and y directions. The equations of equilibrium then take the form

$$\frac{\partial s}{\partial x} + \frac{\partial \sigma}{\partial x} + \frac{\partial \tau}{\partial y} = 0, \tag{8}$$

$$\frac{\partial s}{\partial y} - \frac{\partial \sigma}{\partial y} - \frac{\partial \tau}{\partial x} = 0. \tag{9}$$

The four fundamental equations (6)–(9) contain six unknown functions of position : ϵ, γ, ω, s, τ, and σ ; they must therefore be supplemented by two further equations. These are furnished by the stress-strain law of the considered incompressible solid ; they relate the components s, τ of the stress deviation to the components ϵ, γ of the strain. To avoid premature specialization of the discussion, no specific stress-strain relations will be considered at this stage.

We now proceed to derive equations that will be useful in formulating boundary conditions. Let dx, dy be the components of the line element leading from a generic point P to a neighbouring point Q. With the aid of (5), the x component du of the relative displacement of Q with respect to P can then be written in the form

$$du = \frac{\partial u}{\partial x}\,dx + \frac{\partial u}{\partial y}\,dy = \epsilon\,dx + \gamma\,dy - \omega\,dy. \tag{10}$$

Similarly, the y component of this relative displacement is given by

$$dv = \gamma\,dx + \omega\,dx - \epsilon dy. \tag{11}$$

Consider now the infinitesimal force transmitted from the right to the left side of the oriented line element dx, dy. The components dX, dY of this force are

$$dX = s\,dy + \sigma\,dy - \tau\,dx, \tag{12}$$

$$dY = \tau\,dy + s\,dx - \sigma\,dx. \tag{13}$$

3. The Duality Principle

Consider two problems of plane strain in incompressible solids, using the notations and numbers of the preceding section for the variables and equations of the first problem, and indicating the variables and equation numbers of the second problem by primes. A review of equations (6)–(13) then shows that the substitutions

$$\left.\begin{aligned} &x \to y', \quad y \to x', \\ &\epsilon \to \tau', \quad \gamma \to s', \quad \omega \to \sigma', \\ &s \to \gamma', \quad \tau \to \epsilon', \quad \sigma \to \omega', \\ &du \to dY', \quad dv \to dX', \\ &dX \to dv', \quad dY \to du' \end{aligned}\right\} \tag{14}$$

transform the fundamental equations of the first problem in the following manner into the equations of the second problem :

$$\left.\begin{aligned} &(6) \to (9'), \quad (7) \to (8'), \\ &(8) \to (7'), \quad (9) \to (6'), \\ &(10) \to (13'), \quad (11) \to (12'), \\ &(12) \to (11'), \quad (13) \to (10'). \end{aligned}\right\} \tag{15}$$

If, in addition, the substitutions (14) transform the stress-strain relations and boundary conditions of the first into those of the second problem, there exists a complete dual correspondence between the two problems*.

One example of corresponding stress-strain laws has already been mentioned in the Introduction. The substitutions (14) transforms the stress-strain law of the Maxwell solid,

$$2G\epsilon = s + \alpha \dot{s}, \qquad 2G\gamma = \tau + \alpha \dot{\tau} \tag{16}$$

into the stress-strain law of the Voigt solid,

$$\tau' = 2G' (\gamma' + \alpha \dot{\gamma}'), \qquad s' = 2G' (\epsilon' + \alpha \dot{\epsilon}'), \tag{17}$$

where $G' = 1/(4G)$, the dot indicates the time derivative, and α is a relaxation time.

The correspondence between the boundary conditions of the two problems indicated in Fig. 1. To the line element PQ of the boundary of the first problem corresponds the line element $P'Q'$ of the boundary of the second problem ; $P'Q'$ is obtained from PQ by symmetry with respect to the bisector of the first and third quadrants. The same symmetry transforms the infinitesimal force (dX, dY) transmitted from the right to the left side of the oriented element PQ into the infinitesimal relative displacement (du', dv') of Q' with respect to P'. Stress boundary conditions are therefore mapped into displacement boundary con-

* Professor R. Hill has drawn the author's attention to the following modified version of this dual correspondence: $x \to x'$, $y \to y'$, $\epsilon \to -\tau'$, $\gamma \to s'$, $\omega \to -\sigma'$, etc. ; $du \to dX'$, $dv \to dY'$, etc. ; (6) $\to$ (8'), (7) $\to$ (9'), (10) $\to$ (12'), (11) $\to$ (13'), etc. This follows more closely the lines adopted in Hill's original paper (1955), and avoids any change in co-ordinates, but introduces some changes of sign in the correspondence between the mechanical variables.

ditions and *vice versa*. In particular, to a stress-free boundary corresponds a boundary that undergoes a rigid-body translation, to a boundary that is subjected to a uniformly distributed normal pressure corresponds a boundary that undergoes a rigid-body rotation, and to a straight boundary that is subjected to a uniformly distributed shearing stress corresponds a straight boundary that is being uniformly extended or compressed. The stress-strain laws may imply the dependence of the instantaneous stress or strain on the history of surface deformation or loading. The duality then requires that the complete history of surface loading of the original corresponds to the complete history of surface deformation of the dual. This remark applies in particular to the stress-strain laws (16) and (17).

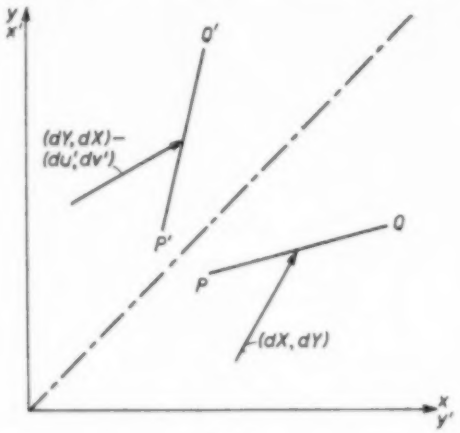

Fig. 1.

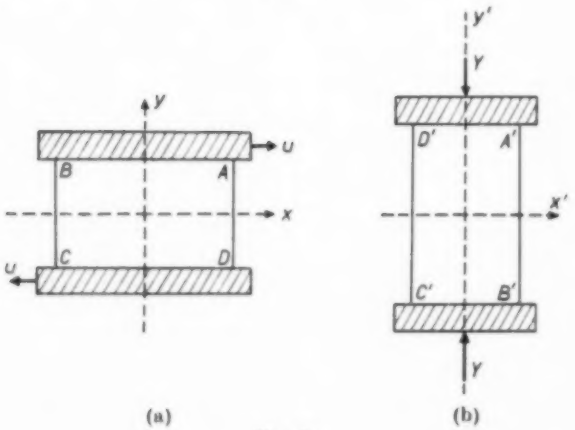

Fig. 2.

Fig. 2 shows two sets of boundary conditions in plane strain that correspond to each other in this manner. In Fig. 2a two opposite faces of a long rectangular prism are cemented to rigid dies, the other two faces being free. The dies are then given the small displacements u indicated in the figure. The dual problem is indicated in Fig. 2 (b) : the faces that were previously free are now cemented

to rigid dies and the other faces are left free. Compressive forces of the intensity $Y = 2u$ are then applied to the dies. This example of corresponding boundary conditions is taken from HILL's paper. Whereas there both solids were supposed to be perfectly elastic, with shear moduli G and G' related by $G' = 1/(4G)$, this restriction has now been shown to be unnecessary. If, for instance, one of the solids obeys Maxwell's stress-strain law, (16), the other must obey Voigt's law, (17).

ACKNOWLEDGMENT

The results presented in this paper were obtained in the course of research conducted under Contract Nonr 562 (10) between the Office of Naval Research and Brown University.

REFERENCE

HILL, R. 1955 *J. Mech. Phys. Solids* **4**, 1.

Journal of the Mechanics and Physics of Solids, 1956, Vol. 4, pp. 172 to 188. Pergamon Press Ltd., London.

THE TEARING OF ALUMINIUM FOILS

By J. Hennephof
Laboratorium voor Technische Physica, Delft

(*Received 5th December,* 1955)

Summary

To investigate the tearing of foils, thin hard aluminium foils (thickness 0·0188 cm) were provided with two parallel cuts. The part of the foil between these two cuts was torn out while the rest was clamped against a flat surface. The base angle of the triangular part that is torn out was measured, and also the tearing-force. The angle under which the tearing takes place was variable and appeared to be of great importance.

The energy for tearing a unit length out of the foil is the essential quantity (and not the tearing force). This energy is made up of two parts : the energy for bending the foil and the energy for the plastic deformation of the borders of the tear. The first quantity was determined separately; it was also calculated in good agreement with the measurements ; it proved to be the greater part of the total tearing energy. The energy necessary for forming the fresh surfaces is thought to be negligible.

1. Introduction

In the theories on the fracture of materials it is generally supposed that micro-cracks exist in the material. At a certain stress these cracks open and propagate through the material. Griffith and others have calculated the stress for crack propagation for a brittle material. For a ductile material the fracture mechanism

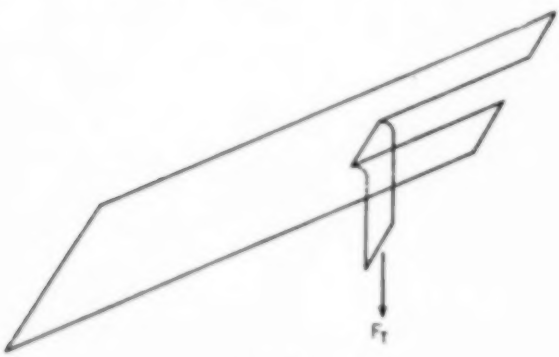

Fig. 1.

is more complicated, as plastic flow can occur in the neighbourhood of the crack. We thought it interesting to study experimentally on a macroscopic scale the propagation of a crack in a ductile material. Our experiments were executed with hard aluminium foils. The circumstances were chosen in such a way that

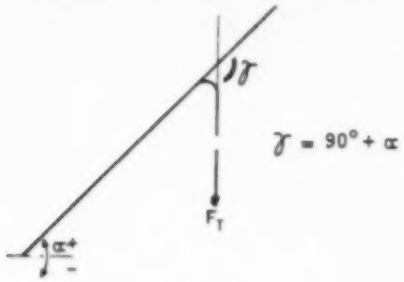

Fig. 2.

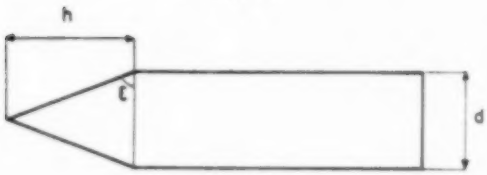

Fig. 3.

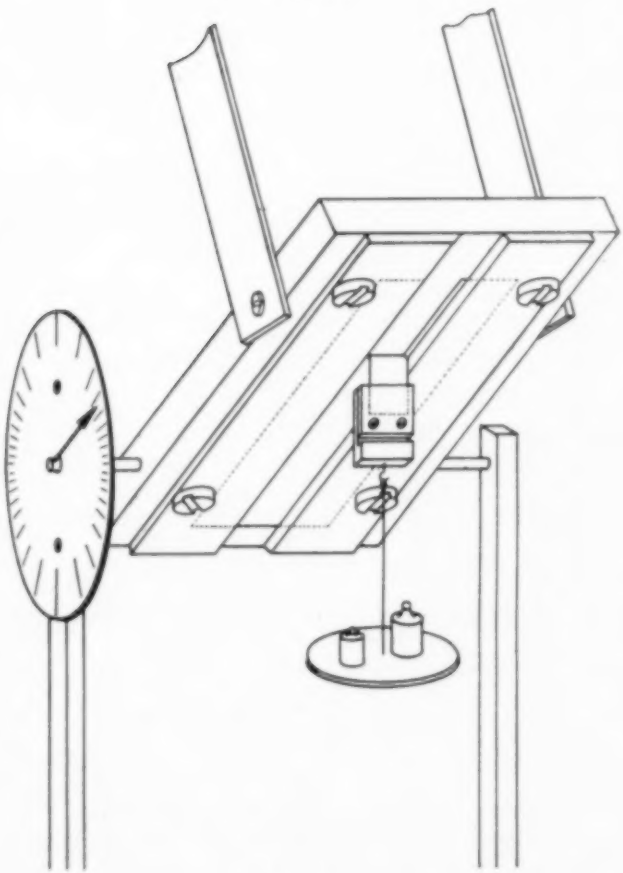

Fig. 4.

the essential parameters of the tearing mechanism could be measured in a reproducible way.

2. THE TEARING OF THE FOILS

(i) *Method.* To get reproducible tearing, foils are provided with two parallel cuts. A lip is set free which can be torn out of the foil (Fig. 1). For this purpose

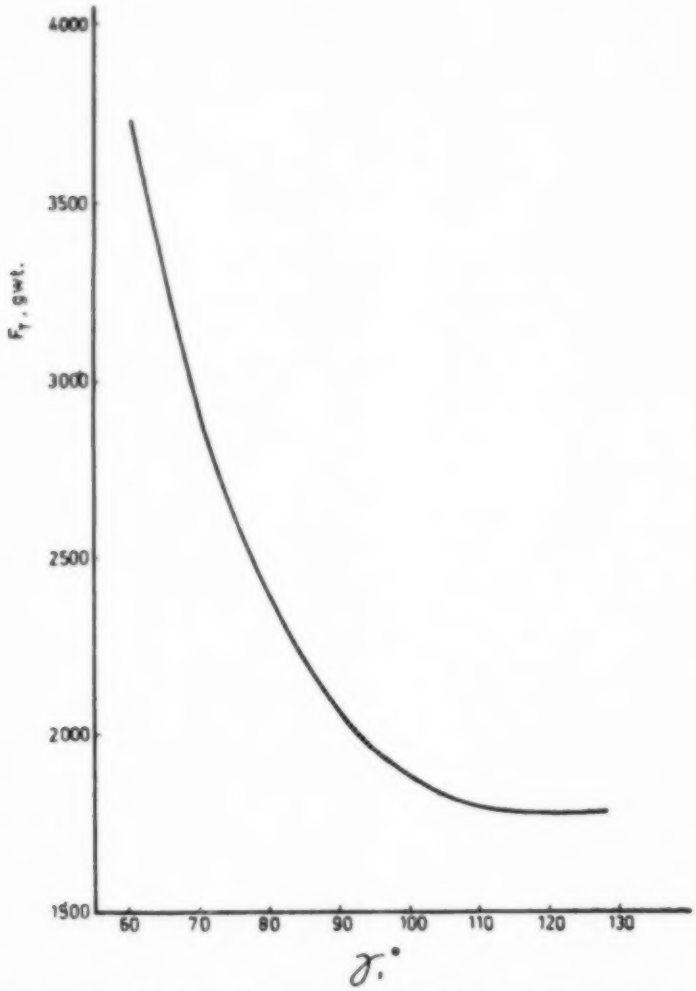

Fig. 5. The tearing force F_T (gwt) as a function of γ, the angle under which the lip is torn out of the foil.

the foil is forced against a flat wooden surface with the help of two metal strips parallel to the above-mentioned cuts. Fig. 4 shows the mounting of the foil in more detail. The distance between the metal strips and the parallel cuts is of secondary importance, and was of the order of magnitude of 0·05 cm. Fig. 2 out-

lines the situation seen from the side. The force F_T necessary to tear the lip out of the material is obtained by the use of weights. The angle γ, under which the lip is torn out of the material, can be varied by varying the elevation angle α of the foil. Fig. 3 reproduces a (flattened) torn out lip, the torn out piece of metal being always triangular.

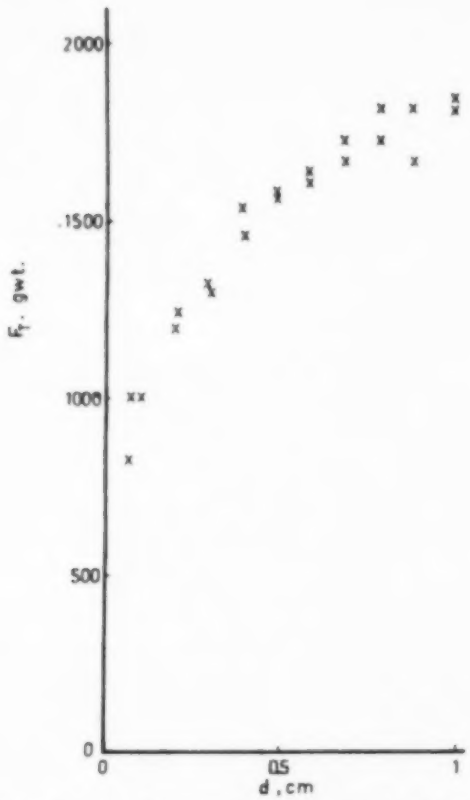

Fig. 6. The tearing force F_T (gwt) as a function of the distance d (cm.) between the parallel cuts.

(ii) *Results.* Fig. 5 shows that the force F_T necessary to tear the lip out of the material depends largely on the angle γ under which the lip is torn out. The distance d between the two parallel cuts was held constant (0·92 cm). As the experiment approaches the tensile test ($\gamma = 0$), F_T rises fast. For $\gamma > 130°$, F_T increases again.

Fig. 6 shows the dependence of F_T on the distance d between the two parallel cuts. Here γ was constant (108°). The smallest distance d was 0·07 cm.

The base angle ϵ of the torn out triangle (Fig. 3) was also determined and appeared to depend on the angle γ. As the angle γ changed from 60° to 130°, ϵ increased from 70° to 80°. It proved, however, that the base angle ϵ was independent of the distance d between the parallel cuts ($d > 0{\cdot}07$ cm.).

Thus Fig. 6 demonstrates the decrease of the force F_T during a single test. As a matter of fact the used quantity F_T is the maximum load which occurs when

a lip is torn out. As we start loading, small but already visible cracks appear at both sides of the lip. The situation however rests in stable equilibrium until the load F_T is reached. Then the lip is torn out all at once.

The material used was fine-grained hard aluminium foil with a thickness of 0·0188 cm. Coarse-grained soft aluminium of the same thickness showed a lack of reproducibility. There the torn out pieces of metal had fanciful forms. The rents were no longer straight lines but broken lines which altered their direction each time they crossed a crystal border. However, sometimes they also changed their direction in the middle of a crystal.

3. The Bending Effect

In our case the energy necessary to tear the lip out of the foil is used partly to bend the lip to a certain radius of curvature and straighten it again. We will now describe the determination of this bending effect both by calculation and by experiment.

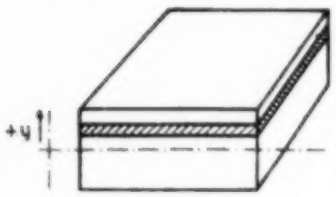

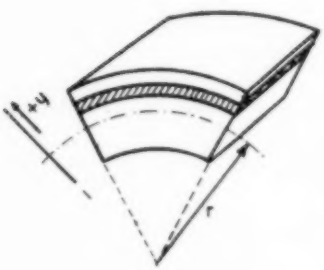

Fig. 7.

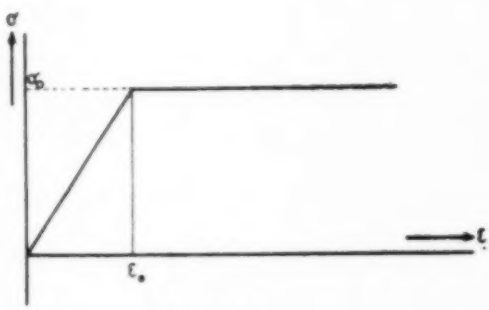

Fig. 8.

(i) *Calculation.* When the deformation of a foil is known, the deformation of a single layer can be determined (e.g. the hatched layer in Fig. 7). The forces necessary to elongate this layer can be calculated from the stress-strain curve of the material. So the deformation energy of the single layers can be calculated. And the energy necessary to deform the whole foil is found by simple addition.

The determined stress-strain curve of the material could easily be schematized to the one represented in Fig. 8 with an ultimate stress $\sigma_0 = 11{\cdot}9\ \mathrm{kg/mm^2}$ and a Young's modulus $E = 5500\ \mathrm{kg/mm^2}$. The simplification will introduce an error to the extent of a few per cent.

In describing the mainly plastic behaviour of the single layers, we assumed that the neutral zone would remain in the middle of the foil. This limits the

exactness of the calculation only to about 1% in our case (WOLTER 1952). Now if the foil is bent in such a way that the neutral zone has a radius of curvature of r, the strain in a layer at a distance y of the neutral zone is given by $\epsilon = y/r$. We can determine the energy used to get this result with the help of the surfaces $S_E + S_P = \frac{1}{2}\sigma_0 \epsilon_0 + \sigma_0 [\epsilon (y) - \epsilon_0]$ (Fig. 9). When the foil is straightened again

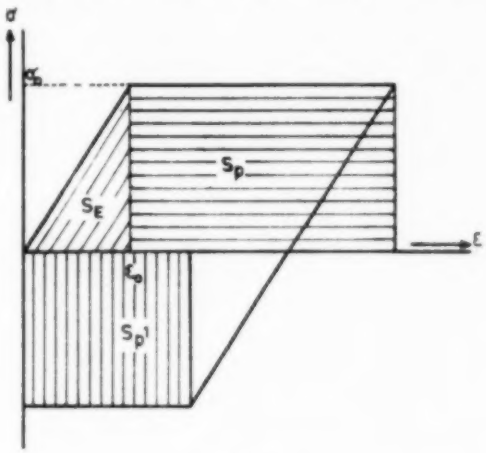

Fig. 9.

our layer is pressed back to its original length. This needs an energy represented by $-S_E + S_E + S_{P'} = S_{P'} = S_P - 2S_E$. So the energy $W(y)$ per unit of volume necessary to elongate our layer and push it back is represented by $W(y) = 2 S_P - S_E$ or

$$W(y) = 2\sigma_0 [\epsilon (y) - \epsilon_0] - \tfrac{1}{2}\sigma_0 \epsilon_0$$

where : σ_0 represents the ultimate stress of the material,
$\epsilon (y)$ the strain of a layer at a distance y from the neutral zone
ϵ_0 the elastic strain ; here σ_0/E by definition.

Hence the total energy W_B per unit length of the foil necessary to bend the foil till the neutral zone has a radius of curvature of r and straighten it again is

$$W_B = 2b \int_{2y_0}^{t/2} W(y)\, dy = b \left[\frac{t}{2} \left(\frac{\sigma_0 t}{r} - \frac{\sigma_0^2}{E} \right) \left(1 - 4 \frac{y_0}{t} \right) \right]$$

where : b represents the width of the foil,
t the thickness of the foil,
y_0 ($= \epsilon_0 r$) the distance from the neutral zone of the layer with a strain ϵ_0,
E Young's modulus.

The layers with a distance y to the neutral zone given by $y_0 < |y| < 2 y_0$, in which $y_0 = \epsilon_0 r$, are not taken into account, as their total contribution here is less than 0·2%. The layers with a distance $|y| < y_0$ do not contribute at all to the energy W_B, as their deformation is purely elastic.

It may be remarked that with $E = \infty$ our expression changes into

$$W_B = b \cdot \frac{\sigma_0 t^2}{2r} : \quad \text{a first approximation of the problem.}$$

Some data are given for a foil 2·00 cm wide, 0·0188 cm thick. Data with $E = 7400$ kg/mm², the Young's modulus for aluminium, are also listed. As the material was not 100% hard, these data give certainly too high values for W_B. It is remembered that $E = 5500$ has been introduced by schematizing the stress-strain curve.

	W_B, *gm. cm/cm foil*		
r *cm.*	$E = \infty$,	$E = 7400$	$E = 5500$
0·109	3850	3670	3600
0·134	3130	2960	2890
0·159	2640	2470	2410
0·209	2010	1850	1750

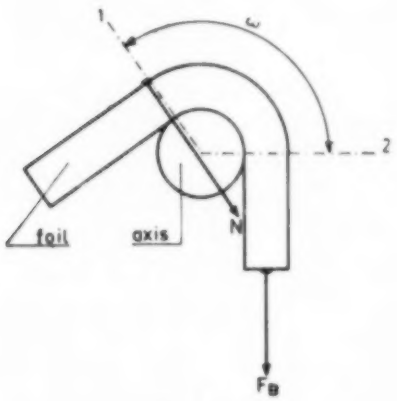

Fig. 10.

(ii) *Experiment.* The energy per unit of length of the foil necessary to bend the foil and straighten it again is determined by forcing a foil to roll over a (revolving) axis. Fig. 10 outlines the situation seen from the side. To realize this situation two forces are needed : N to keep the foil in its place and F_B to draw it over the axis. At 1 (Fig. 10) the foil is bent, at 2 straightened again. When the foil is pressed against the axis the radius of curvature is known to be half the sum of the diameter of the axis and the thickness of the foil. And, as F_B is the only force that supplies energy, the numerical value of F_B must be equal to that of W_B, the energy necessary to bend the unit of length of our foil to the above-mentioned radius of curvature and straighten it again. So

$$|F_B| \equiv |W_B|.$$

The experiment can be carried out as designed in Fig. 11. The force N ($\simeq \frac{1}{2} \cdot L \cos \delta$, which is always about 600 gm) is obtained by a variable load L which is supported by two axles revolving in ball-bearings. The top axle is the axle mentioned before (Fig. 10). The load L is held in equilibrium by a tare-weight $T = L \sin \delta$. In principle there is no force acting on the foil in a direction perpendicular to N. A correction has to be made for the friction of the ball-bearings. The force F_B is obtained by weights attached to one end of the foil. In measuring F_B, a starting-effect is observed which can be suppressed by bending the foil round the axle at the commencement of the experiment. The angle δ can be changed. In principle F_B is independent of ω ($\omega = 90° + \delta$) and thus of δ.

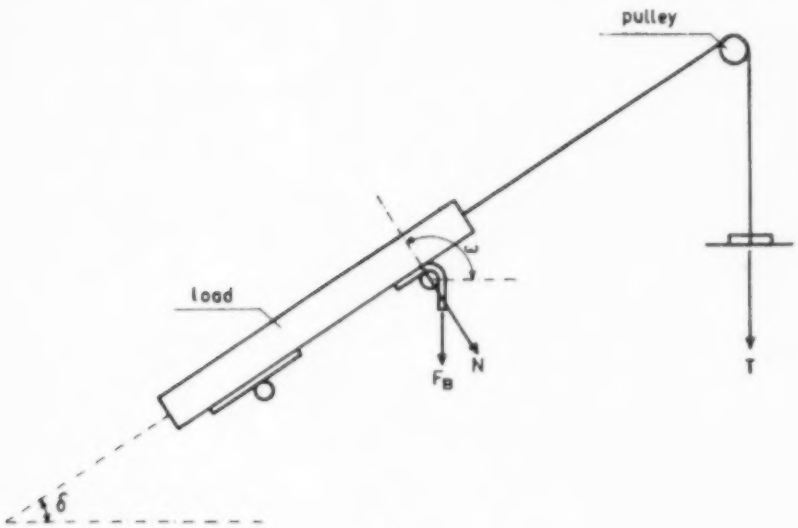

Fig. 11.

(iii) *Results.* Measurements were carried out on foils with a breadth of 2·00 cm and a thickness of 0·0188 cm. The results are plotted in Fig. 12. The radius of curvature r acts as a parameter. For each value of r two calculated values of W_B are given, the lowest one calculated with $E = 5500$ kg/mm², and the highest one with $E = 7400$ kg/mm². These calculated values are independent of δ. The small crosses are mean values. The vertical lines drawn through these crosses give the highest and lowest measurements. The discrepancy for $\delta = 15°$ may be due to the fact that in this case the foil does not follow the axle surface. Indeed for negative angles δ such an effect was remarked.

On the whole a reasonable agreement between calculated and measured values is obtained. Thus, for our purpose, a fair approximation of the energy necessary to bend and straighten a foil can be given now by calculation.

4. The Effect of Bending on Tearing

We return to our starting-point : the tearing of lips out of foils. Such lips do not describe an arc of a circle being torn out but this is unimportant, for if a

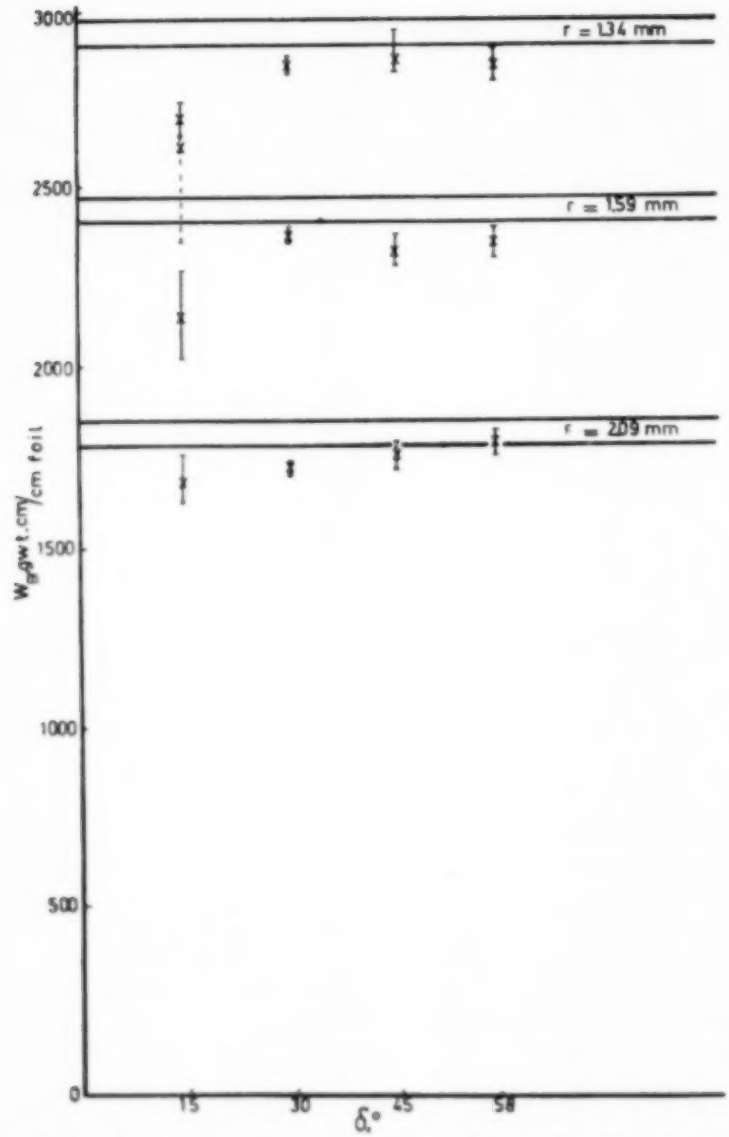

Fig. 12. The energy W_B necessary to bend and straighten a unit length of the foil as a function of the angle δ (Fig. 11).

minimum radius of curvature does exist this radius determines the bending energy. When this radius is known we can calculate the energy necessary to bend and straighten the lip and compare it with the energy necessary to tear the lip out of the foil.

To determine the minimum radius of curvature r, the load F_T is taken away as soon as tearing takes place. This, however, causes the lip to spring back elastically somewhat, with the effect that the radius of curvature increases by a few per cent. For this effect a correction has to be made. The radii of curvature were measured with the aid of a set of bars with decreasing diameters.

The energy W_B necessary to bend and straighten the unit length of a lip can now be calculated with the aid of the formula :

$$W_B = b\left[\frac{t}{2}\left(\frac{\sigma_0 \cdot t}{r} - \frac{\sigma_0^2}{E}\right)\left(1 - 4\frac{y_0}{t}\right)\right]$$

where $E = 5500$ kg/mm², $\sigma_0 = 11{\cdot}9$ kg/mm², $t = 0{\cdot}0188$ cm, and $b = d \simeq 0{\cdot}94$ cm.

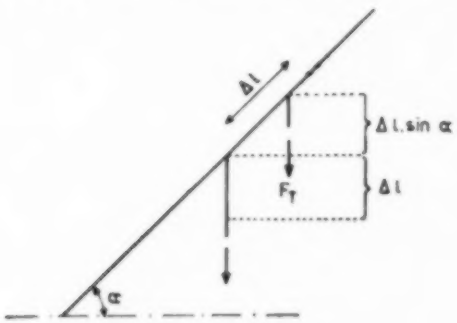

Fig. 13.

The energy W_T necessary to tear out a lip, per unit length of that lip, can be calculated with the help of the elevation angle α of the foil and the tearing force F_T. The work the force F_T performs when a length Δl of the foil is torn out amounts to $F_T \cdot \Delta l \cdot (1 + \sin \alpha)$ as Fig. 13 illustrates. So $W_T = F_T\,(1 + \sin \alpha)$ per unit of length of the lip.

Measurements were executed on foils with a thickness $t = 0{\cdot}0188$ cm and a distance between the parallel cuts $d = 0{\cdot}94$ cm.

It appeared that the radius of curvature decreased with increasing angle γ under which the lip was torn out of the material. The lower curve of Fig. 14 gives the energy W_B per unit length of the lip necessary to bend and straighten this lip while being torn out. The upper-curve in Fig. 14 represents the tearing energy W_T per unit lip length as a function of γ. By comparing this curve with that of Fig. 5 the influence of the factor $(1 + \sin \alpha)$ on W_T can be noticed. Low values for the tearing force F_T correspond here with high values for the tearing energy W_T, and vice versa. It is obvious that the increase of the tearing energy W_T with increasing angle γ is caused by the increase in energy necessary to bend and straighten the lip.

Concerning the difference $W_T - W_B$ between the two curves little can be said. There is, however, no evidence to show that in first approximation this difference

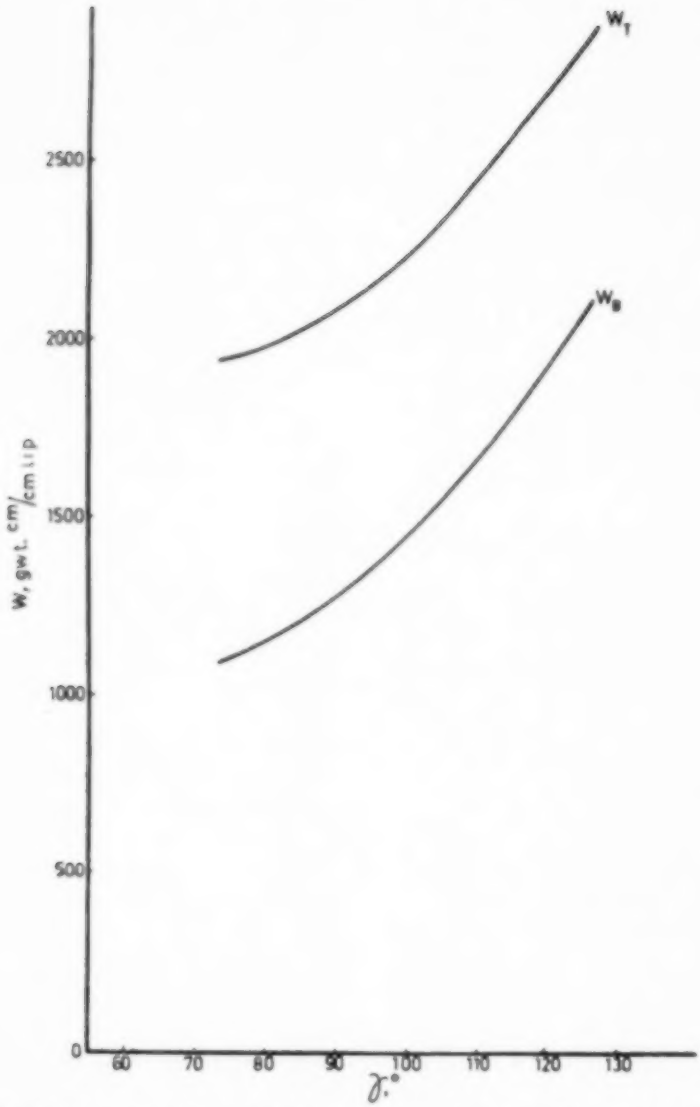

Fig. 14. The tearing energy W_T and the bending energy W_B, per unit length of the lip, as a function of the angle γ under which the lip is torn out of the foil.

should not be constant. In our range of measurements the base angle ϵ of the torn out triangle (Fig. 3) changes only from 70° to 80° with increasing angle γ. So here the length of the rents, per unit torn-out length of the lip, can be regarded as being nearly constant (2·19 cm/cm lip) compared to the error of some 10% in the difference $W_T - W_B$. This very low accuracy of $W_T - W_B$ is chiefly caused by the error (10%) in the determination of the radii of curvature of the lip. As the energy necessary to enlarge the edge surfaces of the newly formed rents is negligible compared to the energy $W_T - W_B$ (some 800 gm cm/cm lip), this latter energy may be regarded as the deformation energy per unit torn-out lip length along the newly formed rents.

So we may conclude with the following remarks.

(1) The tearing force, and consequently the tearing energy, depends largely on the angle γ under which the lip is torn out.

(2) In our case the tearing force is less essential than the tearing energy.

(3) The tearing energy consists of two parts: one part for bending the foil and straightening it again, and the other (here almost constant) part for deforming the material at the borders of the tears. The latter is the smallest part.

These conclusions are only valid in our circumstances.

Acknowledgment

The author is grateful to Prof. M. J. Druyvesteyn for his advice and encouragement throughout the work.

Reference

Wolter, K. H. 1952 *V.D.I. Forschungsheft*, 435.

Journal of the Mechanics and Physics of Solids, 1956, Vol., 4 pp. 184 to 190. Pergamon Press Ltd., London.

COMPARISON OF AN UNSYMMETRIC SLIP-LINE SOLUTION IN EXTRUSION WITH EXPERIMENT

By T. F. JORDAN* and E. G. THOMSEN†

(*Received* 23*rd December*, 1955)

SUMMARY

EXPERIMENTALLY determined velocity vectors obtained from the extrusion of tubes of commercially pure lead from solid billets under axial symmetry and plane strain are compared with an unsymmetric slip-line solution. It was found that qualitative agreement existed and that the slip-line solution is good to a first approximation. A new mechanical slip-line integrator is discussed.

1. INTRODUCTION

THE detailed study of the behaviour of a metal during certain steady-state forming processes has been made possible through an experimental technique developed during recent years in the laboratories of the University of California at Berkeley. This technique, called *visioplasticity*, consists of obtaining instantaneous velocity vectors of metal particles as represented by motion of intersections of grid lines placed on a central plane during incremental deformation steps. From these velocity vectors, strain rates, strains and pressure and stress distribution have been calculated, when the flow properties of the metal were also known. This method has been used to analyse axially-symmetric indirect-extrusion processes with lead by THOMSEN, YANG and BIERBOWER (1954) and with commercially pure aluminium by THOMSEN and FRISCH (1955). These metals were extruded at atmospheric temperature and with essentially zero external friction. There is evidence to substantiate the belief that the method can be used for other steady state forming processes, with or without external friction, and for metals affected by either strain-rate or strain.

It should be understood that the visioplasticity method is not intended to replace, but rather to augment, a purely analytical approach : it offers a check of the applicability of certain assumptions required for specific solutions for which experimental data are not now available. Such a comparison of plane strain and axially symmetric approximate solutions with data obtained by the visioplasticity method on cold-extruding commercially pure aluminium was recently made by THOMSEN (1955). It was found that the ideal plastic solid subjected to plane strain appeared to be a suitable model for describing approximately the behaviour of the aluminium for the particular extrusion ratio investigated. The transition zone from the elastic to the fully plastic state, however, extended beyond the boundaries of the plastic sector of the ideal plastic solid.

* Technical Institute, Hanover, Germany.
† University of California, Berkeley.

2. Experiment

It is the purpose of the present paper to extend the comparison of slip line solutions with experimental data to the specific problem of extruding a tube from a solid billet of commercially pure lead under conditions of both axial symmetry and of plane strain. The problem is of particular interest because of the fact that the dimensions of tube and billet, as shown in Fig. 1, may be so chosen that the geometric centre of the extruded tube wall does not coincide with a line in the billet along which the radial velocity is zero. Hence the present problem involves unsymmetrical plastic flow of the kind discussed by Green (1955).

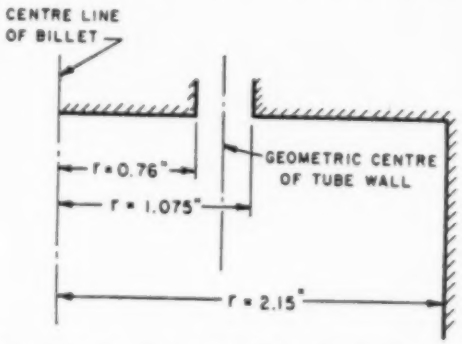

Fig. 1. Configuration of billet and extruded tube on central plane.

Fig. 2 shows typically deformed grid lines during steady-state extrusion of the commercially pure lead billets used in the present investigation. The dimensions of billet and tube for axial symmetry and plane strain were identical with those given in Fig. 1, except that the billet for the plane strain extrusion experiments was square instead of round. The particle velocity vectors were determined from incremental displacements of grid line intersections placed on the central planes of the split billets.

3. Slip-Line Solutions

The slip-lines obtained for the tube extrusion in plane strain are shown in Fig. 3. These slip-lines are directions of maximum shear and are shown as solid lines. For comparison, maximum shear directions obtained experimentally by Thomsen (1955) for an axially symmetric extrusion are shown as crosses on the same Figure. Examination of these results reveals that the maximum shear directions are in close agreement with the theory in the plastic zone, but that the extent of deformation is greater in the actual case. The apparent good agreement with experiment within the plastic zone, however, should increase confidence in the application of slip-line solutions to practice.

The solution given in Fig. 3 was carried out in the same manner as Green's (1955) solution for unsymmetric solid strip extrusions, i.e., by combining two symmetric centred fan solutions into one. This can be done because the centre line of the tube may be regarded as a frictionless or smooth container wall and slip lines must cross it at angles of 45°. Hence the tube extrusion in plane strain reduces to an unsymmetrical strip extrusion.

Several methods of obtaining centred fan solutions were used, and the final solution given in Fig. 3 agrees well with Hill's (1950) tabular values for centred fan solutions with a deviation of less than 2%. The solution was obtained by several methods, i.e. graphical and numerical, all of which agreed closely with each other. One of the graphical methods employed was with the use of a new

mechanical integrator. This device reduces appreciably the time required for obtaining an equiangular network of slip lines. Consequently its operational features are briefly described in the following.

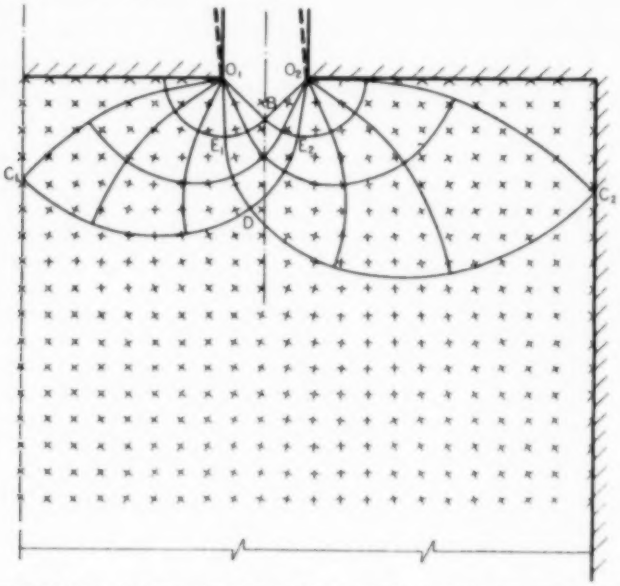

Fig. 3. Slip-line field for tubular extrusion in plane strain (crosses are experimental maximum shear direction for axial symmetry).

4. SLIP-LINE INTEGRATOR

Fig. 4a shows a photograph of the mechanical integrator in action. It is operated on a steel table and its centres, as well as the arm lengths, are clamped by electromagnets which are operated by remote push-button control. An exploded view of the integrator is shown in Fig. 4b.

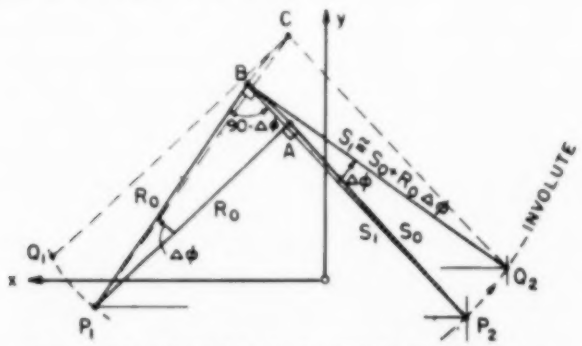

Fig. 5. Principle used in mechanical slip-line integrator.

The principle of the mechanical integrator is illustrated in Fig. 5. If point A is a known intersection of an α- and β-slip-line, and points P_1 and P_2 are instantaneous centres with radii R_0 and S_0, then point B can be determined by drawing

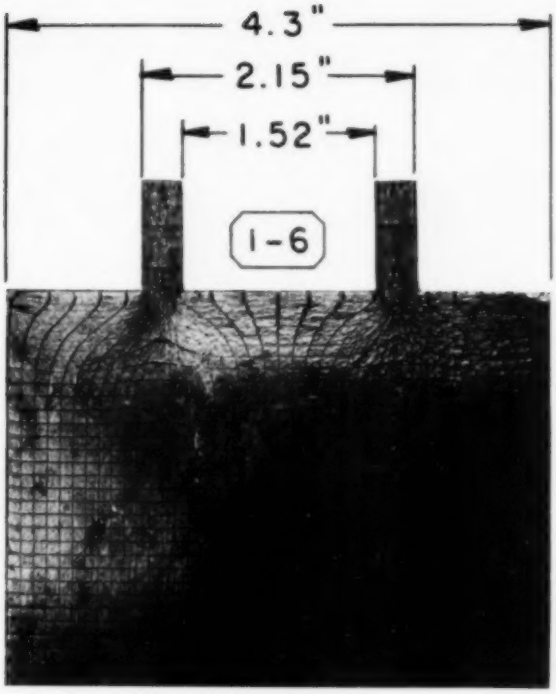

(a)

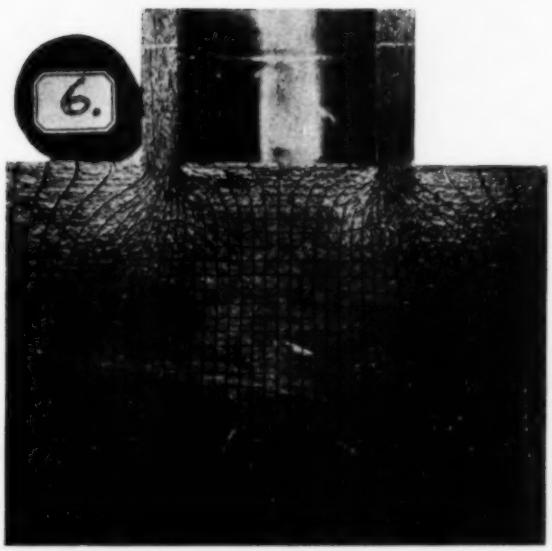

(b)

Fig. 2. Photographs of distorted grid lines of commercially pure lead extruded at atmospheric temperatures and with negligible external friction for the plane and axially symmetric case.

(a) Plane strain area ratio = 6·83.

(b) Axial symmetry area ratio = 7·95.

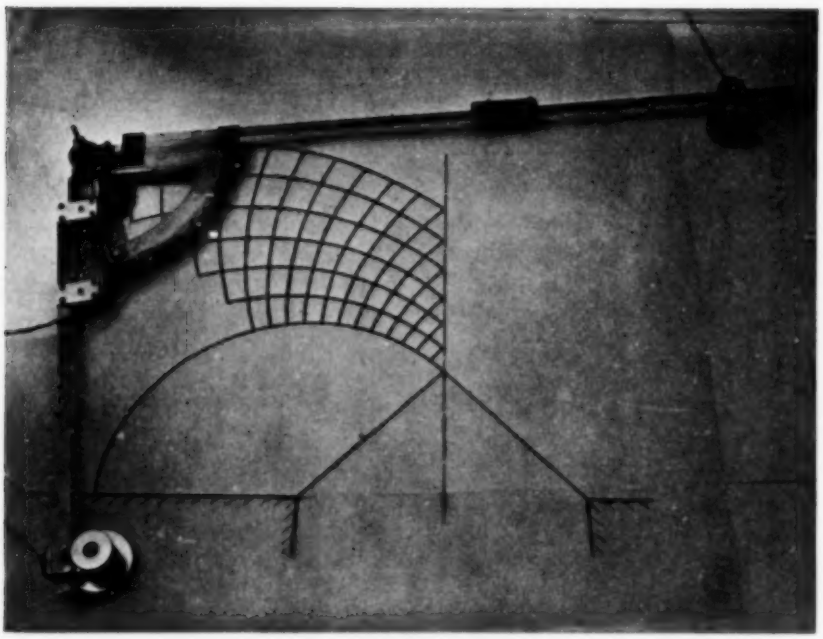

(a)

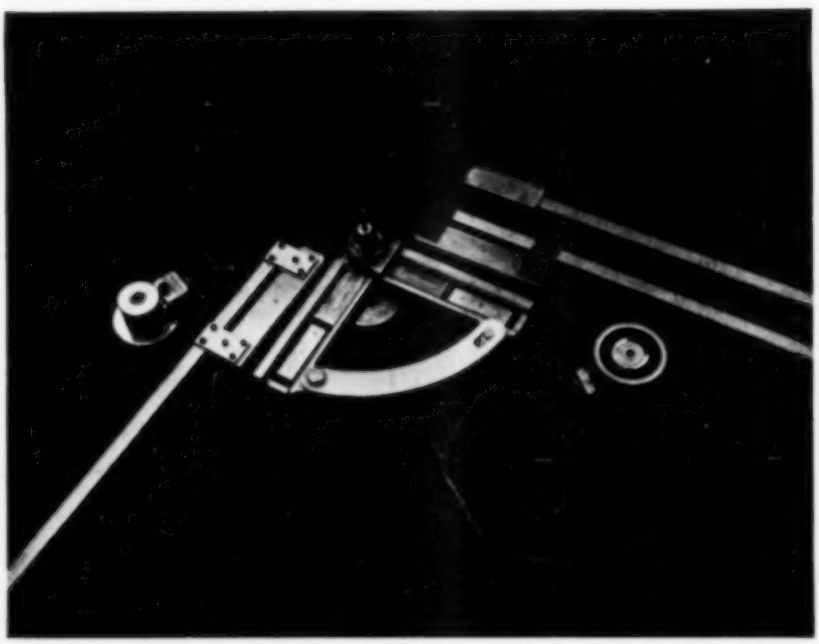

(b)

Fig. 4. Photographs of mechanical slip-line integrator

a circle with radius R_0 about P_1. If centre P_2 is kept fixed and radius R_0 is permitted to change to S_1, then $S_1 \simeq S_0 + R_0 \Delta\phi$. If after drawing the arc AB the new radius S_1 is kept fixed in the instrument and P_2 is allowed to move along the involute to point Q_2, letting point B be the centre, until angle $P_1 BP_2$ again is 90°, then the instrument is in position to draw another arc such as BC, and so on. Hence, this device will draw alternate segments of α- and β-lines by keeping the angle between slip lines fixed between each step.

In order to draw an arc manually, as, for example, AB in Fig. 5, the interlocked magnets P_1 and P_2 are energized and hence clamped to the table. Also the magnet fixing the arm length R_0 is energized at the same time. After the penpoint has reached point B, which is determined by the limited angle of rotation fixed in the instrument, magnet B as well as the magnet in arm S_0 is energized, while centre P_2 is released from the table. This permits moving centre P_2 to position Q_2 where it is again energized and clamped to the table. Segment BC and other consecutive arcs are drawn in a similar manner.

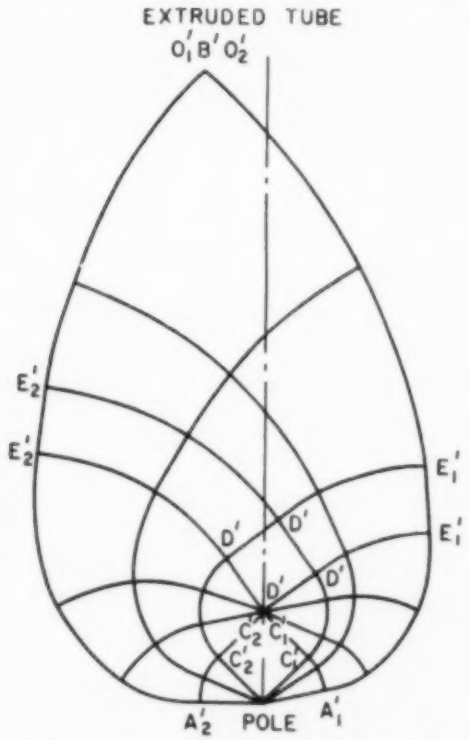

Fig. 6. Hodograph of slip-line field of Fig. 3.

5. Comparison of Velocity Vectors

Fig. 6 shows the hodograph which satisfies continuity and the slip line field of Fig. 3. This diagram permits obtaining of velocity vectors throughout the plastic zone. These vectors are given in terms of direction and magnitude in Figs. 7 and 8 respectively, and are compared with experimental velocities.

It is at once evident that only qualitative agreement exists. The directions of the velocity vectors of Fig. 7 show that no abrupt change in direction in the actual metal flow occurs along the limiting slip lines $C_1 DC_2$ of Fig. 3. Furthermore, the actual extrusions leave the chamber parallel with the centre line of the container instead of at an angle as predicted by the theory. This latter disagreement between theory and experiment was also observed by GREEN (1955)

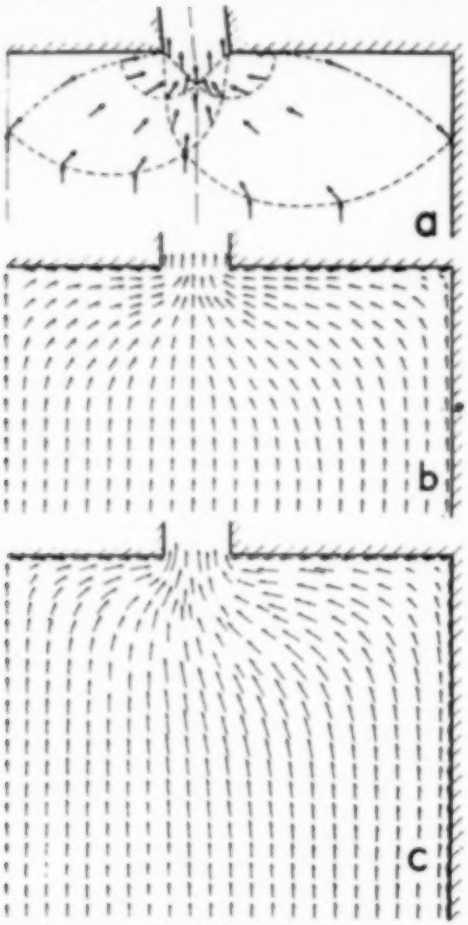

Fig. 7. Direction field of velocity vectors :
(a) approximate solution, ideal plastic solid, plane strain.
(b) experimental, lead, plane strain.
(c) experimental, lead, axial symmetry.

in his plasticine extrusion experiments. It is of further interest to note that some flow across a geometric centre line of the tube wall occurs in the axially symmetric extrusion of Fig. 7 (c), while in the experimental plane strain case of Fig. 7 (b) such cross flow appears to be essentially absent.

The magnitudes of the velocity vectors are given in Fig. 8. These magnitudes are constant along the solid curves. A magnitude of unity has been assigned to

the metal flowing toward the orifice in the undeformed state. The magnitude of the velocity in the orifice, because of continuity, is given by the ratio of the area of billet to area of the extruded product. It follows from this that the exit

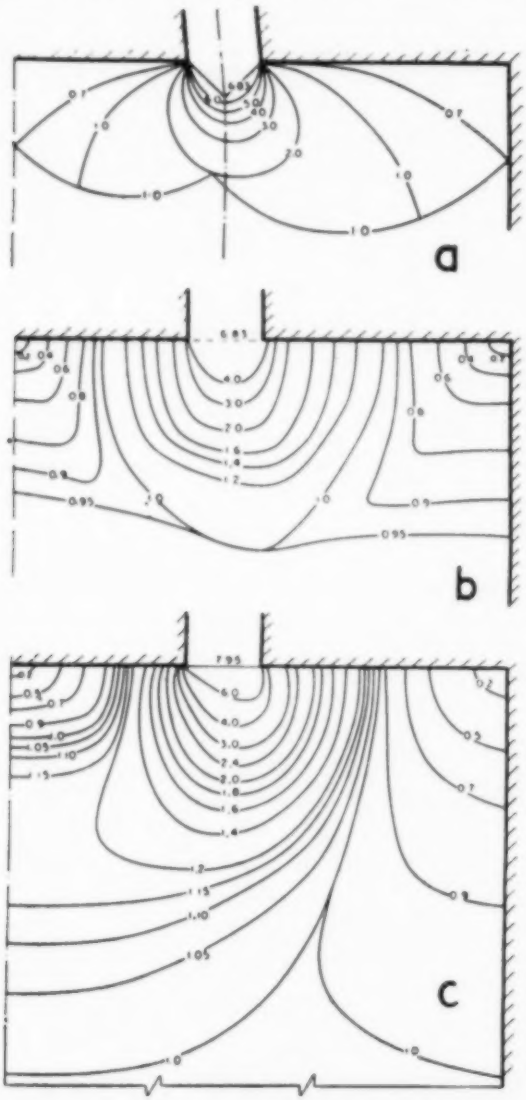

Fig. 8. Magnitude of velocity vectors :
(a) approximate solution, ideal plastic solid, plane strain.
(b) experimental, lead, plane strain.
(c) experimental lead, axial symmetry.

velocities in the orifices for the plane strain and axially symmetric extrusions cannot be the same since the area of the central plane was kept constant. These velocities differ by only about 15%, however, so that a qualitative comparison is

still possible. Hence, examining the velocity patterns of Fig. 8 under these conditions reveals the following likenesses and differences :

(a) A magnitude of 2 occurs in approximately the same billet location upstream from the orifice in all three cases.

(b) Stagnation points for the lead extrusion occur at the intersections of die with cylinder wall and billet centre line, while for the ideal plastic solid it is an area above the 0·7 limiting velocity line.

(c) The velocity in Fig. 8 (c) goes through a maximum on the billet centre line, while no such maximum exists for the velocity of Fig. 8 (b).

(d) Limiting shear lines in the theoretical case, as mentioned earlier, occur in the actual extrusions as transition regions extending over a considerable area, being largest for the axially symmetric case.

6. CONCLUSIONS

The slip-line solution of an ideal plastic solid, although failing to account fully for all observed experimental facts, permits prediction at least to a first approximation of maximum shear directions and magnitude and direction of velocity vectors. There can be no doubt that most of the disagreement lies in the fact that the theory assumes an artificial solid, whose elastic strains are neglected so that a rigid material transforms to a plastic material over an infinitesimal region. However, if such elastic strains as occur in the real metal are taken into account, the advantage of a simple theory is undoubtedly lost. Under this condition it is unlikely that simple graphical techniques will be available to solve forming problems.

ACKNOWLEDGMENTS

The authors wish to thank the National Science Foundation (Grant NSF-G-1002) and the University of California for making funds and facilities available for carrying out the investigation. They also wish to thank Mr. R. ARMSTRONG, undergraduate, and Mr. W. SEIFERT, graduate, students at the University of California for their assistance in the experimental phases of the project.

REFERENCES

HILL, R. 1950 *The Mathematical Theory of Plasticity* (Clarendon Press).
GREEN, A. P. 1955 *J. Mech. Phys. Solids*, **3**, 189.
THOMSEN, E. G., YANG, C. and BIERBOWER, J. B. 1954 *Univ. Calif. Pub. Eng.*, **5**, 89.
THOMSEN, E. G. and FRISCH, J. 1955 *Trans. Amer. Soc. Mech. Eng.*, **77**, 1343.
THOMSEN, E. G. 1955 A.S.M.E. Preprint, 55-A-51, 1.
1955 *Trans. Amer. Soc. Mech. Eng.*, **77**, 515.

Journal of the Mechanics and Physics of Solids, 1956, Vol. 4, pp. 191 to 198. Pergamon Press Ltd., London.

EXTRUSION THROUGH SQUARE DIES OF LARGE REDUCTION

By W. Johnson
Department of Mechanical Engineering, University of Sheffield

(*Received* 1 *February* 1956)

Summary

Slip-line fields for square dies of large reduction are proposed, and results and expressions for calculating the extrusion pressure for extreme values of friction are given.

1. Introduction

When metal is extruded through square dies, dead metal zones are seen to form at the junction of the die and the container wall; Figs. 1, 3 and 4 illustrate this. Hill (1948), using the theory of slip-line fields, calculated the plane-strain extrusion pressure, p for reductions, r, between about 0·12 and 0·88, assuming dead metal

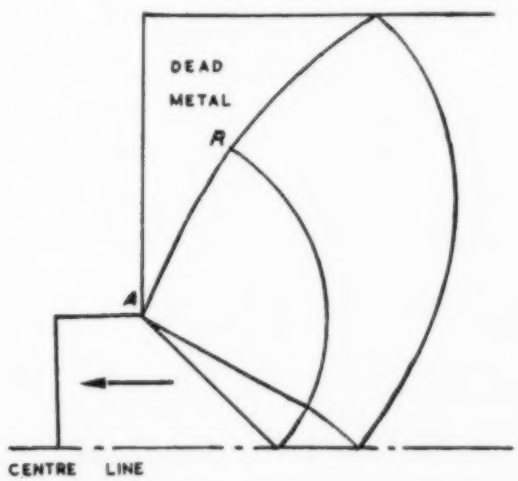

Fig. 1. Dead metal zone extending across all of the die face.

zones to cover the whole of the die face and no friction between the metal and the container wall. In this case of frictionless extrusion, the slip-lines meet the container wall at 45°. Calculations of the extrusion pressure have also been made (Johnson 1955) for the case when there is friction between metal and container wall. The kind of slip-line field used was the same as that of Hill, the slip-lines,

however, meeting the container wall at angles other than 45° ; the greatest reduction attained was about 0·925. The upper limit in both these cases was attained when the radius AR (Fig. 1) coincided with the die face. This paper presents the results of calculations of extrusion pressure when the dead metal zones are lodged in the top-most corner between die and container wall, a situation which often occurs in practice, when the reductions are very large. It will be obvious that these fields and the expressions obtained below could easily be adapted to wedge-shaped dies of semi-angle between 45° and 90°.

2. SMOOTH DIE

The slip-line field shown in Fig. 2 is the application to a square die of the field given by HILL (1950) in connexion with sheet drawing through dies of small

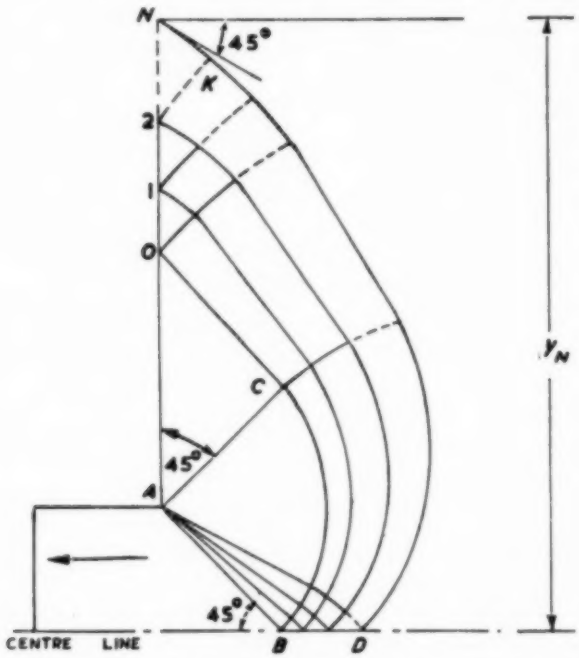

Fig. 2. Slip-line field when the die face and container wall are both smooth (case *i*).

angle. ABC is a circular arc with angle CAB equal to 90°, AB being inclined at 45° to the centre-line of the extruding sheet, and OC at 45° to the die face. This simple pattern is easily extended outwards from ACB, the slip-lines continuing to meet the centre-line between B and D, and the die face from O to N, at 45°. The initial pattern applies for a reduction of 0·667 and the extended fields to reductions larger than this. The slip-lines having been chosen to meet the die face at 45°, and hence the container wall also, means that the assumption of no friction between metal and both the die face and the container wall has been made ; this is case (i).

Suppose now that a slip-line such as NK (see Fig. 3) is continued until it meets the container wall tangentially at M. Then, assuming NKM to be a dead-metal zone, this field satisfies the conditions in which there is no friction between metal and die face but an amount of friction at the container wall sufficient to cause shearing along it; this is case (ii).

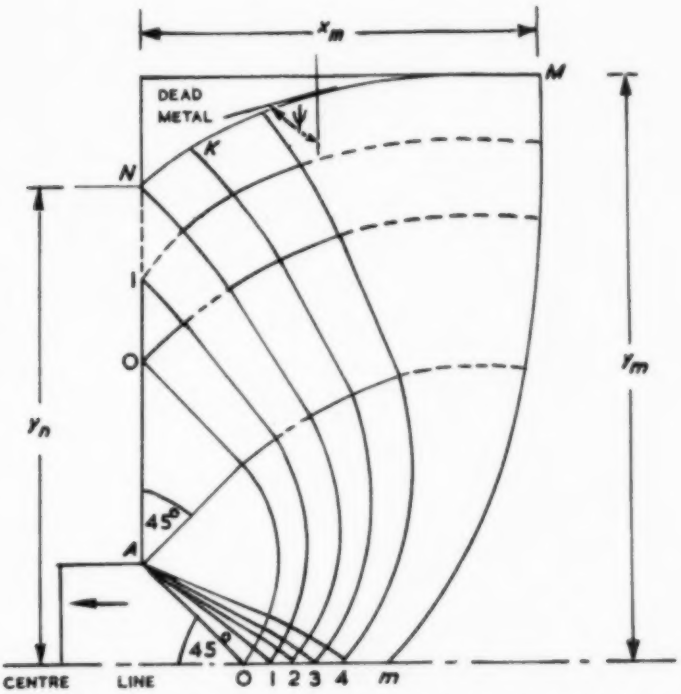

Fig. 3. Slip-line field when the die face is smooth and the container wall rough (case *ii*).

3. Rough Die

If the coefficient of friction between the die face and the metal is greater than 0·176, shearing of the metal occurs along the lower edge of the die face. This case may be regarded as the other extreme from that of a perfectly smooth die face. In Fig. 4, OO is a circular arc and the slip-line field is extended outwards from it as shown. The slip-lines meet the die face either normally or tangentially from O to N. Lines such as NM and mM are chosen to meet the container wall at 45° and the region NPM is taken to be a region of dead metal. In this instance, there is no friction between metal and container wall; this is case (iii).

If, next, NM is extended until it meets the container tangentially, there is shearing friction at the container wall; this is case (iv).

We have thus defined the fields for four extreme cases for extrusion through square dies of large reduction; each field, incidentally, is acceptable from the point of view of velocity conditions.

4. METHOD OF CALCULATION

For each of the four cases described above, slip-line fields of 5° equiangular mesh have been drawn, and by use of the Hencky equations the following expressions were deduced. Measurements from the drawn slip-line fields were inserted in these expressions and provide values of the extrusion pressure for particular values of the reduction.

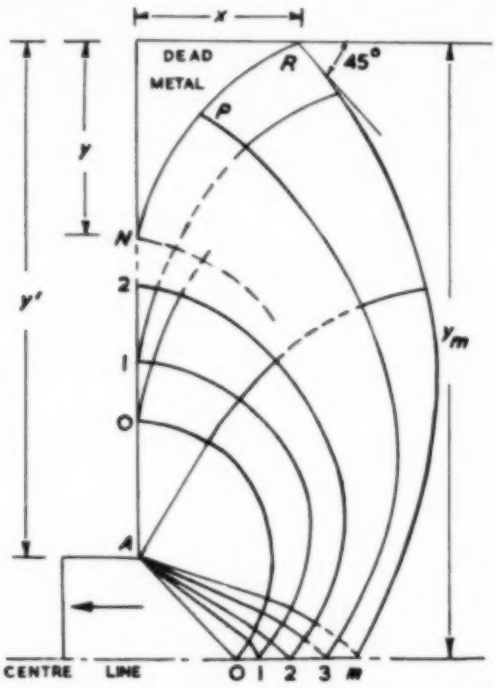

Fig. 4. Slip-line field when the die face is rough and the container wall smooth (case *iii*).

(i) *Smooth Die Face and Smooth Container Wall* (*Fig.* 2)

$$q_N/2k = 1 + \tfrac{1}{2}\pi + 2\,(N-1)\cdot\Delta\phi. \tag{1}$$

q_N is the hydrostatic pressure at N; $\Delta\phi$ is 0·0873 radian for a 5° net.

$$y_N \cdot p/2k = (\overline{AO})\,(1 + \tfrac{1}{2}\pi) + \tfrac{1}{2}\,(\overline{O1})\,(q_1/2k + q_2/2k) + \ldots$$
$$\ldots + \tfrac{1}{2}\,(\overline{N-1\cdot N})\,(q_{N-1}/2k + q_N/2k). \tag{2}$$

$(\overline{N-1\cdot N})$ means the distance between point $(N-1)$ and N on the die face, and p is the extrusion pressure.

(ii) *Smooth Die Face and Rough Container Wall* (*Fig.* 3)

$$y_M\,p/2k = (p/2k)_S \cdot y_N + \tfrac{1}{2}x_M + (y_M - y_N)\,(p_N/2k) + I \tag{3}$$

where $(p/2k)_s$ is equal to the right-hand side of (2), and

$$I = \Sigma(\psi - \tfrac{1}{4}\pi)\sin\psi\cdot\Delta s$$

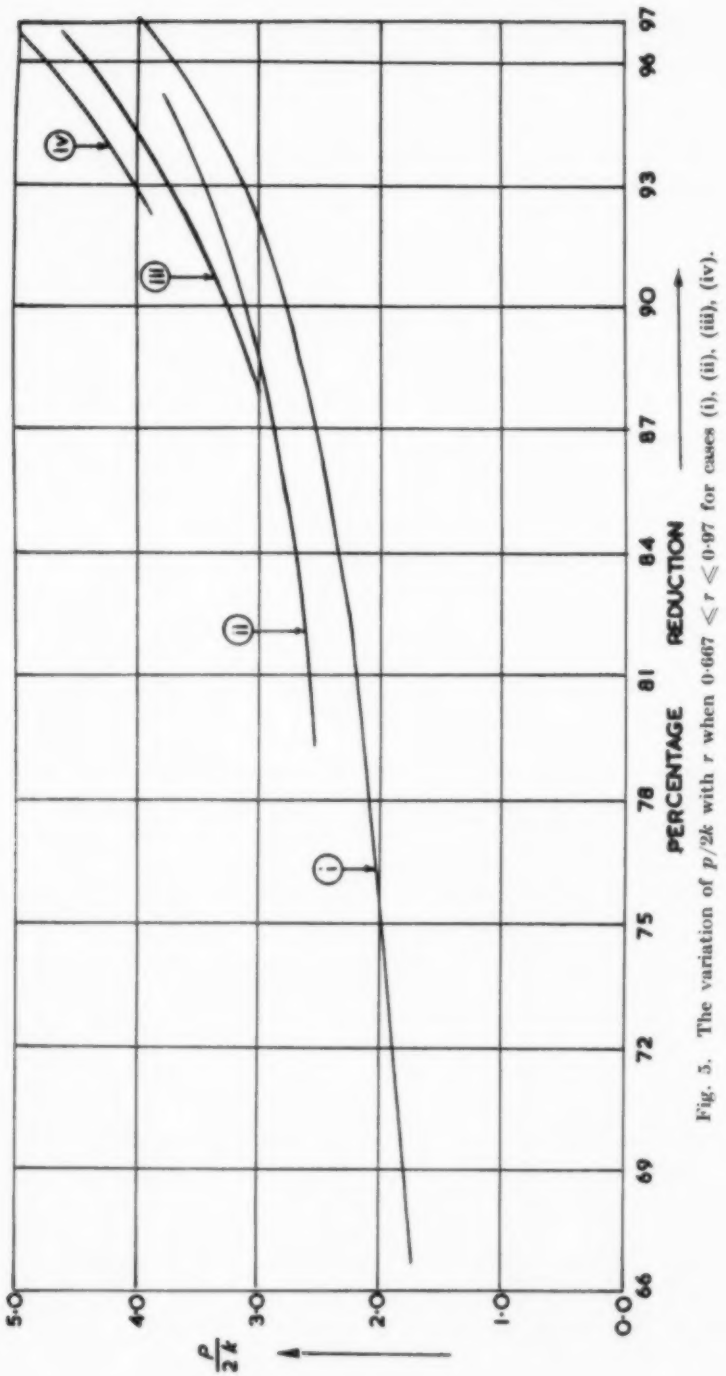

Fig. 5. The variation of $p/2k$ with r when $0{\cdot}667 \leqslant r \leqslant 0{\cdot}97$ for cases (i), (ii), (iii), (iv).

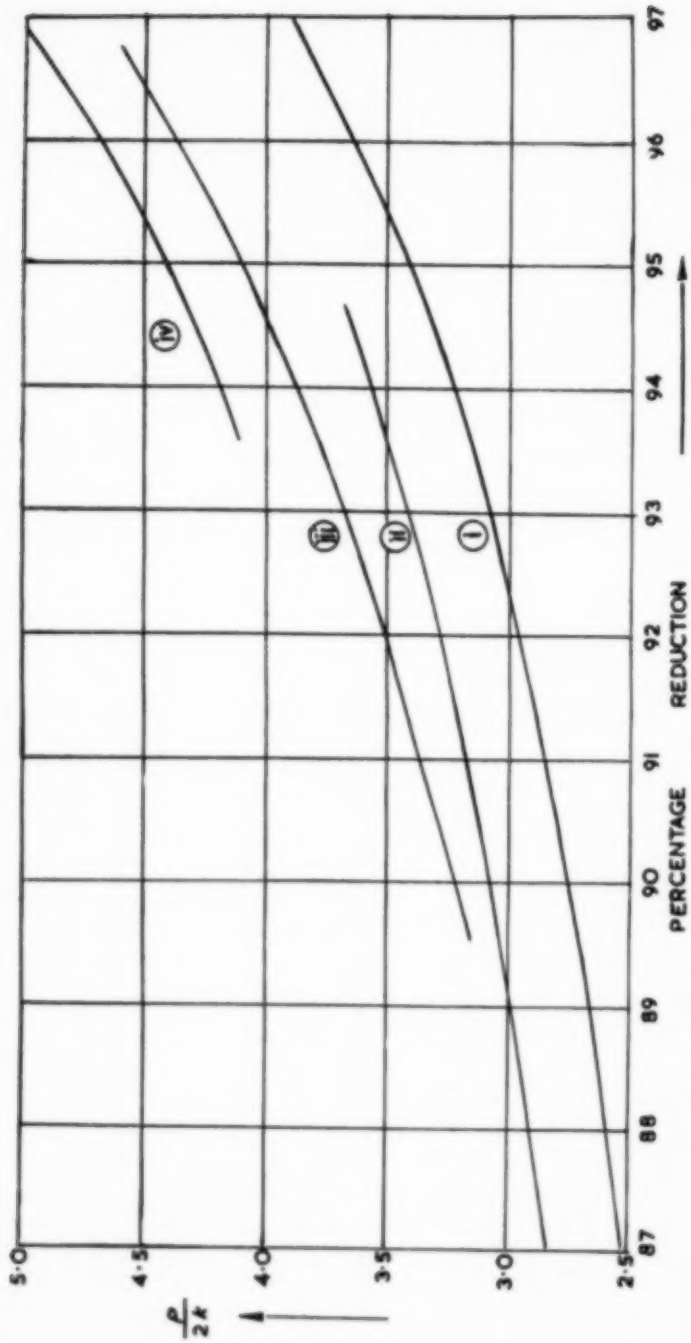

Fig. 6. The variation of $p/2k$ with r when $0{\cdot}87 \leqslant r \leqslant 0{\cdot}97$ for cases (i), (ii), (iii), (iv).

the summation being taken along NM.

The coefficient of friction at the container wall is

$$\mu = 1/(1 + \tfrac{3}{2}\pi + 4m\,\Delta\phi). \tag{4}$$

(iii) *Rough Die Face and Smooth Container Wall* (*Fig.* 4)

$$y_M\,(p/2k) = \tfrac{1}{2}\left[y^1\,(1 + \tfrac{3}{2}\pi) + x + 2\Delta\phi\,\{(01) + 3\,(12) + \ldots \right.$$
$$\left. \ldots + 2\,(\overline{N-1})\,(\overline{N-1\cdot N}) + 2Ny\} + 2I\right] \tag{5}$$

$(\overline{N-1\cdot N})$ is the distance measured along the die face between points $(N-1)$ and N, and

$$I = 2\Sigma\,\psi\cdot\sin\psi\cdot\Delta s$$

the summation being taken along NM.

(iv) *Rough Die Face and Rough Container Wall*

The expression for the extrusion pressure in this case is similar to (5) and the coefficient of friction at the container wall is

$$\mu = 1/(1 + \tfrac{5}{2}\pi + 4m\,\Delta\phi) \tag{6}$$

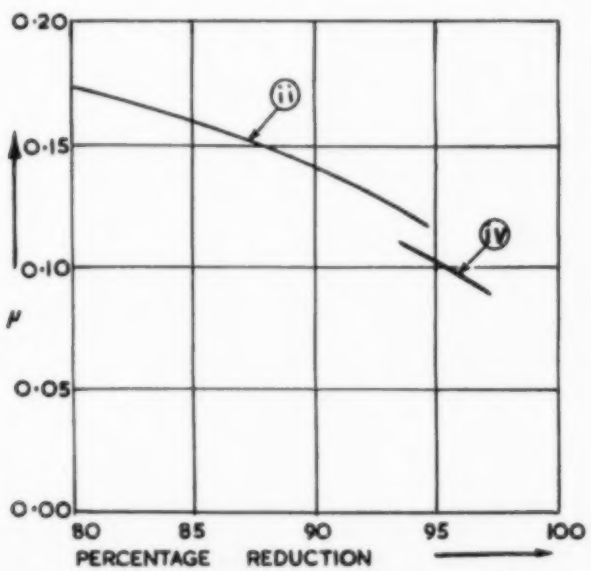

Fig. 7. The variation of μ with r for cases (ii) and (iv).

5. Theoretical Results

The results of the calculations are given in Fig. 5, the values of $p/2k$ for reductions greater than 0·87 being shown to a larger scale in Fig. 6. Curves (iii) and (iv) are continuations of the curves referred to as AB and CD in a previous paper (Johnson 1955a). In Fig. 7, the variation of μ with r for cases (ii) and (iv) is given.

It is interesting to know certain of the proportions of the slip-line fields and these are presented in Table 1. d is the ratio between the length of the dead metal zone at the container wall and the total thickness of the sheet before extrusion. f is the ratio between the greatest width of the field measured from the die face and the total thickness of the sheet before extrusion.

Table 1

	Case (i)	r	*Case (ii)*	r	*Case (iii)*	r	*Case (iv)*	r
f	0·236	0·667	0·496	0·793	0·348	0·879	0·653	0·925
	0·156	0·968	0·457	0·947	0·323	0·967	0·652	0·969
d	0	0·667	0·496	0·793	0·173	0·879	0·653	0·925
	0	0·968	0·457	0·947	0·168	0·967	0·652	0·969

Over the range of reductions given in this paper, the results may be expressed empirically as follows, to an accuracy of better than 2 per cent :

Case (i). $p/2k = 0{\cdot}63 + 0{\cdot}95 \ln \{1/(1-r)\}$.

Case (ii). $p/2k = 1{\cdot}19 + 0{\cdot}83 \ln \{1/(1-r)\}$.

Case (iii). $p/2k = 0{\cdot}37 + 1{\cdot}24 \ln \{1/(1-r)\}$.

Case (iv). $p/2k = 0{\cdot}63 + 1{\cdot}28 \ln \{1/(1-r)\}$.

Acknowledgments

The writer wishes to thank Professor H. W. Swift for his kindly encouragement and Professor R. Hill for a useful private communication on the subject.

Thanks are also due to B.I.S.R.A. for permission to publish these results which are taken from the original report (Johnson 1955b).

References

Hill, R. 1948 *J. Iron Steel Inst.*, **158**, 177.

1950 *Mathematical Theory of Plasticity* (Clarendon Press).

Johnson, W. 1955a *J. Mech. Phys. Solids*, **3**, 218.

1955b *B.I.S.R.A. Report* MW/B/31/55.

Journal of the Mechanics and Physics of Solids, 1956, Vol. 4, pp. 199 to 205. Pergamon Press Ltd., London.

ASSOCIATED PROBLEMS IN TWO-DIMENSIONAL ELASTICITY

By J. E. Adkins
British Rubber Producers' Research Association, Welwyn Garden City

(*Received 2nd March*, 1956)

Summary

A method is outlined for the simultaneous solution of two or more problems, with analytically similar boundary conditions, in two-dimensional elasticity. The procedure is illustrated by examples.

1. Introduction

In the treatment of two-dimensional problems in elasticity it is customary to consider separately the first boundary-value problem, in which values of the stresses are given over the boundaries of the elastic body, and the second boundary-value problem, in which values of the displacements are so prescribed. When the equations for plane strain or generalized plane stress are formulated in complex variable notation, however, the expressions for the displacement at a point, and the force resultant on a curve, assume analytically similar forms. Hill (1955) has observed a similar feature for problems in plane strain, and by making use of this result it is possible, not only to solve corresponding problems of different types simultaneously, but in the subsequent analysis to derive the stresses and displacements from a single function.

The procedure is illustrated by the examples of a circular annulus with prescribed systems of stress and displacement along its boundaries, and of an infinite body containing a single internal circular boundary. In the latter case, a relation noted by Hill for incompressible plane strain is readily obtained. Other applications are briefly discussed.

2. Simultaneous Solution of Associated Problems

We consider an elastic body in plane strain or generalized plane stress, and, in a rectangular Cartesian co-ordinate system denote by u, v, the components of displacement, and by X, Y, the components of the resultant force on a curve, measured from a fixed point to the point x, y. In terms of complex potential functions $\Omega(z)$, $\omega(z)$ (see, for example, Green and Zerna 1954, § 8.1) we then have, in the absence of body forces

$$\left.\begin{aligned} \mu D &= \kappa\Omega(z) - z\overline{\Omega}'(\bar{z}) - \overline{\omega}'(\bar{z}) \qquad (D = u + iv, \qquad z = x + iy), \\ X + iY &= 2i\left\{\Omega(z) + z\overline{\Omega}'(\bar{z}) + \overline{\omega}'(\bar{z})\right\}, \end{aligned}\right\} \quad (1)$$

where $\kappa = 3 - 4\nu$ for plane strain and $\kappa = (3 - \nu)/(1 + \nu)$ for generalized plane stress, μ and ν being the modulus of rigidity and Poisson's ratio respectively.

If we introduce the function

$$\Phi_\alpha = \alpha\Omega(z) + z\overline{\Omega}'(\bar{z}) + \overline{\omega}'(\bar{z}), \tag{2}$$

these results can be written

$$\mu D = -\Phi_{-\kappa} \quad , \quad X + iY = 2i\,\Phi_1 \tag{3}$$

This suggests that if there is a single boundary C, two associated problems may be solved simultaneously by making use of the function Φ_α. Thus, we solve the problem for which Φ_α takes given values

$$\Phi_\alpha = B \text{ (say)}$$

along C, giving the complex potentials as functions of z and the parameter α. From these potentials $\Omega(z, \alpha)$, $\omega(z, \alpha)$ we form the two-parameter function

$$\Phi_{\beta,\alpha} = \beta\Omega(z, \alpha) + z\,\overline{\Omega}'(\bar{z}, \alpha) + \overline{\omega}'(\bar{z}, \alpha). \tag{4}$$

The solutions for two associated problems, one satisfying a boundary-stress condition

$$\Phi_1 = B \text{ along } C,$$

and the other a boundary-displacement condition

$$\Phi_{-\kappa} = B \text{ along } C,$$

are then respectively

$$\left.\begin{aligned} \mu D &= -\Phi_{-\kappa,1} \quad , \quad X + iY = 2i\,\Phi_{1,1}. \\ \mu D &= -\Phi_{-\kappa,-\kappa} \quad , \quad X + iY = 2i\,\Phi_{1,-\kappa}. \end{aligned}\right\} \tag{5}$$

The procedure may evidently be generalized to deal with problems involving several boundaries by assigning a separate function

$$\Phi_{\alpha_r} = \alpha_r\,\Omega(z) + z\,\overline{\Omega}'(\bar{z}) + \overline{\omega}'(\bar{z}) \qquad (r = 1, 2, \ldots n) \tag{6}$$

to each boundary C_r for which separate conditions are prescribed. We then have to satisfy the boundary conditions

$$\Phi_{\alpha_r} = B_r \qquad \text{on} \quad C_r \qquad (r = 1, 2, \ldots n),$$

where $\alpha_r = 1$ or $\alpha_r = -\kappa$ according as a stress or displacement condition is given on C_r. This leads to complex potentials

$$\Omega = \Omega(z, \alpha_r) \quad , \quad \omega = \omega(z, \alpha_r),$$

from which we form the $(n + 1)$-parameter function

$$\Phi_{\beta,\alpha_r} = \beta\Omega(z, \alpha_r) + z\,\overline{\Omega}'(\bar{z}, \alpha_r) + \overline{\omega}'(\bar{z}, \alpha_r). \tag{7}$$

where α_r now denotes, for brevity, the set $\alpha_1, \alpha_2, \ldots \alpha_n$. From this function we obtain

$$\mu D = -\Phi_{-\kappa,\alpha_r} \quad , \quad X + iY = 2i\,\Phi_{1,\alpha_r}. \tag{8}$$

whilst the stresses σ_x, σ_y, τ_{xy} follow from the formulae

$$\sigma_x + \sigma_y = 4\frac{\partial \Phi_{1,\alpha_r}}{\partial z} \quad , \quad \sigma_x - \sigma_y + 2i\,\tau_{xy} = -4\frac{\partial \Phi_{1,\alpha_r}}{\partial \bar{z}}. \tag{9}$$

In this case the method yields, in general, 2^n distinct solutions obtained by giving each of the constants α_r the values 1 and $-\kappa$.

For a simply connected body in equilibrium with no body forces, X, Y, u and v, and hence also Φ_α and $\Phi_{\beta,\alpha}$, must be single-valued functions of position. For a multiply connected body, the complex potentials may be multi-valued, and $\Phi_{\beta\,\alpha_r}$ may then change in value during a complete circuit of a given boundary C_k. For $\alpha_k = 1$ this implies a resultant force on C_k; for $\alpha_k = -\kappa$ it indicates a translational dislocation of the Weingarten type (see, for example, Love, 1952, § 156A). The two cases are not mutually exclusive.

3. The Circular Ring

The procedure of § 2 may be illustrated by considering the deformation of an elastic body bounded by concentric circles of radii a and b ($b = \lambda a > a$) surrounding the origin. Since problems of this type have been considered in some detail by Timpe (1905), Muskhelishvili (1953), Simpson (1955) and others, only a brief treatment will be given for the case where there is neither a dislocation nor a resultant force on either boundary. We therefore suppose the boundary conditions to be given in the form

$$\left.\begin{aligned} \Phi_{\alpha_1} &\equiv \alpha_1\,\Omega(z) + z\,\overline{\Omega}'(\bar{z}) + \overline{\omega}'(\bar{z}) = \sum_{-\infty}^{\infty} A_n \left(\frac{z}{a}\right)^{n+1} \quad \text{on} \quad z\bar{z} = a^2, \\ \Phi_{\alpha_2} &\equiv \alpha_2\,\Omega(z) + z\,\overline{\Omega}'(z) + \overline{\omega}'(\bar{z}) = \sum_{-\infty}^{\infty} B_n \left(\frac{z}{a}\right)^{n+1} \quad \text{on} \quad z\bar{z} = b^2, \end{aligned}\right\} \tag{10}$$

where A_n and B_n are constants which may be real or complex. It is easily seen, by writing $z = r\,e^{i\theta}$, that these expressions represent Fourier series expansions for the distributions of stress or displacement around the circles $r = a$, $r = b$.

The problem may be solved in the usual manner by assuming series expansions of the type

$$\Omega(z) = \sum_{-\infty}^{\infty} a_n \left(\frac{z}{a}\right)^{n+1} \quad , \quad \omega'(z) = \sum_{-\infty}^{\infty} b_n \left(\frac{z}{a}\right)^{n-1} \tag{11}$$

for the complex potential functions. When these are introduced into the second of equations (10) we obtain at $\bar{z} = b^2/z$

$$\alpha_2 \sum_{-\infty}^{\infty} a_n \left(\frac{z}{a}\right)^{n+1} + \sum_{-\infty}^{\infty} (n+1)\,\lambda^{2n}\,\bar{a}_n \left(\frac{a}{z}\right)^{n-1} + \sum_{-\infty}^{\infty} \lambda^{2n-2}\,\bar{b}_n \left(\frac{a}{z}\right)^{n-1} = \sum_{-\infty}^{\infty} B_n \left(\frac{z}{a}\right)^{n+1},$$

or alternatively

$$\sum_{-\infty}^{\infty} \{\alpha_2\,a_{-n} + (n+1)\,\lambda^{2n}\,\bar{a}_n + \lambda^{2n-2}\,\bar{b}_n - B_{-n}\} \left(\frac{a}{z}\right)^{n-1} = 0.$$

Since the coefficient of each power of z must vanish separately we have

$$\alpha_2\,a_{-n} + (n+1)\,\lambda^{2n}\,\bar{a}_n + \lambda^{2n-2}\,\bar{b}_n - B_{-n} = 0, \tag{12}$$

whilst the complex conjugate of the equation obtained by replacing n by $-n$ is

$$(n-1)\,\lambda^{-2n}\,a_{-n} - \alpha_2\,\bar{a}_n - \lambda^{-(2n+2)}\,b_{-n} + \overline{B}_n = 0. \tag{13}$$

The corresponding relations for the first boundary condition may be obtained from (12) and

(13), by putting $\lambda = 1$ and replacing α_2 and B_n by α_1 and A_n respectively. We thus have four linear algebraic relations for a_{-n}, $\bar{a}_n$, b_{-n} and $\bar{b}_n$ which may be solved to yield

$$\left.\begin{aligned} a_n &= \{(\alpha_1 - \lambda^{-(2n-2)}\alpha_2)(A_n - \lambda^{2n+2}B_n) \\ &\qquad + (n-1)(1-\lambda^2)(\bar{A}_{-n} - \lambda^{-(2n-2)}\bar{B}_{-n})\}/\Delta \\ &= a_n(\alpha_1, \alpha_2), \\ b_n &= \lambda^2\{(n+1)(\alpha_2 - \lambda^{2n}\alpha_1)(\lambda^{-2n}A_n - \lambda^2 B_n) \\ &\qquad - (n^2-1)(1-\lambda^2)(\bar{A}_{-n} - \lambda^{-2n}\bar{B}_{-n}) \\ &\qquad - (\lambda^{-2n}\alpha_1 - \lambda^2\alpha_2)(\alpha_2\bar{A}_{-n} - \alpha_1\bar{B}_{-n})\}/\Delta \\ &= b_n(\alpha_1, \alpha_2), \end{aligned}\right\} \tag{14}$$

provided that

$$\Delta \equiv \alpha_1^2 - \lambda^2(\lambda^{2n} + \lambda^{-2n})\alpha_1\alpha_2 + \lambda^4\alpha_2^2 + (n^2-1)(1-\lambda^2)^2 \neq 0. \tag{15}$$

The stresses and displacements may be derived by combining the three-parameter function

$$\Phi_{\beta,\alpha_1,\alpha_2} = \sum_{-\infty}^{\infty}\{\beta a_n(\alpha_1,\alpha_2)z^{n+1} + (n+1)\bar{a}_n(\alpha_1,\alpha_2)z\bar{z}^n + \bar{b}_{n+2}(\alpha_1,\alpha_2)z^{n+1}\}/a^{n+1}$$

with (8) and (9). By putting $\alpha_1 = \alpha_2 = 1$ we then have the solution for prescribed systems of stress on the outer and inner boundaries. Similarly if $\alpha_2 = \alpha_2 = -\kappa$ the displacement conditions are known on these two surfaces, whilst the choice $\alpha_1 = 1$, $\alpha_2 = -\kappa$ implies that the stress distribution is given on the surface $r = a$ and the displacements are prescribed on the outer boundary $r = b$. Allowing for differences in notation, it may be shown that the results thus obtained agree with those derived separately for the three cases by SIMPSON (1955).

Solutions for problems with a uniform distribution of stress on the two boundaries follow by taking A_0 and B_0 to be real in (10) and allowing the remaining coefficients A_n and B_n for $n \neq 0$ to become zero. Equations (12) and (13) are then identical and yield

$$(\alpha_2 + 1)a_0 + b_0/\lambda^2 = B_0,$$

the corresponding relation derived from the first boundary condition being

$$(\alpha_1 + 1)a_0 + b_0 = A_0.$$

Solving for a_0 and b_0 we have

$$a_0 = (A_0 - \lambda^2 B_0)/\Delta_0 \quad , \quad b_0 = \lambda^2\{(\alpha_1+1)B_0 - (\alpha_2+1)A_0\}/\Delta_0,$$

with

$$\Delta_0 = \alpha_1 + 1 - \lambda^2(\alpha_2 + 1),$$

and the three-parameter function for the associated problems becomes

$$\Phi_{\beta,\alpha_1,\alpha_2} = \frac{(\beta+1)(A_0 - \lambda^2 B_0)z\bar{z} + \{(\alpha_1+1)B_0 - (\alpha_2+1)A_0\}\lambda^2 a^2}{\{\alpha_1 + 1 - \lambda^2(\alpha_2+1)\}az}. \tag{16}$$

When the boundaries are subject to all-round tensions T_1 and T_2, we put $A_0 = \frac{1}{2}aT_1$, $B_0 = \frac{1}{2}aT_2$, $\alpha_1 = \alpha_2 = 1$, and obtain from (16)

$$\mu D = -\Phi_{-\kappa,1,1} = \tfrac{1}{4}\{(\kappa-1)(T_1 - \lambda^2 T_2)z\bar{z} + 2(T_1 - T_2)\lambda^2 a^2\}/\{(1-\lambda^2)z\},$$

$$X + iY = 2i\Phi_{1,1,1} = i\{(T_1 - \lambda^2 T_2)z\bar{z} - (T_1 - T_2)\lambda^2 a^2\}/\{(1-\lambda^2)z\}.$$

Again, if the outer boundary $r = b$ is under all-round tension T and the inner boundary is cemented to the rigid disc $r = a$, we put $A_0 = 0$, $B_0 = \frac{1}{2}aT$, $\alpha_1 = -\kappa$, $\alpha_2 = 1$ giving

$$\mu D = -\Phi_{-\kappa,-\kappa,1} = \frac{(\kappa-1)\lambda^2 T}{2(\kappa-1+2\lambda^2)}\left(z-\frac{a^2}{\bar{z}}\right),$$

$$X+iY = 2i\Phi_{1,-\kappa,1} = \frac{i\lambda^2 T}{\kappa-1+2\lambda^2}\left\{2z+(\kappa-1)\frac{a^2}{\bar{z}}\right\}.$$

Other cases may be considered similarly.

4. Infinite Body containing a Circular Boundary

Consider an infinite elastic body bounded internally by the circle $|z| = a$ and subjected to a uniform distribution of stress at infinity. For large $|z|$ the complex potentials take the forms

$$\Omega(z) = Az \quad , \quad \omega'(z) = Bz,$$

where A and B are, in general, complex constants. If $\Phi_\alpha = 0$ on the internal boundary, we may obtain by the method of the preceding section

$$\Omega(z,\alpha) = Az - \overline{B}\frac{a^2}{\alpha z} \quad , \quad \omega'(z,\alpha) = Bz - (A+\alpha\overline{A})\frac{a^2}{z} - \overline{B}\frac{a^4}{\alpha z^3},$$

and the two-parameter function $\Phi_{\beta,\alpha}$ becomes

$$\Phi_{\beta,\alpha} = (\beta A+\overline{A})z - (\alpha A+\overline{A})\frac{a^2}{\bar{z}} + B\frac{a^2}{\alpha\bar{z}^2}\left(z-\frac{a^2}{\bar{z}}\right) - \overline{B}\left(\frac{\beta a^2}{\alpha z}-\bar{z}\right). \tag{17}$$

For $\alpha = 1$, the internal boundary is a stress-free circular hole; for $\alpha = -\kappa$ it is a fixed boundary. Expressions for the stresses and displacements in these two cases now follow directly from equations (8) and (9).

If T_1 and T_2 are the principal stresses at infinity and are oriented so that T_1 makes a positive angle γ with the x axis, A and B are given by

$$4(A+\overline{A}) = T_1+T_2 \quad , \quad 4B = -(T_1-T_2)e^{-2i\gamma}, \tag{18}$$

the imaginary part of A merely contributing a rigid-body rotation of magnitude

$$\tfrac{1}{2}\left(\frac{\partial v}{\partial x}-\frac{\partial u}{\partial y}\right) = \frac{1}{2i}\left(\frac{\partial D}{\partial z}-\frac{\partial \overline{D}}{\partial \bar{z}}\right) = \frac{\kappa+1}{2i\mu}(A-\overline{A}). \tag{19}$$

For plane strain of incompressible materials, where $\kappa = 1$, Hill (1955) has shown that there exists a pair of related states for which, in the present notation

$$X+iY = 2\mu(u^*+iv^*) \quad \text{and} \quad 2\mu(u+iv) = -(X^*+iY^*)$$

or, in terms of the function $\Phi_{\beta,\alpha}$,

$$\Phi_{1,1} = i\Phi^*_{-1,-1} \quad , \quad \Phi_{-1,1} = i\,\Phi^*_{1,-1},$$

corresponding quantities for the two states being denoted by unstarred and starred quantities respectively. From (17), there now follow immediately the relations

$$A^* = iA \quad , \quad B^* = iB \tag{20}$$

between the corresponding coefficients for the two states. The particular case quoted by Hill for which the stress distribution at infinity in the unstarred state is a uniform tension in the y-direction of magnitude T, is derived by taking $T_1 = 0$, $T_2 = T$ and $\gamma = 0$ in (18), giving $2A = B = T/4$. The starred state then becomes, at infinity, a combined shear and rigid body rotation. Similarly, if the stress distribution at infinity is a uniform all-round tension T, we have $T_1 = T_2 = T$, $4A = T$, $B = 0$ so that, from (19) and (20) the starred state there reduces to a rigid body rotation.

5. Other Applications

The foregoing procedure may evidently be applied to a variety of other problems. Thus Green and Zerna (1954, § 8.19) have considered the effect of a stress-free circular hole upon more general distributions of stress in an infinite body. To do this, they make use of the Hilbert problem in a manner which depends upon the extension of the definition of the complex potentials $\Omega(z)$, $\omega(z)$ to the region $|z| < a$ not containing elastic material. This definition is normally based on the expression for the derivative of the Airy stress function obtained by putting $\varkappa = 1$ in equation (2), and it is then necessary for problems involving stress and displacement boundary conditions considered separately. This duplication of effort can be avoided, however, by making use of the function $\Phi_\varkappa$ and extending the definition of the complex potentials by writing

$$\varkappa\,\Omega(z) + z\,\overline{\Omega}'\left(\frac{a^2}{z}\right) + \overline{\omega}'\left(\frac{a^2}{z}\right) = 0 \quad \text{for} \quad |z| < a,$$

$\overline{\Omega}(a^2/z)$ being obtained from $\overline{\Omega}(\bar{z})$ by replacing $\bar{z}$ by a^2/z and leaving any complex constants in this function unchanged. The subsequent analysis follows the lines indicated by Green and Zerna. Similar modifications can be made for problems in which the internal boundary curve C is not circular in shape, but can be mapped on to a circle by means of a conformal transformation.

Problems involving groups of holes have been considered by Howland (1935), Green (1940), Schulz (1941) and others. Corresponding solutions based on the functions $\Phi_{\varkappa r}$ of § 2 would enable any one of the internal boundaries to be made a stress-free hole or fixed boundary at will.

Acknowledgments

This work forms part of a programme of research undertaken by the Board of the British Rubber Producers' Research Association. The author wishes to thank Mr. A. C. Stevenson for valuable comments on an earlier draft of this paper, and for drawing attention to Simpson's work.

References

Green, A. E. 1940 *Proc. Roy. Soc.* A, **176**, 121.
Green, A. E. and Zerna, W. 1954 *Theoretical Elasticity* (Clarendon Press, Oxford).
Hill, R. 1955 *J. Mech. Phys. Solids*, **4**, 1.
Howland, R. C. J. 1935 *Proc. Roy. Soc.* A, **148**, 471.

Love, A. E. H.	1952	*A Treatise on the Mathematical Theory of Elasticity*, 4th Edition (Cambridge University Press).
Muskhelishvili, N. I.	1953	*Some Basic Problems of the Mathematical Theory of Elasticity*, 3rd Edition (Noordhoff Ltd., Groningen).
Schulz, K. J.	1941	*Over den Spanningstoestand in Doorboorde Platen* (Doctor's Thesis, Delft).
Simpson, M. G.	1955	*Generalized plane stress in an elastic annulus*, Ph.D. Thesis, University of London.
Timpe, A.	1905	*Z. Math. Phys.*, **52**, 348.

BOOK REVIEWS

W. PRAGER: **Probleme der Plastizitätstheorie.** *Birkhauser Verlag, Basel und Stuttgart,* 1955. *pp.* 100.

THIS little book is based on a course of lectures given by the author on a visit to the Technical High-School in Zürich. The topics treated were chosen primarily because of the author's particular research interests, but also to avoid overlapping those fields that Swiss workers have especially studied (e.g. plastic instability). The Chapter headings are (freely translated): Mechanical Properties of Plastic Bodies; Behaviour of Structures in the Plastic Range; Limit Analysis; Finite Plastic Straining. There is no index, but the content of each Chapter is summarized (in English). The printing and quality of paper are excellent.

Professor PRAGER has a reputation of long standing as a particularly lucid and methodical expositor, both when writing and lecturing. This book also is a model of clarity (with, however, one exception to be mentioned), and it is a pleasure to read. Although no prior acquaintance with the subject is assumed, the treatment is taken to the limit of present knowledge; the references, not complete but representative, are remarkably up-to-date (end of 1954). Of course, no attempt has been made to do more than touch on a small fraction of the subject of plastic flow. For example, no experimental work is mentioned in the first Chapter, and the theory itself is presented only in outline and indirectly, the author preferring to indulge his taste for mechanical models. (These make amusing light reading for the specialist, but their didactic value may be doubted: too often the difficulties of understanding how a model works, and in what respect it is or is not a proper analogy, are merely superimposed on the intrinsic difficulties of the subject).

The important part of the book is the Chapter on Limit Analysis, which recapitulates the notable contributions to plastic plate and shell theory by the author and his colleagues, and also discusses the practical significance of limit analysis in general. It is here that the author's customary clarity is lacking, particularly where he speaks of two definitions of load-capacity (p. 40). The first (attributed to this reviewer) is the yield point of a hypothetical rigid-plastic solid. Actually I did not define carrying capacity of an *actual* structure in this way, but pointed out that the numerical value furnished by *limit analysis* is *in fact* the yield-point load of a geometrically similar rigid-plastic structure. Moreover, theoretical and experimental investigations have indicated in what circumstances this latter quantity can be taken as a close approximation to the load that produces intolerable deformation of an actual elastic-plastic solid. It is this load, which in general is necessarily incapable of precise definition, that Professor PRAGER presumably has in mind in his second definition. Yet this is given only (p. 28) in the highly special case of an elastic-plastic structure of simple tension members, in each of which the load remains constant once the strain at the elastic limit is exceeded. In the general case, where the plastic zone spreads progressively from a nucleus, the load *never* settles down to a steady value. I could find no explicit statement of this essential restriction on the practical significance of limit analysis. Towards the end of the Chapter (p. 67) it is possibly hinted at in the discussion of some unpublished American experimental work on plastic bending of a supported plate by a point load. Incidentally, this seems to be the only reference to experimental data in the book and it actually shows limit analysis of plates in a most unfavourable light! Professor PRAGER could have referred with profit to the published English work on combined bending and torsion of bars and tubes, which strikingly demonstrates the significance of rigid-plastic theory (i.e. limit analysis) in more favourable circumstances.

The final Chapter is concerned with the well-known theory of plane plastic strain, together with some representative examples (extrusion, wedge-indentation, and extension of a notched bar). Professor PRAGER departs from the standard presentation of the essential properties of the slip-line field and introduces an auxiliary geometric representation involving the concept of the pole of a Mohr's circle. This seems disadvantageous: a simple result (Hencky's equations) is derived by a comparatively lengthy procedure in which it is always easy to make mistakes about signs and about senses of rotation. The time taken to master this representation, together

with the further 'cycloid property,' does not appear to be justified by any advantages as a research tool; at least, the author does not mention any new problems solved in this way. In the subsequent account of the calculations of the velocity field, Professor PRAGER lays emphasis on the use of the hodograph plane. In this case the auxiliary construction is well justified in certain problems, as A. P. GREEN in particular has shown by some remarkable new solutions.

R. HILL

X-Ray Diffraction by Polycrystalline Materials: H. S. Peiser, H. P. Rooksby and A. S. C. Wilson (Technical Editors). The Institute of Physics, 1955, pp. 725 with 263 figures, 63s. net.

IN this book the three editors, with the help of some 28 other authors, aim to cover the whole field of the application of X-ray diffraction methods to the study of polycrystalline materials. The book, although giving over 1,000 references to original papers, is intended to be self-contained, and to describe sufficient practical and theoretical details to enable a reader to apply the various techniques without recourse to other publications. The complete fulfilment of this counsel of perfection is almost certainly not possible, but those concerned in writing the book are to be congratulated on the high standards they attain.

In the first Chapter many details of basic crystallography are tersely summarized, and this Chapter fulfils the declared aim of serving "as a reminder or as a reference to the elements and formulae of the subject." However, as the Editors anticipate, those readers with no prior knowledge of crystallography will find this Chapter too compressed. Rather surprisingly, there is no similar summary of the theory of X-ray emission, nor of some important features of X-ray absorption.

The remaining eleven Chapters of Part I are concerned with the techniques of recording X-ray diffraction effects, both in the usual types of camera and in special circumstances. This part of the book will be of immense value to those who, although well versed in routine matters, have to develop a special technique for a particular application. The details given will obviate much tedious searching of published work and, because the various authors are experts in their fields, there is often a clear indication given of the best technique.

Chapters 13-22 constitute Part II, and are concerned with the interpretation of X-ray diffraction data. This material here more closely corresponds to that usually covered in the normal text-books, but here the treatment is more extensive and often fills gaps left by the more usual treatments.

Part III, embracing Chapters 23-32, takes the form of a series of essays on the application of X-ray diffraction methods to the study of particular phenomena. Some of these essays will be of interest to a large number of readers, but others are more specialized. The difficult task of selecting the features which should be included, and avoiding overlapping with other portions of the book, has been successfully accomplished. A correct balance has also been maintained by restricting this portion to roughly one fifth of the whole book.

A very useful series of Tables of X-ray wavelengths, trigonometrical functions for lattice parameter correction, etc., is appended. The subject index also appears to be extensive and complete.

It is rather invidious to select portions of such a far-ranging book as this, for particular praise or condemnation since appreciation depends on the rather capricious knowledge of the reviewer. Sufficient to say that this reviewer was surprised to find no mention of balanced filters under monochromators, nor sufficient discussion of extraction techniques for, say, carbides from alloys steels. One wonders too whether there is sufficient on stereographic projection in Chapters 1 and 12 to enable the uninitiated to construct a pole figure, and whether there was a need for Chapter 31 on the powder method in atomic energy research. A particularly praiseworthy feature is that the mathematics is usually expressed in simple terms. Many readers will find that, although this may lead to long and cumbersome equations, they are more readily assimilated than the same equations expressed more elegantly and briefly using an advanced mathematical notation.

Most of the criticisms that can be made are of a minor nature, and this book can, without hesitation, be strongly recommended as an essential reference book for any person whose work involves the use of X-ray diffraction techniques. The book is well printed and illustrated and its price attractive, for which the Institute of Physics deserve thanks.

G. B. GREENOUGH

M. REINER (Editor): **Building Materials, Their Elasticity and Inelasticity.** North-Holland Publishing Co., Amsterdam, 1954. pp. 500.

Two books have appeared recently under the title of "Materials of Construction," and the appearance of another on a similar subject is at first a little disconcerting. But this book is quite different as it illustrates the many materials that exhibit rheological properties and the way in which rheological knowledge has to be applied to a variety of problems. The present trend of engineering industry requires the engineer to be increasingly scientific, and engineering students will welcome a book in which the deformation phenomena of materials, so diverse as steel, concrete, clay, and paint, are presented on some kind of common theoretical basis. Rheology is a branch of physical science which deals with the flow and deformation of all materials used in structural engineering and engineering processes. Materials can vary widely in their physico-chemical structure; and any reader, after having studied this book, cannot help being impressed by the fact that the knowledge and experience obtained on only one class of materials are also very relevant to most of the other building materials.

The book is divided into five parts, A, B, C, D and E. Part A deals with theoretical rheology, physical and chemical aspects, structural engineering; Part B with metals and wood; Part C with plaster, mortar, plain and reinforced concrete, road asphalt; Part D with soils, clay products; Part E with paints, mastics, putties, building board. The book is the combined effort of sixteen contributors; and such a large number, though essential in this case, inevitably results in some inconsistencies in the definitions, and in differences of opinion on some of the ideas expressed on a particular topic in a few of the chapters. On p. 6, for instance, concerning the deflection of a reinforced concrete slab, no attempt is made to explain the difference between instantaneous and immediate strains, or how the velocity of the propagation of stress enters into any attempt to record instantaneous strain. An erroneous impression is also given, in different chapters, that very little creep occurs during the actual loading of a specimen. On p. 113 the present standard method in this country of determining structural safety is condemned on the ground that not all of the irrecoverable deformation produces any structural damage. There is no evidence whatever to justify this statement. On p. 146 it is stated that no real metal is elastic and at the same time use is made of the term elastic limit. Inelasticity and elastic limit are incompatible terms when used together. The value of Chapter 4 on metals would have been enhanced if more attention had been devoted to the application of the given data to the design of structures. On p. 220 it is suggested that concrete exhibits no lateral creep; whereas more recent experiments than those quoted show that concrete, like all other building materials, does creep transversely in both tension and compression. On p. 350 concrete is stated to be so weak in tension that the results of tests to observe creep effects are not reliable. There is overwhelming experimental evidence to show that such a statement is incorrect.

The most interesting and useful chapters are those dealing with structural engineering, metals, wood, concrete and soils, and all these well merit serious study. The chapter on theoretical rheology is over-worked and rather confusing. The most important feature of the book is that it gives a comprehensive survey of the whole field of the fundamentals and knowledge contained in rheology. This unifying characteristic of the book will be greatly welcomed by all students and practising engineers. It can be confidently recommended to all those who wish to acquire a basic knowledge of the rheological behaviour of the materials which are common in engineering practice.

R. H. EVANS

Journal of the Mechanics and Physics of Solids, 1956, Vol. 4, pp. 209 to 229. Pergamon Press Ltd., London.

ELASTOPLASTIC THICK-WALLED TUBES OF WORK-HARDENING MATERIAL SUBJECT TO INTERNAL AND EXTERNAL PRESSURES AND TO TEMPERATURE GRADIENTS

By D. R. Bland
Department of Mathematics, King's College, London

(*Received* 22 *March* 1956)

Summary

Using Tresca's yield criterion and its associated flow rule, solutions are obtained for the stresses, the elastic and plastic strains and the displacements when a thick-walled tube of work-hardening material is subject to internal and external pressures and its surfaces are maintained at different temperatures. In general a numerical integration is necessary, but the solutions can be expressed explicitly when the work-hardening law is linear. On removal of the pressures and the temperature difference plastic flow may or may not occur. In both cases the residual stresses can be calculated. Specific examples are given.

1. Introduction

Koiter (1953) discusses the many solutions to the problem of stress distribution in an elasto-plastic thick walled tube which have been put forward; e.g. by Hill (1950), Hodge and White (1950), Allen and Sopwith (1951), and by Steele (1952). These solutions differ in the yield criterion and the plastic stress-strain relations which they assume.

Koiter himself adopts the Tresca yield criterion and its associated flow rule, i.e. the stress plastic strain-increment relation which follows from making the plastic potential and the yield criterion coincide. On the assumption that the axial stress σ_{zz} is the intermediate principal stress – it is shown later in this paper that this is true under a wide range of conditions – the axial plastic strain increment $d\epsilon_{zz}^{\,p}$ is zero. It follows that the axial strain ϵ_{zz} is purely elastic and that σ_{zz} can be expressed in terms of ϵ_{zz} and of the radial and circumferential stresses σ_{rr} and $\sigma_{\theta\theta}$ by means of Hooke's law. In other solutions of this problem, the calculation of σ_{zz} was a real difficulty; (see Hill (1950) p. 111).

Koiter determines the stresses σ_{rr}, $\sigma_{\theta\theta}$ and σ_{zz} for a tube of non-work-hardening material in both the elastic and plastic regions. He then proceeds to determine the radial displacement u in both regions by making use of the fact that the dilatation is purely elastic. He shows that his solutions agree well with the few available rigorous solutions based on the Mises yield criterion and the associated Reuss flow rule except for the axial stress and strain. However, as the axial stress and strain are small compared to the radial and tangential stress and strain, the differences are of minor practical importance.

The author of the present paper calculates the components of the total strain from the dilatation and the elastic parts of these components from the stress. The differences are the plastic parts of the components of strain. From these last components, the equivalent plastic strain, on which depends the yield stress for a work-hardening material, can be found. This provides the additional equation which is necessary to solve the expanding tube problem for a work-hardening material.

Temperature effects can be included in the classical theory of elasticity by the addition of a term to the generalised Hooke's law. The specifically plastic equations of the elasto-plastic material, namely the yield criterion and the plastic stress-strain increment relations are unaffected by variations of temperature provided that the variations are not large enough to appreciably affect the value of the yield stress. This is assumed to be the case in this paper. It is also assumed that the values of all the other physical constants which occur are effectively independent of temperature. Temperature effects are therefore included in this theory of elastoplastic tubes only by their inclusion in the generalized Hooke's law which connects the stress with the elastic part of the strain.

It is assumed that the tube is sufficiently long for the stress and strain not to vary along the tube. In these circumstances plane sections normal to the axis remain plane and the axial strain ϵ_{zz} is the same throughout the tube at any one time. As the problem is also axisymmetric, it follows that if cylindrical polar co-ordinates r, θ, z are employed the principal directions of stress and strain are radial, circumferential and axial. No confusion will arise if single suffixes are used to denote the principal conponents, i.e. σ_r instead of σ_{rr}, ϵ_z instead of ϵ_{zz} etc.

The analysis of this paper will not be taken beyond the point at which the whole tube becomes plastic. At this point the displacement at the bore, where it is a maximum, is about 3% of the internal radius for an external-internal radius ratio of 4 : 1. For smaller radius ratios it is less. No great error will therefore be introduced if, on calculating the stresses and displacements, the boundary conditions are referred to the original shape of the tube.

2. Analysis

The equation of stress equilibrium in the radial direction

$$\sigma_\theta = \sigma_r + r\frac{d\sigma_r}{dr} \tag{1}$$

and the strain-displacement relations (u is the radial displacement)

$$\epsilon_r = \frac{du}{dr} \tag{2}$$

and

$$\epsilon_\theta = \frac{u}{r} \tag{3}$$

are satisfied in both the elastic and plastic parts of the tube. The strain-stress-temperature relations in the elastic part are (Love, 1927, p. 108),

$$\epsilon_r^e = \frac{1}{E}\sigma_r - \frac{\nu}{E}\sigma_\theta - \frac{\nu}{E}\sigma_z + \alpha T, \tag{4}$$

$$\epsilon_\theta^e = -\frac{\nu}{E}\sigma_r + \frac{1}{E}\sigma_\theta - \frac{\nu}{E}\sigma_z + \alpha T, \tag{5}$$

and

$$\epsilon_z^e = -\frac{\nu}{E}\sigma_r - \frac{\nu}{E}\sigma_\theta + \frac{1}{E}\sigma_z + \alpha T, \tag{6}$$

where E is Young's modulus, ν Poisson's ratio and α the linear coefficient of expansion. The superfix e is employed as the same equations are satisfied by the elastic part of the strain in the plastic region. In the elastic region the whole strain is elastic and the superfix can be dropped.

Subject to $\sigma_\theta \geqslant \sigma_z \geqslant \sigma_r$, Tresca's criterion states that yielding occurs when

$$\sigma_\theta - \sigma_r = k. \tag{7}$$

k is the yield stress. For a work-hardening material it will depend, for any material element, on the total plastic deformation of the element.

The associated flow rule states that, subject to $\sigma_\theta > \sigma_z > \sigma_r$

$$d\epsilon_\theta^p = -d\epsilon_r^p \geqslant 0 \quad \text{and} \quad d\epsilon_z^p = 0. \tag{8}$$

$d\epsilon_z^p$ is an increment of plastic strain. It is defined by

$$d\epsilon_z^p = d\epsilon_z - d\epsilon_z^e \tag{9}$$

where $d\epsilon_z$ and $d\epsilon_z^e$ are increments of total and elastic strain respectively; see Hill (1950, p. 25). Since $d\epsilon_z^p = 0$,

$$d\epsilon_z = d\epsilon_z^e$$

and therefore

$$\epsilon_z = \epsilon_z^e. \tag{10}$$

ϵ_z satisfies (6) in both the elastic and plastic regions. ϵ_z has already been shown to be constant. Its value is now found.

The total axial force on any section is

$$P = 2\pi \int_a^b r\sigma_z \, dr. \tag{11}$$

Substitute for σ_z from (6) and then for σ_θ from (1), whence

$$P = 2\pi\nu (a^2 p - b^2 q) + \pi E (b^2 - a^2) \epsilon_z - 2\pi E\alpha \int_a^b rT \, dr \tag{12}$$

where p and q are the internal and external pressures respectively, i.e. $p = -(\sigma_r)_{r=a}$, $q = -(\sigma_r)_{r=b}$. There are three cases of importance. Firstly plane strain, $\epsilon_z = 0$. Secondly a tube with open ends, $P = 0$. And thirdly a tube with closed ends, $P = \pi a^2 p$. In the latter two cases substitution into (12) determines ϵ_z.

Since ϵ_z is now known, (6) and (1) can be used to express σ_z in terms of σ_r. Whence

$$\sigma_z = E\epsilon_z + 2\nu\sigma_r + \nu r \frac{d\sigma_r}{dr} - E\alpha T. \tag{13}$$

The inequalities $\sigma_\theta \geqslant \sigma_z \geqslant \sigma_r$ demand in the plastic region that

$$(1 - 2\nu)\sigma_r + (1 - \nu)k - E\epsilon_z + E\alpha T \geqslant 0 \tag{14}$$

and
$$-(1-2\nu)\,\sigma_r + \nu k + E\epsilon_z - E\alpha T \geqslant 0. \tag{15}$$

The radial displacement u and the equivalent plastic strain $\bar{\epsilon}^p$ will be determined in terms of σ_r. Since the dilatation is purely elastic,

$$\frac{du}{dr} + \frac{u}{r} + \epsilon_z = \frac{1-2\nu}{E}(\sigma_r + \sigma_\theta + \sigma_z) + 3\alpha T.$$

Substituting from (1) and (13)

$$\frac{du}{dr} + \frac{u}{r} = \frac{(1-2\nu)(1+\nu)}{E}\left(2\sigma_r + r\frac{d\sigma_r}{dr}\right) - 2\nu\epsilon_z + 2(1+\nu)\alpha T.$$

On integration,

$$ru = \frac{(1-2\nu)(1+\nu)}{E} r^2\sigma_r - \nu\epsilon_z r^2 + 2(1+\nu)\alpha\int^r Tr\,dr + C \tag{16}$$

where C is a constant. The strain component, ϵ_θ, is

$$\epsilon_\theta = \frac{u}{r} = \frac{(1-2\nu)(1+\nu)}{E}\sigma_r - \nu\epsilon_z + 2(1+\nu)\alpha\frac{1}{r^2}\int^r Tr\,dr + \frac{C}{r^2}. \tag{17}$$

The strain component, ϵ_r, is

$$\left.\begin{aligned}\epsilon_r = \frac{du}{dr} = \frac{(1-2\nu)(1+\nu)}{E}\left(\sigma_r + r\frac{d\sigma_r}{dr}\right) - \nu\epsilon_z \\ + 2(1+\nu)\alpha\left(T - \frac{1}{r^2}\int^r Tr\,dr\right) - \frac{C}{r^2}.\end{aligned}\right\} \tag{18}$$

The plastic strain component, ϵ_θ^p, is defined by $\epsilon_\theta^p = \epsilon_\theta - \epsilon_\theta^e$. Substituting from (17) for ϵ_θ and from (5), (1), and (13) for ϵ_θ^e,

$$\epsilon_\theta^p = -\frac{1-\nu^2}{E} r\frac{d\sigma_r}{dr} + \alpha(1+\nu)\left(\frac{2}{r^2}\int^r Tr\,dr - T\right) + \frac{C}{r^2}. \tag{19}$$

Similarly

$$\epsilon_r^p = \frac{1-\nu^2}{E} r\frac{d\sigma_r}{dr} - \alpha(1+\nu)\left(\frac{2}{r^2}\int^r Tr\,dr - T\right) - \frac{C}{r^2}. \tag{20}$$

Alternatively we could have used $\epsilon_\theta^p + \epsilon_r^p = 0$ to derive (20).

The equivalent plastic strain (HILL 1950, p. 30) is

$$\bar{\epsilon}^p = \int d\bar{\epsilon}^p = \sqrt{\tfrac{2}{3}}\int\{(d\epsilon_\theta^p)^2 + (d\epsilon_r^p)^2\}^{\frac{1}{2}}$$

Since, by (8), the ratio $d\epsilon_\theta^p/d\epsilon_r^p = -1$,

$$\bar{\epsilon}^p = \frac{2}{\sqrt{3}}\int|d\epsilon_\theta^p|$$

$$\therefore\ \bar{\epsilon}_p = \frac{2}{\sqrt{3}}\epsilon_\theta^p.$$

It has been assumed that the sign of $d\epsilon_\theta^p$ is the same throughout the deformation and that it is positive. This will be the case when the internal pressure is the

major external force and it is increasing. When $d\epsilon_\theta{}^p$ is always negative, a negative sign appears on the right-hand side of the above equation. Substituting from (19) for $\epsilon_\theta{}^p$,

$$\bar{\epsilon}^p = \frac{2}{\sqrt{3}}\left\{\frac{C}{r^2} - \frac{1-\nu^2}{E}\, r\,\frac{d\sigma_r}{dr} + \alpha(1+\nu)\left(\frac{2}{r^2}\int^r rT\,dr - T\right)\right\}. \tag{21}$$

The constant C is determined by the condition that $\bar{\epsilon}^p = 0$ in the elastic region. When no elastic region exists, another condition will be needed – such as the value of u at either $r = a$ or $r = b$. But in this case it is doubtful whether the analysis of this paper would be sufficiently accurate. Changes in the geometry of the tube would need to be considered when applying the boundary conditions.

In the plastic region, by (1) and (7),

$$r\,\frac{d\sigma_r}{dr} = k. \tag{22}$$

Therefore, in the plastic region,

$$\bar{\epsilon}^p = \frac{2}{\sqrt{3}}\left\{\frac{C}{r^2} - \frac{1-\nu^2}{E}\,k + \alpha(1+\nu)\left(\frac{2}{r^2}\int^r Tr\,dr - T\right)\right\}. \tag{23}$$

The yield stress curve gives k as a function of $\bar{\epsilon}^p$. Taken with equation (23), this curve enables k and ϵ^p to be found for each point (co-ordinate r) in the plastic region.

When the temperature T is not varying with respect to time, it satisfies Laplace's equation. For dependence on the cylindrical polar co-ordinate r only, the equation is

$$\frac{d^2T}{dr^2} + \frac{1}{r}\,\frac{dT}{dr} = 0 \tag{24}$$

with the solution

$$T = M + N\ln r \tag{25}$$

where the constants M and N are determined by the conditions on the inner and outer surfaces of the tube. If the inner and outer radii are a and b respectively and the corresponding temperatures T_a and T_b, then

$$M = \frac{T_a \ln b - T_b \ln a}{\ln b - \ln a}, \tag{26}$$

$$N = \frac{T_b - T_a}{\ln b - \ln a}. \tag{27}$$

It is assumed that equation (24) remains valid when the tube is under stress in both the elastic and plastic states, i.e. that the coefficient of heat conductivity is independent of whether the material is under stress or not. The heat conducted across the tube per unit length $= 2\pi\sigma N$ where σ is the coefficient of heat conductivity.

We now proceed to determine σ_r, first in the elastic and then in the plastic region. In the elastic region substitute for ϵ_r from (2) into (4) and for ϵ_θ from (3) into (5). Eliminate u from the resulting two equations and substitute for σ_θ and σ_z from (1) and (13). This gives the following differential equation for σ_r:

$$\frac{d^2\sigma_r}{dr^2} + \frac{3}{r}\frac{d\sigma_r}{dr} + \frac{E\alpha}{1-\nu}\frac{1}{r}\frac{dT}{dr} = 0. \tag{28}$$

Substitute for T from (25) and integrate :

$$\sigma_r = \frac{C_1}{r^2} + C_2 - \frac{E\alpha N}{2(1-\nu)}\ln r \tag{29}$$

where C_1 and C_2 are constants. Yielding occurs, from (1) and (7), when

$$r\frac{d\sigma_r}{dr} = k_0 \tag{30}$$

where k_0 is the initial yield stress. On substitution from (29) into (30),

$$-\frac{2C_1}{r^2} - \frac{E\alpha N}{2(1-\nu)} = k_0.$$

If ρ is the radius at the plastic-elastic interface,

$$C_1 = -\tfrac{1}{2}\left(k_0 + \frac{E\alpha N}{2(1-\nu)}\right)\rho^2$$

and in the elastic region

$$r\frac{d\sigma_r}{dr} = \left(k_0 + \frac{E\alpha N}{2(1-\nu)}\right)\frac{\rho^2}{r^2} - \frac{E\alpha N}{2(1-\nu)}.$$

Provided

$$k_0 + \frac{E\alpha N}{2(1-\nu)} > 0 \tag{31}$$

$r\,d\sigma_r/dr$ increases as r decreases. Therefore, if both elastic and plastic regions exist in the tube, the elastic region will be the outer one. On the outer surface of the tube $r = b$, $\sigma_r = -q$. This determines C_2. Substituting for C_1 and C_2,

$$\frac{\sigma_r}{k_0} = -\tfrac{1}{2}(1+\theta)\left(\frac{\rho^2}{r^2} - \frac{\rho^2}{b^2}\right) + \theta\ln\frac{b}{r} - \frac{q}{k_0}, \qquad \rho \leqslant r \leqslant b \tag{32}$$

where

$$\theta = \frac{E\alpha N}{2(1-\nu)k_0}. \tag{33}$$

From (31), $\theta > -1$. Substitute for σ_r in (1) and (13) to obtain σ_θ and σ_z in the elastic region,

$$\frac{\sigma_\theta}{k_0} = \tfrac{1}{2}(1+\theta)\left(\frac{\rho^2}{r^2} + \frac{\rho^2}{b^2}\right) + \theta\ln\frac{b}{r} - \theta - \frac{q}{k_0}, \tag{34}$$

$$\frac{\sigma_z}{k_0} = \frac{E\epsilon_z}{k_0} + \nu(1+\theta)\frac{\rho^2}{b^2} + 2\nu\theta\ln b - 2\theta\ln r - \nu\theta - \frac{E\alpha M}{k_0} - \frac{2\nu q}{k_0}. \tag{35}$$

Substitute for σ_r and T into (21). The condition $\bar{\epsilon}^p = 0$ in the elastic region determines C as

$$C = \frac{1-\nu^2}{E}\left(k_0 + \frac{E\alpha N}{2(1-\nu)}\right)\rho^2 = \frac{(1-\nu^2)k_0}{E}(1+\theta)\rho^2 \tag{36}$$

where the lower limit of the integral has been taken as zero. Substituting for σ_r, T and C in (17),

$$\left.\begin{aligned}\frac{E}{k_0}\frac{u}{r} = \frac{1+\nu}{2}(1+\theta)\frac{\rho^2}{r^2} + (1-2\nu)(1+\nu)\left\{\tfrac{1}{2}(1+\theta)\frac{\rho^2}{b^2} + \theta\ln\frac{b}{r} - \frac{q}{k_0}\right\} \\ - \frac{\nu E\epsilon_z}{k_0} + (1+\nu)\frac{E\alpha M}{k_0} + (1-\nu^2)\,\theta\,(2\ln r - 1).\end{aligned}\right\} \quad (37)$$

In the plastic region, from (1) and (7),

$$r\frac{d\sigma_r}{dr} = k. \quad (22)$$

On integration

$$\sigma_r = \int^r \frac{k}{r}\,dr + K, \qquad K \text{ constant.}$$

Since σ_r is continuous at the plastic-elastic interface, i.e. at $r = \rho$, equate values of σ_r from the above equation and from equation (32) at $r = \rho$ to determine K. Whence

$$\frac{\sigma_r}{k_0} = -\tfrac{1}{2}(1+\theta)\left(1 - \frac{\rho^2}{b^2}\right) + \theta\ln\frac{b}{\rho} - \frac{q}{k_0} - \frac{1}{k_0}\int_r^\rho \frac{k}{r}\,dr, \qquad a \leqslant r \leqslant \rho. \quad (38)$$

The internal pressure p is equal to $-(\sigma_r)_{r=a}$. Substituting from (38),

$$\frac{p}{k_0} = \frac{q}{k_0} + \frac{1}{k_0}\int_a^\rho \frac{k}{r}\,dr + \tfrac{1}{2}(1+\theta)\left(1 - \frac{\rho^2}{b^2}\right) - \theta\ln\frac{b}{\rho} \quad (39)$$

When the internal pressure is given, (39) determines ρ.

Substitute for T and C from (25) and (36) into (23):

$$\frac{E\bar{\epsilon}^p}{k_0} = \frac{2(1-\nu^2)}{\sqrt{3}}\left\{(1+\theta)\frac{\rho^2}{r^2} - \frac{k}{k_0} - \theta\right\}. \quad (40)$$

The yield stress curve expresses k as a function of $\bar{\epsilon}^p$,

$$k = k(\bar{\epsilon}^p). \quad (41)$$

Equations (40) and (41) determine $\bar{\epsilon}^p$ and k for each r once ρ is known. To determine ρ we proceed as below.

In the integral $\int_r^\rho k\,dr/r$ which occurs in equations (38) and (39), we change the variable of integration from r to $\bar{\epsilon}^p$. MANNING (1945) adopted this procedure in the case of a tube of plastic-rigid work-hardening material under internal pressure only. We first differentiate (40) with respect to $\bar{\epsilon}^p$ to give

$$\frac{2(1-\nu^2)k_0}{\sqrt{3}E}\left\{-2(1+\theta)\frac{\rho^2}{r^2}\frac{1}{r}\frac{dr}{d\bar{\epsilon}^p} - \frac{1}{k_0}\frac{dk}{d\bar{\epsilon}^p}\right\} = 1.$$

Eliminate $\frac{\rho^2}{r^2}$ from the above equation using (40)

$$\frac{1}{r}\,dr = -\tfrac{1}{2}\,\frac{\dfrac{\sqrt{3}E}{2(1-\nu^2)} + \dfrac{dk}{d\bar{\epsilon}^p}}{\dfrac{\sqrt{3}E\bar{\epsilon}^p}{2(1-\nu^2)} + k + \theta k_0}\,d\bar{\epsilon}^p. \quad (42)$$

Whence

$$\int_r^p \frac{k\,dr}{r} = \int_0^{\bar{\epsilon}^p} \frac{\dfrac{\sqrt{3}\,E}{2(1-\nu^2)} + \dfrac{dk}{d\bar{\epsilon}^p}}{\dfrac{\sqrt{3}\,E\bar{\epsilon}^p}{2(1-\nu^2)} + k + \theta k_0}\, d\bar{\epsilon}^p \tag{43}$$

or

$$\int_r^p \frac{k\,dr}{r} = K(\bar{\epsilon}^p), \tag{44}$$

where $K(\bar{\epsilon}^p)$ is defined as the integral on the right-hand side of (43). Note that $K(\bar{\epsilon}^p)$ is a function of $\bar{\epsilon}^p$ which depends only on the properties of the material of the tube and on N. Equations (38) and (39) can be written

$$\frac{\sigma_r}{k_0} = -\tfrac{1}{2}(1+\theta)\left(1-\frac{\rho^2}{b^2}\right) + \theta \ln\frac{b}{\rho} - \frac{q}{k_0} - \frac{1}{k_0}K(\bar{\epsilon}^p) \tag{45}$$

and

$$\frac{p}{k_0} = \tfrac{1}{2}(1-\theta)\left(1-\frac{\rho^2}{b^2}\right) - \theta \ln\frac{b}{\rho} + \frac{q}{k_0} + \frac{1}{k_0}K_a(\bar{\epsilon}^p) \tag{46}$$

where $K_a(\bar{\epsilon}^p)$ denotes the value of $K(\bar{\epsilon}^p)$ at $r = a$.

The function $K(\bar{\epsilon}^p)$ must in general be determined by numerical integration making use of the yield stress curve, $k = k(\bar{\epsilon}^p)$. Once this has been done, the remaining computations are simple. Guess a value of $\bar{\epsilon}^p$ and $r = a$. Find k_a and K_a. Using (40) at $r = a$, determine ρ from

$$\rho^2 = \frac{a^2}{1+\theta}\left(\frac{\sqrt{3}\,E(\bar{\epsilon}^p)_{r=a}}{2(1-\nu^2)k_0} + \frac{k_{r=a}}{k_0} + \theta\right). \tag{47}$$

Substitute ρ and K_a into (45) to give a value of p. Repeat for a number of guesses of $\bar{\epsilon}^p$ at $r = a$. Plot p against $(\bar{\epsilon}^p)_{r=a}$ and determine the value of $(\bar{\epsilon}^p)_{r=a}$ for which p is the given internal pressure. Find the value of ρ corresponding to this value of $(\bar{\epsilon}^p)_{r=a}$. The numerical integration of $K(\bar{\epsilon}^p)$ will need to be taken as far as the highest guessed value of $(\bar{\epsilon}^p)_{r=a}$.

Once ρ has been found, the values of σ_r, σ_θ, σ_z and u in the elastic region can be found from (32), (34), (35) and (37). To determine these quantities for a particular value of r in the plastic region, (40) and (41) are solved for $\bar{\epsilon}^p$ and k – the intersection of the straight line, equation (40), in the $\bar{\epsilon}^p$, k plane with the yield stress curve. σ_r is evaluated from (45), then σ_θ from (7) and σ_z from (6). Substituting for T and C into (17),

$$\frac{E}{k_0}\frac{u}{r} = (1-2\nu)(1+\nu)\frac{\sigma_r}{k_0} - \frac{\nu E\epsilon_z}{k_0} + \frac{(1+\nu)\,EaM}{k_0} + (1-\nu^2)\,\theta\,(2\ln r - 1). \tag{48}$$

This completes the solution apart from verifying that $\sigma_\theta > \sigma_z > \sigma_r$ in the plastic region, that no difference between two principal stresses exceeds or equals k inside the elastic region, and that the inequality (31) is satisfied.

The internal pressure p_e at which plasticity commences at the bore is found from equation (39) by putting $\rho = a$. It is

$$\frac{p_e}{k_0} = \frac{q}{k_0} + \tfrac{1}{2}(1+\theta)\left(1-\frac{a^2}{b^2}\right) - \theta\ln\frac{b}{a}. \tag{49}$$

The internal pressure p_f at which the whole tube becomes plastic is found from equation (45) by putting $\rho = b$. It is

$$p_f = q + (K_a(\bar{\epsilon}^p))_{\rho=b} \quad \text{or} \quad p_f = q + \int_a^b \frac{k\,dr}{r}. \tag{50}$$

It is seen from (50) that p_f is independent of N for a non-work-hardening material and from (43) that it is dependent on N for a work-hardening material.

The dimensionless quantity θ can be expressed in terms of the heat conducted through unit length of tube, $H = 2\pi\sigma N$, as

$$\theta = \frac{E\alpha H}{4\pi(1-\nu)\sigma k_0}. \tag{51}$$

θ is a measure of the effect of the temperature differences on the stress system.

3. A Linear Work-hardening Material

Since the equivalent plastic strain rarely exceeds 5%, the yield stress curve can often be replaced with sufficient accuracy by a straight line,

i.e. $$k = k_0(1 + \eta\,\bar{\epsilon}^p). \tag{52}$$

Using this equation, explicit expressions will now be found for the stresses and displacements.

Equations (40) and (52) are solved for k and $\bar{\epsilon}^p$. This gives

$$\bar{\epsilon}^p = \beta\left(\frac{\rho^2}{r^2} - 1\right) \tag{53}$$

and $$k = k_0\left\{1 + \eta\beta\left(\frac{\rho^2}{r^2} - 1\right)\right\} \tag{54}$$

where $$\beta = \frac{1+\theta}{\eta + \dfrac{\sqrt{3}\,E}{2(1-\nu^2)k_0}}. \tag{55}$$

It follows that

$$\int_r^\rho \frac{k}{r}\,dr = k_0(1-\eta\beta)\ln\frac{\rho}{r} + \frac{k_0\eta\beta}{2}\left(\frac{\rho^2}{r^2} - 1\right),$$

and, by substitution into (45), that in the plastic region

$$\frac{\sigma_r}{k_0} = -\tfrac{1}{2}(1+\theta)\left(1 - \frac{\rho^2}{b^2}\right) + \theta\ln\frac{b}{\rho} - \frac{q}{k_0} - (1-\eta\beta)\ln\frac{\rho}{r} - \frac{\eta\beta}{2}\left(\frac{\rho^2}{r^2} - 1\right). \tag{56}$$

Since $\sigma_\theta - \sigma_r = k$ in the plastic region,

$$\frac{\sigma_\theta}{k_0} = \tfrac{1}{2}\left(1 + \frac{\rho^2}{b^2}\right) - \frac{\theta}{2}\left(1 - \frac{\rho^2}{b^2}\right) + \theta\ln\frac{b}{\rho} - \frac{q}{k_0} - (1-\eta\beta)\ln\frac{\rho}{r} + \frac{\eta\beta}{2}\left(\frac{\rho^2}{r^2} - 1\right). \tag{57}$$

Substituting for σ_r and σ_θ in (6), and using (10),

$$\left.\begin{aligned}\frac{\sigma_z}{k_0} = \nu\frac{\rho^2}{b^2} - \nu\theta\left(1 - \frac{\rho^2}{b^2}\right) + 2\nu\theta\ln\frac{b}{\rho} - \frac{2\nu q}{k_0} - 2\nu(1-\eta\beta)\ln\frac{\rho}{r} \\ + \frac{E\epsilon_z}{k_0} - \frac{E\alpha M}{k_0} - 2(1-\nu)\theta\ln r\end{aligned}\right\} \tag{58}$$

Substitution from (56) into (48) gives $\dfrac{E}{k_0}\dfrac{u}{r}$. An alternative expression to (53) for $\bar{\epsilon}^p$ is obtained by substituting for β from (55),

$$\frac{E\bar{\epsilon}^p}{k_0} = \frac{2(1-\nu^2)}{\sqrt{3}}(1+\theta-\eta\beta)\left(\frac{\rho^2}{r^2}-1\right). \tag{59}$$

ρ is determined by substituting $r = a$, $\sigma_r = -p$ into (56), i.e.

$$-\frac{p}{k_0} = -\tfrac{1}{2}(1+\theta)\left(1-\frac{\rho^2}{b^2}\right) + \theta\ln\frac{b}{\rho} - \frac{q}{k_0} - (1-\eta\beta)\ln\frac{\rho}{a} - \frac{\eta\beta}{2}\left(\frac{\rho^2}{a^2}-1\right). \tag{60}$$

Examination of equations (56) to (60) shows that the effects of linear work-hardening is expressed in the equations for stress and strain through the parameter $\eta\beta$ or

$$\frac{\eta(1+\theta)}{\eta + \dfrac{\sqrt{3}}{2(1-\nu^2)}\dfrac{E}{k_0}}.$$

4. The Inequalities for Non-Work-hardening Material, Closed Ends and $q = 0$.

When the yield stress does not increase with plastic working, $k = k_0$. The stresses are obtained from equations (56) to (58) by putting $\eta = 0$. When the ends are closed, the total axial force $P = \pi a^2 p$. Substitute for P, put $q = 0$ and $T = M + N\ln r$ in (12). This gives

$$E\epsilon_z = (1-2\nu)\frac{a^2}{b^2-a^2}p + E\alpha M + 2(1-\nu)k_0\theta\left(\frac{b^2\ln b - a^2\ln a}{b^2-a^2} - \tfrac{1}{2}\right). \tag{61}$$

Substituting into (58) and putting $\eta = 0$ and $q = 0$,

$$\left.\begin{aligned}\frac{\sigma_z}{k_0} = \nu\frac{\rho^2}{b^2} - \nu\theta\left(1-\frac{\rho^2}{b^2}\right) + 2\nu\theta\ln\frac{b}{\rho} - 2\nu\ln\frac{\rho}{r} + (1-2\nu)\frac{a^2}{b^2-a^2}\frac{p}{k_0} \\ + 2(1-\nu)\theta\left(\frac{b^2\ln b - a^2\ln a}{b^2-a^2} - \tfrac{1}{2} - \ln r\right).\end{aligned}\right\} \tag{62}$$

The stress distribution must satisfy $\sigma_\theta > \sigma_z > \sigma_r$ in the plastic region and no difference between two stresses must exceed k_0 in the elastic region.

Suppose the tube is subject in the first place to a temperature gradient only. The internal pressure is increased until plasticity commences at the bore and then increased further until the whole tube finally becomes plastic. The condition for the inequalities to be satisfied throughout this process will now be found.

In the elastic region the stresses produced by the temperature difference and by the internal pressure are additive. Plasticity commences when $\sigma_\theta - \sigma_r$ reaches the value k_0 at the bore and the effect of increasing internal pressure is to increase $\sigma_\theta - \sigma_r$. Therefore the tube will not be plastic at any radius for any $p < p_c$, where p_c is given by (49), unless p_c is negative. If p_c is negative, the tube will have yielded due to the stresses produced by the temperature difference alone. The condition that $p_c > 0$ is, from (49),

$$\tfrac{1}{2}(1+\theta)\left(1-\frac{a^2}{b^2}\right) > \theta\ln\frac{b}{a}.$$

This is satisfied for all $\theta < 0$. For $\theta > 0$ it is

$$\frac{R\ln R}{R-1} < \frac{1+\theta}{\theta}, \tag{63}$$

where

$$R = \frac{b^2}{a^2}. \tag{64}$$

The inequalities once the tube has become plastic at the bore are now considered. In the plastic region the inequalities to be satisfied are (14) and (15). If the left hand side of (14) is differentiated with respect to r, it can be shown that

$$\frac{d\,(\text{L.H.S. of (14)})}{dr} > 0 \qquad \text{if} \qquad (1-2\nu)\,k_0 + E\alpha N > 0 \qquad \text{or} \qquad 1 + \frac{2\,(1-\nu)}{1-2\nu}\,\theta > 0$$

when σ_r is given by (56) with $\eta = 0$, T by (5) and ϵ_z by (61). It follows that if (14) is satisfied at $r = a$, it is satisfied for all r, $a \leqslant r \leqslant \rho$.

At $r = a$, the inequality (14) becomes

$$-(1-2\nu)\,p + (1-\nu)\,k_0 - E\epsilon_z + E\alpha T_a \geqslant 0. \tag{65}$$

The Left-hand side of (65) is differentiated with respect to ρ. Only the first term depends on ρ. Since $dp/d\rho \geqslant 0$, $d\,(\text{L.H.S. of (65)})/d\rho \leqslant 0$. Therefore if the inequality is satisfied at $\rho = b$, it will be satisfied for all ρ, $a \leqslant \rho \leqslant b$.

This gives the condition

$$\frac{R \ln R}{R-1} \leqslant \frac{1+\theta}{\frac{1}{2}\dfrac{1-2\nu}{1-\nu} + \theta}. \tag{66}$$

When $(1-2\nu)\,k_0 + E\alpha N < 0$, if (14) is satisfied at $r = \rho$, it is satisfied for all r, $a \leqslant r \leqslant \rho$. At $r = \rho$, the inequality (14) becomes

$$(1-2\nu)\,(\sigma_r)_{r=\rho} + (1-\nu)\,k_0 - E\epsilon_z + E\alpha T_\rho \geqslant 0. \tag{67}$$

It can be shown that if this inequality is satisfied at $\rho = b$, it is satisfied for all ρ, $a \leqslant \rho \leqslant b$, and that, at $\rho = b$, (67) is satisfied for all values of the ratio b/a.

The inequality (15) is treated in a similar manner. It is first found at what values of r, $a \leqslant r \leqslant \rho$, the left-hand side of (15) is a minimum. Then for these values of r, it is found for what value of ρ the L.H.S. is a minimum. The following inequalities are derived

$$\frac{\ln R}{R-1} > \frac{\theta - \dfrac{\nu}{1-\nu}}{\frac{1}{2}\dfrac{1-2\nu}{1-\nu} + \theta} \qquad \text{for} \qquad \theta - \frac{\nu}{1-\nu} > 0, \tag{68}$$

and

$$\frac{R \ln R}{R-1} < \frac{1-\theta}{-\theta} \qquad \text{for} \qquad -\frac{1-2\nu}{2\,(1-\nu)} < \theta < -1. \tag{69}$$

When (66) is satisfied, so clearly is (63). It can also be shown that, when (66) is satisfied, so is (68) and so is (69) when $\theta \geqslant -(1-2\nu)/(3-2\nu)$. For $-(1-2\nu)/(3-2\nu) \geqslant \theta > -1$, when (69) is satisfied so is (66). The inequalities (63), (66), (68) and (69) can therefore be replaced by

$$\frac{R \ln R}{R-1} < \frac{1+\theta}{\frac{1}{2}\dfrac{1-2\nu}{1-\nu} + \theta}, \qquad \theta \geqslant -\frac{1-2\nu}{3-2\nu}, \tag{70}$$

and

$$\frac{R \ln R}{R-1} < \frac{1-\theta}{-\theta}, \qquad -\frac{1-2\nu}{3-2\nu} \geqslant \theta > -1. \tag{71}$$

In the part of the tube which remains elastic once plasticity commences at the bore, the inequalities to be satisfied are $|\sigma_\theta - \sigma_r| \leqslant k_0$, $|\sigma_\theta - \sigma_z| < k_0$ and $|\sigma_z - \sigma_r| < k_0$, where the equality can exist only at the plastic-elastic interface. These relations must be satisfied at the interface because otherwise inequalities in the plastic region would be violated.

In the elastic region, from (32) and (34),

$$\frac{\sigma_\theta}{k_0} - \frac{\sigma_r}{k_0} = (1+\theta)\frac{\rho^2}{r^2} - \theta.$$

$\sigma_\theta - \sigma_r$ decreases as r increases from ρ to b. It is therefore sufficient that

$$\sigma_\theta - \sigma_r > -k_0 \text{ at } r = b.$$

i.e.
$$(1+\theta)\frac{\rho^2}{b^2} - \theta + 1 > 0$$

The left-hand side of this inequality increases as ρ increases from a to b. It is sufficient that it is satisfied for $\rho = a$, i.e.

$$\frac{1}{R} > \frac{\theta - 1}{\theta + 1}. \tag{72}$$

It can be shown that (72) is satisfied whenever (70) is satisfied.

The analysis of the other two inequalities proceeds in the same manner although there turn out to be a large number of special cases to consider. The difference, $\sigma_\theta - \sigma_z$ say, is first differentiated with respect to r. Its maxima and minima in the range $\rho < r \leqslant b$ are determined. At the maxima $\sigma_\theta - \sigma_z$ must be $< k_0$, at the minima $> -k_0$. The left-hand side of these new inequalities is then differentiated with respect to ρ, bearing in mind that the position of the extremum itself may depend on ρ. If the left-hand side is to be $> k_0$, then the inequality must be satisfied at the minima of the left-hand side, with respect to ρ in the range $a \leqslant \rho \leqslant b$, to be satisfied throughout the range and, conversely, if the left-hand side is to be $< k_0$ then the inequality must be satisfied at the maxima. It can be shown that the inequalities so derived are satisfied when the inequalities (70) and (71) are satisfied.

The maximum values of the radius ratio b/a for $|\theta| \leqslant 1$ have been calculated from equations (70) and (71). The results are given in Table 1.

TABLE 1. *Maximum radius ratio b/a for $|\theta| \leqslant 1$.*

θ	-1	$-0{\cdot}68$	$-0{\cdot}51$	$-0{\cdot}425$	$-0{\cdot}365$	$-0{\cdot}025$	0
max b/a	2·22	3	4	5	6	6	5·43
θ	0·08	0·20	0·43	0·56	0·71	0·86	1
max b/a	4	3	2·22	2	1·82	1·71	1·62

5. EXAMPLES

In the first three examples a tube of non-work-hardening material with radius ratio 2 is chosen. Three values of the temperature stress factor θ are chosen : $\theta = 0$, $\frac{1}{2}$ and $-\frac{1}{2}$. The state of

TABLE 2. *Stresses in a closed-end tube, $b/a = 2$, $\rho/a = \sqrt{3}$, $\theta = 0$, $\eta\beta = 0$.*

r/a	1·0	1·2	1·4	1·6	$\sqrt{3}$	1·85	2·0
σ_r/k_0	$-$ ·674	$-$ ·492	$-$ ·338	$-$ ·204	$-$ ·125	$-$ ·063	0
σ_θ/k_0	0·326	0·508	0·662	0·796	0·875	0·813	0·750
σ_z/k_0	$-$ ·014	0·095	0·187	0·268	0·315	0·315	0·315
$\frac{E}{k_0}\frac{u}{a}$	2·35	1·93	1·67	1·49	1·42	1·37	1·31
$\frac{E}{k_0}\bar{\epsilon}^p$	2·10	1·13	0·56	0·18	0	0	0

stress is evaluated for $\rho/a = \sqrt{3}$ in each case. As uniform thermal expansion is not of interest, the mean temperature $2(b^2 - a^2)^{-1} \int_a^b Tr\, dr$ is taken as zero in the calculation of u/r; ν is taken as 0·3. The results are given in Tables 2, 3 and 4.

TABLE 3. *Stresses in a closed-end tube,* $b/a = 2$, $\rho/a = \sqrt{3}$, $\theta = \frac{1}{2}$, $\eta\beta = 0$.

r/a	1·0	1·2	1·4	1·6	$\sqrt{3}$	1·85	2·0
σ_r/k_0	− ·665	− ·483	− ·329	− ·195	− ·116	− ·055	0
σ_θ/k_0	0·335	0·517	0·671	0·805	0·884	0·759	0·625
σ_z/k_0	0·287	0·268	0·254	0·240	0·231	0·166	0·089
$\frac{E}{k_0}\frac{u}{a}$	2·88	2·26	1·90	1·68	1·63	1·59	1·57
$\frac{E}{k_0}\bar{\epsilon}^p$	3·16	1·71	0·84	0·27	0	0	0

TABLE 4. *Stresses in a closed-end tube,* $b/a = 2$, $\rho/a = \sqrt{3}$, $\theta = -\frac{1}{2}$, $\eta\beta = 0$.

r/a	1·0	1·2	1·4	1·6	$\sqrt{3}$	1·85	2·0
σ_r/k_0	− ·683	− ·501	− ·347	− ·213	− ·134	− ·071	0
σ_θ/k_0	0·317	0·499	0·653	0·787	0·866	0·867	0·875
σ_z/k_0	− ·316	− ·079	0·121	0·295	0·399	0·464	0·541
$\frac{E}{k_0}\frac{u}{a}$	1·82	1·60	1·44	1·30	1·21	1·14	1·05
$\frac{E}{k_0}\bar{\epsilon}^p$	1·04	0·56	0·28	0·09	0	0	0

The stresses σ_r and σ_θ are roughly the same in all three cases. They become identical when $\rho = b$. σ_z varies most for $\theta = -\frac{1}{2}$. The real differences however are in the displacements and in the equivalent plastic strains. They increase with θ, in fact $\bar{\epsilon}^p$ is proportional to $1 + \theta$.

In the last two examples a tube of radius ratio 4 not subject to temperature gradients is chosen. The two examples differ in that the one is non-work-hardening and the other is work-hardening with $\eta\beta = 1/30$. In both cases the tube has just become completely plastic, i.e. $\rho = b$. ν is again taken as 0·3. The results are given in Tables 5 and 6.

The effect of work-hardening is mainly evident in the values of σ_r and σ_θ at the bore. The yield stress increases 50% from the outside to the bore. The internal pressure p increases 15%.

The inequalities satisfied by the stresses break down for a non-work-hardening material when $\theta = 0$ for $b/a > 5{\cdot}43$. They break down because σ_z becomes greater than σ_θ at the bore. Examination of Tables 5 and 6 shows that the difference $\sigma_\theta - \sigma_z$ at the bore is larger for the work-hardening material. It appears likely, therefore, that the inequalities will be satisfied for larger values of b/a for a work-hardening material than are given in Table 1.

Table 5. *Stresses in a closed-end tube, $b/a = 4$, $\rho = b$, $\theta = 0$, $\eta\beta = 0$.*

r/a	1·0	1·5	2·0	2·5	3·0	3·5	4·0
σ_r/k_0	− 1·386	− ·981	− ·693	− ·470	− ·287	− ·133	0
σ_θ/k_0	− ·386	0·019	0·307	0·530	0·713	0·867	1
σ_z/k_0	− ·495	− ·252	− ·079	0·055	0·165	0·237	0·337
$\frac{E}{k_0}\frac{u}{a}$	10·65	7·30	5·70	4·78	4·23	3·85	3·60
$\frac{E}{k_0}\varepsilon^p$	15·77	6·43	3·15	1·64	0·82	0·32	0

Table 6. *Stresses in a closed-end tube, $b/a = 4$, $\rho = b$, $\theta = 0$, $\eta\beta = 1/30$.*

r/a	1·0	1·5	2·0	2·5	3·0	3·5	4·0
σ_r/k_0	− 1·590	− 1·050	− ·720	− ·480	− ·290	− ·134	0
σ_θ/k_0	− ·090	0·154	0·380	0·572	0·736	0·876	1
σ_z/k_0	− ·462	− ·227	− ·060	0·069	0·176	0·265	0·342
$\frac{E}{k_0}\frac{u}{a}$	10·54	7·24	5·66	4·75	4·23	3·85	3·60
$\frac{E}{k_0}\varepsilon^p$	15·24	6·12	3·05	1·59	0·79	0·31	0
k/k_0	1·500	1·204	1·100	1·052	1·026	1·010	1

6. Elastic Unloading

The effect of removing the temperature differences and the internal and external pressures is now investigated.

If the deformation on loading has been purely elastic, on unloading the tube will return to its initial state, i.e. unstressed and no deformation. (By "loading" is meant the application not only of internal and external pressures but also of the temperature differences, and by "unloading" the removal of the pressures and of the temperature differences). The final state can be considered as the superposition on the initial elastic stress system of the elastic stress system obtained on changing the signs of the originally imposed pressures and temperatures. This second system, denoted by a prime, is given (for closed ends, $q = 0$ and $\int_a^b Tr\,dr = 0$) by

$$\frac{\sigma_r'}{k_0} = (p/k_0 + \theta \ln b/a)\left(\frac{1}{a^2} - \frac{1}{b^2}\right)^{-1}\left(\frac{1}{r^2} - \frac{1}{b^2}\right) - \theta \ln b/r, \tag{73}$$

$$\sigma_\theta'/k_0 = -(p/k_0 + \theta \ln b/a)\left(\frac{1}{a^2} - \frac{1}{b^2}\right)^{-1}\left(\frac{1}{r^2} + \frac{1}{b^2}\right) - \theta \ln b/r + \theta, \tag{74}$$

$$\sigma_z'/k_0 = -(p/k_0 + 2\theta \ln b/a)\frac{a^2}{b^2 - a^2} - 2\theta \ln b/r + \theta, \tag{75}$$

$$\left.\begin{aligned}\frac{E}{k_0}\frac{u'}{r} = &-(1-2\nu)\frac{p}{k_0}\frac{a^2}{b^2-a^2} + (1+\nu)\theta \ln b/r - (1+\nu)(p/k_0 \\ &+ \theta \ln b/a)\left(\frac{1}{a^2} - \frac{1}{b^2}\right)^{-1}\frac{1}{r^2} + (1+\nu)\theta\frac{a^2}{b^2-a^2}\ln b/a,\end{aligned}\right\} \tag{76}$$

and

$$\bar{\epsilon}'^p = 0, \tag{77}$$

TABLE 7. *Residual stresses – elastic unloading of tube of Table 2.*

r/a	1·0	1·2	1·4	1·6	$\sqrt{3}$	1·85	2·0
σ_r''/k_0	0	− ·093	− ·104	− ·077	− ·050	− ·025	0
σ_θ''/k_0	− ·798	− ·341	− ·022	0·219	0·350	0·325	0·300
σ_z''/k_0	− ·239	− ·130	− ·038	0·043	0·090	0·090	0·090
$\frac{E}{k_0}\frac{u''}{a}$	1·09	0·85	0·71	0·61	0·59	0·57	0·55

TABLE 8. *Residual stresses – elastic unloading of tube of Table 3.*

r/a	1·0	1·2	1·4	1·6	$\sqrt{3}$	1·85	2.0
σ_r''/k_0	0	− ·139	− ·156	− ·116	− ·076	− ·037	0
σ_θ''/k_0	− 1·196	− ·513	− ·032	0·328	0·526	0·489	0·451
σ_z''/k_0	− ·359	− ·196	− ·056	0·064	0·134	0·135	0·136
$\frac{E}{k_0}\frac{u''}{a}$	1·64	1·27	1·06	0·91	0·89	0·85	0·82

where p and θ refer to the loading not to the unloading process. The residual stress system, which will be denoted by two primes, is the sum of the system produced by loading and that produced by unloading, i.e.

$$\sigma_r'' = \sigma_r + \sigma_r', \qquad \text{etc.} \tag{78}$$

When the loading was purely elastic, $\sigma_r'' = \sigma_\theta'' = \sigma_z'' = u'' = \bar{\epsilon}''^p = 0$.

Now suppose the loading has been such that a small region of the tube around the bore has become plastic. On unloading, the stresses will not return to zero, but it will not be expected that they will be sufficiently large to violate the yield criterion at any point. In this case the unloading will be elastic and will be given by equations (73) to (77). The residual stress system is given by (78).

In Tables 7, 8 and 9 the residual stresses are given, on the basis of elastic unloading, for the first three examples of the last section.

TABLE 9. *Residual stresses – elastic unloading of tube of Table 4.*

r/a	1·0	1·2	1·4	1·6	$\sqrt{3}$	1·85	2·0
σ_r''/k_0	0	− ·045	− ·051	− ·037	− ·024	− ·013	0
σ_θ''/k_0	− ·398	− ·169	− ·011	0·111	0·176	0·163	0·151
σ_z''/k_0	− ·120	− ·065	− ·019	0·021	0·046	0·045	0·044
$\frac{E}{k_0}\frac{u''}{a}$	0·54	0·42	0·36	0·32	0·29	0·29	0·28

Examination of Tables 7, 8 and 9 shows that the residual stress distributions do not violate the yield criterion, maximum principal stress difference less than k_0, except that at $r = a$ in Table 8 $\sigma_r'' - \sigma_\theta'' = 1{\cdot}196\,k_0$. Tables 7 and 9 therefore give the correct residual stress distributions; Table 8 is incorrect as the tube again becomes plastic at the bore. This requires further analysis.

7. UNLOADING WITH FURTHER PLASTIC FLOW

A work-hardening tube is considered, which when loaded is plastic for $a \leqslant r \leqslant \rho$ and elastic for $\rho \leqslant r \leqslant b$. On unloading yielding again occurs for $a \leqslant r < \rho'$, but no further yielding occurs for $\rho' \leqslant r \leqslant b$. Since yielding on unloading occurs only after yielding on loading but need not necessarily occur in this circumstance, it is reasonable to suppose that $\rho' < \rho$.

Let a double prime denote a component in the residual state, and a single prime the addition during unloading to the loaded value of the component, which in its turn is unprimed. For $a \leqslant r \leqslant \rho'$,

$$\sigma_r'' - \sigma_\theta'' = k'', \tag{79}$$

assuming that $\sigma_r'' \geqslant \sigma_z'' \geqslant \sigma_\theta''$. The position of σ_r and σ_θ are interchanged compared with loading. The equation of equilibrium, (1), must be satisfied. Eliminating σ_θ'' from (1) and (79)

$$r\frac{d\sigma_r''}{dr} = -k''. \tag{80}$$

k'' in general is a function of $\bar{\epsilon}''^{p}$.

$$\bar{\epsilon}''^{p} = \bar{\epsilon}^{p} + \bar{\epsilon}'^{p}, \tag{81}$$

where $\bar{\epsilon}^p$ is the equivalent plastic strain during loading and $\bar{\epsilon}'^p$ that during unloading.

In deriving (21) for $\bar{\epsilon}^p$ it was assumed that $d\epsilon_\theta{}^p$ has the same sign throughout the deformation and that it was positive. In unloading $d\epsilon_\theta{}'^p$ has the same sign throughout and it is negative. Therefore

$$\bar{\epsilon}'^p = -\frac{2}{\sqrt{3}}\epsilon_\theta{}'^p. \tag{82}$$

The equations developed in earlier sections for loading are valid for unloading, except equations involving the yield stress or the equivalent plastic strain. The reason is that the former equations are based solely on the theory of elasticity. Equation (19) is still valid, and so

$$\bar{\epsilon}'^p = -\frac{2}{\sqrt{3}}\epsilon_\theta{}'^p = -\frac{2}{\sqrt{3}}\left(-\frac{1-\nu^2}{E}r\frac{d\sigma_r'}{dr} + \alpha(1+\nu)\left(\frac{2}{r^2}\int^r T'\,r\,dr - T'\right) + \frac{C'}{r^2}\right).$$

The temperature differences are removed on unloading, i.e. $T' = -T$. Substituting for $\bar{\epsilon}'^p$ and for $T' = -T = -M - N\ln r$ into (81)

$$\frac{E\bar{\epsilon}''^p}{k_0} = \frac{E\bar{\epsilon}^p}{k_0} + \frac{2}{\sqrt{3}}\left(\frac{1-\nu^2}{k_0}r\frac{d\sigma_r'}{dr} - (1-\nu^2)\theta - \frac{C'}{r^2}\right). \tag{83}$$

From (7) and (79),

$$\sigma_r' - \sigma_\theta' = (\sigma_r'' - \sigma_r) - (\sigma_\theta'' - \sigma_\theta) = k'' + k$$

in the plastic region. At the plastic elastic interface, $r = \rho'$, $k'' = k = k_{\rho'}$, and

$$-\frac{1}{r}\frac{d\sigma_r'}{dr} = \sigma_r' - \sigma_\theta' = 2k_{\rho'} \text{ at } r = \rho'. \tag{84}$$

Using (84) and $\sigma_r' = q$ at $r = b$ as boundary conditions for the differential equation (28) in the elastic region,

$$\frac{\sigma_r'}{k_0} = \left(\frac{k_{\rho'}}{k_0} + \frac{\theta}{2}\right)\left(\frac{\rho'^2}{r^2} - \frac{\rho'^2}{b^2}\right) - \theta\ln\frac{b}{r} + \frac{q}{k_0}. \tag{85}$$

$\bar{\epsilon}''^p = \bar{\epsilon}^p$ for $r \geqslant \rho'$. Substituting for σ_r' from (85) into (83), C' is determined. Whence

$$\frac{E\bar{\epsilon}''^p}{k_0} = \frac{E\bar{\epsilon}^p}{k_0} + \frac{2(1-\nu^2)}{\sqrt{3}}\left(\frac{r}{k_0}\frac{d\sigma_r'}{dr} - \theta + \left(2\frac{k_{\rho'}}{k_0} + \theta\right)\frac{\rho'^2}{r^2}\right).$$

In the plastic region,

$$r\frac{d\sigma_r'}{dr} = r\frac{d\sigma_r''}{dr} - r\frac{d\sigma_r}{dr} = -k'' - k, \tag{86}$$

$$\frac{E\bar{\epsilon}''^p}{k_0} = \frac{E\bar{\epsilon}^p}{k_0} + \frac{2(1-\nu^2)}{\sqrt{3}}\left(-\left(\frac{k}{k_0} + \frac{k''}{k_0}\right) - \theta + \left(2\frac{k_{\rho'}}{k_0} + \theta\right)\frac{\rho'^2}{r^2}\right), \quad a \leqslant r \leqslant \rho'. \tag{87}$$

Equations (80) and (87) taken with $k = k(\bar{\epsilon}^p)$ suffice to determine σ_r'' in the plastic region. The boundary condition on (80) is that σ_r'' is continuous at $r = \rho'$. Substitute $r = a$, $\sigma_r'' = 0$ into the equation for σ_r'' to find ρ'. The solution for a

general yield stress curve proceeds as formerly in the development of equation (43). In the following the linear work-hardening law

$$k = k_0 (1 + \eta \bar{\epsilon}^p) \tag{52}$$

will be used.

Substitute for k'' from (52), for k and $k_{\rho'}$ from (54) and for $\bar{\epsilon}^p$ from (59) into (87).

$$\bar{\epsilon}''^p = \beta \left(\frac{\rho^2}{r^2} - 1\right) + \beta \frac{2 + \theta - 2\eta\beta}{1 + \theta} \left(\frac{\rho'^2}{r^2} - 1\right) \tag{88}$$

or

$$\left.\begin{aligned} \frac{E\bar{\epsilon}''^p}{k_0} = {} & \frac{2(1-\nu^2)}{\sqrt{3}} (1 + \theta - \eta\beta) \left(\frac{\rho^2}{r^2} - 1\right) \\ & + \frac{2(1-\nu^2)}{\sqrt{3}} \frac{(1 + \theta - \eta\beta)(2 + \theta - 2\eta\beta)}{1 + \theta} \left(\frac{\rho^2}{r^2} - 1\right). \end{aligned}\right\} \tag{89}$$

Substituting for $\bar{\epsilon}''^p$ from (88) into (52),

$$\frac{k''}{k_0} = 1 + \eta\beta \left(\frac{\rho^2}{r^2} - 1\right) + \eta\beta \frac{2 + \theta - 2\eta\beta}{1 + \theta} \left(\frac{\rho'^2}{r^2} - 1\right). \tag{90}$$

Substitute for k'' and k from (90) and (54) into (86) and integrate.

$$\left.\begin{aligned} \frac{\sigma_r'}{k_0} = {} & \left(-2 + 2\eta\beta + \eta\beta \frac{2 + \theta - 2\eta\beta}{1 + \theta}\right) \ln r \\ & + \left(\eta\beta\rho^2 + \eta\beta \frac{2 + \theta - 2\eta\beta}{2(1 + \theta)} \rho'^2\right) \frac{1}{r^2} + A \end{aligned}\right\} \tag{91}$$

where A is a constant determined by making σ_r' continuous at $r = \rho'$. Equation (91) is valid for $a \leqslant r \leqslant \rho'$. Substitute $\frac{k_{\rho'}}{k_0} = 1 + \eta\beta \left(\frac{\rho^2}{\rho'^2} - 1\right)$ into (85) to give

$$\frac{\sigma_r'}{k_0} = \eta\beta \left(\frac{\rho^2}{r^2} - \frac{\rho^2}{b^2}\right) + \left(1 - \eta\beta + \frac{\theta}{2}\right) \left(\frac{\rho'^2}{r^2} - \frac{\rho'^2}{b^2}\right) - \theta \ln \frac{b}{r} + \frac{q}{k_0}, \quad \rho' \leqslant r \leqslant b. \tag{92}$$

Equating (91) and (92) at $r = \rho'$ determines A. Substituting back in (91),

$$\left.\begin{aligned} \frac{\sigma'_r}{k_0} = {} & \left(-2 + 2\eta\beta + \eta\beta \frac{2 + \theta - 2\eta\beta}{1 + \theta}\right) \ln \frac{r}{\rho'} - \theta \ln \frac{b}{\rho'} + \eta\beta \left(\frac{\rho^2}{r^2} - \frac{\rho^2}{b^2}\right) \\ & + \eta\beta \frac{2 + \theta - 2\eta\beta}{1 + \theta} \left(\frac{\rho'^2}{r^2} - 1\right) + \frac{2 + \theta - 2\eta\beta}{2} \left(1 - \frac{\rho'^2}{b^2}\right) + \frac{q}{k_0}, \quad a \leqslant r \leqslant \rho'. \end{aligned}\right\} \tag{93}$$

ρ' is determined by substituting $r = a$, $\sigma_r' = p$ into (93).

σ_θ' is found by substituting for σ_r' in the equation of equilibrium (1), i.e.

$$\sigma_\theta' = \sigma_r' + r \frac{d\sigma_r'}{dr}. \tag{94}$$

σ_z' is found by substituting σ_r' and σ_θ' into equation (6),

$$\sigma_z' = \nu(\sigma_r' + \sigma_\theta') - E\epsilon_z + E\alpha T \tag{95}$$

since $\epsilon_z' = -\epsilon_z$ and $T' = -T$; and u' by substituting σ_r' and C'' into equation (17),

$$\left.\begin{aligned}\frac{E}{k_0}\frac{u'}{r} = (1-2\nu)(1+\nu)\frac{\sigma_r'}{k_0} + \frac{\nu E\epsilon_z}{k_0} - \frac{(1+\nu)\,E\alpha M}{k_0} \\ -(1-\nu^2)\,\theta\,(2\ln r - 1) - (2+\theta-2\eta\beta)\frac{\rho''^2}{r^2} - 2\eta\beta\frac{\rho^2}{r^2}.\end{aligned}\right\} \quad (96)$$

The residual stresses and the residual displacement are found by addition:

$$\sigma_r'' = \sigma_r + \sigma_r', \quad \sigma_\theta'' = \sigma_\theta + \sigma_\theta', \quad \sigma_z'' = \sigma_z + \sigma_z' \quad \text{and} \quad u'' = u + u'. \quad (97)$$

In Tables 10, 11 and 12 the residual stresses are given for the unloading of the tubes, whose loaded stresses are given in Tables 3, 5 and 6.

TABLE 10. *Residual stresses in a closed-end tube, $b/a = 2$, $\rho/a = \sqrt{3}$, $\theta = \frac{1}{2}$, $\eta\beta = 0$, $\rho'/a = 1{\cdot}041$.*

r/a	1·0	1·2	1·4	1·6	$\sqrt{3}$	1·85	2·0
σ_r''/k_0	0	− ·136	− ·155	− ·116	− ·075	− ·036	0
σ_θ''/k_0	− 1	− ·51	− ·04	0·32	0·52	0·49	0·44
σ_z''/k_0	− ·30	− ·19	− ·06	0·06	0·13	0·13	0·13
$\frac{E}{k_0}\frac{u''}{a}$	1·64	1·28	1·06	0·91	0·88	0·87	0·81
$\frac{E}{k_0}\bar{\epsilon}''^p$	3·37	1·71	0·84	0·27	0	0	0

TABLE 11. *Residual stresses in a closed-end tube, $b/a = 4$, $\rho = b$, $\theta = 0$, $\eta\beta = 0$; $\rho'/a = 1{\cdot}276$.*

r/a	1·0	1·276	1·5	2·0	2·5	3·0	3·5	4·0
σ_r''/k_0	0	− ·244	− ·359	− ·388	− ·312	− ·208	− ·102	0
σ_θ''/k_0	− 1	− 1·244	− ·807	− ·202	0·168	0·430	0·632	0·796
σ_z''/k_0	− ·300	− ·446	− ·350	− ·177	− ·043	0·067	0·159	0·239
$\frac{E}{k_0}\frac{u''}{a}$	8·42	6·73	5·89	4·56	3·83	3·40	3·10	2·90
$\frac{E}{k_0}\bar{\epsilon}''^p$	17·09	9·28	6·43	3·15	1·64	0·82	0·32	0

It is seen from Tables 10, 11 and 12 that σ_z'' is the intermediate principal stress in that part of the tube that is plastic on unloading and that the yield criterion is not violated in that part which is elastic.

Provided $\theta \geqslant 0$ the method of unloading is unimportant, i.e. it is immaterial whether the internal pressures are removed first and then the temperature gradient or vice-versa or both together. If $\theta < 0$, the internal pressure and temperature gradient produce stress distributions which differ in sign. In this case on unloading one external effect must not be removed by itself if the other external effect is sufficient to produce plasticity by itself. For example, if this were not done in the example of Table 4 and the temperature gradient were removed first, the the stress system would become that of Table 2 and, on removal of pressure, would be that of Table 7, not that of Table 9.

TABLE 12. *Residual stresses in a closed-end tube.* $b/a = 4$, $\rho = b$, $\theta = 0$, $\eta\beta = 1/30$; $\rho'/a = 1{\cdot}107$.

r/a	1·0	1·107	1·5	2·0	2·5	3·0	3·5	4·0
σ_r''/k_0	0	− ·148	− ·394	− ·398	− ·312	− ·206	− ·101	0
σ_θ''/k_0	− 1·514	− 1·550	− ·716	− ·156	0·190	0·438	0·629	0·786
σ_z''/k_0	− ·454	− ·509	− ·333	− ·166	− ·037	0·070	0·159	0·236
$\frac{E}{k_0}\frac{u''}{a}$	8·16	7·53	5·69	4·46	3·75	3·36	3·08	2·88
$\frac{E}{k_0}\bar{\epsilon}''^p$	15·68	12·48	6·12	3·05	1·59	0·79	0·81	0
k''/k_0	1·514	1·402	1·204	1·100	1·052	1·026	1·010	1

8. FURTHER CONSIDERATIONS

Suppose a tube not subject to temperature gradient has been loaded and unloaded and, that during the latter process, some plastic flow has occurred. On the assumption that on reloading plasticity commences again at the bore, at what internal pressure will plasticity recommence?

Plasticity recommences when $\sigma_\theta - \sigma_r = k''$ at the bore. The residual stress distribution had $\sigma_r'' - \sigma_\theta'' = k''$ at the bore. Since the stress distribution superimposed on reloading is additive, plasticity commences when the superimposed stress distribution, denoted by a bar, is such that at the bore $\bar{\sigma}_\theta - \bar{\sigma}_r = 2k''$. If in the initial state, the tube had commenced to yield at internal pressure p, then on reloading it commences to yield at an internal pressure $\frac{2k''}{k_0}p$. For a non-work-hardening material the internal pressure at which yielding recommences is just double that which caused yielding in the initial state, irrespective of the amount of yielding which had previously taken place.

In the presence of temperature gradients the above remarks require modification as the strseses in the completely elastic state are no longer proportional to p (see equations 73 and 74).

There are a number of interesting problems which suggest themselves as extensions of the matter of this paper; for example shakedown, solutions for values

of b/a greater than those given by (70) and (71), solutions for large plastic deformations of the whole tube, and the effect of transient temperature gradients.

Shakedown is a state achieved in continuous loading and unloading. At first plasticity occurs but after a certain number of reversals plastic flow ceases and the stresses and displacements are superimposed elastically. Does this occur with thick tubes? It does for the example of Tables 2 and 4 for no plasticity occurs on unloading, and on reloading the states of Table 2 or 4 would be reached again. For the other examples further plastic flow occurs on reloading and it is necessary to follow each loading and unloading separately until no further plastic flow occurs.

Solutions for large values of b/a have been obtained by KOITER (1953) for non-work-hardening tubes not subject to temperature gradients. He finds that an inner plastic region is formed where $\sigma_z = \sigma_\theta$. It needs to be investigated whether this remains true for the more general case considered in this paper.

In considering the effect of large plastic deformation, it is necessary to take into account the change in radii of the outer and inner surfaces of the tube when applying the boundary conditions. This was done in the solution for the problem of the expansion of a hole in a plate by ALEXANDER and FORD (1954). For a closed-end tube the amount of expansion permissible is limited by the ends. If the centre sections expand too far, the assumption of uniform conditions along the length of the tube is no longer valid. For open ends or plane strain this objection does not apply.

The effect of a varying temperature is easy to assess if it does not produce plasticity at any stage. If it does, then a step by step analysis of each variation is necessary. It is to be assumed that the temperature varies slowly enough for elastic and plastic wave effects to be neglected. If this is not the case, it is necessary to add an additional term to the equilibrium equation (1). The mathematical problem is then so different as hardly to be classified as an extension to the results of this paper.

ACKNOWLEDGMENTS

This paper was written while the author was the holder of an I.C.I. Research Fellowship. He wishes to thank Professor H. FORD of Imperial College, London, for stimulating his interest in this problem.

REFERENCES

ALEXANDER, J. M. and FORD, H. 1954 *Proc. Roy. Soc. A*, **226**, 543.

ALLEN, D. N. de G. and SOPWITH, D. G. 1951 *Proc. Roy. Soc. A*, **205**, 69.

HILL, R. 1950 *Mathematical Theory of Plasticity* (Clarendon Press).

HODGE, P. G. and WHITE, G. N. 1950 *J. Appl. Mech.* **17**, 180.

KOITER, W. T. 1953 *Biezeno Anniversary Volume*, Stam, Haarlem, 232-251.

LOVE, A. E. H. 1927 *Mathematical Theory of Elasticity*, 4th edition (C.U.P.).

MANNING, W. R. D. 1945 *Engineering* **159**, 101 and 183.

STEELE, M. C. 1952 *J. Appl. Mech.* **19**, 133.

Journal of the Mechanics and Physics of Solids, 1956, Vol. 4, pp. 230 to 234. Pergamon Press Ltd., London.

CREEP OF POLYCRYSTALLINE ALUMINIUM AS DETERMINED FROM STRAIN RATE TESTS

By J. Weertman
Naval Research Laboratory, Washington, D.C.

(*Received 6th March*, 1956)

Summary

Polycrystalline samples of high purity aluminium have been tested in a strain rate machine over a wide temperature range. The relationship which exists between the maximum stress, strain rate, and temperature is

$$\text{strain rate} = A\,(\text{stress})^{4.4} \exp(-Q/RT)$$

where A is a constant, R is the gas constant, T is the absolute temperature, Q is an activation energy equal to 36,000 cal/mole.

The results are compared with those of Servi and Grant on constant stress creep tests and shown to be almost identical.

1. Introduction

There are two general methods for stressing specimens under uniaxial stress in high temperature creep studies. The more common way is to deform a sample under constant load or stress conditions; the less common way is to deform a specimen at a constant strain rate. In the first method, the strain rate varies during a test, and reaches a steady or almost steady rate for a large portion of the extension. In the second method, the stress varies during the test and, if the load is low enough, it also reaches a steady or almost steady value. Now, if the stress corresponding to a steady-state creep rate (at some particular temperature) for a constant-stress experiment is appreciably different from the steady-state stress found in a constant strain rate experiment, that the difficulties in the problem of explaining high-temperature creep will be greatly magnified.

The purpose of this experiment was to obtain data for strain rate tests on high purity polycrystalline aluminium and to compare this data with the extensive data which exists for constant stress tests on high purity polycrystalline aluminium (Servi and Grant, 1951). Comparison is also possible with constant stress tests on aluminium single crystals, tests which were carried out during the same time as the strain rate tests (Weertman, 1956).

2. Experiments

Specimens 0·505 inches in diameter and 2 inches in gauge length were machined out of bars of high purity aluminium (99·996%). These specimens were annealed

at 500°C for four hours to produce a grain size of approximately 4 mm.*. The samples were pulled in a constant strain-rate machine which uses a strain-gauge load cell to measure the load continuously. This machine was actually designed to pull specimens of one-inch gauge length at a constant true strain rate. In order to obtain the low stresses desired in this experiment it was necessary to use a 0·505 inch-diameter-specimen. For this diameter, a two-inch gauge length is more suitable. Our strain rates are therefore not perfectly constant. However, the variation in stress because of this nonuniformity in the strain rate is only of the order of 5% and thus is not serious. The variation in strain rate is large ($\sim 25\%$), but in a plot such as Fig. 2 or 3 the error is small.

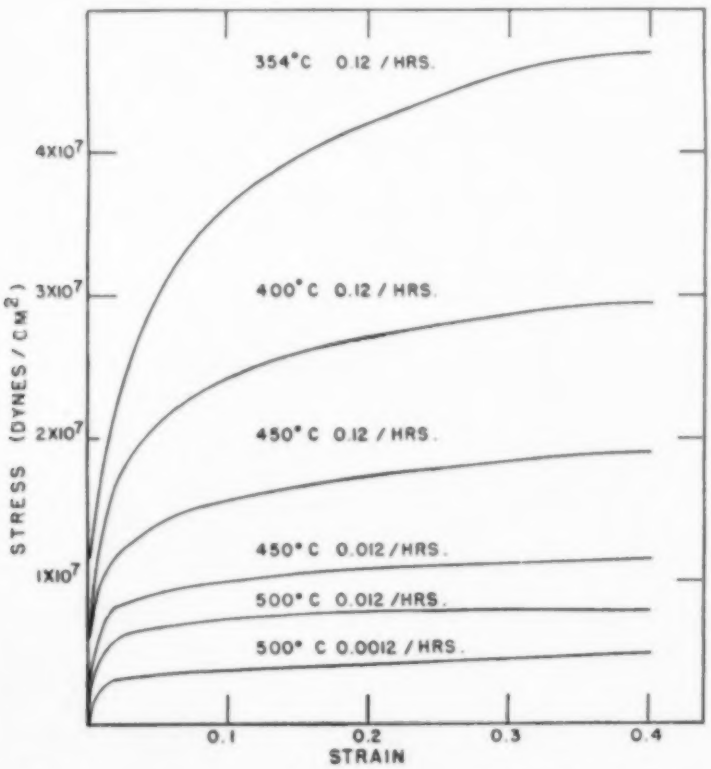

Fig. 1. Stress strain curve for various temperatures and strain rates.

3. Results

Fig. 1 shows the types of stress-strain curves which were obtained. In general the lower the applied stress the longer is the region where the stress is almost constant. It was not possible to go to as high stresses as did Servi and Grant because in the higher stress tests, the stress was still rising sharply up to the highest strain (see Table 1). The data from all tests are listed in Table 1.

*Note that some tests were run at 550°C, Table 1. The value of these tests is, of course, doubtful.

4. DISCUSSION

A creep law derived from a dislocation model (WEERTMAN, 1955), which should be applicable in the present case for polycrystalline samples, is

$$\text{steady state creep rate} = A\sigma^{1.11} \sinh (B\sigma^{1.78}/RT) \exp (-Q/RT) \qquad (1)$$

TABLE 1.

Temperature °C	*Average strain rate* h^{-1}.	*Steady state*** *stress dynes/cm*^{2}
150	0·012	$2{\cdot}8 \times 10^{8}$*
150	0·0012	$2{\cdot}2 \times 10^{8}$*
150	0·00012	$9{\cdot}8 \times 10^{7}$†
200	0·12	$2{\cdot}7 \times 10^{8}$*
200	0·012	$1{\cdot}75 \times 10^{8}$*
250	1·2	$2{\cdot}3 \times 10^{8}$*
250	0·12	$1{\cdot}6 \times 10^{8}$*
250	0·012	$9{\cdot}5 \times 10^{7}$
300	1·2	$1{\cdot}4 \times 10^{8}$
300	0·12	$9{\cdot}0 \times 10^{7}$
300	0·012	$5{\cdot}6 \times 10^{7}$
350	1·2	$8{\cdot}4 \times 10^{7}$
354	0·12	$4{\cdot}6 \times 10^{7}$
354	0·12	$4{\cdot}7 \times 10^{7}$
400	1·2	$5{\cdot}2 \times 10^{7}$
400	0·12	$3{\cdot}0 \times 10^{7}$
450	1·2	$3{\cdot}3 \times 10^{7}$
450	0·12	$1{\cdot}9 \times 10^{7}$
450	0·012	$1{\cdot}16 \times 10^{7}$
500	1·2	$2{\cdot}4 \times 10^{7}$
500	0·12	$1{\cdot}3 \times 10^{7}$
500	0·012	$8{\cdot}0 \times 10^{6}$
500	0·0012	$5{\cdot}0 \times 10^{6}$
550	1·2	$1{\cdot}7 \times 10^{7}$
550	0·12	$9{\cdot}5 \times 10^{6}$
550	0·012	$6{\cdot}2 \times 10^{6}$
550	0·0012	$3{\cdot}7 \times 10^{6}$‡

*Stress at largest strain. The stress was still rising sharply at the highest strain.
†Crept only to a strain of 0·11 instead of 0·4. Stress at the strain of 0·11.
‡The stress cycled during the test between this value and a value approximately half of this.
**Measured at strain of 0·4.

where σ is the stress, R is the gas constant, T is the absolute temperature, A and B are constants, and Q is the activation energy of self-diffusion. At low stress this equation reduces to

$$\text{creep rate} = K = AB (\sigma^{2.89}/RT) \exp (-Q/RT). \qquad (2)$$

In the present experiment, the strain rate would correspond to the steady state creep rate and the stress would be steady state stress.

In Fig. 2 is given a log-log plot of the data. It can be seen that the data lie on a straight line with a slope of 4·4. The activation energy of creep is 36,000

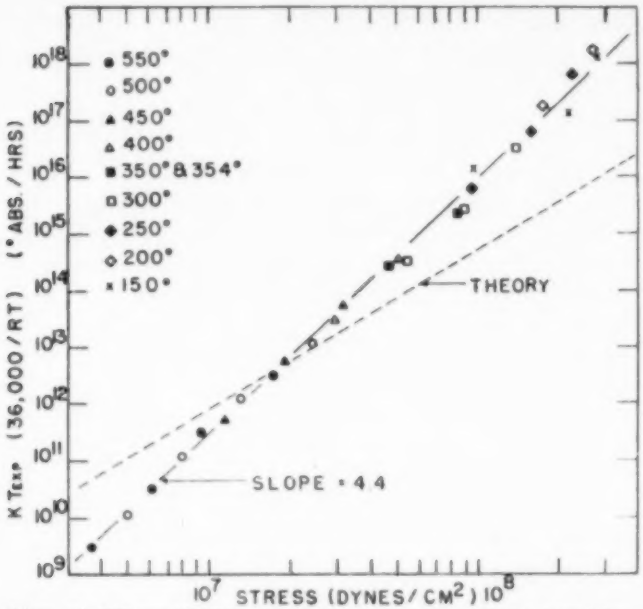

Fig. 2. Logarithm of $KT\exp(Q/RT)$ plotted as a function of the logarithm of the stress.

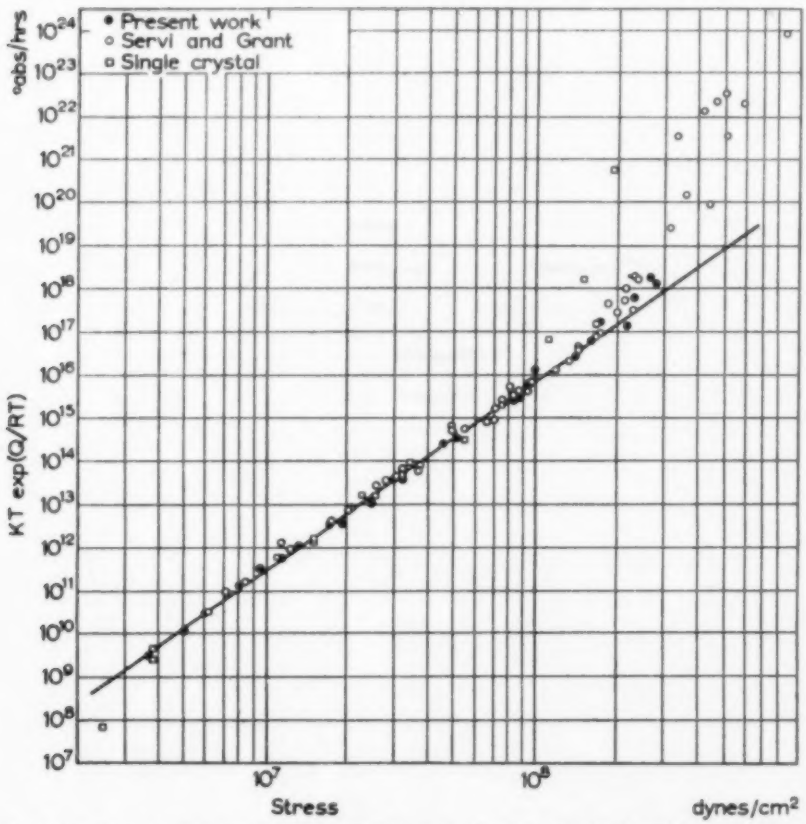

Fig. 3. Logarithm of $KT\exp(Q/RT)$ plotted as a function of the logarithm of the stress.

cal/mole. The dashed line shows theoretical values calculated from equation (2). Agreement between theory and experiment is to within an order of magnitude. In calculating the theoretical curve, the same values were used for the terms entering into the expression AB as were used previously (WEERTMAN, 1955) except that a grain size of 4 mm was used instead of 1 mm and the critical shear stress was taken to be 10^6 dynes/cm^2 instead of 3×10^6 dynes/cm^2. The higher value cannot be used since creep is observed at stresses lower than this in single crystals.

In Fig. 3 is given another log-log plot of the data. Also included in this plot is the constant stress data of SERVI and GRANT and data on single crystals of aluminium. The single crystals were made from the same stock of aluminium as were the strain-rate samples. The purity of this aluminium is about the same as that used by SERVI and GRANT. It can be seen that there is good agreement between the three types of experiments over most of the stress range. Theory would predict (WEERTMAN, 1955), however, that the single crystals should have a temperature compensated creep rate of a factor ten greater than the polycrystalline samples.

Since the grain size of our specimens is about the same as that of most of SERVI and GRANT's samples, we may conclude that constant-strain-rate tests and constant-stress tests lead to the same results. In other words, the path through which a specimen is led into the steady-state region has no effect on the relationship between stress and creep rate in this region. This demonstrated insensitivity to the type of creep test, then, is the main result of this paper.

ACKNOWLEDGMENTS

The author wishes to thank Mr. J. T. ATWELL and Mr. R. L. SAUNDERS for carrying out these tests.

REFERENCES

SERVI, I. S. and GRANT, N. J. 1951 *J. Metals* **3**, 909.

WEERTMAN, J. 1955 *J. Appl. Phys.* **26**, 1213.

1956 *Bull. Amer. Phys. Soc.*, Series II, 1, 45. To be published in J. Appl. Phys.

Journal of the Mechanics and Physics of Solids, 1956, Vol. 4, pp. 235 to 246. Pergamon Press Ltd., London.

FLANGE WRINKLING IN DEEP-DRAWING OPERATIONS

By B. W. Senior
University of Sheffield

(*Received* 31*st March*, 1956)

Summary

The critical dimensions of a deep-drawn flange and the number of waves into which it will collapse on wrinkling are predicted on the bases of the stress/strain curve of the material and the flange geometry.

Further terms are introduced to allow for blankholding pressure of different types and the results obtained are shown to agree well with experimental observations.

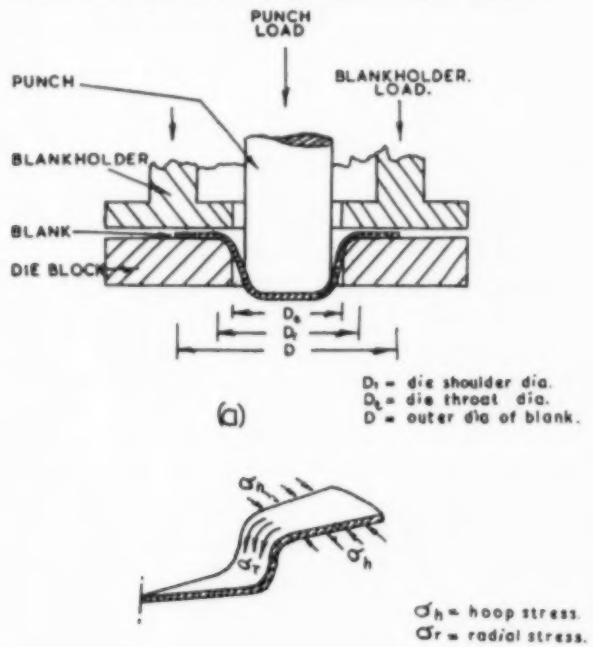

Fig. 1. (a) Deep-drawing tools.
(b) Stresses in a flange segment.

1. Introduction

In the deep-drawing operation an initially flat blank is drawn over a radiused die by a profiled punch, the shape of which governs the form of the finished com-

ponent. Fig. 1 (a) shows a typical arrangement for the drawing of a cylindrical shell or cup from an initially flat circular blank. During the drawing operation, the outer flange of material is subjected to a radial drawing stress, σ_r, and an induced hoop stress, σ_h, as shown in Fig. 1 (b). Under the influence of this combined stress system the material yields and plastic flow results.

For particular drawing-tool dimensions and material thickness there is a critical blank diameter, above which the flange collapses into waves or wrinkles under the influence of the induced hoop stresses. In drawing blanks smaller than this critical diameter the blankholder, as shown in Fig. 1 (a), is unnecessary. In the drawing of deeper shells where this critical blank diameter is exceeded, a blankholder is employed to restrain the wrinkled wave form by providing a lateral surface pressure to the flange.

In general, the blankholder load may be applied in either of two separate ways, or by a combination of the two. In the first case a constant load is applied by pneumatic or hydraulic pressure so that the total load on the flange surface is substantially independent of any lateral deflection of the flange surface. In the second case the loading is provided by springs or by the stiffness of the holding down bolts of the blankholder plate giving rise to a surface load which is a linear function of the lateral flange surface deflection.

2. Use of Energy Method to Determine Critical Conditions

In general there are two ways in which stability problems may be solved. In the first the differential equations for the system in equilibrium are set up and solved to give the critical load conditions directly. This method is typified by the Euler solution for the buckling of longitudinally loaded struts (e.g. Westergaard and Osgood 1942). Alternatively, a deflected form may be assumed for the system and the component quantities of potential energy related to a small deflection evaluated. When the total energy tending to restore equilibrium is greater than that due to the forces displacing it the system remains stable. Equating the two energy values gives the critical condition.

In the wrinkling of a deep-drawn flange due to lateral collapse under the induced hoop stresses, the energy terms involved are of three main types :

E_B, the energy due to bending into a half-wave segment of the wrinkled flange.

E_H, the energy due to the circumferential shortening of the flange under the hoop stress,

and E_L, the energy due to the lateral loading of the flange surface.

During the drawing operating the inner flange periphery is, in effect, firmly clamped between the punch and die radii. Thus the effective resistance of the flange to wrinkling is increased. In considering the deflections of an annular flat plate rigidly constrained around the inner edge and uniformly loaded around its mean radius Morley (1954) has shown that the deflection at the mean radius is proportional to the load applied according to the relation

$$y = \frac{Cqb^5}{8EI} \tag{1}$$

where q is the transverse pressure, b the flange breadth, E is Young's Modulus and I is the second moment of area of the flange section about a radius through the centre of the section. C is a constant depending on Poisson's ratio and the ratio of the flange outer and inner radii, r. GECKELER (1928) has calculated values of the constant C over the range of values of r from 3 to 10 and shown that it varies between 1·03 and 1·11. Thus, for the purposes of the present work, a mean value of 1·07 is assumed. Rearranging (1) and substituting this value of C, we obtain

$$\frac{q}{y} = 7{\cdot}47\,\frac{EI}{b^3} = K. \tag{2}$$

It follows that the effect of the constraint around the inner flange periphery can be simulated by a transverse loading around the flange centre line proportional to the deflection at the point considered.

In addition, lateral loading components are introduced by the use of a blankholder and where the blankholder is of the spring type, the load is proportional to the lateral deflection, whilst a hydraulic or pneumatic blankholder exerts a load substantially independent of the deflection.

3. Selection of Assumed Deflected Wave Form in Wrinkling

In the most general case the deflected form of a buckled bar or flange segment of length l can be expressed in the form

$$y = \sum_{n=1}^{n\to\infty} \gamma_n \sin\frac{n\pi x}{l}. \tag{3}$$

TIMOSHENKO (1936) has shown that for a straight strut the use of the first term alone in this equation predicts the critical load sufficiently accurately so that it is considered adequate to assume a wrinkled wave form

$$y = \gamma \sin\frac{\pi x}{l} \tag{4}$$

where x is the co-ordinate direction along the circumference at the mean flange radius and y is the lateral deflection.

It is also assumed that the number of waves n is sufficiently large for the axis of a half-wave segment to be considered straight and that twisting of the flange section during buckling may be neglected.

4. Energy Components in Buckled Half-wave Segment : No Bankholder

Due to lateral elastic bending, the energy stored in a half-wave segment is

$$E_B = \tfrac{1}{2}\int_0^l EI\,\frac{d^2y}{dx^2}\,dx. \tag{5}$$

VON KARMAN (1909) has shown that the conventional elastic bending theory can be extended to cover plastic bending by the substitution for Young's Modulus E of a Plastic Buckling Modulus, E_0 where

$$E_0 = \frac{4EP}{(\sqrt{E} + \sqrt{P})^2}.$$

P being the slope of the stress/strain curve of the material in simple tension at a particular value of strain; it follows that E_0 is a function of strain.

That the effect of the radial stress may be neglected is confirmed by tests carried out by BALDWIN and HOWALD (1947).

The length of a half-wave segment l is given by

$$l = \frac{a\pi}{n} \tag{6}$$

where a is the mean flange radius and n the total number of waves formed. Hence, evaluating (5) by means of (4) and then using (6), we obtain

$$E_B = \frac{E_0 I \gamma^2 \pi n^2}{4a^3}. \tag{7}$$

The buckling of a half-wave segment reduces its length by

$$\tfrac{1}{2}\int_0^l \left(\frac{dy}{dx}\right)^2 dx$$

so that the energy released by the hoop stresses is

$$E_H = \frac{\sigma_h bt}{2}\int_0^l \left(\frac{dy}{dx}\right)^2 dx \tag{8}$$

where σ_h is the mean hoop stress in the flange, b is the flange breadth and t the thickness. (It is assumed that the slight thickening of the flange which occurs as the drawing operation proceeds may be neglected).

On evaluating (8) by substituting from (4) and (6) it is found that

$$E_H = \sigma_h bt \,.\, \frac{\gamma^2 \pi n}{4a}. \tag{9}$$

Due to the assumed lateral loading of the flange surface q which simulates the clamping of the inner flange periphery between the punch and die, the remaining energy component is

$$E_L = \int_0^l \int_0^y bq \, dy \, dx. \tag{10}$$

In practice it is uncertain whether a loading proportional to the deflection at any particular point in the segment should be taken,

$$q = Ky, \tag{11}$$

or one proportional to the amplitude of the wave,

$$q = K\gamma. \tag{12}$$

For this reason it is preferable to substitute in (10) for both conditions and so obtain limits between which a transition from stability to wrinkling takes place. Using (11) the lower limit becomes

$$E_L = \frac{bK\gamma^2 a\pi}{4n}, \tag{13}$$

and from (12) follows the upper limit

$$E_L = \frac{2b\,K\gamma^2\,a}{n}. \tag{14}$$

The critical condition is reached when

$$E_B + E_L = E_H.$$

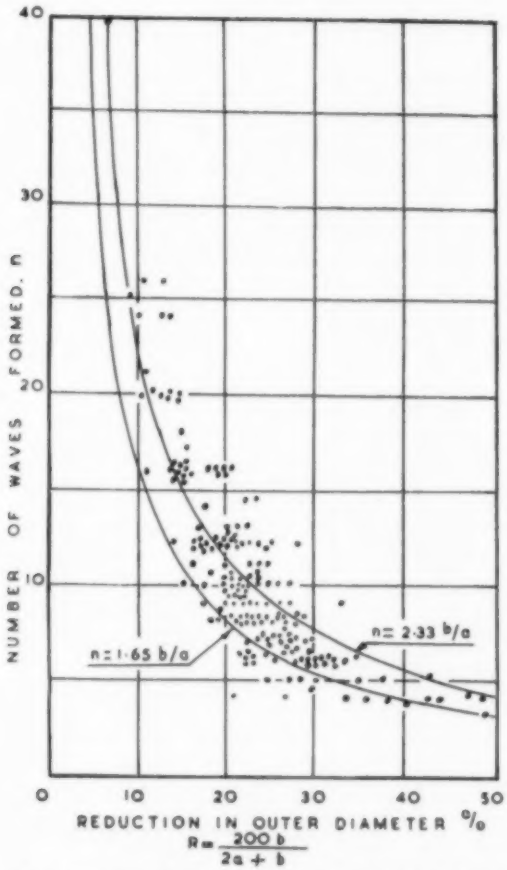

Fig. 2. Number of waves formed in deep-drawing tests without blankholder.

For the lower limit this gives

$$\sigma_h\,bt = E_0\,I\,\frac{n^2}{a^2} + bK\,\frac{a^2}{n^2} \tag{15}$$

and for the upper limit

$$\sigma_h\,bt = E_0\,I\,\frac{n^2}{a^2} + \frac{8}{\pi}\,bK\,\frac{a^2}{n^2}. \tag{16}$$

Equations (15) and (16) are now differentiated with respect to n to find the condi-

tion of minimum hoop stress at the onset of buckling. It appears that the number of waves into which the flange would wrinkle is given by

$$1{\cdot}65\,\frac{a}{b} \leqslant n \leqslant 2{\cdot}33\,\frac{a}{b}, \tag{17}$$

and the hoop stress at which instability occurs follows from

$$0{\cdot}46\left(\frac{t}{b}\right)^2 \leqslant \frac{\sigma_h}{E_0} \leqslant 0{\cdot}64\left(\frac{t}{b}\right)^2. \tag{18}$$

It is interesting to note that the result (17) for the critical number of waves n is dependent only on the flange dimensions a and b and is independent both of the flange thickness and the mechanical properties of the material.

The theoretically predicted limits are shown in Fig. 2 in comparison with experimentally observed values of the numbers of waves formed in wrinkled pressings in pure aluminium (of five different hardnesses), soft 70/30 brass, and commercial quality killed steel in thicknesses ranging from 0·033 in. to 0·125 in. Punch diameters of 0·75 in. and 2 in. were used in these tests.

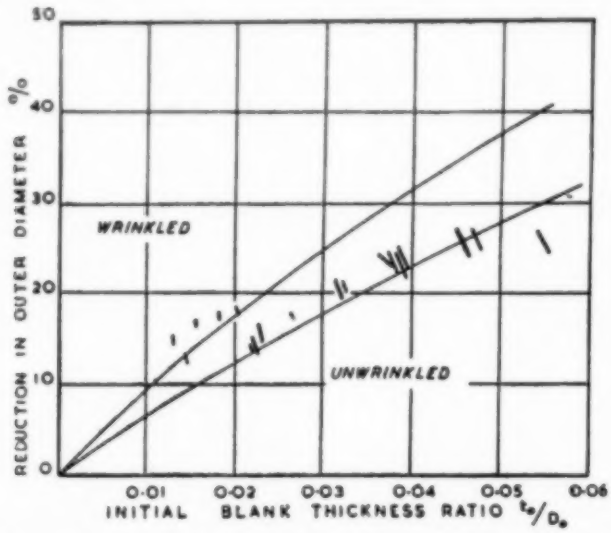

Fig. 3. Critical curves for soft 70/30 brass without blankholder showing the upper and lower theoretical limits. Bars indicate the experimentally observed transition from fold-free to wrinkled flanges.

From (18) it is clear that the factor σ_h/E_0 is a function of terms depending only on the stress/strain properties of the material, while the other factor (t/b) is governed by the geometry of the flange itself. σ_h/E_0 can therefore be evaluated as a function of strain for a particular material from an experimentally determined stress/strain curve. The variation in (t/b) with the mean strain in the flange can be calculated for particular values of (t_0/b_0), t_0 and b_0 being the initial values of flange thickness and breadth respectively. Thus, both factors in (18) can be represented as a function of strain. It has been shown by BALDWIN and HOWALD

(1947) that by superimposing the curves of σ_h/E_0 and (t_0/b_0) against strain plotted on the same scale, and adjusting them relative to one another at right angles to the strain axis, the points of tangency for particular values of (t_0/b_0) can be obtained. Thus, a relationship between (t_0/b_0) and mean strain is derived. For convenience in experimental work this is converted to a graph of reduction in outer diameter of blank $R = 2b/(2a + b)$ against initial blank thickness to diameter ratio, t_0/D_0, as shown in Fig. 3. The upper and lower theoretically predicted limits shown here are for soft 70/30 brass drawn with a 0·75 in. diameter punch. The experimentally observed demarkation between wrinkled and fold-free pressings is shown for comparison. The length of the bar in the figure denotes the range of the observed transition. In these tests the material thickness ranged from 0·022 in. to 0·080 in. Similar results have been obtained for all the materials quoted above in connection with the observed number of waves, the correlation between theory and experiment being in all cases of the order of that demonstrated in Fig. 3.

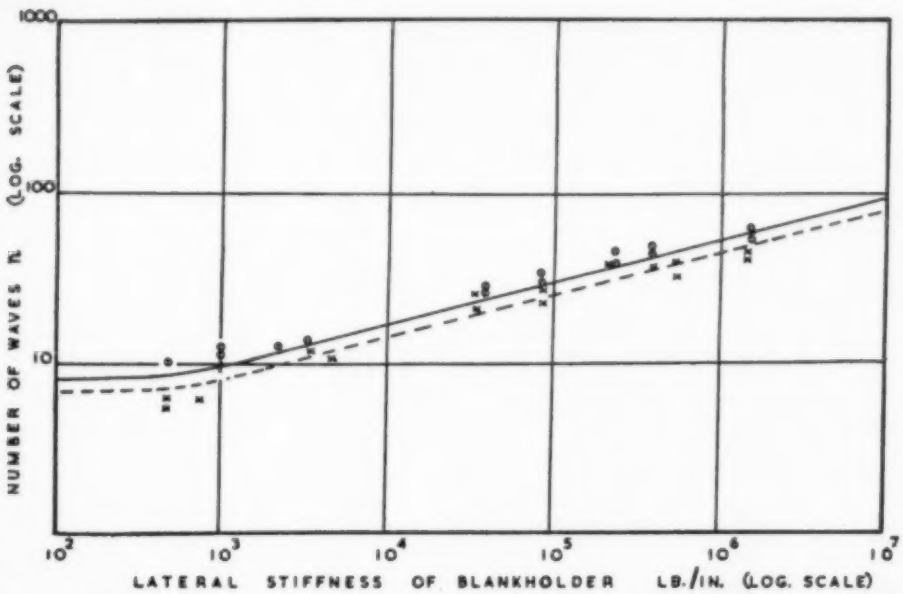

Fig. 4. The effect of material properties on the number of waves formed under spring blank holding.

Theoretical curves	Soft 70/30 brass	————
	Rimming steel	- - - - - -
Experimental results	Soft 70/30 brass	o
	Rimming steel	x

5. Modification of Stability Equation for Spring-type Blankholder.

In practice, flanges greater than the critical size are drawn with a blankholder. This provides a lateral loading of the flange surface and gives rise to configurations of stability other than the initially plane condition. Where a spring-type blankholder is used, the loading is proportional in general to the lateral deflection of the flange surface. The surface pressure on the flange is

$$q_1 = \frac{S\gamma}{\pi ab}, \tag{19}$$

γ being the amplitude of the wrinkled wave form and S the spring stiffness of the blankholder. When this is added to the lateral pressure simulating the clamping of the inner edge, the energy component due to the total lateral loading becomes, following (9),

$$E_L = \int_0^l \int_0^y b\,(q + q_1)\,dy\,dx. \tag{20}$$

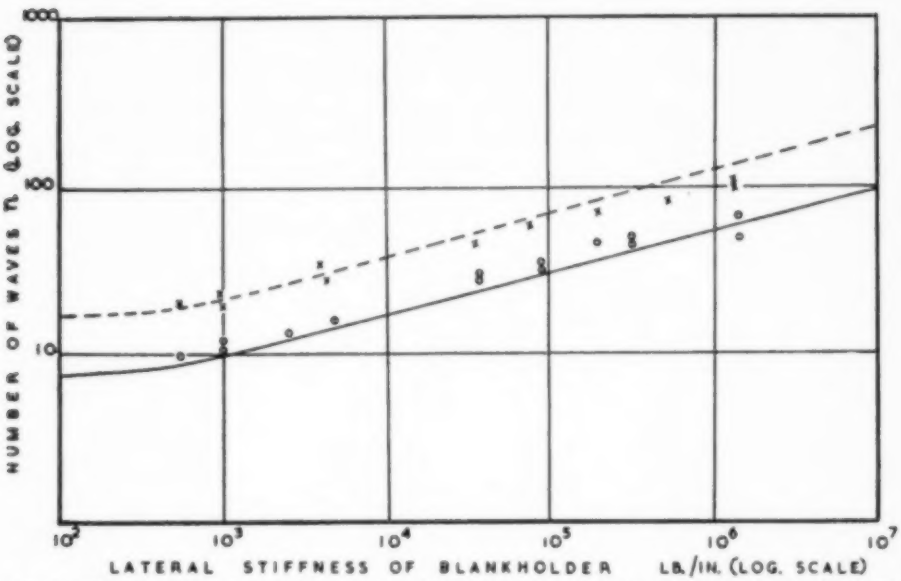

Fig. 5. The effect of material thickness on the number of waves formed (under spring holding) in drawing test on soft 70/30 brass.

Theoretical curves	0·036″ material	- - - - - -
	0·012″ material	————
Experimental results	0·036″ material	o
	0·012″ material	x

Using the upper limit stated in (12), this becomes

$$E_L = b\left(K + \frac{S}{\pi ab}\right)\frac{\gamma^2 a\pi}{4n}, \tag{21}$$

whence, using $E_B + E_L = E_H$, E_B and E_H being as stated in (7) and (8), it follows that

$$\sigma_n = \frac{a}{bt\,\pi n}\left(\frac{E_0 I \pi n}{a^3} + \frac{\pi a}{n}\left(\frac{8\,E_0 I}{b^4} + \frac{S}{\pi a}\right)\right). \tag{22}$$

This is stationary with respect to n when

$$n = a\left(\frac{14}{b^4} + \frac{3{\cdot}8\,S}{E_0\,bat^3}\right)^{\frac{1}{4}}. \tag{23}$$

The first term due to the lateral loading representing the peripheral clamping is negligible except at very low values of S and for practical purposes the equation may be written as

$$n = 1{\cdot}4\, a \left(\frac{S}{E_0\, bat^3}\right)^{\frac{1}{4}}. \tag{24}$$

In evaluating this equation it is necessary to idealize the stress strain curve for the material, assuming a constant strain hardening rate.

Fig. 4 shows the theoretically predicted variation in the number of waves between 0·012-in. and 0·036-in. soft 70/30 brass drawn on 2-in. diameter tools, for a wide range of blankholder stiffnesses.

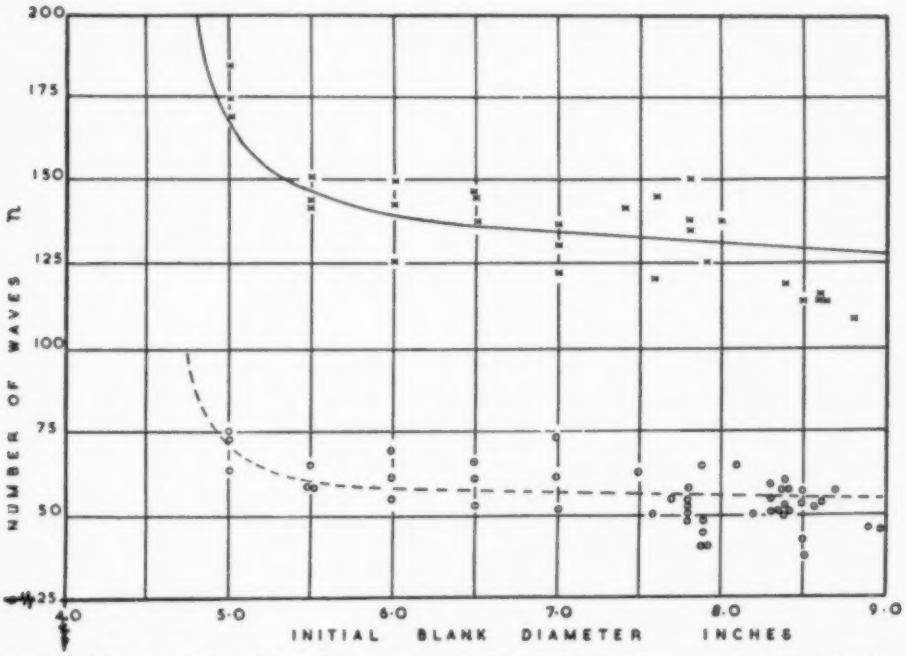

Fig. 6. Effect of variation in initial blank diameter on the number of waves formed in the drawing of 0·036″ half-hard 70/30 brass over a 4·00″ – diameter die under clearance blank holding conditions.

Theoretical curves	Initial elastic waves	- - - - - -
	Final plastic waves	———
Experimental results	Initial elastic waves	o
	Final plastic waves	x

Fig. 5 demonstrates the effect of different materials, 0·036-in. soft 70/30 brass and rimming steel, on the number of waves formed using the same tools. The experimental results lie in two distinct groups. Those on the left were obtained using coil springs of various sizes behind the blankholder plate, while for those to the right long studs of varying diameters were used to give the higher stiffness values required.

Fig. 6 demonstrates the effect of the variation of initial blank diameter on the number of waves formed in 4-in.-diameter cups drawn from 0·036-in. half-hard

70/30 brass. These tests were carried out on a 100-ton-capacity hydraulic press fitted with a clearance type blankholder. The spring stiffness of the blankholder plate clamping mechanism was calculated and checked experimentally. The upper curve is obtained using an idealized strain-hardening characteristic and corresponds to the plastic wrinkles formed in the latter stage of the drawing operation. The lower curve is based on the elastic modulus of the material and is compatible with the lower number of waves formed elastically in the initial stages of wrinkling. These separate phases of wrinkling may be clearly discerned on drawn cups and the experimental points agree well with the theoretical predictions.

It is important in all deep-drawing operations that the number of waves developed in wrinkling be relatively large in order that the resulting wave amplitude shall be small. This permits ironing out of the wave tips as the drawn body passes through the die throat without causing an unduly high built-up of punch load.

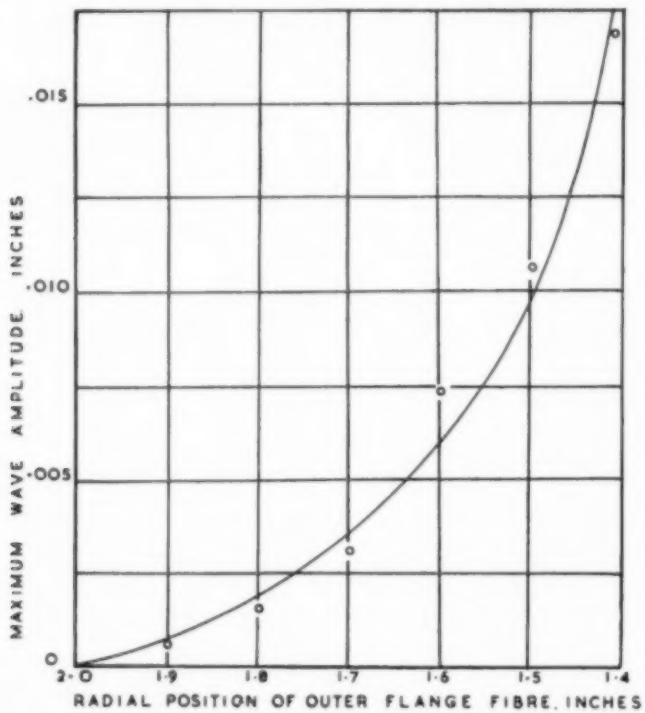

Fig. 7. Theoretically predicted variation in maximum wave amplitude during the drawing of a 4″-diameter blank of 0·036″ rimming steel into a 2″-diameter cup. ———— Experimental measurements o

6. Blankholders Exerting a Constant Load.

In the previous Sections the lateral pressure on the flange surface has been considered proportional to the deflection of the surface. Where a pneumatic- or hydraulic-type blankholder is used the surface pressure is usually very nearly constant.

Thus, a further energy term must be added to the stability equation

$$E_Q = 2\gamma \frac{Q}{n} \tag{25}$$

where Q is the total load exerted by the blankholder. The stability equation then becomes

$$E_B + E_L + E_Q = E_H$$

Substituting for E_B, E_L, and E_H from (7), (9) and (13) as before, we derive

$$\sigma_h = 0{\cdot}083 \frac{E_0 bt^3}{a^2} \cdot n^2 + \frac{0{\cdot}69\, a^2 E_0 t^3}{b^3 n^2} + 1{\cdot}27\, a \frac{Q}{\gamma} \cdot \frac{1}{n^2}.$$

Proceeding as before, we find

$$n = \left[\frac{1{\cdot}34\, E_0 a^4 t^3 + 2{\cdot}54\, a^3 b^3 Q/\gamma}{E_0 b^4 t^3}\right]^{\frac{1}{4}}. \tag{26}$$

It can be seen that in this case the number of waves and the wave amplitude are interdependent.

Rearranging (26):

$$\gamma = \frac{15{\cdot}3\, Q b^3 a^3}{E_0 t^3 (b^4 n^4 - 8{\cdot}04\, a^4)}. \tag{27}$$

Fig. 7 shows the theoretically predicted wave amplitude for a particular case based on the number of waves counted at each stage of the operation and the experimentally measured wave amplitudes are included for comparison.

7. Conclusions

It has been shown that the conditions of stability in a deep-drawn flange without a blankholder may be predicted by an energy method. From the resulting equations it is apparent that the number of waves formed is independent of the mechanical properties of the material and of the material thickness and that it tends towards infinity as stability is approached.

It is found that, while the critical flange dimensions are dependent on the material properties, there is little difference between the normally used strain-hardening materials and that the critical diameter is affected to a far greater extent by the geometry of the drawing tools and the material thickness.

The introduction of a term representing the stiffness of a spring-type blankholder leads directly to a solution for the number of waves formed and this number tends to increase as the blankholder stiffness increases. The effect of material properties is again shown to be slight.

For a constant-load blankholder where the surface pressure is independent of the wave amplitude, it is shown that the number and amplitude of the waves are interrelated. Comparison with experimental results shows that, while this leads to no directly useful result, the relationship observed agrees well with that predicted theoretically.

ACKNOWLEDGMENTS

The author wishes to express his thanks to Professor H. W. SWIFT and Mr. W. JOHNSON for their kindly advice and encouragement during the course of this work.

REFERENCES

BALDWIN W. M. and HOWALD T. S.	1947	*Trans. Amer. Soc. Mech. Engrs.* **38**, 757.
GECKELER J. W.	1928	*Z. angew. Math. Mech.* **8**, 341.
KARMAN T. VON	1909	*Z. Ver. dtsch. Ing.*, **81**.
MORLEY A.	1954	*Strength of Materials*, Longmans.
TIMOSHENKO S.	1936	*Theory of Elastic Stability*, McGraw-Hill.
WESTERGAARD H. B. and OSGOOD W. R.	1942	*Trans. Amer. Soc. Civil Engrs.* **107**, 965.

Journal of the Mechanics and Physics of Solids, 1956, Vol. 4, pp. 247 to 255. Pergamon Press Ltd., London.

ON THE PROBLEM OF UNIQUENESS IN THE THEORY OF A RIGID-PLASTIC SOLID—1

By R. Hill
Department of Mathematics, University of Nottingham

(*Received 6th April*, 1956)

Summary

The yield point of a rigid-plastic solid is defined by specifying the velocity $\boldsymbol{v}$ over a part S_v of the surface and traction $\boldsymbol{F}$ over the remainder S_F. It is known that these boundary conditions uniquely determine the state of stress in a certain part of the plastic zone but not usually the instantaneous mode of deformation. In that event it is shown here that it is also necessary to specify the traction-rate $\dot{\boldsymbol{F}}$ over S_F, and that this is sufficient to define the mode uniquely (with certain continuity restrictions) when the material work-hardens and when changes in geometry are negligible. The appropriate mode in a nonhardening solid is obtained by a limiting process in which the rate of hardening is made vanishingly small.

1. Outline of Basic Concept

The solid under consideration is work-hardening and rigid-plastic with an identical yield function and plastic potential at each point. It has been shown that the state of stress is uniquely determined in a certain zone when the traction $\boldsymbol{F}$ is specified over a part S_F of the surface and the velocity $\boldsymbol{v}$ over the remainder S_v (Hill, 1951).* This zone forms part (or sometimes all) of the plastic region and contains all material that can deform at this instant in conformity with *these* boundary conditions; a method for delimiting the zone has been described by Bishop, Green and Hill (1956). On the other hand, the mode of deformation in the zone *may* not be uniquely determined by these boundary conditions alone. A classic example is indentation of a plane surface by a flat punch, for which there exists a single infinity of competing modes (Hill, 1950, p. 255). Another example is a body in a uniform plastic state of stress under suitable surface tractions; the corresponding set of modes has been stated by Prager (1954a). Many writers (myself included), when remarking on this indeterminacy, have suggested ad hoc hypotheses for its removal or have vaguely speculated that it might not occur if work-hardening were somehow to be taken into account. However, in the absence of a valid general criterion, the situation has remained obscure and the treatment of problems of continued deformation has been seriously impeded.

The present discussion of this difficulty is restricted to situations where it is permissible to neglect positional changes and rotations of material elements

*This is true also for other natural boundary-conditions, e.g. normal component of $\boldsymbol{F}$ (or $\boldsymbol{v}$) and tangential component of $\boldsymbol{v}$ (or $\boldsymbol{F}$) specified over the same part of the surface. The modifications in the statements and proofs of subsequent theorems are sufficiently obvious.

in the ensuing distortion.* The restriction does not, however, affect the basic concept in the principle proved in Section 2. For a work-hardening material this states that, when more than one mode is compatible with the boundary conditions on $\boldsymbol{F}$ and $\boldsymbol{v}$, the physically possible mode is singled out by the following additional requirement: there must exist an equilibrium distribution of stress-rate compatible with the implied rate of hardening everywhere in the body and with the given traction-rate $\dot{\boldsymbol{F}}$ on S_F. All other modes are merely kinematically possible at the instant and imply a hardening-rate for which this requirement cannot be satisfied. In short, there is no inherent indeterminacy in general: previous difficulties were due simply to inadequate formulation of the problem. (It is reiterated that this conclusion does not apply without modification when the effects of positional changes are paramount, e.g. the necking of a tension specimen). Certain exceptional cases with discontinuities require further investigation, however.

When $S_v \neq 0$, the stress-rate components individually are, however, not uniquely determined in the deformation zone until reference is made to yet a further boundary condition, namely the "acceleration" $\dot{\boldsymbol{v}}$ on S_v (which may be thought of pictorially as specifying the "curvature" of the "strain-path").† This, indeed, becomes obvious by regarding the problem of determining the stress-rate as equivalent to determining the actual stress at an infinitesimal time dt later; the uniqueness theorem of HILL can be applied to this later instant, having regard to the new distribution of hardness produced by the unique mode and to boundary conditions specifying the traction $\boldsymbol{F} + \dot{\boldsymbol{F}}dt$ on S_F and velocity $\boldsymbol{v} + \dot{\boldsymbol{v}}dt$ on S_v. When $S_v = 0$, the same theorem shows, as would be expected, that the stress-rate *is* uniquely determined in the deforming zone by given $\boldsymbol{F}$ and $\dot{\boldsymbol{F}}$ all over the surface.

A nonhardening material, on the other hand, is on a different footing. No uniqueness theorem for the mode can be proved, even with the problem formulated in terms of given $\boldsymbol{F}$ and $\dot{\boldsymbol{F}}$ on S_F and $\boldsymbol{v}$ on S_v. It seems necessary, therefore, to import into the analysis an extraneous physical consideration, namely that the proper mode is to be obtained as a limit approached by the unique mode in a work-hardening solid as the hardening rate is uniformly diminished everywhere. This appears appropriate when the rigid-plastic nonhardening solid is regarded as a convenient approximation to a work-hardening metal at temperatures where creep and other time effects are negligible. If it is introduced for other purposes, however, it may be more appropriate to regard it as a degenerate case of some different solid, for instance a viscoplastic material in which the viscosity is reduced indefinitely. In Section 4 we describe the precise manner in which this limiting process is to be carried out.

2. UNIQUENESS THEOREM

To simplify the notation the components of the stress and strain-rate tensors are regarded as constituting "vectors" in a space of 9 dimensions and are denoted

*A full analysis incorporating these factors is to be given elsewhere.

†This is in marked contrast to the uniqueness theorem for an elastic-plastic solid (work-hardening or not), where the stress-rate *is* uniquely determined by given $\dot{\boldsymbol{F}}$ on S_F and $\boldsymbol{v}$ on S_v (see, for example, HILL 1950, pp. 53-8). The analysis in Section 2 has a certain formal resemblance to that in the proof of the uniqueness theorem for an elastic-plastic solid, but the interpretation and conclusions are fundamentally different. Relations between the two solids, and the transition from one to the other, are to be discussed elsewhere.

by $\boldsymbol{\sigma}$ and $\boldsymbol{\epsilon}$.* The scalar product of two vectors is indicated by placing them in juxtaposition; for example, the rate of work per unit volume is written $\boldsymbol{\sigma\epsilon}$.

The body may be anisotropic and inhomogeneous, but at every point the yield surface in stress space is assumed to be convex and to contain the origin (zero stress) and to have a unique normal everywhere. The unit outward normal is denoted by $\boldsymbol{n}$ ($\boldsymbol{n}^2 \equiv \boldsymbol{nn} = 1$) and is a function of stress and strain-history. On the hypothesis that the yield function and plastic potential coincide, the relations between stress $\boldsymbol{\sigma}$, strain-rate $\boldsymbol{\epsilon}$, and stress-rate $\dot{\boldsymbol{\sigma}}$ in a *plastic* element are

$$h\,\boldsymbol{\epsilon} = \begin{cases} (\boldsymbol{n}\,\dot{\boldsymbol{\sigma}})\,\boldsymbol{n} & \text{when} \quad \boldsymbol{n}\,\dot{\boldsymbol{\sigma}} > 0 \\ 0 & \text{when} \quad \boldsymbol{n}\,\dot{\boldsymbol{\sigma}} \leqslant 0 \end{cases} \tag{1}$$

where h is a positive scalar function of stress and strain-history, expressing the work-hardening properties of the material.† (For an account of the physical basis of these relations, see HILL, 1956.) $\boldsymbol{n}$ would be found experimentally from the measured ratios of the strain-rate components in a plastic state $\boldsymbol{\sigma}$, while h could be obtained as the ratio of any of the corresponding components of stress-rate and strain-rate when the stress is increased from $\boldsymbol{\sigma}$ along $\boldsymbol{n}$. From (1) and the relation $\boldsymbol{n}^2 = 1$ we deduce

$$\dot{\boldsymbol{\sigma}}\,\boldsymbol{\epsilon} = \begin{cases} h^{-1}\,(\boldsymbol{n}\,\dot{\boldsymbol{\sigma}})^2 & \text{for} \quad \boldsymbol{\epsilon} \neq 0 \text{ only} \\ h\,\boldsymbol{\epsilon}^2 & \text{for all} \quad \boldsymbol{\epsilon}. \end{cases} \tag{2}$$

Note that $\boldsymbol{\epsilon} = 0$ and $\boldsymbol{n}\,\dot{\boldsymbol{\sigma}} < 0$ if an element unloads from a plastic state, and that $\boldsymbol{\epsilon} = 0$ with $\boldsymbol{n}\,\dot{\boldsymbol{\sigma}}$ unrestricted if an element is nonplastic. Also, when $\boldsymbol{\epsilon} \neq 0$, $\boldsymbol{n}\,\dot{\boldsymbol{\sigma}} = h\,|\boldsymbol{\epsilon}|$.

Suppose there could be two physically possible modes $\boldsymbol{\epsilon}_1$ and $\boldsymbol{\epsilon}_2$ such that $\boldsymbol{v}_1 = \boldsymbol{v}_2$ on S_v, associated with equilibrium distributions of stress-rate $\dot{\boldsymbol{\sigma}}_1$ and $\dot{\boldsymbol{\sigma}}_2$ such that $\dot{\boldsymbol{F}}_1 = \dot{\boldsymbol{F}}_2$ on S_F, with

$$h\,\boldsymbol{\epsilon}_1 = (\boldsymbol{n}\,\dot{\boldsymbol{\sigma}}_1)\,\boldsymbol{n} \quad \text{and} \quad \boldsymbol{n}\,\dot{\boldsymbol{\sigma}}_1 > 0 \quad \text{where} \quad \boldsymbol{\epsilon}_1 \neq 0,$$

$$h\,\boldsymbol{\epsilon}_2 = (\boldsymbol{n}\,\dot{\boldsymbol{\sigma}}_2)\,\boldsymbol{n} \quad \text{and} \quad \boldsymbol{n}\,\dot{\boldsymbol{\sigma}}_2 > 0 \quad \text{where} \quad \boldsymbol{\epsilon}_2 \neq 0;$$

$$\boldsymbol{n}\,\dot{\boldsymbol{\sigma}}_1 \leqslant 0 \quad \text{where} \quad \boldsymbol{\epsilon}_1 = 0, \qquad \boldsymbol{n}\,\dot{\boldsymbol{\sigma}}_2 \leqslant 0 \quad \text{where} \quad \boldsymbol{\epsilon}_2 = 0,$$

in the uniquely stressed zone. For the moment we exclude from consideration any mode that involves a velocity discontinuity (see Section 5). Discontinuities in the stress-rate components are contemplated, subject to the restriction that in general the traction-rate $\dot{\boldsymbol{F}}$ across any such surface must be continuous for equilibrium.‡ This situation arises, for instance, where the strain rate is discontinuous; as can easily be seen from (1) this is possible only where the stress at each point of the surface of discontinuity is such that the strain-rate components

*No confusion need be caused by using the same type for the 3-dimensional vectors $\boldsymbol{F}$ and $\boldsymbol{v}$.

†Note that stress-rate in (1) strictly refers to the change of stress in a material element, but can here be evaluated at a fixed station since positional changes are neglected. In evaluating $\dot{\boldsymbol{F}}$ rotations of the surface normal are also neglected.

‡This may readily be shown by examining the discontinuities in stress gradient allowed by the equilibrium and continuity relations for the stress, coupled with the observation that a discontinuity in stress-rate accompanies one in stress gradient when the discontinuity surface moves.

Exceptionally, the tangential component of $\dot{\boldsymbol{F}}$ can be discontinuous across a surface of discontinuity in the existing stress or in the strain-rate (the stress being incipiently discontinuous). The theorems of Sections 2 and 3 (a) are still valid when all competing modes have the same tangential velocity.

in the tangent plane vanish.† Again, there may be points on the surface of the body where the strain rate increases without limit as these are approached (e.g. in plane strain, at the centre of a fan of slip lines); a classification of the various possibilities is not attempted here. It is merely remarked that the following proof applies without modification when all the competing modes have identical singularities (e.g. in the Prandtl indentation problem); that is the *differences* between the respective strain rates, stress rates and velocities of any pair of modes are finite everywhere or at least such that the following integrals exist. With these restrictions the virtual work principle may be applied in the form

$$\int (\dot{\boldsymbol{F}}_2 - \dot{\boldsymbol{F}}_1)\,(\boldsymbol{v}_2 - \boldsymbol{v}_1)\,dS = \int (\dot{\boldsymbol{\sigma}}_2 - \dot{\boldsymbol{\sigma}}_1)\,(\boldsymbol{\epsilon}_2 - \boldsymbol{\epsilon}_1)\,dV$$

where S is the surface of the body and V its interior.

Consider the integrand, I say, in the volume integral, remembering that the existing stress is unique (and known in principle) wherever either $\boldsymbol{\epsilon}_1$ or $\boldsymbol{\epsilon}_2$ is nonzero. Four regions may be distinguished as requiring separate treatment:

(i) $\boldsymbol{\epsilon}_1 \neq 0, \quad \boldsymbol{\epsilon}_2 \neq 0. \quad I = h^{-1}\{\boldsymbol{n}\,(\dot{\boldsymbol{\sigma}}_2 - \dot{\boldsymbol{\sigma}}_1)\}^2 \geqslant 0$

with equality if and only if $\boldsymbol{\epsilon}_1 = \boldsymbol{\epsilon}_2$.

(ii) $\boldsymbol{\epsilon}_1 \neq 0, \quad \boldsymbol{\epsilon}_2 = 0. \quad I = -h^{-1}\,(\boldsymbol{n}\,\dot{\boldsymbol{\sigma}}_1)\{\boldsymbol{n}\,(\dot{\boldsymbol{\sigma}}_2 - \dot{\boldsymbol{\sigma}}_1)\} > 0$

since $\boldsymbol{n}\,\dot{\boldsymbol{\sigma}}_1 > 0$, $\boldsymbol{n}\,\dot{\boldsymbol{\sigma}}_2 \leqslant 0$ (the existing stress being already at the yield point where $\boldsymbol{\epsilon}_1 \neq 0$).

(iii) $\boldsymbol{\epsilon}_1 = 0, \quad \boldsymbol{\epsilon}_2 \neq 0. \quad I = h^{-1}\,(\boldsymbol{n}\,\dot{\boldsymbol{\sigma}}_2)\{\boldsymbol{n}\,(\dot{\boldsymbol{\sigma}}_2 - \dot{\boldsymbol{\sigma}}_1)\} > 0$

since $\boldsymbol{n}\,\dot{\boldsymbol{\sigma}}_2 > 0$, $\boldsymbol{n}\,\dot{\boldsymbol{\sigma}}_1 \leqslant 0$ (the existing stress being already at the yield point where $\boldsymbol{\epsilon}_2 \neq 0$).

(iv) $\boldsymbol{\epsilon}_1 = 0, \quad \boldsymbol{\epsilon}_2 = 0. \quad I = 0 \quad$ for any $\quad \dot{\boldsymbol{\sigma}}_1,\ \dot{\boldsymbol{\sigma}}_2$.

In view of the boundary conditions on $\dot{\boldsymbol{F}}$ and $\boldsymbol{v}$ the surface integral vanishes. Since contributions (i)–(iv) to the volume integral are positive or zero they must separately vanish. It follows that $\boldsymbol{\epsilon}_1 = \boldsymbol{\epsilon}_2$ in region (i) and that regions (ii) and (iii) cannot exist since their contributions would be definitely positive. In other words, only one mode of deformation is compatible with the boundary conditions for $\dot{\boldsymbol{F}}$. On the other hand, only the combination of stress-rate components involved in $\boldsymbol{n}\,\dot{\boldsymbol{\sigma}}$, and not the components individually, is necessarily unique in the zone of deformation.

However, while the values of $\dot{\boldsymbol{F}}$ on S_v depend on the assigned values of $\dot{\boldsymbol{v}}$ there, the quantity $\int \dot{\boldsymbol{F}}\,\boldsymbol{v}\,dS_v$ is dependent solely on $\boldsymbol{v}$ on S_v and $\boldsymbol{F}, \dot{\boldsymbol{F}}$ on S_F. For, from (2),

$$\int \dot{\boldsymbol{F}}\,\boldsymbol{v}\,dS_v = \int h\,\boldsymbol{\epsilon}^2\,dV - \int \dot{\boldsymbol{F}}\,\boldsymbol{v}\,dS_F$$

and this only involves quantities which are given or do not depend on $\dot{\boldsymbol{v}}$ on S_v. In particular, when S_v consists of areas where the assigned distributions of $\boldsymbol{v}$

†This has been noticed by several writers in the case of a LEVY-MISES solid: see, for instance, PRAGER (1954b). It was known to the author in 1946 (unpublished); the method of proof was later given in relation to the axially-symmetric problem (HILL, 1950, p. 263).

constitute rigid-body translations or rotations, this result can be interpreted in terms of rates of loading. Note that when the actual mode involves a strain-rate singularity of such order that the integrals diverge, the loading rate is momentarily infinite, i.e. the characteristic load-distortion curve has a vertical tangent initially.

3. Extremum Principles

(a) Consider the set of modes compatible with the boundary conditions for $\boldsymbol{v}$ on S_v and with the existing stress $\boldsymbol{\sigma}$. Let $\boldsymbol{\epsilon}^*$ denote any member of this set derivable from a continuous velocity $\boldsymbol{v}^*$. Then, where $\boldsymbol{\epsilon}^* \neq 0$,

$$\boldsymbol{\epsilon}^* = \lambda^* \boldsymbol{n}\,, \qquad \lambda^* > 0. \tag{3}$$

Any such mode will be called *virtual*.

If $\boldsymbol{\epsilon}$ is the actual mode (supposed derivable from a continuous velocity $\boldsymbol{v}$) and $\dot{\boldsymbol{\sigma}}$ is the actual stress-rate compatible with given $\dot{\boldsymbol{F}}$ on S_F,

$$\int \dot{\boldsymbol{F}}\,(\boldsymbol{v}^* - \boldsymbol{v})\,dS_F = \int \dot{\boldsymbol{F}}\,(\boldsymbol{v}^* - \boldsymbol{v})\,dS = \int \dot{\boldsymbol{\sigma}}\,(\boldsymbol{\epsilon}^* - \boldsymbol{\epsilon})\,dV.$$

In evaluating the integrand, I say, in the volume integral we distinguish four regions as before:

(i) $\boldsymbol{\epsilon} \neq 0$, $\boldsymbol{\epsilon}^* \neq 0$. $I = \lambda^*\,(\boldsymbol{n}\,\dot{\boldsymbol{\sigma}}) - h\boldsymbol{\epsilon}^2 = h\boldsymbol{\epsilon}\,(\boldsymbol{\epsilon}^* - \boldsymbol{\epsilon}) \leqslant \frac{1}{2}h\,(\boldsymbol{\epsilon}^{*2} - \boldsymbol{\epsilon}^2)$

with equality if and only if $\boldsymbol{\epsilon}^* = \boldsymbol{\epsilon}$.

(ii) $\boldsymbol{\epsilon} \neq 0$, $\boldsymbol{\epsilon}^* = 0$. $I = -h\boldsymbol{\epsilon}^2 < \frac{1}{2}h\,(\boldsymbol{\epsilon}^{*2} - \boldsymbol{\epsilon}^2)$.

(iii) $\boldsymbol{\epsilon} = 0$, $\boldsymbol{\epsilon}^* \neq 0$. $I = \lambda^*\,(\boldsymbol{n}\,\dot{\boldsymbol{\sigma}}) \leqslant 0 < \frac{1}{2}h\,(\boldsymbol{\epsilon}^{*2} - \boldsymbol{\epsilon}^2)$

since $\lambda^* > 0$ and $\boldsymbol{n}\,\dot{\boldsymbol{\sigma}} \leqslant 0$ (the existing stress being at the yield point).

(iv) $\boldsymbol{\epsilon} = 0$, $\boldsymbol{\epsilon}^* = 0$. $I = 0 = \frac{1}{2}h\,(\boldsymbol{\epsilon}^{*2} - \boldsymbol{\epsilon}^2)$.

Hence
$$\int \dot{\boldsymbol{F}}\,(\boldsymbol{v}^* - \boldsymbol{v})\,dS_F \leqslant \tfrac{1}{2}\int h\,(\boldsymbol{\epsilon}^{*2} - \boldsymbol{\epsilon}^2)\,dV$$

or

$$\int h\,\boldsymbol{\epsilon}^{*2}\,dV - 2\int \dot{\boldsymbol{F}}\,\boldsymbol{v}^*\,dS_F \geqslant \int \dot{\boldsymbol{F}}\,\boldsymbol{v}\,dS_v - \int \dot{\boldsymbol{F}}\,\boldsymbol{v}\,dS_F \tag{4}$$

with equality if and only if $\boldsymbol{\epsilon}^*$ is the actual mode.

If $S_F = 0$, or if $\dot{\boldsymbol{F}} = 0$ on S_F, this reduces to

$$\int h\,\boldsymbol{\epsilon}^{*2}\,dV \geqslant \int \dot{\boldsymbol{F}}\,\boldsymbol{v}\,dS. \tag{5}$$

If $S_v = 0$, or if $\boldsymbol{v} = 0$ on S_v, there is a disposable *positive* factor in $\boldsymbol{v}$. For any selected virtual mode we choose this factor so that the left-hand side of (4) is as small as possible. This leads to

$$\int \dot{\boldsymbol{F}}\,\boldsymbol{v}\,dS \geqslant \left(\int \dot{\boldsymbol{F}}\,\boldsymbol{v}^*\,dS\right)^2 \Big/ \int h\,\boldsymbol{\epsilon}^{*2}\,dV \quad \text{provided} \quad \int \dot{\boldsymbol{F}}\,\boldsymbol{v}^*\,dS > 0. \tag{6}$$

If the distribution $\dot{\boldsymbol{F}}$ produces further flow in the actual mode, then

$$\int \dot{\boldsymbol{F}}\,\boldsymbol{v}\,dS > 0 \tag{7}$$

since

$$\int \dot{\boldsymbol{F}}\,\boldsymbol{v}\,dS = \int \dot{\boldsymbol{\sigma}}\,\boldsymbol{\epsilon}\,dV \qquad \text{and} \qquad \dot{\boldsymbol{\sigma}}\,\boldsymbol{\epsilon} = h\,\boldsymbol{\epsilon}^2 > 0$$

where $\boldsymbol{\epsilon} \neq 0$, by (2). In this case, there is certainly at least one virtual mode satisfying the requirement in (6). There may also be virtual modes such that $\int \dot{\boldsymbol{F}}\,\boldsymbol{v}^*\,dS \leqslant 0$ and these merely lead to (7) (zero being the best possible choice of the factor). If, now, $\dot{\boldsymbol{F}}$ produces no further flow, then $\boldsymbol{v} \equiv 0$ and the integral in (7) vanishes. In this case

$$\int \dot{\boldsymbol{F}}\,\boldsymbol{v}^*\,dS \leqslant 0 \tag{8}$$

for *all* virtual modes, since $\dot{\boldsymbol{\sigma}}\,\boldsymbol{\epsilon}^* = \lambda^*\,(\boldsymbol{n}\,\dot{\boldsymbol{\sigma}})$ wherever $\boldsymbol{\epsilon}^* \neq 0$ and this is negative since $\lambda^* > 0$ and $\boldsymbol{n}\,\dot{\boldsymbol{\sigma}} \leqslant 0$ where $\boldsymbol{\epsilon}^* \neq 0$. Equation (8) may be regarded as the necessary and sufficient condition that flow ceases.

(b) Let $\dot{\boldsymbol{\sigma}}^*$ be an equilibrium distribution of stress-rate such that $\dot{\boldsymbol{F}}^* = \dot{\boldsymbol{F}}$ on $S_{\boldsymbol{F}}$. Then, by virtual work,

$$\int (\dot{\boldsymbol{F}}^* - \dot{\boldsymbol{F}})\,\boldsymbol{v}\,dS_{\boldsymbol{v}} = \int (\dot{\boldsymbol{F}}^* - \dot{\boldsymbol{F}})\,\boldsymbol{v}\,dS = \int (\dot{\boldsymbol{\sigma}}^* - \dot{\boldsymbol{\sigma}})\,\boldsymbol{\epsilon}\,dV.$$

The integrand in the volume integral vanishes where $\boldsymbol{\epsilon} = 0$ while where $\boldsymbol{\epsilon} \neq 0$ it equals

$$h^{-1}\,(\boldsymbol{n}\,\dot{\boldsymbol{\sigma}})\,\{\boldsymbol{n}\,(\dot{\boldsymbol{\sigma}}^* - \dot{\boldsymbol{\sigma}})\} \leqslant \tfrac{1}{2}\,h^{-1}\,\{(\boldsymbol{n}\,\dot{\boldsymbol{\sigma}}^*)^2 - (\boldsymbol{n}\,\dot{\boldsymbol{\sigma}})^2\}.$$

The equality holds when $\boldsymbol{n}\,(\dot{\boldsymbol{\sigma}}^* - \dot{\boldsymbol{\sigma}}) = 0$; note that this could be achieved with $\dot{\boldsymbol{\sigma}}^* \neq \dot{\boldsymbol{\sigma}}$. Then

$$2\int \dot{\boldsymbol{F}}^*\,\boldsymbol{v}\,dS_{\boldsymbol{v}} - \int h^{-1}\,(\boldsymbol{n}\,\dot{\boldsymbol{\sigma}}^*)^2\,dV \leqslant \int \dot{\boldsymbol{F}}\,\boldsymbol{v}\,dS_{\boldsymbol{v}} - \int \dot{\boldsymbol{F}}\,\boldsymbol{v}\,dS_{\boldsymbol{F}}. \tag{9}$$

The equality is obtained with any *actual* $\dot{\boldsymbol{\sigma}}^*$ distribution associated with the actual mode (i.e. corresponding to different $\dot{\boldsymbol{v}}$ on $S_{\boldsymbol{v}}$). Strictly, the volume integral in (9) need extend only over the zone $\boldsymbol{\epsilon} \neq 0$, but in practice this would usually not be known in advance. The integral would then have to be taken over the whole deformable zone defined by $\boldsymbol{v}$ on $S_{\boldsymbol{v}}$ and $\boldsymbol{F}$ on $S_{\boldsymbol{F}}$; this would tend to weaken the inequality.

If $S_{\boldsymbol{F}} = 0$, or if $\dot{\boldsymbol{F}} = 0$ on $S_{\boldsymbol{F}}$, there is a disposable factor of arbitrary sign in $\dot{\boldsymbol{\sigma}}^*$. With the best choice of this, the inequality is improved to

$$\int \dot{\boldsymbol{F}}\,\boldsymbol{v}\,dS \geqslant \left(\int \dot{\boldsymbol{F}}^*\,\boldsymbol{v}\,dS\right)^2 \Big/ \int h^{-1}\,(\boldsymbol{n}\,\dot{\boldsymbol{\sigma}}^*)^2\,dV. \tag{10}$$

All imposed surface velocities necessarily produce further flow (with the trivial exception of rigid-body motions, for which both sides of (10) vanish). If $S_{\boldsymbol{v}} = 0$, or if $\boldsymbol{v} = 0$ on $S_{\boldsymbol{v}}$,

$$\int h^{-1}\,(\boldsymbol{n}\,\dot{\boldsymbol{\sigma}}^*)^2\,dV \geqslant \int \dot{\boldsymbol{F}}\,\boldsymbol{v}\,dS. \tag{11}$$

By combining (4) and (9) a continued inequality is obtained which can be used to approximate the quantity $\int \dot{\boldsymbol{F}}\,\boldsymbol{v}\,dS_v - \int \dot{\boldsymbol{F}}\,\boldsymbol{v}\,dS_F$ from above and below; as proved in Section 2 this quantity is independent of $\dot{\boldsymbol{v}}$. Similar remarks apply to (5) and (10), and to (6) and (11).

4. Nonhardening Solid

Suppose that the nonhardening solid is introduced with a view to approximating, or being in context with, a work-hardening solid having a certain h-distribution at the moment under consideration. In order to characterize the appropriate solution for the nonhardening solid by a limiting process, substitute μh for h in (1), where μ is a constant which is to be made vanishingly small. We recall that the set of virtual modes depends only on the existing hardness distribution and that a definite member of this set corresponds to each μ. A unique sequence of actual modes is thereby obtainable for decreasing values of μ, and if the sequence approaches a limit this is taken to be the appropriate mode for the non-hardening solid; it is of course dependent on the specified h distribution.

When $\boldsymbol{v} \neq 0$ on S_v and $\dot{\boldsymbol{F}} \neq 0$ on S_F it is clear – for example from the extremum property (4) – that the sequence of modes depends on μ in a way that cannot be foreseen, and requires detailed calculation before the existence of a limit can be examined. When $S_F = 0$ or $\dot{\boldsymbol{F}} = 0$ on S_F the procedure is much simplified since the actual velocity and strain rate are then independent of μ; $\boldsymbol{n}\,\dot{\boldsymbol{\sigma}}$ is proportional to μ in the zone of deformation but not necessarily the individual components of stress rate. Only one member of the sequence need be considered since the actual mode is the same for all. It can be found from the field equations or through the property of minimizing $\int h\,\boldsymbol{\epsilon}^{*2}\,dV$ in the set of virtual modes; in particular, if h is uniform, $\int \boldsymbol{\epsilon}^{*2}\,dV$ is minimized.

Special consideration is required by the case $S_v = 0$ or $\boldsymbol{v} = 0$ on S_v. In a nonhardening solid the prescribed $\dot{\boldsymbol{F}}$ must be such that $\int \dot{\boldsymbol{F}}\,\boldsymbol{v}^*\,dS \leqslant 0$ for *all* virtual modes since $\boldsymbol{n}\,\boldsymbol{\sigma} \leqslant 0$ wherever $\boldsymbol{\epsilon}^*$ is non-zero. On the other hand, from (8), flow is only possible in a work-hardening solid when the prescribed $\dot{\boldsymbol{F}}$ are such that $\int \dot{\boldsymbol{F}}\,\boldsymbol{v}\,dS > 0$. One might therefore take the view that the nonhardening solid must be considered to stay rigid under any permissible $\dot{\boldsymbol{F}}$, since no flow would be possible in a material that could harden, however slightly. But this view would prevent the nonhardening solid being put to any use when $\dot{\boldsymbol{F}}$ is such that $\int \dot{\boldsymbol{F}}\,\boldsymbol{v}^*\,dS > 0$ for one or more virtual modes. Instead, the following procedure is suggested. A sequence of solutions for decreasing $\mu \leqslant 1$ is defined such that traction rates $\mu\dot{\boldsymbol{F}}$ are applied to the solid with hardening rate μh. Then the actual velocity and strain-rate are independent of μ, while $\boldsymbol{n}\,\dot{\boldsymbol{\sigma}}$ in the deformation zone is proportional to μ (and also $\dot{\boldsymbol{\sigma}}$ itself when $S_v = 0$). All members of the sequence have the same mode, which may therefore be adopted as appropriate for the

nonhardening solid. According to (6) the mode has the property of maximizing

$$\left(\int \dot{F}\, v^*\, dS\right)^2 \Big/ \int h\, \epsilon^{*2}\, dV$$

among those virtual modes for which $\int \dot{F}\, v^*\, dS > 0$.

5. Discontinuities of Velocity*

In a work-hardening material a velocity discontinuity can occur at a single instant only (or at a discrete number of instants in a process of distortion consisting of distinct phases). For otherwise the discontinuity would persist and either remains stationary relative to the material or travel through it. The first alternative is tantamount to fracture, and solutions of the field equations with this feature are purely formal and must be rejected ; the second alternative violates equilibrium since it implies discontinuities in strain, hardness, and traction on the discontinuity surface. Thus, the discontinuity immediately begins to diffuse so that the velocity is continuous during a succeeding interval of time.

Not only is a discontinuity in velocity momentary but (as is well known) it is only possible at all in special circumstances. Take, for illustration, an incompressible solid : the state of stress at every point of the surface of discontinuity must be that corresponding to a simple strain-rate parallel to the tangent plane and in the direction of the discontinuity in tangential velocity. In a general 3-dimensional state of distortion, internal surfaces having this property are probably uncommon and mainly restricted to the interfaces between plastic and rigid regions.

The situation is otherwise in special states where the distortion is pure shear at all points of the body (for example, torsion and plane strain). The field equations are hyperbolic and every characteristic surface is potentially a surface of discontinuity of velocity and strain rate.

We now inquire whether the actual mode in a workhardening solid does in fact ever involve a velocity discontinuity. The answer is in the affirmative : examples are known, and many more could be constructed, where there is *only one* virtual mode and this mode involves a discontinuity. However, this case poses no problem of selection.

There remains the situation where, at a certain instant, the set of virtual modes contains discontinuous, in addition to continuous, velocity fields. The uniqueness theorem of Section 2 shows only that one continuous mode at most can be actual. The question whether there could be two (or more) physically-possible modes, one continuous and one (or more) discontinuous, is left for further study.

References

Bishop, J. F. W., Green, A. P. and Hill, R. 1956 *J. Mech. Phys. Solids.* **4**, 256.

*We consider here only discontinuities that are possible in a genuinely 3-dimensional state of stress and are not due simply to approximations, as in generalized plane stress or plate theory ; these call for separate treatment.

HILL, R.	1950	*Mathematical Theory of Plasticity* (Clarendon Press).
	1951	*Phil. Mag.*, **42**, 868.
	1956	Mechanics of Quasi-static Plastic Deformation in Metals : article in *Surveys in Mechanics*, G. I. Taylor 70th Anniversary Volume (Cambridge University Press).
PRAGER, W.	1954a	*Rev. Fac. Sci. Univ. Instanbul*, **19**, 28.
	b	2nd U.S. Nat. Cong. Appl. Mech., Ann Arbor.

Note added in proof :—

All theorems proved here remain true if the yield surface contains areas which are plane (i.e. have the same normal $\boldsymbol{n}$ at every point), provided that h has the same value at every point of each such area. In this case it is $\boldsymbol{n}$, and not necessarily $\boldsymbol{\sigma}$, that is uniquely determined in the deformable zone for given $\boldsymbol{F}$ on S_F and $\boldsymbol{v}$ on S_v. In a material element whose associated $\boldsymbol{n}$ is normal to one of the plane areas on the yield surface, the existing stress can correspond to any point of the area.

Journal of the Mechanics and Physics of Solids, 1956, Vol. 4, pp. 256 to 258. Pergamon Press Ltd., London.

A NOTE ON THE DEFORMABLE REGION IN A RIGID-PLASTIC BODY

By J. F. W. Bishop*, A. P. Green† and R. Hill‡

(*Received 20th April*, 1956)

Summary

It is established that the deformable region in a rigid-plastic body yielding under given boundary conditions can be determined from an examination of one complete solution. Particular methods are suggested for determining this region, and are illustrated by a consideration of indentation under conditions of plane strain, plane stress, and axial symmetry.

1. Introduction

The following considerations relate to an ideal work-hardening rigid-plastic material whose yield function and plastic potential are identical. Consider a body of such material under given stress and velocity boundary conditions such that part of it is yielding plastically. A so-called complete solution to such a problem consists of an equilibrium stress distribution satisfying the stress boundary conditions and nowhere violating the yield criterion, together with one or more modes of deformation satisfying the velocity boundary conditions and compatible with the stress distribution. A theorem due to Hill (1951) proves that in a region of deformation the stress is uniquely defined; no statement, however, is made about possible deformation modes except that they must be compatible with the stress. In certain classes of problem this theorem enables the yield-point *loads* to be determined uniquely if a complete solution can be constructed. However, without further consideration, it cannot be said whether the known deformation mode or modes form the complete set satisfying the velocity boundary conditions, or indeed whether they cover the region containing the complete set.

In this note we consider only the problem of isolating the domain which is occupied by the complete set of modes; this domain will be called the *deformable region*. If there is more than one mode, the isolation of the domain is only the first step towards selecting the mode that will actually operate, a problem outside the scope of this note.

A theorem and corollary established in the following Section provide the general basis for determining the deformable region.

2. Basis

Theorem. A deformation mode associated with the stress field in one complete solution is compatible with the stress field in any other complete solution.

* Mechanical Engineering Research Laboratory, East Kilbride.
† Tube Investments Research Laboratories, Hinxton Hall, Cambridge.
‡ Department of Mathematics, Nottingham University.

Corollary. Any region of the stress field in a known complete solution which is shown to be necessarily rigid for *that* field (i.e. by arguments based solely on the geometrical and other properties of that field) must be rigid in all complete solutions.

The truth of the theorem follows from the uniqueness property mentioned above. For where deformation can occur in *any* mode, the state of stress is unique, i.e. identical in all complete solutions. To establish the corollary, suppose that the region shown to be necessarily rigid in the known solution were not so in another solution. By the theorem, the corresponding deformation mode would be compatible with the stress field in the known solution. Since, however, this region is shown to be necessarily rigid the supposition that it could deform in another solution must be erroneous.

It follows from the theorem and the corollary that the complete set of modes associated with the totality of complete solutions is associable with each solution. Thus, in determining the deformable region, it is necessary to consider *only one complete solution.*

3. Methods

In general a complete solution includes (i) a plastic region in which the strain-rate in some mode is everywhere non-zero; (ii) a region stressed to the yield point and into which no mode is known to extend; (iii) a region stressed below the yield point.

The non-plastic region (iii) is necessarily rigid in the known solution and hence by the corollary it must be rigid in all possible complete solutions. It remains to deal with the plastic region (ii) in which no modes are known. Normally this is bordered by a non-plastic region. The following method is applicable to such a situation when the velocity equations are hyperbolic with distinct characteristics. Consider for definiteness the situation in plane strain where the characteristics are the slip-lines of the stress field in a region stressed to the yield point. Suppose that this is bordered by a non-plastic region along a curve AB which is not a characteristic. Let AC and BC be the concurrent slip-lines in the plastic region terminating in A and B. Then the velocity boundary conditions on AB uniquely determine the velocity in ACB. But the velocity must be continuous across AB and so a consistent velocity field is the rigid motion of ACB. This is the unique field in ACB, which is therefore necessarily rigid.

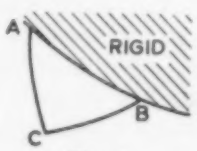

Fig. 1.

A different situation may arise in problems of axial symmetry. Here, elimination of the velocities and the scalar constant from the stress/strain-rate relations leads to a differential equation of compatibility involving only the stresses. The restriction imposed by this equation on the stresses may be sufficient to establish the necessary rigidity of a region.

4. Examples

Consider the indentation by a smooth flat die of a semi-infinite slab under plane strain conditions. Prandtl (1923) and Hill (1947) have proposed partial solutions

involving different modes, while a complete solution corresponding to both has been given by Bishop (1958). One half of the complete solution is shown in Fig. 2.

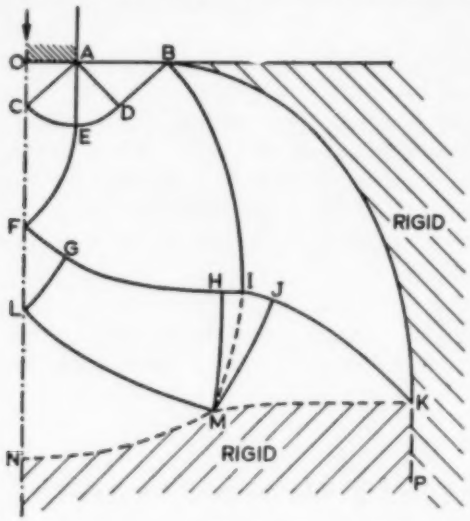

Fig. 2.

The material to the right of BK is unstressed and the material lying below the stress discontinuity NMK is stressed below the yield point (except along the line KP). Modes of deformation are known covering the region $OABDC$.

From the corollary it follows that the material lying outside $BKMN$ is rigid. The remaining material in $CDBKMN$ is readily shown to be rigid, bearing in mind that velocity discontinuities cannot occur across the stress discontinuity IM. The proof consists of applying the method described in Section 3 successively to the regions KMJ, BKI, MJI, MIH, MLN, $MLGH$, LGF, $BIFE$ and EFC. Hence the Prandtl field $OABDC$ covers the whole deformable region. Analogous results can be proved for the corresponding problem in plane stress for which a complete solution has been given by Hill (1952) and Bishop (1953), and also for indentation by a smooth flat cylindrical die, starting with the complete solution due to Shield (1955) which is based on a Tresca yield criterion and plastic potential.

Acknowledgments

We are indebted to the Director of the Mechanical Engineering Research Laboratory and to Tube Investments Ltd. for permission to publish.

References

Bishop, J. F. W.	1953	*J. Mech. Phys. Solids* **2**, 43.
Hill, R.	1947	*J. Iron and Steel Inst.*, **156**, 513.
	1951	*Phil. Mag.*, **42**, 868.
	1952	*J. Mech. Phys. Solids* **1**, 19.
Prandtl, L.	1923	*Z. ang. Math. Mech.*, **3**, 401.
Shield, R. T.	1955	*Proc. Roy. Soc.* A, **233**, 267.

Journal of the Mechanics and Physics of Solids, 1956, Vol. 4, pp. 259 to 268. Pergamon Press Ltd., London.

THE PLASTIC YIELDING OF SHALLOW NOTCHED BARS DUE TO BENDING

By A. P. Green
Tube Investments Research Laboratories, Hinxton Hall, Cambridge

(*Received 30th April*, 1956)

Summary

Previous plane strain solutions for the bending of deeply notched bars (Green 1953; Green and Hundy 1956) are modified for bars in which the notch is shallow, so that plastic deformation extends to the notched face. The critical minimum depth of notch for which the solution for a deep notch is still valid is calculated for (a) pure bending of a bar with a 60° V notch and (b) the Izod test.

1. Introduction

Slip-line field solutions * have been proposed for the initial yielding of a deeply notched bar of rigid-plastic material bent under conditions of plane strain, either by pure couples (Green 1953), or by a combination of bending moment and shear force (Green and Hundy 1956). The strain was assumed to be zero in the direction parallel to the length of the notch. If the notch is sufficiently deep, as was assumed in these solutions, initial deformation does not extend to the surface of the bar on either side of the notch. The shape of the slip-line field then depends only on the shape of the root of the notch (or notches) and the loading conditions; it is independent of the ratio b/a of the depth of the notch b to the thickness a of the bar at its minimum section.

The theory is extended in the present paper to shallow notches. Modifications of the slip-line fields are suggested which involve the extension of deformation to the surface of the bar on one or both sides of the notch. The minimum value of b/a for which the solution for a deep notch is valid is calculated in particular cases. The theory is supported by previously published experimental work (Hundy 1954); (Green and Hundy 1956).

2. Form of the Slip-line Field

Let us first consider the problem of the bending by pure couples of a parallel-sided bar with a single V-shaped notch on one side, since this clearly exemplifies the two main types of slip-line field (Fig. 1) which have been constructed for bars with deep notches. The shape of the slip-line field in the immediate vicinity of any stress-free surface is determined uniquely by the shape of this surface.

*For an account of the theory of plane plastic strain see R. Hill, *The Mathematical Theory of Plasticity*, 1950, Ch.VI (Clarendon Press); the standard notation used there is used in this paper.

When the total notch angle $2\beta > 114{\cdot}6°$, the part of the field determined by the surface of the notch is connected to the part determined by the opposite flat surface at the singular point N (Fig. 1a), across which there is a discontinuity in the hydrostatic pressure component of stress. When however $2\beta < 114{\cdot}6°$, the connection between the two parts is made by a pair of circular slip lines PQ (Fig. 1b).

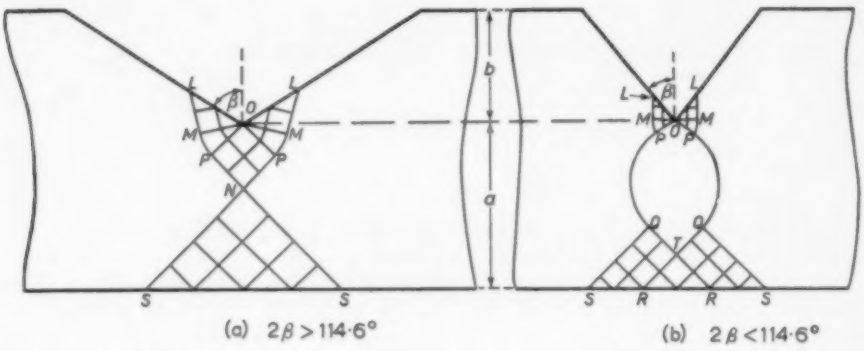

Fig. 1. Slip-line fields for pure bending of a bar with a deep V notch.

The modification of these fields for shallow notches was first indicated by certain experiments of HUNDY (1954), in which the regions of plastic deformation were revealed by an etching technique in bars of mild steel with shallow 60° notches, bent under four-point loading. The patterns obtained (Fig. 2) correspond with remarkable clarity to the kind of slip-line field shown in Fig. 3a. This is a modification of the field in Fig. 1b, and involves deformation of the surface GK on each side of the notch. It is envisaged that deformation extends over the whole field, and that, taking the central rigid " pivot " $OPQTQPO$ to be stationary, the rigid ends of the bar rotate about this pivot in opposite directions with angular velocity ω_1, say, while each rigid part $WGHEULW$ rotates in the same direction as the end of the bar to which it is adjacent, with angular velocity ω_2, say, where $\omega_2 < \omega_1$. To fix ideas it will be assumed that the bar is bent to open the notch.

Before discussing other possible modifications it will first be shown that, assuming this form, the dimensions of the slip-line field are uniquely determined by the shape of the bar and by stress and velocity considerations. Since the problem is symmetrical about OT, only the right hand half of the slip-line field in Fig. 3a will be discussed.

In the regions LOP, QRS and GIK, the field is determined by the shape of the stress-free surface to which it is adjacent. Hence, LM, OM, GI, KI, RQ and SQ are all straight lines inclined to their respective surfaces at 45°, while the region OMP consists of concentric circular arcs and their radii. The size of these regions depends on the following four unknowns, $LM = d_1$, $GI = d_2$, $QR = d_3$, and $\angle\, MOP = \theta$. Furthermore, by HENCKY's first theorem on the geometrical property of slip-line fields (HILL 1950a, p. 136), the slip-line segments connecting the pair of slip lines UF and MD are all straight and have the same length, and

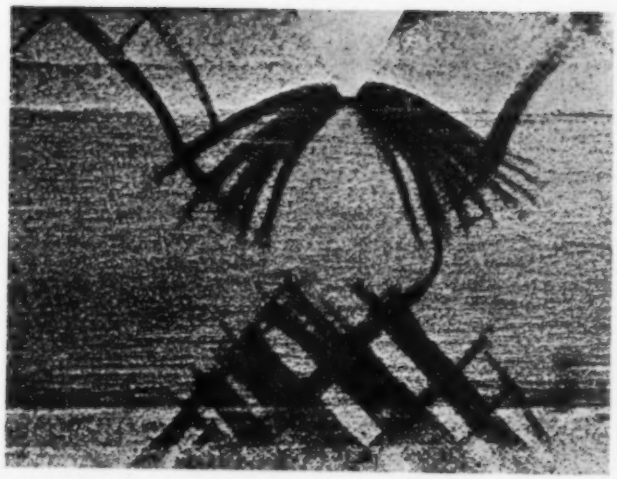

(a)

$b/a = 0{\cdot}24$

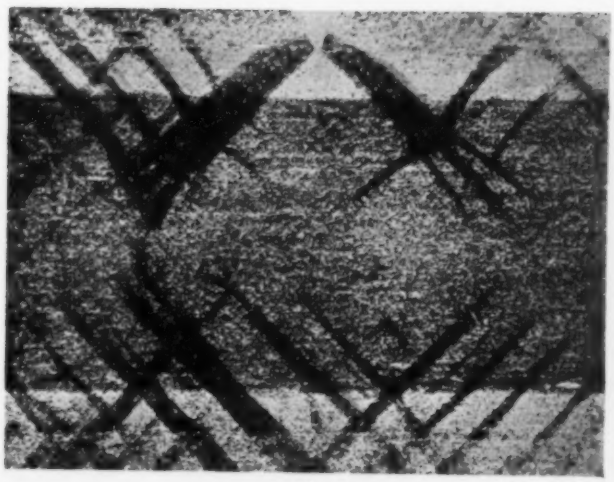

(b)

$b/a = 0{\cdot}1$

Fig. 2. Deformation patterns for pure bending of bars with shallow V notches.

so likewise are the segments connecting AH and BI. The lengths of these segments, $UM = d_4$ and $AB = d_5$, are two additional unknowns.

Turning for the moment to velocity conditions, since the rigid end of the bar rotates relative to the central pivot by sliding over BQ, this must be a circular arc, the radius and angular span of which will be denoted by R_1 and λ_1 respectively. There is a velocity discontinuity across the slip lines $OPABQTR$ which for positive

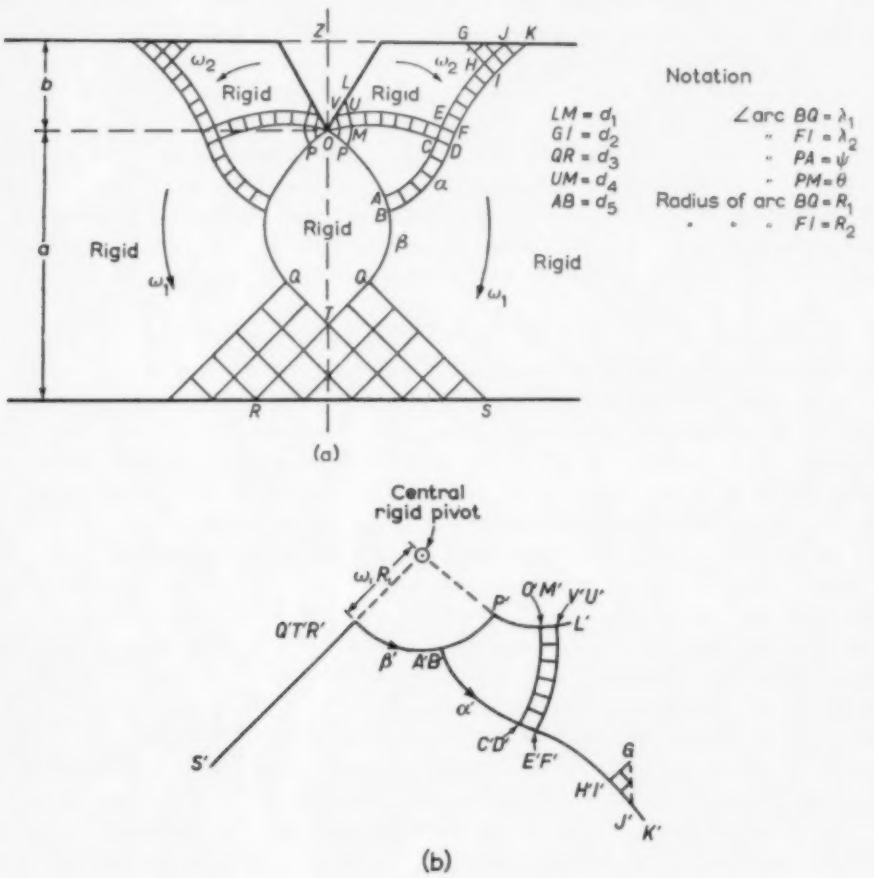

Fig. 3. Pure bending of a bar with a shallow V notch.
(a) Form of the slip-line field.
(b) Hodograph.

plastic work must be a β line. This determines which slip lines are α and which β lines throughout the field, as indicated in Fig. 3a. Further consideration of velocity conditions is facilitated by the construction of a hodograph for the velocity distribution (Green 1954, Prager 1953). The hodograph for the right-hand half of the bar is shown in Fig. 3b. Points and lines in the hodograph are indicated by the same notation as their counterparts in the slip-line field with an addition of a dash after the symbols. The main properties of the hodograph are :

(i) A line element in the hodograph is perpendicular to its corresponding line

element in the slip-line field. Thus, angular variations are identical in the two figures.

(ii) A nonrotating rigid region is plotted as a point in the hodograph. Thus, the origin of the hodograph represents the stationary central pivot. Furthermore, taking $\omega_1 = 1$, the constant-velocity discontinuity R_1 across the slip line $PABQT$ leads to the line $P'(A'B')(Q'T')$ in the hodograph being a circular arc of radius R_1.

(iii) The boundaries of a rotating rigid region in the slip-line field are represented by geometrically similar boundaries in the hodograph, the ratio of the dimensions of the latter to the former being the angular speed of rotation. Hence, with $\omega_1 = 1$, the boundaries $S'Q'B'D'F'I'K'$ and $SQBDFIK$ are identical, while the boundary $L'U'E'H'G'$ is similar to $LUEHG$ and ω_2 times its size.

One immediate deduction from (iii) is that the slip lines EH and FI must be circular arcs. For, owing to the coincidence of A' and B' in the hodograph, the lines $E'H'$ and $F'I'$ also coincide, and this single line is, from (iii), geometrically similar to both EH and FI. Hence these two lines are similar to each other, which is only possible if they are both circular arcs. It also follows that

$$\omega_2 (R_2 + d_5) = \omega_1 R_1 \tag{1}$$

R_2 being the radius of curvature, and λ_2 the angular span of the arc FI.

The shape of the region $PUFB$ is governed in a more complex way by velocity conditions, or by what is the same thing, the necessary geometrical similarities between slip-line field and hodograph. Again taking $\omega_1 = 1$, we find the radius of the arc $P'A'$ is then R_1 as already noted in (ii). Let us suppose for the moment that d_1, d_4, d_5, R_1, ω_2, θ, and the angular span of the slip line PA, denoted by ψ, are known. Then, by the geometrical properties of the slip-line field, the sliplines UE and BF are determined by PM and PA. PM is a circular arc of radius d_1, but the shape of PA is as yet unspecified. Knowing ω_1 and ω_2, and using (iii), we observe that UE and BF determine the corresponding lines $U'E'$ and $B'F'$ in the hodograph. The latter in turn determine $P'A'$ and $P'U'$. Thus, there is a one-to-one relationship between PA and $P'A'$ which, since $P'A'$ is known to be a circular arc of radius R_1, determines the shape of PA. In other words, by taking into account all necessary velocity conditions, the region $PUFB$ has been shown to be determined by the unknowns, d_1, d_4, d_5, R_1, ω_2/ω_1, θ and ψ.

The determination of the whole slip-line field is now reduced to finding the values of the 12 unknowns, d_1, d_2, d_3, d_4, d_5, R_1, R_2, λ_1, λ_2, θ, ψ, and ω_2/ω_1. For this purpose there exist equation (1) and the following additional 11 independent conditions, which uniquely determine the unknowns :

Geometrical considerations

Given values of a and b. (2) and (3).

Angular variations along the slip lines

$$LMPQR, \quad \beta + \theta + \lambda_1 + \psi = \pi; \tag{4}$$

and $$JEV, \quad \beta + \lambda_2 + \psi = \pi/2. \tag{5}$$

Hencky stress relations along the slip lines

$$LMPQR, \qquad \lambda_1 + \psi - \theta = 1 \tag{6}$$

and $$JEV, \qquad \psi = \lambda_2 \tag{7}$$

Stress equilibrium equations

Zero resultant tensile and shear forces across the minimum section of the bar. (8) and (9)

Three equations of equilibrium for the rigid region $WGHEULW$. (10), (11) and (12)

There are several changes which can be made in the slip-line field of Fig. 3a which still result in uniquely determined fields. These are :

(a) $d_4 = 0$. We must then envisage that the slip-line boundary of the rigid region adjacent to the notch lies somewhere within $OMCD$, and the variable d_4 is then replaced by the angle, γ say, which this slip line boundary makes with PO at O.

(b) In addition to the above, it may happen that for very small notch angles $d_1 = 0$ (it is known already that $d_1 = 0$ for deep notches when $\beta < 3{\cdot}2°$). The Hencky stress relation (6) along $LMPQR$ is then not valid, and there remain 11 equations and unknowns.

(c) $R_1 = 0$. We must then envisage the possibility of a stress discontinuity at the point B, now coinciding with Q. The field can be considered as a modification of that for deep notches shown in Fig. 1a, having two singular points B instead of the one central one N. Again the Hencky stress relation (6) along $LMPQR$ is not valid, and there remain 11 equations and unknowns. By analogy with the solution shown in Fig. 1a, this situation is likely to arise with obtuse notches. It also seems likely to occur for very shallow notches whatever the notch angle, since this would provide a continuous transition to the slip-line field for an unnotched bar as the notch is made progressively shallower, whereas from a slip-line field of the kind shown in Fig. 3a there is no such continuous transition.

No attempt has been made to calculate any of the slip-line fields described for shallow notches except in the special case when the notch is of the critical depth at which the transition to the solution for a deep notch takes place. This is discussed in the following section. Clearly, similar types of slip-line fields can be constructed for bars of different shape with different shapes of notch, and or/for bars subjected to different loading systems, e.g. the Izod test in which the resultant forces across the minimum section are a combination of shear force and bending moment. For the latter the slip-line field (Green and Hundy, 1956) is not, of course, symmetrical, but lies mainly on the same side of the notch as the line of action of the applied shear load (Fig. 5).

8. Critical Notch Depth

It could be argued that the critical notch depth corresponds to the limiting form, as b/a is increased, of the slip-line fields proposed in the previous section for shallow notches. For example, considering the slip-line fields shown in Fig. 3a,

it is to be expected that, as b is increased, keeping a constant, the length of AB ($= d_s$) will decrease, eventually becoming zero so that $ACEHJ$ coincides with $BDFIK$. The dashed part of the resulting slip-line field (Fig. 4) to the right of $LUMPB$ is then, with $\omega_1 = 1$, identical to the hodograph, which implies that it is rigid. Thus the solution reduces to that for a deep notch shown in Fig. 1b, with PQ a continuous circular arc. However, since the set of slip-line fields corresponding to increasing values of b/a has not been calculated, it still remains to prove that the limiting field shown in Fig. 4 does in fact correspond to the critical notch depth. The following proof makes use of the uniqueness and limit theorems for a rigid-plastic body (HILL 1951). The only assumption made is that there is a complete solution associated with the limiting field, i.e. that there exists an associated equilibrium stress distribution in the rigid regions which nowhere violates the yield criterion.

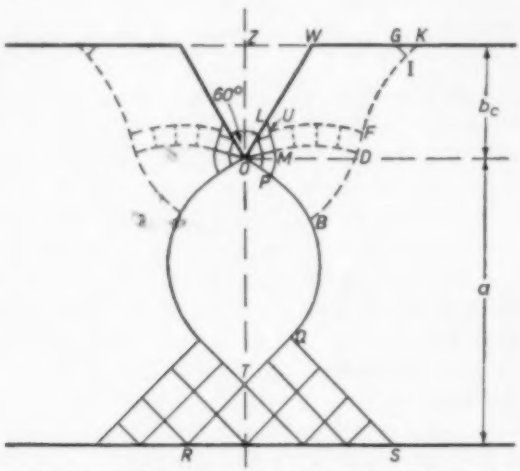

Fig. 4. Limiting slip-line field corresponding to the critical depth of notch ($2\beta = 60°$).

It is convenient to regard a as fixed, and to vary b/a by adding or substracting uniform layers of material on the notched surface of the bar. Let M be the yield-point bending moment per unit width of bar, and M_d be its value for deep notches. The critical notch depth b_c is defined as the minimum depth for which $M = M_d$ and below which M falls below M_d. Since the removal of material cannot cause an increase in M, M must be less than M_d for *all* $b < b_c$. It follows immediately that for all $b < b_c$ deformation extends to the notched surface of the bar. For, if this were not so, the deformation mode for $b < b_c$ would provide an upper bound to M for the notch depth b_c, so that $M_b \geqslant M_{b_c} = M_d$, which is contrary to the definition of b_c.

The depth of notch corresponding to the slip-line field shown in Fig. 4 is denoted by b_0. As was remarked above, deformation does not extend to the notched surface. If, however, we imagine that the part of the bar to the left of the slip-line $OPBQR$ were removed but the forces exerted by this part on the remainder of the bar remain unchanged, then deformation could extend to the notched surface.

For, with the rigid pivot removed, a velocity discontinuity is permissible across the slip-line *KIFDB*, and a mode exists extending over the regions *OLUFBO*, *FI* and *GIK*. It follows that the stress is unique in these regions, even though in the complete bar they constitute part of the rigid zone. If, now, b_0 is reduced by an infinitesimal amount, a " shaving " is removed from this mode along *GK*. Hence, the reduced body cannot withstand the same surface forces over *OB*, since the internal rate of work in the remainder of the mode is now *less* than the rate of work done by these surface forces, which is contrary to one of the limit theorems.

Thus, considering again the complete bar, the slip-line field for a deep notch leads to a violation of the yield criterion in some parts of the rigid region if $b < b_0$, and would only be valid if the material was sufficiently harder in those parts. Hence M_b must be less than M_d if $b < b_0$. For, if M_b was equal to M_d, it would follow from the uniqueness of the stress distribution in the deforming regions of the appropriately hardened bar that the stress field of any solution valid for the unhardened bar was identical to that given by the slip-line field for a deep notch in the deforming region covered by the latter. But this is contrary to what has been proved, since it implies that a stress field which does not violate the yield criterion anywhere in the unhardened bar can be associated with the slip-line field for a deep notch. Finally, since $M_b < M_d$ and, if the assumption that the solution shown in Fig. 4 can be completed is correct, $M_{b_0} = M_d$, it follows that b_0 is the critical notch depth b_c (if the assumption is not correct $M_{b_0} < M_d$ and $b_0 < b_c$, though this seems most unlikely).

The limiting slip-line field is readily calculated, starting with the known solution for the deep notch. The five parameters describing the extension of the slip-line field to the surface at *GK* are d_2, d_4, R_2, λ_2, and ψ. To determine these there are the three equations of equilibrium for the rigid region *WGIFULW*, and equations (5) and (7), which give λ_2 and ψ immediately.

Calculations have been made for a bar with a 60° V notch bent by pure couples. The slip-line field in the region *PBDM* was calculated numerically, using $(\bar{x}, \bar{y})$ co-ordinates and a 5° equiangular network (Hill 1950a, p. 143). Resultant forces were numerically integrated over the boundaries of the rigid regions in terms of the unknown lengths d_2, d_4, and R_2. The results were $\beta = \lambda_2 = \psi = 30°$, $d_2/a = 0{\cdot}042$, $d_4/a = 0{\cdot}077$, $R_2/a = 0{\cdot}59$. It was deduced that $b_c/a = 0{\cdot}39$ and $ZK/a = 0{\cdot}59$, ZK being the perpendicular distance from K to the axis of symmetry. This numerical calculation of the limiting field was somewhat lengthy and was only practicable because all the angles in the slip-line field could be readily calculated without recourse to the conditions of overall equilibrium, and the problem was thus reduced to finding the three unknown lengths. However, this method is not possible when $d_1 = d_4 = 0$, (as in the modification (b) suggested in the previous section), for then the angle γ appears as an unknown in place of d_4. This situation occurs in the slip-line field for the Izod test (Fig. 5), in which a square bar with a 45° V notch on one face is firmly clamped at one end up to its minimum cross-section, and is loaded as a cantilever by a concentrated force applied to the notched face towards the other end.

An alternative method was used, therefore, which avoided exact calculation of the limiting slip-line field. The accuracy of this method was first checked against

the above numerical calculation and was then applied to the Izod test. The method is based on the construction of a fully plastic stress field of the kind suggested by BISHOP (1958), which has stress-free boundaries lying inside the actual body. Considering again the problem of the bar with a sharp V notch bent by pure couples, the slip-line field for the deep notch was uniquely extended, with a stress-free surface LK as shown in Fig. 6. This surface was continued on from OL until it became parallel to the flat surface of the bar at K. The resulting field was, of course, different from that shown in Fig. 4. The construction was carried out

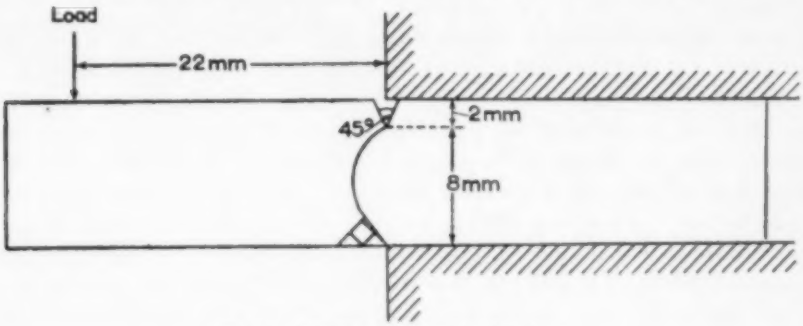

Fig. 5. Slip-line field for the Izod test.

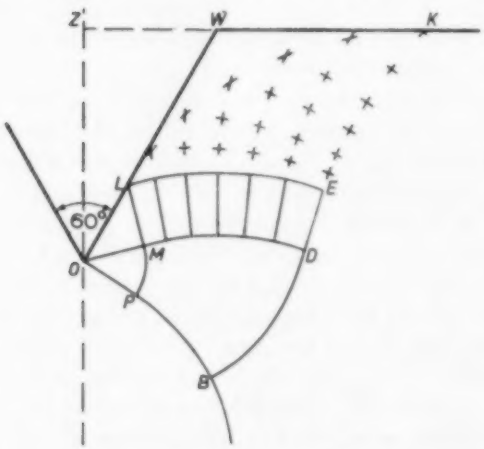

Fig. 6. Stress field giving a close estimate of the critical notch depth ($2\beta = 60°$).

graphically, using a 5° equiangular network, and substituting a straight line having the mean slopes at the mesh points for each segment between two adjacent mesh points. This is much more rapid than numerical calculation, and remarkably accurate if done on a large scale.

The critical notch depth was taken to be ZO in Fig. 6, where Z is the foot of the perpendicular from K on to the axis of symmetry. The resulting estimates of b_c/a and of ZK/a were exactly the same as those already calculated by the first method. This coincidence must be regarded as somewhat fortuitous since it will now be shown that the method may be expected to overestimate b_c/a at

least by a small amount*. It seems reasonable to suppose that the stress field shown in Fig. 6 could be extended over the whole bar without violating the yield criterion. If so, $M = M_d$ and $b \geqslant b_c$, and the same would be true for a bar with the stress-free regions LWK removed. But the removal of these regions from a bar for which $b = b_c$ would involve cutting off a part of the region GIK of the slip-line field shown in Fig. 4, thus lowering M. Hence b must be greater than b_c, though clearly it need not be much greater.

A similar stress field was constructed for the Izod test, starting with the previously calculated slip-line field shown in Fig. 5. The results were $b_c/a = 0{\cdot}22$, and $ZK/a = 0{\cdot}46$. For a standard Izod test piece $b/a = 0{\cdot}25$, and therefore yielding would not be expected to extend to the notched face until some deformation has occurred.

4. Remarks

The solution for a bar with a notch of critical depth (Fig. 4) shows an interesting feature not hitherto exemplified. It contains a region where deformation does not occur but where the stress is uniquely determined by the given boundary conditions. Such a region can only be demonstrated in a particular problem by imagining the removal of the velocity constraints, but not the forces, transmitted across the boundary of some rigid region (in the present problem, the central rigid " pivot "), thereby permitting an extension of the deforming region. Thus in a rigid-plastic body yielding plastically, the region over which the stress distribution is unique may be larger than the total region covered by deformation modes.

Furthermore, the original yield-point loads can no longer be supported if any part of the uniquely stressed region is weakened or removed, whether or not it is covered by a deformation mode in the unweakened body. In proving this it has been shown that, if a tentative solution for a rigid-plastic body yielding under given boundary conditions is complete except for the construction of an associated equilibrium stress distribution in the rigid regions, and if in fact *no* such stress distribution can be constructed without violating the yield criterion, then the yield-point load † will *definitely* be overestimated. If, however, as Hill (1951) has remarked, an associated equilibrium stress distribution is constructed in the rigid regions which does locally exceed the yield condition in certain parts, all that can be said is that the solution is valid for a body sufficiently harder in those parts, and that the yield-point load for the body under consideration *tends* to be overestimated.

Acknowledgment

The author would like to thank the Chairman of Tube Investments Ltd. for permission to publish this paper.

References

Bishop, J. F. W. 1953 *J. Mech. Phys. Solids*, **2**, 43.

*c.f. the estimates of the critical dimensions of a bar indented by a smooth flat die. Hill's (1950b) slip-line field gives a slightly lower estimate of the critical width of bar than Bishop's (1953) stress field.

†More strictly, the minimum work principle as stated by Hill (1951, equation 6) will be a definite inequality.

GREEN, A. P.	1953	*Q. J. Mech. Appl. Maths.*, **6**, 223.
	1954	*J. Mech. Phys. Solids*, **2**, 73.
GREEN, A. P. and HUNDY, B. B.	1956	*J. Mech. Phys. Solids*, **4**, 128.
HILL, R.	1950a	*The Mathematical Theory of Plasticity* (Clarendon Press).
	1950b	*Phil Mag.*, **41**, 745.
	1951	*Phil. Mag.*, **42**, 868.
HUNDY, B. B.	1954	*Metallurgia*, **49**, 109.
PRAGER, W.	1953	*Trans. Royal Inst. Tech. Stockholm*, No. 65.

Journal of the Mechanics and Physics of Solids, 1956, Vol. 4, pp. 269 to 282. Pergamon Press Ltd., London.

EXPERIMENTS IN PLANE-STRAIN EXTRUSION

By W. Johnson
Department of Engineering, University of Manchester

(*Received 27th May*, 1956)

Summary

The results of experiments in the plane-strain extrusion of lead and aluminium with dies of semiangle 30°, 45°, 60°, 75° and 90° at various reductions are presented, and a comparison of the experimental values with those predicted by the use of slip-line field methods is made. Conclusions are drawn about the nature of the process and the predictive value of the theory.

1. Introduction

A great amount of experimental work on the hot and cold extrusion of metals has been performed since the pioneer work of Siebel and Fangmeier (1931), but the process still cannot be said to be well understood. Attention has usually been focused on the relationship between reduction and extrusion pressure for certain boundary conditions and these have generally been related in a simple empirical fashion which was not always illuminating. In particular, to obtain such relationships homogeneous straining was generally assumed though this was well known to be far from the truth.

Hill (1948) considered the plane-strain extrusion of an ideal rigid perfectly plastic material and was able to account for both inhomogeneous deformation of the extruded material and approximately for the order of pressure encountered.

The aim of the experiments described and reported below was, primarily, to compare the predictions of extrusion pressure for a given reduction as given by the theory of slip-line fields, with that obtained under experimental conditions. It was felt that if confidence in the predictive value of the theory could be established, and provided its limitations were appreciated, a better understanding of the much more common industrial process of axisymmetric extrusion would be obtained.

The only plane-strain extrusion hitherto carried out with metals is that by Purchase and Tupper (1953) who extruded lead through 90° dies of various reductions, r. The procedure they adopted was to determine, experimentally, the extrusion pressure p for each value of r. Then, assuming a reasonable value of k, where k is the yield shear stress of the material in plane strain, they showed that their results conformed well with those predicted by Hill for extrusion through a square die when the container walls are perfectly smooth and the face of the die supports a region of dead metal.

The procedure followed in the present work was different. The value of k is derived experimentally from a true stress-logarithmic strain curve, p is measured experimentally, and the quantity $p/2k$ then deduced. This magnitude is then

compared with that derived for certain theoretical conditions. The results of these experiments lead to results and conclusions different from those of PURCHASE and TUPPER. They stated that there was a " remarkable consistency between theory and experiment . . . ," which appears to imply among other things that they believed they had attained states of frictionless extrusion. However, nearly all workers dealing with metal-forming operations usually assume or deduce, that with lubricated work, the coefficient of friction μ is seldom less than 0·08. Even in a comparable working operation when drawing wire under conditions of hydrodynamic lubrication, WISTREICH (1955) found (experimentally) μ to be 0·02 to 0·03. As has been indicated (JOHNSON 1955a) values of μ between 0·08 to 0·15 (though dependent on the reduction attained) are often quite sufficient to cause shearing friction in extrusion processes.

In respect of flow-pattern studies, PURCHASE and TUPPER confirmed that the dead-metal zones for lubricated extrusion at small reductions, are in section, nearly isosceles triangles, as the theory assumes. The existence and shape of the dead-metal zones at high reductions are approximately confirmed by their photographs.

GREEN (1955) has investigated the modes of deformation in the plane-strain extrusion of plasticine, in the use of both symmetrically and unsymmetrically situated dies. He has shown quite convincingly in his photographs that the assumed shapes of the dead-metal zones at high reduction are in close agreement with those required theoretically.

2. EXPERIMENTAL WORK

(i) *Apparatus and Tools.* A drawing of the plane-strain extrusion apparatus which was made in mild steel, is shown in Fig. 1. It was designed to extrude rectangular specimens 1·9 in. wide and 1 in. thick through wedge-shaped dies of various semiangles. The extrusion container proper consists of four segments

TABLE 1

Die angle in degrees, α	*Reduction* r	*Die angle in degrees*, α	*Reduction* r	*Die angle in degrees*, α	*Reduction* r
20	0·300	60	0·500	90	0·500
			0·635		0·667
30	0·414		0·667		0·800
	0·500				0·882
	0·667	75	0·500		0·920
			0·659		0·950
45	0·500		0·667		0·960
	0·584				
	0·667				

tapered on the outside and joined by light steel dowels, pressed into an outer container; an interference fit of 0·0075 in. was thought sufficient to prevent any infiltration of metal between the segments during the course of an extrusion. A land was ground on the bottom of the container and the top of the dies to prevent infiltration of the metal between die and container wall.

The dies were a light drive fit finally located by a die plate which was fastened to the outer container with cup-head screws. In all about twenty sets of dies were used, their form being as shown in Fig. 2 and the reductions for the various semiangles α being given in Table 1.

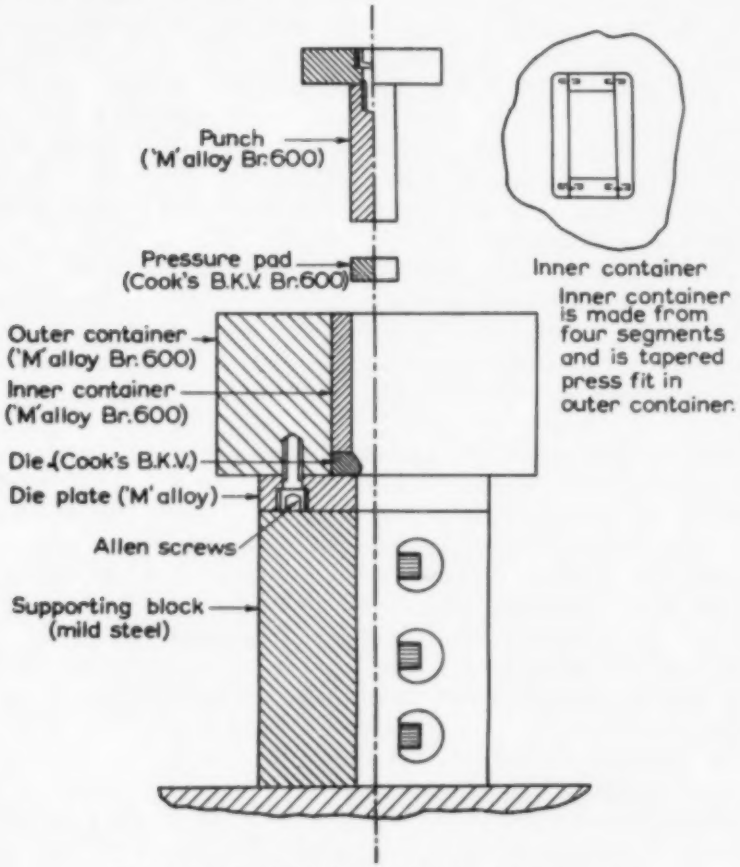

Fig. 1. Details of the plane-strain extrusion apparatus.

Fig. 2. Form of wedge-shaped die.

The pressure pad was a hardened mild-steel block, 0·5 in. thick × 1·9 in. × 1·0 in., carrying a land round its leading edges for the purpose of securing adequate protection against " flashing," or the movement of metal between the pad and the container wall.

(ii) *Compression Tests.* These tests were performed on the materials extruded. two specimens of each being compressed to a logarithmic strain of more than 3, The tests were carried out at the same speed as that of the extrusion, i.e. 0·1 in. per min. The compression platens were of hardened metal lapped and polished to a surface roughness of 2 to 3 microinches and their hardness was Vickers Pyramid Number 649. The strain measurement was made using two dial gauges placed on stands on either side of the specimen.

The specimens used were originally of 1 in. diameter and 1·5 in. long, this length being short enough to avoid tilting of the specimens during compression. Grooves were turned in the ends of the specimens to facilitate retention of the lubricant; 60 grooves, 0·01 in. deep spaced at 30 to the inch diameter were used following the practice of LOIZOU and SIMS (1953). The grooving had negligible effect on the length during compression.

The procedure in a test was first to lubricate the ends of the specimen well, carefully ensuring that the lubricant had been forced well down into the grooves; the lubricant used was graphite in tallow. A load of about 100 lb. was applied to the specimen when it had been centred on the platens to align the specimen and squeeze out superfluous lubricant. The load was then taken off and the dial gauges set.

Simultaneous readings of load and both dial gauges were recorded after each 0·025 in. travel of the crosshead. The first stage of compression continued until the specimen height was reduced to 0·75 in. and its diameter increased to 1·25 in. The specimen was then turned down to 0·80 in. diameter and compressed to a height of 0·35 in. Again it was turned down, this time to 0·563 in. diameter. The final height of the compressed specimen was 0·075 in. It was not found necessary to turn fresh grooves after each stage of the compression.

(iii) *Materials Extruded.* The materials used were (a) pure lead, (b) 0·065% tellurium lead, (c) super-pure aluminium, (d) 99·5%-pure aluminium, 99·7%-pure aluminium.

(iv) *Specimens.* These consisted of two blocks, 0·95 in. × 1·0 in. × 1·1 in. which when inserted side by side just fitted the container. The use of two such blocks allowed the inner face of one of them to be stamped with a square grid for the purpose of studying the subsequent pattern of metal flow.

All the lead specimens were hammered to refine the grain size.

(v) *Test Procedure.* Before commencing a test the specimen container, die and pressure pad face, were cleansed with carbon tetrachloride. The lubricant used (if any) was always graphite and tallow, and the loads were recorded every 0·05 in. of punch travel for a distance of about 1 in.

3. EXPERIMENTAL RESULTS

(i) *Stress-Strain Curves.* True stress (σ), log-strain (ϵ), curves as calculated from the compression tests for all materials are shown in Fig. 3; the individual points obtained were too numerous to mark and the smooth curves through them were almost identical for the two tests made on each material. The curves for both aluminiums were found to be identical. Comparison of these curves with those obtained for the same materials by CHANG (1950), is, as far as his extend, good.

(ii) *Autographic Diagrams.* This diagram is a record of the variation of punch load with punch travel and from it the " true " extrusion pressure is ultimately deduced. Nearly all the autographic diagrams obtained have been given elsewhere (JOHNSON and COLLINS, 1954 and JOHNSON 1955b and c), and only selected

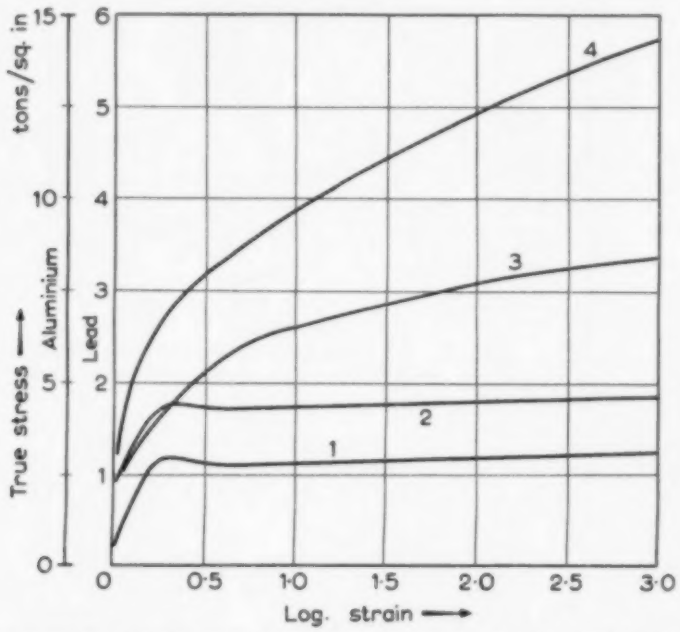

Fig. 3. True stress-logarithmic strain curves for (1) Pure Lead, (2) 0·065% Tellurium Lead, (3) Super-pure Aluminium; (4) 99·7% Pure Aluminium.

ones are presented in Fig. 4. Repeat tests performed on lubricated and unlubricated specimens in respect of pressures generally agreed to better than 3% for the former and about 6% for the latter.

(iii) *Flow Patterns.* Many flow pattern tests were carried out but in metals these are difficult to interpret precisely.

4. Interpretation of Experimental Data

(i) *Autographic Diagrams.* Fig. 4 (b) represents a typical autographic diagram. When experimental readings are being noted as the extrusion load decreases with punch travel, a time when the rate of decrease is greatly accelerated is observed; this is quite discernable in practice with a sensitive testing machine. These readings when plotted, however, are usually on such a small scale that their significance tends to be overlooked. If a test is stopped immediately or very soon after this point of accelerated load decrease is observed (i.e. at the points marked in Fig. 4 b) and the slug examined, it is very clear that piping or coring is commencing; a gap between the material and the pressure pad is opening up over a short distance on either side of the slug axis. Extrusion proper has thus ceased

and there is no longer pressure over the whole of the pressure pad. The process at this point becomes one of nonsteady motion and as such is thereafter not comparable with the theory; the slip-line field region associated with steady motion has been invaded. It is the load applied at this instant, minus an amount due

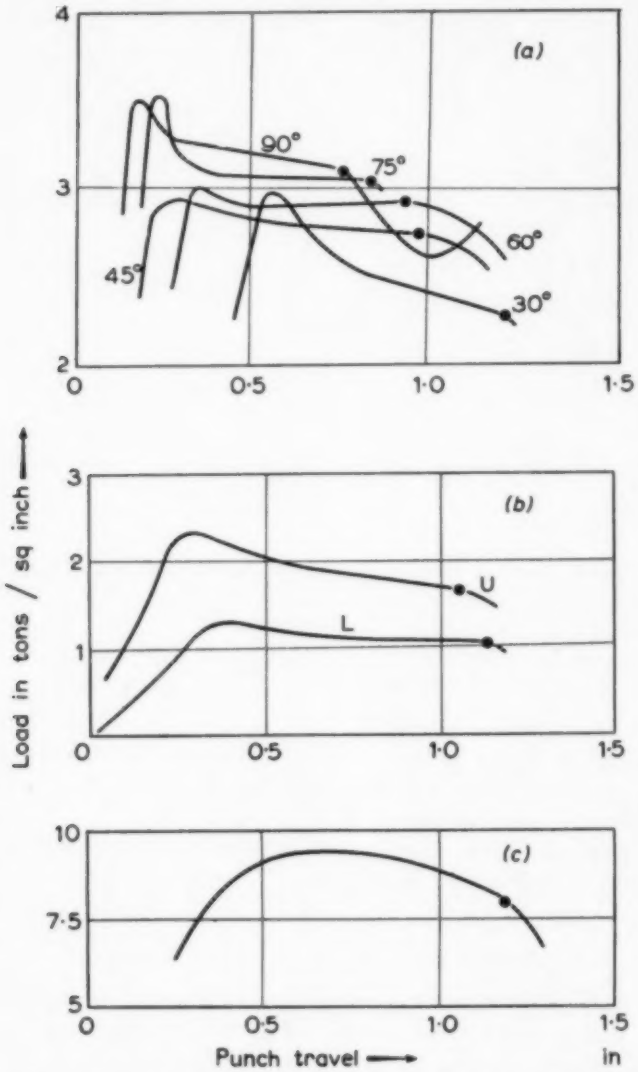

Fig. 4. Autographic diagrams for the extrusion of (a) Lubricated Pure Lead : $r = 0{\cdot}50$, (b) Pure Lead : $r = 0{\cdot}30$ and $\alpha = 20°$, U – Unlubricated, L – Lubricated, (c) Lubricated Super-pure Aluminium, $r = 0{\cdot}30$ and $\alpha = 20°$.

to friction between the rigid material and the container wall, that must be used to determine the true extrusion pressure. When there is slip over the die face this net load can be obtained graphically by extrapolating the portion of the line

of steady load decrease before the coring to intersect the point of entry to the die. When a dead-metal zone is present, its extent is generally indefinite and the load at the end of steady-state extrusion has then to be accepted for the sake of consistency.

This experimentally observed feature is of great importance since it points to the physical existence of two qualitatively different forms of flow. Specimens may be subjected either to a steady- or an unsteady-state extrusion depending on their current length. It may be remarked that the same feature is observable in axisymmetric or rod extrusion. The load at which steady-state extrusion is considered to cease and the one used for comparison with theoretical values is clearly indicated in the autographic diagrams reproduced in Fig. 4. It will be observed that while it is comparatively easy to discern the onset of the unsteady state with lead, it is a matter of some uncertainty with a material that has a high strain-hardening rate such as aluminium.

(ii) *The Yield Shear Stress k.* To obtain the experimental value of $p/2k$ it is necessary, besides determining the pressure p, to find a value of k. The value of k is assumed constant in theory but when strain-hardening materials are treated it is essential to make a consistent and rational allowance for this fact. This was done following in principle the method described by HILL (1950), by determining a mean value of $2k$ from the stress-strain curves. A strain of at least $\ln\{1/(1-r)\}$ must be acquired by the extruded product since this is the strain required if the change of shape is achieved homogeneously. The mean strain actually imparted is larger than this, but it is not known *a priori*. From the theoretical curves available, this mean strain for a given r is seen to be $p/2k$ and accordingly $2k$ may be easily obtained by deriving the mean true stress $k\sqrt{3}$ over the range of logarithmic strain 0 to $(2/\sqrt{3})\cdot(p/2k)$ from the true stress – logarithmic strain curves of Fig. 3. It is assumed that a Mises yield criterion obtains and that the form of the strain-hardening characteristic of the material does not seriously affect the true strain imparted.

In the experiments in lubricated extrusion the mean strain is obtained by reference to the curves for frictionless extrusion and since some degree of friction is obviously present, this must in fact be underestimated. Similarly, in the unlubricated experiments the mean strain is assumed to be given by the shearing friction theoretical curves and the probability then is that this is overestimated.

In deducing the value of the extrusion load it may be noted that dead metal zones are nearly always associated with the 90° and 75° dies and slip over the die face for 30° dies. It is not always clear which mode of extrusion prevails for dies of intermediate semiangle and it was necessary to carry out many experiments to determine which mode applied for each particular reduction. It is against this background of knowledge about the manner of deformation that the final results have been interpreted.

5. Comparison of Experimental and Theoretical Results

The theoretical values of $p/2k$ for particular values of r, α and degree of friction as required for comparison with this experimental work have been calculated and presented in earlier papers (JOHNSON 1955a and 1956).

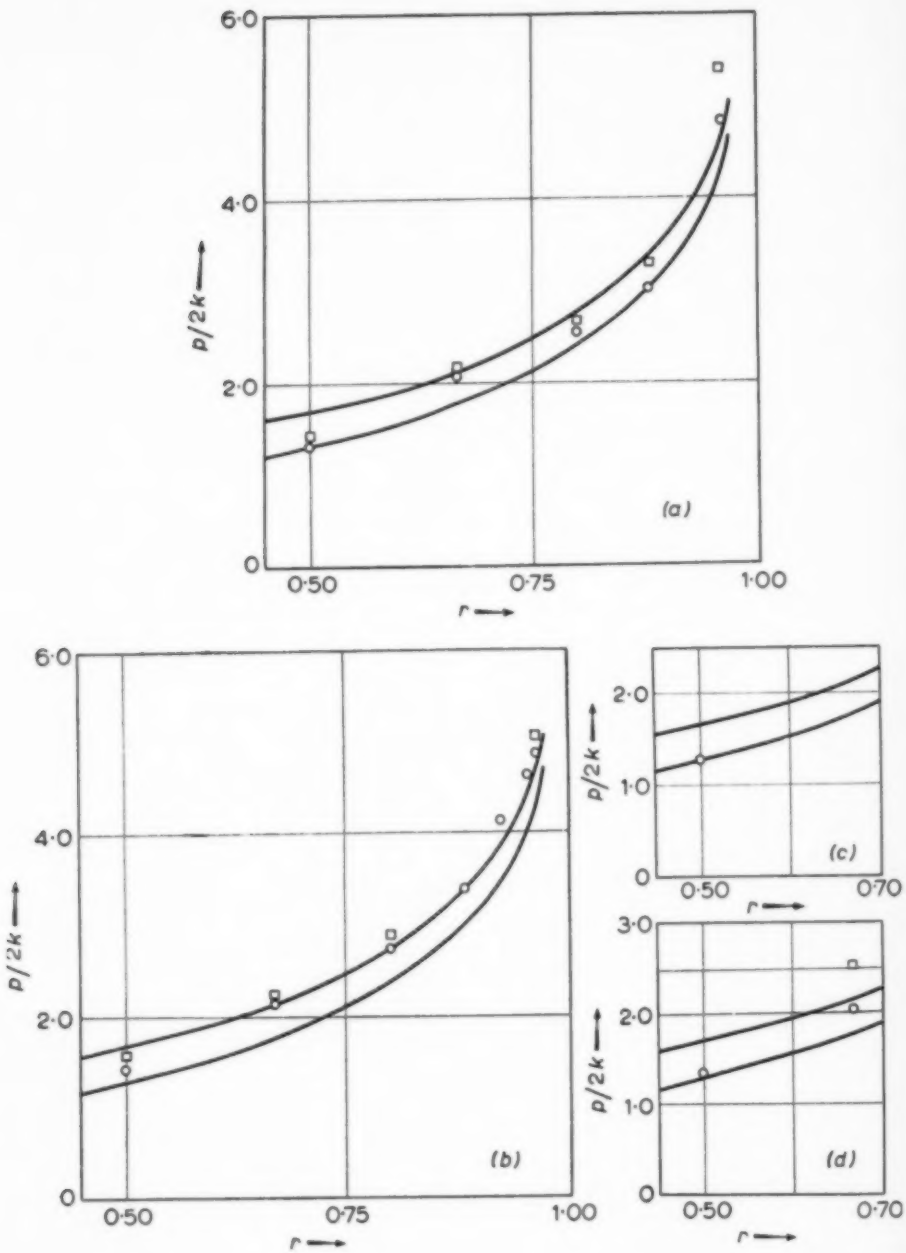

Fig. 5. Comparison of theoretical and experimental results for $\alpha = 90°$. Upper curve refers to a perfectly rough container wall and lower curve to a smooth container wall with a dead metal zone on the die face. ○ Experimental point for lubricated extrusion ; ⊡ Experimental point for unlubricated extrusion. (a) Pure Lead ; (b) Tellurium Lead ; (c) 99·7% Pure Aluminium ; (d) Super-pure Aluminium.

In practice the square die is most frequently used and those of small semiangle, i.e. 20° and 30°, the least; dies of intermediate angle are commonly used but no particular angle merits special attention.

Square die, $\alpha = 90°$

In Fig. 5 the results of the experimental values of $p/2k$ for the various values of r for all materials are compared with the two theoretical curves which assume a dead-metal zone over the whole die face or, at very high reductions with that associated with shearing along the lower edge of the die, when the container wall is smooth or perfectly rough.

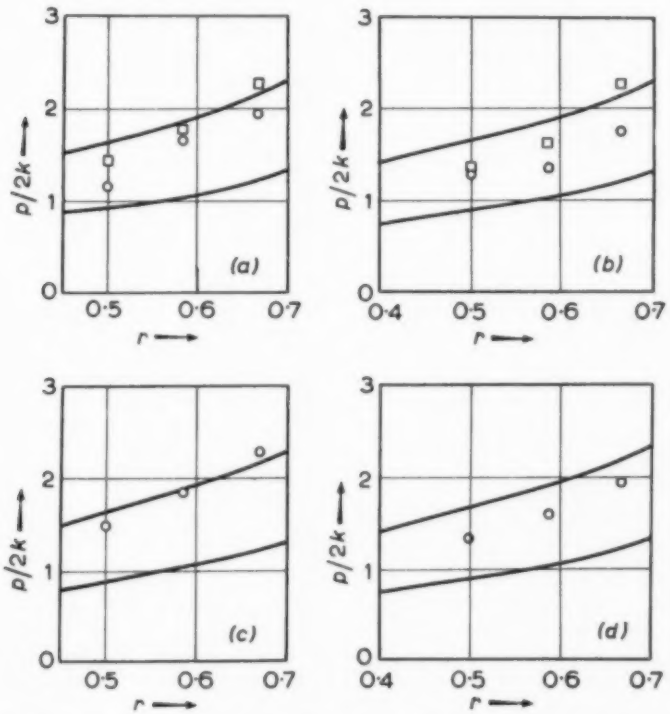

Fig. 6. Comparison of theoretical and experimental results for $\alpha = 45°$. Upper curve refers to a perfectly rough container wall and shearing along the die face. Lower curve refers to slip along a smooth die face. ○ Experimental points for lubricated extrusion; ⊡ Experimental points for unlubricated extrusion. (a) Pure Lead; (b) Tellurium Lead; (c) Super-pure Aluminium (d) 99·7% Pure Aluminium.

There is reasonable agreement except at high reductions where the pressure is consistently underestimated. Much of this was attributed to "flashing" – the movement of metal past the pressure pad or its lodgement between pad and container wall. The few results obtained with lubricated aluminium are surprisingly good.

$\alpha = 45°$, $60°$ and $75°$

The results of experiments at these angle dies are given in Figs. 6, 7 and 8, in which the lower curve is for frictionless extrusion and the upper curve the worst conditions, viz. rough container wall and a rough die face supporting a small dead metal zone. Almost all the results are bounded by these curves, the tendency for them being to approach the upper curve at the higher reductions

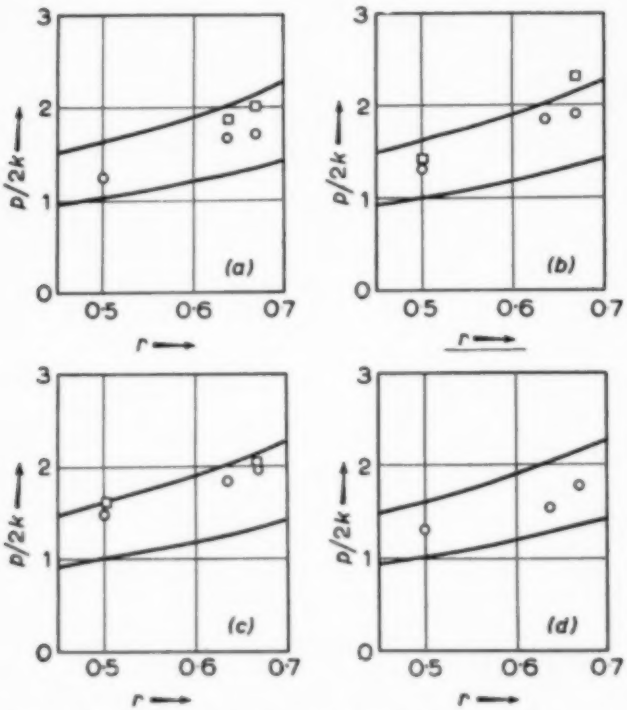

Fig. 7. Comparison of theoretical and experimental results for $\alpha = 60°$. Upper curve refers to a perfectly rough container wall and shearing along the die face. Lower curve refers to slip along a smooth die face. ○ Experimental points for lubricated extrusion, □ Experimental points for unlubricated extrusion. (a) Pure Lead; (b) Tellurium Lead; (c) Super-pure Aluminium; (d) 99·7% Pure Aluminium.

$\alpha = 20°$ *and* $30°$

The upper theoretical curve in Figs. 9 and 10 was derived on the assumption that the die was perfectly rough or that shearing along the whole of the die face occurred. The lower curve corresponds to frictionless conditions. For both kinds of lead, lubricated extrusions are bounded by these two curves but the indications are that considerable friction is encountered. With unlubricated lead the upper curves tend to underestimate the pressure. The lubricated aluminium extrusions are well summarized by the upper curves but much of this tendency is probably associated with the well rounded nature of the stress-strain curves for the comparatively small strains imposed.

6. Discussion on the Limitations to the Use of the Theory

There is no reason to doubt that the model suggested by the theory is largely correct. Early work on extrusion had need of empirically determined constants to match its experimental and theoretical results. The early theoretical work was thought of entirely by reference to homogeneous deformation and in consequence, without empirical constants, gave pressure predictions which were in

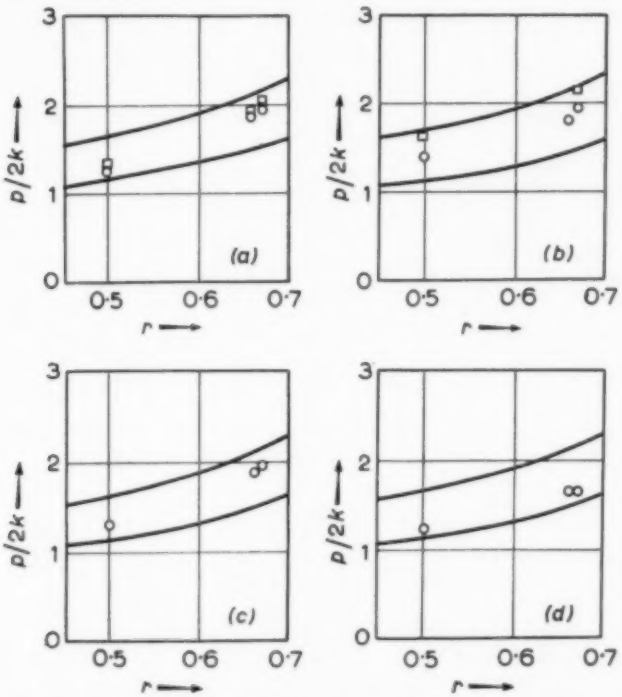

Fig. 8. Comparison of theoretical and experimental results for $\alpha = 75°$. Upper curve refers to a perfectly rough container wall and shearing along the die face. Lower curve refers to slip along a smooth die face. ○ Experimental points for lubricated extrusion ; ⊡ Experiental points for unlubricated extrusion. (a) Pure Lead ; (b) Tellurium Lead ; (c) Super-pure Aluminium ; (d) 99·7 % Pure Aluminium.

error by a very considerable amount ; in particular no attempt was made to predict in detail how a grid would distort. The emergence of slip-line field techniques has removed or very greatly reduced – in the field of plane strain – the magnitude of these failings. Nonetheless it is not amiss to summarize the weaknesses and limitations of the new methods.

(a) Perhaps foremost is the not very satisfactory method of allowing for strain-hardening by means of an averaged strain. However, though the differences in behaviour between the ideal and real industrial materials may appear large enough to appear to discredit the application of this theory to strain-hardening materials, yet very reasonable experimental results are obtained.

(b) Effective lubricated extrusion is very difficult to achieve. This implies that the curves relating to extrusion through smooth dies are something of an ideal,

and not likely to be approached in experiment. These lowest limits, however, demonstrate quite clearly that great savings in power could be made if the lubrication was effective to a high degree.

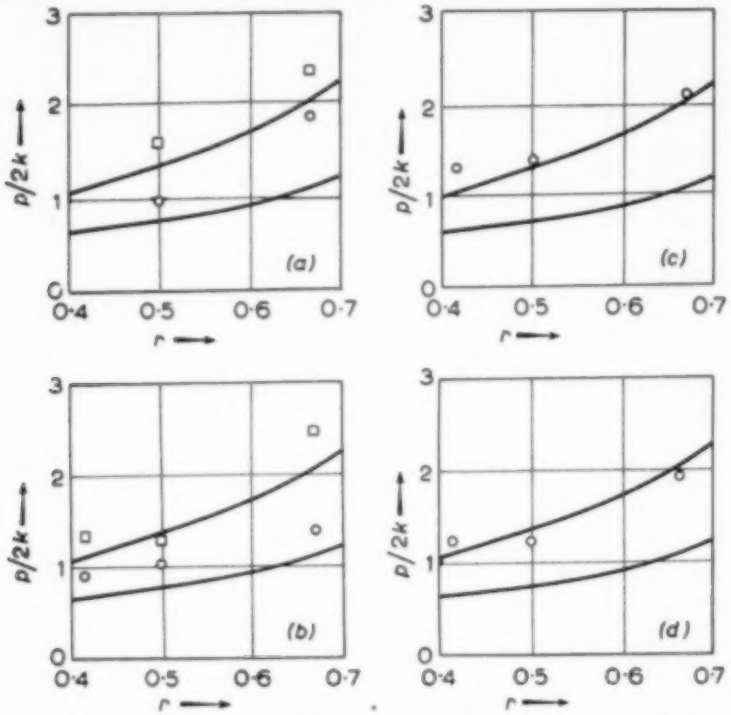

Fig. 9. Comparison of theoretical and experimental results for $\alpha = 30°$. Upper curve refers to shearing along whole die face and lower curve to frictionless conditions. ○ Experimental points for lubricated extrusion ; ⊡ Experimental points for unlubricated extrusion. (a) Pure Lead; (b) Tellurium Lead ; (c) Super-pure Aluminium ; (d) 99·7% Pure Aluminium.

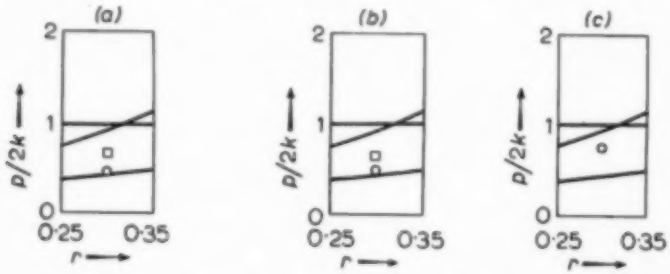

Fig. 10. Comparison of theoretical and experimental results for $\alpha = 20°$. Upper curve refers to shearing along whole die face and lower curve to frictionless conditions. ○ Experimental points for lubricated extrusion ; ⊡ Experimental points for unlubricated extrusion. (a) Pure Lead ; (b) Tellurium Lead ; (c) Super-pure Aluminium.

(c) The theory nowhere takes account of the effect of the proximity of the punch to the slip-line field. It would be useful to know how the condition of a punch face (or pressure pad) affects the metal flow and the extrusion pressure.

(d) A limitation to the use of the theory is set by the experimental difficulties of closely defining the conditions under which an operation is proceeding. Thus far no detailed measurement of the coefficient of friction prevailing in an experiment has been made, and it is very doubtful if this can be made to a high degree of accuracy. The extrusion process is a dynamic one, and involves many and various factors. Extrusion, by comparison with wire-drawing, the nearest comparable process, covers a much larger range of working conditions from small die-angles and small reductions to square dies with very large reductions; wire drawing is concerned only with slip over a die face but extrusion includes this and also requires the consideration of dead metal zones. In one, a container wall is absent and in the other is a source of uncertain effects. In extrusion the contribution to the total load of the pressure pad as it bears on the container wall cannot be evaluated. Wire-drawing experiments require lighter die loads (when other things are the same) and are also capable of being established to give long runs at steady conditions.

(e) Considering the factors given above, the method of deciding where on an autographic diagram one should read off the extrusion pressure or load, is not entirely satisfactory though it is believed that the identification of the coring point on the autographic diagram is a new and worthwhile observation.

7. Conclusions

It is unfortunate that experiments are not repeatable with a high degree of accuracy and this, together with theoretical shortcomings, make it possible only to reach broad conclusions. These are

(1) lubricated extrusions are accompanied by coefficients of friction that are not small;

(2) in the case of lubricated slip over the die face, which occurs for semi-angles of die up to about 60°, pressures can be reasonably well predicted if a high value of μ is assumed;

(3) with large angle or square dies, pressures will be predicted to better than about 15% by the curves associated with the dead metal zone hypotheses with a rough container wall;

(4) the method of allowing for strain-hardening by using an averaged value of the yield stress is quite satisfactory for practical purposes;

(5) distorted grids as predicted by the theory, though not exact, certainly provide very good first approximations;

(6) the term extrusion pressure is only fully meaningful when due regard is paid to the length of the slug extruded.

Acknowledgments

The author wishes to thank Mr. A. G. Collins for his assistance in performing some of the experiments, Professor H. W. Swift for his encouragement, and

B.I.S.R.A. for permission to publish results taken from the original reports (JOHNSON and COLLINS 1954, JOHNSON 1955 b and c).

REFERENCES

CHANG, T. M.	1950	*D.S.I.R., M.E.R.O. Report MF/MS* 41.
GREEN, A. P.	1955	*J. Mech. Phys. Solids*, **3**, 189.
HILL, R.	1948	*J. Iron Steel Inst.*, **158**, 177.
	1950	*Mathematical Theory of Plasticity* (Clarendon Press).
JOHNSON, W.	1955a	*J. Mech. Phys. Solids*, **3**, 218.
	1955b	*B.I.S.R.A. Report MW/B/51/55.*
	1955c	*B.I.S.R.A. Report MW/E/49/55.*
	1956	*J. Mech. Phys. Solids*, **4**, 191.
JOHNSON, W. and and COLLINS, A. G.	1954	*B.I.S.R.A Report MW/E/54/54.*
LOIZOU, N. and SIMS, R. B.	1953	*J. Mech Phys. Solids*, **1**, 234.
PURCHASE, N. W. and TUPPER, S. J.	1953	*J. Mech. Phys. Solids*, **1**, 277.
SIEBEL, E. and FANGMEIER, E.	1931	*Mitt. Kais. Wilh. Eisenf.*, **13**, 28.
WISTREICH, J. G.	1955	*Proc. Inst. of Mech. Engrs.*, **169**, 654.

Journal of the Mechanics and Physics of Solids, 1956, Vol. 4, pp. 283 to 293. Pergamon Press Ltd., London.

CREEP RELAXATION FOR COMBINED STRESSES

By J. E. Griffith* and Joseph Marin†

(*Received 6th June*, 1956)

Summary

This paper develops a theory for predicting stress relaxation-time relations for creep in the case of combined stresses based on an assumed constant stress-creep-time relation. The accuracy of the theoretical prediction is checked experimentally by conducting some preliminary creep relaxation tests on thin-walled circular tubes subjected to combined axial tension and torsion. The material tested was an aluminium alloy 3S-0 and the experiments were conducted at room temperature.

1. Introduction

Many studies have been conducted on the mechanics of creep for simple stresses as indicated by reviews prepared by Hoff (1955), Marin (1951) and Schwope (1952). However, most investigations have considered the condition where the stresses remain constant and do not change with time. The general condition, however, is that of stress relaxation in which stresses change as creep deformations occur. Some creep stress relaxation studies have been made for special cases and simple stresses. Relaxation relations for creep in simple tension have been derived based on constant-stress creep relations by Davis (1943), Nadai (1952), Oding (1950), Pao (1952), Popov (1942), Roberts (1949), Robinson (1939) and Soderberg (1939). The authors were unable to find any published papers on experimental studies on creep relaxation for combined stresses. A theoretical analysis on creep relaxation under a combined state of stress was made by Davis (1952). Davis considered the stress relaxation of radial and tangential stresses in an ideal elastic-viscous thick-walled tube.

This paper presents theories for creep relaxation under combined stresses based upon a selected constant stress creep-stress-time relation for simple tension. To develop this theory, the constant stress creep strain-stress-time relations for combined stresses must first be determined.

2. Constant Creep Strain-Stress-Time Relations under Combined Stresses

For simple tension creep, a good approximation to the actual creep strain-stress-time relations in various materials is obtained by considering the deformation as made up of four parts. That is,

$$\epsilon = \epsilon_e + \epsilon'_p + \epsilon''_p + \epsilon'''_p \tag{1}$$

* Department of Civil Engineering, Yale University.
† Department of Engineering Mechanics, Pennsylvania State University.

where ϵ_e is the elastic component, ϵ'_p is the plastic component, ϵ''_p is the transient component and ϵ'''_p is the steady-state (or constant creep rate) component. Furthermore, it will be assumed that the foregoing strain components may be expressed in terms of stress and time as follows

$$\epsilon = \frac{\sigma}{E} + k_1 \sigma^n + k_2 \sigma^n (1 - e^{-qt}) + k_3 t \sigma^n \tag{2}$$

where σ = stress, t = time, e = base for natural logarithms, and E, k_1, k_2, k_3, q and n = material constants. Each term on the right-hand side of (2) corresponds respectively to each term on the right-hand side of (1).

For the case of combined stresses, it will be assumed that each principal strain may also be expressed in terms of four components as defined in (1). That is, if ϵ_1, ϵ_2, and ϵ_3 are the three principal total strains,

$$\left.\begin{aligned} \epsilon_1 &= \epsilon_{e1} + \epsilon'_{p1} + \epsilon''_{p1} + \epsilon'''_{p1} \\ \epsilon_2 &= \epsilon_{e2} + \epsilon'_{p2} + \epsilon''_{p2} + \epsilon'''_{p2} \\ \epsilon_3 &= \epsilon_{e3} + \epsilon'_{p3} + \epsilon''_{p3} + \epsilon'''_{p3} \end{aligned}\right\} \tag{3}$$

The elastic part of the strain in (3) is, in terms of the principal stresses,

$$\left.\begin{aligned} \epsilon_{e1} &= \frac{1}{E}\left[\sigma_1 - \nu(\sigma_2 + \sigma_3)\right] \\ \epsilon_{e2} &= \frac{1}{E}\left[\sigma_2 - \nu(\sigma_3 + \sigma_1)\right] \\ \epsilon_{e3} &= \frac{1}{E}\left[\sigma_3 - \nu(\sigma_1 + \sigma_2)\right] \end{aligned}\right\} \tag{4}$$

To determine the nonelastic strain components in terms of the principal stresses, it will be assumed, as in the total strain theory of plasticity, that (1) the nonelastic strains produce no volume change, and (2) the ratios of the principal shear strains to shear stresses are equal. By assumption (1),

$$\epsilon_{p1} + \epsilon_{p2} + \epsilon_{p3} = 0 \tag{5}$$

where

$$\epsilon_{p1} = \epsilon'_{p1} + \epsilon''_{p1} + \epsilon'''_{p1} \quad \text{etc.}$$

By assumption (2)

$$\frac{\epsilon_{p1} - \epsilon_{p2}}{\sigma_1 - \sigma_2} = \frac{\epsilon_{p2} - \epsilon_{p3}}{\sigma_2 - \sigma_3} = \frac{\epsilon_{p3} - \epsilon_{p1}}{\sigma_3 - \sigma_1} = c. \tag{6}$$

From the three equations defined in (5) and (6) it can be shown that

$$\left.\begin{aligned} \epsilon_{p1} &= c'\left[\frac{(\sigma_1 - \sigma_2) - (\sigma_3 - \sigma_1)}{2}\right] = \left(\frac{\bar{\epsilon}_p}{\bar{\sigma}}\right)\left[\frac{(\sigma_1 - \sigma_2) - (\sigma_3 - \sigma_1)}{2}\right] \\ \epsilon_{p2} &= c'\left[\frac{(\sigma_2 - \sigma_3) - (\sigma_1 - \sigma_3)}{2}\right] = \left(\frac{\bar{\epsilon}_p}{\bar{\sigma}}\right)\left[\frac{(\sigma_2 - \sigma_3) - (\sigma_1 - \sigma_2)}{2}\right] \\ \epsilon_{p3} &= c'\left[\frac{(\sigma_3 - \sigma_1) - (\sigma_2 - \sigma_3)}{2}\right] = \left(\frac{\bar{\epsilon}_p}{\bar{\sigma}}\right)\left[\frac{(\sigma_3 - \sigma_1) - (\sigma_2 - \sigma_3)}{2}\right] \end{aligned}\right\} \tag{7}$$

where $\bar{\epsilon}_p$ and σ are the nonelastic effective stress and effective strain and have values

$$\left.\begin{aligned} \epsilon_p &= \sqrt{\tfrac{2}{3}\left(\epsilon^2_{p1} + \epsilon^2_{p2} + \epsilon^2_{p3}\right)} \\ \bar{\sigma} &= \frac{1}{\sqrt{2}}\sqrt{(\sigma_1 - \sigma_2)^2 + (\sigma_2 - \sigma_3)^2 + (\sigma_3 - \sigma_1)^2} \end{aligned}\right\} \tag{8}$$

Applying the first of (7) to simple tension and noting by (2) that

$$\epsilon_p = \sigma^n\left[k_1 + k_2(1 - e^{-qt}) + k_3 t\right],$$

$$\frac{\epsilon_p}{\sigma} = \frac{\bar{\epsilon}_p}{\bar{\sigma}} = \bar{\sigma}^{n-1}\left[k_1 + k_2(1 - e^{-qt}) + k_3 t\right]. \tag{9}$$

From (7) and (9) the nonelastic strains in terms of the stresses can now be completely defined. That is

$$\left.\begin{aligned} \epsilon_{p1} &= \bar{\sigma}^{n-1}\left[k_1 + k_2(1 - e^{-qt}) + k_3 t\right]\left(\sigma_1 - \frac{\sigma_2}{2} - \frac{\sigma_3}{2}\right) \\ \epsilon_{p2} &= \bar{\sigma}^{n-1}\left[k_1 + k_2(1 - e^{-qt}) + k_3 t\right]\left(\sigma_2 - \frac{\sigma_3}{2} - \frac{\sigma_1}{2}\right) \\ \epsilon_{p3} &= \bar{\sigma}^{n-1}\left[k_1 + k_2(1 - e^{-qt}) + k_3 t\right]\left(\sigma_3 - \frac{\sigma_1}{2} - \frac{\sigma_2}{2}\right) \end{aligned}\right\} \tag{10}$$

where $\bar{\sigma}$ is defined by (8).

The nonelastic strains in (10) may be combined with the elastic strains in (4) to give the total principal strains in terms of the principal stress. Then,

$$\left.\begin{aligned} \epsilon_1 &= \frac{1}{E}\left[\sigma_1 - \nu(\sigma_2 + \sigma_3)\right] + \bar{\sigma}^{n-1}\left[k_1 + k_2(1 - e^{-qt}) + k_3 t\right]\left(\sigma_1 - \frac{\sigma_2}{2} - \frac{\sigma_3}{2}\right) \\ \epsilon_2 &= \frac{1}{E}\left[\sigma_2 - \nu(\sigma_3 + \sigma_1)\right] + \bar{\sigma}^{n-1}\left[k_1 + k_2(1 - e^{-qt}) + k_3 t\right]\left(\sigma_2 - \frac{\sigma_3}{2} - \frac{\sigma_1}{2}\right) \\ \epsilon_3 &= \frac{1}{E}\left[\sigma_3 - \nu(\sigma_1 + \sigma_2)\right] + \bar{\sigma}^{n-1}\left[k_1 + k_2(1 - e^{-qt}) + k_3 t\right]\left(\sigma_3 - \frac{\sigma_1}{2} - \frac{\sigma_2}{2}\right). \end{aligned}\right\} \tag{11}$$

3. Theoretical Relaxation Creep Relations for Combined Stresses

The condition of stress relaxation is defined by expressing the change in the principal strains with time. Since these changes are dependent upon the time and the changes in all three principal stresses, the differential changes in the principal strains may be expressed in general form by the following three equations,

$$\left.\begin{aligned} d\epsilon_1 &= \left.\frac{\partial\epsilon_1}{\partial\sigma_1}\right| d\sigma_1 + \left.\frac{\partial\epsilon_1}{\partial\sigma_2}\right| d\sigma_2 + \left.\frac{\partial\epsilon_1}{\partial\sigma_3}\right| d\sigma_3 + \left.\frac{\partial\epsilon_1}{\partial t}\right| dt \\ d\epsilon_2 &= \left.\frac{\partial\epsilon_2}{\partial\sigma_1}\right| d\sigma_1 + \left.\frac{\partial\epsilon_2}{\partial\sigma_2}\right| d\sigma_2 + \left.\frac{\partial\epsilon_2}{\partial\sigma_3}\right| d\sigma_3 + \left.\frac{\partial\epsilon_2}{\partial t}\right| dt \\ d\epsilon_3 &= \left.\frac{\partial\epsilon_3}{\partial\sigma_1}\right| d\sigma_1 + \left.\frac{\partial\epsilon_3}{\partial\sigma_2}\right| d\sigma_2 + \left.\frac{\partial\epsilon_3}{\partial\sigma_3}\right| d\sigma_3 + \left.\frac{\partial\epsilon_3}{\partial t}\right| dt. \end{aligned}\right\} \tag{12}$$

The vertical lines following each partial derivative in (12) indicates that the initial values of σ_1, σ_2, σ_3, and t are to be substituted after differentiation. The partial derivatives in (12) can be determined by means of (11). For example, from (11),

$$\frac{\partial \epsilon_1}{\partial \sigma_1} = \frac{1}{E} + \left[k_2 (1 - e^{-qt}) + k_3 t\right] \left[\bar{\sigma}^{n-2}\right] \left[(n-1)\left(\sigma_1 - \frac{\sigma_2}{2} - \frac{\sigma_3}{2}\right)^2 + \bar{\sigma}^2\right]. \quad (13)$$

The substitution of other derivatives similar to (13) in (12) yields three equations which cannot be solved directly for the stresses since they appear in mixed terms and are raised to various values of the exponents. To obtain an approximate direct solution (12) can be expressed in terms of increments in place of differentials Then by Taylor's series expansion, the equation corresponding to the first of (12) becomes

$$\epsilon_1 \left[\sigma_{10} + \Delta\sigma_1, \sigma_{20} + \Delta\sigma_2, \sigma_{30} + \Delta\sigma_3, t_0 + \Delta t\right] =$$

$$\epsilon_1 (\sigma_{10}, \sigma_{20}, \sigma_{30}, t_0) + \left(\Delta\sigma_1 \frac{\partial}{\partial \sigma_1} + \Delta\sigma_2 \frac{\partial}{\partial \sigma_2} + \Delta\sigma_3 \frac{\partial}{\partial \sigma_3} + \Delta t \frac{\partial}{\partial t}\right) \epsilon_1 \Big| + R_1 \quad (14)$$

where

$$R_1 = \tfrac{1}{2} \left[\Delta\sigma_1 \frac{\partial}{\partial \sigma_1} + \Delta\sigma_2 \frac{\partial}{\partial \sigma_2} + \Delta\sigma_3 \frac{\partial}{\partial \sigma_3} + \Delta t \frac{\partial}{\partial t}\right]^2 \epsilon_1'.$$

In this equation the values of ϵ_1' are those values for $(\sigma_{10} + \theta\Delta\sigma_1)$, $(\sigma_{20} + \theta\Delta\sigma_2)$, $(\sigma_{30} + \theta\Delta\sigma_3)$, and $(t_0 + \theta\Delta t_0)$, where θ has some value between zero and one.

Equations similar to (14) may also be written for the strains ϵ_2 and ϵ_3 in which there are remainders R_2 and R_3 in place of R_1. Equation (14) and similar equations for ϵ_2 and ϵ_3 will now be used to define stress relaxation for special cases.

Case 1 – *Three principal strains constant*

For this condition $d\epsilon_1 = 0$, and by (14)

$$\left.\begin{aligned} \frac{\partial \epsilon_1}{\partial \sigma_1}\Big| \Delta\sigma_1 + \frac{\partial \epsilon_1}{\partial \sigma_2}\Big| \Delta\sigma_2 + \frac{\partial \epsilon_1}{\partial \sigma_3}\Big| \Delta\sigma_3 + \frac{\partial \epsilon_1}{\partial t}\Big| \Delta t + R_1 = 0 \\ \frac{\partial \epsilon_2}{\partial \sigma_1}\Big| \Delta\sigma_1 + \frac{\partial \epsilon_2}{\partial \sigma_2}\Big| \Delta\sigma_2 + \frac{\partial \epsilon_2}{\partial \sigma_3}\Big| \Delta\sigma_3 + \frac{\partial \epsilon_2}{\partial t}\Big| \Delta t + R_2 = 0 \\ \frac{\partial \epsilon_3}{\partial \sigma_1}\Big| \Delta\sigma_1 + \frac{\partial \epsilon_3}{\partial \sigma_2}\Big| \Delta\sigma_2 + \frac{\partial \epsilon_3}{\partial \sigma_3}\Big| \Delta\sigma_3 + \frac{\partial \epsilon_3}{\partial t}\Big| \Delta t + R_3 = 0. \end{aligned}\right\} \quad (15)$$

The partial derivatives in (15) can be obtained from (12). When the time Δt is selected, (15) then gives three simultaneous equations which can be solved for the unknown stress increments $\Delta\sigma_1$, $\Delta\sigma_2$, and $\Delta\sigma_3$ using an iterative process. The solution can be simplified by noting that approximations may be made depending upon whether the times are short or long.

Case 2 – *Principal strain* ϵ_1 *and stresses* σ_2 *and* σ_3 *constant*

By the first of (12) for ϵ_1 constant $d\epsilon_1 = 0$ and

$$\frac{\partial \epsilon_1}{\partial \sigma_1}\Big| \Delta\sigma_1 + \frac{\partial \epsilon_1}{\partial \sigma_2}\Big| \Delta\sigma_2 + \frac{\partial \epsilon_1}{\partial \sigma_3}\Big| \Delta\sigma_3 + \frac{\partial \epsilon_1}{\partial t}\Big| \Delta t = 0. \quad (16)$$

The solution of (16) for the stress changes will depend on the stress condition considered. For the principal stress σ_2 and σ_3 constant and σ_1 varying, (16) becomes

$$\left.\frac{\partial \epsilon_1}{\partial \sigma_1}\right| \Delta\sigma_1 + \left.\frac{\partial \epsilon_1}{\partial t}\right| \Delta t = 0. \tag{17}$$

Placing the value of ϵ_1 as defined by (11) in (12),

$$\Delta\sigma_1 \left[\frac{1}{E} + \{k_1(1 - e^{-qt}) + k_3 t\}\, \bar{\sigma}^{n-3}\left\{(n-1)\left(\sigma_1 - \frac{\sigma_2}{2} - \frac{\sigma_3}{2}\right)^2 + \bar{\sigma}^2\right\}\right] =$$

$$= -\bar{\sigma}^{n-1}\left(\sigma_1 - \frac{\sigma_2}{2} - \frac{\sigma_3}{2}\right)(k_2 q\, e^{-qt} + k_3)\, \Delta t. \tag{18}$$

Equation (18) can now be used to find the stress change $\Delta\sigma_1$, for the time change Δt. A graphical solution for this case is simpler than the analytical solution. The graphical solution requires the following procedure :

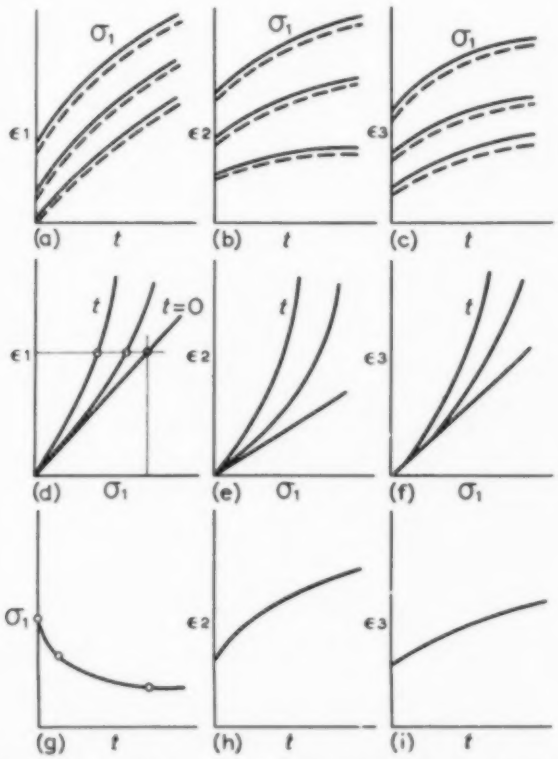

Fig. 1. Graphical solution of stress-time relation when only one principal stress varies.

1. Based upon (11), the strain-time curves are plotted as shown in Figs. 1 (a) and (b) and (c) for different values of σ_1 and the same values of σ_2 and σ_3. Subtracting the assumed nonrecoverable initial plastic strain gives the dotted curves in Figs. 1 (a), (b) and (c).

2. Vertical lines representing selected time values are next drawn in Figs. 1 (a), (b), and (c). The intersection of these time lines and the dotted creep-time curves gives a series of values to enable the plotting of the strain-stress curves shown in Figs. 1 (d), (3) and (f).

3. Knowing the initial value of $\sigma_1 = \sigma_{10}$, a horizontal line is drawn in Fig. 1 (d) through a point defining $\sigma_1 = \sigma_{10}$ (the stress at $t = 0$). A series of values of stress σ_1 corresponding to various times can then be obtained for which the strain ϵ_1 remains constant as indicated in Fig. 1 (d). With these stress and time values known, the relaxation stress-time curve of Fig. 1 (g) can be plotted. In a similar manner using Figs. 1 (e) and (f) the relations of Fig. 1 (h) and (i) may be plotted.

Case 3 – Principal strain ϵ_1 and principal stress ratios σ_2/σ_1 and σ_3/σ_1 constant.

For the condition where the principal stress ratios $\sigma_2/\sigma_1 = \alpha$ and $\sigma_3/\sigma_1 = \beta$ are constant, placing the partial derivatives from (11) in (16) gives

$$\Delta\sigma_1 \left[c_1 + c_2\, n\, \sigma_1^{n-1} \left\{k_2 (1 - e^{-qt}) + k_3\, t\right\}\right] = - c_2\, \sigma_1^{n} (k_2\, q\, e^{-qt} + k_3)\, \Delta t \qquad (19)$$

where

$$c_1 = \frac{1 - v\,(\alpha + \beta)}{E} \text{ and } c_2 = (\alpha^2 + \beta^2 + 1 - \alpha - \beta - \alpha\beta)\, \frac{n-1}{2} \left(1 - \frac{\alpha}{2} - \frac{\beta}{2}\right).$$

Equation (19) may now be used to find changes $\Delta\sigma_1$ in σ_1 for changes in time Δt. Direct solutions can also be determined for the short time values by neglecting the transient and steady-state strains. For long time values, the elastic strains may be neglected to provide a direct solution of (19). A graphical solution of the problem can also be made by using a procedure similar to that employed for Case 2.

4. Combined Stress-Relaxation Tests

In order to determine the accuracy of the combined stress-relaxation theory proposed in this paper, some preliminary experiments were conducted on thin-walled tubular specimens of an aluminium alloy 3S-0 (Fig. 2). The material tested has the properties shown in Table 1 :

TABLE 1

Average Mechanical Properties of Aluminium Alloy 3S-0

Ultimate tensile strength	16,000 psi
Tensile yield strength	6,000 psi
Compressive yield strength	6,000 psi
Modulus of elasticity	10,300,000 psi
Brinell number	28
Ultimate shear strength	11,000 psi
Shear field strength	4,000 psi

The combined stresses were produced by applying torsion and axial tension to the thin-walled tubular specimen. Both the tensile and torsion loads were applied

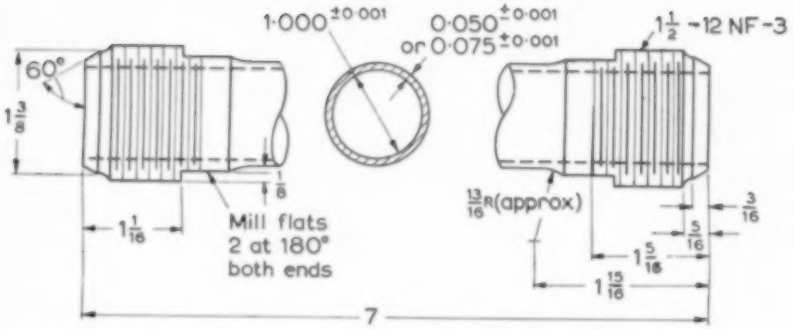

Fig. 2. Test specimen.

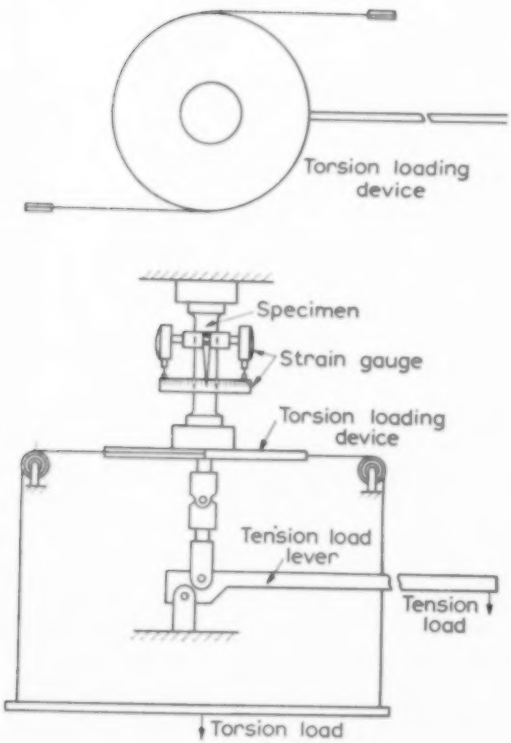

Fig. 3. Combined tension-torsion creep machine.

by dead weights as shown in Fig. 3. The tensile load was placed at the end of a lever (A) which is connected to the bottom of the specimen (S). The torsion load is applied by dead weights supported by cables passing over pulleys to a disk (B). By wrapping the two cables around the disk on opposite sides of the disk, a twisting moment is produced on the specimen. The axial and torsional stresses are determined from the known applied loads and the dimensions of the specimen.

Axial strains were measured by two mechanical averaging dial gauges (Fig. 3). The gauge length used was 2 in. and the dial gauges read to within 0·0002 in. The angle of twist was measured by a graduated disk which had inscribed markings for each degree. A vernier made it possible to read angles of twist within 0·05 degrees for the 2 in. gauge length used. The specially designed combined stress-strain gauge used for measurement of the axial strains and angles of twist was attached directly to the specimens as indicated in Fig. 3.

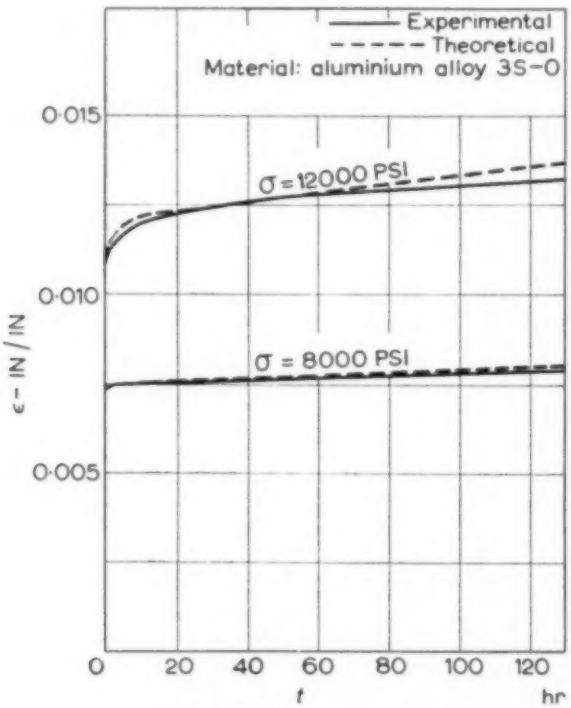

Fig. 4. Tension creep curves.

Preliminary constant-stress tensile creep tests were conducted to determine the creep constants in (2). These material constants were found to be :

$k_1 = 0, k_2 = 5{\cdot}53 \times 10^{-17}, k_3 = 6{\cdot}92 \times 10^{-20}, q = 0{\cdot}12, E = 10{\cdot}6 \times 10^6$ psi, $n = 3{\cdot}33$.

The actual creep time curves and their comparisons with theoretical relations based on (2) are shown in Fig. 4.

Three preliminary relaxation creep tests were conducted including simple tension, pure torsion and combined tension and torsion tests. In the case of the

simple tension and pure torsion tests, the initial axial strain and angle of twist were respectively maintained constant while the loads were reduced. For the combined tension-torsion relaxation test, the axial strain and principal stress ratio were maintained constant. The results of these tests are shown in Figs. (5) and (6).

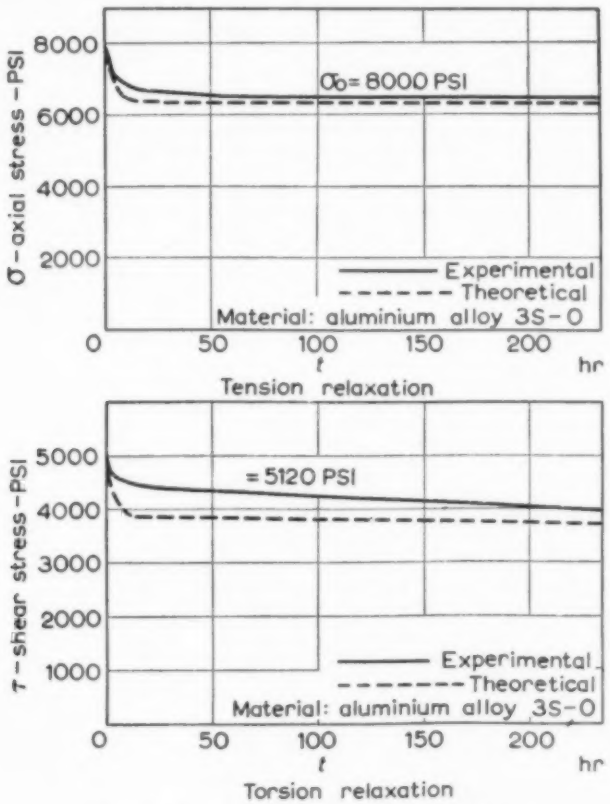

Fig. 5. Tension and torsion relaxation curves.

For the case of tension and torsion relaxation, the graphical procedure described in this paper was used to obtain the theoretical creep-relaxation relations indicated by the dotted lines in Fig. (5). However, the analytical procedure was used to obtain the theoretical creep-relaxation relations shown in Fig. (6). A comparison of the dotted and solid curves in Figs. (5) and (6) indicate approximate agreement between tests and theory.

5. Conclusions

This paper develops a theory for creep relaxation in the case of combined stresses. Some preliminary combined-stress creep-relaxation experiments were conducted that indicate for the material tested approximate agreement between the theory

proposed and test results. To the authors' knowledge, this is the first time creep-relaxation experiments have been conducted for combined states of stress.

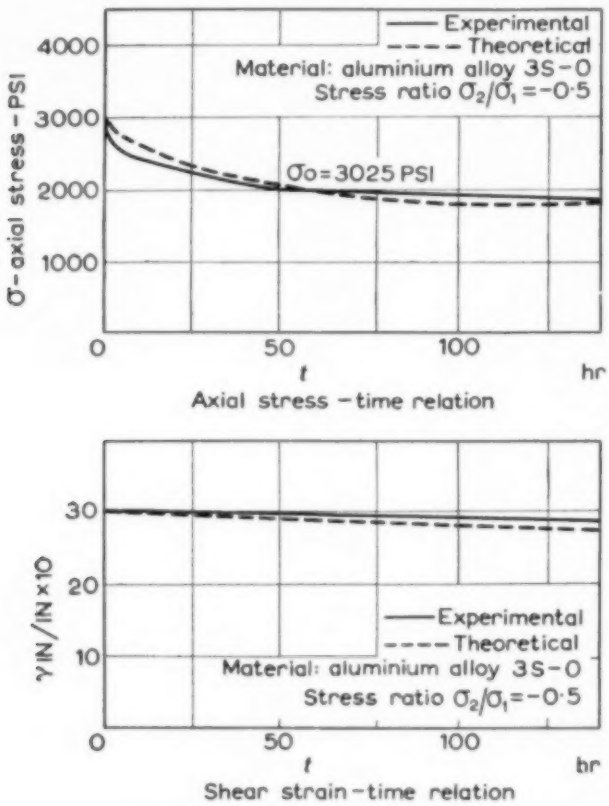

Fig. 6. Tension-torsion relaxation curves.

Acknowledgments

This study represents in part a Ph.D. Thesis conducted by J. E. Griffith under the supervision of Joseph Marin. The financial assistance of the National Science Foundation and the du Pont Company in making possible this project is greatly appreciated. The authors also acknowledge the valuable suggestions of Dr. L. W. Hu, Assistant Professor of Engineering Research.

References

Davis, E. A.	1943	*J. Appl. Mech.*, **10**, A101.
	1952	*Trans. Amer. Soc. Mech. Eng.*, **74**, 381.
Hoff, N. J.	1955	*Appl. Mech. Rev.*, **8**, 453.
Marin, J.	1951	*Appl. Mech. Rev.*, **4**, 633.
Nadai, A.	1952	*Trans. Amer. Soc. Mech. Eng.*, **74**, 403.
Oding, I. A.	1950	*Doklady Akad. Nauk, U.S.S.R.*, **75**, 197.

Pao, Y. H.	1952	Thesis, Pennsylvania State University.
Popov, E. P.	1947	*J. Appl. Mech.*, **14**, 135.
Roberts, I.	1949	*J. Appl. Mech.*, **16**, 208.
Robinson, E. L.	1939	*Trans. Amer. Soc. Mech. Eng.*, **61**, 543.
Schwope, A. D., Schober, F. R. and Jackson, L. R.	1952	*N.A.C.A. Tech. Note* 2618.
Soderberg, C. R.	1939	*Plastic Flow and Creep in Polycrystalline Materials*, pp. 238-244 (Wiley & Sons).

Journal of the Mechanics and Physics of Solids, 1956, Vol. 4, pp. 294 to 299. Pergamon Press Ltd., London.

MINIMUM WEIGHT DESIGN OF CIRCULAR PLATES

By Walter Freiberger and Bekir Tekinalp
Brown University

(*Received 7th May*, 1956)

Summary

The theory of minimum weight design of circular thin plates and circular sandwich plates obeying v. Mises's yield condition is discussed. It is shown that the minimum weight design admits a failure mechanism for which the mechanical energy dissipated per unit volume has a constant value throughout the plates. The distribution of the bending moments and thickness throughout the plates are determined.

1. Introduction

This paper is concerned with the minimum weight design of circular solid and sandwich plates. Only rotationally symmetric types of loading and simple edge support are considered. The plate material is supposed to obey v. Mises's yield condition and flow rule, and the failure criterion of limit analysis is used. Except for the use of another yield condition, problems of this type have been treated by Hopkins and Prager (1955) minimum weight design of noncircular plates has been discussed by Craemer (1955) and Prager (1955b).

Under the rotationally symmetric conditions considered here, the mechanical behaviour of an element of the rigid, plastic plate is described in terms of the radial and circumferential bending moments as the generalized stresses, and the rates of radial and circumferential curvature as the generalized strain rates (see, for instance, Prager (1954)). Denote the radial and circumferential bending moments by M and N, respectively, and the rates of radial and circumferential curvature by κ and λ. On account of the rotational symmetry, all four quantities depend only on the distance r from the plate centre. In terms of the rate of deflection, $v = v(r)$, the rates of curvature are defined by

$$\kappa = -v'', \qquad \lambda = -v'/r, \tag{1}$$

where the prime indicates differentiation with respect to r.

The yield condition of the solid plate will be assumed to have the form

$$F(M, N) = M_0^{1/2}, \tag{2}$$

where F is homogeneous of the order $\frac{1}{2}$ in M and N and continuously differentiable with respect to these arguments, and M_0 is the fully plastic moment of the plate. If σ_0 is the yield stress in simple tension or compression,

$$M_0 = \tfrac{1}{4}\,\sigma_0 H^2 \tag{3}$$

for a solid plate of the thickness H.

In addition to the yield condition (2), the bending moments M and N must satisfy the equation of equilibrium

$$(rM)' - N = -\int_0^r r\,p\,dr, \tag{4}$$

where $p = p(r)$ is the intensity of the distributed load.

According to the theory of the plastic potential, the yield condition (2) is associated with the flow rule

$$\kappa = \alpha \frac{\partial F}{\partial M}, \qquad \lambda = \alpha \frac{\partial F}{\partial N}, \tag{5}$$

where α is an arbitrary positive factor of proportionality. The rate D at which mechanical energy is dissipated per unit area of the plate is given by

$$D = M\kappa + N\lambda = \alpha\left(M\frac{\partial F}{\partial M} + N\frac{\partial F}{\partial N}\right) = \tfrac{1}{2}\,\alpha M_0^{1/2}, \tag{6}$$

where the last term follows from Euler's theorem on homogeneous functions and equation (2). With α from (6), the flow rule (5) can be rewritten as

$$\kappa = \frac{2D}{M_0^{1/2}}\frac{\partial F}{\partial M}, \qquad \lambda = \frac{2D}{M_0^{1/2}}\frac{\partial F}{\partial N}, \tag{7}$$

2. Minimum Weight Design of Solid Plate

In view of (3) the weight of a solid plate of variable thickness $H = H(r)$ will be proportional to

$$\int_0^R r\,M_0^{1/2}\,dr, \tag{8}$$

where R is the radius of the plate. To minimize the integral (8) under the subsidiary conditions (2) and (4) is a problem that can be treated by standard techniques of the calculus of variations. If $\mu = \mu(r)$ and $\nu = \nu(r)$ are the Lagrangian factors applied to (2) and (4) respectively, the Euler equations corresponding to the variables M_0, M and N are

$$r - \mu = 0, \tag{9}$$

$$\mu\frac{\partial F}{\partial M} - r\nu' = 0, \tag{10}$$

$$\mu\frac{\partial F}{\partial N} - \nu = 0. \tag{11}$$

Elimination of μ and ν between these equations yields

$$\frac{\partial F}{\partial M} = \left(r\frac{\partial F}{\partial N}\right)'. \tag{12}$$

On account of (7), (12) can be written as

$$\frac{M_0^{1/2}}{D}\kappa = \left(\frac{M_0^{1/2}}{D}r\lambda\right)'. \tag{13}$$

In view of (1) and (8), this equation is equivalent to

$$\frac{H}{D} = \text{const.} \tag{14}$$

Equation (14) indicates that the minimum weight design must admit a failure mechanism for which the rate of energy dissipation in each plate element is proportional to the weight of this element. This finding extends to solid plates a result that FOULKES (1954) obtained for structural frames.

3. Minimum Weight Design of Sandwich Plate

The sandwich plate considered here has a light-weight core of given constant thickness H and equal faces of variable thickness h, which has to be designed for minimum weight. The fully plastic moment M_0 is now given by

$$M_0 = \sigma_0 hH, \tag{15}$$

and the weight of the plate is proportional to

$$\int_0^R r\, M_0\, dr. \tag{16}$$

Accordingly, the yield condition is best written in the form

$$F(M, N) = M_0, \tag{17}$$

where F is homogeneous of the order 1 in M and N. This change in the yield condition requires the following changes in (6) and (7):

$$D = \alpha\, M_0, \tag{6'}$$

$$\kappa = \frac{D}{M_0}\frac{\partial F}{\partial M}, \qquad \lambda = \frac{D}{M_0}\frac{\partial F}{\partial N}. \tag{7'}$$

Minimizing the integral (16) under the subsidiary conditions (17) and (5), we obtain (12) as before, and from this, by means of (6') and (7'), the relation

$$\frac{h}{D} = \text{const.}, \tag{18}$$

which replaces (14).

4. The von Mises Yield Condition

The von Mises yield condition is

$$M^2 + N^2 - MN = M_0^2. \tag{19}$$

(a) *The solid plate.* From (19) and (2) we have, for the solid plate,

$$F(M, N) \equiv (M^2 + N^2 - MN)^{1/4} \tag{20}$$

and from (19) and (3)

$$M^2 + N^2 - MN = \tfrac{1}{16}\,\sigma_0^2\, H^4. \tag{21}$$

With $F(M, N)$ from (20), Eq. (12) becomes

$$\left.\begin{aligned} M'(2M^2 + 2N^2 - 11MN) + N'(5M^2 - 4N^2 + 4MN) \\ + \frac{12}{r}(N - M)(M^2 + N^2 - MN) = 0. \end{aligned}\right\} \tag{22}$$

For uniform transverse load the equilibrium equation (5) becomes

$$rM' + M - N = -\tfrac{1}{2} r^2 p. \tag{23}$$

The solution of (22) and (23) for M and N has been found numerically and is plotted in Fig. 1. The thickness distribution was then obtained from (21); it is plotted in Fig. 2.

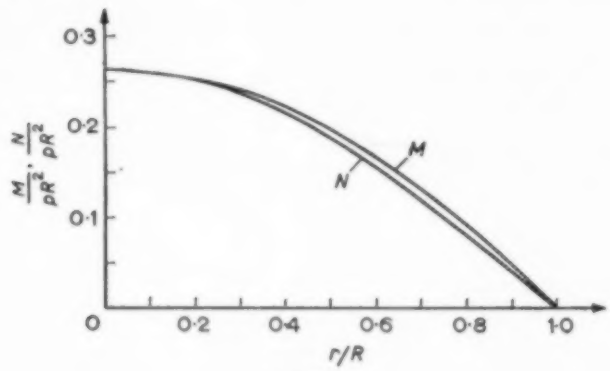

Fig. 1.

(b) *The sandwich plate.* From (19) and (17) we have, for the sandwich plate,

$$F(M, N) = (M^2 + N^2 - MN)^{1/2} \tag{24}$$

and from (19) and (15)

$$M^2 + N^2 - MN = \sigma_0^2 h^2 H^2. \tag{25}$$

With $F(M, N)$ from (24), equation (12) now yields

$$M' MN - N' M^2 + \frac{3}{r}(M - N)(M^2 + N^2 - MN) = 0 \tag{26}$$

which is satisfied by

$$M = N \text{ for all } r. \tag{27}$$

Substitution of (27) into the yield condition (19) shows that

$$|M| = |N| = M_0 \tag{28}$$

everywhere in the plate. The equilibrium equation (23) and the boundary condition $M(R) = 0$ then furnishes

$$M = \frac{p}{4}(R^2 - r^2), \tag{29}$$

for the simply supported plate. Consequently

$$M_0^2 = \sigma_0^2 h^2 H^2 = \frac{p^2}{16}(R^2 - r^2)^2,$$

and the thickness distribution is given by

$$h(r) = \frac{pR^2}{4\sigma_0 H}\left(1 - \frac{r^2}{R^2}\right). \tag{30}$$

Equation (27) could also be obtained from (18) and the fact that $D = \sigma_0 Hh(\kappa^2 + \lambda^2 + \kappa\lambda)^{1/2}$.

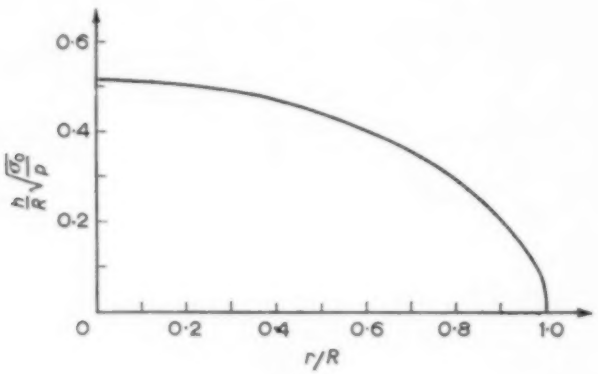

Fig. 2.

5. REMARKS

The results expressed by (14) and (18) seem to be special cases of a general principle in limit design : a minimum weight design admits a failure mechanism for which the mechanical energy dissipated per unit volume has a constant value throughout the structure.

HOPKINS and PRAGER (1955) and PRAGER (1955a) have shown the Tresca yield condition to lead to a minimum weight design for a solid plate in which the radial and circumferential bending moments are both equal to the fully plastic moment at each point. When the VON MISES yield condition is used, this equality of the bending moments is still obtained for the sandwich plate considered here but no longer for the solid plate, though the difference between the two bending moments in this case is nowhere large.

ACKNOWLEDGMENT

The results presented in this paper were obtained in the course of research sponsored by the Ballistic Research Laboratories of Aberdeen Proving Ground under Contract DA-19-020-ORD-798.

References

Craemer, H.	1955	*Ingenieurarchiv* **23**, 151.
Foulkes, J.	1954	*Proc. Roy. Soc.* A, **223**, 482.
Hopkins, H. G. and Prager, W.	1955	*J. Appl. Mech.* **22**, 372.
Prager, W.	1954	*Proc. 2nd U.S. National Congress Appl. Mech.*
	1955a	*Bull. Tech. Suisse Romande*, **81**, 85, sect. 5.
	1955b	*De Ingenieur*, **67**, 046.

Journal of the Mechanics and Physics of Solids, 1956, Vol. 4, pp. 300. Pergamon Press Ltd., London.

CORRIGENDA

The Propagation of Dynamic Stresses in Visco-elastic Rods

(D. S. Berry and S. C. Hunter, *J. Mech. Phys. Solids.*, 1956, **4**, 72)

The second limit on p. 87, for the integral around γ_2, is given incorrectly. In the approximation for $\alpha - \beta \ll \beta$, the limit should read

$$\lim_{\rho \to 0} \int_{\gamma_2} Ids = 2\pi i \, \sigma_0 (\alpha - \beta) \, \kappa x \sinh (\beta \kappa x) \, e^{-\beta t} \left[1 + O(\alpha - \beta)\right]$$

The corrected expressions (10.4), (10.7) resulting from this are

$$-\frac{\sigma(x,t)}{\sigma_0} = 1 - (\alpha - \beta)\, \kappa x \sinh(\beta \kappa x)\, e^{-\beta t}\left[1 + O(\alpha - \beta)\right]$$

$$- \frac{2(\alpha - \beta)}{\pi} \int_0^\infty \frac{\xi}{(1+\xi^2)(\alpha + \beta\xi^2)} \sin\left[\kappa\left(\frac{\alpha - \beta\xi^2}{1+\xi^2}\right)\xi x\right] \exp\left[-\left(\frac{\alpha + \beta\xi^2}{1+\xi^2}\right) t\right] d\xi \qquad (10.4)$$

$$\sigma(x,t) = -\sigma_0 \left[1 - \tfrac{1}{2}(\alpha - \beta)\, \kappa x\, e^{-\beta(t - \kappa x)}\right] H(t - \kappa x) + O\left[(\alpha - \beta)^2\right] \qquad (10.7)$$

Correction of a similar error in evaluating the displacement integral leads to

$$u(x,t) = \sigma_0 \kappa \left\{\left(\frac{\alpha}{\beta}\right)^{\frac{1}{2}}\left[t - \left(\frac{\alpha}{\beta}\right)^{\frac{1}{2}} \kappa x - \frac{\alpha - \beta}{2\alpha\beta}\right] + \frac{\alpha - \beta}{\beta^2}\left[\sinh(\beta\kappa x) + \right.\right.$$

$$\left. + \beta \kappa x \cosh(\beta \kappa x)\right] e^{-\beta(t - \kappa x)}\left[1 - O(\alpha - \beta)\right]$$

$$\left. + \frac{2(\alpha - \beta)}{\pi} \int_0^\infty \frac{\xi^2}{(\alpha + \beta\xi^2)^2} \cos\left[\kappa\left(\frac{\alpha + \beta\xi^2}{1+\xi^2}\right)\xi x\right] \exp\left[-\left(\frac{\alpha + \beta\xi^2}{1+\xi^2}\right) t\right] d\xi \right\} H(t - \kappa x) \qquad (10.6)$$

$$u(x,t) = \sigma_0 \kappa \left\{\left(\frac{\alpha}{\beta}\right)^{\frac{1}{2}}\left[t - \left(\frac{\alpha}{\beta}\right)^{\frac{1}{2}} \kappa x - \frac{\alpha - \beta}{2\beta^2}\right] + \frac{\alpha - \beta}{2\beta^2}(1 + \beta\kappa x)\, e^{-\beta(t - \kappa x)} \right\} H(t - \kappa x)$$

$$+ O\left[(\alpha - \beta)^2\right] \qquad (10.8)$$

in place of the existing expressions.

The paragraph at the top of p. 88 is no longer applicable and should be replaced by the following: "It is easily shown that, neglecting the $O\left[(\alpha - \beta)^2\right]$ terms, the approximate solutions (10.7) and (10.8) satisfy the equation of motion exactly, and also the stress-strain relation (3.15) to the required degree of approximation, provided $\alpha - \beta \ll \beta$ and $(\alpha - \beta)\, \kappa x \ll 1$."

END OF VOL.